LOCAL SHELL-SIDE COEFFICIENTS IN SHELL AND TUBE HEAT EXCHANGERS - THE USE OF A MASS TRANSFER TECHNIQUE

A thesis submitted for the degree of

Doctor of Philosophy

by

Nigel Vivian Mackley

Department of Chemical Engineering

University of Aston in Birmingham

November 1973

SUMMARY

A diffusion-controlled electrochemical mass transfer technique has been employed in making local measurements of shell-side coefficients in segmentally baffled shell and tube heat exchangers. Corresponding heat transfer data are predicted through the Chilton and Colburn heat and mass transfer analogy.

Mass transfer coefficients were measured for baffle spacing lengths of individual tubes in an internal baffle compartment. Shell-side pressure measurements were also made.

Baffle compartment average coefficients derived from individual tube coefficients are shown to be in good agreement with reported experimental bundle average heat transfer data for a heat exchanger model of similar geometry. Mass transfer coefficients of individual tubes compare favourably with those obtained previously by another mass transfer technique.

Experimental data are reported for a variety of segmental baffle configurations over the shell-side Reynolds number range 100 to 42 000.

Baffles with zero clearances were studied at three baffle cuts and two baffle spacings. Baffle geometry is shown to have a large effect on the distribution of tube coefficients within the baffle compartment. Fluid "jetting" is identified with some baffle configurations. No simple characteristic velocity is found to correlate zonal or baffle compartment average mass transfer data for the effect of both baffle cut and baffle spacing.

Experiments with baffle clearances typical of commercial heat exchangers are also reported. The effect of leakage streams associated with these baffles is identified.

Investigations were extended to double segmental baffles for which no data had previously been published. The similarity in the shell-side

characteristics of this baffle arrangement and two parallel single segmental baffle arrangements is demonstrated.

A general relationship between the shell-side mass transfer performance and pressure drop was indicated by the data for all the baffle configurations examined.

ACKNOWLEDGEMENTS

The author wishes to express his gratitude to:-

The Heat Transfer and Fluid Flow Service, AERE Harwell, for sponsoring the work.

Dr B Gay and Dr J D Jenkins for their supervision

Professor G V Jeffreys for provision of research facilities in the Department of Chemical Engineering, University of Aston in Birmingham.

The Reactor Development Division, AEE Winfrith for provision of research facilities and the technical and workshop staff for their assistance in the construction and operation of the equipment.

Dr R V Macbeth for his guidance.

AUTHOR

The author graduated with first class honours in Chemical Engineering from the University of Aston in Birmingham July 1970.

At the time of submitting this thesis, the author is about to take up the position of Petroleum Engineer with the Shell International Petroleum Company.

PREVIOUS PUBLICATION OF THE WORK

"Design Data for Shell-Side Heat Transfer in Shell and Tube Heat Exchangers - The Use of a Mass Transfer Modelling Technique."

B Gay, J D Jenkins, N V Mackley

Paper presented by N V Mackley at the International Centre for Heat and Mass Transfer 1972 International Seminar - "Recent Developments in Heat Exchangers", Trogir, Yugoslavia.

The Work was exhibited at ACHEMA '73 Frankfurt, W Germany, June 1973.

CONTENTS

INTRODUCTION

Detailed knowledge of the features of shell-side heat transfer in shell and tube heat exchangers is generally lacking. Previous work in this field has been devoted almost entirely to the effect of the geometrical parameters on the bundle average heat transfer coefficient.

The need for local shell-side heat transfer data has been created by the advent of precise design procedures for predicting shell-side performance. One such prediction method is being developed by the Heat Transfer and Fluid Flow Service (HTFS), AERE Harwell, the sponsors of this work.

Section 1 of this thesis reviews the literature on shell-side heat transfer.

The use of mass transfer modelling techniques in predicting local shell-side heat transfer coefficients had been demonstrated by Williams (32). In the present work a diffusion-controlled electrochemical mass transfer method was employed. The potassium ferri-ferrocyanide electrochemical system was chosen. Heat transfer data were predicted through the Chilton and Colburn heat and mass transfer analogy. The analogy is examined in Section 2. The electrochemical method is described in Section 3.

The research work was divided into two parts. The first part constituted developing the electrochemical technique in making local measurements of shell-side mass transfer coefficients in a segmentally baffled shell and tube heat exchanger and demonstrating the analogy between these data and actual heat transfer data. This work was performed in the Department of Chemical Engineering of the University of Aston and is described in Section 4 and associated Appendices.

Through the success of the development work, HTFS decided to adopt the electrochemical mass transfer modelling technique in an extensive

research programme to determine local shell-side heat transfer data for a wide variety of segmentally baffled shell and tube heat exchanger geometries. The research work was transferred to the Atomic Energy Establishment, Winfrith. The experimental investigations during this, the second part of the author's research work, are described in Sections 5, 6, 7 and 8. The author's own interpretation of the experimental results from this section of the work is presented in this thesis.

1. SHELL-SIDE HEAT TRANSFER IN SHELL AND TUBE HEAT EXCHANGERS

1.1 INTRODUCTION

Flow across banks of tubes is, from both physical and constructional considerations, one of the most effective means of heat transfer. The repeated expansion and contraction of the flow path across the tubes and the separation of the boundary layer on the downstream side of the tubes cause strong eddying producing excellent mixing in the bulk of the fluid and high heat transfer coefficients.

The baffled shell and tube heat exchanger implements flow normal to tube banks in a configuration which is sturdy enough for industrial use and which provides a large heat transfer surface area to volume ratio. This is accomplished by inserting the tube-bank longitudinally into a cylindrical shell and providing baffles normal to the tube-bank to guide the flow. The essential features of a segmentally baffled shell and tube heat exchanger are shown in Figures 1. and 2. Such an arrangement however destroys the ideal case of purely normal flow. While the flow through the baffle window is predominantly parallel to the tubes, the flow between the baffles is neither uniform nor in fact normal to the tubes. In addition mechanical assembly requirements dictate that there be clearances between the baffles and the shell and between the baffles holes and tubes (see Fig. 2). Since there exists a pressure difference across the baffles, leakage streams are produced through the clearances thus distorting the flow distribution. Some exchangers are constructed such that there is a substantial clearance between the outer row of tubes and the shell which unless blocked leads to significant bypassing of the tubes and a subsequent decrease in exchanger effectiveness.

A complete thermal and hydraulic design of a shell and tube

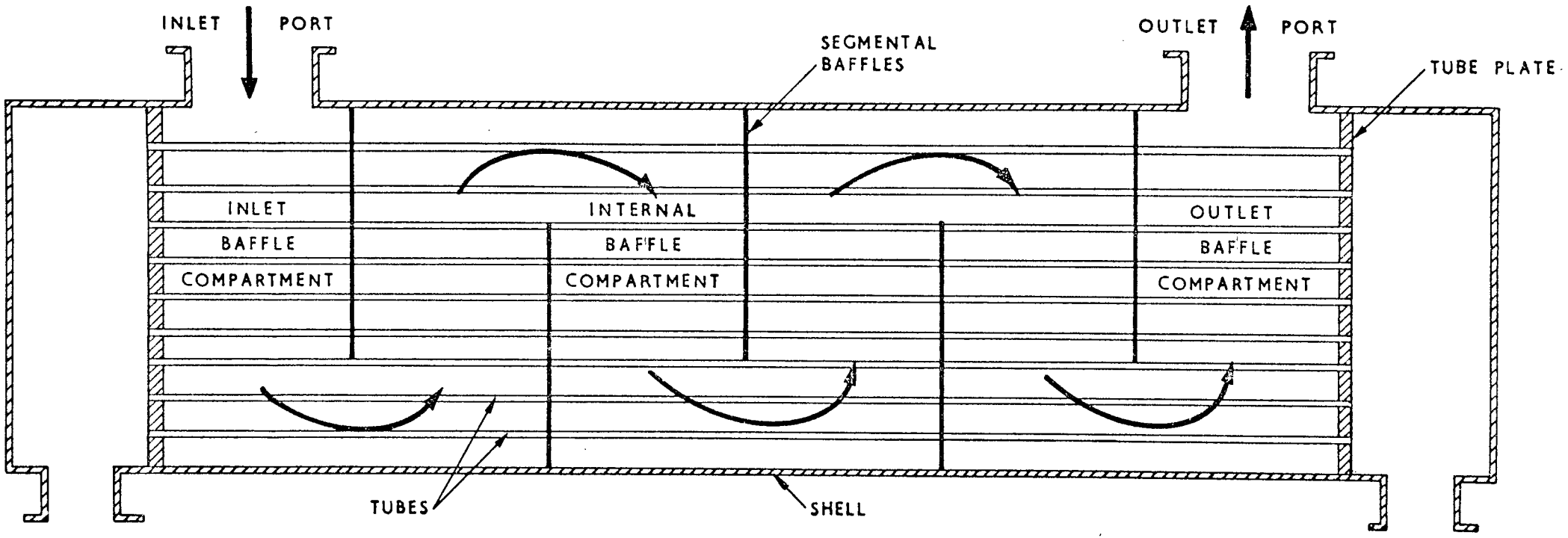

FIG. 1. SEGMENTALLY BAFFLED SHELL AND TUBE HEAT EXCHANGER WITH SINGLE PASS SHELL

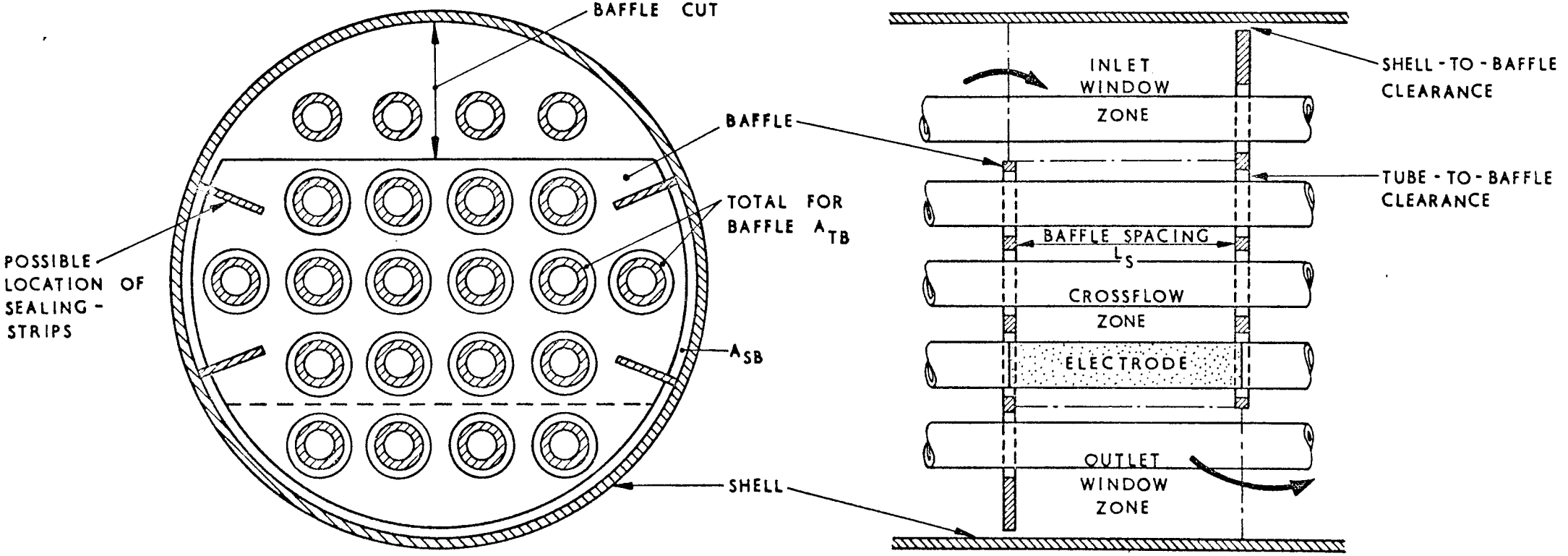

FIG. 2. SHELL-SIDE GEOMETRY NOMENCLATURE

(TUBE-ARRANGEMENT NOT TYPICAL OF THAT USED IN PRESENT WORK)

heat exchanger, or indeed heat transfer equipment generally, requires detailed knowledge of the following:

(i) Heat transfer coefficient data for "clean" surfaces.

(ii) Fluid fouling characteristics.

(iii) Temperature driving force; a log-mean temperature difference (LMTD) is commonly used.

(iv) Pressure drop data.

The present work deals essentially with aspect (i) and to a lesser extent with (iv). Temperature profiles and the estimation of log-mean temperature differences are however briefly discussed in section 1.3.

Fouling, although not included in this work, is of equal if not greater importance compared with the other design aspects. Most heat transfer processes result in deposition of undesirable scale on the transfer surfaces. The thermal resistance of such deposits can reach dominant magnitude, sometimes completely overwhelming the accuracy of heat transfer predictions. Furthermore the deposits can cause blockage of the baffle clearances thus modifying the flow distribution and related phenomena. Taborek (1) in a recent review on fouling in heat transfer systems recommended that greater attention be paid to this phenomenon which in the past has been the subject of few quantitative investigations.

The present work is further confined to the case of single phase flow.

The geometrical complexity of baffled shell and tube heat exchangers resulting in equally complex flow patterns and temperature profiles, makes reliable prediction of the shell-side heat transfer and pressure drop characteristics extremely

difficult. The analysis of the tube-side is however comparatively simple.

The analysis of shell-side phenomena requires consideration of the following geometrical features:

(i) Tube diameter and arrangement

(ii) Baffle spacing

(iii) Baffle cut

(iv) Baffle plate thickness

(v) Baffle leakage clearances: these may be sub-divided into tube-to-baffle clearance and shell-to-baffle clearance

(vi) Bundle bypass channel dimensions.

The effect of the baffle plate thickness (aspect (iv)), is rarely appreciated, being more often than not inadvertently omitted from design calculations. It is probable that the baffle plate thickness would have little effect on the flow as it passed over the baffle in the window zone (see Fig. 2.). The flow through the leakage areas associated with the baffles is however dependent on the flow resistance characteristics of these channels which are in turn functions of the channel length. Thus both the baffle clearances and baffle plate thickness must be incorporated in any rigorous analysis.

The effects of the geometrical features may be taken account of by the definition of a suitable mass velocity or simply correlated as dimensionless groups. This will be demonstrated in the following sections.

The shell and baffles in shell and tube heat exchangers occur in a variety of types. The most common design and that dealt with in the present work comprises:

Shell - single pass with inlet and outlet nozzles located

at the extremities. This corresponds to the T.E.M.A. "E" type shell (2).

Baffles - single segmental although investigations are extended to double segmental in section 8.

Such a configuration is depicted in Fig. 1.

Although the majority of shell-side heat transfer and pressure drop investigations have been confined to this particular design type, simple modifications can often be made to the correlations to make their extension to other designs possible. Evidence of this is shown for the case of double segmental baffles in the present work.

In the following sections the presently available prediction methods for shell-side heat transfer in segmentally baffled shell and tube heat exchangers will be surveyed. The experimental investigations on which the calculation methods were established are also examined in order to elucidate the principles behind shell-side flow phenomena and more particularly to identify inadequacies in the analyses.

The investigations of the present work were conceived out of the recommendations made from the survey.

A preliminary section examines the existing literature on heat transfer associated with the flow across ideal tube-banks.

1.2 HEAT TRANSFER IN IDEAL TUBE-BANKS

The characteristics of rectangular tube-banks in crossflow provide a simple basis for the study of heat transfer and pressure

drop in more complex tube bundle geometries such as those encountered in baffled shell and tube heat exchangers. Furthermore the analytical shell-side heat transfer prediction methods to be discussed in section 1.3.3, use these tube-bank correlations as a basis in the analyses.

Rectangular tube-banks may be classified into:

(i) Ideal tube-banks in which the tube arrangement is geometrically regular throughout the bank and the bank is effectively laterally infinite. Laterally infinite tube-banks are closely approximated experimentally by using half tubes as the side walls, the remaining wall effect being negligible.

(ii) Uniform tube-banks with bypass streams in which the tube arrangement is geometrically regular but in which a clearance exists between the outer row of tubes and the wall.

The review in this present section will be confined to the case of ideal tube-banks. The effect of bypass flow will however be discussed in section 1.3.2.2.

Heat transfer by forced convection for flow normal to tube-banks may be represented by the general equation:

$$Nu = c\ Re^m\ Pr^n \qquad \ldots\ldots (1.1)$$

with Re : based on a characteristic tube outside diameter and flow area

m : often recommended as 0.6 for ideal tube-banks

n : 0.33, taken from tube-side correlations

c : constant, dependent on tube arrangement.

Numerous investigations into crossflow heat transfer in tube-banks have studied the effects of such geometrical variables as tube arrangement, tube diameter and spacing and have derived

corresponding experimental values for the constants in equation (1.1). Some workers, as a result of their investigations, have however proposed slightly different forms of correlating equations.

Colburn (3) published in 1933 a correlation of the existing data for the flow of gases normal to staggered tube-banks in which the term $Nu(Pr)^{-\frac{1}{3}}$ was plotted against the Reynolds number. The characteristic dimension was the tube diameter and the velocity was determined from the minimum free area for flow. Between Reynolds numbers of 2 000 and 32 000 the curve was well represented by the equation:

$$\frac{h\, d_t}{k_f} = 0.33 \left[\frac{Cp\,\mu}{k}\right]_f^{0.33} \left[\frac{G_{max}\, d_t}{\mu_f}\right]^{0.6} \qquad \ldots\ldots (1.2)$$

For in-line arrangements Colburn suggested a similar equation with the value of the constant 0.33 reduced to 0.26.

Grimison (4) correlated the extensive data of Huge (5) and Pierson (6) in the Reynolds number range 2 000 to 40 000, for both staggered and in-line arrangements with air in the form of the equation:

$$\frac{h\, d_t}{k_f} = b \left[\frac{G_{max}\, d_t}{\mu_f}\right]^n \qquad \ldots\ldots (1.3)$$

with tabulated values of b and n for different tube arrangements. These values are reproduced by McAdams (7). For the case of a 1.25 tube pitch to diameter ratio staggered square arrangement, Grimison gives the value of the exponent, n, as 0.56.

There is evidence to show that neither the Grimison nor the Colburn correlations may be safely extrapolated beyond a Reynolds number of 70 000. Sheehan et al. (8) found that in a tube-bank of equilateral triangular pitch, the Colburn curve fitted well with

water up to a Reynolds number of 70 000. Whereas in this region the heat transfer coefficient was proportional to $Re^{0.6}$, for Reynolds numbers between 70 000 and 1 000 000 the value of the Reynolds number exponent rose to 0.8.

Crossflow data at low Reynolds numbers were obtained as part of the extensive shell and tube heat exchanger investigations at the University of Delaware. In the initial investigations, Bergelin et al. (9) examined three tube arrangements of the same tube diameter and pitch over the Reynolds number range 1 to 1 000. Average heat transfer coefficients were obtained for a rectangular tube-bank, seven $\frac{3}{8}$ in. (9.5 mm) diameter tubes wide by ten rows deep. These data and those from pursuing investigations were all correlated in the j-factor form originally employed by Colburn (3). The data thus presented showed a steeper slope than the higher Reynolds number data correlated by Colburn. For the case of a staggered square arrangement, for Reynolds numbers less than 100, the data correlated on a straight line with a corresponding value of 0.32 for the Reynolds number exponent in equation (1.2). Bergelin however confirmed Colburn's findings that the data for in-line tube-banks fell about 40 per cent below that for staggered tube-banks and that staggered square and triangular arrangements correlated on the same curve. No correlating function could be found to correlate all the data over the whole range of flows studied. Whereas data in the laminar region, arbitrarily defined by Bergelin as Reynolds numbers less than 100, could be represented by straight parallel lines, a distinctive curvature existed in the transition and turbulent regions.

In another series of investigations Bergelin et al. (10)

varied the tube diameter and spacing for three tube arrangements. For staggered arrangements, the data for the large and small tube diameters coincided. The in-line arrangements however showed a considerable spread of data and were lower than those for staggered arrangements. Moreover while the staggered arrangements produced smooth transition zone characteristics, the in-line data showed an abrupt "dip" at a Reynolds number of about 1 000. This is attributable to the fact that for staggered arrangements, turbulent eddies first appear at the downstream row of tubes and slowly move upstream as the Reynolds number increases. With in-line arrangements however, turbulent eddies appear throughout the tube-bank at a well defined Reynolds number.

In later work Bergelin et al. (11) extended the investigations to the range of Reynolds numbers 100 to 10 000. Staggered and in-line square and equilateral triangular tube arrangements were again studied at two pitch to diameter ratios. For the square patterns, while the data for the staggered and in-line orientations were coincident at Reynolds numbers above about 4 000, at lower Reynolds numbers the data diverged with the in-line arrangement being inferior to the staggered case. There was evidence however that the data converge again for Reynolds numbers less than 100. It is perhaps significant that the Delaware workers arbitrarily defined the laminar flow region as existing for Reynolds numbers less than 100 and the turbulent region for those greater than 4 000. The onset of the turbulent region was however supported by accompanying visual studies (12).

Zukauskas (13) in a recent survey on heat transfer for flow over tube-banks made the following recommendations for the average value of the Reynolds number exponent in equation (1.1).

Reynolds number range	Value of exponent	
	Staggered	In-line
< 100	0.40	0.40
1 000 to 200 000	0.60	0.63
> 200 000	0.84	0.84

The Reynolds number range 100 to 1 000 was found to exhibit exponent values fluctuating between 0.4 and 0.5. While the value of the Reynolds number exponent was found to be independent of the tube spacing the value of the constant, c, in equation (1.1) was shown to have a definite value for every tube arrangement.

The preceding correlations have all been based on the minimum velocity in the tube-bank. Weisman (14), however, using the void-fraction concept defined a Reynolds number based on the average velocity through the tube-bank. By introducing a further void-volume term to the Colburn j-factor he correlated heat transfer data in the form:

$$j\varepsilon^{\phi b} = \text{function}\left[\frac{d_t\ G}{\mu\ \varepsilon}\right] \qquad \ldots\ldots (1.4)$$

where ε is the void-fraction in the tube-bank and ϕ and b are coefficients dependent on the tube arrangement and Reynolds number respectively. In this form, Weisman correlated the tube-bank data of Pierson (6), Bergelin et al. (9, 10, 11), Sheehan et al. (8) and Kays et al. (15). A very good correlation was found, the data for staggered arrangements showing no deviation from the curve in excess of 10 per cent while in-line data were within 15 per cent. The staggered-tube data were found to lie above the data for in-line banks until a Reynolds number of 30 000 was reached. From this point on, the two curves were coincident. The tube-bank data

were compared with data for single cylinders recommended by McAdams (7). It is interesting to note that while both tube-bank correlations lay above the single cylinder data in the fully turbulent region, in the laminar region the staggered-tube correlation was above but the in-line correlation was below the single cylinder data.

Whitaker (16), in very recent work, proposed a new general form of correlation for packed bed and tube-bank heat transfer data based on the additive effects from model and boundary layer theories. The Nusselt number was thus expressed by the equation:

$$Nu = (0.5\ Re^{\frac{1}{2}} + 0.2\ Re^{\frac{2}{3}})\ Pr^{\frac{1}{3}} \qquad \ldots\ldots (1.5)$$

Using this form of equation Whitaker correlated the data of Bergelin et al. (9, 10, 11), Pierson (6), Kays et al. (15) and Fairchild and Welch (17). While he was able to correlate the staggered-tube data well, the use of the same equation for in-line arrangements produced a fairly wide scatter. Furthermore the correlation was found to be restricted to compact tube arrangements with void-fractions less than 0.65. Pierson (6), Kays et al. (15) and Sheehan et al. (8) and others have shown that the first few rows of a tube-bank have a lower heat transfer coefficient than the tubes of later rows; for staggered-tube arrangements the coefficient in the first row is approximately 0.63 times the mean coefficient in an infinite number of rows. Bergelin et al. (18) found that for tube-banks of up to 10 rows deep, the mean heat transfer coefficient of the tube-bank varied inversely as $N_T^{0.18}$ where N_T is the number of tube rows. The higher coefficients of the rows in the rear of the bank are attributed to increased turbulence.

Comparatively little work has been done to confirm the use of the $\frac{1}{3}$ Prandtl number exponent in correlations for heat transfer

in tube-banks. Limited investigations by Weisman (14) showed that the use of the $\frac{1}{3}$ exponent did not adequately correlate data obtained for Prandtl numbers of 3 and 1. Weisman himself admits that the results should be regarded as being only tentative. The more recent investigations of Zukauskas (19) into 27 tube-banks of different tube arrangements using fluids with Prandtl numbers in the range 0.7 to 500, showed that the power index of the Prandtl number had the value 0.36. For practical purposes, the use of the Colburn $\frac{1}{3}$ exponent is thus justified. A similar conclusion for the Schmidt number exponent in mass transfer was established experimentally in the present work (see Appendix 2.1).

1.3 SHELL-SIDE HEAT TRANSFER PREDICTION METHODS

The methods of prediction of shell-side heat transfer (and pressure drop) in segmentally baffled shell and tube heat exchangers may be classified into four distinct types. It is convenient that this classification also provides a more or less chronological division.

1.3.1 Integral Methods

These methods, using the simple types of equation already described for cross flow in ideal tube-banks, are termed "integral" as they consider the total shell-side flow as effective and introduce only simplied correction factors to account for the effects of bundle geometry. The two representative methods of this group are due to Donohue (20) and Kern (21).

1.3.1.1 Donohue Method

Donohue (20) in 1949 correlated the data of Short (22), Heinrich and Stuckle (23), Bowman (24), Gardner and Siller (25) and Tinker (26) for both bored and unbored shells over the range of Reynolds numbers 100 to 40 000. Donohue found that, in any of Short's heat exchanger models, variations in baffle spacing could be correlated by an equation of the

form originally proposed by Colburn (3) for ideal tube-banks:-

$$\frac{h\, d_t}{k} = C \left[\frac{G_z\, d_t}{\mu}\right]^{0.6} \left[\frac{C_p\, \mu}{k}\right]^{0.33} \qquad \ldots\ldots (1.6)$$

The characteristic mass velocity G_z was taken as the geometric mean of the crossflow velocity at the widest section of the shell and the velocity through the baffle window i.e.

$$G_z = (G_c . G_w)^{\frac{1}{2}} \qquad \ldots\ldots (1.7)$$

Short however, when originally correlating his own data used an average mass velocity that consisted of three equally weighted parts:-

$$G_{AV} = \frac{1}{3} (G_{min} + G_{max} + G_w) \qquad \ldots\ldots (1.8)$$

Variations in baffle cut in the units of Tinker were correlated with a similar equation to that of Equation (1.6) above, provided that the window area was not less than 15 percent of the baffle area.

The effect of tube arrangement was also correlated using Equation (1.6). While the data of Bowman and Tinker gave an essentially constant value for C in Equation (1.6), the data of Short showed a variation from unit to unit. For such cases the value of C was found to be proportional to $De^{0.6}$ where De is the shell equivalent diameter.

Donohue analysed the data from the bored-shell units of Short where a slight variation in baffle-to-shell clearance existed. Previously little attention had been paid to the effects of leakage and in consequence the available

correlations in terms of exchanger geometry were inconsistent because of varying manufacurer's tolerances. Correlating the data in the form of Equation (1.6) showed that there was a significant decrease in the heat transfer coefficient with increase in leakage area, with each clearance case having a distinct value of the constant C. No correlating function for leakage was however proposed. Analysis of the two units tested by Tinker in which the only difference was the clearance area, showed a decrease of 19 percent in heat transfer coefficient as a consequence of the increase in leakage area.

The correlation of the data of Short (22), Tinker (26) and Gardner and Siller (25) prepared by the City and Guilds College for the British Shipbuilding Research Association (27) improves on the Donohue correlation by introducing a "clearance ratio" term. The correlation is defined for Reynolds numbers up to 44 000, where the Reynolds number is based on the mass velocity originally proposed by Short. The full correlating Equation is:-

$$\frac{h\, d_t}{k} = c \left[\frac{P-d_t}{P}\,\frac{d_t}{D_S}\right]^{0.4} \left[\frac{A_w}{A_w+A_{SB}}\right]^{2} \left[\frac{G_{AV}\, d_t}{\mu}\right]^{0.6} \left[\frac{C_p\, \mu}{k}\right]^{0.3} \left[\frac{\mu}{\mu_w}\right]^{0.14} F_E \qquad \ldots\ldots (1.9)$$

The original symbols have been changed in the above equation to preserve continuity in the present work. The term F_E is the end space factor recommended by Tinker (28) to account for the differing characteristics in the heat exchanger end baffle compartments. The correlation was found to represent all Short's data within 18 percent and those of Tinker within 17 percent. The correlation has the deficiency that no account is taken of the effect of tube-to-baffle clearance.

Fluid flowing through this clearance is certainly not, as Tinker (28) suggests, lost as far as heat transfer is concerned. Furthermore the effect of tube arrangment has not been explicitly included, but it would appear that for all normal arrangements the effect is small.

1.3.1.2 Kern Method

Kern (21) correlated "industrial data" in 1950 for baffled shell and tube heat exchangers with a wide variety of shells with "typical" internal leakage areas and a constant baffle cut of 25 percent. He employed a hydraulic mean diameter of the shell D_h for flow parallel to the tubes, as the characteristic dimension in the Reynolds and Nusselt numbers. The shell-side mass velocity, G_K, defined by Kern can be considered as characterising the maximum mass velocity between the tubes near the centre of the tube bundle. He presented a curve representing $Nu.Pr^{-1/3}$ as a function of Reynolds number for the Reynolds number range 10 to 1 000 000. The curve was drawn so that the deviation of the test points (not shown) ranged from 0 to approximately 20 percent high. For Reynolds numbers between 2 000 and 1 000 000 the data was said to be represented by the equation:-

$$\frac{h\,D_h}{k} = 0.36 \left[\frac{G_K\,D_h}{\mu}\right]^{0.55} \left[\frac{C_p\,\mu}{k}\right]^{1/3} \left[\frac{\mu}{\mu_w}\right]^{0.14} \quad \ldots\ldots (1.10)$$

While it undoubtedly has the merit of simplicity, it must be recognised that Equation (1.10) takes no account of effects due to variations in baffle cut, baffle spacing, leakage between the baffles and the shell and the tubes and bundle bypass area. For example Tinker (28) has estimated that the flow through the tube bundle varies between 12 and 60 percent

of the total shell-side flow in liquid coolers, which are very sensitive to changes in leakage or bypass streams; Kern's correlation gives no assistance in predicting the results of such changes.

It is significant to note that until recently the prediction methods of Donohue and Kern were used extensively in design offices, sometimes to the exclusion of all other methods for calculating shell-side heat transfer coefficients.

1.3.2 Semi-Analytical Methods

It was recognised in the late 1940's (28), that better account must be taken of the actual flow distribution in the complex geometry of a baffled exchanger.

The first practical application using this approach was due to Bell (29) who published a concise account of the recommendations from an extensive experimental programme at Delaware University. In an adjusted form his method can be represented as a modification of the "integral" type equation, using a number of correction factors which account for the non-ideality of baffled flow:-

$$\frac{Nu}{Re\ Pr} = St = j_I\ \phi\ \zeta\ \gamma\ \lambda\ \ Pr^{-2/3}\ \left(\frac{\mu}{\mu_w}\right)^{0.14} \qquad \ldots\ldots\ (1.11)$$

where

j_I ideal tube bank j-factor for any given tube layout,

ϕ the baffle window correction factor which accounts for the different effectiveness of crossflow versus window flow,

ζ the shell-to-bundle bypass stream correction factor,

γ the tube-row number correction factor,

λ the combined correction factor for baffle-to-shell and baffle-to-tube leakage streams.

The combined effect of these correction factors can range from almost the full effectiveness of an ideal tube-bank (approximately 0.6) for a well designed tube bundle to as low as 0.1 for poorly designed baffle geometry.

The derivation of the ideal tube bundle heat transfer correlations by Bergelin et al. has already been dealt with in Section 1.2.

The non-ideality correction factors in the Bell equation and their associated underlying experimental investigations will now be examined.

1.3.2.1 Baffle Geometry

The Delaware University experimental investigations into heat transfer and pressure drop in unbaffled ideal rectangular tube-banks, were first extended by Bergelin et al.(30) to a cylindrical baffled exchanger designed so that internal leakage was essentially absent.

The heat exchanger model had 80 $\frac{3}{8}$ in.(9.5 mm) OD tubes arranged on a staggered square pattern inside a $5\frac{1}{4}$ in.(133 mm) ID shell. Tube-to-baffle and shell-to-baffle leakage was eliminated by rubber seals and bundle bypassing was minimised by thoughtful tube arrangement and location of the tie-bars. The model is however described in more detail in Section 4. The tube-side fluid was water while various types of oil were passed through the shell. In the investigations, bundle average shell-side heat transfer coefficients were obtained for three baffle cuts and four baffle spacings.

In the theoretical analysis of shell-side heat transfer, Bergelin divided the fluid flow into a crossflow zone and a window zone (see Fig. 2). The overall heat transfer

coefficient, h_o of the exchanger was thus considered as having two components:-

$$h_o S_T = h_B S_B + h_W S_W \qquad \ldots\ldots (1.12)$$

where subscripts B and W refer to the crossflow zone and window zone respectively, or:-

$$h_B = h_o \Big/ 1 - r + r \frac{h_W}{h_B} \qquad \ldots\ldots (1.13)$$

where

$$r = \frac{S_W}{S_T}$$

Assuming that the crossflow zone characteristics fall close to those of an ideal tube-bank, then from previous studies of the latter:-

$$h_B = \alpha u_M^{0.6} \qquad \ldots\ldots (1.14)$$

and it was further assumed that the same type of relationship held in the baffle window when the geometric mean velocity was used:-

$$h_W = \beta u_Z^{0.6} = \beta u_M^{0.3} u_W^{0.3} \qquad \ldots\ldots (1.15)$$

This led to the equation:-

$$h_o = h_B \left[1 - r + \frac{r\beta}{\alpha} \left(\frac{A_B}{A_W}\right)^{0.3} \right] \qquad \ldots\ldots (1.16)$$

Correlating the experimental results for the varying baffle geometry Brown (31) found that:-

$$\beta = 108 \left(\frac{A_B}{A_W}\right)^{-0.27} r^{-0.68} \qquad \ldots\ldots (1.17)$$

and

$$\alpha = 205.$$

Substituting these values into Equation (1.16) gives:-

$$h_o = h_B \left[1 - r + 0.524\, r^{0.32} \left(\frac{A_B}{A_W}\right)^{0.03} \right] \qquad \ldots\ldots (1.18)$$

Defining a correction factor, ϕ by:-

$$h_o = \phi\, h_B \qquad \ldots\ldots (1.19)$$

gives:-

$$\phi = 1 - r + 0.524\, r^{0.32} \left(\frac{A_B}{A_W}\right)^{0.03} \qquad \ldots\ldots (1.20)$$

Because ϕ was such a weak function of A_B/A_W, the latter may be taken as unity and

$$\phi = 1 - r + 0.524\, r^{0.32} \qquad \ldots\ldots (1.21)$$

Williams (32) in his studies of individual tube coefficients for a heat exchanger of identical geometry, obtained a correction factor to relate the baffle compartment overall coefficient to the average value for the crossflow zone:-

$$\phi = 1 - r + 1.025\, r \left(\frac{A_B}{A_W}\right)^{0.27} \qquad \ldots\ldots (1.22)$$

The differing powers on the function A_B/A_W in Equations (1.20) and (1.22) casts doubt on the validity of the assumptions behind Equation (1.14). However the correction of Williams should be regarded as tentative as only one baffle spacing was investigated.

The baffle geometry correction factors of both Brown and Williams, do not include the shell diameter as a direct

variable, probably because the investigations in both cases were devoted to one and the same shell diameter. It would however be expected that the flow characteristics in a baffled bundle would be affected by the baffle spacing to shell diameter ratio for a certain baffle cut.

1.3.2.2 Bundle Bypassing

If any spacing exists between the outer tubes in a tube bundle and the walls, a disproportionate fraction of the flow will proceed through this bypass area and significantly reduce the effective heat transfer rate and the pressure drop.

Bergelin et al.(33) modified the ideal tube-bank models of previous investigations to study the characteristics of bundle bypassing and in particular the effect of using sealing strips (see Fig. 2). By varying the bypass area and measuring the pressure drop and mass flow rate they were able to estimate the amount of fluid passing through the bypass and tube bundle respectively.

In the laminar flow range for a tube-bank with a 30 percent bypass flow area, the pressure drop was 22 percent while the shell-side heat transfer coefficient was 63 percent of that for an ideal tube-bank. The results were very similar in the turbulent regime. Blocking the bypass stream with one sealing strip gave pressure drops of 67 percent and heat transfer coefficients of about 90 percent of the ideal bundle values. It is significant that the shell-side coefficient based on the mass velocity through the actual tube bundle (as distinct from combined bundle and bypass area), correlated about 10 percent above that for the ideal tube-bundle without bypass.

Bell (29) expressed the results in terms of an ideal tube-bundle correction factor:-

$$\zeta = \frac{h_{BP}}{h_I} = e^{-1.25\, F_{BP}\, (1 - \frac{2N_S}{N_T})} \qquad \ldots\ldots (1.23)$$

where N_T and N_S are the number of tube rows and sealing strips respectively and F_{BP} the fraction of the total minimum cross-flow area that is in the bypass channel.

1.3.2.3 Number of Tube Rows

When correcting non-leakage baffled tube bundle data for effects of baffle geometry and bypassing, it was found that this so formed correlation compared favourably with that for an ideal tube-bank in the turbulent region, but showed considerable deviation in the laminar regime. This was attributed to the variation of the heat transfer coefficient with tube row already discussed for the case of ideal tube-banks in Section 1.2.

The total effective number of crossflow tubes in series in the exchanger was defined:-

$$N_C' = (N_B + 1)\, N_C + (N_B + 2)\, N_W \qquad \ldots\ldots (1.24)$$

From ideal tube-bank results Bergelin et al.(18) had shown:-

$$j \propto N_C^{-0.18} \qquad \ldots\ldots (1.25)$$

Thus to compare results for the 13 row ideal tube-bank with those from the baffled exchanger a correction factor was proposed:-

$$\lambda = \left(\frac{13}{N_C'}\right)^{0.18} \qquad \text{for } Re_M < 100 \qquad \ldots\ldots (1.26)$$

The baffled exchanger data when replotted using this correction factor, fell within 15 percent of the ideal tube-bank data.

1.3.2.4 Leakage

In later work Bergelin et al.(34) examined the effect of clearances between the baffle and the shell and between the tubes and the baffle.

In this series of tests two heat exchanger models were used. One was the 80 tube model previously employed in the no-leakage studies (designated Model 9 by the Delaware workers), while the other was the larger Model 10 consisting of 470 $\frac{1}{4}$ in.(6.3 mm) tubes arranged on an equilateral triangular pattern within a 8.378 in.(213 mm) diameter shell. Bundle bypassing was minimised as in the case of Model 9. Both the individual and combined effects of shell-to-baffle and tube-to-baffle clearances on the overall heat transfer coefficient and baffle compartment pressure drops were investigated. The following general conclusions were drawn out of the investigations:-

(i) Internal leakage had a far greater effect on pressure drop than on heat transfer. Nominal internal clearances were shown to reduce the pressure drop to 25 percent of the non-leakage value while the heat transfer coefficient was only reduced to about 50 percent.

(ii) Shell-to-baffle leakage was found to have a greater effect than leakage round the tubes.

(iii) The addition of tube-to-baffle leakage to the case of shell-to-baffle leakage though reducing the pressure drop, may in some instances enhance the heat transfer.

(iv) In the turbulent flow zone the relative effects of leakage do not vary appreciably with the flow rate.

(v) The amount of leakage area is the major factor in determining the effect of leakage upon heat transfer and pressure drop.

The leakage heat transfer data were correlated by plotting the ratio of heat transfer coefficients with and without leakage against the ratio of leakage area to cross-flow area i.e. $(1 - h_L/h_{NL})$ against A_L/A_M.

Investigations into the individual effect of the sources of leakage, showed that at a given A_L/A_M the value of $(1 - h_L/h_{NL})$ for shell-to-baffle leakage was about twice the value for tube-to-baffle leakage. Thus a single curve of $(1 - h_L/h_{NL})_o$ versus A_L/A_M is obtained if the values of $(1 - h_L/h_{NL})$ for shell-to-baffle leakage only are divided by 2 and the corresponding values for tube-to-baffle leakage by unity. Bell (29) thus proposed the following equation to account for the effect of leakage:-

$$\left[1 - \frac{h_L}{h_{NL}}\right]_{EXCHANGER} = \left[1 - \frac{h_L}{h_{NL}}\right]_o \left[\frac{A_{TB} + 2\,A_{SB}}{A_L}\right] \quad .. (1.27)$$

where the total leakage area $A_L = A_{TB} + A_{SB}$.

Rearranging, the combined leakage correction factor λ is defined by:-

$$\lambda = \frac{h_L}{h_{NL}} = 1 - \left[1 - \frac{h_L}{h_{NL}}\right]_o \left[\frac{A_{TB} + 2\,A_{SB}}{A_L}\right] \quad ..... (1.28)$$

The value of the term $\left[1 - \frac{h_L}{h_{NL}}\right]_o$ is obtained for a given value of A_L/A_M using the correlation expressed graphically in (29).

In the derivation of the leakage correction factor, it was assumed that the effects of individual leakages were additive if each leakage was weighted by its corresponding area. However Bergelin et al.(34) themselves concluded from their experimental investigations that one leakage stream may modify the effect of another leakage stream.

Sullivan (35) obtained an analytical solution of the effect of leakage upon pressure drop using an idealised single baffle exchanger to verify his mathematical model. Although the analysis was too complex for practical design purposes, the leakage path orifice coefficients experimentally obtained therein have proved to be of valuable use in "Stream Analysis" prediction techniques (see Section 1.3.3).

In the final appraisal, the Bell semi-analytical method shows definite advantages and weaknesses. With a minimum amount of additional work, the efficiency factors of the individual streams account much more closely for effects of baffle geometry and manufacturing tolerances than can be accomplished by the pure "integral" methods. Despite the apparent complexity, the method is, with appropriate graphical simplifications, relatively easy to use.

The individual correction factors derived are independent of each other and therefore their interaction cannot be reflected in a way as the theoretical flow model suggests. While additional refinements could be made, the overall approach would seem less effective than the "Stream Analysis" method now described.

1.3.3 Stream Analysis Methods

The Stream Analysis method is based on the original work of Tinker (28) who recognised that a solution to shell-side flow

could be obtained if the shell stream were divided into a number of separate streams as shown in Fig. 3.

Defining an "effective" crossflow velocity, the bundle average heat transfer coefficient was obtained by substituting this velocity value in heat transfer correlations for ideal tube-banks.

The individual streams, in order of decreasing heat transfer and pressure drop efficiency as considered by Palen and Taborek (36) are:-

B-Stream: This is the true crossflow stream and is considered fully effective for both heat transfer and pressure drop.

A-Stream: This stream is created by the pressure differential driving force on the two sides of a baffle forcing fluid through the gap between tubes and baffle holes. Very high heat transfer coefficients were observed in the annular spaces and this stream can be considered fully effective for heat transfer but decreasing the overall pressure drop.

C-Stream: The bundle bypass stream can attain very substantial values for pull-through bundles without sealing devices. The stream is only partially effective for heat transfer as it contacts the heat transfer surface on one side of the channel only.

F-Stream: Tube layout partitions of multitube pass bundles create open passages if located in the direction of the main crossflow stream. The effectiveness of this stream is higher than for C-Stream.

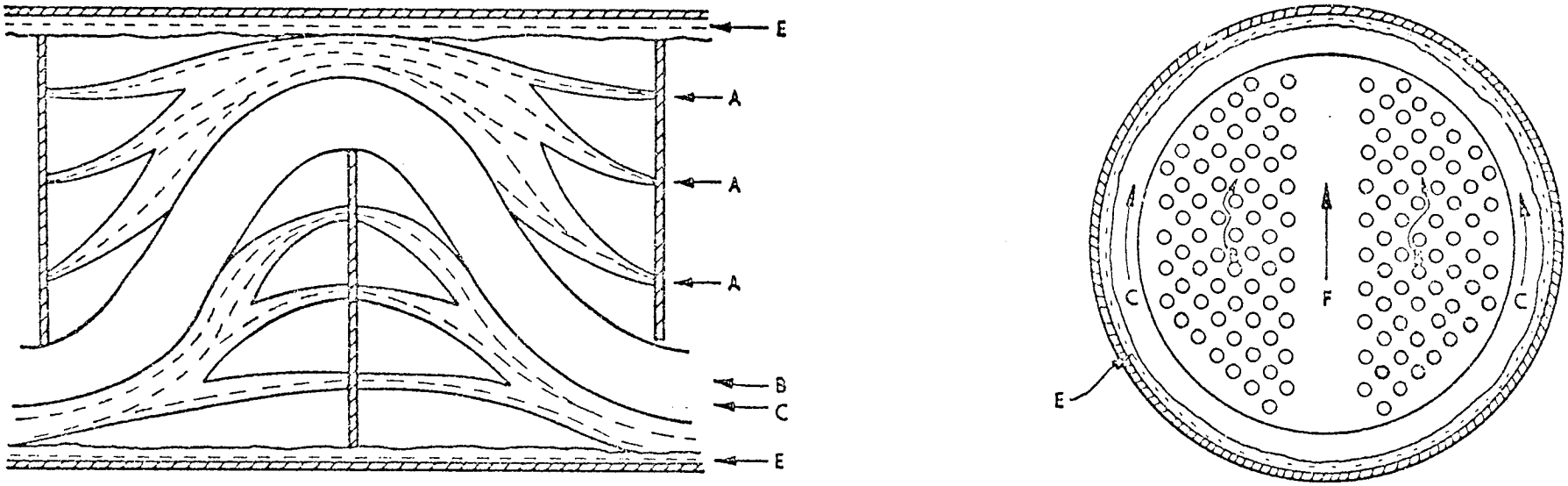

FIG. 3. ILLUSTRATION OF THE SHELL-SIDE FLUID STREAMS

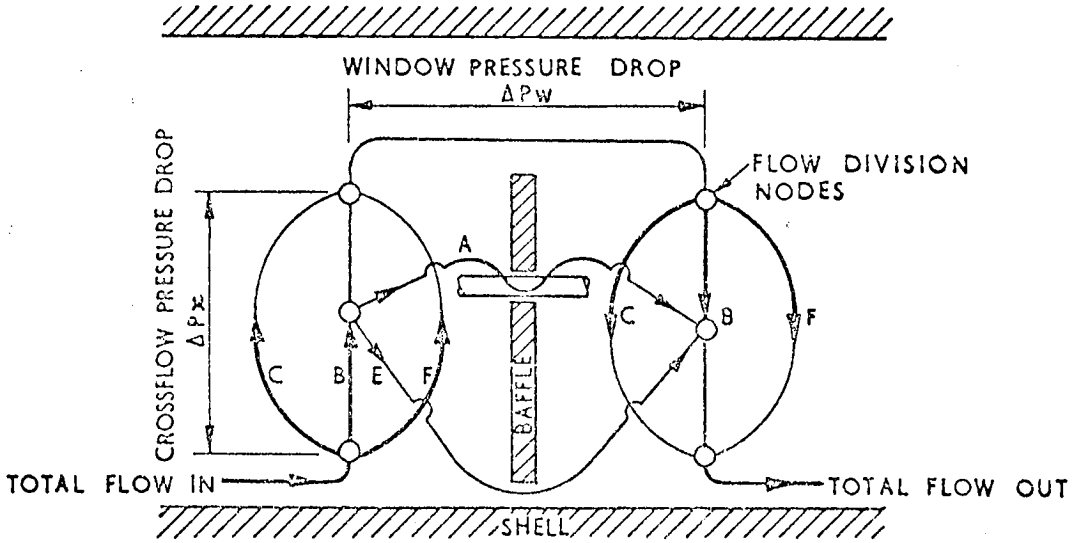

FIG. 4. SCHEMATIC MODEL OF SHELL-SIDE FLOW PATHS AND RESISTANCES ACROSS ONE BAFFLE SPACING

E-Stream: The baffle-to-shell leakage stream is not only considered ineffective but can contribute to considerable distortion of the temperature profile.

No distinct window flow stream is defined for, as will be appreciated, this is composed of varying proportions of the above mentioned streams.

The relative magnitudes of the stream velocities are calculated by considering the individual stream pressure differentials and the conservation of mass. One such solution is given by Palen and Taborek (36) who represented the individual flow streams as a piping network as shown in Fig. 4. Referring to this figure, the pressure drop relations may be expressed as:-

$$\Delta P_C = \Delta P_B = \Delta P_F = \Delta P_X \qquad \ldots\ldots (1.29)$$

and

$$\Delta P_A = \Delta P_E = \Delta P_X + \Delta P_W \qquad \ldots\ldots (1.30)$$

where ΔP_X and ΔP_W are the crossflow and window pressure drops respectively and the subscripts refer to the particular flow stream. The mass flow rate for a stream j, is given implicitly by the pressure drop equation:-

$$\Delta P_j = C\, K_j \left[\frac{W_j}{A_j}\right]^2 \qquad \ldots\ldots (1.31)$$

where K_j is the flow resistance factor, A_j is the associated flow area and C is a constant. The final equation required is the mass balance of the total flow W:-

$$W = W_A + W_B + W_C + W_E + W_F \qquad \ldots\ldots (1.32)$$

When the representative cross-sectional flow areas A_j are defined, Equation (1.29) to (1.32) can be solved with knowledge

of the flow resistance factors for each stream. As the flow resistances are themselves functions of the mass flow rates the method of solution is iterative. The flow resistance factors, are in most cases derived from established ideal tube-bank pressure drop correlations e.g. Grimison (4) and the leakage and bypass channel pressure drop data from the investigations under Bergelin at Delaware University.

A shell-side heat transfer coefficient is calculated by first defining an "effective" crossflow velocity for use in ideal tube-bank heat transfer correlations.

In the original work of Tinker and some later Stream Analysis versions by Parker and Mok (37) and Devore (38), the "effective" crossflow velocity was taken as that for the B-Stream when flowing through the actual crossflow region of the bundle. By not taking the bypass and leakage streams into account when determining the bundle heat transfer coefficient, it was assumed that these streams were completely ineffective as regards heat transfer. Although this may be the case for the bypass and shell-to-baffle leakage streams, experimental evidence shows it to be grossly inaccurate for the tube-to-baffle leakage stream. For Ambrose and Knudsen (39) and Gurushankariah and Knudsen (40) showed that high values of local heat transfer coefficients occurred at the baffle holes. Furthermore Bergelin et al.(34) found that introducing leakage between the tubes and the baffles in one of their experiments increased the shell-side heat transfer coefficient over that obtained with shell-to-baffle leakage only.

A more rigorous approach has been adopted by the Heat Transfer Research Incorporated, California (HTRI), reported by Palen and Taborek (36). In their analysis a heat transfer "effectiveness" value is assigned to each flow stream defined separately for pure

crossflow and window flow, based on experimental values obtained under various baffle geometry designs. Thus while the crossflow stream B is considered to be totally effective, the bundle bypass stream C effectiveness ranges from about 0.1 of that of the B-stream to equal that of the B-stream as bypass channel sealing strips are increased from zero to the optimum number. Streams A and F have an intermediate effectiveness. Thus a nett "effective" flow rate, Q, for use in ideal tube-bank crossflow correlations is defined:-

$$Q_{EFFECTIVE} = \alpha' Q_B + \beta' Q_A + \gamma' Q_C + \zeta' Q_F \qquad \ldots\ldots (1.33)$$

where $\alpha', \beta', \gamma', \zeta'$ are the "effectiveness" factors.

The crucial values of the "effectiveness" factors for each stream were developed for the best overall data fit.

The identification of individual flow streams has shown that considerable distortion of the true mean temperature profile can occur due to the effect of the bypass and more especially the shell-to-baffle leakage stream. As these streams are not essentially in contact with the heat transfer surface, their temperatures alter only by interchange of fluid with the cross-flow and perhaps the tube-to-baffle leakage streams. In consequence for cases of considerable bypassing and leakage a correction to the log mean temperature difference (LMTD) is required. This fact was first recognised by Short (41) who derived such a correction factor for the case of laminar flow. Recently various other workers (42, 36) have proposed more rigorous forms of LMTD correction factors.

1.3.4 Numerical Methods

A new approach to the solution of shell-side heat transfer, pressure drop and temperature distribution is at present being

developed by Spalding (43).

It is shown that the three dimensional differential equations which describe the flow of a continuous fluid may be solved by constructing a finite-difference grid sufficiently fine to represent realistically the details of the tube wall configurations. Solution of a series of energy equations is performed in a similar manner. The iterative procedure involved is particularly suited to computer application.

Up until the present the numerical analysis has only been applied to a simple rectangular baffled exchanger unit without leakage. Furthermore no comparisons have been made with experimental data. Although Spalding points out that because of its flexibility, the method could be applied to geometries of almost infinite complexity, the accuracy of the analysis ultimately depends on the reliability of existing data on flow resistance characteristics of the leakage and bypass channels.

1.3.5 Recommendations

Many of the previously published prediction methods have made claims to varying degrees of accuracy. However no direct comparison of the practical performances of these methods has been made until recently.

Heat Transfer Research Incorporated (HTRI) evaluated the existing prediction methods using their large bank of computer-stored data. The general results from 100 cases published by Taborek (44) are presented in the following table:-

Method	ΔP Data Within ± 30%	Heat Transfer Data Within ± 25%
Kern	10	30
Donohue	20	40
Bell	50	60
Stream Analysis	80	90

The Heat Transfer and Fluid Flow Service (HTFS), the sponsors of the present work, while developing their own Stream Analysis method made comparisons between this method and those of Kern and Bell for which they had written commercially-available computer programs. Although only a limited amount of data were available, their general conclusions echoed those of HTRI in that the Stream Analysis technique possessed superior accuracy for both heat transfer and pressure drop predictions.

Again, in a survey on shell-side heat transfer and pressure drop Emerson (45) concluded that although the Bell rating method was simpler to use than Stream Analysis procedures, the latter were fundamentally more sound and capable of improvement as better data become available.

Industry, in particular heat exchange equipment manufacturers, have in the past relied on the prediction methods of Donohue and Kern and to some extent that of Bell for design purposes. It has been the practice however to place greater emphasis on "experience" in that design of new equipment was, if possible, closely matched to that of existing equipment of proven performance. Manufacturers are now being faced to an increasing extent with the design of equipment for novel heat transfer duties. In this absence of previous design data, they are forced to depend solely on the accuracy of the available prediction methods. In such cases the

use of large design safety factors is common. The use of the Steam Analysis method would thus be justified by virtue of its superior accuracy; furthermore the formal and precise analysis readily lends itself to computerisation.

1.4 THE EXPERIMENTAL DEVELOPMENT OF THE HTFS STREAM ANALYSIS METHOD

The Heat Transfer and Fluid Flow Service (HTFS) are developing a Stream Analysis method which will later be made commercially available. However in order that the method be accepted by industry, stringent performance tests must first be made.

While comparison of overall heat transfer and pressure drop predictions with actual measured performances would naturally be of interest, a more informative approach would involve experimental testing of the individual component correlations within the general analysis. Thus any weaknesses in the analysis could be identified and subsequently corrected.

Measurements of localised values of heat transfer coefficients and pressure drops would thus provide the following general information:-

(i) The knowledge of individual baffle compartment average heat transfer coefficients and pressure drops would provide a means of discriminating between the effects of the internal and the entrance and exit end compartments.

(ii) Average values for the crossflow and window zones provide suitable data for rigorous testing of tentative correlations for heat transfer and pressure drop in these regions.

(iii) Individual tube average heat transfer coefficients give a general picture of the distribution of heat transfer throughout the bundle and would indicate areas of fluid stagnation or maldistribution leading possibly to the design of more efficient exchanger geometries. Such studies would be

particularly useful in analysing the effect of leakage and bundle bypassing.

(iv) Studies of the distribution of heat transfer along a tube would provide information on the heat transfer rates around areas of leakage, the presence of eddy streams behind the baffles and other characteristic flow patterns in the bundle.

(v) Pressure drop measurements made within the bundle when suitably analysed would provide vital friction factor data for the leakage and bypass streams. Such existing data is rather sparse and not too reliable.

The following section reviews the previous investigations into the distribution of shell-side flow and heat transfer.

1.5 PREVIOUS EXPERIMENTAL STUDIES OF THE DISTRIBUTION OF SHELL-SIDE HEAT TRANSFER

Previous investigations into the distribution of shell-side heat transfer in shell and tube heat exchangers are very few in number. Furthermore the majority of these studies have been restricted to bundles of small numbers of large diameter tubes constituting heat exchanger geometries not generally encountered in industrial units. However the results from such investigations provide useful qualitative information about the characteristics of shell-side flow and heat transfer.

It was flow visualisation studies that originally identified characteristic flow patterns in baffled exchangers. Gunter et al.(46) in their simple investigations using a baffled rectangular model without internal leakage showed that the eddy currents or "whirlpools" created behind the baffles were reduced by increasing the number of baffles. Gupta and Katz (47) by observing the motion of coloured beads introduced into the fluid stream of a leak-tight cylindrical glass

exchanger, divided the resulting flow into zones of three different flow characteristics:- longitudinal flow, true crossflow and eddy or dead zones. Unsuccessful attempts were made to correlate the eddy zone heat transfer using established equations for both crossflow and longitudinal flow.

Ambrose and Knudsen (39) were the first to make detailed measurements of local heat transfer coefficients in a cylindrical baffled unit. Using an electrically heated sensing probe they obtained values of heat transfer coefficients for increments of tubes at various positions in the bundle. Studies were made in the presence of leakage for five baffle spacings and two tube pitches. Gurushankaria and Knudsen (40) supplemented this work with more detailed investigations in a single baffle compartment. The results from the combined investigations indicated that:-

(i) The local heat transfer coefficient where the tubes passed through the baffle was between two and four times that at the centre of the crossflow region (i.e. mid-way between baffles) in the same tubes.

(ii) In those tubes which passed through the baffle windows, the local heat transfer coefficient in the plane of the window was higher than in the between-baffle sections of the same tubes.

(iii) There were indications of a large eddy zone in the lee of each baffle. The heat transfer coefficients in these zones was estimated by Gurushankaria and Knudsen to be between 1 and 28 percent higher than that of the average for the pure crossflow zone. It can be suggested that this increase is due to the high velocity jets issuing through the annular spaces in the baffle holes. It is of interest to note that Stachiewicz and Short (50) from studies in an exchanger with

no internal leakage, found that the heat transfer coefficients in the eddy zones in the lee of the baffles were inferior to those for pure crossflow regions.

The heat exchanger model used in the above mentioned series of experiments had a 6 in.(152 mm) diameter shell and 1 in.(25.4 mm) diameter tubes. Two bundles comprising four and fourteen tubes were tested. Ambrose and Knudsen found lower heat transfer coefficients in the fourteen tube bundle, even though the velocity through the exchanger was higher and they attributed this to turbulent effects in the tube bundle. On examination of the tube bundle dimensions it is evident that while the tube separation differed by a factor of about 5 in the two bundles, the clearance between the outer tubes and the shell was kept constant. Thus the bypass flow in the tighter packed fourteen tube bundle may be expected to be much greater than in the four tube bundle, with a consequent effect on the heat transfer coefficient similar to that observed.

Narayanan (51) later extended the work to a tube bundle containing eighteen $\frac{3}{4}$ in.(19 mm) diameter tubes. Segmental baffles of 25 percent cut (diameter based) with leakage clearances were studied for a single spacing and a constant shell-side air flow rate. In order to determine the effect of exchanger geometry on the bundle average coefficient, it was proposed that the exponent of the Reynolds number in the Nusselt type equation be plotted against a term containing the number of tubes, tube pitch and diameter and the number of baffles. Although such a correlation was possible in the case of some similar tests performed using orifice baffles, for segmental baffle investigations there were an insufficient number of variables studied. While obtaining similar heat transfer distribution patterns to those of Ambrose and Knudsen, both local and bundle average heat transfer coefficients were found to be lower than those encountered by these same workers. Narayanan

attributed this to bundle geometry effects, pointing out that his was a more compact bundle. As mentioned earlier, a more feasible explanation could be the existance of differing degrees of bundle bypassing.

Stachiewicz and Short (50) examined local heat transfer coefficients in a baffled rectangular unit without leakage using a coiled-wire heat probe. They presented the distribution patterns in the form of contours indicating that the highest coefficients occurred around the baffle tips, with very low coefficients in the lee of the baffles. The experimental results indicated that heat transfer coefficients in the window zone could be correlated by a crossflow equation if the window velocity was based on the geometric mean of the crossflow and longitudinal velocities as originally proposed by Donohue (20).

The most relevant study of local heat transfer coefficients to shell and tube heat exchanger design was that of Williams (32 , 52). A mercury evaporation mass transfer technique was utilised, giving the corresponding heat transfer data through the Chilton and Colburn heat-mass analogy. The cylindrical exchanger employed was of identical geometry to the eighty-tube Model 9 unit utilised in the Delaware heat transfer investigations (30). As in the Model 9 exchanger, internal leakage was eliminated using rubber seals and bundle bypassing was minimised by thoughtful tube arrangement and location of tie bars. Measurements were made of average coefficients for baffle-spacing lengths of tubes within a central baffle compartment. Investigations were made for three baffle cuts viz. 18.4, 31.0 and 43.7 percent of shell diameter but only a single baffle spacing.

Individual tube coefficients when averaged over the baffle compartment showed good agreement with the actual bundle overall heat transfer coefficient data obtained by Bergelin et al.(30). Average coefficients were calculated for the window and crossflow zones. Correlations for the zonal average coefficients were derived accounting

for the effects of baffle cut. These correlations took the form of a plot of Chilton and Colburn j-factors against a suitably defined Reynolds number. The crossflow data were also correlated in a modified form of that proposed by White and Churchill (53) by plotting the j-factors against $Re_M^{-0.5}$.

In the case of the crossflow a simple velocity based on the minimum flow area at the centre row of tubes was found adequate for use in the Reynolds number. However the window zone data were successfully correlated only when a velocity derived from the geometric mean of the crossflow and window velocities was used.

Analysis of individual tube coefficient values indicated that the distribution of heat transfer in a segmentally baffled unit is affected not only by the bundle geometry but also the shell-side flow rate. While for low flow rates (e.g. $Re_M = 54$) the highest coefficients were found to be around the perimeter of the bundle in the crossflow zone, for the case of large flow rates (e.g. $Re_M = 1625$) these high coefficients were distributed throughout the crossflow zone. It would seem that at the low flow rates the flow resistance in the bundle bypass channel is less than that of the bundle pure crossflow region but these resistances become comparable as the flow rate is increased.

In accordance with the findings from flow visualisation studies, Williams showed that increasing the baffle cut produces maldistribution of flow with an associated reduction in heat transfer coefficients particularly in the extremities of the window zone where stagnant regions would exist.

Roberts (54, 55) utilised the individual tube coefficient data of Williams to determine the distribution of local velocities within the bundle. From comparisons of proportionality constants and the Reynolds number exponents in correlations of individual tube j-factors against Reynolds numbers, he derived velocity ratio terms. In these terms the

apparent crossflow velocity at any tube was related to that of a tube in the middle of the bundle which was considered to possess ideal crossflow characteristics. Such an approach however assumes that variations in tube heat transfer coefficients are due only to changes in the local fluid velocity and not for example due to variations in the direction of fluid flow. Due to turn-round of the shell-side fluid in the baffle window this assumption will hold less validity in the window zones.

The resulting velocity distribution patterns gave further evidence of flow distribution being affected mainly by bundle bypassing. For the extreme values of the baffle cut (18.4 and 43.7 percent) regions in the bundle were produced where the velocity ratio term decreased or increased with the flow rate. However with the intermediate 31.0 percent baffle cut case, there were fewer tubes of this type and the flow distribution was more uniform. In general, the lowest velocities, and hence lowest heat transfer coefficients were found in the outlet window zone.

Although the investigations of Williams went far towards modelling a typical commercial heat exchanger unit, they were however, restricted to the case of no internal leakage. Furthermore the Reynolds number range covered (54 to 1625) merely represents the lower end of those encountered in industrial heat exchangers.

1.6 THE USE OF A MASS TRANSFER MODELLING TECHNIQUE FOR STUDIES OF SHELL-SIDE HEAT TRANSFER

The absence of local shell-side heat transfer data for exchanger geometries representative of commercial units warranted a new series of experimental investigations in this field.

The non-leakage investigations of Williams (32) using an eighty tube bundle provide however, a sound basis for extending the studies in a systematic manner to other geometrical parameters. Furthermore

the bundle average heat transfer coefficient measurements made by the Delaware University workers e.g. (29) for an identical exchanger configuration, afford a convenient source of data for comparison purposes.

The adoption of heat probes for measurements of local shell-side heat transfer coefficients have been found to necessitate the use of large diameter tubes and bulky instrumentation. Moreover great difficulty is experienced in making accurate measurements of local shell-side fluid temperatures. Also the insertion of thermocouples into the tube bundle could possibly disturb the fluid flow.

An alternative is to employ a mass transfer modelling technique for such measurements. Williams (32) has already established the viability of this method in the study of local coefficients in shell and tube heat exchangers.

The mercury evaporation mass transfer technique employed by Williams has however been found to possess the following detrimental features:-

(i) The method is very laborious, with investigations on any tube necessitating prior tube bundle removal. In consequence the technique is totally inadequate for rapid data acquisition.

(ii) The instrumentation is unsuited to the employment of data logging facilities.

(iii) The mercury evaporation technique possesses inaccuracies associated with representative fluid sampling and deposition of mercury in the bundle. These will however be discussed in greater detail in Section 4.4.2.6.

A diffusion-controlled electrochemical mass transfer technique was shown from a literature study to exhibit no such inadequacies (see Section 3.1). Furthermore recent utilisation of this technique at Aston University provided first-hand knowledge of its practical features.

It was thus decided to adopt a diffusion-controlled mass transfer modelling technique in the study of local shell-side heat transfer coefficients utilising the analogy between heat and mass transfer.

The subsequent two chapters examine in detail the analogy between heat and mass transfer and the diffusion-controlled electrochemical technique.

2 THE HEAT AND MASS TRANSFER ANALOGY

2.1 INTRODUCTION

Analogies between momentum, mass and heat transfer make it possible to derive expressions for heat and mass transfer coefficients using fluid friction data and to calculate heat transfer coefficients from experimental data on mass transfer and vice versa.

Analogies between mass and heat transfer processes can be deduced theoretically from similarity of the differential equations describing transfer across the boundary layer, providing the boundary conditions are equivalent.

For the case of steady flow, the differential equations governing convection of heat and mass simplify in their vector form to:-

for heat transfer $$C_p . \rho . u . \nabla T = k \nabla^2 T \qquad \ldots\ldots (2.1)$$

for mass transfer $$u . \nabla C = D_V \nabla^2 C \qquad \ldots\ldots (2.2)$$

From the solution of these differential equations under dynamically similar conditions, various forms of heat and mass analogies have been proposed.

Complete analytical solution of these equations is however generally impossible, necessitating that the anologies be of a semi-empirical form.

One such semi-empirical analogy, chosen for this work, was that proposed by Chilton and Colburn (56).

2.2 THE CHILTON-COLBURN ANALOGY

An analogy between heat and momentum transfer in a turbulent fluid was first suggested by Reynolds (57). By making the assumption that the fluid was turbulent right up to the solid surface, he showed that:-

$$\frac{\tau}{\rho u^2} = \frac{h}{\rho u C_p} \qquad \ldots\ldots (2.3)$$

This relationship is however applicable only to cases with Prandtl numbers of unity.

Taylor (58) and Prandtl (59) modified Reynolds analogy to account for the existance of a laminar sublayer. In their treatment they assumed that the simple Reynolds analogy was applicable to the transfer of heat and momentum from the main stream to the edge of the laminar sublayer. In this region outside the laminar sublayer, molecular diffusion processes were assumed negligible and the turbulent eddy diffusivities for momentum and heat were of equal magnitude. Transfer through the laminar sublayer was then presumed to be attributable solely to molecular diffusion in the complete absence of eddy diffusion. Taylor and Prandtl derived the equation:-

$$St = \frac{h}{C_p \rho u} = \frac{\tau / \rho u^2}{1 + \nu (Pr-1)} \qquad \ldots\ldots (2.4)$$

The term, ν, is the ratio of the velocity at the edge of the laminar sublayer to the stream velocity. For the case of Pr=1, the relationship simplifies to the Reynolds analogy.

A corresponding equation for the analogy between momentum and mass transfer was shown by Sherwood (60) to be:-

$$\frac{K_c}{u} = \frac{\tau / \rho u^2}{1 + \nu (Sc-1)} \qquad \ldots\ldots (2.5)$$

The theory behind these equations assumes an abrupt transition from turbulent to laminar flow at the boundary of the laminar sublayer, thus neglecting the existance of an intermediate buffer zone.

For turbulent flow in pipes, Colburn (3) found that heat transfer data when correlated in terms of j-factors showed approximately the same characteristics as a friction factor correlation. He defined a heat transfer j-factor and represented the heat-momentum relationship

by the equation:-

$$j_h = \frac{h}{C_p \rho u} Pr^{2/3} = \tau / \rho u^2 = 0.023 Re^{-0.2} \quad \ldots\ldots (2.6)$$

Comparing this equation with that of the Prandtl-Taylor analogy shows that $Pr^{2/3}$ replaces the term $\left[1 + \nu(Pr-1)\right]$ as the correction factor for the Reynolds analogy.

Chilton and Colburn (56) extended the Colburn principle to the analogy between heat and mass transfer, defining a corresponding mass transfer j-factor:-

$$\frac{K_c}{u} Sc^{2/3} = j_m = j_h = \text{function (Reynolds number)} \quad \ldots\ldots (2.7)$$

They showed from experimental data that this empirical analogy was applicable to not only turbulent flow in pipes, but also flow across tubes and over plane surfaces. The analogy between heat or mass and momentum is however restricted to systems where no flow separation occurs; for heat and mass transfer have no analogous process to form drag.

The analogy requires dynamic similarity and similarity of boundary conditions. The condition of dynamic similarity is fulfilled by the use of the Reynolds number. The second provision implies that the type of boundary condition, such as constant heat flux or concentration is the same in both cases. Thus utilising an electrochemical modelling technique having a characteristic constant surface concentration would, in the case of heat transfer studies, require an analogous boundary condition in the heat transfer system. However Lucas (61) in his studies of rapid heating furnaces, showed that the analogy still held for the case of a constant heat flux system being modelled by such an electrochemical method.

2.3 PROPERTY NUMBER EXPONENT

Many theoretical and semi-empirical analyses have been proposed in which the existance of a buffer layer and the presence of eddy diffusivity in regions close to the surface have been taken into account. Such phenomena are neglected in the derivation of the Prandtl-Taylor and Chilton-Colburn analogies. However many of these analyses e.g. Murphree (62) and Von Karman (63) have been shown to be accurate only in cases where property numbers (i.e. Prandtl number in heat transfer and Schmidt number in mass transfer) were near unity.

Inadequacies in expressions for eddy diffusivity would be particularly significant in cases of high Prandtl and Schmidt numbers where the associated thin boundary layers produce extremely large temperature and concentration gradients. The effect of expressions for eddy diffusivity is generally reflected in the value of the property number exponent obtained in the analyses. Thus Lin et al.(64) proposed that for the case of large Schmidt and Prandtl numbers, the property number exponent varied with the Reynolds number. In crossflow over tubes, for Reynolds numbers less than 10 000, the value of the exponent approximated to that in the Chilton-Colburn analogy. The theoretical analysis of Deissler (65) however recommended a value of 3/4 for the exponent. For large Prandtl and Schmidt numbers, Mizushina (66) verified both theoretically and experimentally the 2/3 exponent in the Chilton-Colburn analogy.

Mixon and Carberry (67) in their analyses of developing laminar boundary layers, deduced that the property number exponent under these conditions must lie between 1/2 and 2/3 in any transfer correlation. They recommended the use of the 2/3 exponent for a property number greater or equal to 1.0 and an exponent of 1/2 for a property number less than 0.05.

Hubbard and Lightfoot (68) in their study of mass transfer at high Schmidt and Reynolds numbers, made a critical test of the semi-empirical models currently used to describe heat, mass and momentum transfer. These included, in addition to those already mentioned, the analysis of Vieth et al.(69). Their experimental results indicated that for practical purposes, the Chilton-Colburn relation was equivalent, if not superior, to the best of the more sophisticated semi-empirical models. On the other hand the results cast considerable doubt on the analysis of Deissler.

Lucas (61) gave a rigorous experimental test of the Chilton-Colburn analogy in his rapid heating furnace studies. Results from two mass transfer and a heat transfer modelling technique with property numbers of 1600, 2.46 and 0.7 respectively, were shown by the analogy to be in good agreement with each other. Another example of the successful utilisation of the Chilton-Colburn analogy was the tube-bank studies of Williams (32).

The large Schmidt number associated with the electrochemical technique utilised in the present work warranted experimental investigations into the value of the property number exponent in correlations of mass transfer for flow over tube bundles (see Appendix 2.1).

The results showed that for practical purposes the 2/3 exponent in the Chilton-Colburn relationship adequately describes the mass transfer process.

2.4 RANGE OF APPLICATION

The analogies between momentum, mass and heat transfer have all been derived for turbulent flow conditions. Indeed, Colburn originally defined the similarity between heat transfer and fluid friction for flow in smooth pipes to be true only for Reynolds numbers greater than 10 000. In consequence previous use of the Chilton-Colburn analogy has been restricted to cases of essentially turbulent flow.

In laminar flow where transport is essentially by conduction or diffusion, thermal gradients in the case of heat transfer, distort the velocity profile. In mass transfer the analogous phenomenon would be far less significant; for the fluid viscosity would not alter appreciably with variations in concentration. This inadequacy does not arise to any significant extent in turbulent flow where the hydrodynamic boundary layer is much thinner. The case of laminar flow is further complicated by the presence of eddy currents produced by natural convection, the extent to which these are present being characterised by the Grashof number.

In consequence no simple general relationship has been found to adequately describe an analogy between heat and mass transfer by forced convection in laminar flow. However some investigators e.g. (70), have found that for systems of approximately equal property number, under dynamically similar conditions, the Nusselt number in heat transfer falls close to the corresponding Sherwood number in mass transfer.

3. THE ELECTROCHEMICAL TECHNIQUE

3.1 ADVANTAGES AND LIMITATIONS

In the electrochemical technique the transfer surface under investigation is replaced by an electrode of the same dimensions and a source of external potential is applied between this, the test electrode, and another electrode positioned elsewhere in the system. A suitable electrolyte solution is the flow medium. Under diffusion-controlled conditions, the mass transfer coefficient associated with the transfer rate of ions to the test electrode, is obtained directly from current measurements.

The diffusion-controlled electrochemical technique has definite advantages over other mass transfer modelling techniques and methods of direct heat transfer measurement. The electrochemical technique enables the measurement of not only space averaged values but also local values of transfer rates. Furthermore because the response of the electrochemical process is very fast, fluctuation values as well as time-smoothed values can be obtained.

The relative simplicity of the method facilitates economic construction of experimental equipment with the minimum of instrumentation. The accuracy of the technique is inherently high owing to the current being effectively the only measured variable (see Section 3.4). In contrast to other mass and heat transfer techniques where sampling of a fluid stream is necessary, the electrochemical method has its measurements confined to the locality of the transfer surface thus avoiding the difficulties incurred in obtaining representative samples.

The electrochemical technique however, has the limitation of being only directly applicable to the study of transport phenomena associated with liquids, where the Schmidt number is generally high. Furthermore the choice of liquid mixtures is restricted to those that exhibit diffusion-controlled electrochemical reaction characteristics.

3.2 PREVIOUS UTILISATION

Although electrochemists had studied electrode processes in connection with polarographic analysis for many years, it was not until the work of Levich (71) and Agar (72), that the usefulness of diffusion-controlled electrode processes in studies of transport phenomena generally, was recognised.

Since that time the diffusion-controlled electrochemical technique has found successful application in a variety of convective heat and mass transfer investigations. Mizushina (73) gives an appraisal of the use of the electrochemical method in transport phenomena.

The electrochemical technique was first applied to the study of transport phenomena of relatively simple systems e.g. rotating cylindrical electrodes (74, 75). Other workers were soon extending its use to investigations into more practical systems. These studies included flow in pipes (76, 77, 68), pipe flow at abrupt expansions (79, 93), flow in annuli (80, 81, 82), flow over cylinders (77, 83, 84, 70), flow around spheres (85, 86) and through packed and fluidised beds (87, 88, 89).

The technique has been utilised in studies of two-phase systems, in particular climbing and falling films (90, 91, 92). These applications produced the problem of electrolyte degradation by the air present; this being a characteristic of the particular electrochemical system utilised and which for the case of single phase situations can be essentially eliminated (see Appendix 1.1).

The utilisation of the electrochemical technique has not been restricted to forced convection studies. The literature reveals the increasing application of the technique in the field of natural convection. Particular attention has been given to natural convection at horizontal and vertical plates (94, 95, 96, 97) and cylinders (98,99). The mass transfer correlations from such investigations have shown very

close agreement with those obtained using conventional direct heat transfer measurement methods.

A recent publication of Russian work by Shulman et al.(100) shows how the electrochemical technique has been utilised in the study of transfer processes associated with non-Newtonian fluids.

In the last few years, industry's acceptance of the electrochemical technique as a valuable tool in transport phenomena, has been evident from the adoption of the technique in detailed performance analyses of actual industrial equipment. The heat exchanger studies of the present work fall into this very category. Another example is that of rapid heating furnaces (61). In this context it is perhaps of interest to note that since making first publication of this present work (101), the author has been approached on numerous occasions by industrial research departments wishing to employ the electrochemical technique in detailed analyses of the performances of extended heat transfer surfaces.

The electrochemical technique has been further utilised in making direct measurements of velocity gradients close to a surface. The high Schmidt number incurred with electrolyte solutions has meant that because of the associated thin concentration boundary layer, the velocity gradient in this region can be assumed to be linear, thus simplifying the situation. Furthermore a micro-electrode embedded in the wall does not disturb the flow characteristics. Mitchell (102) developed a sheer-stress meter on these principles, for the study of turbulence at a wall.

3.3 VIABILITY AS A MODELLING TECHNIQUE

The following discussions while demonstrating the viability of the electrochemical method as a mass transfer modelling technique, at the same time give further evidence of the accuracy of the Chilton-Colburn heat mass analogy.

Examples are given of four independent investigations into flow over cylinders where the electrochemical data have been compared with

corresponding data from other mass and heat transfer techniques. The case of forced convection for flow over cylinders was chosen because of its particular relevance to the tube bundle studies of the present work.

Dobry (83) showed excellent agreement between his electrochemical data from studies of rates of mass transfer from thin wires with the data obtained from an electrical heating technique. In these two cases the property numbers of the fluids were however of the same order of magnitude.

Grassmann (77) compared his electrochemical data for flow over thick cylinders with correlations produced by various investigators utilising other techniques. These included an evaporation mass transfer technique, two cases of an electrical heating technique and a case where the cylinder was steam-heated. The data when compared by means of the Chilton-Colburn analogy showed remarkably good agreement taking into consideration the wide variation in the Schmidt and Prandtl numbers with technique. For while the evaporation technique had a Schmidt number of near unity, both the electrochemical and heating methods had respective Schmidt and Prandtl numbers up to the order of a thousand.

Mizushina (73) compared his crossflow data with not only similar electrochemical data of Grassmann (77), Dobry (83) and Vogtlander (70) and the electrical heating technique data of Comings (104) and Hilpert (105) but also the correlation of van der Hegge Zijnen (103) compiled from results of many investigators, mainly on heat transfer. This comparison is shown in Fig. 5.

In the cylindrical billet rapid heating furnace studies of Lucas (61) transfer rates were measured using an electrochemical technique, a sublimation technique and an electrical heating technique. The three sets of data, although being subject to scatter particularly

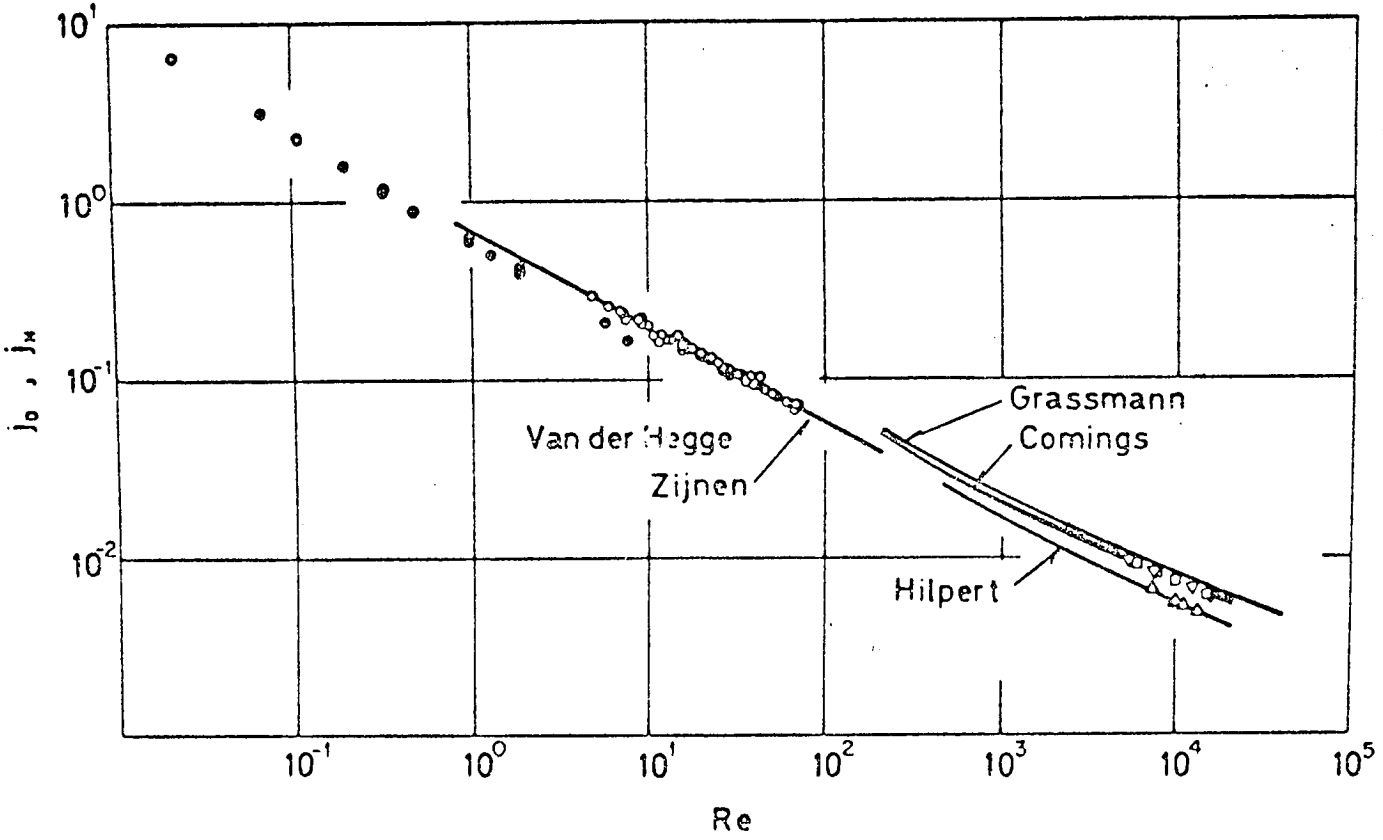

FIG 5 Mass transfer coefficients in cross flow. Key: (⊕) Dobry *et al.*; (○) Vogtländer *et al.*; (△, ▽, □) Mizushina *et al.*

in the sublimation work, fell within about 15 percent of each other when correlated using Chilton-Colburn j-factors.

3.4 THEORY OF ELECTROCHEMICAL TECHNIQUE

3.4.1 Introduction

Since the original foundation work of Agar (72) and Levich (71), the theory of the diffusion controlled electrochemical technique has been given substantial coverage in the literature by the previous users of the technique. Such theoretical treatments while dealing in great depth with the underlying principles of electrode reaction kinetics and polarisation, in general have failed to give attention to the practical aspects of interest to the potential user of the technique. Thus such features as the technique's inherent inaccuracies through theoretical assumptions and its useful range of application have been of conflicting nature or excluded completely.

In the present work a concise explanation of the principles behind the electrochemical technique is presented. Details of the more established electrochemical aspects while perhaps being omitted here are however given by Levich (71).

3.4.2 Mechanism of Diffusion Control

The passage of current through an electrolytic cell can be viewed as a special case of a heterogeneous chemical reaction in that ions move from the bulk of the electrolyte solution to the surface of the electrode where chemical and physical changes occur.

The rate of the overall process may be controlled by the rate of transfer of ions to the electrode surface to replace those that have been removed by the electrode reaction. This is called concentration polarisation as it is associated with a decrease in concentration of the electrolyte in the immediate vicinity of the electrode. Alternatively chemical polarisation may exist whereby the overall process rate is controlled by the electrochemical

reaction on the electrode surface. In measuring the rates of mass transfer by the use of electrochemical reactions it is convenient to make the chemical polarisation negligible because the mass transfer coefficients are more easily obtained from limiting current measurements when the concentration at the liquid-solid interface can be assumed to be zero.

An electrode reaction proceeding at a finite rate involves movement of reacting ions between the electrode and the solution surrounding it.

The transport of such ions is principally by:-

(i) Migration due to the potential field.

(ii) Diffusion due to the concentration gradient.

(iii) Convection by the fluid flow.

Whereas the potential field extends throughout the electrolyte up to the electrode surfaces, the diffusional process, for the case of turbulent forced convection, is confined to an essentially laminar boundary layer adjacent to the electrode surface. Nernst (106) originally postulated a stagnant diffusion layer, but modern boundary layer theory predicts a "mass transfer boundary layer" which allows for fluid motion to extend up to the solid-fluid interface.

Convection although being the predominant mode of transport in the region outside the boundary layer, is however negligible in comparison with diffusional processes within the boundary layer. Thus the "bulk" concentration of the electrolyte solution may be considered to be uniform with any ion concentration gradients being confined to within the mass transfer boundary layer. The overall rate of ion transfer from the "bulk" of the solution to the electrode surface is thus controlled by the diffusion and migration

processes within the boundary layer. Fig. 6 gives a pictorial representation of the transport mechanisms in terms of the electrochemical system used in this work.

The case of laminar forced convection may be treated in the same manner as above realising that the mass transfer is now entirely by diffusion and migration under the potential field. Natural convection effects may however become significant and must be taken into account when analysing experimental data.

For the case of steady and unidirectional mass transfer in the y-direction perpendicular to the surface of the electrode, the rate of transfer of a reacting ionic species, i, may be represented by:-

$$N_i = - n_{e_i}(D_i + \varepsilon_\psi) \frac{F C_i}{RT} \frac{\partial \psi}{\partial y} - (D_i + \varepsilon_D) \frac{\partial C_i}{\partial y} \qquad \ldots\ldots (3.1)$$

the two terms on the right of the equation being the contributions made by migration and diffusion respectively, and ε_ψ and ε_D are those made by turbulence-induced eddies.

The current density, I, at the electrode is expressed by:-

$$\frac{I}{n_{e_i} F} = N_i \qquad \ldots\ldots (3.2)$$

A simplification can be achieved concerning the migration term by adding to the solution of reacting ions a large excess of an indifferent (i.e. unreactive) electrolyte whose decomposition potential is above that used in the experiment and which consequently does not participate in the electrode reaction. The indifferent ions compensate for any potential gradients produced by heterogeneity in the reacting ions, particularly in the region close to the electrode surface. Thus the electrostatic potential gradient, $\frac{\partial \psi}{\partial y}$ will be approximately zero and the migration term may be neglected. The justification in the neglect of migration in

SYSTEM - Cathodic Reduction of Potassium Ferricyanide

$Fe(CN)_6^{3-} + e \longrightarrow Fe(CN)_6^{4-}$ —— Cathode Reaction

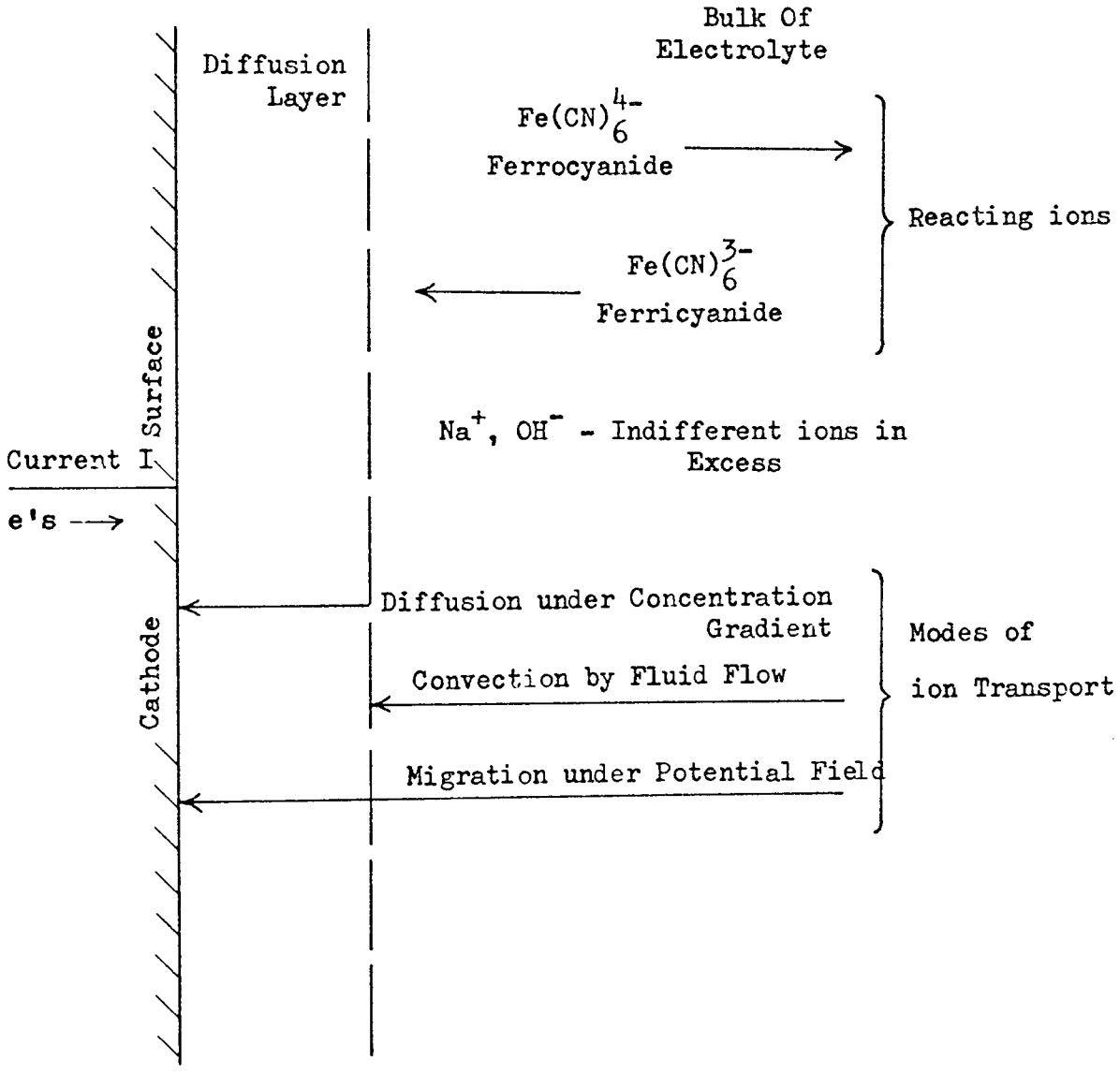

FIG 6 MECHANISM OF DIFFUSION-CONTROLLED ELECTROCHEMICAL TECHNIQUE

the presence of indifferent ions was investigated by Sutey and Knudsen (107). Based on their findings, the migration effects in the electrochemical system used in the present work was estimated to be less than 0.5%.

Thus in Equation (3.1) only the diffusion term remains:-

$$N_i = -(D + \varepsilon_D)\frac{\partial C_i}{\partial y} \qquad \ldots\ldots (3.3)$$

The rate of mass transfer may alternatively be expressed in terms of a mass transfer coefficient K_C, defined by:-

$$N_i = K_C (C_b - C_s) \qquad \ldots\ldots (3.4)$$

where C_b and C_s are concentrations in the fluid bulk and at the electrode surface respectively.

From Equations (3.2) and (3.4):-

$$I = K_C n_e F (C_b - C_s) \qquad \ldots\ldots (3.5)$$

In this case, I, being associated with pure diffusion mass transfer is termed the "diffusion current".

The electrochemical reaction rate increases with increase in the applied potential until it equals the rate of diffusion of the reacting ions to the electrode surface. At the same time the surface concentration of the reacting ion gradually falls towards zero.

The maximum rate of mass transfer or "limiting current density" can be seen from Equation (3.5) to exist when C_s is zero. This assumes the absence of chemical polarisation in that reacting ions having diffused through the boundary layer are immediately removed from the surface of the electrode by the electrochemical reaction. The limiting current is given by a plateau on a current-potential plot such as those shown in Fig. 7. Further increases in current

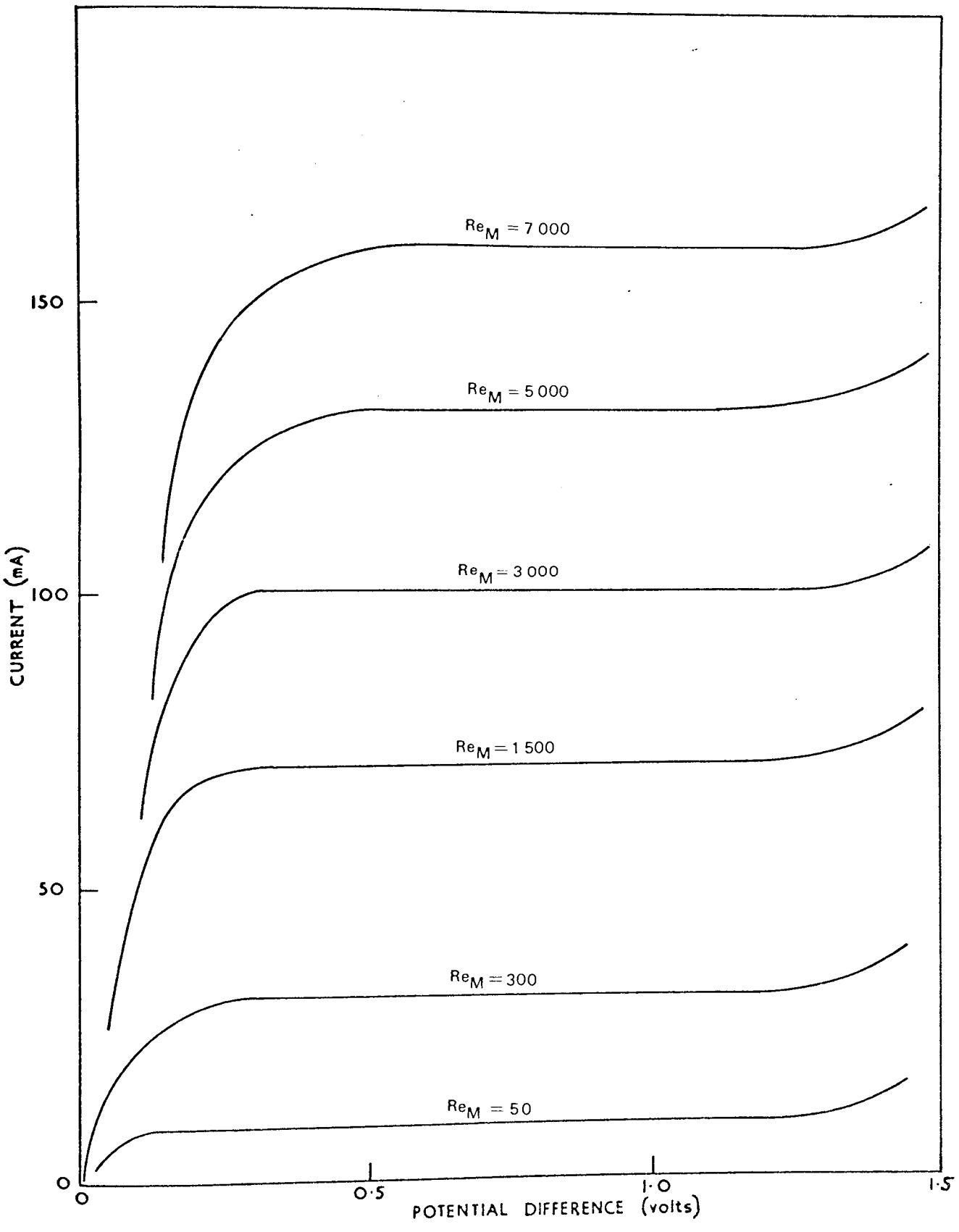

FIG 7 Specimen Current — Voltage Curves

can be achieved only by the occurrence of secondary electrode reactions e.g. hydrogen evolution on the cathode.

Thus with the knowledge of the bulk concentration of the reacting ion C_b, mass transfer coefficients are obtained directly from limiting currents, I_L, using Equation (3.5):-

$$K_C = \frac{I_L}{n_e F C_b S} \qquad \ldots\ldots (3.6)$$

The theoretical limiting current density cannot be fully reached in practice because of the development of chemical polarisation associated with the depletion of the reacting ions in the region of the electrode. However Wilke et al.(108) found that a value of 10^{-3} for the ratio C_s to C_b was obtainable, thus giving justification to the assumption of C_s being zero for practical purposes.

A critical fluid velocity exists for every electrochemical system and electrode geometry, which if exceeded causes the disappearance of the characteristic plateau on the polarisation curve. In such situations chemical polarisation occurs whereby the electrode reaction rate is insufficient to remove the ions reaching the electrode surface by the enhanced diffusion rate. Thus the surface concentration of the reacting ions is no longer zero.

For any electrochemical system, electrochemical reactions and transport processes occur simultaneously at the two electrodes. The study of diffusion-controlled phenomena at a particular electrode requires that the other electrode be made non-controlling. This is achieved by employing a "non-controlling" electrode of considerably greater surface area than that of the test (or controlling) electrode. Such an arrangement produces a comparatively smaller current density at the "non-controlling" electrode, with the result

that the process at this electrode has no noticeable effect on the polarisation curve at the test electrode. An alternative solution adopted by Lucas (61), is generally applicable to situations where the system geometry imposes limits on electrode size. For the case of Redox systems, the limiting current can be controlled by diffusion at only one electrode by employing a greater concentration of the ions reacting at the "non-controlling" electrode compared to that of ions reacting at the test electrode.

3.5 THE POTASSIUM FERRI-FERROCYANIDE SYSTEM

The particular electrochemical system chosen for this work was the cathodic reduction of Potassium Ferricyanide on nickel electrodes.

The electrolyte solution consists of equimolar concentrations of Potassium Ferricyanide and Potassium Ferrocyanide with a large excess of sodium hydroxide as the indifferent electrolyte. The principal electrochemical reactions of this Redox system are:-

$$\underset{\text{Ferricyanide}}{Fe(CN)_6^{3-}} + e \longrightarrow Fe(CN)_6^{4-} \qquad \text{at the cathode} \qquad \ldots\ldots (3.7)$$

$$\underset{\text{Ferrocyanide}}{Fe(CN)_6^{4-}} \longrightarrow Fe(CN)_6^{3-} + e \qquad \text{at the anode} \qquad \ldots\ldots (3.8)$$

The accompanying secondary reactions and their associated discharge potentials for the sake of continuity are dealt with in Section 3.5.1.

The advantages of the Potassium Ferro-Ferricyanide system over other electrochemical systems, particularly those involving deposition or dissolution processes, are numerous:-

(i) The electrodes remain physically unaltered during the electrochemical process.

(ii) Steady state electrode potentials are attained in much shorter times than in deposition reactions (see Appendix 1.10).

(iii) Electrochemical reactions involving an electron transfer are very rapid and in consequence chemical polarisation is usually negligible even at high mass transfer rates.

(iv) The bulk concentrations of the reacting ions remain constant by virtue of the complimentary reactions at the electrodes.

(v) Competing electrochemical reactions and decomposition of the electrolyte can be avoided if suitable precautions are taken (see Appendix 1.1).

(vi) The surface roughness of polished nickel electrodes is low (see Appendix 1.5).

(vii) Simple and accurate analytical methods exist for the determination of the ferricyanide and ferrocyanide ion concentrations (see Appendix 1.14).

(viii) The system has a high critical velocity. Eisenberg et al. (75) in their work on rotating disc electrodes, reported the critical velocity to be 4.26 m/s. The pipe flow studies of Hubbard and Lightfoot (68), however showed successful application of the electrochemical system up to velocities of 5.5 m/s, this being the limit of their experimental equipment. It is of interest to note here that in the present work involving flow over cylinders, satisfactory polarisation curves were obtained throughout the experimental flow rate range corresponding to velocities of up to 4.0 m/s. The differing surface geometries investigated in the above three cases, would for the same suitably defined velocity, produce varying boundary layer characteristics and hence mass transfer rates. It would, thus, be more generally applicable if the critical limit were expressed in terms of the actual mass transfer rate, this being independent of the particular geometry of the system.

3.5.1 Discharge Potentials

When a voltage is applied between the electrodes of an alkaline Ferri-Ferrocyanide solution two reactions are possible at each electrode. Standard oxidation potentials (volts) are shown for each reaction.

At the cathode:-

$$Fe(CN)_6^{3-} + e \longrightarrow Fe(CN)_6^{4-} \qquad E^\circ = -0.356 \qquad \ldots\ldots (3.9)$$

$$H^+ + e \longrightarrow \frac{1}{2} H_2 \qquad E^\circ = 0.000 \qquad \ldots\ldots (3.10)$$

At the anode:-

$$Fe(CN)_6^{4-} \longrightarrow Fe(CN)_6^{3-} + e \qquad E^\circ = 0.356 \qquad \ldots\ldots (3.11)$$

$$2OH^- \longrightarrow \frac{1}{2} O_2 + H_2O + 2e \qquad E^\circ = 0.401 \qquad \ldots\ldots (3.12)$$

The oxidation potential, E, in any state other than the standard state is given by the equation:-

$$E = E^\circ - \frac{RT}{n_e F} \ln Q' \qquad \ldots\ldots (3.13)$$

where Q' is the equilibrium constant in terms of activities for the reaction considered.

In order to produce electrolytic decomposition at an electrode the oxidation potential of the particular ionic species must be exceeded. In practice it is also necessary to overcome an additional potential, characteristic of the electrode, known as overpotential. The discharge potential is thus the sum of the oxidation or reduction potential and the overpotential. For the case of reduction of Ferricyanide ions and the oxidation of Ferrocyanide ions the overpotentials are negligibly small.

The table below gives the discharge potentials (volts) for the anodic and cathodic reactions.

Reaction		Oxidation/Reduction Potential	Overpotential	Discharge Potential
$Fe(CN)_6^{3-}$	Reduction	0.34	0.00	0.34
$Fe(CN)_6^{4-}$	Oxidation	- 0.34	0.00	- 0.34
H^+	Reduction	- 0.83	- 0.21	- 1.04
OH^-	Oxidation	- 0.40	- 0.06	- 0.46

The oxidation and reduction potentials are evaluated for the electrolyte composition used in this work at 25°C.

The EMF of a cell is the sum of the reduction discharge potential at the cathode and the oxidation discharge potential at the anode. For the case of the Redox reaction this is zero and hence any applied voltage will cause a flow of current. When the cathode potential reaches - 1.04 volts hydrogen evolution begins. Oxygen is similarly evolved when the anode potential is - 0.46 volts. Therefore gas is evolved at both electrodes when a voltage of 1.50 volts is applied. The discharge characteristics of the reacting and indifferent ions are shown in Fig. 8.

3.5.2 Ohmic Potential

The treatment in the foregoing section has assumed a negligible cell ohmic potential drop. This assumption is valid for most practical cases where the electrode separation is small, particularly in the presence of an excess of an indifferent electrolyte.

In the present work however, the complex geometrical characteristics of the heat exchanger model necessitated the location of the anode distant from the cathodes.

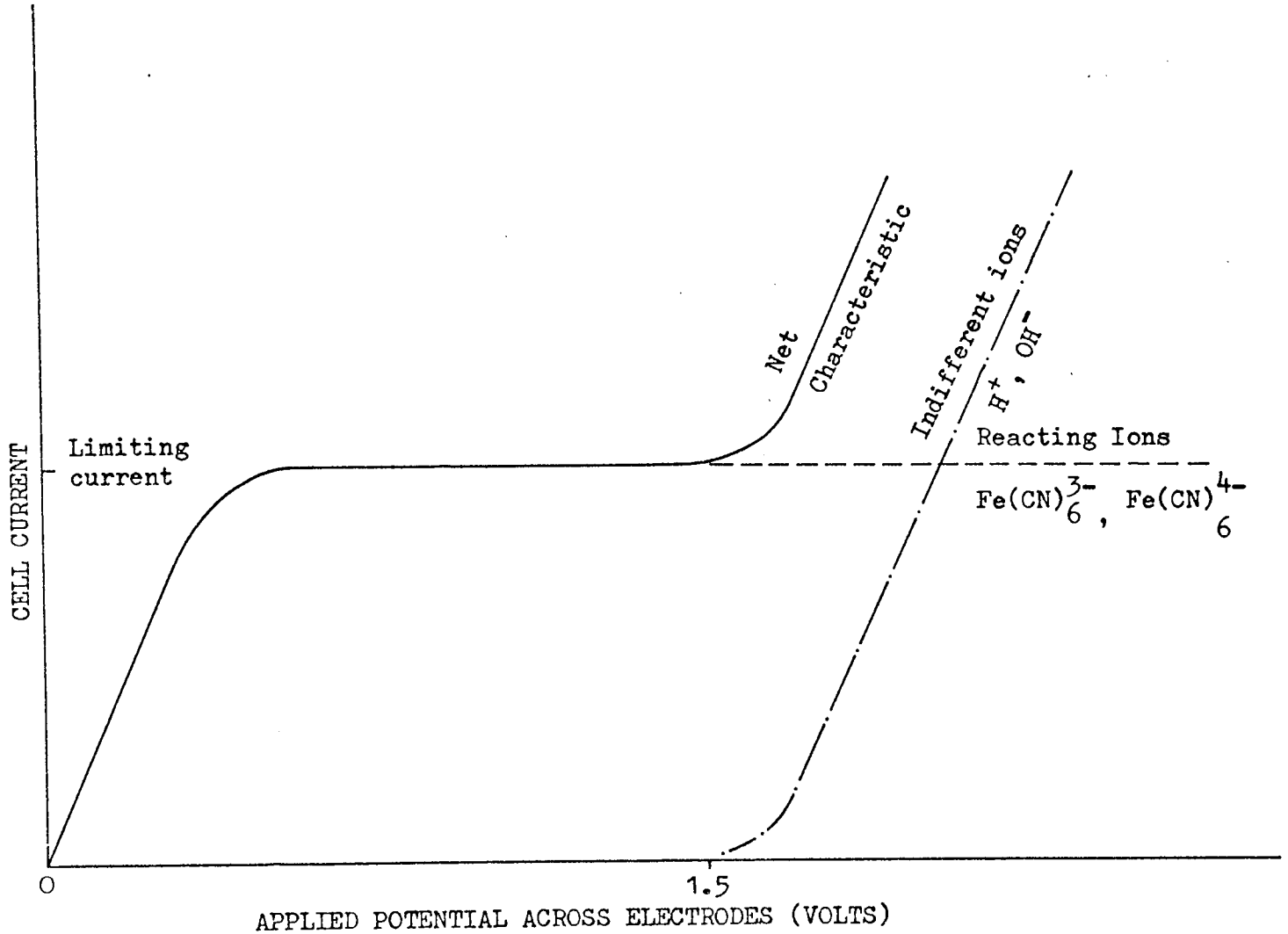

FIG 8 DISCHARGE CHARACTERISTICS OF IONS IN THE REDOX SYSTEM

In such systems with a significant ohmic resistance, the applied potential must first overcome the ohmic potential drop, before electrolytic decomposition can occur at the electrodes. Thus the actual applied potential necessary to produce evolution of gases at the electrodes will be in excess of the 1.50 volts cited in the previous section. A similar situation exists for the onset of the plateau on the polarisation curve. The nett result is a shift of the plateau to a range of higher applied potential.

The shift of the polarisation curve plateau will be more evident at high mass transfer rates, where the associated rise in current increases the "cell" ohmic resistance proportionally.

It is clear that in the evaluation of mass transfer coefficients using the electrochemical technique, the value of the ohmic potential drop is immaterial, since limiting current values are independent of potential difference under pure diffusion-controlled conditions. Thus contrary to the recommendations of Runchal (93), the presence of redundant inert metallic conductors in the "cell", while perhaps reducing the cell ohmic resistance, will not however affect the limiting current value. This is verified experimentally in Appendix 1.7.

4. DEVELOPMENT OF THE ELECTROCHEMICAL MASS TRANSFER MODELLING TECHNIQUE

4.1 INTRODUCTION

The utilisation of the electrochemical technique in making measurements of local shell-side mass transfer coefficients required much developing. The complexity of the shell-side geometry necessitated detailed investigations into various practical aspects of the electrochemical method. Electrode arrangement was one such feature. The scale of the equipment and experimental programme made examination of methods for prolonging the operational life of electrolyte batches economically justifiable. The development of these and other practical aspects of the electrochemical technique is discussed in greater detail in Appendix 1.

The shell-side mass transfer data obtained by the electrochemical technique were compared with corresponding data from other sources. Comparisons with reported heat transfer results from a similar exchanger provided a means of testing the heat and mass transfer analogy. Measurements of shell-side pressure drop were used in establishing that leakage was not evident in the exchanger model of this work.

The electrochemical technique has been extended to the study of residence times of the shell-side fluid. This work is summarised in Appendix 2.5.

4.2 EXPERIMENTAL EQUIPMENT

4.2.1 Essential Features

The electrolyte solution, constituting the shell-side fluid, was circulated through the shell and tube heat exchanger model. Measurements of mass transfer coefficients on the outside of the tubes were made using the electrochemical technique. The nature of the technique requires no tube-side fluid. General views of the experimental rig are shown in Figs. 9 and 10.

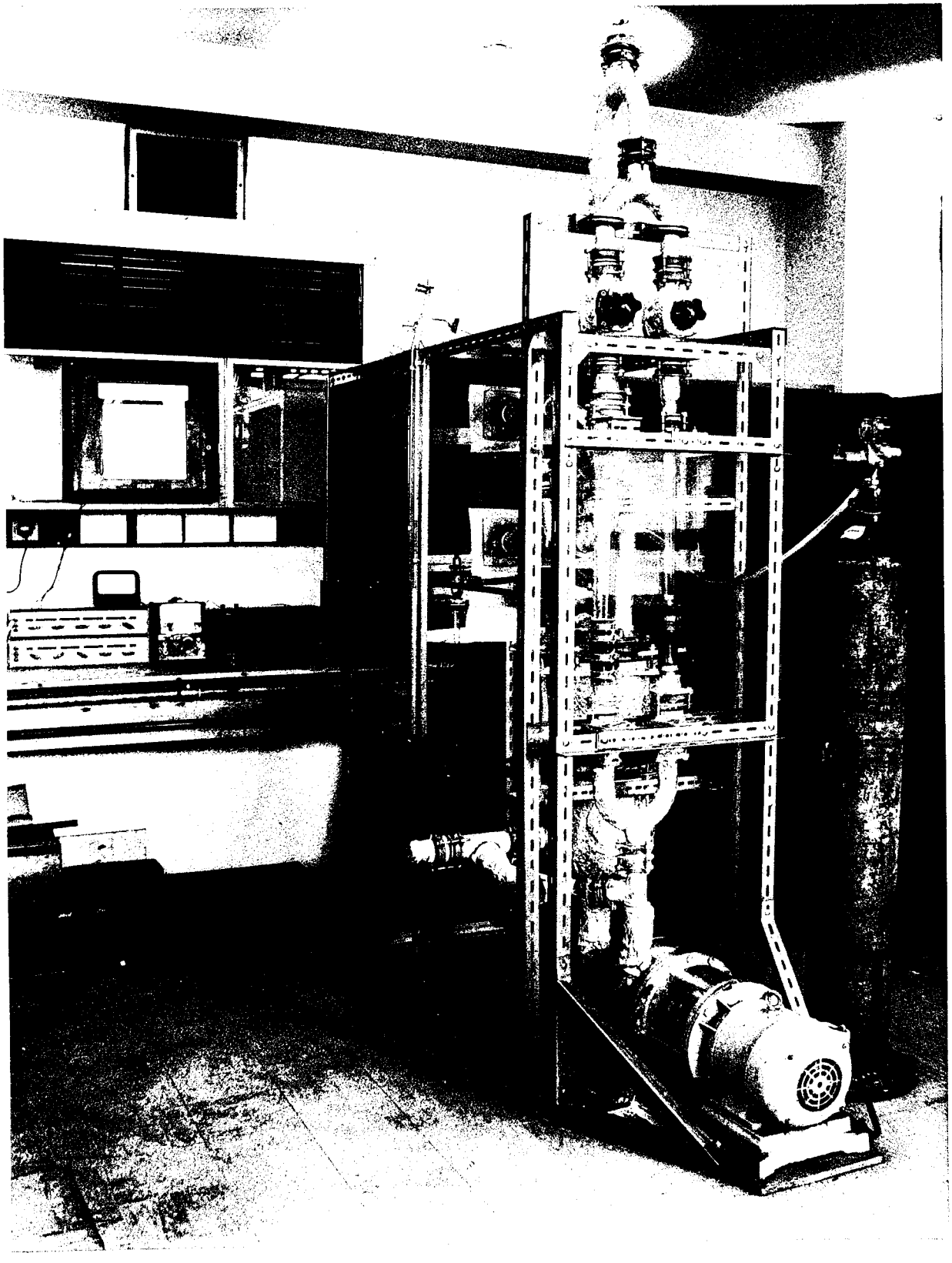

FIG 9 GENERAL VIEW OF THE RIG

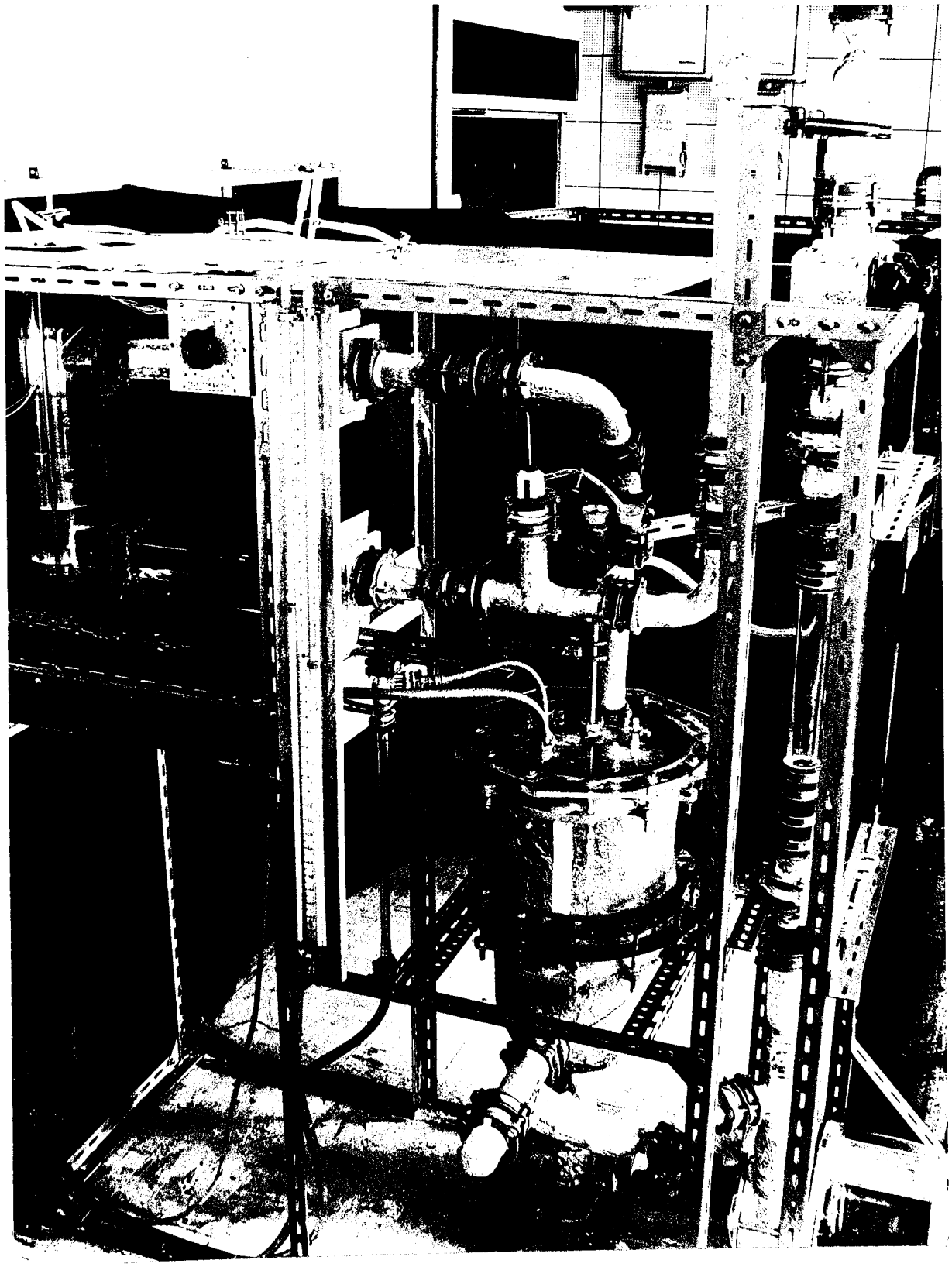

FIG 10 CLOSE-UP VIEW OF THE RIG

The choice of materials of construction was based on the recommendations given in Appendix 1.15.

The equipment was limited to a maximum electrolyte flow rate of 50 l/min corresponding to a shell-side Reynolds number (Re_M) of 2 000. This limit was imposed by structural weakness in the heat exchanger model which had originally been designed by Roberts (54) to operate at atmospheric pressures. Flow rates of up to 180 l/min were however reached for short periods when investigating aspects of diffusion control. Serious seepage from the exchanger model shell occurred at these high flow rates.

4.2.2 Electrolyte Flow Circuit

The electrolyte solution was drawn from a storage tank and delivered by a pump to the heat exchanger model. The solution was then returned to the tank thus completing the flow circuit. A schematic representation of the flow circuit is shown in Fig. 11. The pipework, pump and the storage tank were all constructed from standard QVF glassware. The pipework was of $1\frac{1}{2}$ in. (38 mm) ID. Neoprene jointing gaskets were used throughout.

The electrolyte storage tank was 12 in. (305 mm) ID with a capacity of 45 litres. A helical glass cooling coil supplied with mains water was located inside the tank. A stainless steel sparge pipe introduced nitrogen into the tank. The electrolyte return pipe, cooling coil feed-water lines and the sparge pipe all passed through the $\frac{1}{2}$ in. (12.7 mm) thick perspex tank lid by means of compression bulkhead fittings. The lid was provided with a gas venting valve and an electrolyte filling point. The return pipe dipped below the electrolyte surface thus providing a liquid seal and reducing gas entrainment. A draining pipe was attached to the bottom of the tank.

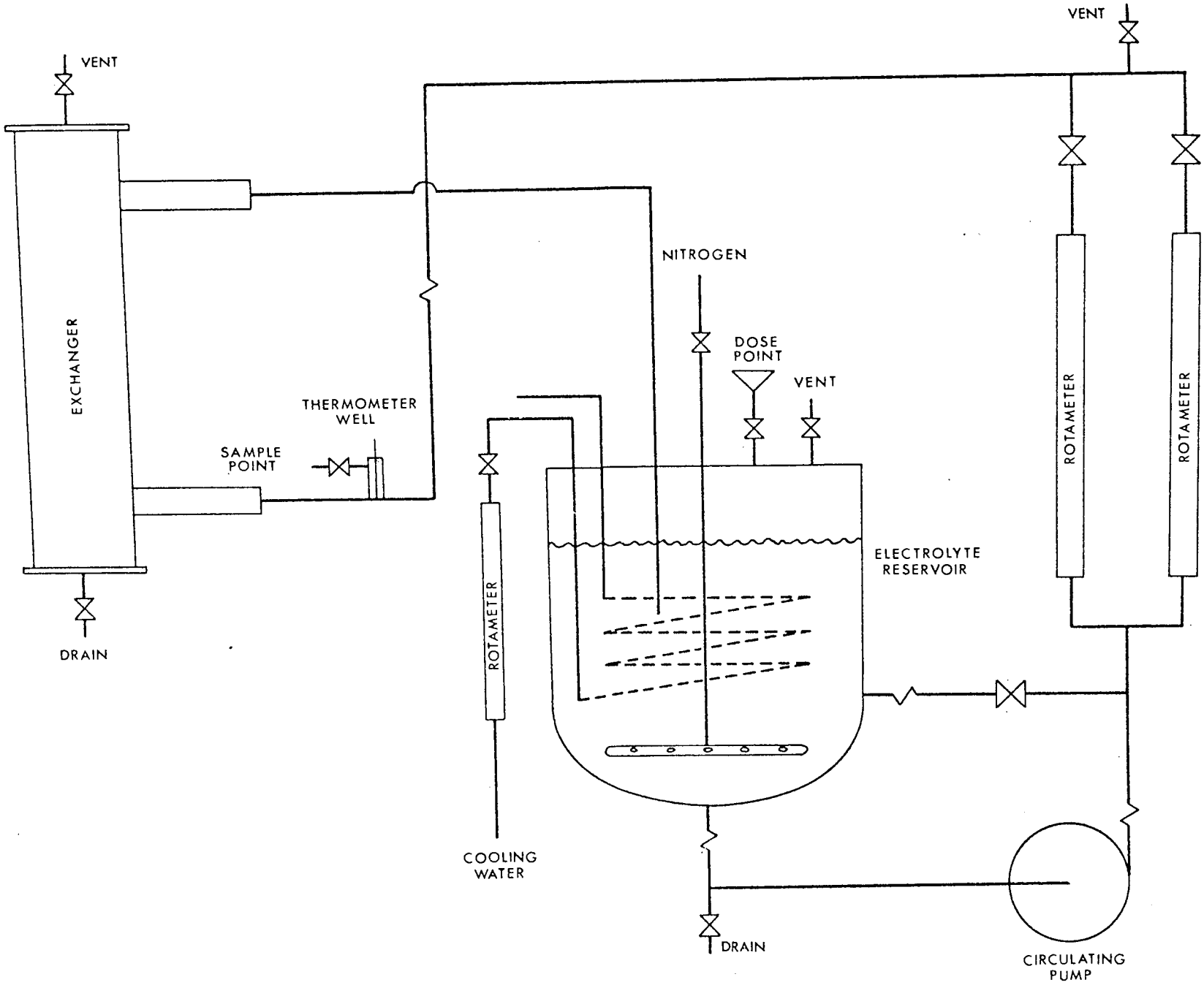

FIG 11 FLOW CIRCUIT

A QVF centrifugal pump capable of delivering 350 l/min against a 30 ft. (9.9 m) head was used. The pump impeller and casing were both glass while the gland was PTFE. A bypass line was incorporated in the pump delivery line to prevent the pump being overloaded at low flow rates.

The flow delivery rate to the exchanger model was controlled by diaphragm valves. Globe valves were originally employed but were found to produce serious cavitation characteristics.

The flow was metered by a pair of rotameters arranged in parallel. The rotameters were the metric 35 and 65 sizes produced by the Rotameter Manufacturing Company. Using stainless steel floats, flow rates up to 50 and 200 l/min respectively could be measured. For studies at very low flow rates the metric 65 size was replaced by a metric 14 size giving accurate metering up to 5 l/min. The rotameters were calibrated using the charts recommended by the manufacturers. The accuracy of this calibration procedure has been confirmed by Akers (119).

A thermometer-well was incorporated in the pipework at a point just upstream of the exchanger model. The temperature of the electrolyte solution was measured using a mercury thermometer to an estimated accuracy of $\pm$ 0.2°C.

The pump, model exchanger and electrolyte tank were protected from vibration and stresses through pipe misalignment by flexible couplings in the pipework. Vent pipes were located at convenient points in the pipework to allow the complete removal of gas from the system. Samples of electrolyte were obtained from one such bleed line located on the thermometer-well.

In order to protect the electrolyte solution from the adverse effects of sunlight (see Appendix 1.1.1), all the glass pipework and ancillaries were covered with aluminium foil. Removable

covers over the rotameter scales allowed inspection of the flow rates when required.

As a safety precaution against the occurrence of pipe fracture, the exposed glassware was encased in a transparent PVC sheet.

4.2.3 The Exchanger Model

The heat exchanger model employed in the development work was that used by Roberts (54) in previous studies of local shell-side coefficients at Aston University. Several modifications were however necessary before it could be used with the electrochemical technique.

This model was almost identical to that used by Williams (32) in the original utilisation of the mercury evaporation technique in determining shell-side coefficients. Furthermore the exchanger was geometrically similar to the model 9 unit used in the heat transfer research work of Bergelin et al. (30, 34) at the University of Delaware.

The slight differences in the dimensions of these exchanger models are shown in the table below. For convenience the dimensions are given in inches.

Dimension	Delaware	Williams	This Work
End-plate separation	16	$16\frac{1}{8}$	16
Baffle spacing	3.72	3.89	3.89
Tie-bar diameter	3/16	$\frac{1}{8}$	$\frac{1}{8}$

The essential features of these models were the gasketed tube sheets and baffle plates and the extra wide ports. The shell-side fluid leakage between the baffles and the shell and between tubes and the baffles were eliminated by the use of the gasketed baffle plates. In the present work the same result was achieved using

tight-fitting plastic baffles. Bypassing between the tube bundle and the shell, although not eliminated was minimised by positioning the tubes as near the shell wall as possible and by thoughtful location of the baffle tie-bars. The use of large rectangular ports minimised the entrance and exit effects.

4.2.3.1 Tube Bundle Construction

The tube bundle comprised eighty $\frac{3}{8}$ in. (9.5 mm) OD perspex tubes approximately 18 in. (455 mm) long arranged on a staggered-square pattern with a 1.25 pitch to diameter ratio. Baffles and end-plates were constructed of 1/16 in. (1.65 mm) polypropylene sheet. The baffle holes were reamed to a size giving a tight fit for the tubes. The baffles were also made a tight fit within the shell. As already mentioned above and discussed in more detail in Appendix 1.7, some initial experiments were performed with the chrome plated mild steel baffle plates and tubes originally used by Roberts (54). The baffles in this case consisted of a 1/16 in. (1.65 mm) sheet of neoprene rubber sandwiched between two 1/16 in. (1.65 mm) metal baffle plates. Tight seals between tubes and baffles were produced by overdrilling the tube holes in the baffle plates while undercutting the corresponding holes in the rubber sheet. A seal between the baffles and the shell was achieved in a similar manner. It was found however that when inserting tubes into the baffles the rubber sheet distorted between the plates and an efficient seal was not produced. Moreover repeated dismantlings of the bundle caused the rubber to tear. Using a rubber lubricant did not solve the problem. From scrutiny of the tube bundle photographs of Williams (32) and Roberts (54), it would appear that both distortion and tearing of the rubber was experienced in their equipment.

The use of the metal baffles and tubes presented electrical insulation difficulties in the case of the electrochemical technique.

The spacing of the baffles was maintained by eight $\frac{1}{8}$ in. (3.2 mm) diameter threaded stainless steel tie-rods and the separation of pseudo tube plates was fixed at 16 in. (406 mm). Baffles of 31.0 per cent and 43.7 per cent diametrical cut were employed at a constant spacing of 3.89 in. (99 mm).

The tube bundle is shown in Fig. 12.

4.2.3.2 Shell Construction

The shell of the exchanger model was that originally used by Roberts (54). The shell is shown in Fig. 13. A detailed design drawing is given in (54).

The shell was 24 in. (610 mm) long with a 5.25 in. (133 mm) ID constructed in $\frac{1}{4}$ in. (6.3 mm) perspex. Two rectangular ports of internal dimensions $2\frac{1}{4}$ in. (57 mm) by $3\frac{1}{2}$ in. (89 mm) were mounted in line on the shell. The distance between port centres of $14\frac{1}{8}$ in. (359 mm) allowed the inside faces of the tube plates to coincide exactly with the extreme edges of the ports. The tube bundle was located in such a position by means of perspex stops attached to the shell wall. The ends of the shell were sealed by two $\frac{1}{2}$ in. (12.7 mm) thick perspex backing-plates compressed against neoprene gaskets using tie-bars. The original rectangular perspex ducts used by Roberts to reduce the port size to $1\frac{1}{2}$ in. (38 mm) square were retained in the present work.

The positioning of the nickel anodes within the shell is discussed in Appendix 1.3.

The vertical tube bundle orientation of Roberts was retained in this work. This orientation allowed complete

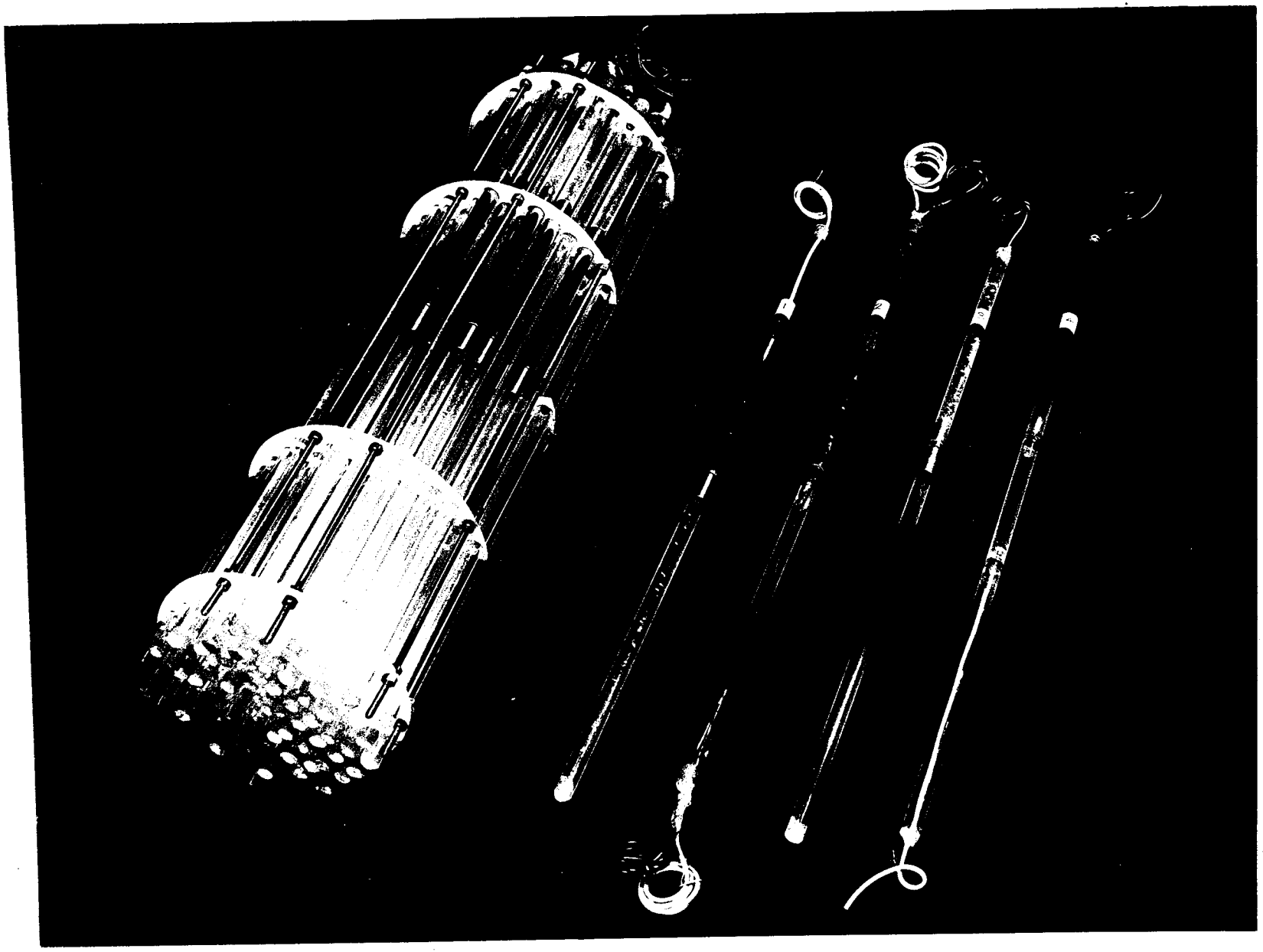

FIG 12 TUBE BUNDLE WITH VARIOUS PROBES

1 Baffle-Spacing Length Electrode 2 Composite Electrode

2 Micro-Electrode 4 Pressure Measuring Tube

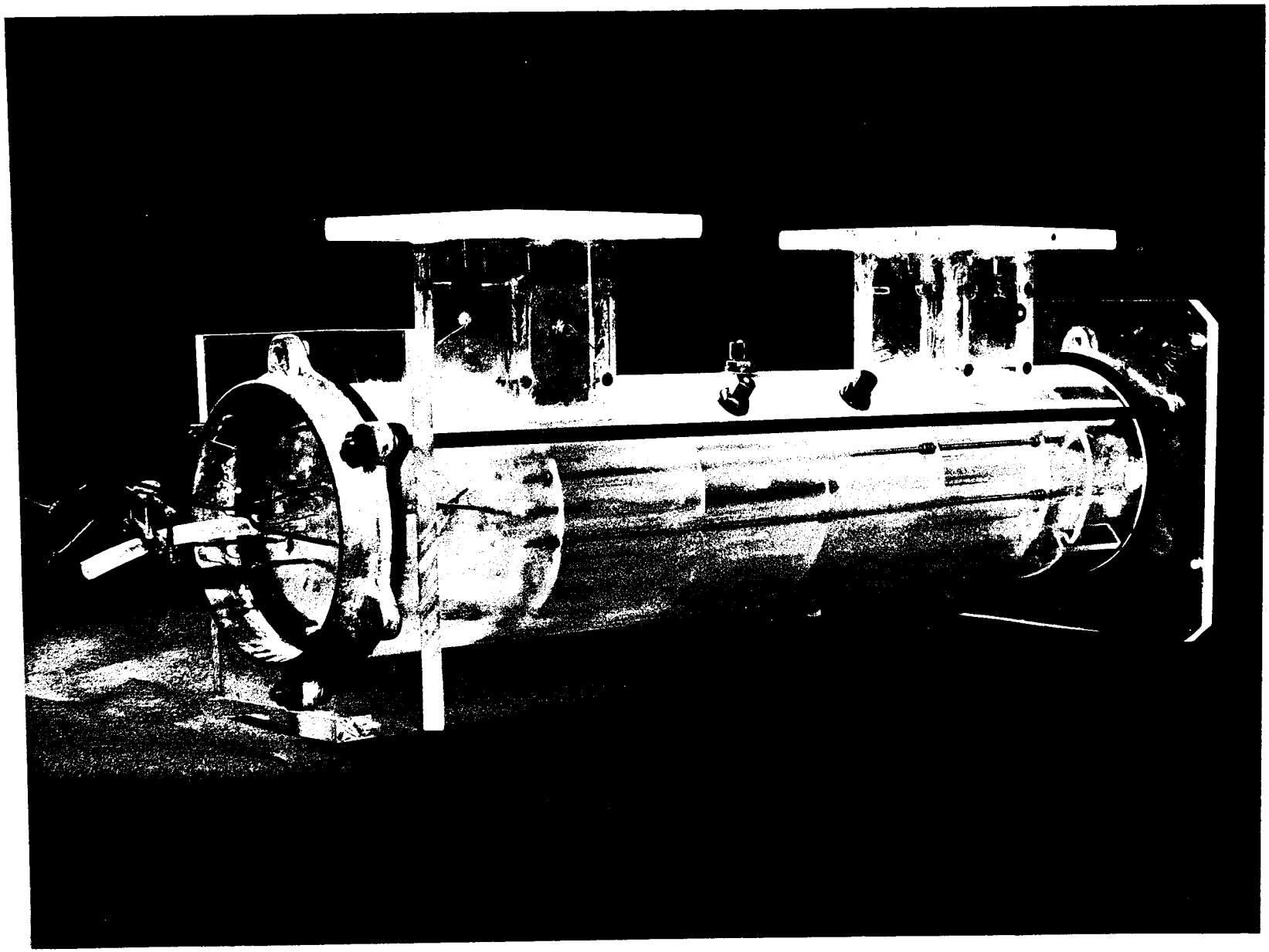

FIG 13 MODEL HEAT EXCHANGER SHELL (Tube Bundle Inserted)

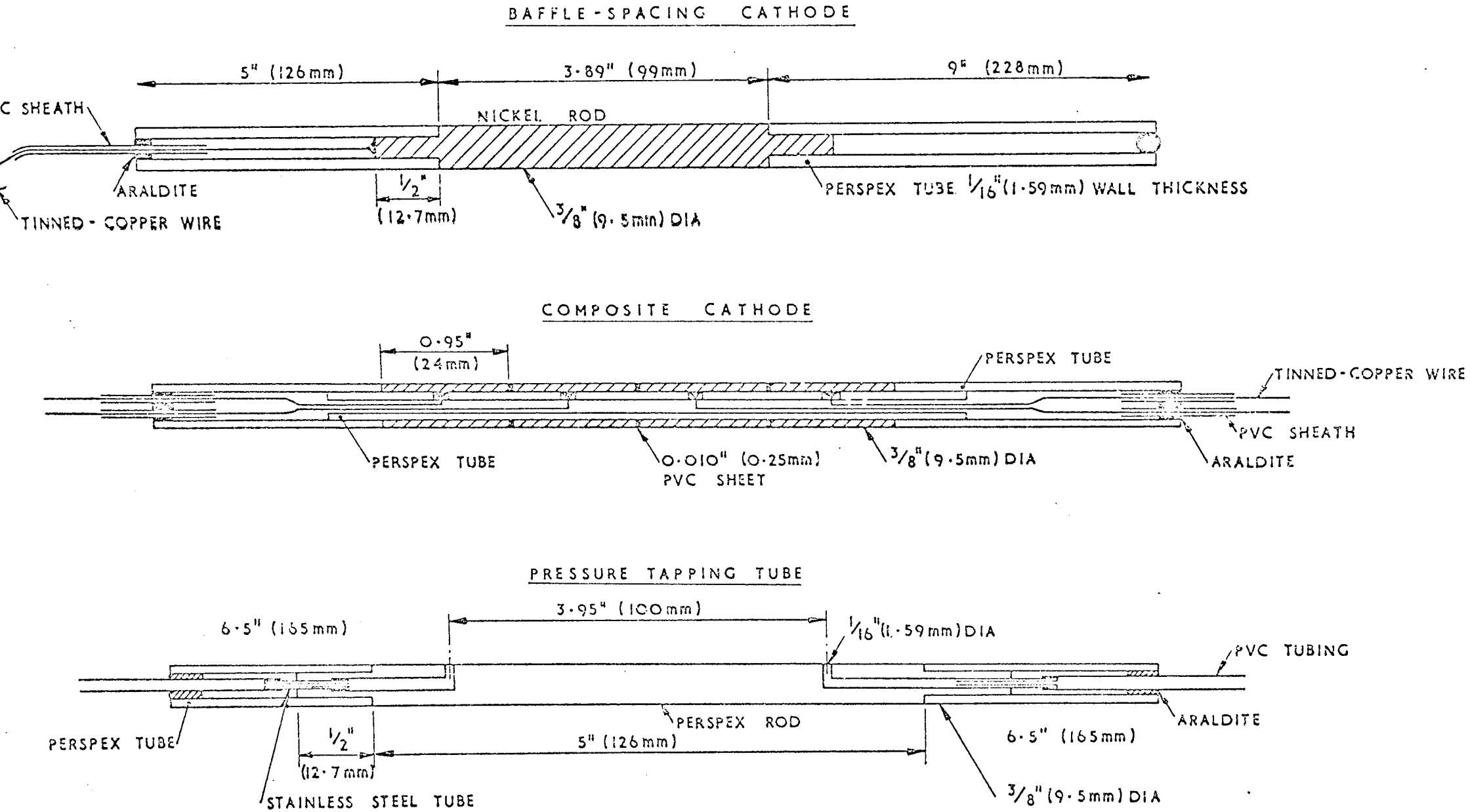

FIG 14 PROBE DESIGN

electrolyte drainage and gas displacement from the exchanger model while providing a more compact pipework layout.

The consequences of comparing data from this model with those from a horizontal unit are discussed in Section 4.4.2.8.

The exchanger model was enclosed in a hardboard light-proof box.

4.2.4.3 Cathode Construction

Tubes under investigation were replaced by probes having a section of nickel rod corresponding to the transfer surface of interest. PVC coated electrical leads soldered to the nickel rods were brought out through the tubular perspex end sections. The leads came out of the exchanger model through the perspex backing-plates using "Araldite" as a sealing compound. Details of the cathodes are given in Fig. 14. Composite electrodes used in other aspects of the work are also shown in Fig. 14. Details of these electrodes are however given in Section 4.4.5.

4.2.4 Electrical Instrumentation

The electrical circuit employed in making limiting current measurements (as distinct from the electrode activation process) is shown in Fig. 15. A variable supply of stabilised DC voltage enabled external potentials of up to 10 volts to be applied across the electrodes.

Currents were measured on a Sangemo Weston 12 in. (254 mm) scale DC ammeter. External shunts afforded a variable instrument range of 0.1 to 2 amps. The ammeter had recently been calibrated by the manufacturers prior to the experimental work. A simple moving coil voltmeter was employed in measuring the potential across the electrodes.

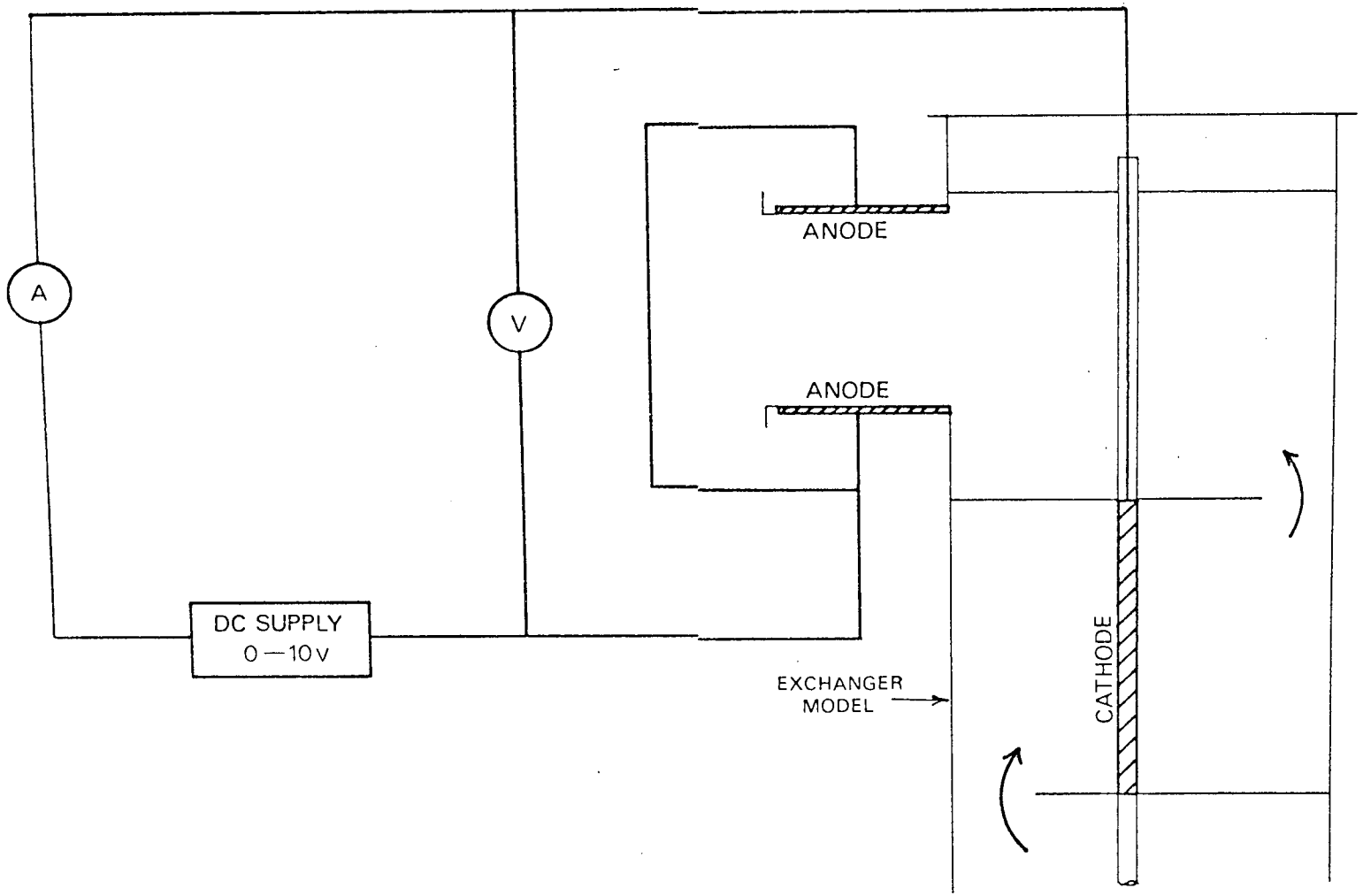

FIG 15 ELECTRICAL CIRCUIT

In the electrode activation process the electrical leads to the operational anodes were switched to the activation anodes. The cathode leads were connected to the appropriate electrode requiring activation.

In the activation process, because of the large currents involved, the Sangemo Weston ammeter was replaced by an Avometer. This instrument was sufficiently accurate for the purpose.

4.2.5 Pressure Instrumentation

Pressure measurements similar to those of Bergelin (30), were made within the tube bundle. A single perspex pressure measuring tube was used having two 1/16 in. (1.59 mm) tappings. The separation of the tappings was such that when the tube was inserted in the bundle the tappings were located midway between the baffles in two adjacent baffle compartments.

Details of the pressure tapping tube are shown in Fig. 14. Pressure differentials were measured using a vertical "U" tube glass manometer with the electrolyte solution over the carbon tetrachloride (sg 1.59) manometer fluid. Venting valves were located in the pressure lines to enable the removal of trapped gas from the system.

4.3 EXPERIMENTAL PROCEDURE

1.3.1 Assembling the Tube Bundle

The baffles and the full-face end-plates were assembled along the tie-bars with the appropriate spacings.

The nickel cathodes were polished and rinsed as described in Appendix 1.2. While the tube bundle was out of the shell, the anodes were given this same treatment.

The cathode tubes and the plain tubes were then inserted into their appropriate positions in the baffle assembly. Distilled water was flushed over the tubes in order to ease their insertion

into the tight-fit baffle holes. In cases where tubes were particularly tight a light smear of glycerol solved the problem. Glycerol was used in preference to other lubricants because of its good miscibility with water.

The tubes were located in the bundle with the nickel sections exactly spanning a baffle spacing. The tight-fitting baffles held the tubes rigidly in this position. In investigations with baffle clearances the tubes were held sufficiently rigid by the tight-fitting end-plates.

The tube bundle was gently lowered into the shell through the top opening until the bottom tube plate was located on the stops. Again distilled water or glycerol was used in the operation to reduce friction. The cathode electrical leads were threaded through holes in the top backing plate and a seal was made with "Araldite". This simple seal while being leak-tight, was easily broken with a sharp implement (e.g. screwdriver) when dismantling the bundle. The top backing plate was then screwed down onto the end of the shell using the tie-bars.

When using the composite electrodes or pressure tapping tubes, the electrical leads and capillary tubes respectively were led out through both the top and bottom backing plates.

Finally the hinged panels of the lightproof box were closed.

4.3.2 Making up the Electrolyte Solutions

The electrolyte solutions were made up in a separate glass mixing tank fitted with a nitrogen sparge pipe. The required amount of distilled water was poured into the tank and nitrogen was bubbled through it for about one hour to remove the majority of the dissolved oxygen. The appropriate weight of sodium hydroxide pellets was then dissolved in the distilled water. The nitrogen purge was continued in order to promote mixing.

The potassium ferricyanide and ferrocyanide salts were made up in a separate solution in a similar manner. This solution was added to the sodium hydroxide solution in the rig after the activation process. Appropriate amounts of the constituents were used in order to produce 45 litres of the final electrolyte mixture of the composition given in Appendix 1.12.

4.3.3 Filling the Rig

Air was first removed from the system using a nitrogen purge discharging through the vent lines. With a steady purge of nitrogen through the sparge pipe the sodium hydroxide solution was poured into the reservoir and the filling cap tightened down. The reservoir was then allowed to pressurise thus forcing the electrolyte solution through the pipework to the remainder of the system. Displaced gas was vented through lines on the top of the exchanger model and at the highest point on the pipework. When the electrolyte issued from these vent lines the valves were closed and the nitrogen supply to the reservoir shut off. Without this prior displacement of gas from the system, serious problems were encountered with entrained gas in the electrolyte solution. The rig was now in an operational condition.

4.3.4 Electrode Activation Process

With both the flow control valves and the pump bypass valves fully shut, the circulating pump was started. The bypass valve was then fully opened. At the same time water was fed to the reservoir cooling coil. By opening the flow control valves, cutting back on the bypass value as required, a flow rate of about 50 l/min was circulated through the exchanger model. Each cathode and the operational anode were then activated by passing a current density of 0.1 mA/mm^2 for 4 or 5 minutes as described in Appendix 1.2. During the activation periods a steady purge of nitrogen was

bubbled through the electrolyte in the reservoir to remove the dissolved oxygen and hydrogen produced as a result of the electrolysis. At the end of the activation period the voltage supply was switched off and the circulating pump stopped after closing the flow control and bypass valves. The filling cap on the reservoir lid was then carefully opened and the make-up solution of the potassium salts was added to the sodium hydroxide solution, maintaining a slight nitrogen purge to prevent influx of air into the system. The filling cap was tightened down and any nitrogen collected in the pipework was displaced by the electrolyte as before.

4.3.5 Experimental Run

With the flow control and bypass valves shut, the circulating pump was started. The bypass valve was then opened and the flow control valves were adjusted to give a flow rate of around 50 l/min.

The electrolyte solution was allowed to circulate at this rate until the analysis of electrolyte samples indicated that the electrolyte solution was homogeneous. This period was usually of the order of 15 minutes. At the same time the water flow rate to the cooling coil was adjusted to produce a steady electrolyte temperature of about 25°C.

The flow control valves were then adjusted to produce the required flow rate and the source of DC potential was connected across the operational anode and the cathode under investigation. The applied potential was gradually increased by increments and the values of the current and voltage were recorded. A short period of about 15 seconds (see Appendix 1.10) was allowed to elapse after each potential adjustment before readings were taken. The polarisation curve was thus plotted. The increase in potential

was halted when a rapid rise in current indicated the evolution of gases at the electrodes (see Section 3.5.1). The value of the limiting current was obtained from the plateau region of the polarisation curve. The temperature of the electrolyte solution was recorded, as was the flow rate. The procedure was then repeated at the same flow rate for the other cathodes under investigation, recording the limiting currents and electrolyte temperatures as before. The investigations were then extended to other flow rates. Samples of the electrolyte solution were taken periodically (usually every hour) and the concentration of the potassium ferricyanide ion and occasionally of the other ions, was determined by titration (see Appendix 1.14).

At the termination of a series of experimental runs the pump was stopped and the nitrogen and cooling water lines were shut off. The electrolyte solution was then drained back into the reservoir where it was either retained for further use or dumped.

4.4 DISCUSSION OF EXPERIMENTAL RESULTS

4.4.1 General

Measurements of average mass transfer coefficients were made for baffle spacing lengths of tubes in the third of a total of four baffle compartments. Two baffle cuts of 31.0 per cent and 43.7 per cent of the shell diameter were studied at a constant baffle spacing of 3.89 in. (99 mm). Tight-fitting baffles prevented tube-to-baffle and shell-to-baffle leakage. A few tests were however performed with shell-to-baffle leakage. The range of Reynolds number (Re_M) studied was 24 to 1 500 in the case of the 43.7 per cent baffle cut while only 300 to 1 500 for the 31.0 per cent cut.

The availability of only 10 electrode tubes necessitated several rebuilds of the bundle when investigating all the 80 tubes.

As originally pointed out by Williams (32) and experimentally confirmed in the present work, symmetry existed about a central vertical plane through the tube bundle. Thus measurements were required from only 44 of the total of 80 tubes in the bundle. This reduced the number of bundle rebuilds for each exchanger configuration to five. The system of tube numbering employed in the following discussions is shown in Fig. 16. The experimental data are tabulated in Appendix 3.1.

Measurements of shell-side pressure drops were also made. These results are also tabulated in Appendix 3.1.

A limited number of investigations were made into the variation of mass transfer rates along the length of tubes within a baffle spacing.

The discussion of the experimental results compares the data from this work with those of Williams (32) and Bergelin et al. (30) who employed similar heat exchanger models. The large differences in the values of the property numbers in these other investigations and in this work (see Appendix 3.4.2) provided a rigorous test for the heat and mass analogy.

For the comparisons, both heat and mass transfer coefficients were expressed in the form of Chilton and Colburn j-factors (see Section 2.2) and correlated with a Reynolds number. The characteristic velocity in the j-factor and Reynolds number although arbitrary, was taken as that based on the minimum flow area at the centre row of tubes in the bundle (see Fig. 16). Bell (29) employed this same characteristic velocity when correlating the University of Delaware heat transfer data.

The mass transfer data were analysed as individual tube, baffle compartment average and zonal average j-factors.

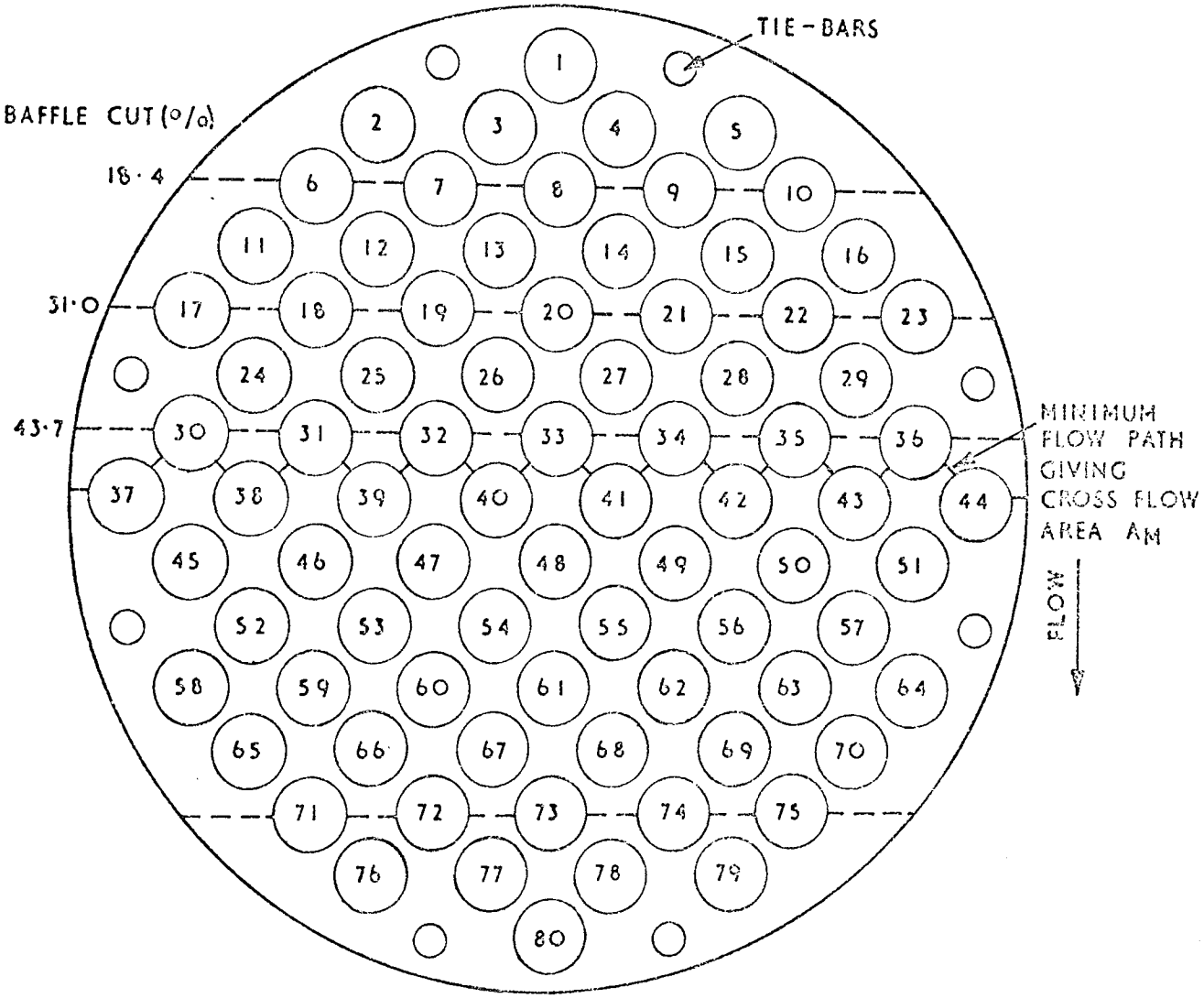

FIG. 16. TUBE ARRANGEMENT

4.4.2 Baffle Compartment Average j-Factors

The constant bulk and surface concentrations of the reacting ions in the electrochemical system is analogous to isothermal conditions in heat transfer. For such systems it is perfectly justifiable to derive average transfer coefficients from local values by an unweighted procedure. Thus baffle compartment average j-factors were calculated from all the individual tube values using a simple arithmetic average.

For non-isothermal heat transfer systems, when computing average heat transfer coefficients from overall heat transfer rates the effect of the temperature distribution is often accounted for by the use of a log mean temperature difference term.

For the case of the 43.7 per cent baffle cut, baffle compartment average j-factors were compared with those similarly obtained by Williams (32) and also bundle average values obtained in the heat transfer studies by Bergelin et al. (30). In the latter case measurements were made for both heating and cooling of the shell-side fluid. The data are shown plotted in Fig. 17.

While the three sets of data showed good agreement at the high Reynolds numbers, a distinct deviation occurred at the lower Reynolds numbers. At a Reynolds number of 54, being the lower limit of Williams's data, the data of Bergelin et al. fell about 7 per cent and those of Williams 24 per cent below the data of the present work. This discrepancy between the results of Bergelin et al. and present work was within the limits of the estimated accuracy of the measurements made in the present work (see Appendix 2.2). However further consultation of Fig. 17 reveals that the discrepancy between these two sets of data increases to as much as 20 per cent at a Reynolds number of around 20.

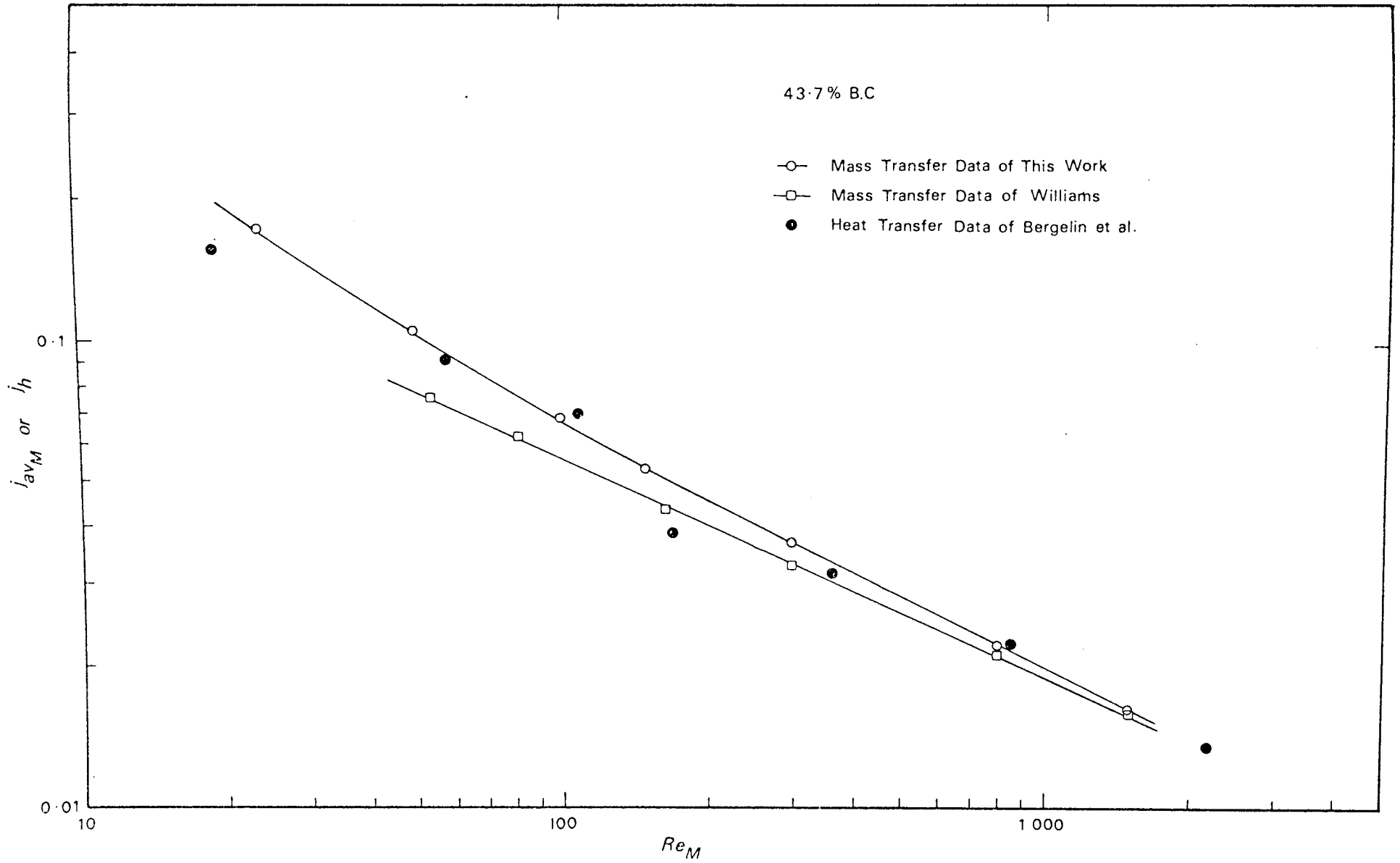

FIG 17 Comparison of Average Coefficients

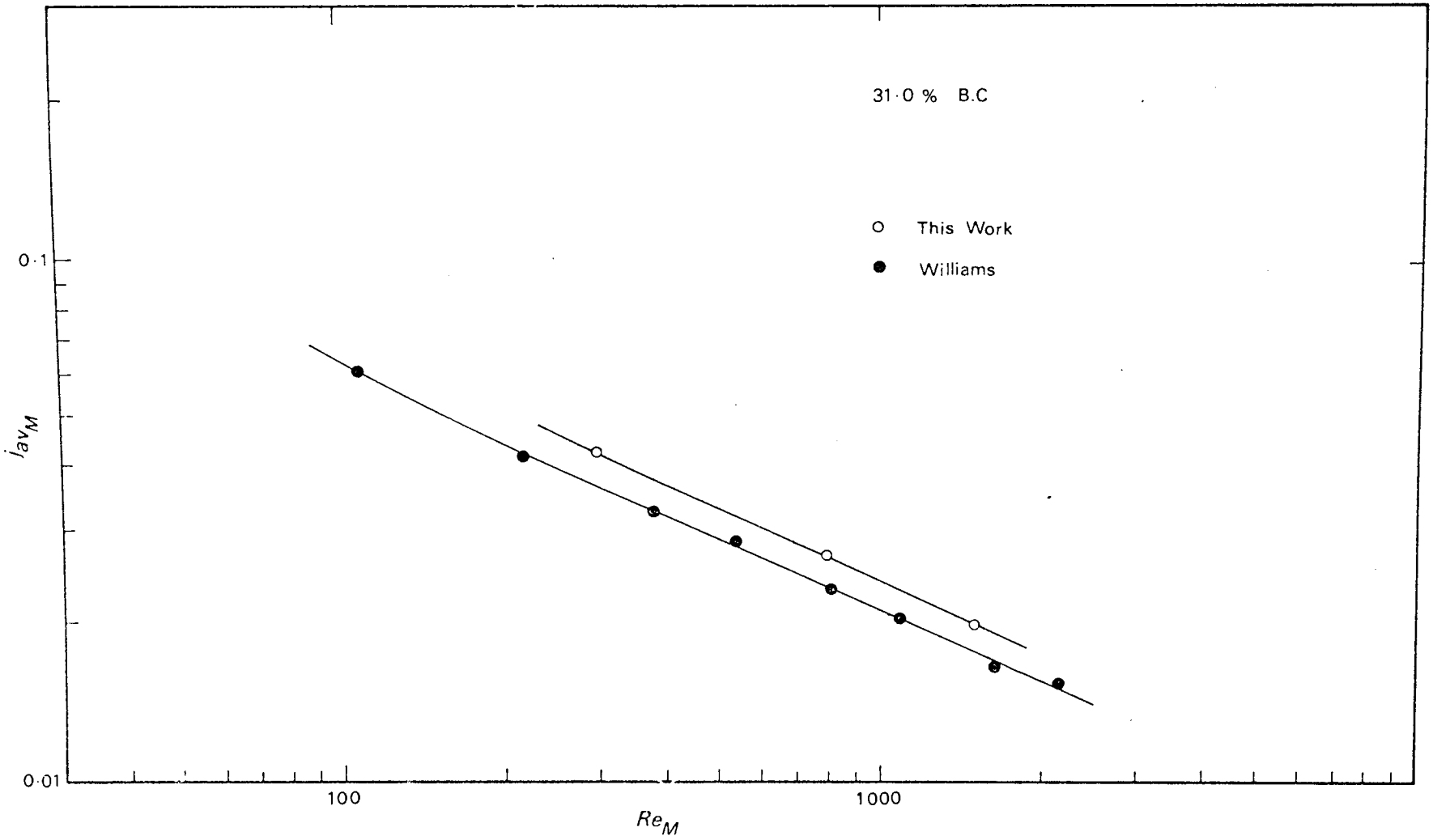

FIG 18 COMPARTMENT AVERAGE COEFFICIENTS

For the case of the 31.0 per cent baffle cut a comparison with only Williams was possible. The two sets of compartment average j-factor data are shown plotted in Fig. 18. The data from the present work fell about 15 per cent higher than the data of Williams.

For complex systems such as shell and tube heat exchangers it is common practice to accept variations in experimentally determined heat transfer data of up to 25 per cent. However the distinct increase in the discrepancy between the 43.7 per cent baffle cut data at low Reynolds numbers requires a rational explanation.

A number of possible explanations for the discrepancies between the data from the three sources are now examined.

4.4.2.1 Derivation of Average j-Factors

Bergelin et al. derived bundle overall heat transfer coefficients from shell-side and tube-side fluid stream temperatures using a log mean temperature difference. The heat balances were reported (30) as being within ± 5 per cent. Established correlations were used to calculate the tube-side coefficients. Shell-side coefficients were subsequently obtained from the overall and tube-side coefficients with the assumption that fouling was negligible. It is however probable that the tubes were not nearly as "clean" as the nickel electrode surfaces in the electrochemical technique. The tube-side coefficients were made a factor of 10 higher than the shell-side coefficients by inserting cores in the tubes to increase the fluid velocity. Slight errors in the tube-side coefficient value would thus have been insignificant. For large fluid stream temperature changes, the corresponding variation in the specific heat may be sufficient to produce

a non-linear fluid temperature versus heat transfer relationship. In such cases the use of a log mean temperature difference in calculating average coefficients is not justified and would lead to errors. Examination of Bergelin's data tabulated in (120) revealed that the water temperature on the tube-side was essentially constant and the shell-side oil temperature altered by up to 20°F (11°C) as it passed through the exchanger. The corresponding variation in the physical properties of both the oils used was not sufficient to invalidate the use of the log mean temperature difference.

In the mercury evaporation technique of Williams, the mercury concentration on the tube surfaces was essentially constant. The relatively low mass transfer rates produced little change in the mercury concentration in the gas stream. As with the electrochemical technique, this system may be regarded as analogous to an isothermal heat transfer situation. Thus Williams's use of an arithmetic mean in calculating the baffle compartment average coefficient was justified.

4.4.2.2 End Baffle Compartments

While the measurements of Williams and the present work were confined to an internal baffle compartment, the average coefficients obtained by Bergelin et al. represented the entire bundle. Thus in comparing the average coefficients from these investigations it was assumed that all the baffle compartments exhibited the same characteristics, with the average coefficient for an internal compartment representing that of the bundle. The two internal baffle compartments, being of identical geometry, would probably have similar average heat transfer coefficients. The inlet and exit baffle compartments, having no effective inlet and outlet window

zones respectively (see Fig. 1) would exhibit heat transfer characteristics different from those of the internal baffle compartments. Although the entrance and exit effects were minimised by the use of large rectangular ports, low coefficients would probably occur in the first few tube rows contacted by the shell-side fluid. This phenomenon was shown by Bergelin et al. (18) to occur in ideal tube banks (see Section 1.2). A simple calculation was performed to estimate the mass transfer coefficients of the tubes contained within the window zones adjacent to the shell inlet and exit ports. The mass transfer j-factor correlation for tube number 48 in the middle of the crossflow zone, was applied to these tubes estimating the appropriate fluid velocities from the geometry of the tube layout. The effect amounted to the average coefficients of the end baffle compartments being about 4 per cent higher than those of internal compartments. However such a correction assumes pure crossflow without any of the entrance effects already discussed.

Bergelin et al. (34) in studies of a heat exchanger with internal leakage, found that the pressure drop in the end baffle compartments was a factor of 5 greater than that in the internal compartments. The excessive pressure losses were attributed to the smaller leakage areas available in the end compartments and the fluid entrance and exit effects.

The need for detailed investigations into the heat transfer and pressure drop characteristics of end baffle compartments is thus demonstrated.

4.4.2.3 Flow Development Through the Bundle

The mass transfer coefficient measurements of both Williams and the present work were confined to the third of

four baffle compartments. The shell-side flow may not have been fully developed by the time it reached this third baffle compartment.

Ideal tube bank studies have shown that while turbulent flow conditions may exist at downstream regions, laminar flow may still be present further upstream with associated lower transfer coefficients. Furthermore the range of the Reynolds number of the data under discussion, according to Bell (29), corresponds to the transitional flow regime. The presence of differing levels of turbulence in the baffle compartments could seriously invalidate the comparison of a bundle average coefficient with a single compartment average value.

Bergelin et al. (18) demonstrated that for staggered tube arrangements turbulent eddies first appear at the downstream tubes and slowly move upstream as the Reynolds number increases. Smooth transition zone characteristics were thus observed in correlations of average heat transfer coefficients. With in-line tube arrangements turbulent eddies appear throughout the tube-bank at a well defined Reynolds number showing a distinct "dip" in heat transfer correlations. It is thus surprising that the data of Bergelin in Fig. 17 show such a "dip"; for a staggered tube arrangement was employed. The complex shell-side geometry could be regarded as constituting both in-line and staggered tube arrangements. When plotting the Bergelin heat transfer data for all the other baffle configurations investigated, it was noticed that no such "dip" occurred in any of these correlations. The Bergelin heat transfer data presented in Fig. 17 were in fact obtained from two series of experiments by two different

co-workers of Bergelin. Brown, using a light oil on the shell-side obtained measurements in the Reynolds number range 170 to 5 720. Tompkins, used a more viscous oil and studied the lower Reynolds number range 3 to 108. It is thus significant that the apparent "dip" in the correlation occurs around the boundary between the two sets of measurements. Furthermore the apparently low data points of Brown represented cases of relatively large shell-side fluid temperature changes. The accuracy of the measurements and the derivation of the bundle average coefficient under such conditions are thus open to question.

4.4.2.4 Baffle Leakage

Investigations into the effect of internal leakage by Bergelin et al. (34) and also in the present work (see Section 4.4.4.2) revealed that both the bundle or baffle compartment average coefficients and pressure drops were reduced as a result of baffle clearances. Although stringent precautions were taken against possible internal leakage in the three exchanger models under discussion, baffle clearances could have occurred through tearing of the rubber sealing sheets or sagging of the bundle. As already discussed in Section 4.2.3.1, problems with rubber baffle seals were encountered in the present work prior to changing to plastic baffles. It is quite feasible that similar problems were encountered by both Bergelin and Williams; photographs of Williams's bundle show definite evidence of tears in the rubber seals.

Later investigations in the present work at AEE Winfrith using a horizontally orientated bundle with plastic baffles, showed serious signs of bundle sagging producing clearances

between the top of the baffles and the shell. Although the metal bundles of both Williams and Bergelin would have been more rigid, slight sagging could have occurred particularly in this case of large baffle cut and baffle spacing. The sealing rubbers may not have been able to contend with the subsequent increased baffle-to-shell clearance.

Detailed examination of the individual tube coefficients (see Section 4.4.4) indicated that some internal leakage was present in the exchanger model of Williams. Bergelin et al. (34) showed that the effect of leakage on heat transfer was more significant at low Reynolds numbers. It would seem that the variation between the compartment average j-factor values in Fig. 17 reflect this phenomenon.

Pressure drop measurements made within the tube bundle in the present work were compared with those obtained by Bergelin and reported in (120) (see Section 4.4.6). The measurements of the present work were found to be coincident with those made by Bergelin at the higher Reynolds numbers while up to 20 per cent higher than Bergelin's data at the lower Reynolds numbers. This would suggest that if any leakage were present it was in the exchanger model of Bergelin. No similar comparison was possible with Williams.

The rubber baffle seals in the exchanger models of both Bergelin and Williams would not have rigorously located the tubes in the centre of the baffle holes. When using a similar sealing arrangement in the initial stages of this work, it was noticed that the tubes generally positioned themselves eccentrically within the oversize baffle plate holes, often actually touching the plate. A similar characteristic was observed with the position of the baffle plates within the

shell. The baffle plates of both Bergelin and Williams had tube holes drilled 1/32 in. (0.79 mm) over the tube diameter and the outer diameter was cut 3/16 in. (4.75 mm) under the shell inside diameter. The minimum clearance between tubes and also between the outer tubes and the shell was nominally 3/32 in. (2.38 mm). It is thus possible through flexibility in tube location, for the minimum clearance between the tubes to vary between 3/32 and 5/32 in. (2.38 and 3.96 mm). Similarly the minimum width of the bundle bypass channel between the outer tubes and the shell could vary between 3/32 and 9/32 in. (2.38 and 7.14 mm). This flexibility in the bundle geometry could result in substantial redistribution of the flow.

4.4.2.5 Trapped Gas

The later experimental investigations at AEE Winfrith using a horizontal exchanger model, revealed that in cases where internal leakage had been eliminated, gas became trapped behind the baffles in the upper window zones. This became a serious problem at low flow rates where there was insufficient turbulence in the shell-side fluid to entrain the trapped gas and carry it out of the exchanger model. The problem was however overcome by increasing the shell-side flow rate for a short period prior to making measurements at low flow rates.

In the metal exchanger model of Bergelin (30) the presence of any trapped gas would not have been evident. Bergelin made no mention of this phenomenon and no gas venting points were incorporated in the flow system. The presence of trapped gas in the bundle would reduce the effective heat transfer surface area with a consequential

decrease in the derived average heat transfer coefficient. The 18.4 per cent baffle cut, 48.5 mm baffle spacing case examined in the later work at AEE Winfrith, revealed that at low Reynolds numbers (around 100) the trapped gas extended over the top 5 tubes in the bundle. The large baffle cut and long baffle spacing configuration under discussion here would be subject to an even greater problem with trapped gas.

The vertically orientated exchanger model used at the University of Aston did not have the problem of trapped gas. In the case of Williams any trapped air would have been removed by the nitrogen purge prior to experimental runs.

4.4.2.6 Accuracy of Williams's Data

Williams (32) made no attempt to estimate the accuracy nor the repeatability of his mass transfer data obtained by the mercury evaporation technique. In measuring mass transfer coefficients from mercury coated sections of tubes, allowance had to be made for mercury that was blown off the tubes and deposited in the bundle. Dummy runs performed after each experimental run showed that the deposits contributed up to 30 per cent of the total mass transfer. The bundle removal between experimental and dummy runs could have dislodged the deposits or produced others as the mercury coated tubes were withdrawn. Some repeatability tests would have provided valuable information on this subject.

The accuracy of the gas sampling system and the mercury vapour concentration measurements is also suspect particularly in cases of low mercury concentrations.

The tube surfaces were saturated with mercury vapour. The saturation concentration was calculated from a rather

complex theoretical equation which involved the assumption of ideal gas behaviour.

4.4.2.7 The Heat and Mass Analogy

The Chilton and Colburn heat and mass transfer analogy was originally defined for fully turbulent flow in pipes, although other workers have since extended this to other systems (see Section 2). For the heat exchanger studies at the University of Delaware, Bell (29) defined laminar shell-side flow as existing for Reynolds numbers (Re_M) less than 100 and fully turbulent flow for Reynolds numbers greater than 4 000. The ranges of Reynolds numbers investigated by Williams and the present work would thus correspond to the transitional and laminar flow regimes.

In the development work the response from a micro-electrode (in this case $\frac{1}{4}$ in. (6.3 mm) long) located in the mid-baffle position on tube number 48, was recorded on a Kent recorder. A shunt converted the instrument to an ammeter. Under diffusion controlled conditions the characteristics of the response were recorded over a range of Reynolds numbers 100 to 1 500. The results of this investigation are shown in Fig. 19. The amplitude of the oscillations give an indication of the turbulence level. The associated stability of the hydrodynamic and mass transfer boundary layers is reflected in these limiting current response characteristics. The smooth response for Reynolds numbers less than 300 would suggest that laminar flow existed. The damping characteristics of the recorder may have concealed oscillations occurring at lower Reynolds numbers. Moreover these results represent the characteristics of a single tube in an internal baffle

Chart Speed = 34 mm/s

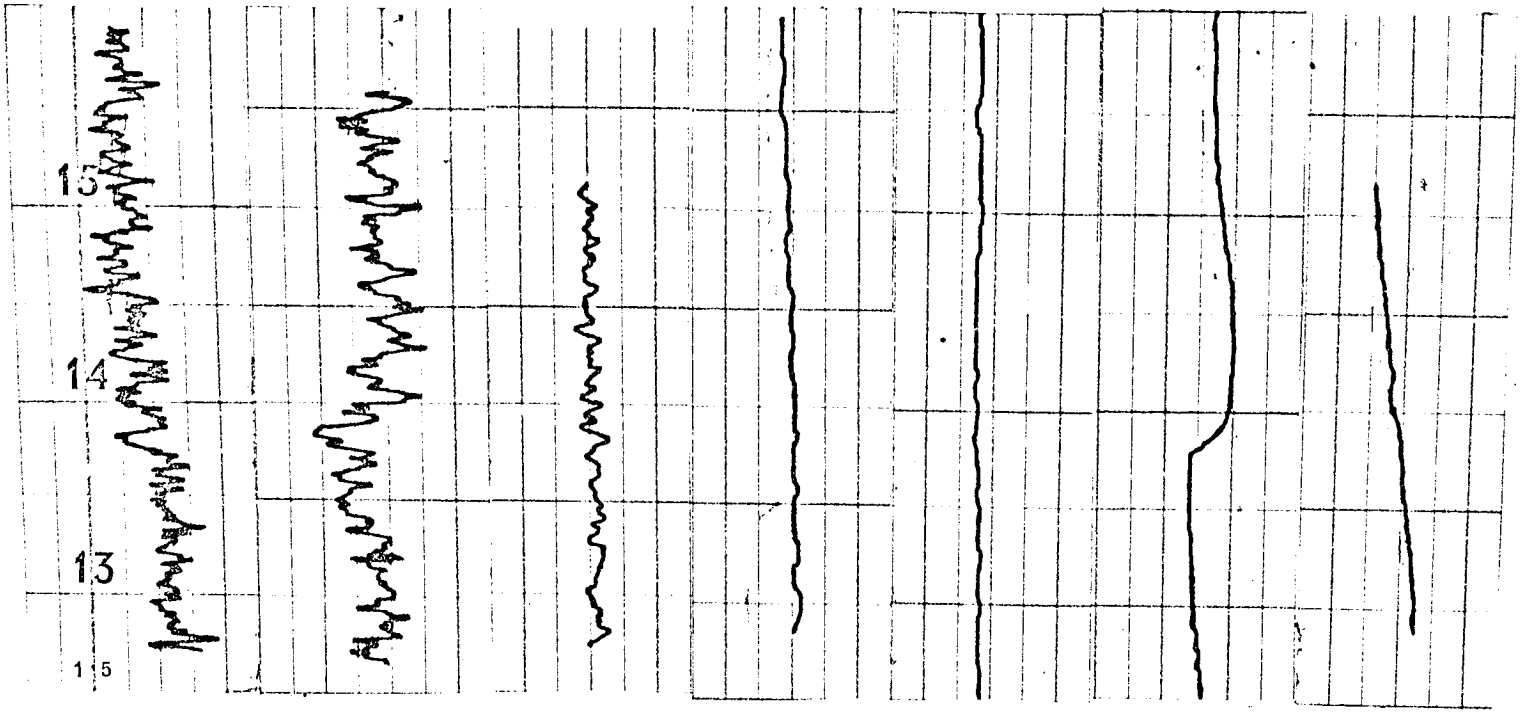

Re_M = 1 500 1 000 500 400 350 300 100

Fig 19 LIMITING CURRENT CHARACTERISTICS

compartment. For as mentioned earlier, the onset of turbulence in staggered tube arrangements varies with position in the bundle. The onset of fully turbulent conditions is not so easily identified in Fig. 19. However the amplitude of the oscillations at Reynolds numbers of 1 000 and 1 500 are roughly equal.

The flow regimes defined by Bell and those demonstrated in the present investigations, both indicate that the use of the Chilton and Colburn analogy in comparing the heat and mass transfer data was not fully justified, particularly at the lower Reynolds numbers.

The following section examines this subject further.

4.4.2.8 Natural Convection

Analogies between heat and mass transfer often breakdown in regions of low Reynolds numbers due to the effects of natural convection. Natural convection in heat transfer is produced by fluid motion brought about solely by differences of density created by temperature gradients. In the case of mass transfer an analogous situation exists where natural convective mass transfer is produced by density differences due to concentration gradients.

In natural convection the product of the Grashof number and Prandtl number (or Schmidt number in the case of mass transfer) known as the Rayleigh number, Ra, replaces the Reynolds number as the dimensionless group characterising the process. The Rayleigh numbers were calculated for the transfer systems in the present work and in those of Bergelin and Williams. Details of the calculations are given in Appendix 3.4.2. The values are shown in the table below.

Work	Rayleigh Number	Critical Reynolds Number
Tompkins	1.4×10^{4}	1×10^{3}
Brown	4.5×10^{5}	1×10^{3}
Williams	4.6×10^{-4}	5×10^{-2}
This work	6.1×10^{7}	2×10^{3}

The University of Delaware investigations under Bergelin have been subdivided into the two series of experiments by Tompkins and Brown.

The Rayleigh numbers were essentially constant in each series of experiments.

The Rayleigh number in the electrochemical process was a factor of 10^{2} higher than those in both of the heat transfer studies under Bergelin. The mercury evaporation technique of Williams exhibited an exceptionally low value.

Engineering Sciences Data Unit (49) have analysed the majority of the existing data on heat transfer from horizontal and vertical cylinders in crossflow. Regions were defined in which the separate modes of convection are dominant (see Fig. 20). In the intermediate "mixed convection" zone it was found that neither the forced or natural convection correlations adequately described the process.

On superimposing the data from the above table onto Fig. 20, it was apparent that in the case of Williams, natural convection would become significant only at Reynolds numbers below 5×10^{-2}. This was well below the range of his work. In the present work and both the heat transfer studies, the effect of natural convection would become significant at Reynolds numbers less than 1 000. These critical Reynolds

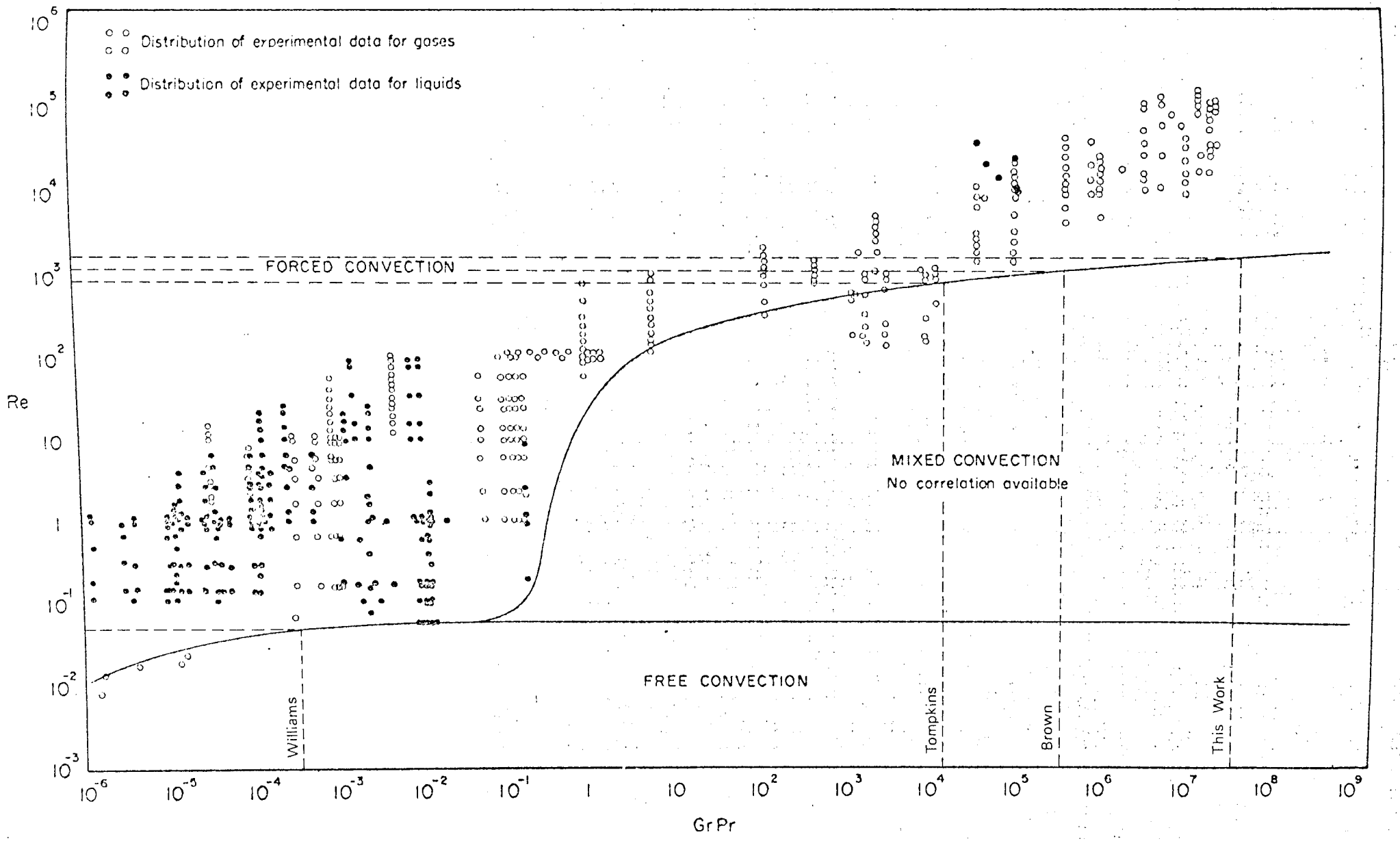

FIG 20 REGIONS OF APPLICATION OF CORRELATIONS FOR CYLINDERS

number values are also recorded in the above table. It would thus seem significant that the discrepancy between heat and mass transfer data presented in Fig. 17 begins to emerge at around a Reynolds number of 1 000. A similar characteristic was produced in a confirmation test at AEE Winfrith (see Section 6.2).

An attempt was made to separate the natural convection components in the heat and mass transfer data and to correlate them. As already shown, the natural convection component in Williams's data would have been negligible. The natural convection components in the heat transfer and electrochemical data were obtained by simply subtracting the j-factors of Williams from their own corresponding j-factor values. This approach assumes that the effects of natural and forced convection are additive. The resulting pure natural convection j-factor values were then converted to Nusselt or Sherwood numbers. These were compared with correlations given by McAdams (7) for natural convection from both horizontal and vertical cylinders (see Figs. 21 and 22).

The Delaware heat transfer data fell close to the correlation for horizontal cylinders particularly at the very low Reynolds number of 20. The data from the present work fell considerably below this correlation as did the data from the confirmation test performed later at AEE Winfrith. The data from the present work would be correlated more justifiably as vertical cylinders (see Fig. 22). Again the data fell below the correlation. This discrepancy could be attributed to errors in the estimation of the densification term in the Grashof number and to differing characteristics between a single tube and a tube bundle. The method of

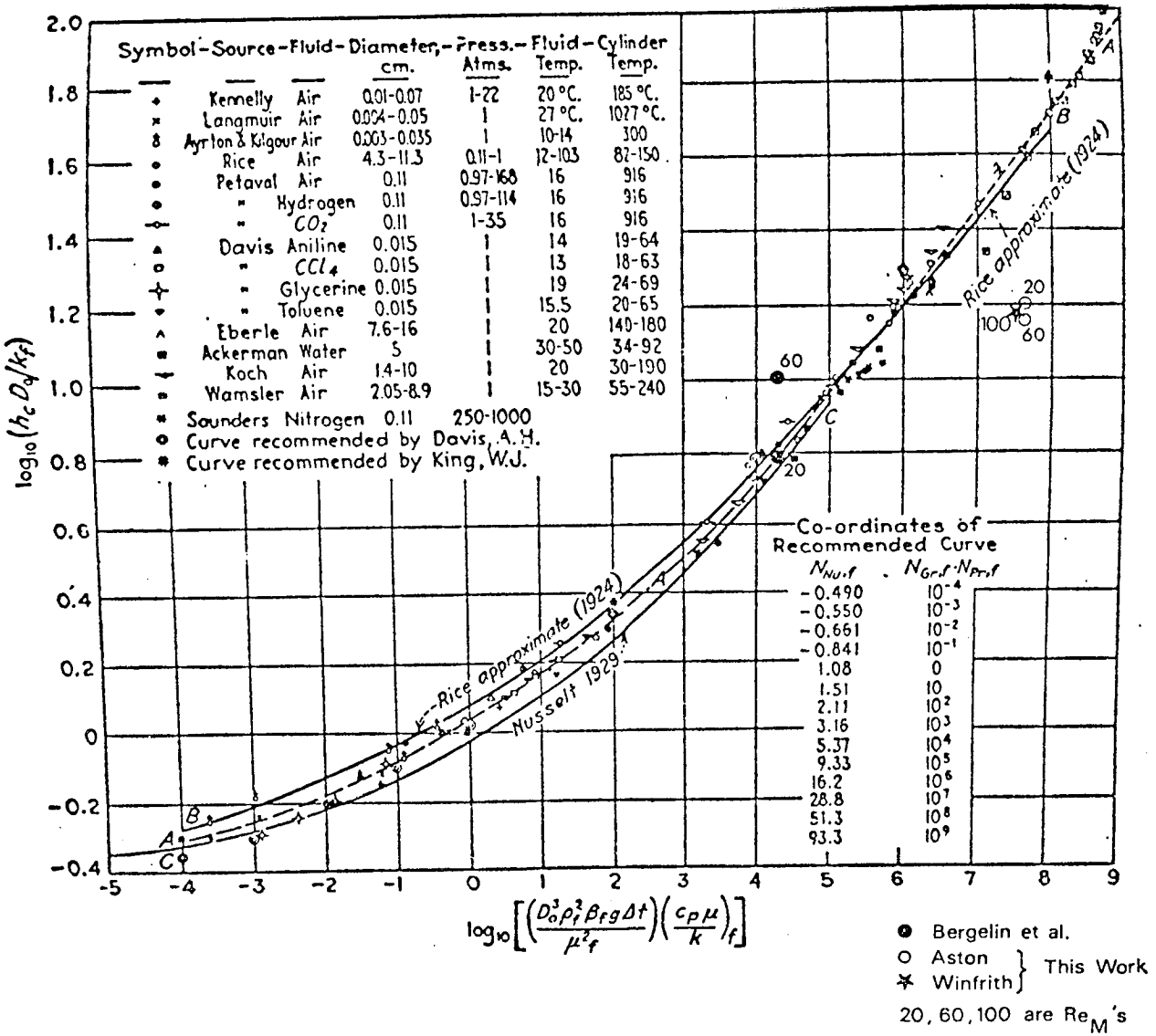

FIG 21 - CORRELATION FOR NATURAL CONVECTION FROM HORIZONTAL CYLINDERS (McAdams)

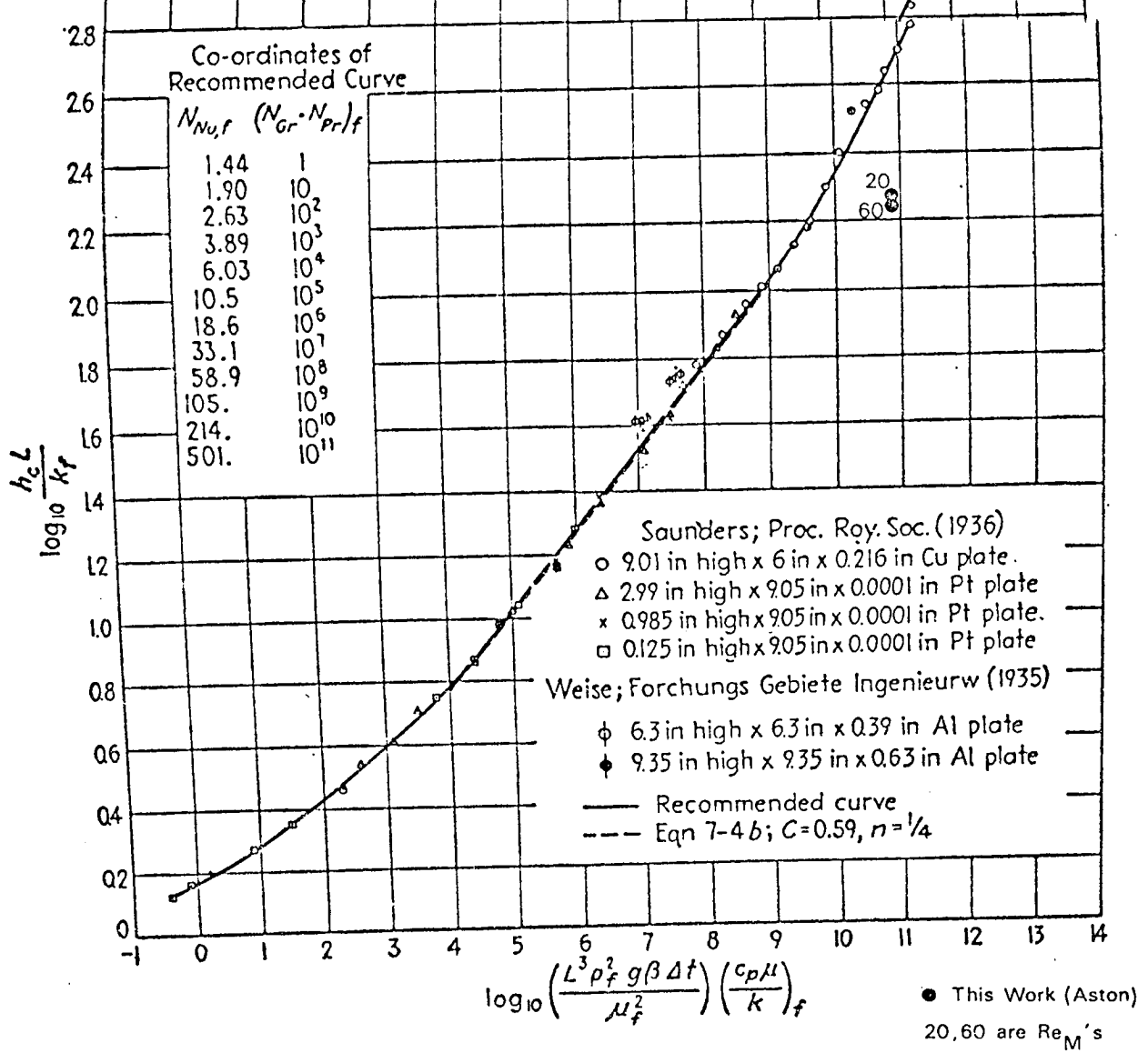

FIG 22 - CORRELATION FOR NATURAL CONVECTION FROM VERTICAL CYLINDERS (McAdams)

deriving the natural convection components may also have been at fault. No general correlation for natural convection in tube-banks was available. The correlations used in the above discussions were for natural convection from a single cylinder. The situation in a baffled tube bundle would be considerably more complicated. The buoyancy effects may cancel out as the fluid flow direction is reversed in alternate baffle compartments. Thus the net effect of natural convection on the overall bundle heat transfer data of Bergelin may have been negligible.

In the present work and that of Williams only one baffle compartment was investigated. Thus any enhancing or suppressing effects of natural convection would be more evident as the flow was essentially in one direction only.

4.4.3 Zonal Average j-Factors

When analysing the distribution of heat transfer through a baffled tube bundle it is convenient to divide the flow area into zones. Bergelin et al. (30) defined a window zone and a cross flow zone with their boundaries determined by the baffle cut and baffle spacing (see Fig. 2). The window zone may then be subdivided into an inlet and outlet window zone depending on the direction of the shell-side fluid flow.

A zonal average j-factor was derived as the arithmetic mean of the j-factors of all the tubes contained within the particular zone. In the case of both baffle cuts employed, the baffle tip coincided with the centre of a row of tubes. Williams (32) overcame this problem in his analysis by defining two additional zones containing the tubes on the inlet and outlet baffle edges. In the present work, for the sake of simplicity, the tubes on the baffle edges were regarded as having half their transfer surfaces

in the crossflow and half in the window zones. When calculating zonal average coefficients the coefficients of the two divided surfaces were assumed to be equal. The validity of the assumption depends on the uniformity of the distribution of heat or mass transfer around the circumference of the tubes. The data of Williams were re-analysed using this simplified zonal definition. The zonal average j-factors of Williams and this work are compared for the two baffle cuts in Figs. 23 and 24.

At the 43.7 per cent baffle cut, the present work gave near equal average j-factors for the two window zones. The crossflow average j-factor was however considerably higher. This was predictable, for the separation of the boundary layers in crossflow produces higher transfer rates than those from longitudinal flow. Furthermore, visual studies (see Section 1.5) have shown that stagnant regions occur in the corners of window zones. Analysis of Williams's data gave distinctly different average j-factor values for the three zones. The inlet window and crossflow j-factors did however converge at low Reynolds numbers. While the crossflow zone gave the highest values, the outlet window zone gave by far the lowest values of average j-factors. The inlet window zone j-factors from the two sets of work compared well. The Williams's crossflow data gradually fell off from that of this work as the Reynolds number was decreased. The outlet window zone values of Williams were however consistently lower than those of the present work. The characteristic manner in which the discrepancies between the corresponding zonal j-factors increased progressively from the inlet window to the outlet window, would suggest that internal leakage was present in Williams's exchanger model. Fluid losses by leakage from the main flow stream as it moved through the baffle compartment, would produce

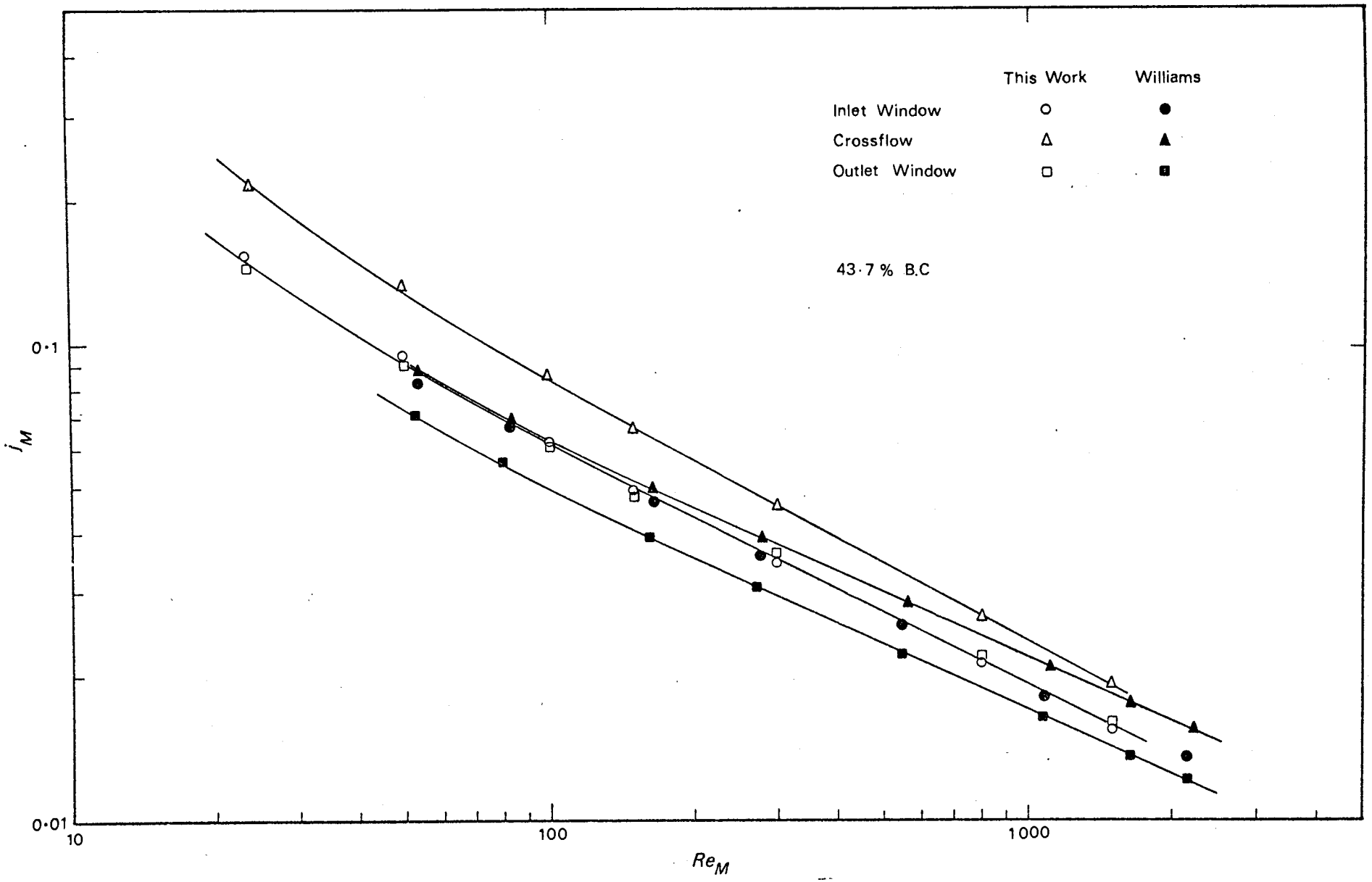

FIG 23 ZONAL AVERAGES

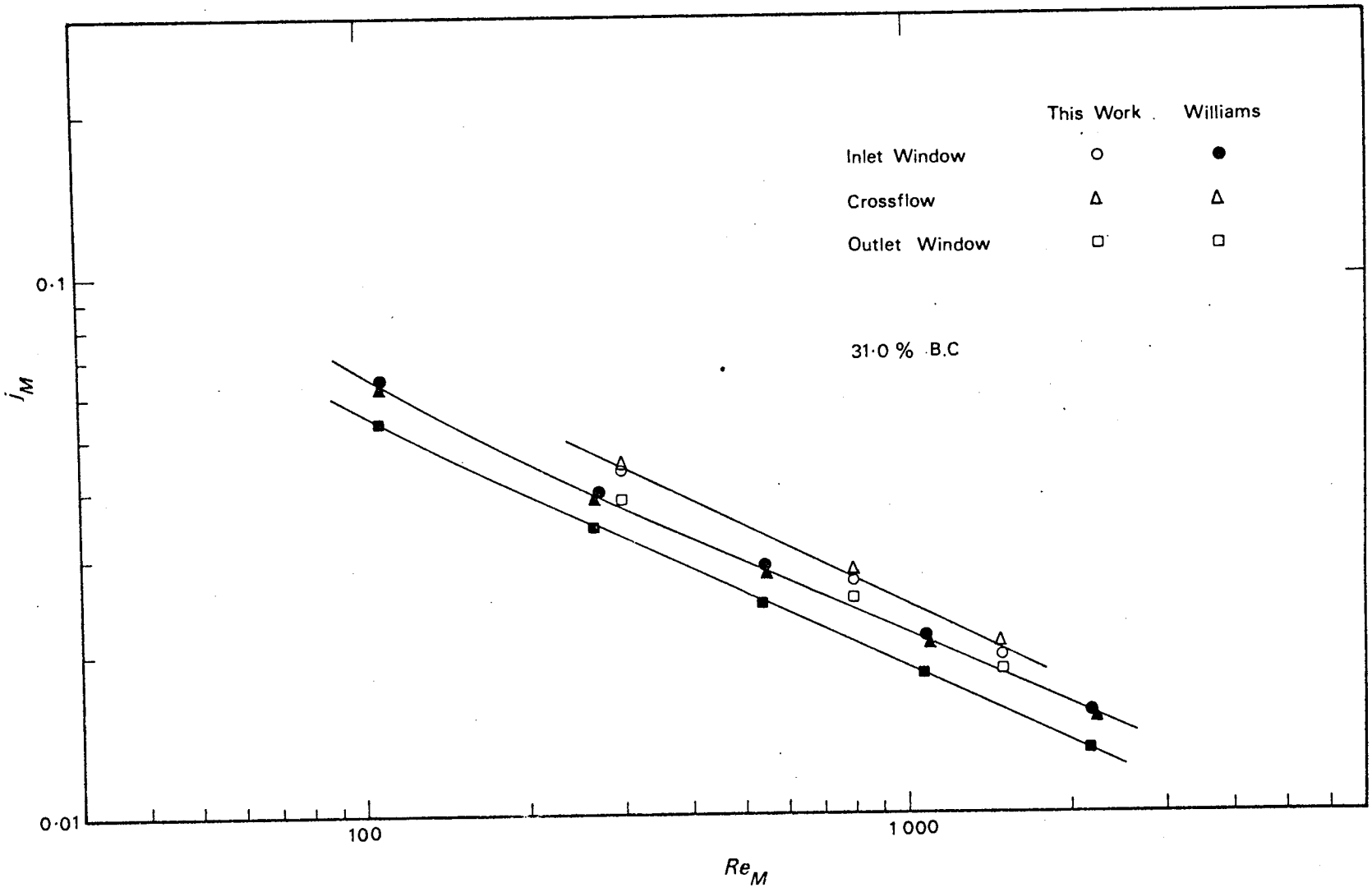

FIG 24 ZONAL AVERAGES

lower mass transfer rates in the downstream compared with the upstream regions. However this explanation requires that leakage be more significant in the downstream than in the upstream baffle of the particular baffle compartment. Localised tearing of the sealing rubbers could have produced leakage in just one baffle. Had leakage been more widespread, discrepancies would probably have also been evident between the inlet window zone coefficients of Williams and this work.

At the 31.0 per cent baffle cut, the inlet window and crossflow zone average j-factors of the present work were roughly equal. The outlet window zone j-factor was inferior to these particularly at lower Reynolds numbers. The inlet window and crossflow zone j-factors of Williams were also nearly equal to each other but were by up to 15 per cent lower than those of the present work. The outlet window zone j-factor was again considerably lower than coefficients in the other two zones. The relationship between zonal j-factors was thus similar in the two investigations.

In the present work the 43.7 per cent cut baffles were made by simply cutting down the baffles used in the investigations at the 31.0 per cent cut. Williams however used two separate sets of baffles. The differing relative characteristics of the two sets of data at the two baffle cuts, reflect the inconsistency of the baffle leakage control in Williams's work.

4.4.4 Individual Tube j-Factors

4.4.4.1 General Analysis

The individual tube mass transfer j-factors were compared with the corresponding data of Williams. The discrepancies (as percentages) between values from this work and those of Williams were determined for each tube investigated.

Williams's results were taken as the datum in these calculations.

The j-factor values and their discrepancies from those of Williams for the 43.7 per cent baffle cut are given in Figs. 25 and 26. Reynolds numbers of 1 500 and 300 were chosen for the illustrations as these represented cases where the compartment average j-factors of the present work and of Williams were in good and bad agreement respectively. The distribution of the tube j-factors revealed that at both Reynolds numbers, the tubes with the highest values occurred in the crossflow zone. Very low j-factors were exhibited by tubes at the top and bottom of the bundle. These low values are attributable to longitudinal flow and the presence of regions of relatively stagnant fluid. The distribution of individual tube discrepancies showed that throughout the inlet window zone the results from the two investigations were in close agreement. In the crossflow and the outlet window zones the results from the present work were consistently higher, in the case of one tube by as much as 50 per cent. Again the general pattern of the discrepancies would suggest the presence of leakage in the Williams exchanger model.

A comparison of actual individual tube coefficient values should be regarded as only tentative. Any random redistributions of the shell-side fluid would result in variations in measured values of local coefficients. This phenomenon would be particularly significant in the regime of mainly transitional flow under examination here. A more informative approach is to compare the distribution patterns of the tube coefficients. Thus the two sets of data were

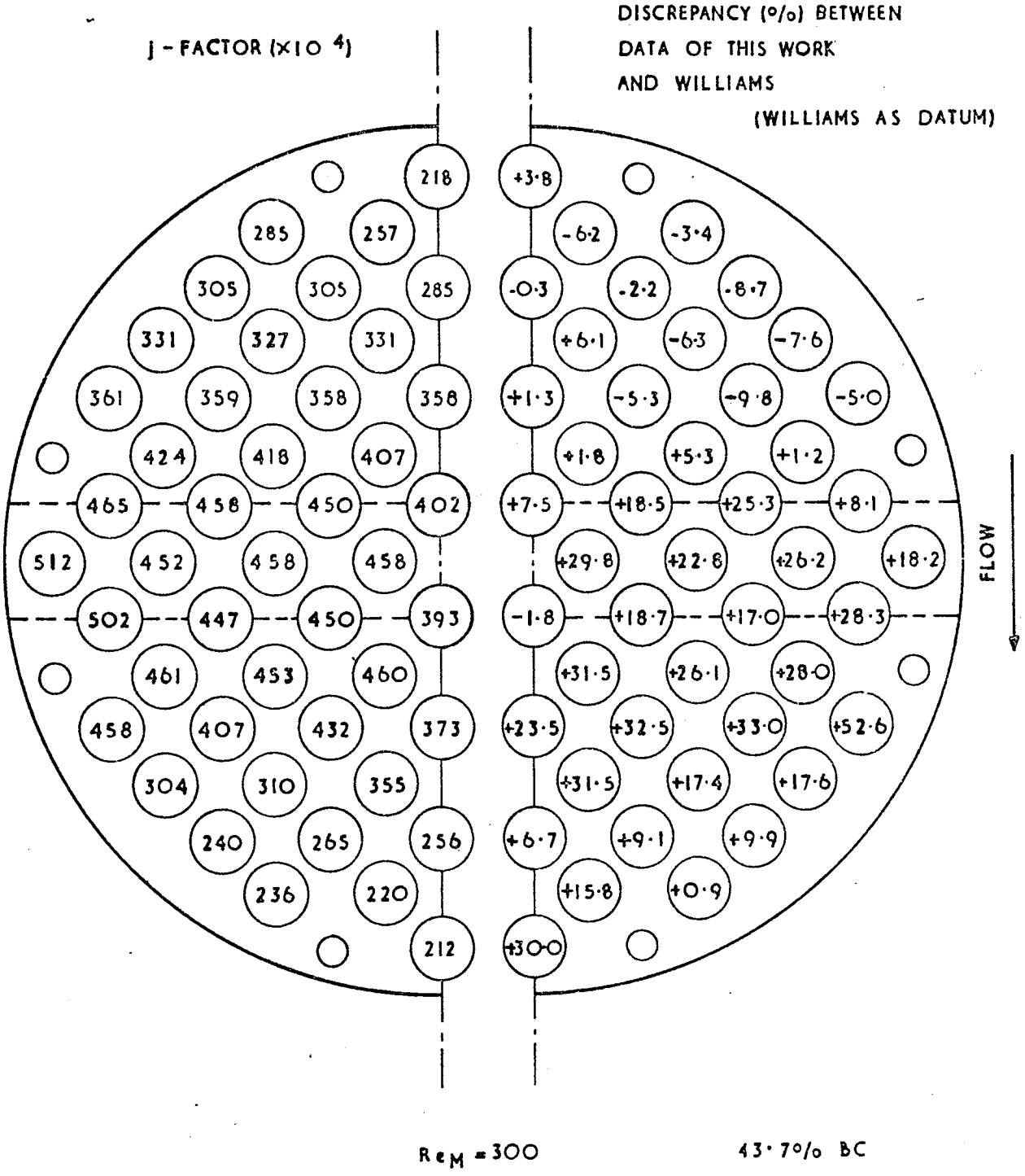

FIG. 25. NO-LEAKAGE

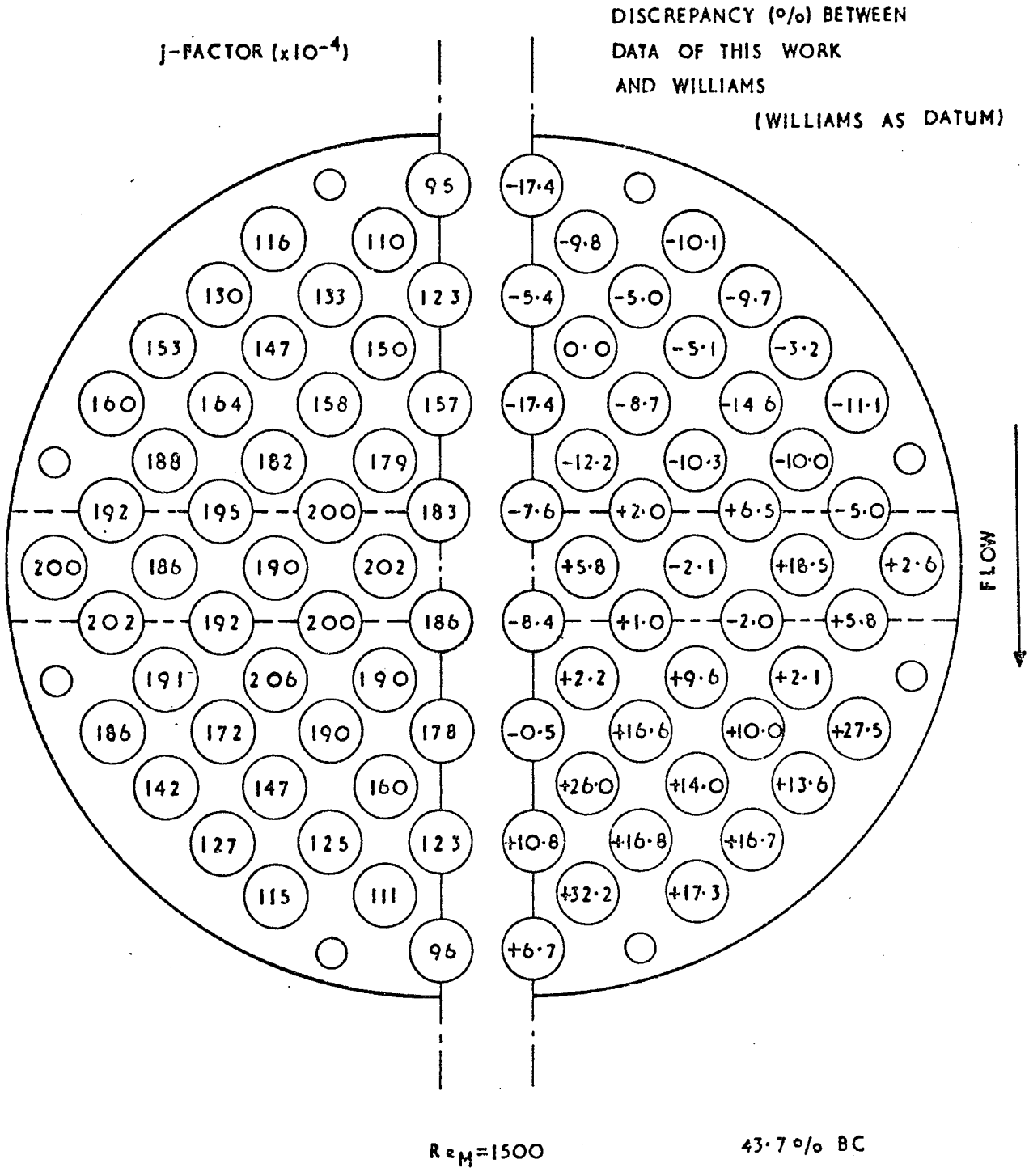

FIG.26. NO-LEAKAGE

expressed as ratios of the individual tube j-factors to the compartment average value. These "normalised" data are shown side by side in Figs. 27 and 28. At the low Reynolds number a distinct variation between the two patterns emerges. In the present work, tubes with above average j-factors (signified by ratio values greater than unity) do not occur until the last row of the inlet window zone. Such tubes extend throughout the crossflow zone to the middle of the outlet window zone. The results of Williams reveal that such tubes occur initially further upstream in the baffle compartment and subsequently terminate after the first full row of tubes in the outlet window zone. Tubes possessing j-factors that exceed the compartment average value by over 20 per cent are more numerous and show greater uniformity of distribution in the case of the present work. At the Reynolds number of 1 500, there is far greater similarity in the limits of tubes having above-average j-factors. The distributions of the lower value j-factors are also very similar in the two cases. These characteristics and the demonstrated equality in compartment average values, indicate that internal leakage was not significant at this value of the Reynolds number. However at the low Reynolds number, Williams's lower compartment average j-factor and the differing individual coefficient distributions patterns suggest that leakage occurred in his exchanger model.

The individual tube coefficient data for the 31.0 per cent baffle cut were analysed in a similar manner. The results of the analysis are given in Figs. 29, 30, 31 and 32. At both Reynolds numbers the tube j-factors again showed a steady decline in value from the edges of the crossflow zone

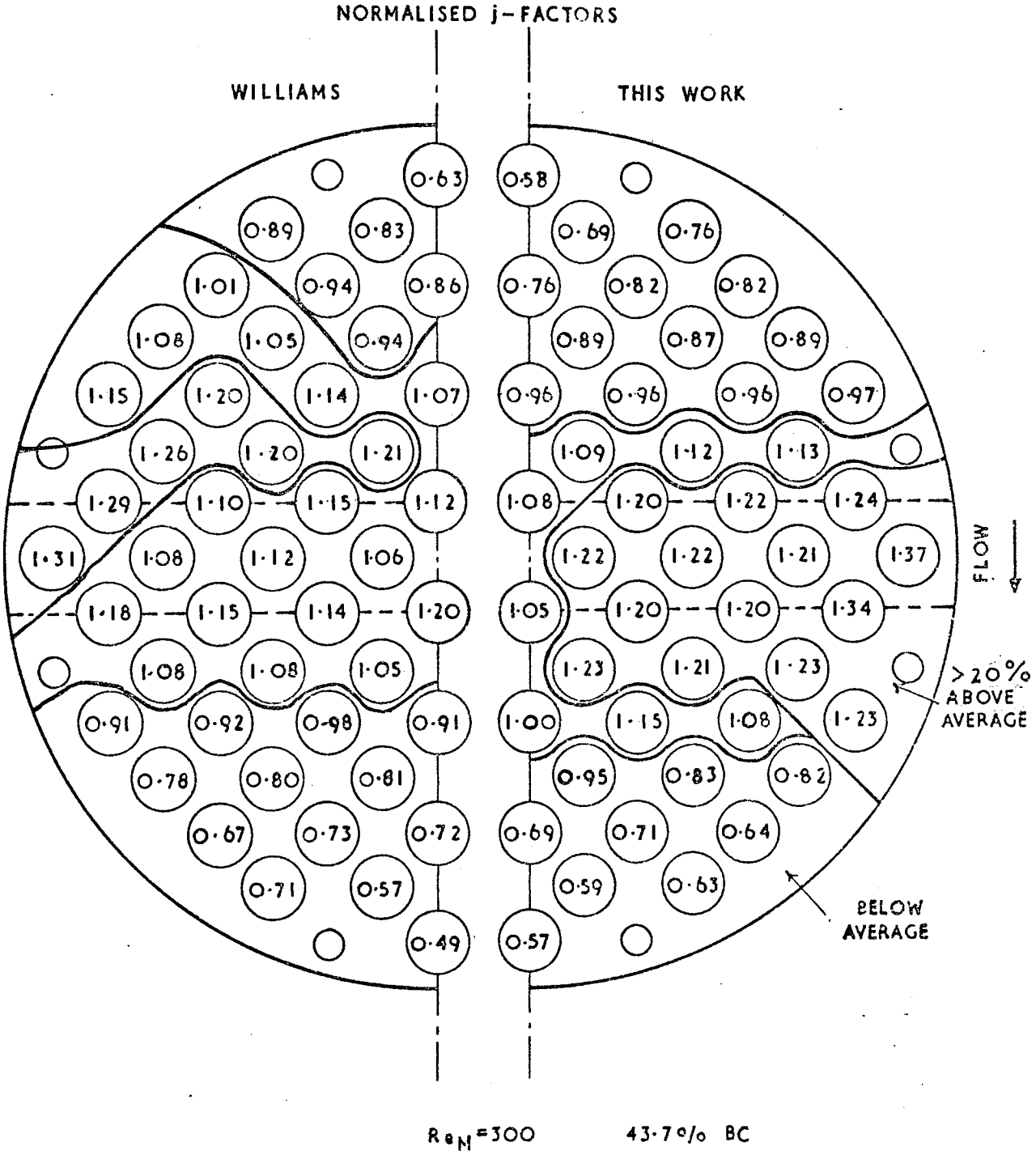

FIG.27. NO-LEAKAGE

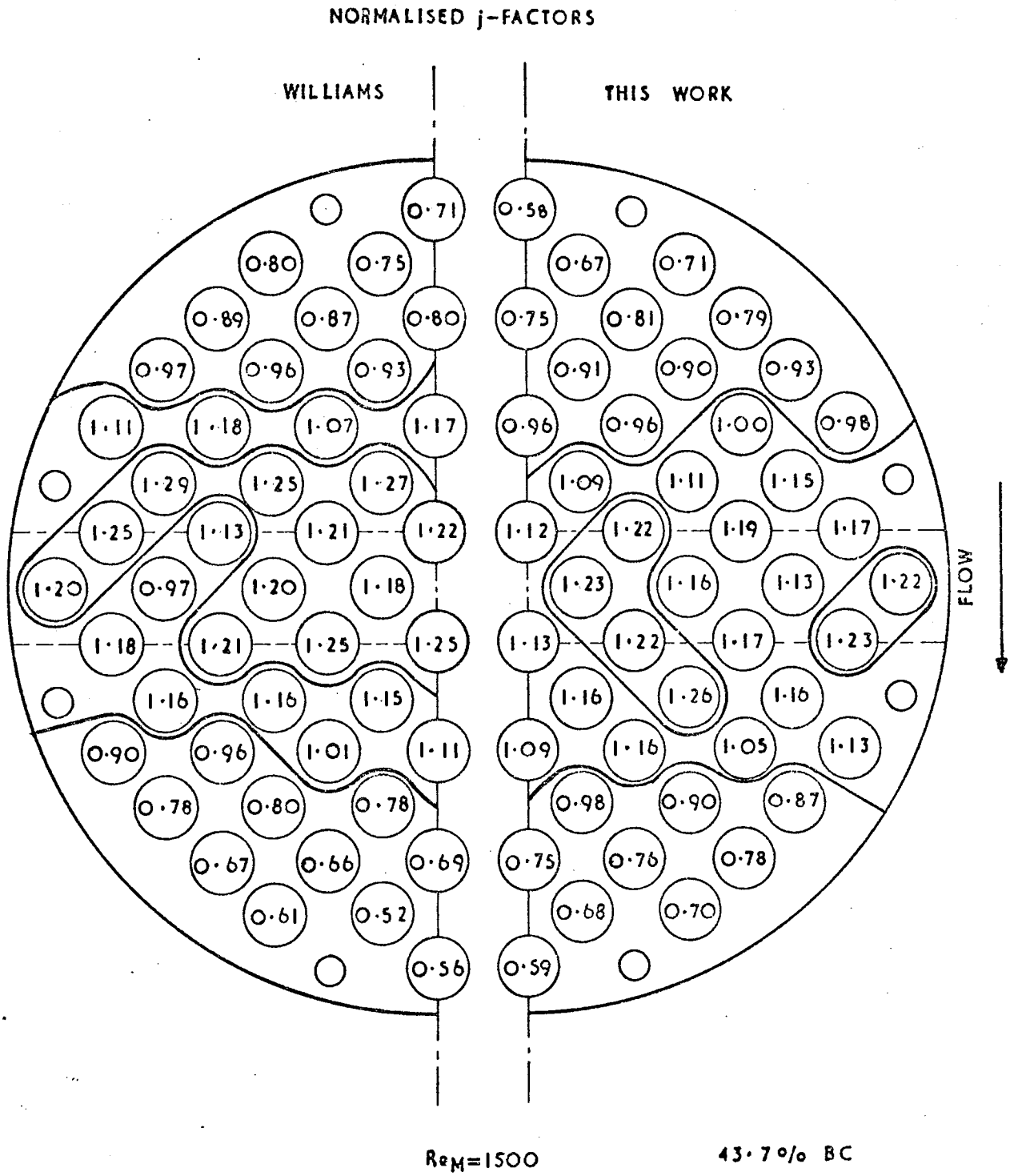

FIG. 28. NO-LEAKAGE

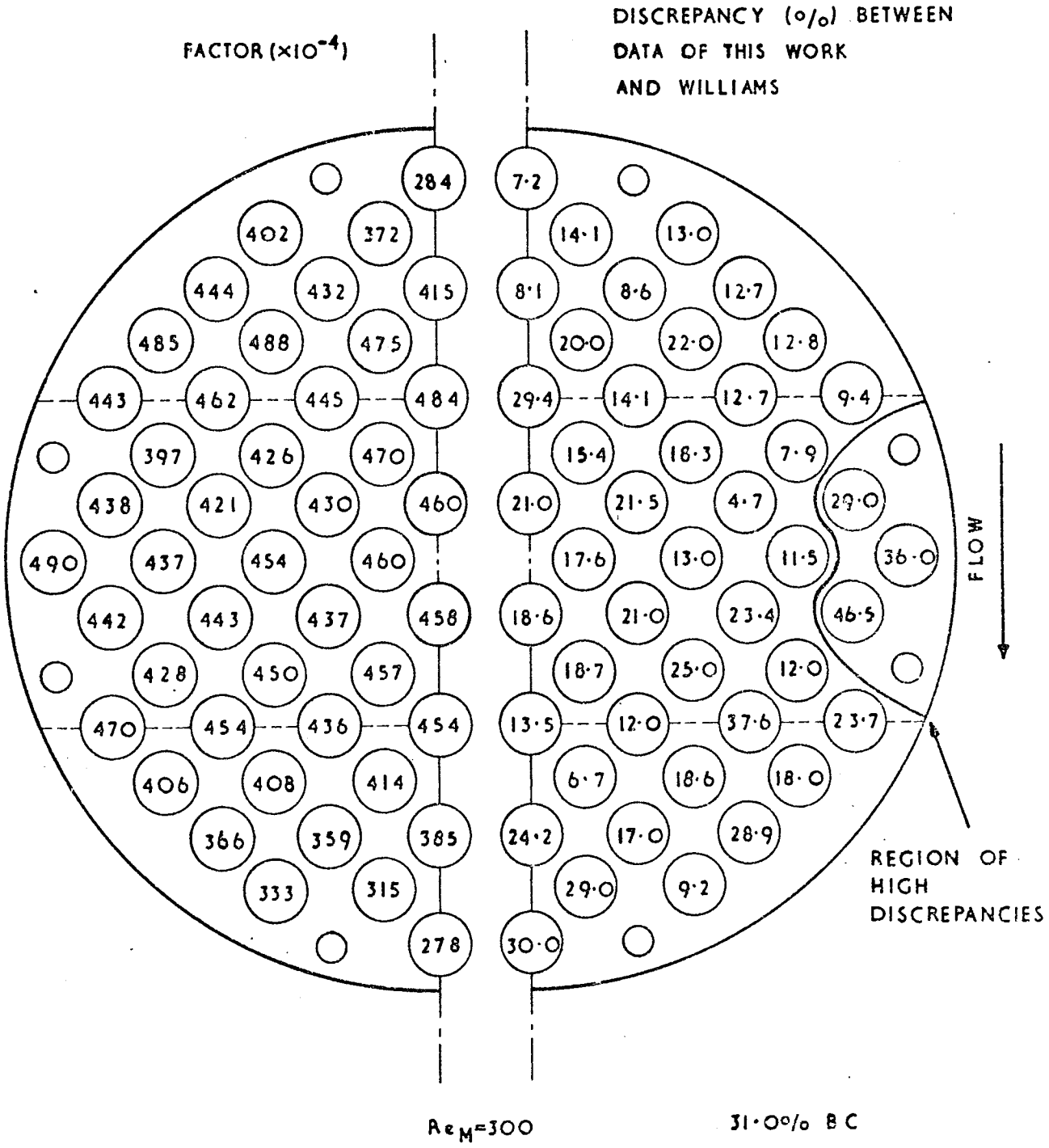

FIG.29. NO-LEAKAGE

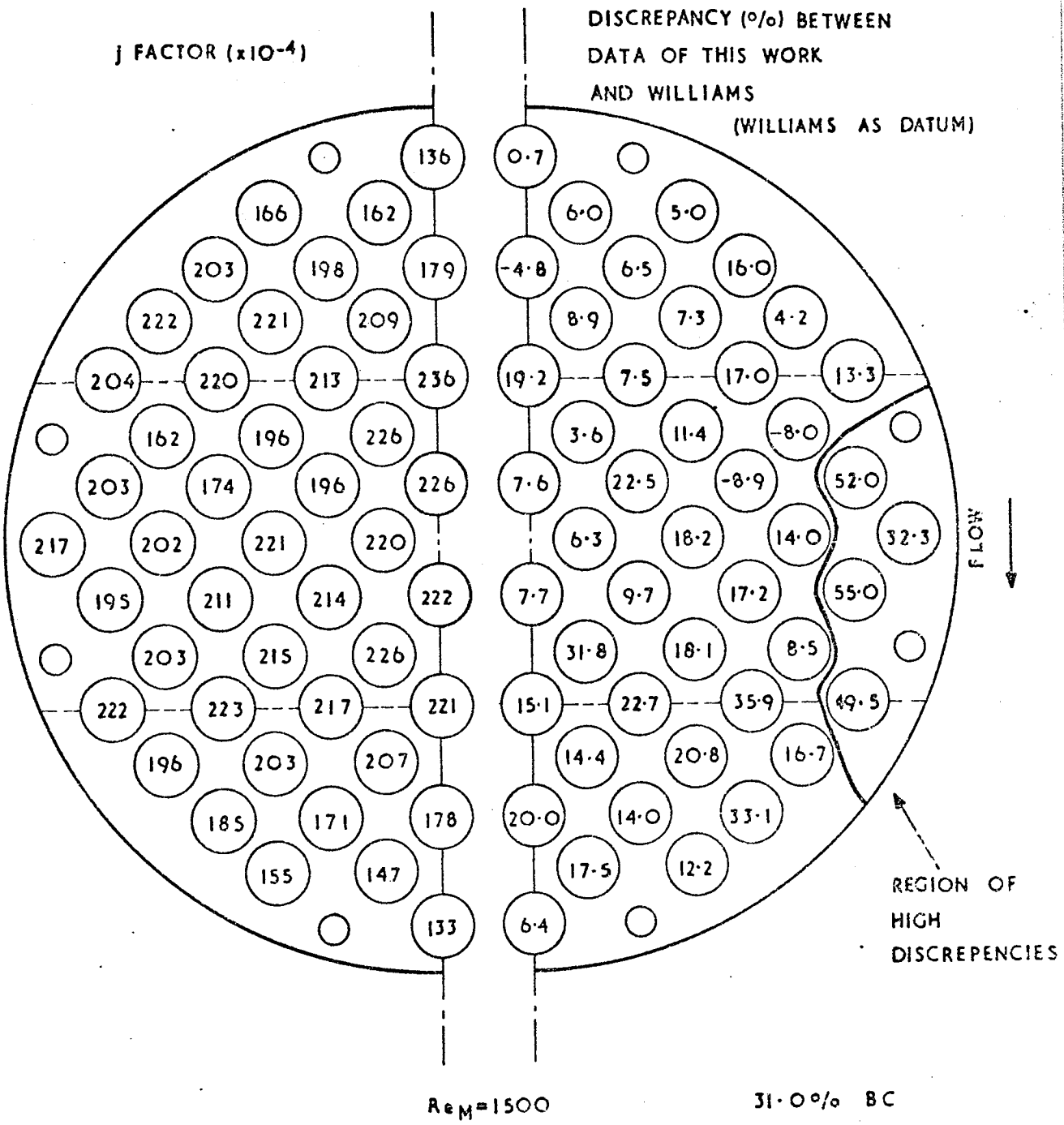

FIG. 30. NO-LEAKAGE

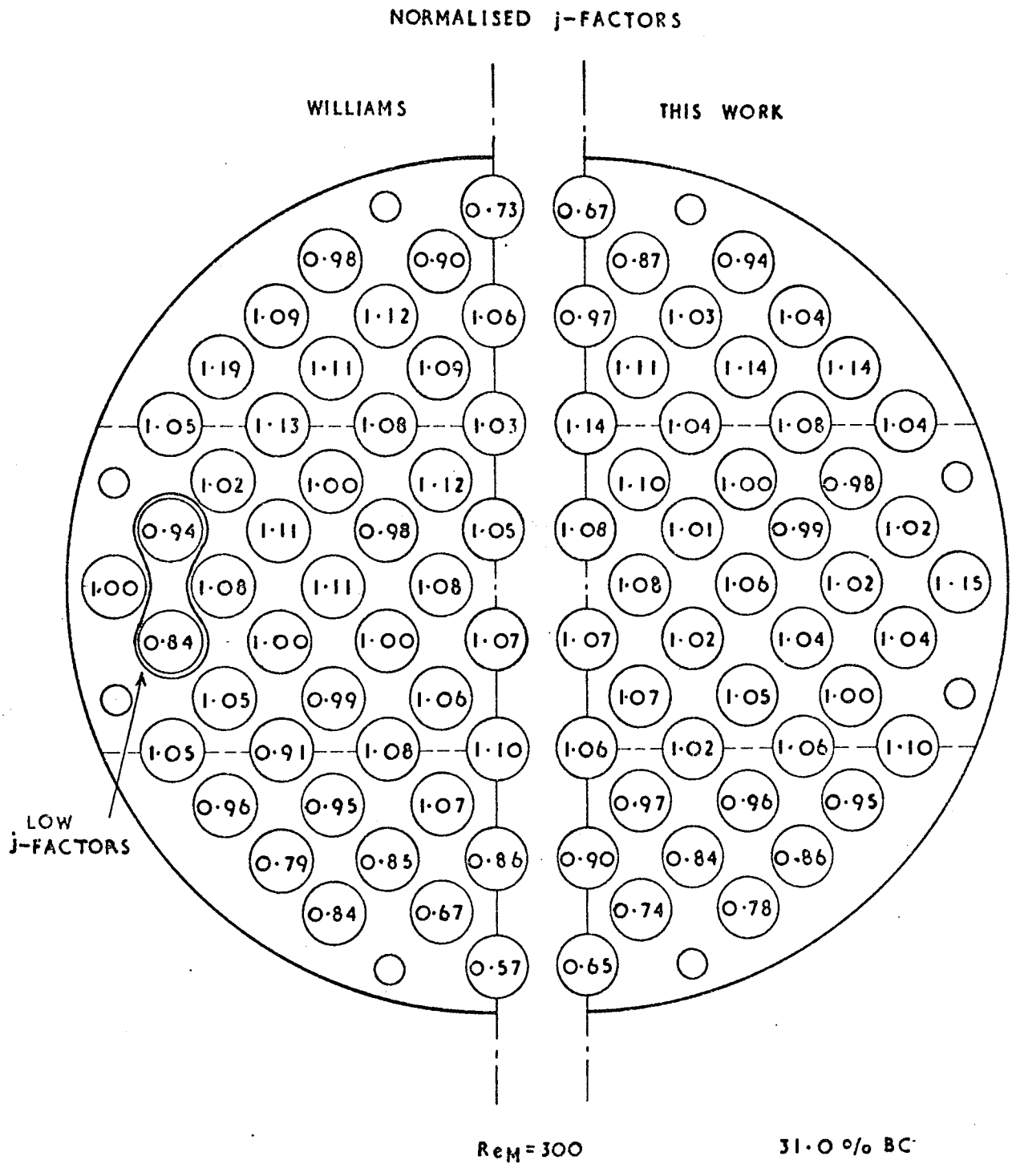

FIG. 31. NO-LEAKAGE

to the top and bottom tubes within the bundle. The variation in tube j-factor values was however less pronounced compared with that for the 43.7 per cent baffle cut. This would indicate that the 31.0 per cent baffle cut represented a more efficient baffle configuration. Comparison with the data of Williams showed that the present work gave generally higher tube j-factor values throughout the bundle. Particularly high discrepancies were revealed for bundle perimeter tubes in the crossflow zone. Here the j-factors of the present work were up to 50 per cent higher than those of Williams. The normalised values of Williams's data were distinctly low in this same region. No such maldistribution was evident in the data of the present work (see Figs. 31 and 32). Localised very low values of transfer coefficients could have occurred as the result of incidental leakage. The location of the tubes with low j-factors would in the case of Williams indicate shell-to-baffle leakage.

The following section describes an experimental investigation into the effects of shell-to-baffle leakage. The study was confined to the 31.0 per cent baffle cut. This baffle configuration possessed a larger potential leakage area and had exhibited more distinctive leakage characteristics in previous analyses.

4.4.4.2 Leakage Analysis

Experiments were performed to investigate the effect of shell-to-baffle leakage on individual tube coefficients. For these tests the original metal baffles of Roberts (54) were employed. Tube-to-baffle leakage was prevented by the use of rubber seals as described in Section 4.2.3.1. The rubber sheet was however trimmed flush with the periphery of

the $5\ ^{1}/_{16}$ in. (128 mm) diameter baffle plates. A shell-to-baffle diametrical clearance of 3/16 in. (4.7 mm) was thus produced. Individual coefficients were measured for 10 tube positions in the bundle. The positions were carefully chosen so as to represent areas of most interest. The results are tabulated in Appendix 3.1.3 . These leakage data were compared with those obtained by Williams under nominally non-leakage conditions. The discrepancies between the data of Williams and both the leakage and non-leakage data of this work are compared at Reynolds numbers of 300 and 1 500 in Figs. 33 and 34. At both Reynolds numbers the discrepancies between Williams's data and the leakage data were considerably less than those between Williams's data and the non-leakage data. As a result of the leakage, the j-factors of tubes on the bundle perimeter in the crossflow zone (i.e. tubes 44 and 51 in Fig. 16) were reduced by a far greater extent than those of the other tubes investigated. At the Reynolds number of 300, as a result of leakage, the j-factor of tube 44 fell from 36 per cent above down to 1.4 per cent below that of Williams. In general the tubes in the window zones showed the least change as a result of leakage. The average values of the individual tube j-factors from the 10 tubes investigated were compared with those of Williams. At the Reynolds number of 300, while the non-leakage data of the present work gave a value for the average j-factor 19.7 per cent above that of Williams, the introduction of shell-to-baffle leakage produced a value 3.5 per cent below that of Williams. At the Reynolds number of 1 500 these values were 16.9 and 3.6 per cent respectively.

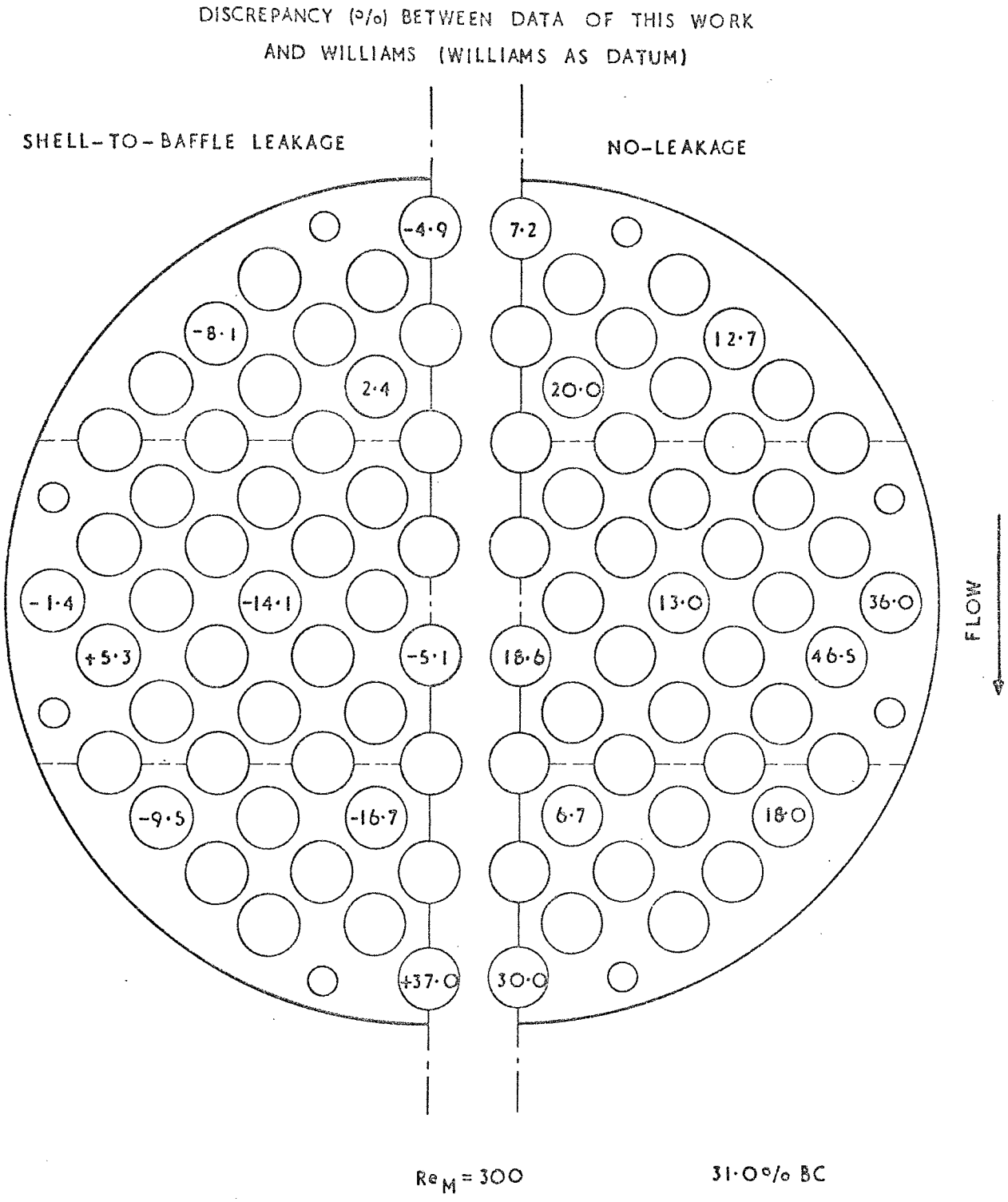

FIG. 33. EFFECT OF LEAKAGE

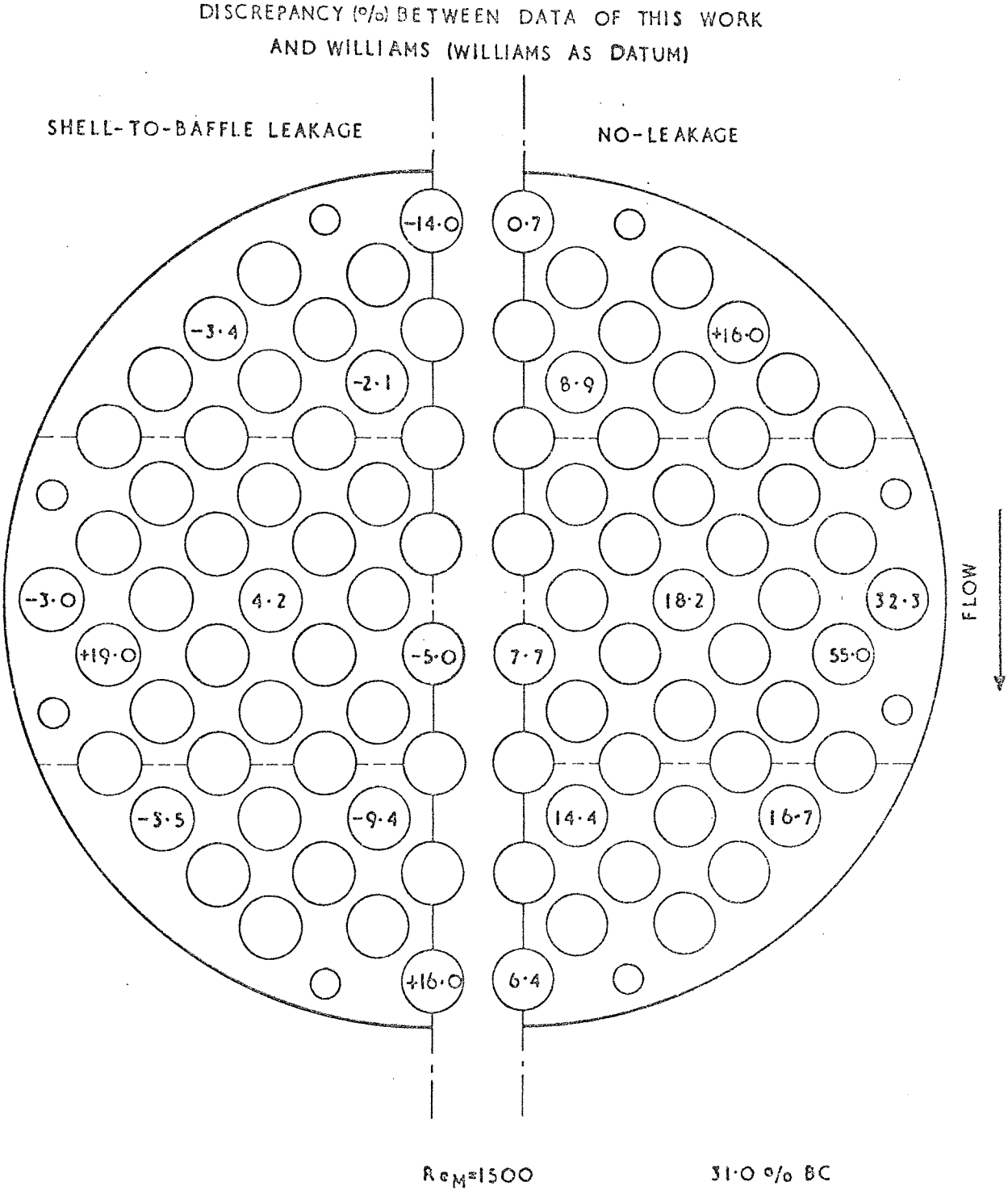

FIG. 34. EFFECT OF LEAKAGE

The leakage experiments thus demonstrated that shell-to-baffle leakage could have produced tube coefficients similar to those obtained by Williams. However any incidental leakage in the Williams model caused by tears in the rubber seals, would not have been as great nor as uniform as the leakage introduced into the present experiments. These controlled leakage tests did however reduce the average j-factors to values lower than those obtained by Williams. Whether the 10 tubes examined truly represented the characteristics of the whole baffle compartment is also open to question.

4.4.5 Variation of Coefficient Along the Tube Length

A limited number of investigations were made into the distribution of mass transfer along the tubes within a baffle compartment. A composite cathode was constructed by dividing a baffle spacing length electrode into four equal length increments electrically insulated from each other. The composite electrode is shown in Fig. 14.

Measurements were made on tubes 23 and 48 (see Fig. 16) at a baffle cut of 31.0 per cent. These particular tube positions were chosen as they represented regions of special interest. Tube 23 being on the edge of a baffle would possess characteristics of both cross and window flow. Tube 48 would be the tube most representative of pure crossflow.

The incremental mass transfer coefficient values for Tube 23 under conditions of no internal leakage are shown in Fig. 35. It was thought unnecessary to convert the mass transfer coefficients to j-factor form. The average of the four incremental coefficients were found to be almost identical to that measured from a single baffle spacing length electrode. This agreement is illustrated

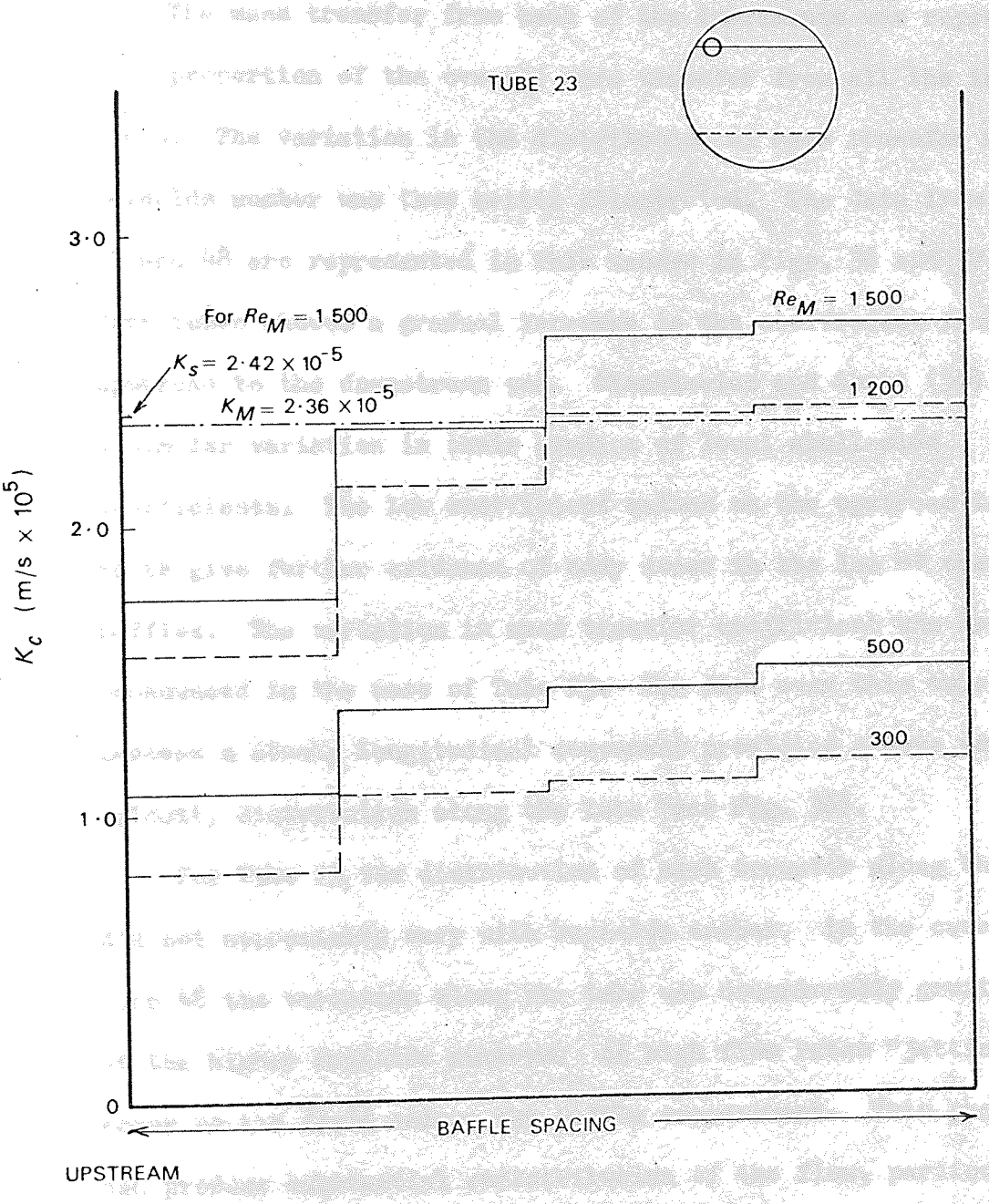

K_M — Arithmetic mean of incremental coefficients

K_s — Coefficient for baffle-spacing length electrode

FIG 35 MASS TRANSFER PROFILE ALONG A TUBE

for the case of a Reynolds number of 1 500 in Fig. 35. This result supports the use of the arithmetic average used in deriving bundle average coefficients from individual tube coefficients.

The mass transfer from each of the increments was represented as a proportion of the overall mass transfer from all the increments. The variation in the distribution of mass transfer with Reynolds number was thus better illustrated. The data from Tubes 23 and 48 are represented in this manner in Figs. 36 and 37. Both tubes showed a gradual increase in the coefficient from the upstream to the downstream end. Stachiewicz and Short (50) found a similar variation in their studies of local shell-side coefficients. The low coefficient values on the upstream increments give further evidence of eddy zones in the lee of the baffles. The variation in mass transfer coefficient was less pronounced in the case of Tube 23. The flow over this tube would possess a strong longitudinal component providing a more uniform velocity distribution along the tube (see Fig. 38).

For Tube 23, the distribution of mass transfer along the tube did not appreciably vary with Reynolds number. In the case of Tube 48 the variation along the tube was considerably greater at the higher Reynolds numbers. At high flow rates "jetting" can occur as the fluid enters the baffle compartment. This phenomenon can produce substantial redistribution of the flow, particularly in the crossflow zone (see Fig. 38).

Measurements were made on Tube 23 in the presence of shell-to-baffle leakage. The degree of leakage was the same as that in the investigations reported in Section 4.4.4.2. The variation of coefficient along the tube is shown in Fig. 39. The profile reveals that the presence of the leakage resulted in a more

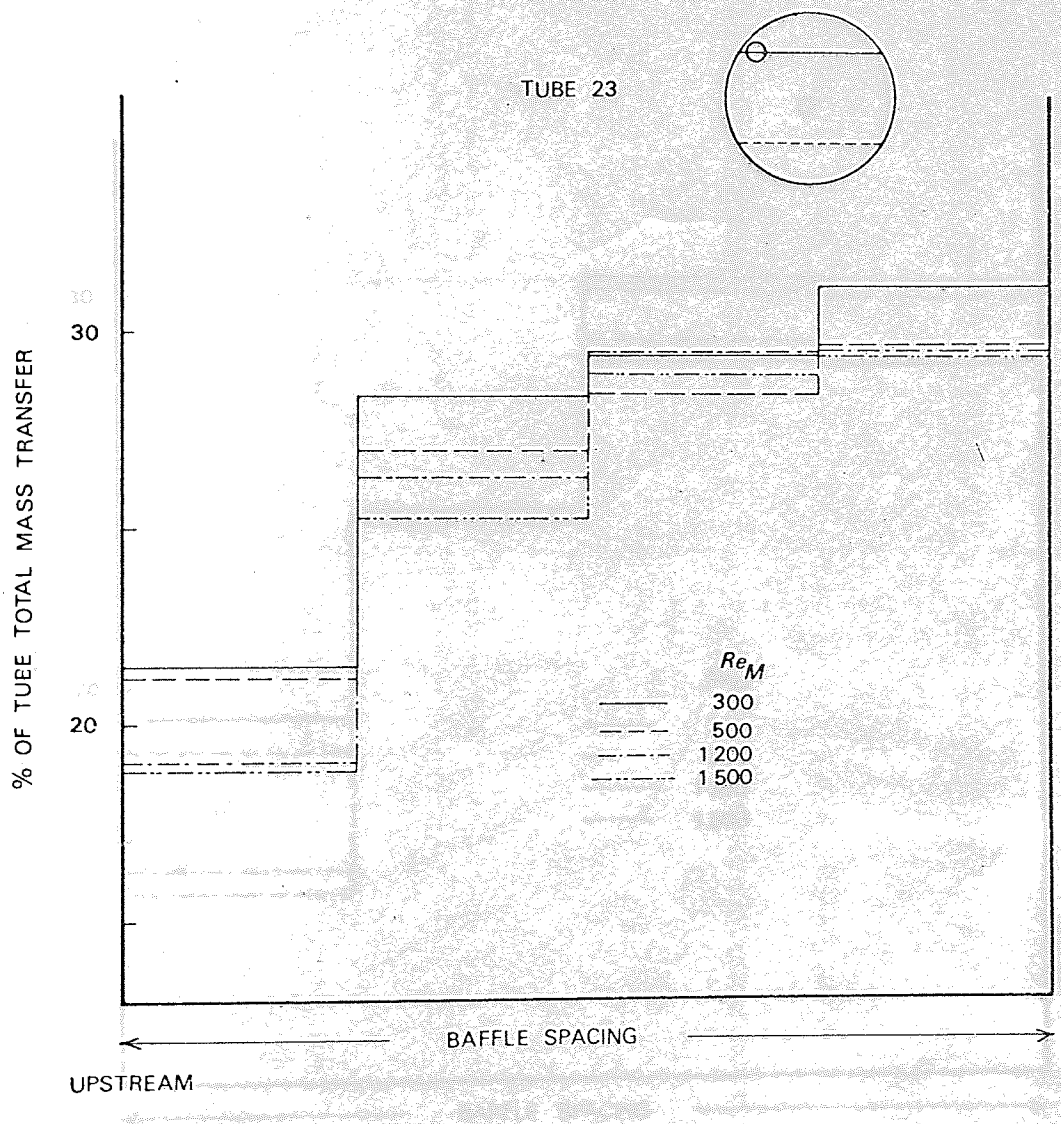

FIG 36 MASS TRANSFER PROFILE ALONG A TUBE

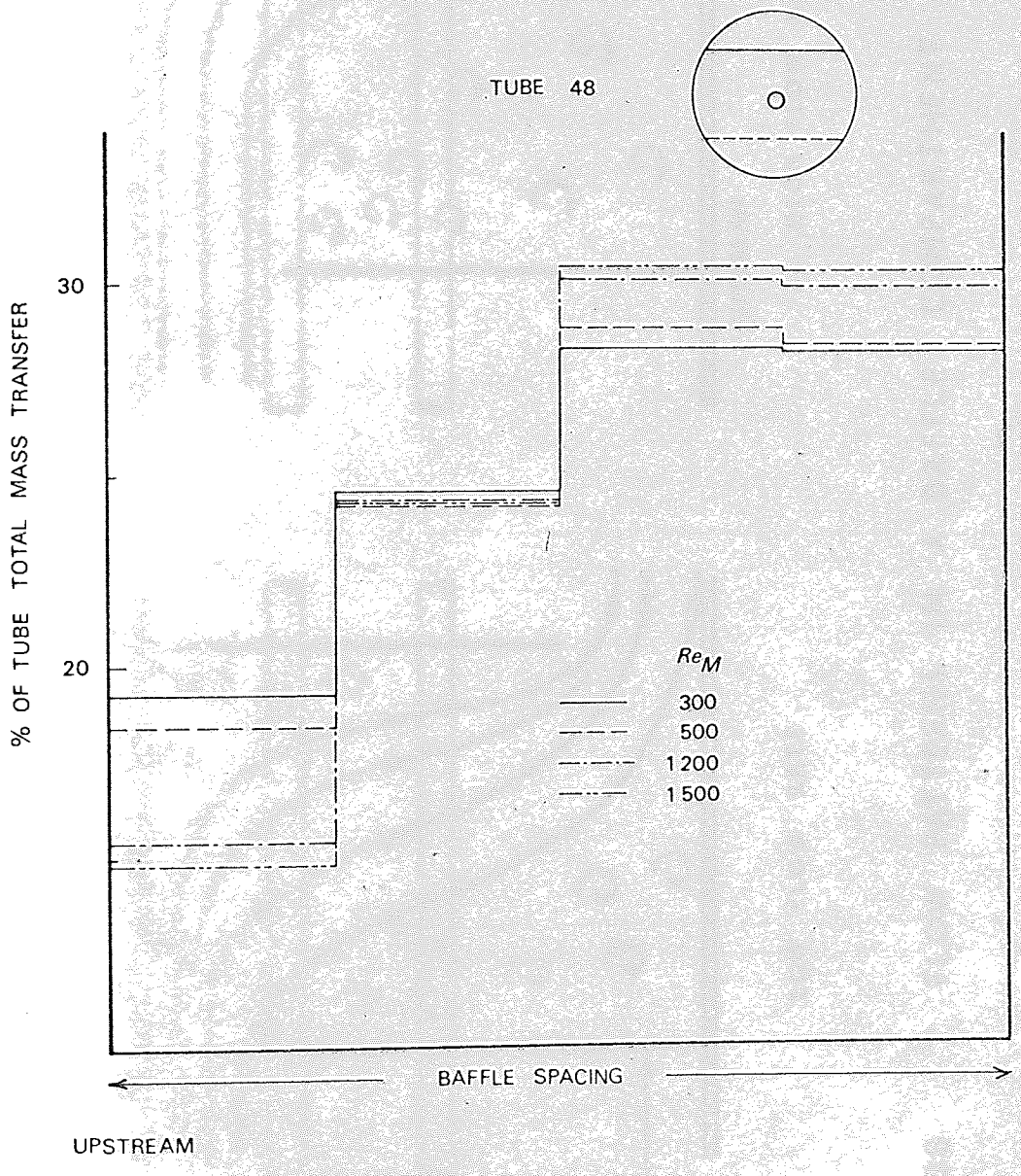

FIG 37 MASS TRANSFER PROFILE ALONG A TUBE

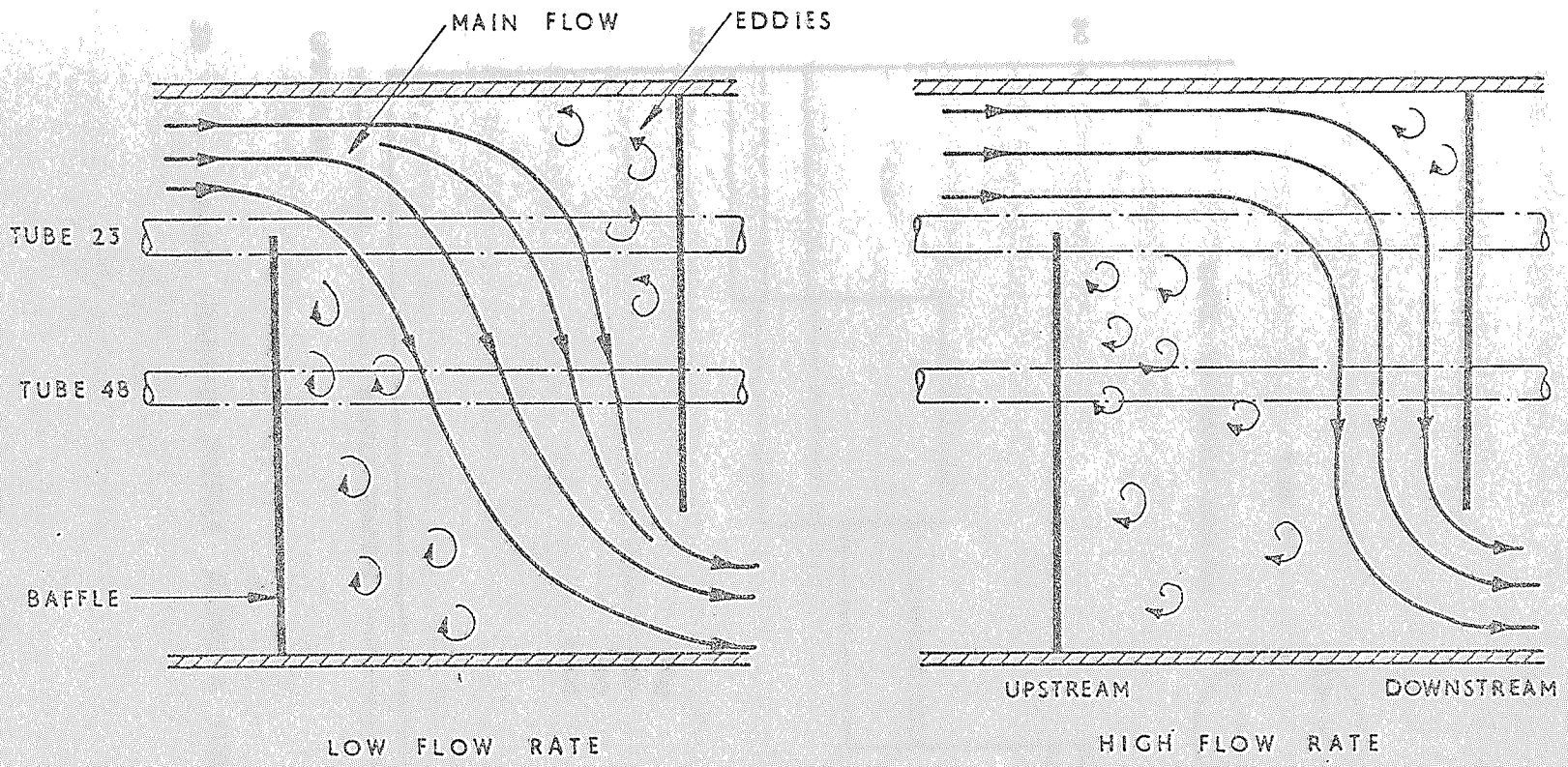

FIG 38 FLOW PATTERNS IN A BAFFLE COMPARTMENT

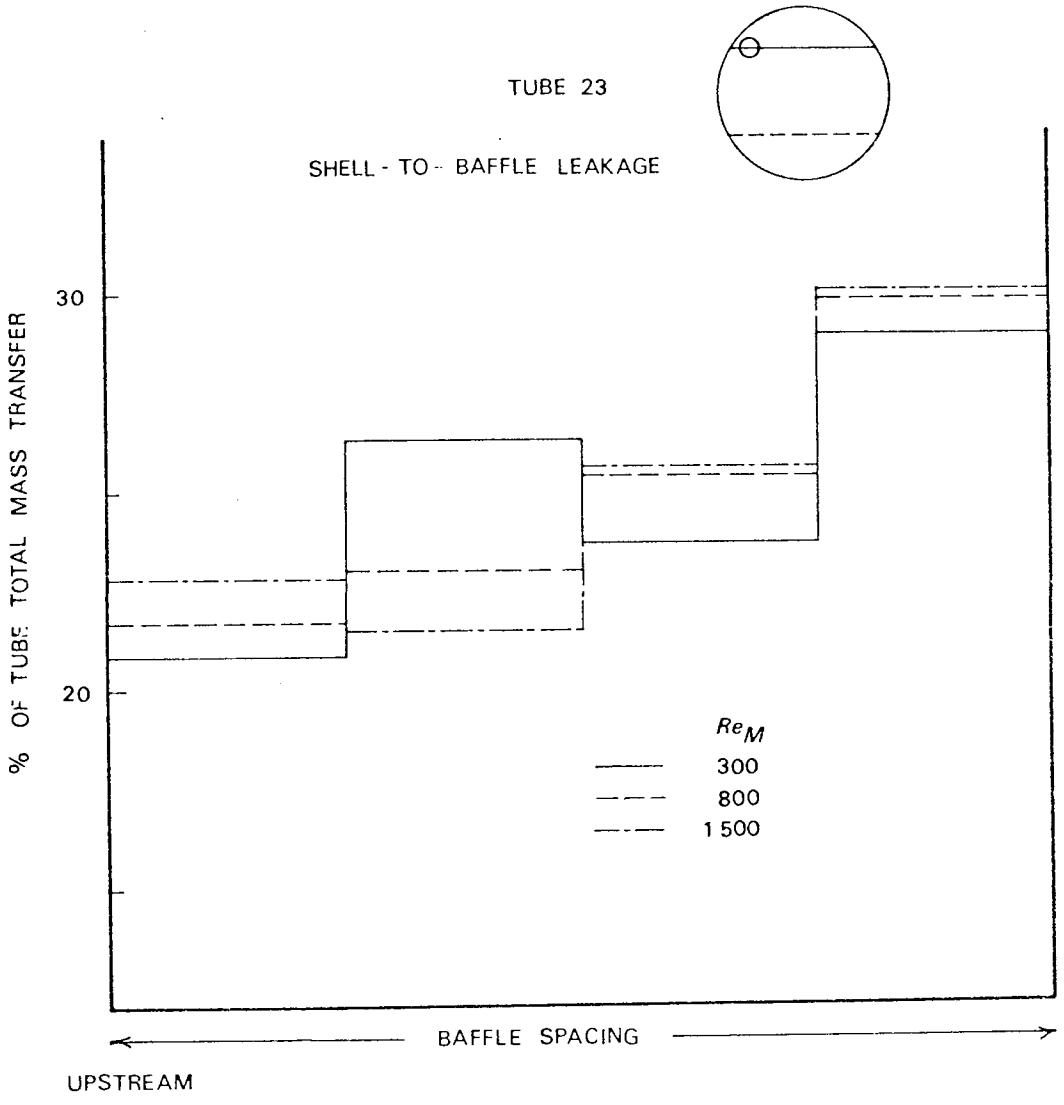

FIG 39 MASS TRANSFER PROFILE ALONG A TUBE

uniform distribution with less evidence of an eddy zone behind the baffle. The profiles varied with the Reynolds number. The higher Reynolds numbers produced profiles similar to those obtained under non-leakage conditions. The profile at the Reynolds number of 300 showed a relatively higher coefficient near the centre of the tube. The difference in the distribution at the low Reynolds number can be attributed to the redistribution of the shell-side flow from changes in the relative flow resistances of the leakage and main streams. The combined shell-to-baffle and tube-to-baffle leakage studies of Gurushankaria and Knudsen (40) revealed that in the crossflow zone the lowest coefficients were to be found near the middle of the tubes. Relatively high Reynolds numbers were employed in this study.

If meaningful measurements of mass transfer rates from increments of a surface are to be made, it is essential that the concentration boundary layer be made continuous as it would be if the adjoining surfaces had also been active. The boundary layers of isolated surfaces would not be fully developed, with the result that higher coefficients would be obtained. The size of the increments in the composite electrode compared with the very thin concentration boundary layer associated with the high Schmidt number, would probably render any such boundary layer discontinuities negligible. Furthermore the effect would only arise from the longitudinal component of the flow over the tubes.

Simple tests were performed to measure the magnitude of these effects in the present work. When making measurements from each of the four incremental electrodes equal potentials were applied to the other electrodes. These results were compared with those obtained when the adjoining electrodes were not activated. For every case the change in the limiting currents was well below

1 per cent. This was considered to be insignificant. The agreement already shown between the average of the four incremental coefficients and that obtained from a single baffle spacing length electrode supports this conclusion.

4.4.6 Shell-side Pressure Measurements

Pressure measurements were made within the tube bundle at both baffle cuts. Pressure data would provide information on:-

(i) The presence of internal leakage.

(ii) The identification of flow regimes.

(iii) General tube bundle flow characteristics.

A pressure tapping tube, shown in Fig. 14, was inserted into the bundle midway along the tube row on the baffle tip. Referring to Fig. 16 these correspond to the tube positions 20 and 33 for the 31.0 and 43.7 per cent baffle cuts respectively. The two tappings were positioned midway between the baffles of the two adjacent internal baffle compartments. These tapping holes were orientated at right angles to the direction of the crossflow.

The pressure differentials measured constituted the sum of the differentials across two crossflow zones and a single window zone (see Fig. 40) i.e.

$$\Delta P_{MEASURED} = 2\ \Delta P_C + \Delta P_W \qquad \ldots\ldots (4.1)$$

where the subscripts C and W refer to the crossflow and window zones respectively.

For any system involving separated flow the pressure drop may be represented by:-

$$\Delta P = c_1 \left[\frac{\rho u^2}{2g}\right] + c_2 \left[\frac{\rho u^2}{2g}\right] \qquad \ldots\ldots (4.2)$$

where c_2 = function (Re, Roughness).

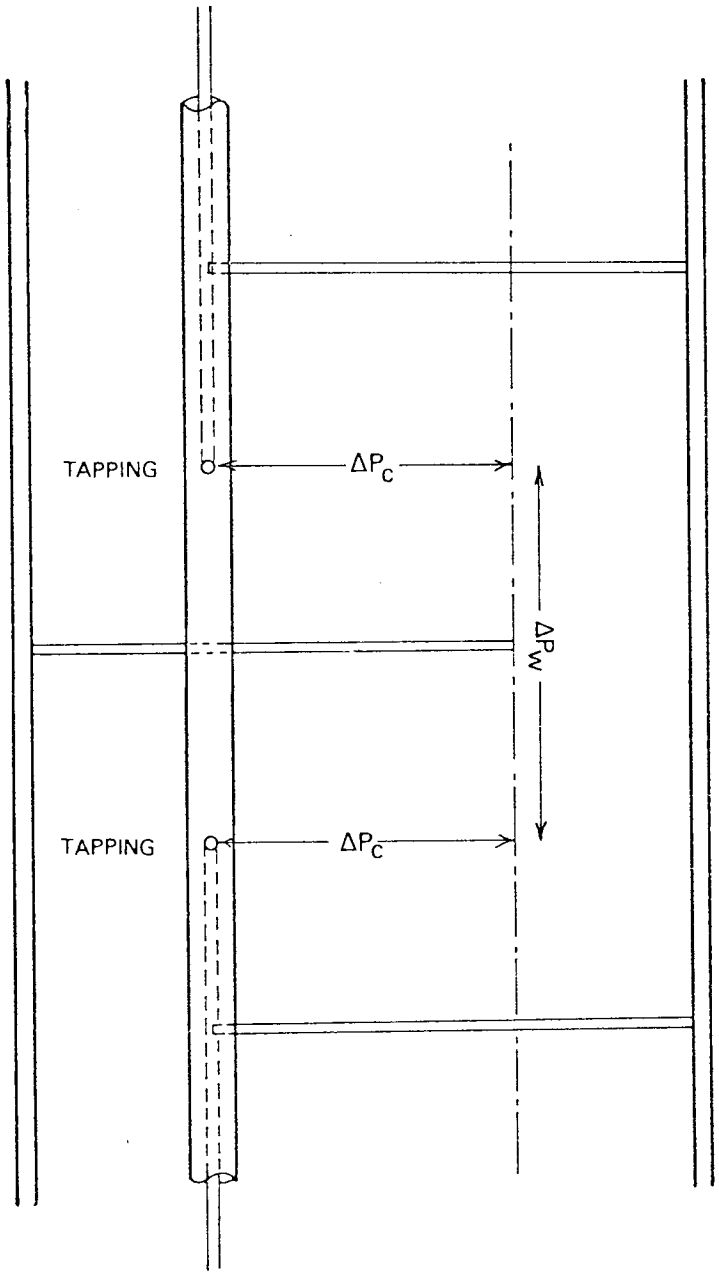

FIG 40 LOCATION OF PRESSURE TAPPINGS

The two terms on the right hand side of Equation (4.2) represent the contributions made by form drag and skin friction respectively.

Equation (4.2) may be rearranged to give the number of velocity heads lost i.e.

$$\left[\frac{\Delta P}{\frac{\rho u^2}{2g}}\right] = c_1 + c_2 \qquad \ldots\ldots (4.3)$$

For laminar flow the term c_2 is inversely proportional to the Reynolds number and is independent of surface roughness. Thus a gradient of minus one would be produced on a plot of Equation (4.3) for this flow regime. In fully turbulent flow form drag predominates and the number of velocity heads is essentially independent of the Reynolds number. Correlating pressure drop results in the form of Equation (4.3) provides not only a basis for comparing different sets of data but also a means of identifying the various flow regimes. The pressure drop data of the present work are shown correlated in this manner in Fig. 41.

The data at the 43.7 per cent baffle cut were compared with those obtained by Bergelin et al. (30) and tabulated in (120). The corresponding pressure drops were obtained from Bergelin's measurements of individual crossflow and window zone components using Equation (4.1). The surface roughness of the tubes and shells were assumed equal in the two cases.

The data of Bergelin and the present work were coincident for Reynolds numbers greater than about 3 000. At lower Reynolds numbers the data of the present work fell between 10 and 20 per cent above those of Bergelin. This discrepancy could be attributed to various phenomena. The low values of the Bergelin pressure drop data could have been due to the presence of internal

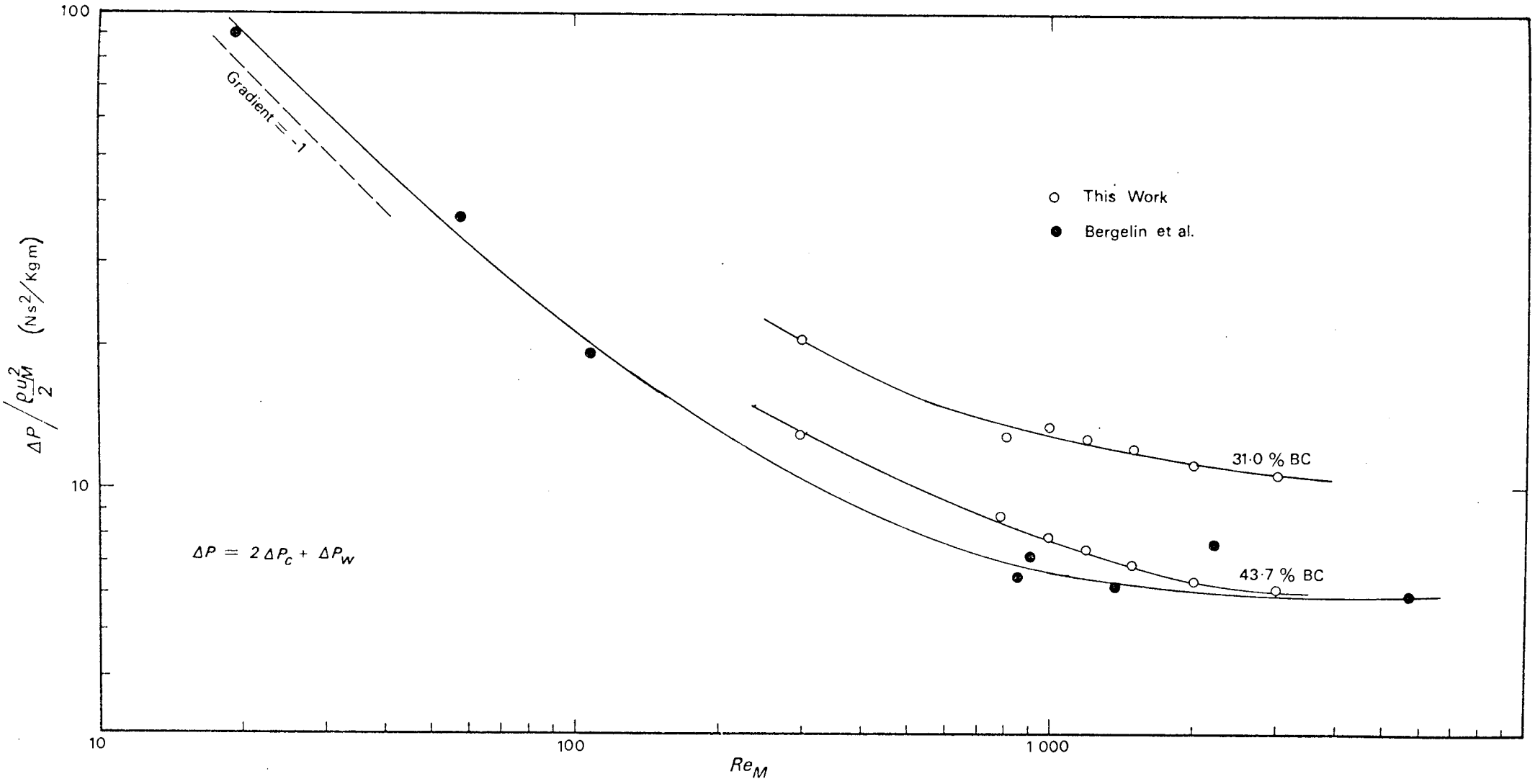

FIG 41 PRESSURE DROP

leakage, the effects of which became insignificant at the higher flow rates. As already discussed in Section 4.4.2.5 trapped gas could have been present in the Bergelin exchanger model. In the present work this was found to be a particularly serious problem at low flow rates. Furthermore pressure measurements made when gas was present in the bundle were found to produce considerably lower results. The sensitivity of the manometers could also have been at fault. Bergelin employed an air-over-oil manometer fluid system with a density difference of 0.79 compared with that of 0.55 in the present work.

In the present work the 31.0 per cent baffle cut gave considerably higher pressure drop results than those of the 43.7 per cent baffle cut. This is attributable to both the higher velocity and tighter flow turn-round in the window zone with the 31.0 per cent baffle cut. The variation of the pressure with Reynolds number was almost identical in the two cases.

The pressure data of both Bergelin and the present work indicate that the flow was fully turbulent at Reynolds numbers above 4 000. This is consistent with the definition of Bell (12) who summarised the research work at the University of Delaware. Laminar flow, characterised by a gradient of minus one in the correlations shown in Fig. 41, would seem from the Bergelin data to exist at Reynolds numbers below 40. However this value is dependent on the shape of the curve that one cares to draw through the data points. Bell recommended a Reynolds number of 100 for the transition. In the present work, pressure measurements were not made at sufficiently low Reynolds numbers to enable the identification of this transition. However similarity in the correlation characteristics of Bergelin and the present work would indicate that the laminar flow regimes were roughly coincident.

The general validity of making local pressure measurements in a system as complex as a baffled tube-bundle is questionable. Any random redistribution of the flow through the bundle could produce significant variations in pressure measurements made on a tube surface. This would be particularly true in the transitional flow regime apparently predominant in the present studies. The orientation of tapping holes at right angles to the theoretical crossflow may not have completely eliminated the dynamic component of the pressure. In measuring a pressure differential any dynamic heads should effectively cancel out. The two pressure measuring points were located at upstream and downstream ends respectively of crossflow zones. The direction of flow onto the two tapping tubes may not have been the same resulting in a difference in the two dynamic heads. The only way that a true static pressure differential could be assured would have been to rotate each tapping point independently to a position that gave the minimum pressure reading. Such a procedure was considered to be impracticable.

4.5 CONCLUSIONS

The general conclusions from the results of the development work are now summarised.

The electrochemical mass transfer modelling technique has been shown to yield values of individual tube coefficients which when suitably averaged were consistent with the bundle average heat transfer data reported by Bergelin et al. (120). At the very low Reynolds numbers however, the Bergelin data fell outside the limits of the estimated accuracy of the electrochemical data. This discrepancy has been shown to be attributable to a variety of phenomena. Natural convection was considered to be the most significant of these phenomena. However this low Reynolds number range represents an area

of comparatively little industrial interest; commercial shell and tube heat exchangers are generally designed to operate under turbulent shell-side flow conditions. The case of viscous oils is a possible exception but here the associated very high fouling factors often make the need for accurate shell-side heat transfer data unnecessary.

Individual tube coefficients showed reasonable agreement with those obtained by Williams (32) using an alternative mass transfer technique. For the 43.7 per cent baffle cut the deviation in the data at the lower Reynolds numbers was attributed to the effect of natural convection. The presence of internal leakage in the Williams exchanger model was also suggested as a possible cause. Experimental investigations in the case of the 31.0 per cent baffle cut gave more positive indications that leakage existed in the Williams model. The discrepancy between the data at this baffle cut was explained in terms of this leakage. The comparison of pressure drop measurements with those of Bergelin established that leakage was not evident in the exchanger model of this work. The general accuracy of the measurements made by Williams was questioned.

The investigations into the variation of coefficients along tube lengths gave experimental evidence of eddy zones in the lee of the baffles. Similar measurements made in the presence of internal leakage gave indications of the redistribution of flow that occurs with leakage. The results from such investigations could provide valuable information about the distribution of shell-side flow leading to the design of more efficient exchanger geometries.

The development work has shown generally that the relative simplicity of the technique makes it readily adaptable to any shell and tube heat exchanger geometry. Furthermore the technique, by virtue of its suitability for instrument automation, provides a valuable tool for rapid data acquisition.

4.6 RECOMMENDATIONS

The ability of the electrochemical technique through the Chilton and Colburn analogy to predict accurate shell-side heat transfer data was established in the development work. The technique was also shown to exhibit attractive experimental features.

The Heat Transfer and Fluid Flow Service, thus decided to adopt the electrochemical mass transfer modelling technique in an extensive research programme to determine local shell-side heat transfer data for a wide variety of segmentally baffled shell and tube heat exchanger geometries.

The research work was transferred to AEE Winfrith where superior laboratory and data-logging facilities existed. The author was similarly transferred to AEE Winfrith in order to continue the research work.

The remaining sections of the thesis describe the experimental investigations made at AEE Winfrith.

5. LOCAL SHELL-SIDE TRANSFER COEFFICIENTS

5.1 EXPERIMENTAL PROGRAMME

The objectives of the experimental programme at AEE Winfrith were two-fold:-

(i) To make local measurements of mass transfer coefficients to allow a detailed study of the characteristics of shell-side heat transfer.

(ii) To provide data for developing and testing the HTFS Stream Analysis prediction method (see Section 1.4).

The latter objective required that measurements of shell-side pressure differentials also be made.

The work reported here is only the initial stage of a long term experimental programme.

Measurements of average mass transfer coefficients were made for the lengths of tubes within a baffle compartment. Shell-side pressure measurements were made simultaneously. A total of thirty-one baffle configurations were examined for a single tube arrangement and shell diameter.

In the preliminary series of experiments internal leakage was prevented by using baffles with zero clearances. The data from these somewhat hypothetical no-leakage cases provided:-

(i) identification of shell-side heat transfer characteristics without the added complication of leakage,

(ii) a comparison with shell-side mass and heat transfer data of other workers,

(iii) a comparison with data from ideal tube-banks,

(iv) a convenient datum for the measurements made with baffle leakage.

In a second series of experiments baffle clearances were introduced. Combined shell-to-baffle and tube-to-baffle clearances were

used. Summation of the effects of leakage shown by independent investigations with each type of baffle clearance, would give a distorted picture of the combined effect of the clearances. The baffle clearances were typical of those in commercial shell and tube heat exchangers. These experiments allowed a detailed examination of the effect of leakage streams on the shell-side performance characteristics.

The versatility of the mass transfer modelling technique and the experimental equipment were exploited in the final series of experiments where investigations were extended to double segmental baffles. No design data for this baffle arrangement have previously been published.

A schematic representation of the experimental programme is shown overleaf. The geometrical parameters of each series of investigations are shown.

The future experimental programme at AEE Winfrith will examine other features of shell-side geometry. These may include:-

(i) Other shell sizes.

(ii) Bundle-bypassing.

(iii) Novel tube arrangements.

(iv) Other multiple segmental baffle designs.

5.2 EXPERIMENTAL EQUIPMENT

5.2.1 Special Features

The experimental rig at AEE Winfrith was modelled on the rig used in the development work at Aston University. The following superior features were incorporated:-

(i) The insertion of liners into the model heat exchanger produced shells of 5.25 in. (133 mm) up to 9.88 in. (250 mm) ID. For the 1.25 pitch-to-diameter ratio staggered-square tube arrangement, these gave tube

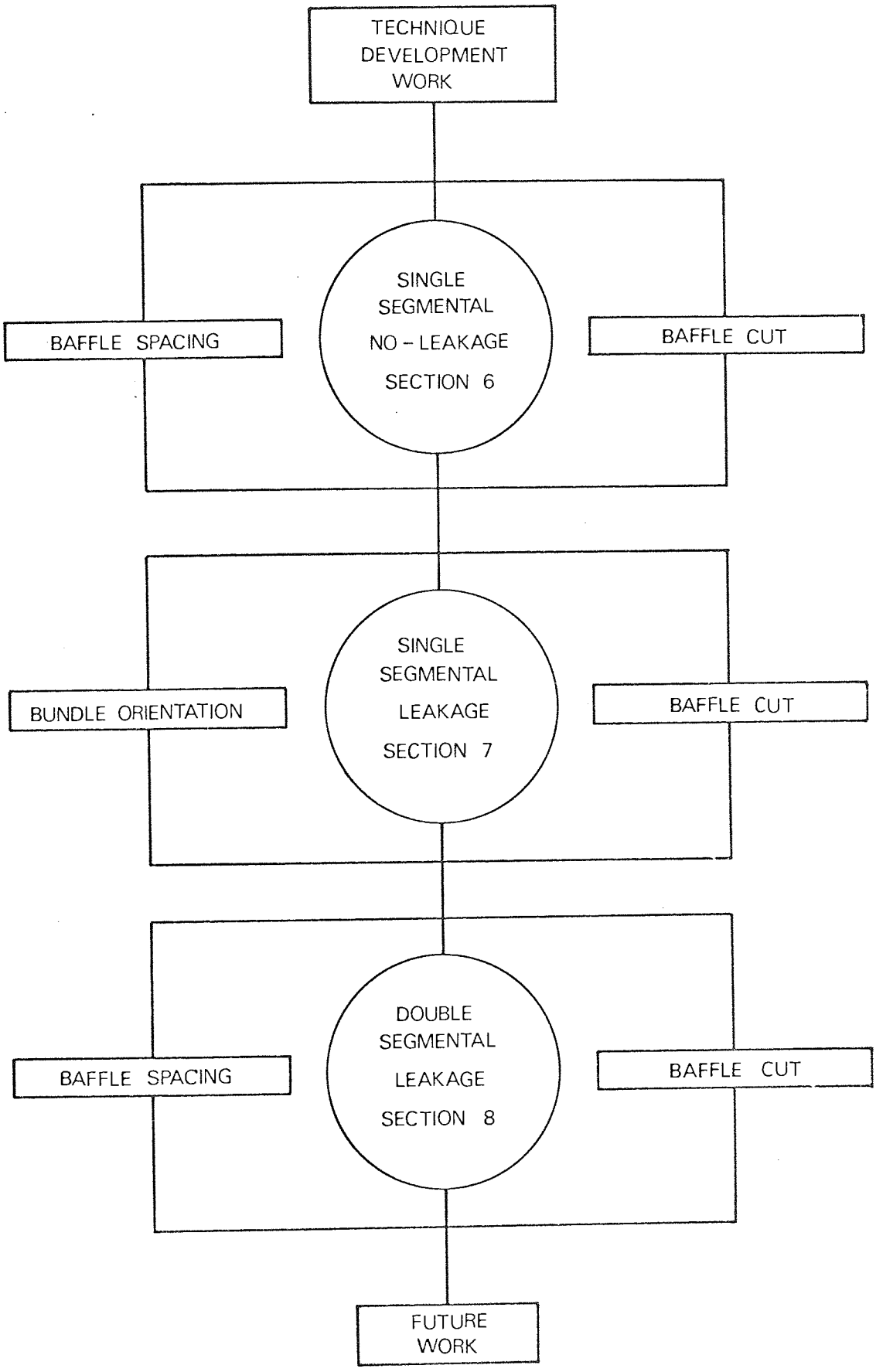

EXPERIMENTAL PROGRAMME

bundles containing 80 to 300 tubes.

(ii) The design of the exchanger body with four ports made studies of different port arrangements possible.

(iii) Cathodes of two different lengths afforded measurements of mass transfer coefficients at two baffle spacings.

(iv) The design of the heat exchanger model provided easy removal and replacement of the tube bundle.

(v) The pumping and flow metering equipment allowed shell-side flow rates of up to 175 gal/min (800 l/min). For the 5.25 in. (133 mm) shell ID and a 1.91 in. (48.5 mm) baffle spacing, this afforded Reynolds numbers (Re_M) of up to 65 000.

(vi) Data-logging facilities provided rapid acquisition of experimental data in a form suited to analysis by computer.

(vii) A separate flow circuit for electrochemically activating the electrodes removed the need to change the electrolyte batch after every series of experiments (see Appendix 1.1).

(viii) Pressure instrumentation gave pressure drop measurements across crossflow and window zones in three adjacent baffle compartments.

In this work the electrode tubes were designed specifically for making measurements in internal baffle compartments. Location of the nickel cathodes at the ends of the tubes would allow studies of the downstream end baffle compartment. The inlet and outlet ports of the exchanger shell could be reversed for studies in the upstream end compartments.

A general view of the experimental rig is shown in Fig. 51. A more informative representation is given in Fig. 52.

5.2.2 Electrolyte Flow Circuits

The experimental rig consisted essentially of two separate flow circuits both incorporating the model heat exchanger. The larger primary circuit was used during experimental runs. The secondary circuit was employed only in the electrode hydrogen activation process. The flow circuitry is shown in Fig. 53.

5.2.2.1 Primary Flow Circuit

The primary circuit consisted of a circulating pump, bank of rotameters, the heat exchanger model and an electrolyte storage tank. The working electrolyte (sodium hydroxide plus the ferri- and ferrocyanide salts) passed from the circulating pump to the model heat exchanger test section via the bank of rotameters. It was then returned to the storage tank through a dip pipe. A bypass line was incorporated around the pump to allow for low flow rate conditions. All pipework, excluding the draining lines, were of 2 in. (51 mm) or 3 in. (76 mm) nominal bore rigid PVC flanged sections.

The circulating pump was on APV Mitchell canned motor stainless steel centrifugal unit rated at 200 gal/min (910 l/min) at a 90 ft. (27.3 m) head. As the bearings of the pump were lubricated by the pumped fluid, it was essential that the electrolyte operating temperature did not rise too high in order to avoid damage to the pump. A temperature trip was located at the pump outlet to trip the pump if the electrolyte temperature rose to 40°C.

The 120 gallon (550 l) capacity cylindrical storage tank was of $\frac{3}{4}$ in. (19 mm) thick polypropylene welded

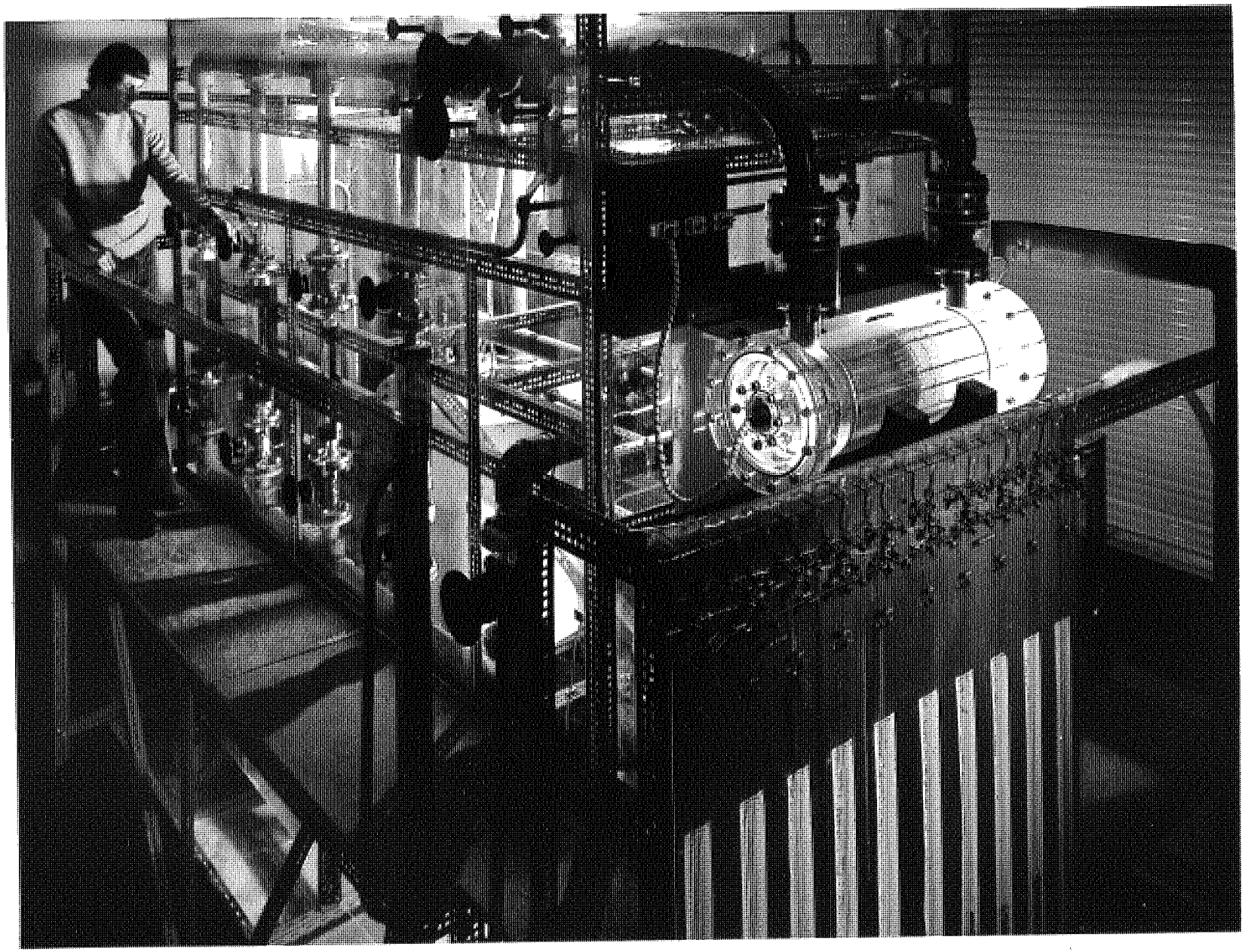

FIG 51 GENERAL VIEW OF THE RIG

FIG 52 GENERAL VIEW OF THE RIG

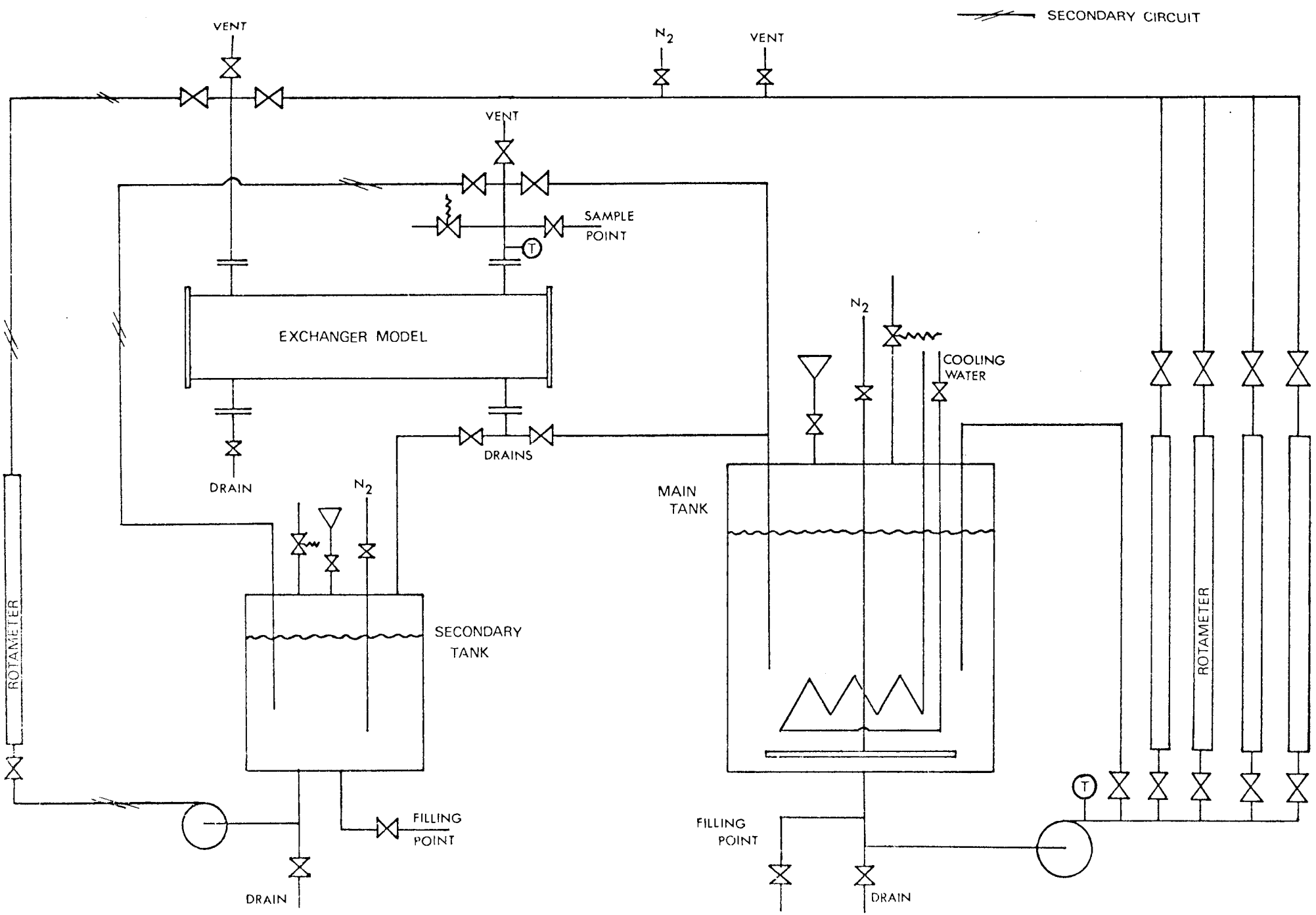

FIG 53 FLOW CIRCUIT

construction. A stainless steel sparge pipe introduced nitrogen into the bottom of the tank. The nitrogen provided a positive pressure over the electrolyte surface and promoted mixing. A stainless steel helical cooling coil supplied with mains low pressure water was immersed in the electrolyte solution. The tank was protected from over-pressure by a relief valve of the lute type, set to relieve at 5 in. (127 mm) wg.

The electrolyte flow rate was metered by a bank of four Fischer and Porter (Series 10A3500) rotameters having the following flow ranges:-

(gal/min)	(l/min)
0 - 5	0 - 22.7
5 - 20	22.7 - 91.0
10 - 50	45.5 - 227
10 - 100	45.5 - 455

The manufacturer's calibrations were checked experimentally in the Winfrith Laboratories. The accuracy of the calibrations was estimated to be within ± 3.0 per cent.

All the flow control valves were 2 in. (51 mm) cast iron Saunders diaphragm valves. The valve ports were glass lined and neoprene diaphragms were used. Other valves were PVC or stainless steel.

The pump and the model heat exchanger were protected from pipe misalignment and vibrations by PTFE bellows couplings. An electrolyte sampling point was located at the outlet of the model heat exchanger. Nitrogen inlet and gas venting lines were located at suitable points in the circuit.

The primary circuit, excluding the storage tank, was subjected to a hydraulic pressure test to 65 lbf/in^2. (0.45 MN/m^2). A pressure relief valve operating at 20 lbf/in^2. (0.14 MN/m^2) was incorporated in the circuit at the outlet of the exchanger model.

5.2.2.2 Secondary Flow Circuit

The secondary circuit was of similar form to the primary circuit. The activating electrolyte solution (sodium hydroxide) was pumped to the heat exchanger model via a single rotameter and then returned to the storage tank. The pipework was in $\frac{3}{4}$ in. (19 mm) rigid PVC flanged sections.

The circulating pump was a stainless steel Stuart Turner centrifugal unit rated at 10 gal/min (45 l/min) at a 70 ft. (21.2 m) head. No bypass line was incorporated around the pump as it was operated at near its maximum capacity. The 20 gallon (91 l) rectangular storage tank was of welded polypropylene construction. Nitrogen was introduced through a sparge pipe. The tank was protected by a lute relief valve operating at 5 in. (127 mm) wg. As the activation time was relatively short and flow rate low, no cooling facilities were incorporated. The electrolyte flow rate was metered by a rotameter with a range 0 to 10 gal/min (0 to 45 l/min). $\frac{3}{4}$ in. (19 mm) rigid PVC diaphragm valves were used throughout.

Perspex sheeting around the rig protected the operator from leaks in the two flow circuits.

5.2.3 Model Heat Exchanger

A general view of the model heat exchanger is shown in Fig. 54. Fig. 55 gives a cut-away view showing details of the internal components.

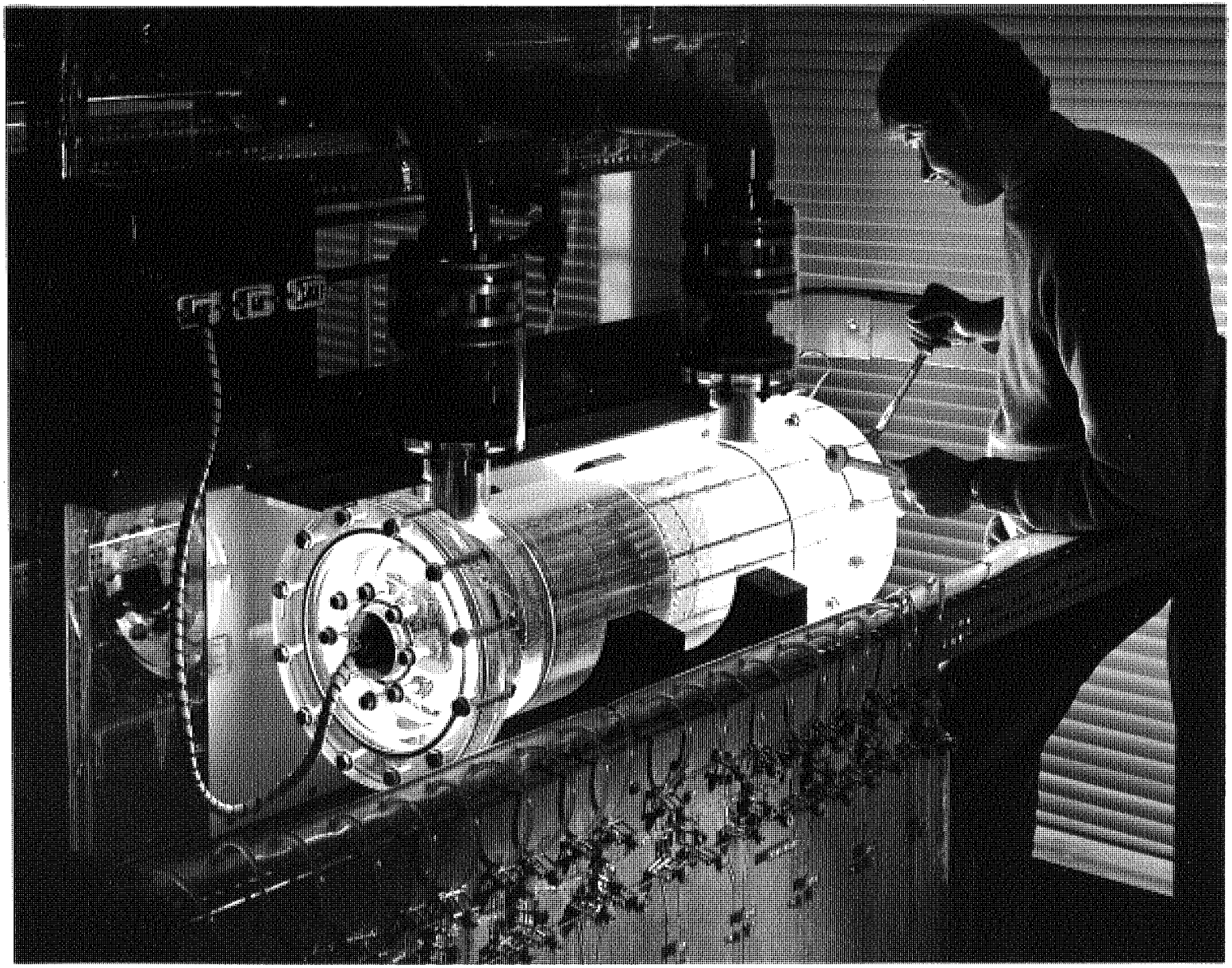

FIG 54 CLOSE-UP VIEW OF THE MODEL HEAT EXCHANGER

FIG 55

5.2.3.1 Shell Construction

The exchanger body was cast in perspex. The body (without the end plates) had an overall length of $36\frac{3}{4}$ in. (934 mm) and a wall thickness of $\frac{3}{4}$ in. (19 mm). Pairs of 2 in. (51 mm) ID perspex ports were located at either end of the shell as shown in Fig. 55. The ID of the exchanger body was 9.875 in. (251 mm). By inserting perspex liners into the outer casing the effective shell inside diameter could be varied. The $29\frac{3}{4}$ in. (757 mm) long liners allowed a full 9.875 in. (251 mm) diameter compartment at the upstream end of the shell. This compartment removed any flow effects from the inlet port and gave additional space for the cathode leads and capillary tubes. O-ring seals around the outside diameter of the liners prevented fluid bypassing the bundle. In this work investigations were confined to a 5.25 in. (133 mm) ID shell.

The electrolyte solution entered and left the model exchanger through the two ports on the upper side of the body. Perspex plates with drain lines were fitted to the ports on the lower side. The downstream end of the exchanger body was sealed with a full-face 1 in. (25 mm) thick perspex plate. A similar plate fitted to the upstream end of the body incorporated a bulkhead fitting to bring out the electrical leads from the cathodes. In the bulkhead fitting the leads passed through drilled holes in a 2 in. (51 mm) diameter rubber bung. A tight seal was achieved by compressing the bung in a tapered hole drilled in a perspex backing-plate. Every set of cathode rods had its own bulkhead fitting which was simply bolted onto the end-plate when inserting a new tube bundle. The attachment bolts were

of $\frac{1}{2}$ in. (12.7 mm) dia. stainless steel fitted with Dowty seals. All other nuts and bolts employed were of $\frac{1}{2}$ in. (12.7 mm) dia. galvanised mild steel.

The model exchanger was enclosed in an opaque rigid PVC box having hinged panels.

5.2.3.2 Tube Bundle Construction

The tube bundle was essentially similar to that used in the development work. This comprised 80, $\frac{3}{8}$ in. (9.53 mm) dia. perspex tubes arranged on a staggered-square pattern with a 1.25 pitch-to-diameter ratio.

The overall length of the tubes was $27\frac{1}{2}$ in. (698 mm). The tubes were centre-ground to fine tolerances (see Appendix 2.2). Details of the cathodes inserted in the tubes are given in Section 5.2.3.3. Baffles were constructed from rigid PVC sheet. The machining properties and rigidity of this material was found to be superior to those of the polypropylene used for the baffles in the development work. The baffles employed in investigations without baffle leakage were nominally 1/16 in. (1.59 mm) thick. Precise measurements of the baffle thicknesses are given in Appendix 3.3.1. Narrow 1/32 in. (0.80 mm) thick neoprene rubber lip-seals were attached to the outer edges of these baffles using "Evostik". The seals were trimmed to extend 1/32 in. (0.80 mm) proud of the baffle edges. In investigations with internal leakage the reduction in the baffle rigidity as a result of the clearances necessitated the use of $\frac{1}{8}$ in. (3.18 mm) thick baffles. The precise control of internal leakage required that the baffles be made to fine tolerances. The baffle spacing was maintained by tie-bars made from stainless steel 4 BA screwed rod. The baffles

were cut segmentally to the dimensions given in Section 5.4.1. A full-face baffle at the extreme downstream end of the tube bundle aided bundle rebuilding and increased the bundle rigidity. The position of the cathodes relative to the baffles was maintained by locating the tubes and tie-bars against the shell downstream end-plate. The pressure of the circulating electrolyte on the exchanger internal components preserved this position.

5.2.3.3 Electrode Construction

The design of the cathodes is shown in Fig. 55. Sections of nickel rod were located between lengths of perspex tube and rod. All three sections were of $\frac{3}{8}$ in. (9.53 mm) dia. The cathodes were of two lengths. These were 1.97 in. (50.0 mm) and 3.89 in. (99.0 mm). PVC-coated copper wires were soldered to the nickel cathodes and passed out through the tubular sections of the tubes. The tubular sections were filled with "Evostik" adhesive to form a seal. The leads from all the cathodes passed through the bulkhead fitting in the exchanger end-plate and were connected to a taper-pin terminal block. Leads from corresponding terminals in the other half of the block fed into the data-logger.

Tubular anodes were located in the ports of the exchanger shell. The operational anode, used when making actual limiting current measurements, was located in the outlet port. The anode used for the hydrogen activation of the electrodes was positioned in the inlet port. Both tubular anodes were $4\frac{1}{2}$ in. (114 mm) long and $1\frac{15}{16}$ in. (49.2 mm) OD constructed from nickel plate. The surface area of the operational anode was increased by inserting four concentric nickel tubes into the existing $1\frac{15}{16}$ in.

(49.2 mm) dia. tube. An effective surface area of 184 in^2. (0.12 m^2) was thus produced, this being over four times the combined surface area of ten cathodes. Nickel flanges welded to the ends of the anodes, were sandwiched between neoprene gaskets at the joints where where the pipework was attached to the exchanger ports. Electrical contact was made through protruding tabs attached to the nickel flanges.

5.2.4 Instrumentation

5.2.4.1 Electrical

The electrical system comprising DC power supplies, timing mechanism and scanning and recording equipment was incorporated in a 250 channel data-logger unit.

The electrical system had three modes of operation:-

(i) Acquisition of limiting current data.

(ii) Cathode activation.

(iii) Anode activation.

The fully automated limiting current data acquisition procedure had the following features. A potential was applied between the anode and ten cathodes at a time. After a preset time period had elapsed, the individual cathodes within the group were automatically scanned and their currents logged. The procedure was then repeated for the other groups of cathodes in sequence until all had been analysed.

The procedure for the cathode activation process was similar. The circuit for anode activation merely included a power supply without any timing mechanism.

The basic circuitry of the electrical system is shown in Fig. 56. The data acquisition or activation modes of

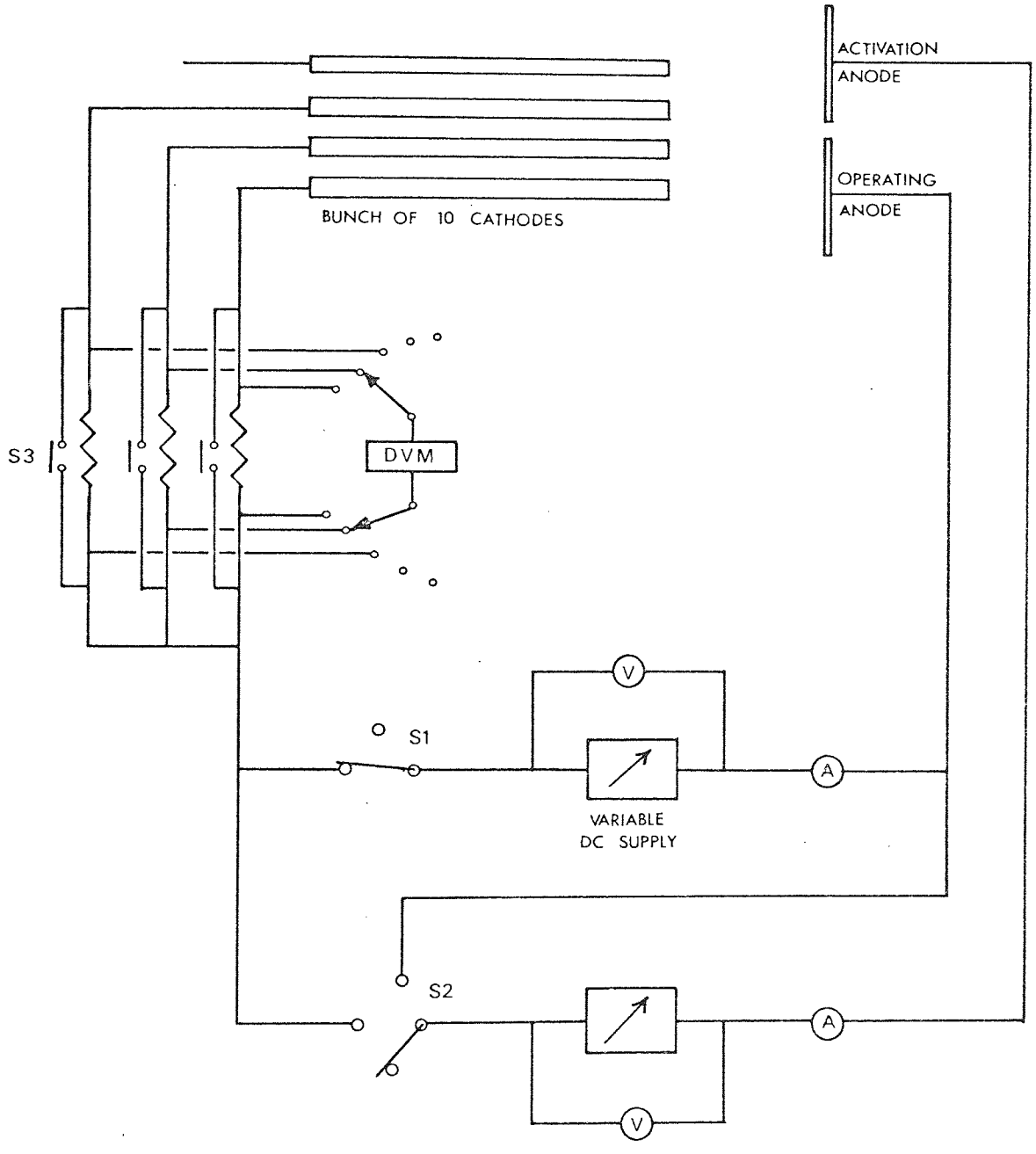

FIG 56 ELECTRICAL CIRCUIT

operation, were selected through the switches S1, S2 and S3 in Fig. 56.

Two variable DC power supplies were available. A stabilised unit providing 0 to 15 volts was used when making limiting current measurements. A 0 to 25 volt range unstabilised unit was used for the electrode hydrogen activation process. Voltmeters gave indication of the applied voltage.

Electrical leads from the cathodes were connected in groups of ten to separate heavy-duty relays. An automatic selector activated the relays in turn, bringing the groups of cathodes into circuit. The period of time that each group of cathodes was in circuit was controlled by an adjustable timing device. When making limiting current measurements sufficient time had to be allowed for equilibrium to be attained (see Appendix 1.10). A far greater time was necessary for the hydrogen activation process (see Appendix 1.2). At the end of the preset time period, the currents from the individual cathodes within the group were scanned and logged. Currents were measured as voltage drops across standard 0.4 ohm resistors. The resistors were shown to be accurate to well within 0.1 per cent. A digital voltmeter gave visual display as well as printed and punched paper tape output. A variable gain amplifier was required to make full use of the 3 bit digital voltmeter tape output. In the hydrogen activation process, the standard measuring resistors were shorted-out (Switch S3 in Fig. 56) during the scanning stage to protect them from the large currents involved.

The size of the tube bundle in the present studies required the use of only 80 of the 250 channels of the

data-logger. These were conveniently arranged in 8 groups of 10. The cathode leads were connected such that the channel identity corresponded to the tube number (see Fig. 16 for tube numeration) in which the cathode was located.

The applied and digital voltmeter output voltages were displayed on the x and y-axes respectively of a graph plotter. Polarisation curves for any manually selected cathode could thus be plotted. Applied voltages for limiting current conditions could be determined for use in the experimental runs.

5.2.4.2 Temperature Readout

The temperature of the circulating electrolyte solution was measured by an electrical resistance thermometer located just downstream of the model exchanger. The temperature (degrees centigrade) was indicated on a Kent chart recorder. A mercury thermometer sited adjacent to the resistance thermometer gave a calibration check.

5.2.5 Pressure Measuring Equipment

Details of the pressure tapping tubes are shown in Fig. 55. Three tappings in each tube allowed pressure measurements to be made in three adjacent baffle compartments. The two baffle spacings investigated required two sets of tapping tubes. The only difference in these tubes was the pitch of the tapping holes.

The location of tapping tubes for the case of the single segmental baffles is shown in Fig. 57 and for the double segmental baffles in Fig. 123.

PVC capillary tubes passed out of the exchanger model through the plate on the upstream lower port.

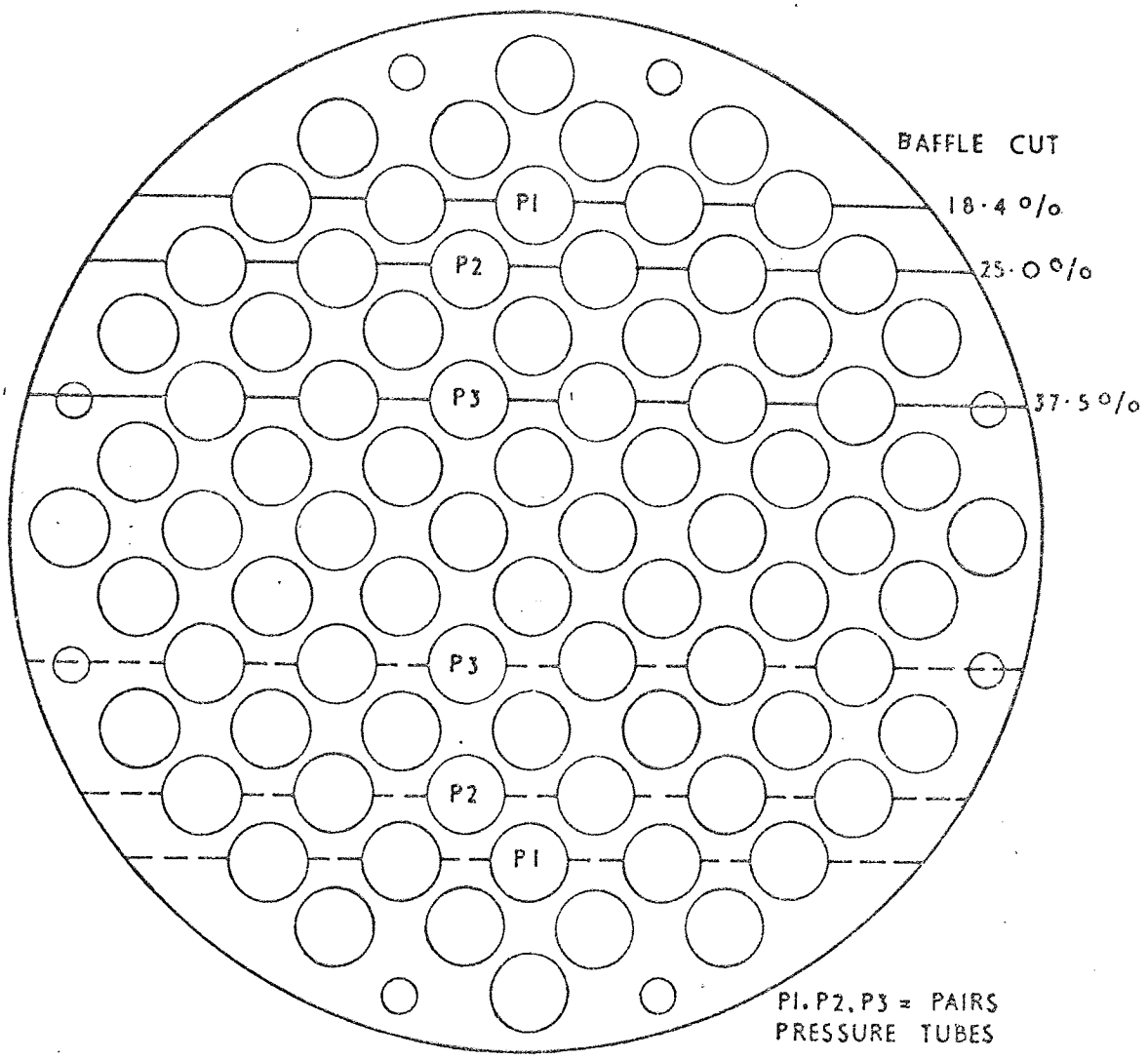

FIG. 57. LOCATION OF PRESSURE TUBES

The five pressure differentials were measured on two banks of vertical U-tube manometers. For the low pressure ranges carbon tetrachloride (sg 1.59) was the manometer fluid while tetrabromoethane (sg 2.96) was used for the higher ranges. Bleed lines were incorporated in the system.

5.3 EXPERIMENTAL PROCEDURE

The following sections describe the features of the experimental procedure leading up to and including the experimental run.

The rig operating routine is described in greater detail in the Safety and Operating Manual compiled by the author for the guidance of future operators of the equipment. The Manual is in the custody of AEE Winfrith.

5.3.1 Assembling the Model Exchanger

The tube bundle was assembled in a manner similar to that described in Section 4.3.1. The pressure tapping tubes were inserted in their appropriate positions. The tube bundle with its bulkhead fitting attached was then inserted into the shell through the upstream end. Both the ends of the tie-bars and the tubes were located against the downstream perspex end-plate. This positioned the nickel cathode sections within the appropriate baffle compartment. The bulkhead fitting was then attached to the upstream end-plate and this whole unit was bolted onto the exchanger body. The cathode leads were connected to the electrical equipment through the terminal block. The pressure capillary tubes were slipped over stainless steel tubes passing through the plate over the lower upstream port. 4 mm bore PVC tubing attached to the outer ends of these metal tubes led to the manometers. The plate was then bolted up. The covers of the light-proof box were closed down over the model exchanger.

5.3.2 Making-up the Electrolyte Solutions

Sodium hydroxide solutions were made up outside the building in a 50 gal (227 l) pressure-tight stainless steel drum. The water used was both deoxygenated and demineralised. A nitrogen atmosphere was maintained in the tank.

The solutions were transferred to the two storage tanks on the rig under nitrogen pressure in the mixing tank. The potassium salts were then added directly to the primary circuit tank.

Electrolyte batches of 80 gal (363 l) were used in the primary circuit. The composition of the electrolyte is given in Appendix 1.12. 20 gal (91 l) batches were used for the activation process. The concentration of the sodium hydroxide solution was approximately 1.0 molar.

5.3.3 Electrode Activation Process

The activation electrolyte was circulated through the exchanger model and the anode activation mode of the electrical equipment was selected. In accordance with Appendix 1.2, a current density of 0.1 mA/mm^2 (12 amp total current) was passed for 5 minutes.

Using the cathode activation mode of the equipment, the cathodes were activated in groups of ten for 5 minutes each. The current density was again 0.1 mA/mm^2.

5.3.4 Experimental Run

The electrolyte flow rate through the primary circuit was set at the desired value and the data acquisition mode of the electrical equipment was selected.

Polarisation curves were plotted for a number of selected cathodes. It was usual to select one cathode from each of the 8 groups of 10. A value of the applied potential was selected which fell on the plateaux from every case. The plateaux in

most of the investigations were fairly coincident. The large applied potential range of the plateaux however allowed for considerable shift in the plateaux from tube to tube. The applied potential between the anode and the cathodes was set at this selected value.

The time period that the potential is applied to each group of cathodes before scanning, was selected on the timing clock. This was normally set at around 15 seconds, although considerably smaller values could have been used at the high electrolyte flow rates. The range level of the digital voltmeter input and the amplifier gain were adjusted to give a suitable 3 digit output for tape punching. The automatic sequence was then started and the limiting currents from all the cathodes were recorded on punched tape. The complete procedure took under 3 minutes.

The average value of the electrolyte temperature during the run time was obtained from the chart recorder. This temperature and details of the particular experimental run were punched manually onto the tape. The precise format of the punched tape data is given in Appendix 2.4.

The experimental procedure was then repeated for other flow rates.

Pressure measurements were made at each flow rate during the acquisition of the limiting current data.

5.4 OUTLINE OF THE EXPERIMENTS

5.4.1 Essential Features

The three series of experiments with the no-leakage single segmental, leakage single segmental and the double segmental baffles are described in Sections 6, 7 and 8 respectively.

All investigations were confined to the 5.25 in. (133 mm) ID shell and the eighty tube bundle. The staggered-square tube

arrangement with a 1.25 pitch-to-diameter ratio represents a common commercial design.

Three baffle cuts were studied with the single segmental baffles. These were 18.4, 25.0 and 37.5 per cent of the baffle (zero clearance) diameter. Baffle cuts in commercial heat exchangers are usually around 25 per cent. The 18.4 per cent cut allowed a comparison of data with those of other work. The baffle cuts are shown in Fig. 57. Only the 18.4 and 25.0 per cent cuts were used with the double segmental baffles.

Two baffle spacings of 1.91 and 3.82 in. (48.5 and 97.0 mm) were studied. A set of ten baffles were used at the short spacing and a set of six at the long spacing. These gave nine and five baffle compartments respectively. Investigations with the leakage single segmental baffles were confined to the short baffle spacing. Both baffle spacings allowed comparisons of data with those of other work. The baffle spacing to shell diameter ratios of 0.36 and 0.73 were typical of commercial designs.

Measurements were confined to central internal baffle compartments. The flow through these compartments was estimated to be free from the bundle entrance and exit effects.

Mass transfer measurements were made on 78 out of the total of 80 tubes. The coefficients of the two tubes replaced by pressure tapping tubes, were estimated from those of adjacent tubes (see Appendix 2.4).

The range of the shell-side flow rate was 0.7 to 100 gal/min (3.2 to 454 l/min). This afforded a shell-side Reynolds number (Re_M) range of 170 to 42 000 with the short baffle spacing. In experiments with the 1/16 in. (1.59 mm) thick baffles the flow rate was restricted to below 60 gal/min (272 l/min).

Details of the bundle geometry for each experiment are listed together in Appendix 3.2.1.

The processing of the experimental mass transfer data is described in Appendix 2.4.

The processed experimental data from all the investigations are tabulated in Appendix 3.2.

Tests were performed to determine the reproducibility of the experimental data. Details of these tests are given in Appendix 2.3.

An estimation of the accuracy of the experimental data is given in Appendix 2.2.

5.4.2 Correlation of the Experimental Data

The experimental mass transfer data are correlated in the form of the Chilton and Colburn j-factor and Reynolds number used in the development work. These are defined by:-

$$j_m = \frac{K_c}{u} (Sc)^{2/3} \qquad \ldots\ldots (2.5)$$

$$Re_M = \frac{d_t \, u_M \rho}{\mu} \qquad \ldots\ldots (5.1)$$

where the fluid velocity u_M is based on the minimum crossflow area A_M at the centre row of tubes (see Fig. 16).

Correlation of data in the form of dimensionless groups is fully justified only where independent variations occur in all the constituent terms. The tube diameter in the Reynolds number (Re_M) was constant in this work. During any series of measurements, the fluid temperature rose within the range 15 to 35°C. The associated change in the fluid viscosity and density would be up to 54.0 and 0.5 per cent respectively. The variation in the

Reynolds number would thus be due largely to the variation in the fluid velocity. The variation in the Schmidt number was produced by variations in all the component physical properties; the variation in the fluid density was however relatively less.

Bell (12) and Williams (32) correlated shell-side data using the j-factor and Reynolds number. The variation in both the fluid viscosity and density in Williams's experiments was only 4 per cent. In the experiments summarised by Bell, the fluid average physical properties did not vary significantly from run to run. However data from two series of experiments using oils of differing physical properties were well correlated. The tube diameter was not varied.

Presenting the experimental data of this work in the form of a j-factor and Reynolds number provided:-

(i) a basis for comparing these data with both mass and heat transfer data from other work,

(ii) a method of correlating data obtained at different fluid temperatures,

(iii) a general correlation from which heat transfer coefficients could be obtained.

6. SINGLE SEGMENTAL BAFFLES WITHOUT LEAKAGE

6.1 SCOPE OF EXPERIMENTS

Baffles with zero clearances eliminated both tube-to-baffle and shell-to-baffle leakage. The baffles were nominally 1/16 in. (1.59 mm) thick.

Mass transfer measurements were made at two baffle spacings and three baffle cuts. These were:-

Baffle spacing - 1.91, 3.82 in. (48.5, 97.0 mm)

Baffle cut (% diameter) - 18.4, 25.0, 37.5.

The measurements were confined to the fifth baffle compartment of nine and the third of five for the short and the long baffle spacings respectively. The second compartment was also investigated for the 37.5 per cent baffle cut at the short baffle spacing.

The tube bundle was arranged in the shell with the flow entering at the top of the test baffle compartment. An investigation was made at one baffle configuration with the bundle rotated through 90 degrees. This is reported in Section 7.4.

6.2 CONFIRMATION TESTS

6.2.1 Comparison with Bergelin et al.

The 1.91 in. (48.5 mm) baffle spacing, 18.4 per cent baffle cut configuration provided a further case for comparing the results of this work with those obtained by Bergelin et al. (30) in the heat transfer studies at the University of Delaware. Baffle compartment average j-factors were compared with the bundle average j-factors of Bergelin obtained from a heat exchanger having eight baffle compartments. This comparison is shown in Fig. 58.

The mass transfer data of this work fell within 5 per cent of Bergelin's heat transfer data for Reynolds numbers above 1 000. At lower Reynolds numbers the two sets of data gradually separated,

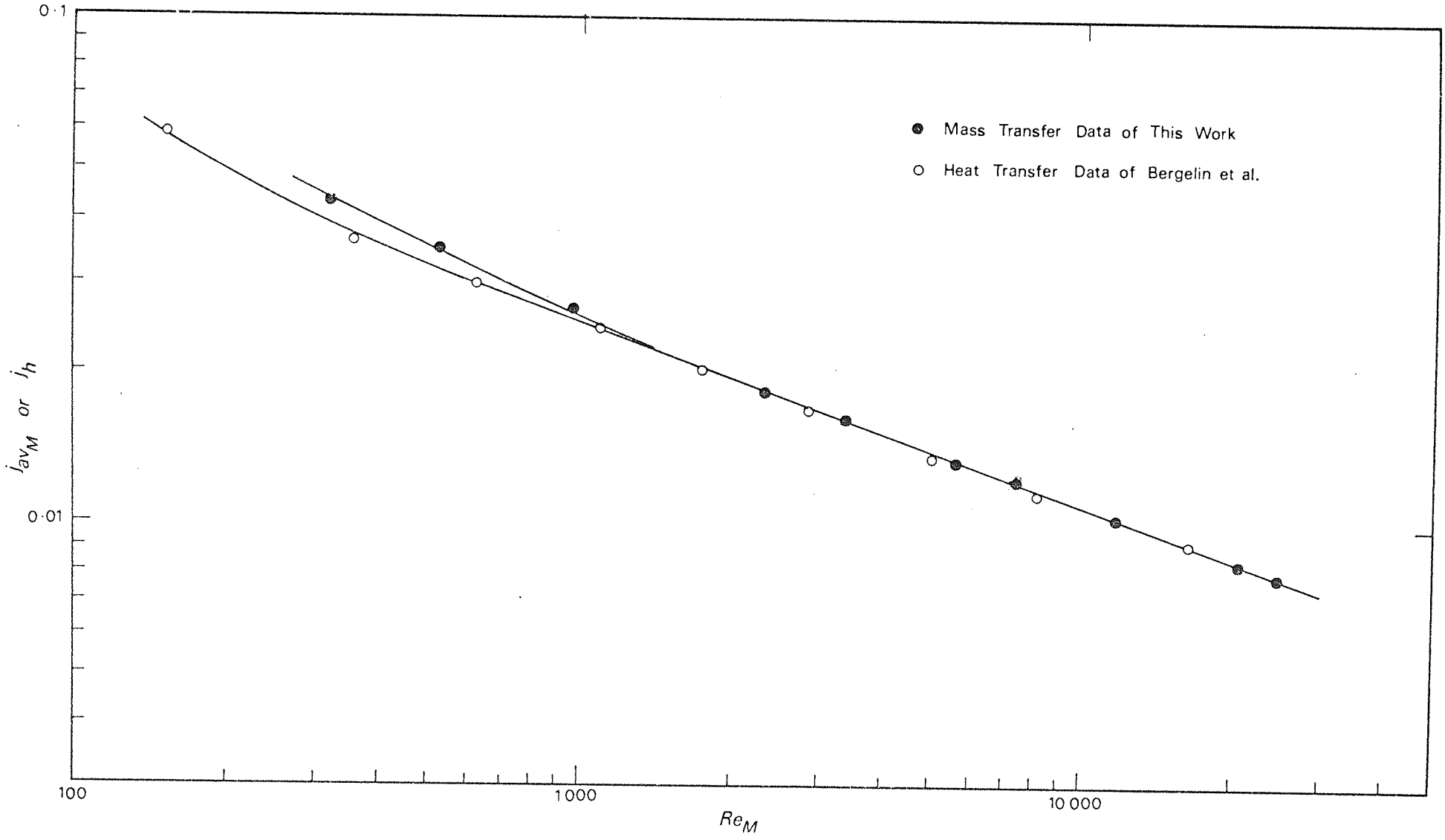

FIG 58 COMPARISON OF AVERAGE COEFFICIENTS

the data of this work falling above those of Bergelin. At the Reynolds number of 320, corresponding to the lower limit of the mass transfer data, the j-factor value from this work was 12 per cent above that of Bergelin. This discrepancy would seem barely significant compared with the estimated accuracy of the data from this work (see Appendix 2.2). However it is significant that the deviation between the two sets of data occurred at around this same Reynolds number of 1 000 in the confirmation test performed in the development work (see Section 4.4.2). In that test the data from this work also fell above those of Bergelin.

In Section 4.4.2 the discrepancy between the heat and mass transfer data was attributed to a variety of phenomena. It was shown that natural convection effects would become significant in both this work and that of Bergelin at Reynolds numbers below 1 000. An attempt to correlate the natural convection component of the data of this work is described in Section 6.2.2. No similar analysis of the heat transfer data was possible.

In this work measurements were made in a typical internal baffle compartment. The average heat transfer coefficients obtained by Bergelin, were for the entire bundle which for this particular baffle spacing contained eight baffle compartments. The effect of the end baffle compartments would be reflected in a comparison of the characteristics of an internal compartment with those of the whole bundle. In Bergelin's heat exchanger model, large rectangular ports were used to minimise the entrance and exit effects.

Variation in the level of fluid turbulence through the bundle has already been put forward as another possible cause of the discrepancy between the baffle compartment and bundle average coefficients (see Section 4.4.2.3). This effect would be

particularly significant in the transitional flow regime defined by the Reynolds number range 100 to 4 000 (see Section 4.4.2.7).

In later experiments, measurements of mass transfer coefficients were made in both the fifth and second baffle compartments. The baffles in this case were at a spacing of 1.91 in. (48.5 mm) and had a 37.5 per cent cut. In order to examine the second compartment the first three upstream baffles were merely removed from the bundle. The total number of baffle compartments was consequently reduced from nine to six. The second compartment was considered to be the most upstream compartment retaining the flow characteristics of an internal compartment. The average j-factors for these two compartments are compared in Fig. 59. The data from the second compartment were consistently around 10 per cent lower than those from the fifth compartment. The estimated accuracy of the data makes this discrepancy barely significant. If there had been a substantial variation in the turbulence level through the bundle the discrepancy between these two sets of data would have been relatively greater at the lower Reynolds numbers corresponding to the transitional flow regime. The discrepancy in the data shown in Fig. 59 may be attributed to the flow through the second compartment still possessing some entrance compartment characteristics. The individual tube coefficients however gave no evidence of differing flow distributions in the two baffle compartments.

Pressure measurements made within the test baffle compartment were compared with those obtained by Bergelin. Bergelin's measurements were made in the fourth of eight baffle compartments. The zonal pressure drops are compared in Fig. 60. The baffle compartment pressure drops also shown are the sum of the crossflow and window pressure drops. The method of correlation is that used

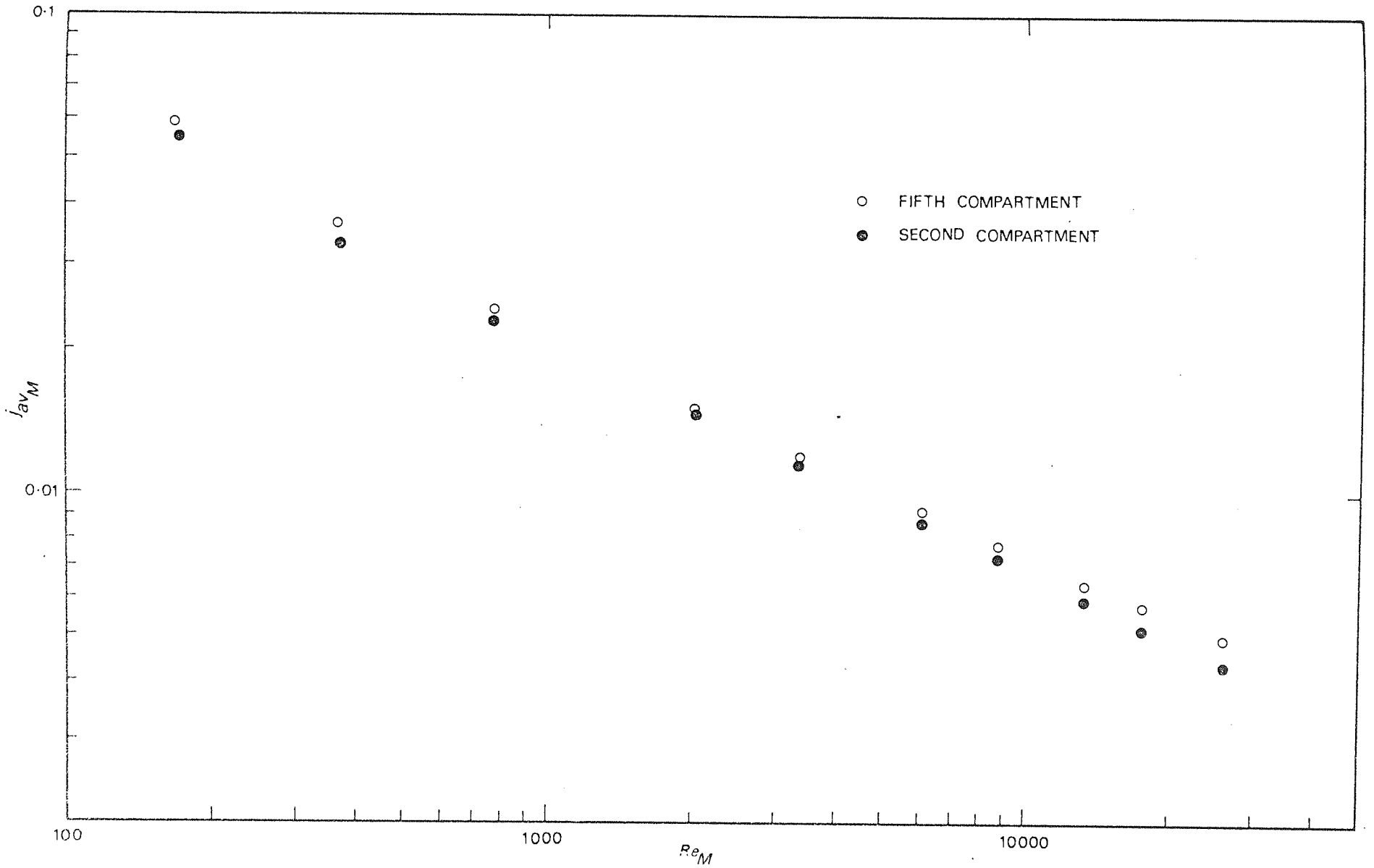

FIG 59 COMPARTMENT AVERAGE COEFFICIENTS

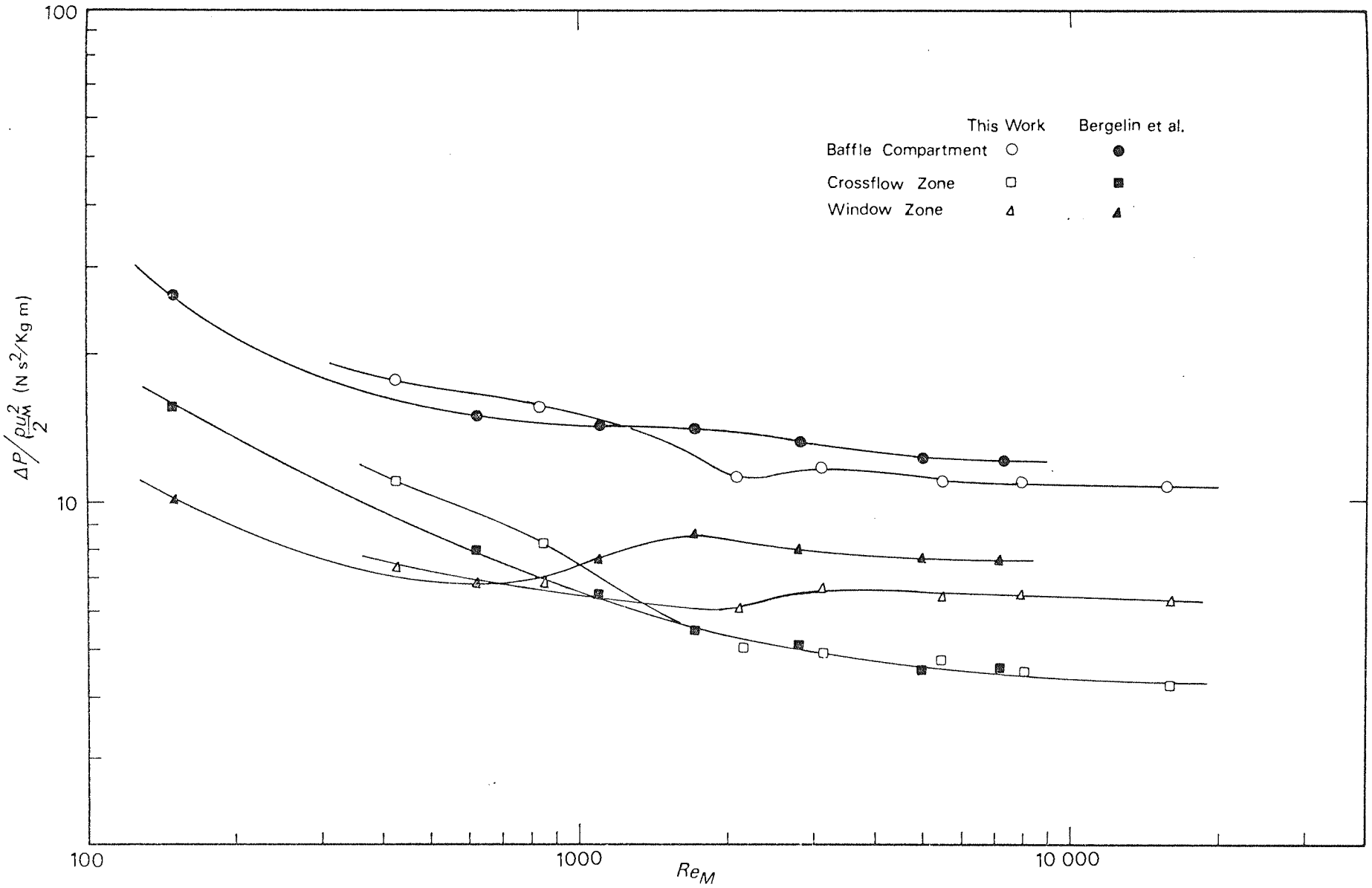

FIG 60 PRESSURE DROP

in Section 4.4.6. The two sets of baffle compartment pressure drop data were generally within 10 per cent of each other. The validity of such local pressure measurements has already been discussed in Section 4.4.6. However, while the data from this work were lower than those of Bergelin at Reynolds numbers above 1 000, the reverse was true for Reynolds numbers below 1 000. The window zone pressure drop components exhibited this same characteristic. The crossflow zone data of the present work fell above those of Bergelin at the lower Reynolds numbers but coincided with these data at the higher Reynolds numbers. It is significant that the transition in the characteristics of this pressure drop comparison and the deviation in the heat and mass transfer data shown in Fig. 58, both emerge at the Reynolds number of 1 000. The lower pressure drops and j-factors of Bergelin at the lower Reynolds numbers, suggest the presence of internal leakage in his exchanger model. However in later studies, Bergelin et al. (34) showed that leakage produced a far greater reduction in pressure drop than in heat transfer. The deviation in the heat and mass transfer data in Fig. 58, may have been augmented by natural convection effects already discussed above.

The low pressure drops and j-factors exhibited by Bergelin at the lower Reynolds numbers could be attributed to the presence of trapped gas in his exchanger model. In the non-leakage experiments of the present work, gas was found to collect in the top of the bundle behind the baffles. This occurred only at the lower flow rates and was overcome by increasing the flow rate for a short time prior to making measurements at a low flow rate. As already mentioned in Section 4.4.2.5, Bergelin would not have been able to identify the presence of trapped gas in his exchanger

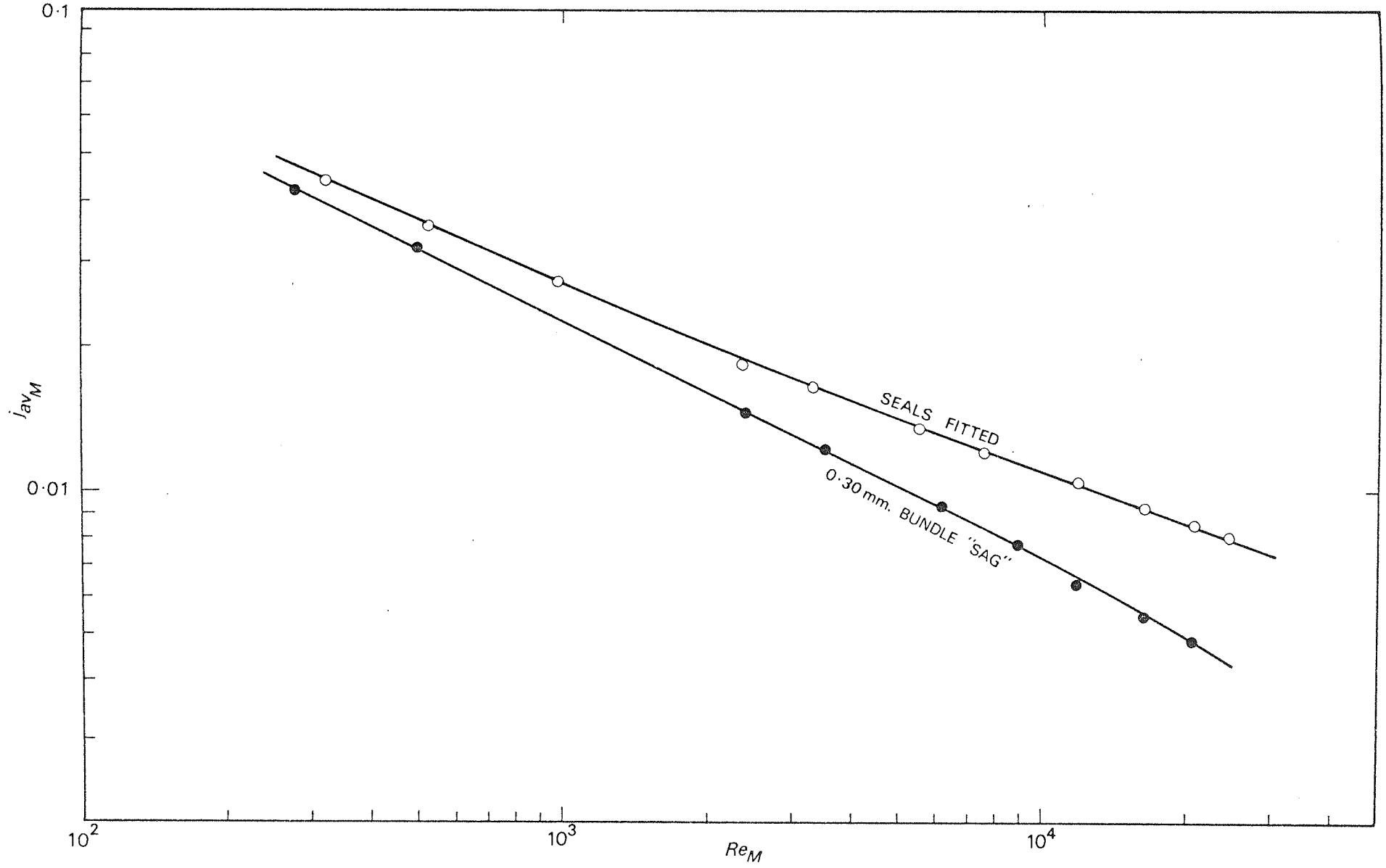

FIG 61 EFFECT OF BUNDLE SAGGING ON COMPARTMENT AVERAGE COEFFICIENTS

model. Furthermore his flow circuit had no provision for venting gas.

Bundle sagging was also found to be a problem in the no-leakage experiments of this work. For the case of the short baffle spacing, the sagging produced clearances between the top of the baffles and the shell of up to 0.012 in. (0.30 mm). The effect of these clearances on the baffle compartment average j-factor is revealed in Fig. 61. This problem was overcome by fitting rubber lip-seals to the edges of the baffles. Although the metal bundle of Bergelin would have been more rigid, the sealing rubbers used may not have been able to contend with any slight increase in the shell-to-baffle clearance at the top of the bundle.

6.2.2 Comparison with Williams

The 3.82 in. (97.0 mm) baffle spacing, 18.4 per cent baffle cut configuration, provided a further case for comparing the results of this work with those obtained by Williams (32) using a mercury evaporation mass transfer technique.

The baffle compartment average j-factors of Williams and this work are compared in Fig. 62. As in the previous comparison with Williams (see Section 4.4.2), a discrepancy between the data gradually emerges at the lower Reynolds numbers, the data of the present work falling above those of Williams. The onset of the discrepancy would appear to occur at a slightly lower Reynolds number than before. However, at a Reynolds number of 100, Williams's data now fall 16 per cent lower than the data of this work compared with a corresponding value of 18 per cent in the earlier confirmation test.

The discrepancy could again be attributed to natural convection. The natural convection component of the electrochemical mass transfer data was derived by the method used earlier in

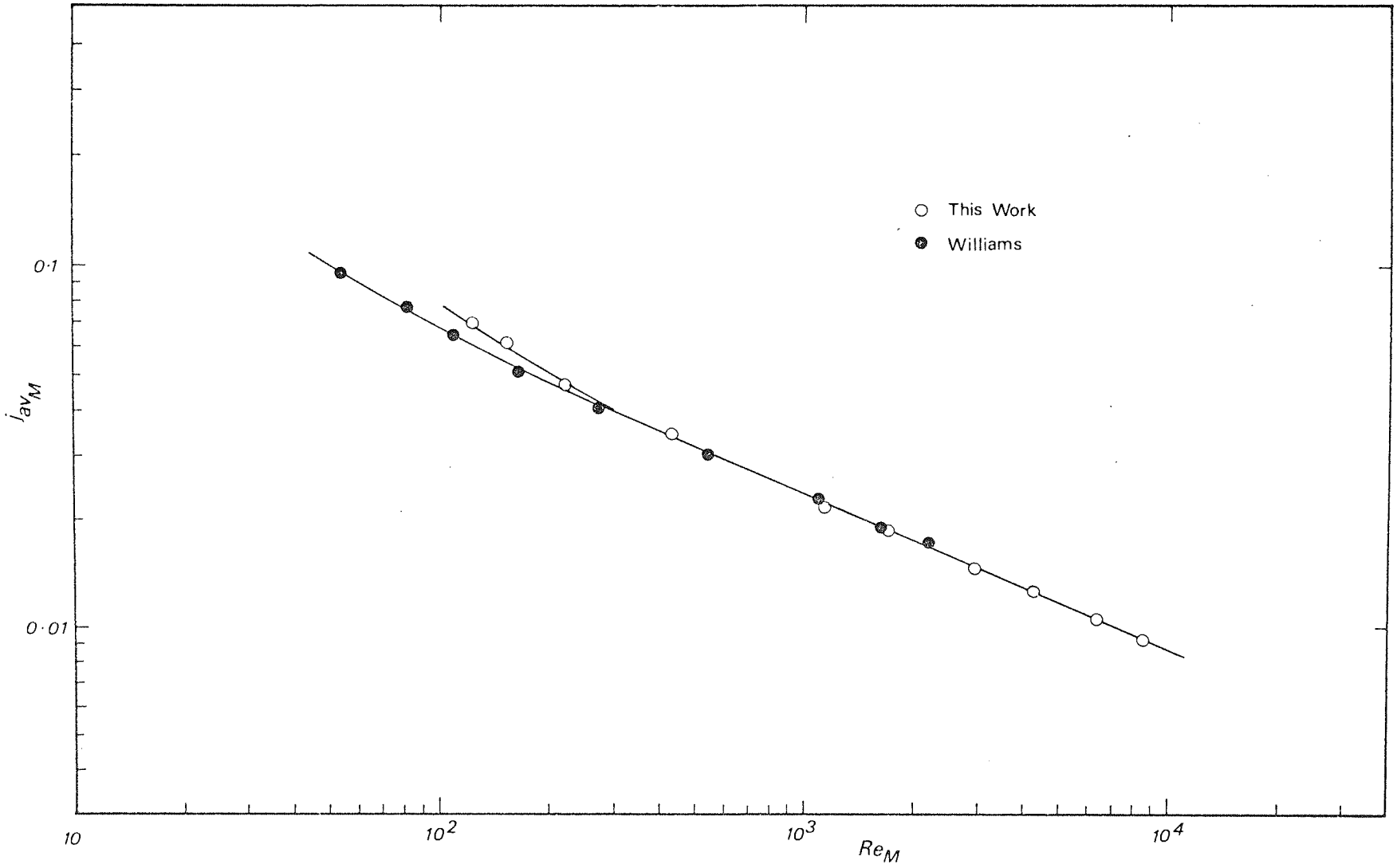

FIG 62 COMPARISON OF COMPARTMENT AVERAGE COEFFICIENTS

Section 4.4.2.8. As before, the natural convection data thus obtained fell considerably below the correlation for single horizontal cylinders recommended by McAdams (see Fig. 21). Differing characteristics between single cylinders and baffled tube bundles and possible errors incurred in deriving the densification term in the Grashof number could again account for this disparity.

The individual tube mass transfer coefficients of this work and Williams are compared for both low and high Reynolds numbers in Figs. 63 and 64. The data have been normalised by dividing the individual tube coefficients by the corresponding baffle compartment average value. The data of this work represent the average of the values from symmetrically positioned tubes. At the high Reynolds number, the distribution of the tube coefficients in the two cases is very similar with the tubes around the side of the bundle showing below-average coefficients. However in the inlet window zone, Williams shows higher tube coefficients than those of this work. Tubes 37 and 44 (see Fig. 16) on the side of the bundle show this same characteristic. At the low Reynolds number, corresponding to the lower limit of the data of this work, greater differences emerge between the two distributions of tube coefficients. The discrepancy between the coefficients of tubes in the inlet window zone is more pronounced. Williams's data show a region of tubes down the centre of the bundle exhibiting above-average coefficients. The present work shows these tubes to have well below-average coefficients. This indicates that in Williams's experiments, a greater proportion of the flow penetrated the centre of the bundle. This could have occurred through random changes in the flow distribution or by the presence of internal leakage. Casual tube-to-baffle leakage could produce local high values of tube coefficients. As already mentioned in Section 4.4.2.4,

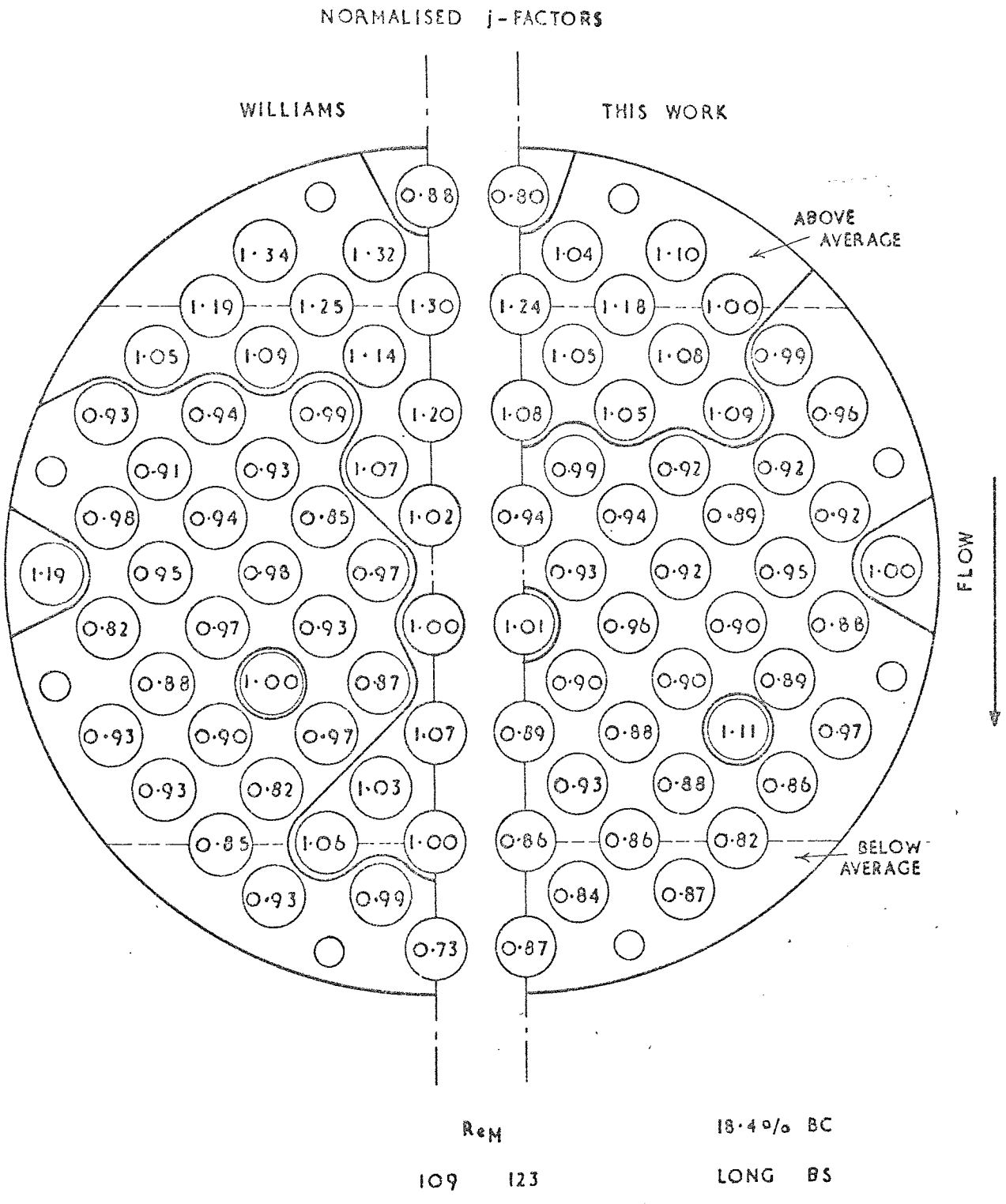

FIG. 63. NO-LEAKAGE

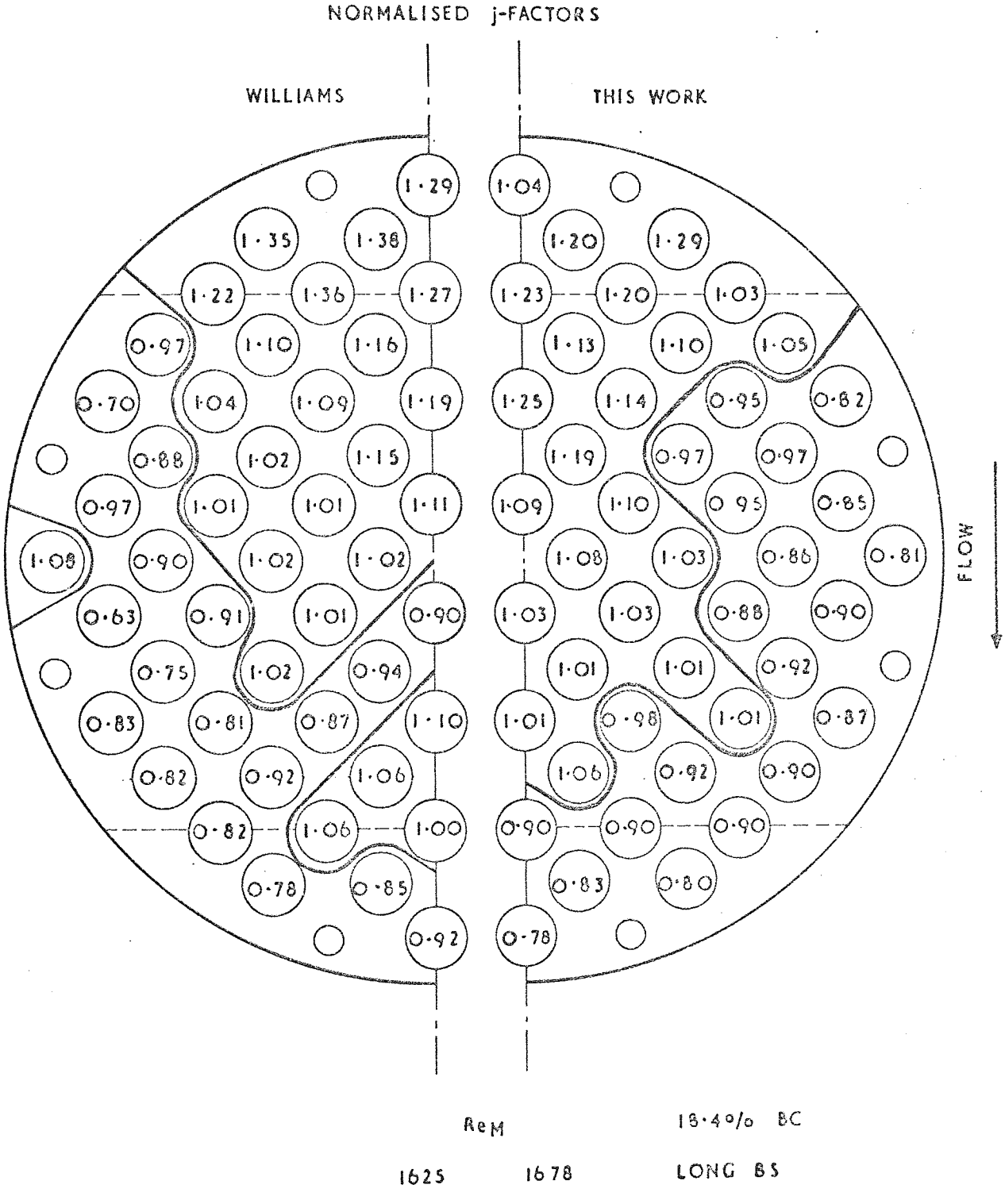

FIG. 64. NO-LEAKAGE

significant variations in the tube pitch could have occurred in Williams's tube bundle. An increase in the tube pitch would produce a preferential flow channel for the shell-side fluid. This constitutes another possible explanation for the differing distributions of tube coefficients.

6.2.3 Conclusions

The mass transfer data of this work have again been shown to be in good agreement with both the mass transfer data of Williams and the heat transfer data of Bergelin et al. The discrepancy in the j-factors at the lower Reynolds numbers has again been attributed to a variety of phenomena of which natural convection would seem to be the most consistent. However, it is recommended that the data at Reynolds numbers less than 500 should be employed with caution. In this region the j-factor data of Bergelin et al. fall outside the limits of the estimated accuracy of the experimental data of the present work.

6.3 INDIVIDUAL TUBE COEFFICIENTS

6.3.1 Symmetry

The no-leakage situation with the baffle windows at the top and bottom of the bundle affords symmetry about the bundle diameter at right angles to the baffle cut. Experimental data from all the six no-leakage baffle configurations showed that the mass transfer coefficients of symmetrically positioned tubes were generally within 5 per cent of each other. Evidence of this is shown in Figs. 65 to 73. Any slight asymmetry could be attributed to random redistributions of the flow within the bundle. The average coefficients of all the tubes in the two symmetrical halves of the bundle were consistently within 2 per cent of each other. Any random flow redistribution effects would appear to have been smoothed out. These results justify the procedure adopted

in the development work of making measurements on tubes in only one half of the bundle.

For the 3.82 in. (97.0 mm) baffle spacing, 37.5 per cent baffle cut case, measurements of tube coefficients were made with the bundle rotated through a right angle (see Section 7.4). The degree of symmetry in the coefficients was shown to be equivalent to that exhibited by a configuration with the window zones at the top and bottom of the bundle.

6.3.2 Distribution of Tube Coefficients

The distribution of individual tube j-factors is best represented by a normalised form of the data. The individual tube j-factors were thus each divided by the baffle compartment average value. These data for all the six no-leakage baffle configurations at a Reynolds number of around 8 000 are shown in Figs. 65 to 70. This particular value of the Reynolds number represented the middle of the range of those studied.

The baffle configurations having 25.0 and 37.5 per cent cuts at the short spacing and a 37.5 per cent cut at the long spacing (Figs. 66, 67 and 70) all show similar distribution characteristics. The tubes in the inlet and outlet windows exhibit the lowest coefficients while the tubes in the crossflow region possess coefficients that are generally above-average (represented by normalised values greater than unity). For the case of the 18.4 and 25.0 per cent cuts at the long baffle spacing (Figs. 68 and 69), tubes with above-average coefficients extend throughout the inlet window zone into the centre of the crossflow zone. Tubes with low coefficients are confined to the outlet window zone and the flanks of the crossflow zone. The 18.4 per cent cut at the short spacing (Fig. 65) would appear to have a combination of these two characteristics.

NORMALISED j FACTORS

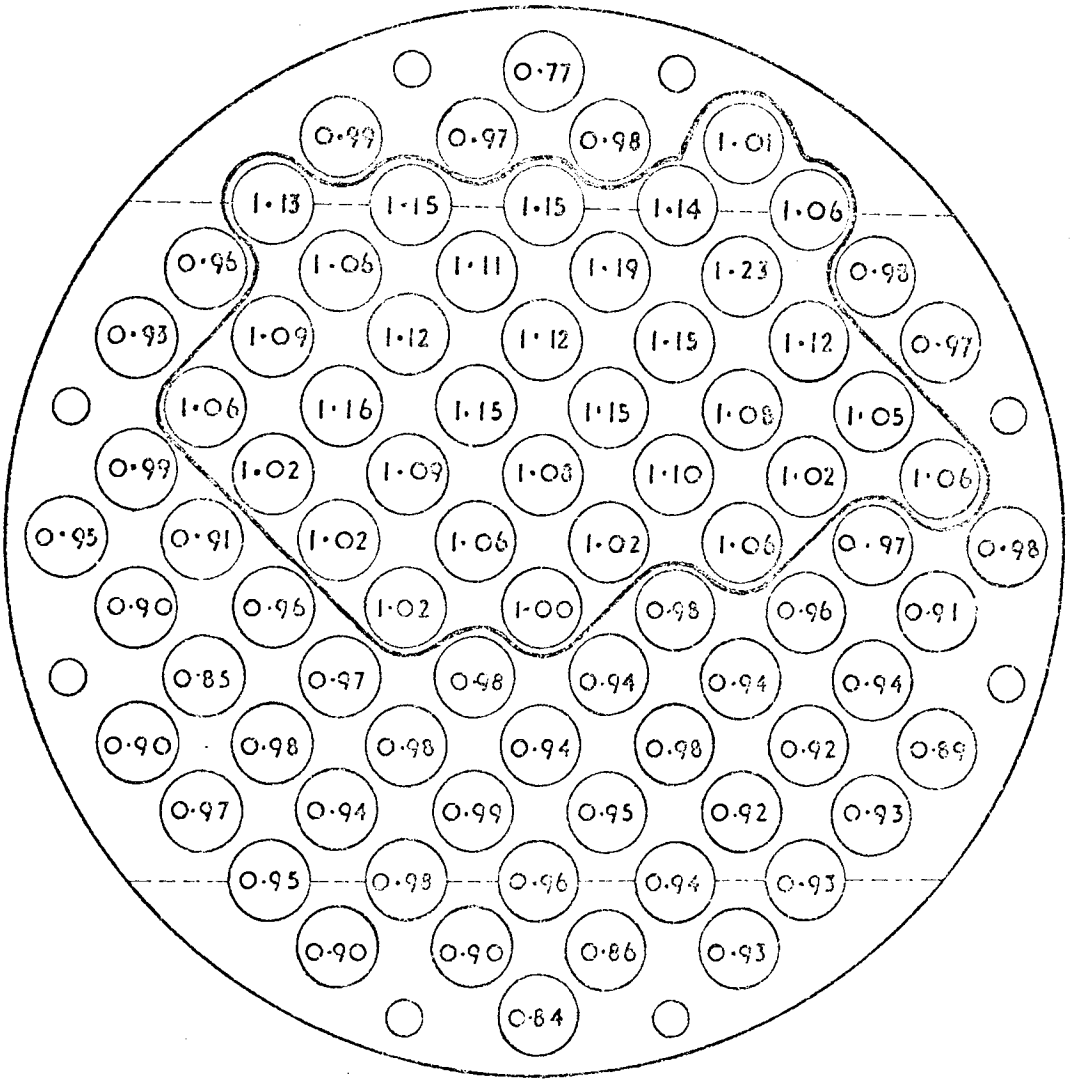

Re_M = 7380

18·4% BC

SHORT BS

AM/AW = 1·74

FIG.65. NO-LEAKAGE

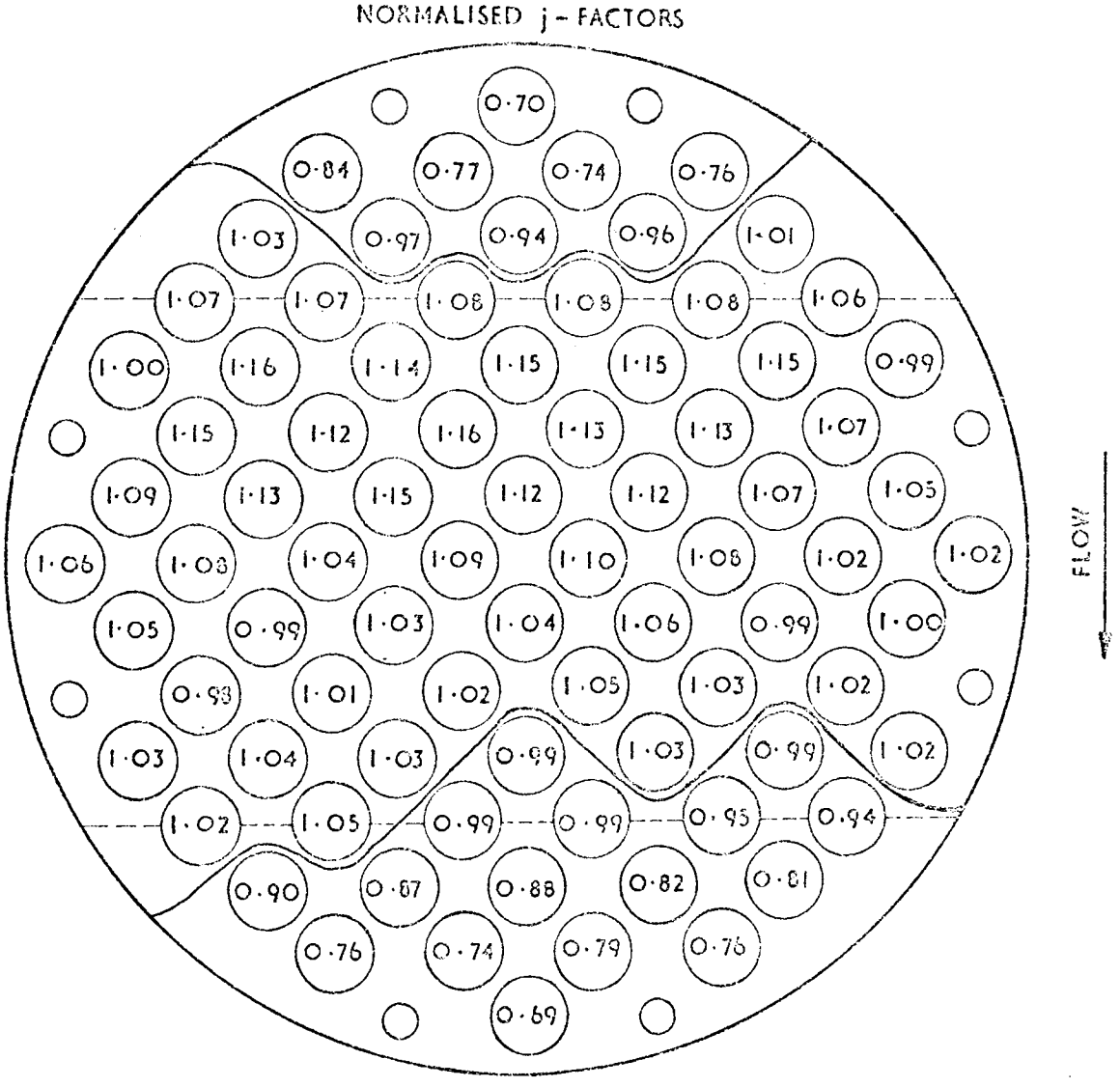

FIG. 66. NO - LEAKAGE

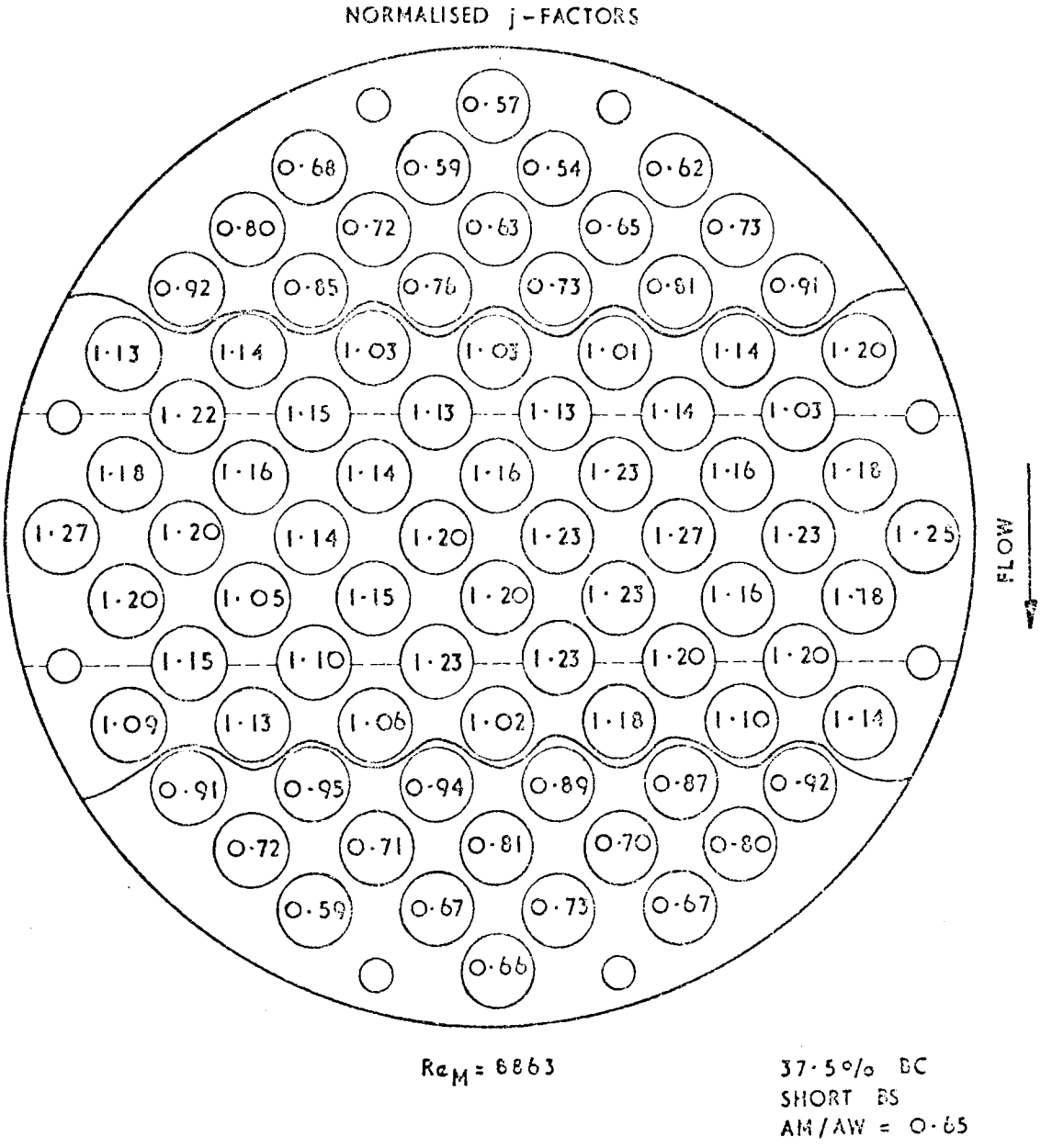

$Re_M = 6863$

37·5% BC
SHORT BS
AM/AW = 0·65

FIG. 67. NO-LEAKAGE

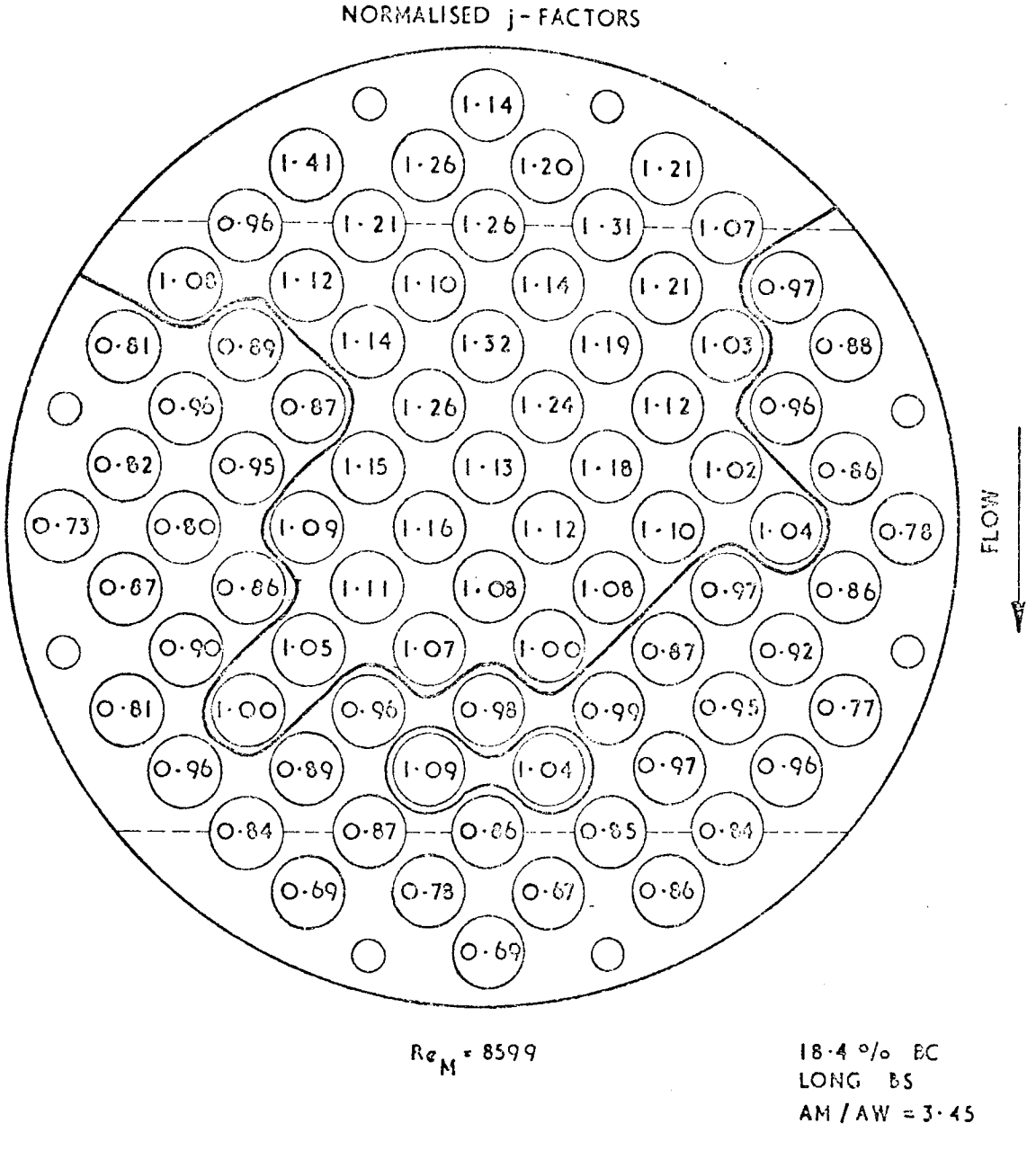

FIG. 68. NO-LEAKAGE

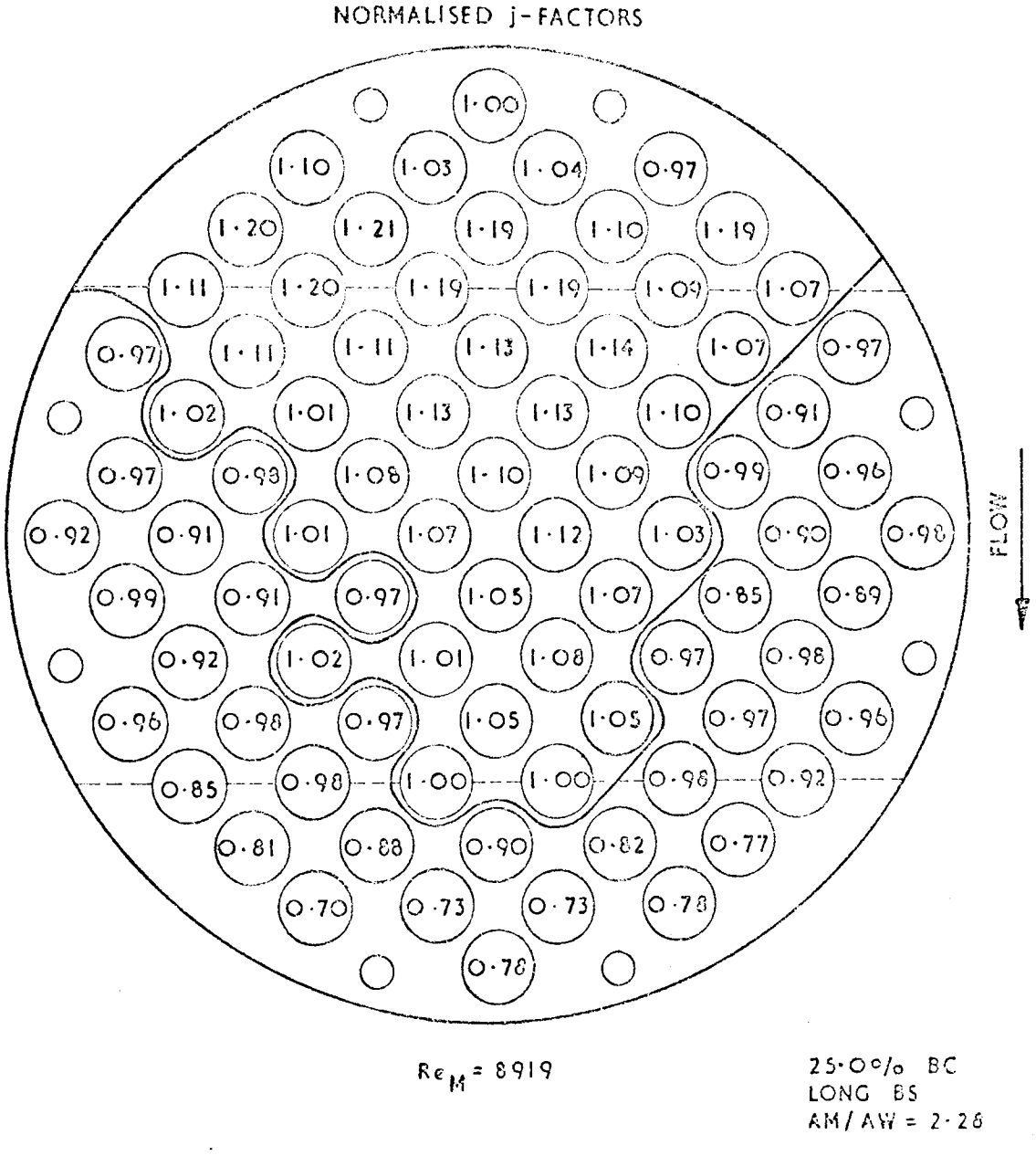

FIG. 69. NO - LEAKAGE

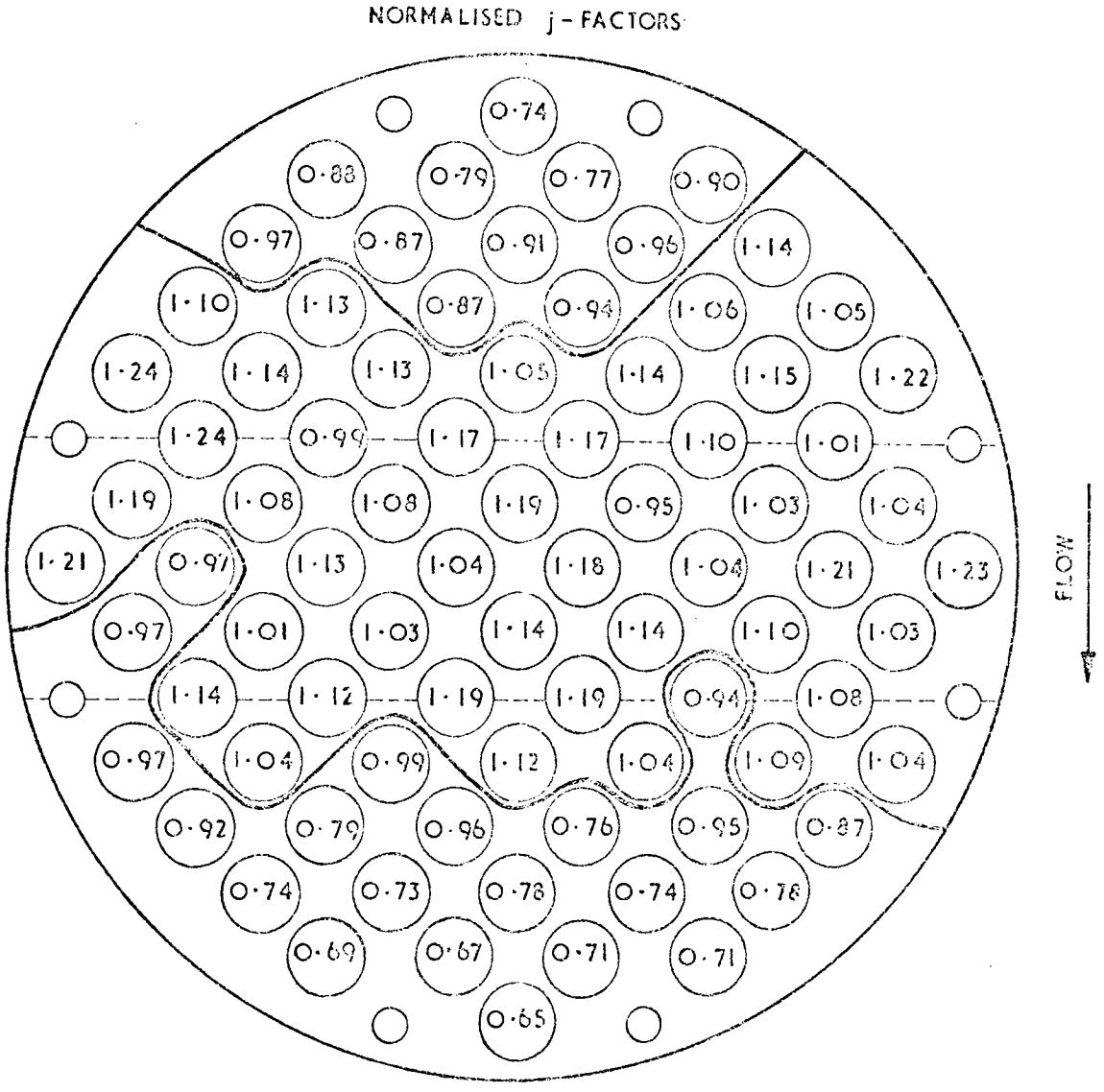

FIG. 70. NO - LEAKAGE

The ratio of the minimum crossflow area at the centre row of tubes to the window flow area through the plane of the baffle, was calculated for each baffle configuration. The values of this term A_M/A_W are given on the figures under discussion. It is evident that the baffle configurations exhibiting the low coefficients in both window zones and high coefficients in the crossflow zone, have lower values of the term A_M/A_W which are not far from unity. The similar flow areas in the crossflow region and the windows would be expected to produce more uniform shell-side flow without any of the effects from sudden enlargements or contractions in the flow channel area. The lower tube coefficients in the window zones may be attributed to the inferior transport characteristics of longitudinal flow and the presence of eddy regions (see Fig. 74).

The configurations that exhibited high tube coefficients in the inlet window zone and in the centre of the crossflow zone (Figs. 68 and 69) have relatively high values of A_M/A_W; these are 3.45 and 2.28 for the 18.4 and 25.0 per cent baffle cuts respectively at the short baffle spacing. In these two cases a sudden contraction in the flow area occurs as the shell-side fluid passes through the baffle window. The fluid would enter the baffle compartment as a jet, penetrating into the eddy regions that normally occur at the downstream corners of the inlet window zones. This flow characteristic is also shown in Fig. 74. The higher jet velocity and the reduction in the eddies would account for the relatively high coefficients exhibited by the tubes in the inlet window zone. The distribution of the tube coefficients indicates that the higher velocity jet penetrates into the middle of the crossflow zone thereby producing higher coefficients. The low coefficients in the flanks of the crossflow zone suggest the

presence of eddy regions created by this redistribution of the shell-side flow. An extensive eddy region would be expected in the outlet window zone (see Fig. 74). The exceptionally low tube coefficients give evidence of this.

The short baffle spacing, 18.4 per cent baffle cut configuration having a value of 1.74 for A_M/A_W, would be expected to have only slight jetting effects. Fig. 65 shows that the coefficients of the tubes in the inlet window zone are not so relatively high and that the jet penetrates only halfway through the crossflow zone.

The variation in the distribution of tube coefficients with Reynolds number is examined for a baffle configuration exhibiting relatively uniform flow and for a case showing severe signs of jetting. The 3.82 in. (97.0 mm) baffle spacing, 37.5 per cent baffle cut configuration was chosen as the former example. Tube coefficient distributions at three Reynolds numbers are shown in Figs. 70, 71 and 72. The distribution patterns are very similar, with the low coefficients being confined to the inlet and outlet window zones. At the higher Reynolds numbers the tubes with above-average coefficients extend further into the sides of both the window zones. The increased turbulence associated with the higher Reynolds numbers, would diminish the eddy regions in the window zones. The consistently low coefficients in the greater part of the window zones, represent tubes with substantially longitudinal flow.

The distributions in the 3.82 in. (97.0 mm) baffle spacing, 18.4 per cent baffle cut configuration are shown at two Reynolds numbers in Figs. 68 and 73. This configuration with a value of 3.45 for A_M/A_W, had shown signs of serious jetting at a high Reynolds number (Fig. 68). At the low Reynolds number (Fig. 73),

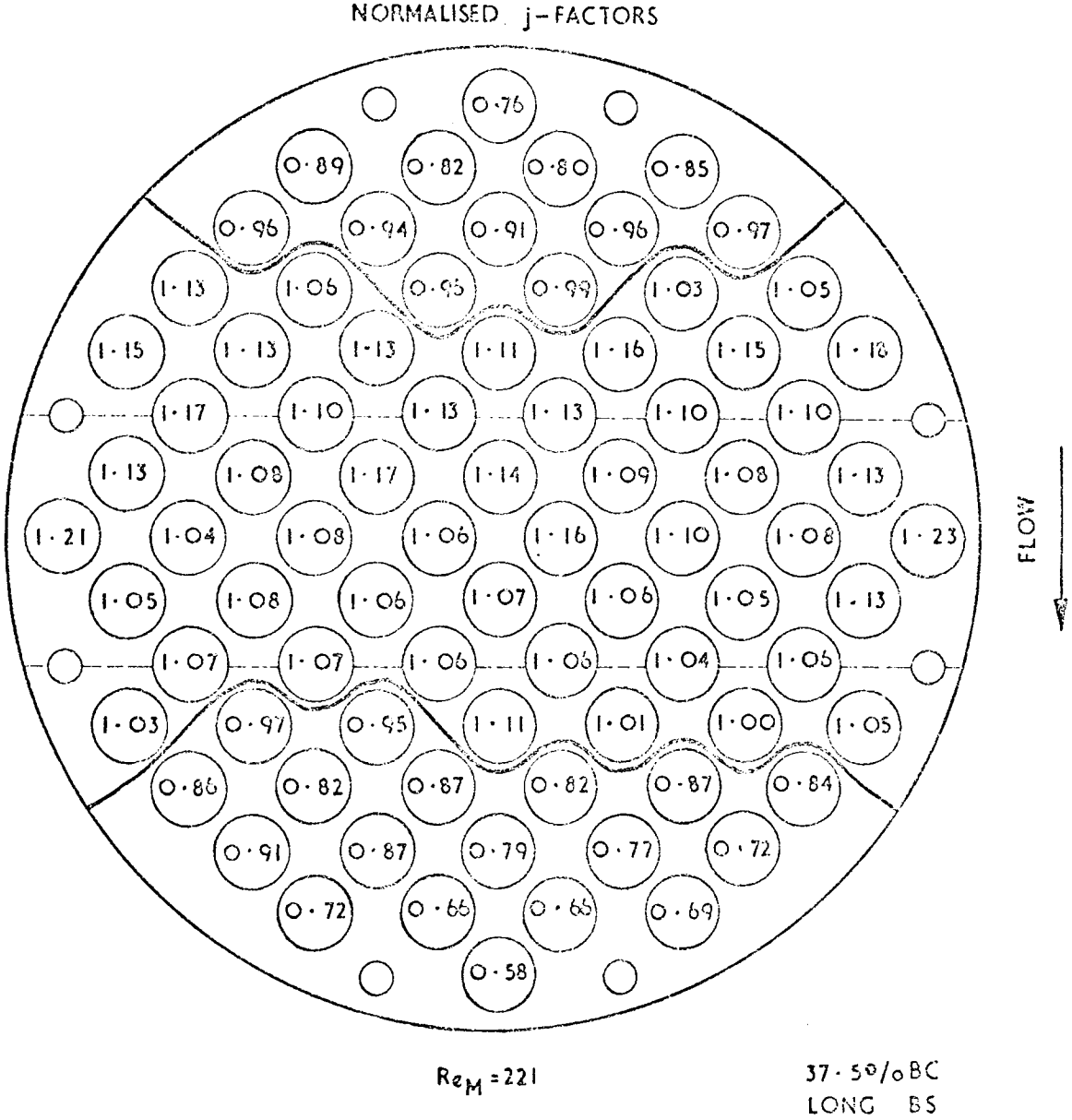

FIG. 71. NO-LEAKAGE

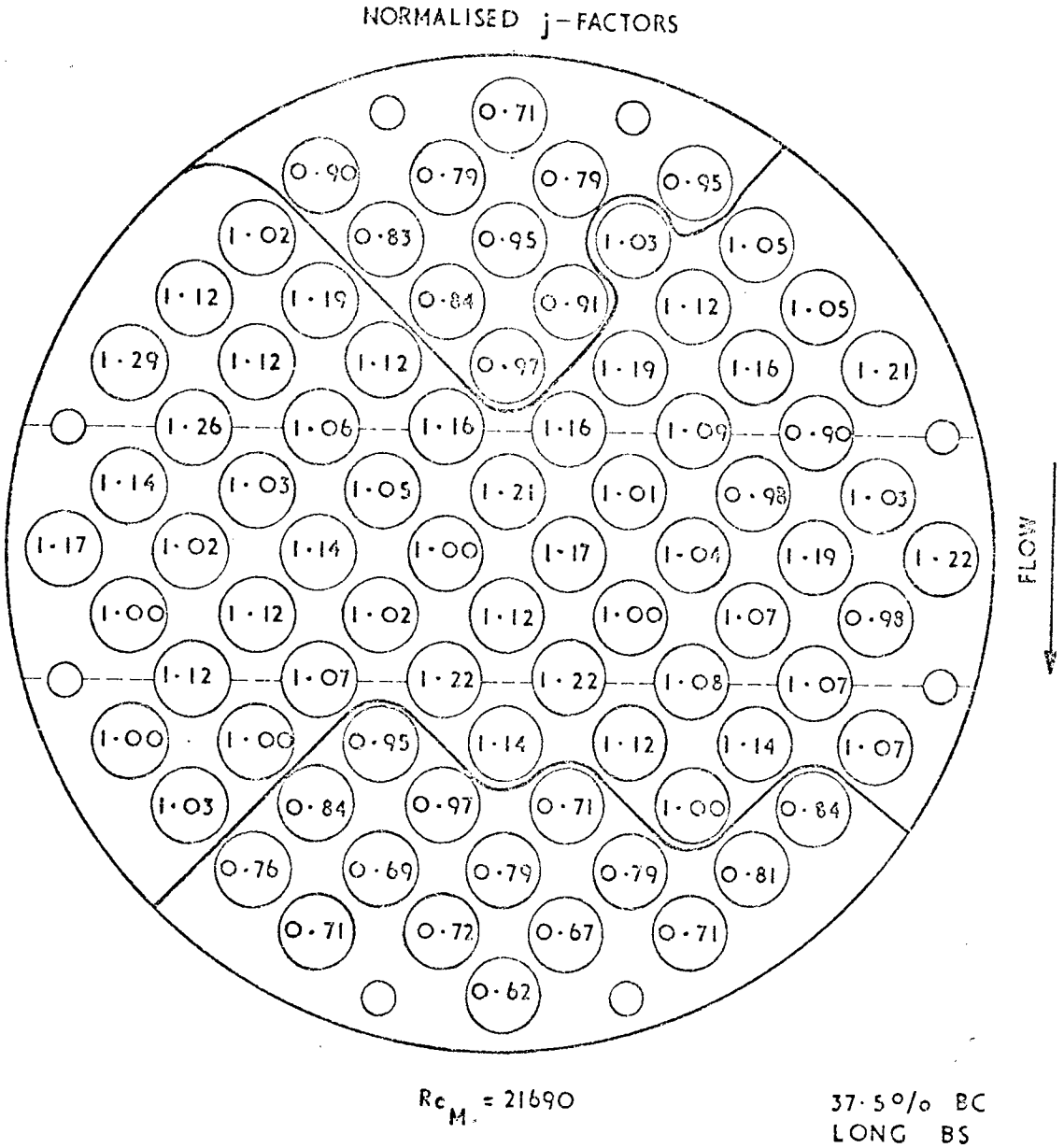

FIG. 72. NO-LEAKAGE

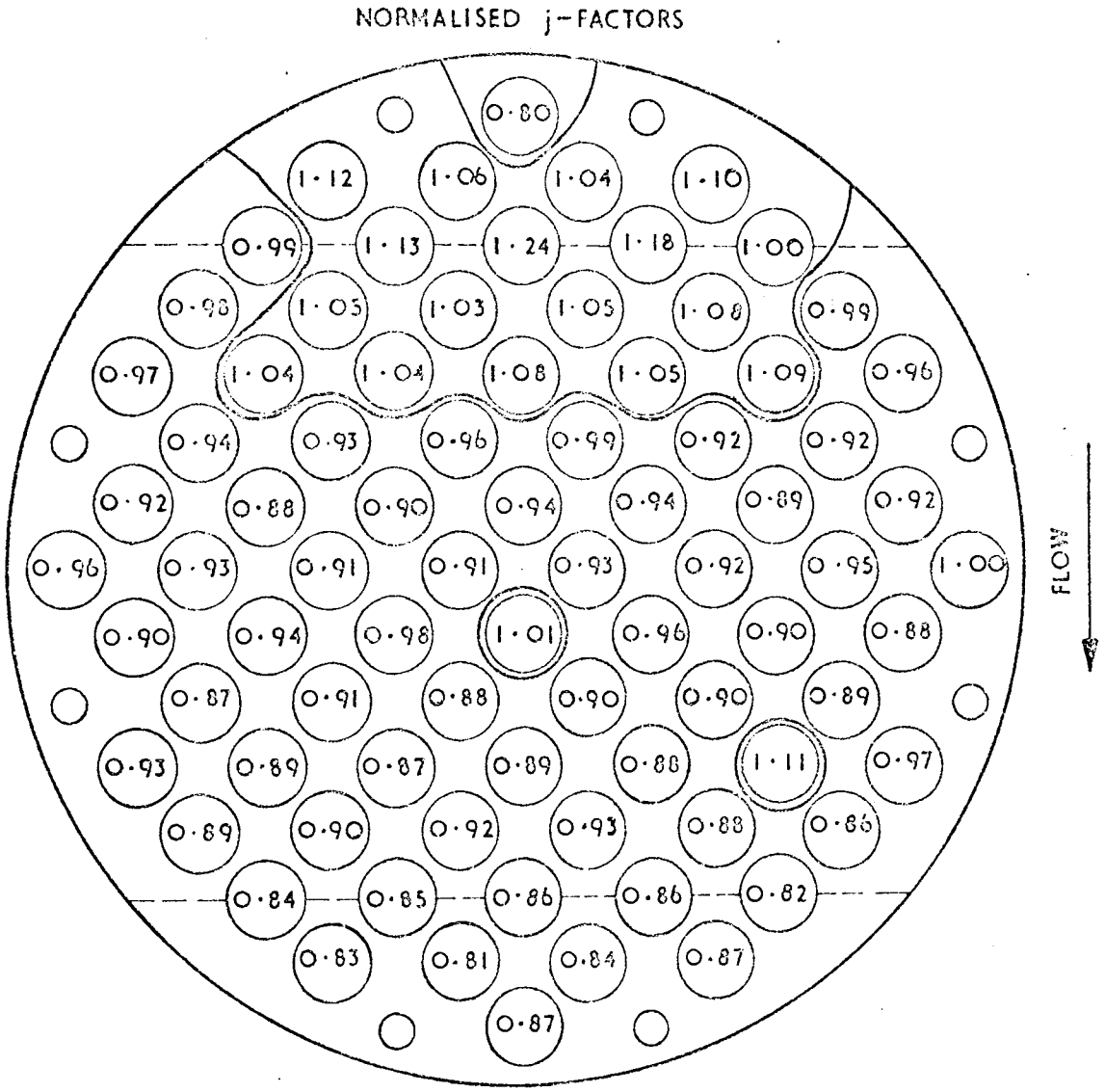

FIG. 73. NO - LEAKAGE

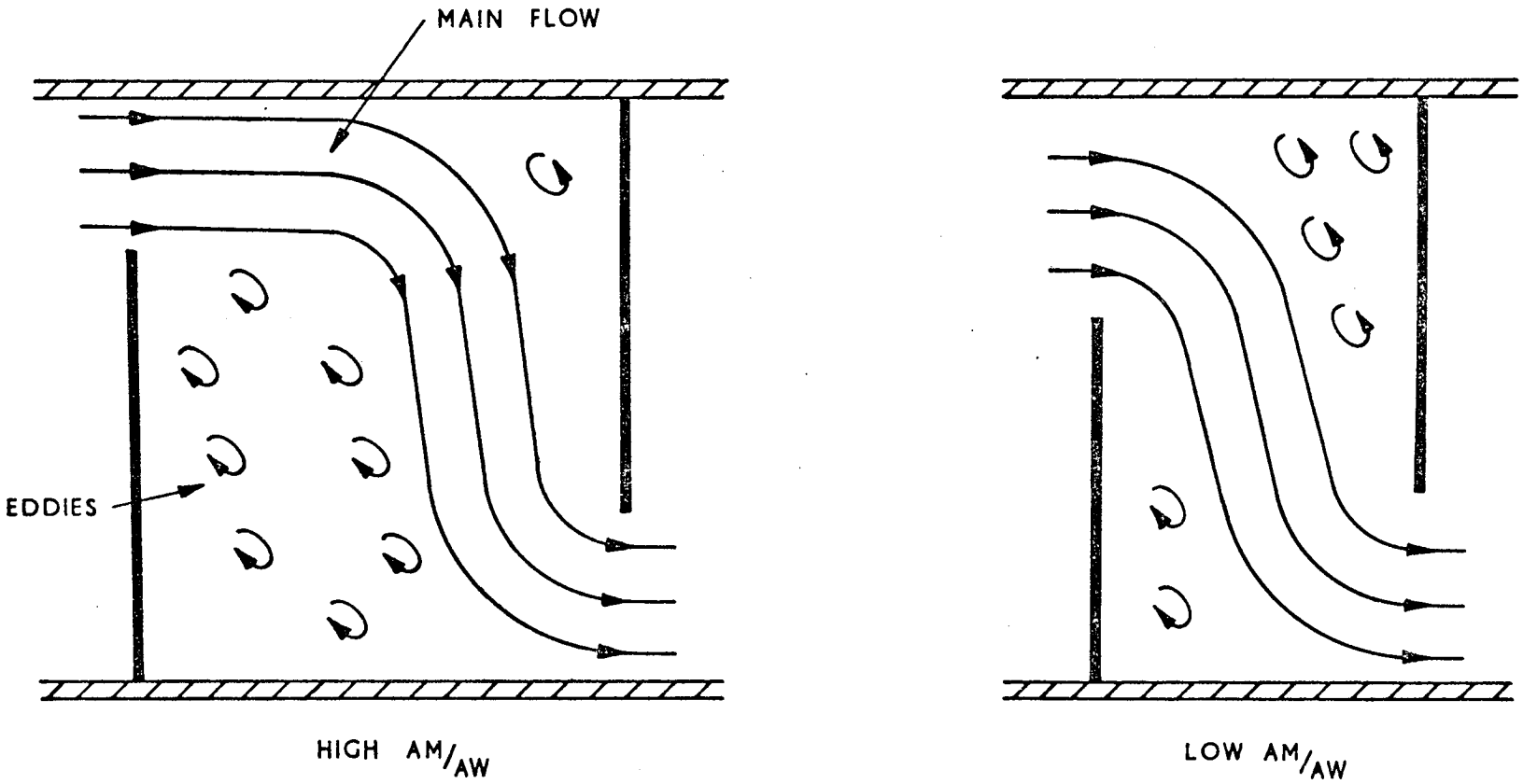

FIG. 74. VARIATION OF FLOW DISTRIBUTION WITH BAFFLE CONFIGURATION

this effect was less significant with the jet apparently penetrating only as far as the second row of tubes in the crossflow zone. The tubes throughout the rest of the bundle show coefficients that are below-average. At very low flow rates the jetting effect may completely disappear as the conversion of pressure to kinetic energy diminishes.

A measure of the variation in the values of tube coefficients through the baffle compartment would provide useful information for the design of baffle geometry. Standard deviations of individual tube coefficients from the baffle compartment arithmetic average were normalised by dividing them by this arithmetic average. For an 80 tube bundle this term is represented by:-

$$\left[\frac{\sum_{1}^{80} \left[\frac{j_i - j_{av}}{j_{av}} \right]^2}{80} \right]^{\frac{1}{2}}$$

where j_i is an individual tube j-factor and j_{av} is the compartment average value. A value of zero for this term implies that all the individual tube mass transfer coefficients are equal or are equally distributed about the arithmetic mean.

Analyses of the individual tube data from the six baffle configurations at three shell-side Reynolds numbers are represented in Fig. 75. The data at the short baffle spacing show increasing uniformity with decreasing baffle cut. There are indications that an optimum condition is reached at a baffle cut lower than those examined in this work. Similar characteristics are exhibited at all the Reynolds numbers. The highest Reynolds number produces the least uniform distribution. There is no obvious explanation for these characteristics; the baffle configuration with the 25.0 per cent cut having a value for A_N/A_W of near unity, would

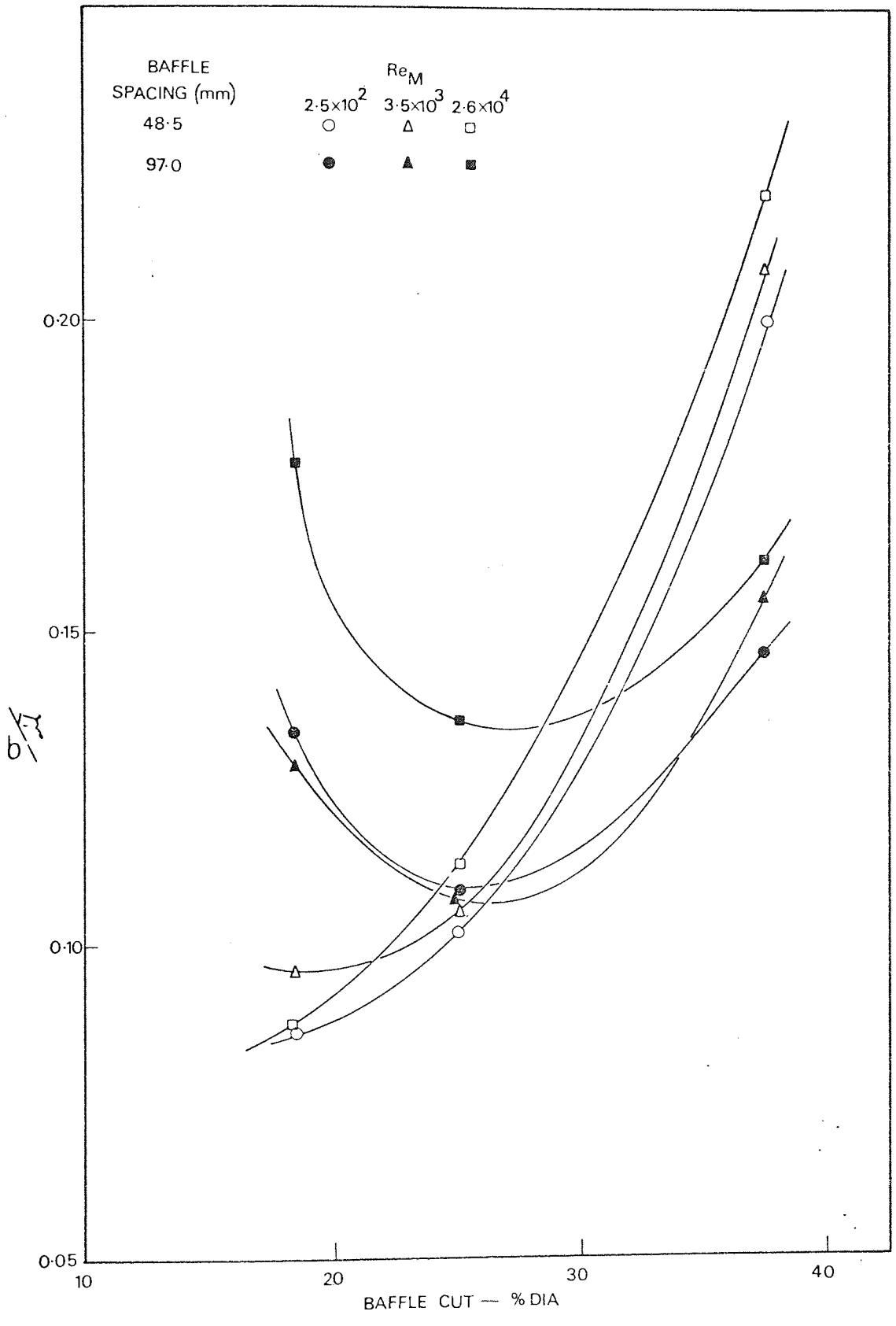

FIG 75 DISTRIBUTION OF TUBE COEFFICIENTS

be expected to produce the most uniform distribution.

The data for the long baffle spacing show an optimum at a baffle cut of around 25 per cent. At baffle cuts above this value, the long baffle spacing produces distributions that are more uniform than those of the short baffle spacing. The reverse is true for baffle cuts below 25 per cent. Again the highest Reynolds number produces the least uniform distribution. There is no obvious explanation in terms of flow characteristics for this optimum occurring at a baffle cut of 25 per cent. This configuration has already been shown to produce jetting characteristics which are compatible with those at the 18.4 per cent baffle cut.

6.3.3 Characteristics of Individual Tubes

The variation in the j-factor with Reynolds number was examined for a few particular tubes and baffle configurations. The cases chosen are shown in the table below:-

Case	Tube Number+	Baffle Configuration*	Zone	Indicated Flow Characteristics
(i)	48	48.5/18.4	Crossflow	Slight jetting
(ii)	48	48.5/37.5	Crossflow	No jetting
(iii)	4	97.0/18.4	Inlet window	Serious jetting
(iv)	8	97.0/37.5	Inlet window	No jetting
(v)	80	97.0/37.5	Outlet window	No jetting

+See Fig. 16

*Baffle spacing (mm)/Baffle cut (% diameter)

The tubes in Cases (i) and (ii) would be those most representative of ideal crossflow. The tubes in Cases (iii) and (iv) being in the centre of the inlet window zone, would be expected to exhibit some characteristics of longitudinal flow. Tube 80

in Case (v) should also show characteristics of longitudinal flow. The j-factor data of the tubes are shown in Fig. 76.

The characteristics of all tubes show a remarkable similarity. The tubes in Cases (ii), (iii) and (iv) have correlations with almost identical gradients. Tube 48 in Case (i) exhibits a slightly flatter slope. Tube 80 has a similar gradient but shows a distinct transition in the correlation at a Reynolds number of around 1 000.

Zukauskas (13) and others (see Section 1.2) showed that in ideal crossflow, the Nusselt number varied as the 0.4 to 0.6 power of the Reynolds number. For water flowing parallel to a tube bundle Miller et al. (48) showed that the value of this Reynolds number exponent was 0.8. The characteristic tube dimension in their Reynolds number was the outside diameter. The corresponding slopes in a j-factor correlation would be minus 0.6 to 0.4 for crossflow and minus 0.2 for longitudinal flow. This interpretation is justified below.

The slope of the correlation for Tube 48 in Case (i) varies between minus 0.43 and 0.34. The slopes in Cases (ii), (iii) and (iv) vary between minus 0.52 and 0.38. This would suggest that the window zone tubes in Cases (iii) and (iv) have crossflow characteristics that are equivalent to those of Tube 48 in Case (ii) while greater than those of this same crossflow zone tube in Case (i). Furthermore none of the window zone tubes show signs of an approach to pure longitudinal flow. This would have been expected, particularly in Case (iii), where serious jetting was indicated in previous analyses.

The presence of eddy regions may distort the crossflow or longitudinal flow characteristics exhibited by an average coefficient from a baffle-spacing length of tube. The correlation

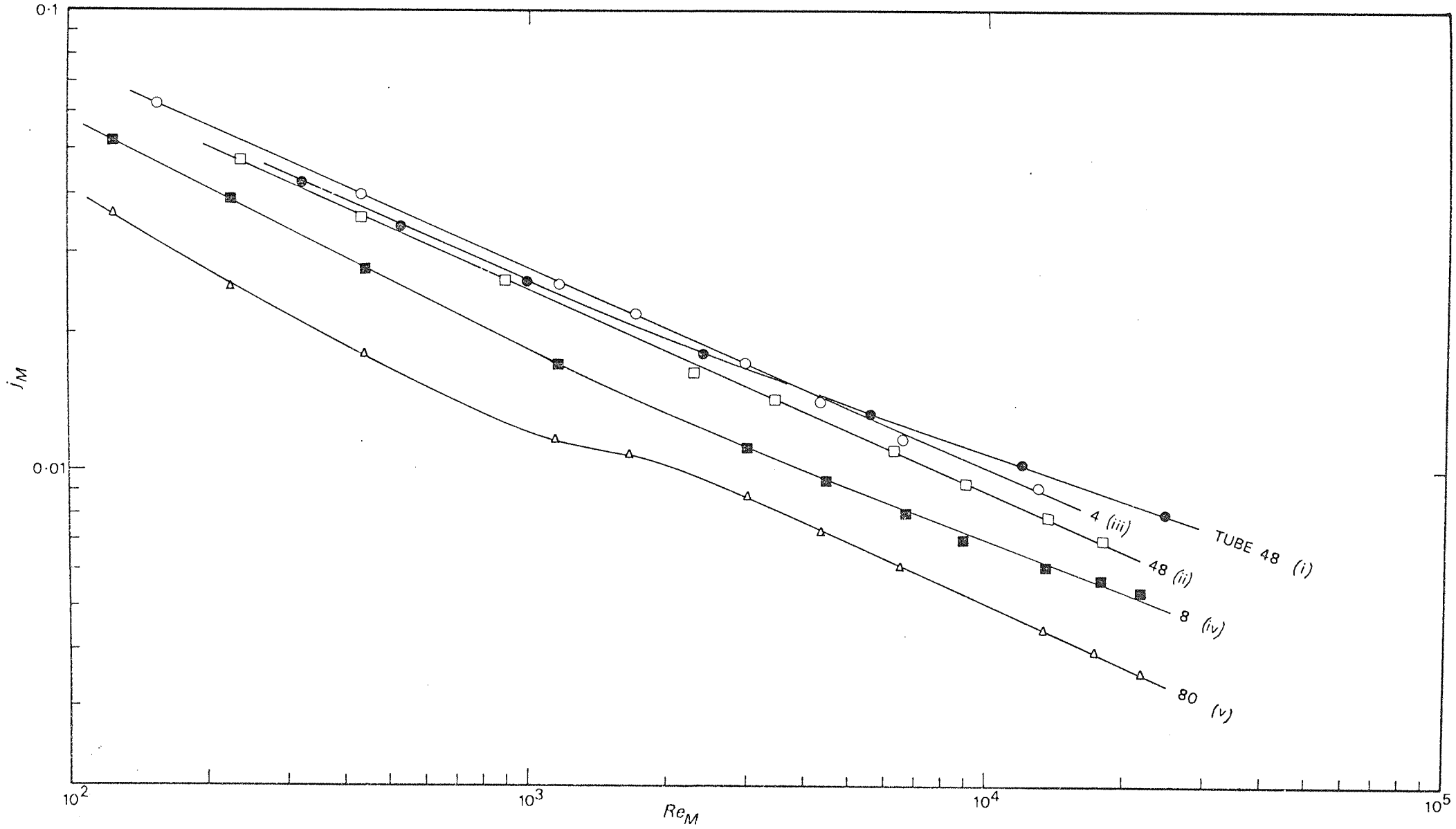

FIG 76 CHARACTERISTICS OF INDIVUAL TUBES

characteristics of average coefficients from smaller increments of tubes would separate the flow characteristics and identify regions of substantially crossflow or longitudinal flow.

The flow characteristics may be further distorted by variations with flow rate in the distribution of velocities through the bundle.

In this form of correlation the velocity term appears in both the Reynolds number and the j-factor (see Section 5.4.2). The Reynolds number exponent in this form of correlation may be derived from that in a Nusselt number versus Reynolds number relationship, only in cases where the variation in the Reynolds number is due solely to variations in the fluid velocity. Conditions in this work approach this situation (see Section 5.4.2). This method of correlation may not effectively combine the correlation characteristics of both crossflow and longitudinal flow; for the velocity is based solely on a crossflow area.

6.4 COMPARTMENT AVERAGE j-FACTORS

The compartment average j-factor data for the six baffle configurations are shown plotted in Fig. 77. The characteristic velocity in the Reynolds number and j-factor is that based on the minimum crossflow area at the centre row of tubes, A_M. The data for each baffle configuration generally fell on separate curves. The data at the short baffle spacing are higher than those at the long spacing having the same baffle cut. For both baffle spacings the j-factor decreases with increasing baffle cut.

The effect of neither baffle spacing nor baffle cut were completely correlated by this method. At the long baffle spacing the effect of baffle cut was negligible for small baffle cuts (viz. 18.4 and 25.0 per cent). At the 37.5 per cent baffle cut the effect of baffle spacing was negligible.

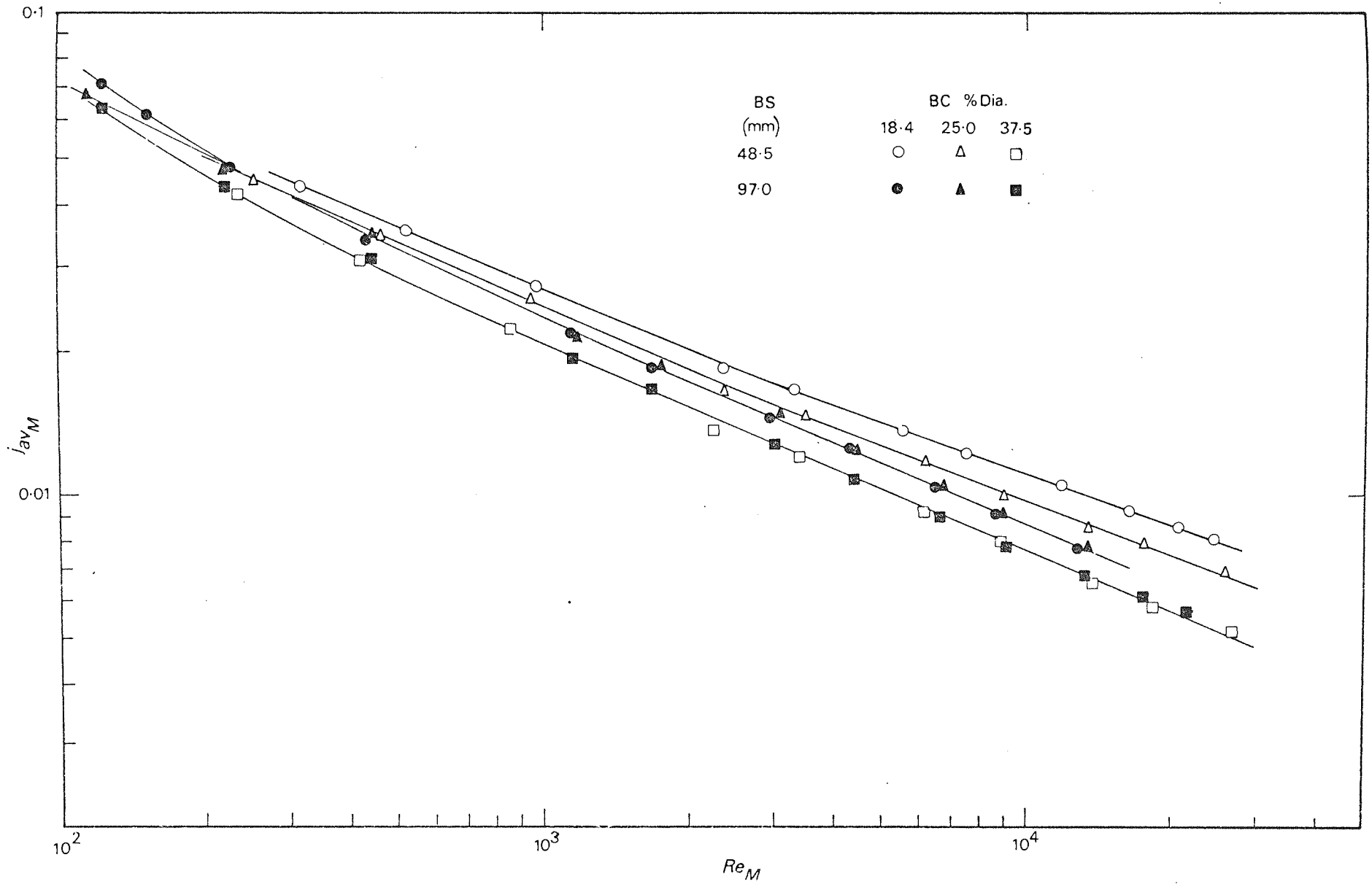

FIG 77 COMPARTMENT AVERAGES

For the same shell-side velocity, the average heat transfer coefficient for the 18.4 and 25.0 per cent baffle cuts at the long baffle spacing, would be identical. Both of these baffle configurations have exhibited "jetting" characteristics (see Section 6.3.2). However Fig. 75 shows that the 25.0 per cent cut baffle configuration produces the more uniform distribution of individual tube coefficients. Furthermore this configuration was found to exhibit a lower shell-side pressure drop across a baffle compartment.

The two 37.5 per cent baffle cut configurations would also produce similar heat transfer coefficients for the same shell-side velocity. Neither of these configurations showed signs of fluid "jetting". Fig. 75 reveals that the long baffle spacing configuration gives the more uniform distribution of tube coefficients. This configuration also produced a lower baffle compartment pressure drop.

Bergelin et al. (30) experienced this same difficulty in correlating the effect of baffle spacing and cut in their bundle average j-factor data. Using the same form of correlation, their plotted data from four baffle spacings and three baffle cuts produced a band extending $\pm$ 25 per cent about a mean. When applying a correction factor accounting for the differing characteristics in the crossflow and window zones, the scatter of the data was reduced to around $\pm$ 20 per cent.

Williams (32) also plotted his compartment average mass transfer j-factor data in this way. The data from three baffle cuts at a 3.89 in. (99.0 mm) baffle spacing fell on separate curves with the data at the smallest baffle cut showing the highest j-factors.

The characteristic velocity employed in all the above correlations takes into account the baffle spacing but not the baffle cut. In Fig. 77 for either of the baffle spacings, the variation in the baffle cut is shown to have a substantial effect on the compartment average

j-factor. A characteristic velocity based on the dimensions of both the crossflow and window flow channels would seem necessary.

Donohue (20) correlated the shell-side heat transfer data of Short (see Section 1.3.1.1) using a weighted velocity defined as the geometric mean of the crossflow velocity at the widest section of the shell and the velocity through the baffle window. Replacing Donohue's crossflow velocity by that based on the minimum area at the centre row of tubes gives a corresponding velocity, u_Z defined by:-

$$u_Z = (u_M \cdot u_W)^{\frac{1}{2}} \qquad \ldots\ldots (6.1)$$

The data in Fig. 77 were re-analysed using this velocity in the Reynolds number and j-factor. These data are plotted in Fig. 78. The effect of baffle spacing was not correlated with the result that the data segregated into two curves. At each baffle spacing the effect of baffle cut was however correlated to within $\pm$ 10 per cent. This scatter is barely significant in relation to the estimated accuracy of experimental data.

At a constant baffle cut of 35 per cent, Donohue was able to correlate variations in baffle spacings to within $\pm$ 10 per cent. The range of the baffle spacings for the 6 in. (152 mm) ID shell was 2.33 to 21.4 in. (58.3 to 543 mm). In Fig. 78 the data at the 37.5 per cent baffle cut fall within 20 per cent of each other. This is similar to the degree of correlation obtained by Donohue. Data at the other baffle cuts show greater separation. Donohue made no attempt to correlate variations in baffle cut using the weighted velocity.

When Short (22) correlated his own data, he employed a weighted velocity derived from the arithmetic mean of the maximum and minimum crossflow velocities and the window velocity. This is represented in Equation (1.8). Short was able to correlate variations in baffle

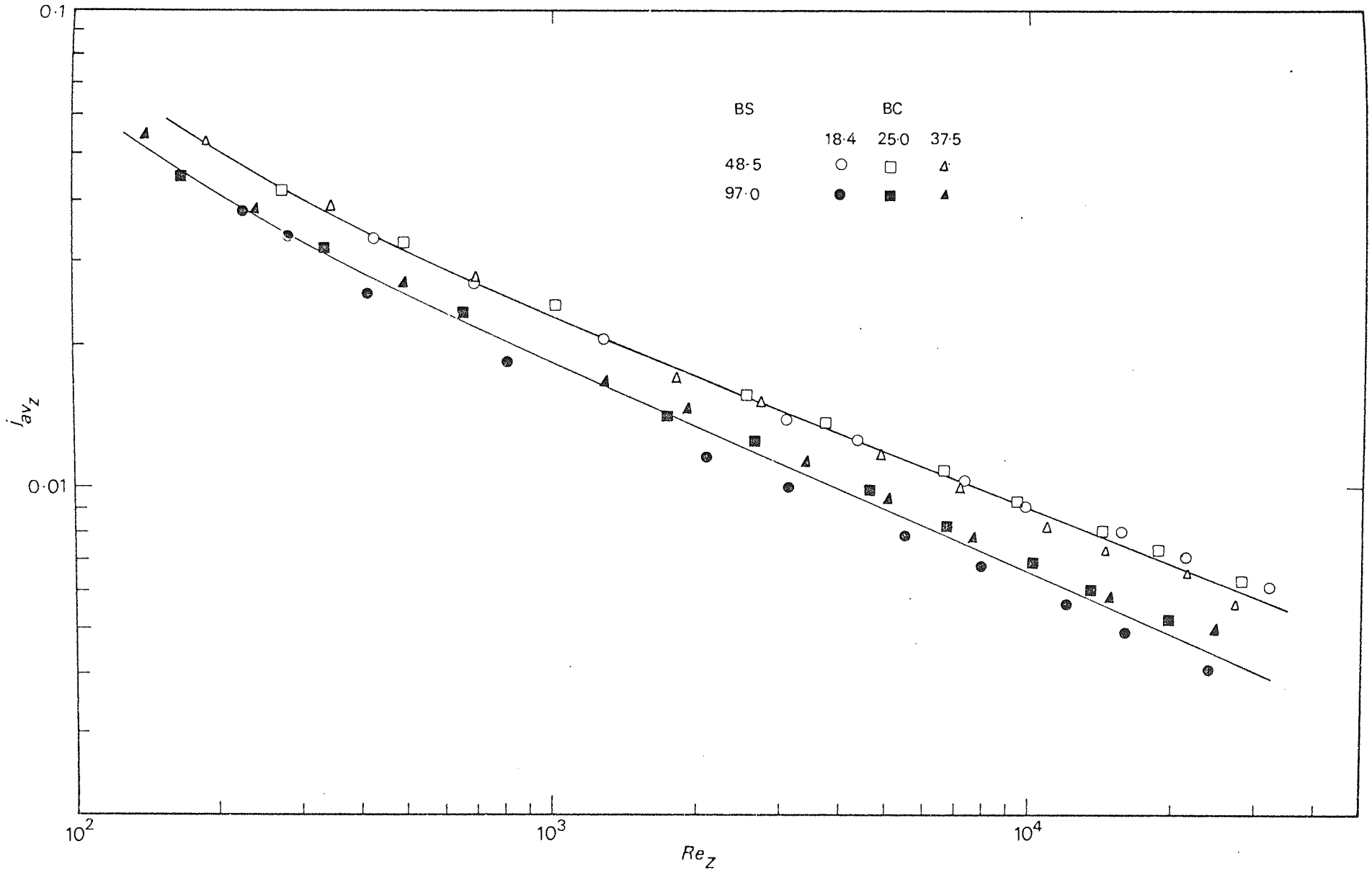

FIG 78 COMPARTMENT AVERAGES

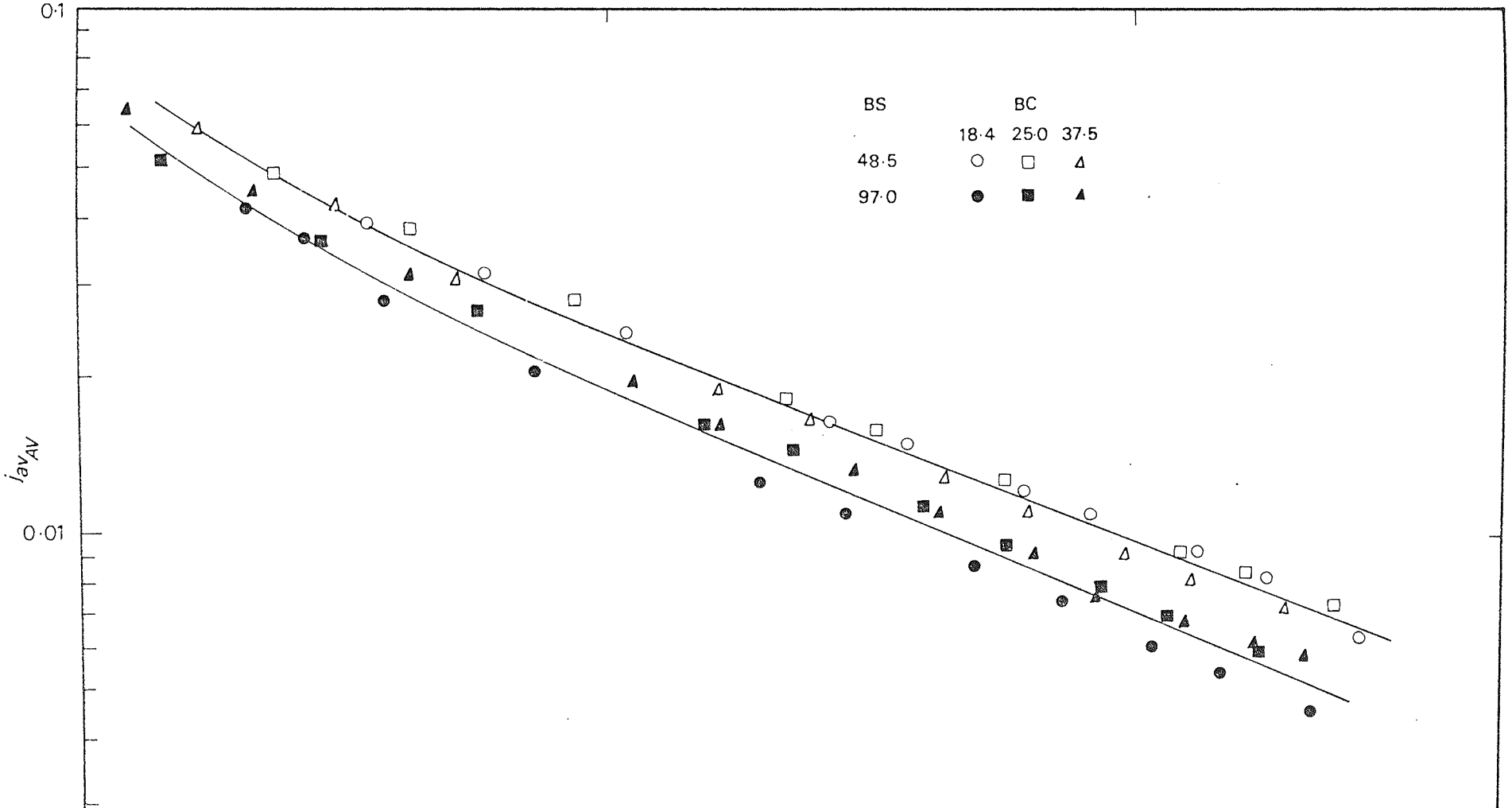

FIG 79 COMPARTMENT AVERAGES

spacing at the 35 per cent baffle cut to within ± 15 per cent.

The original data in Fig. 77 were re-analysed using the characteristic velocity given by Equation (1.8). The data are shown plotted in Fig. 79. As in the previous method of analysis, the effect of baffle spacing was not adequately correlated. At the short baffle spacing, the variation in the baffle cut was correlated to within ± 10 per cent. At the long spacing the correlation was only within ± 15 per cent. Short found that his data at the short baffle spacings, viz. 2.3 and 3.0 in. (58.3 and 76.0 mm), showed the least degree of correlation.

It would thus appear that no simple characteristic velocity can adequately correlate baffle compartment average data for variations in both baffle spacing and baffle cut. The analyses of the individual tube data have already shown that variations in the baffle geometry can produce vast changes in the general shell-side flow characteristics. No simple correlation method could accurately describe such a complex shell-side flow phenomenon as "jetting".

Williams (32) correlated his shell-side data through separate analyses of the crossflow and window zone data. This method is now examined.

6.5 CROSSFLOW ZONE AVERAGE j-FACTORS

The crossflow zone average j-factor data for the six baffle configurations are shown plotted in Fig. 80. The zonal average j-factors were derived in the same way as in the development work (see Section 4.4.3). Details of this procedure are also given in Appendix 2.4. The characteristic velocity in the Reynolds number and j-factor is that based on the minimum crossflow area at the centre row of tubes. All the data at the long baffle spacing and those of the 37.5 per cent baffle cut at the short baffle spacing were correlated to within ± 5 per cent. The data from the two smaller

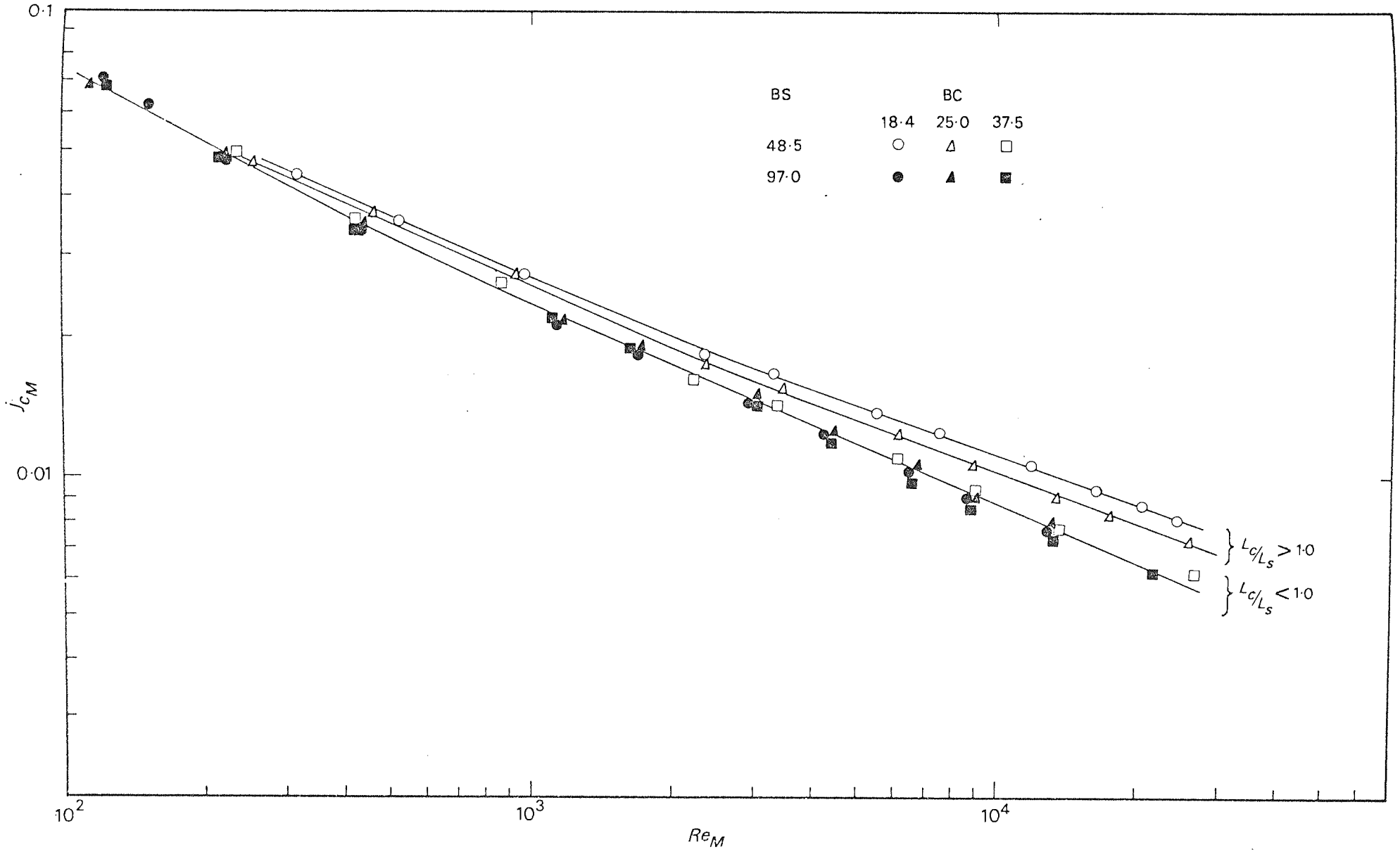

FIG 80 CROSSFLOW ZONE AVERAGES

baffle cuts at the short baffle spacing fell on separate curves both considerably above that of the other data. For the range of the variables studied, the features in Fig. 80 infer that:-

(i) At the long baffle spacing the crossflow zone average j-factor is independent of the baffle window geometry.

(ii) At the 37.5 per cent baffle cut the j-factor is independent of the baffle spacing. The j-factor and Reynolds number contain a velocity which is already a function of the baffle spacing.

(iii) The crossflow zone j-factor at the short baffle spacing varies considerably with baffle cut.

The baffle configurations of the four sets of data showing good correlation had not all exhibited the same flow characteristics in the individual tube analyses. The value of A_M/A_W in these four cases varied between 0.65 and 3.45.

Williams (32) made measurements of individual tube coefficients at three baffle cuts but only one baffle spacing equal to the long spacing in this work. The crossflow zone data at this baffle spacing similarly correlated onto a single curve.

The characteristic velocity u_Z in Equation (6.1) takes account of the geometries of both the crossflow and window flow channels. The crossflow zone j-factor data were re-analysed using this characteristic velocity and plotted in Fig. 81. The data at the short baffle spacing showed good correlation. The correlation was within $\pm$ 5 per cent at the higher Reynolds numbers and $\pm$ 10 per cent at the lower Reynolds numbers. The data at the long baffle spacing now fell onto three separate curves corresponding to each baffle cut.

The characteristic velocity used by Short (22) was also derived from the velocities in both crossflow and window flow (see Equation (1.8)). The crossflow zone j-factor data when analysed using this

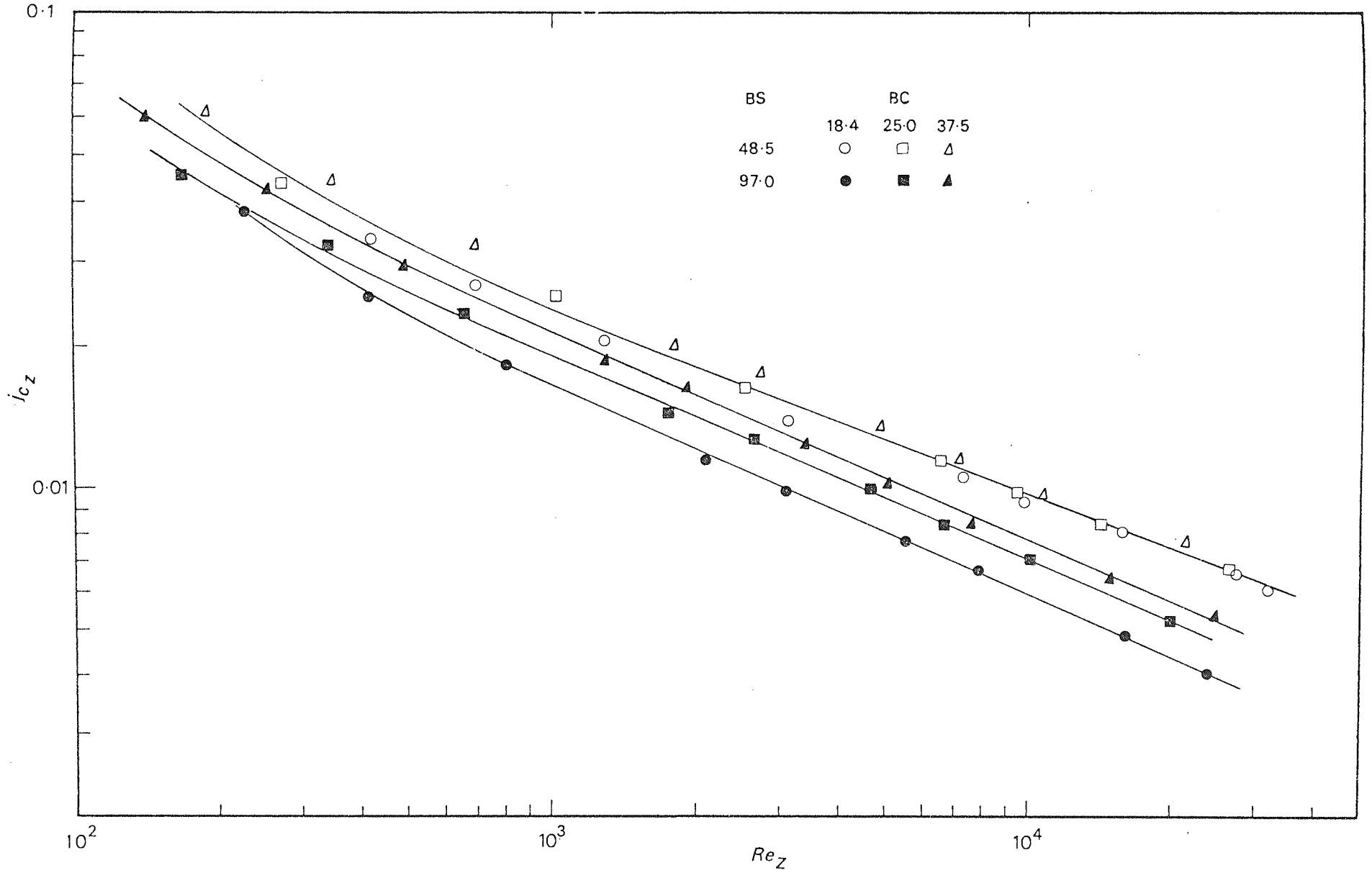

FIG 81 CROSSFLOW ZONAL AVERAGES

velocity (see Fig. 82) produced features that were similar to those already obtained using Donohue's geometric mean velocity.

When the window velocity was introduced into the analyses, the data at the short baffle spacing correlated. The data at the long baffle spacing separated with the smallest baffle cut giving the lowest j-factors. The short baffle spacing data in Fig. 80 had in fact shown the reverse with the smaller baffle cuts producing the higher j-factors. Correlation characteristics intermediate between those of Fig. 80 and those of both Figs. 81 and 82, would be obtained if far greater weight were put on the crossflow velocity component when deriving a weighted velocity. This was demonstrated by defining an arbitrary characteristic velocity u_y where:-

$$u_y = (u_M^2 \cdot u_w)^{\frac{1}{3}} \qquad \ldots\ldots (6.2)$$

The crossflow zone data were analysed using this velocity and plotted in Fig. 83. The variation in the baffle cut was now correlated for both baffle spacings. The data correlated to within $\pm$ 10 per cent at the long spacing while to within $\pm$ 5 per cent at the short spacing. Again, the effect of baffle spacing was not adequately correlated.

It has been shown that no simple characteristic velocity can correlate crossflow zone data for the effect of both baffle spacing and baffle cut. A more empirical approach would seem necessary to describe the variation in the complex crossflow zone characteristics associated with a change in baffle geometry.

The configuration of the crossflow zone may be represented two-dimensionally by the ratio L_C/L_S, where L_C and L_S are the baffle overlap and baffle spacing respectively.

For large values of the ratio L_C/L_S the crossflow zone would be deep and narrow resulting in a large crossflow component (see Fig. 84).

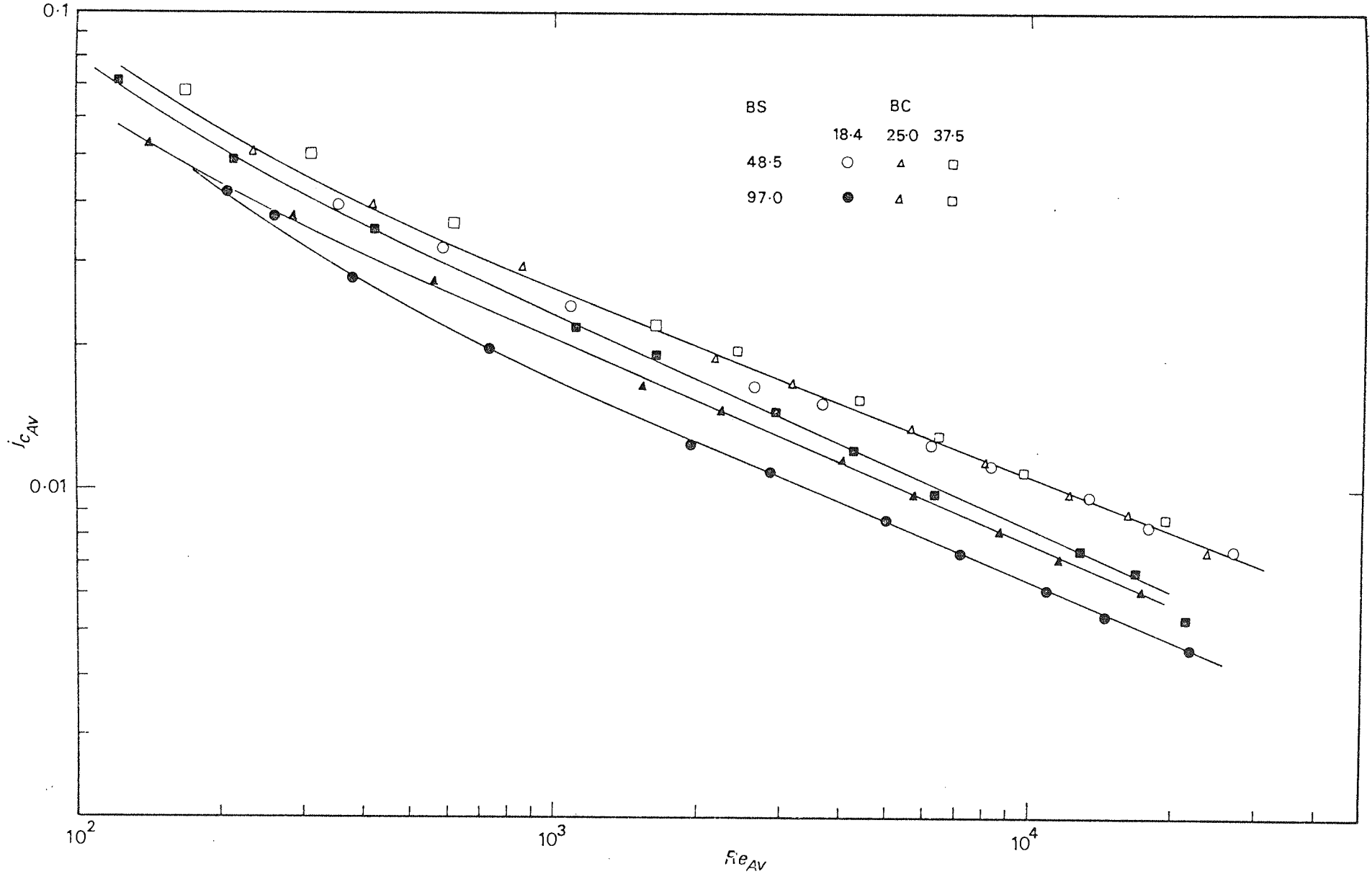

FIG 82 CROSSFLOW ZONAL AVERAGES

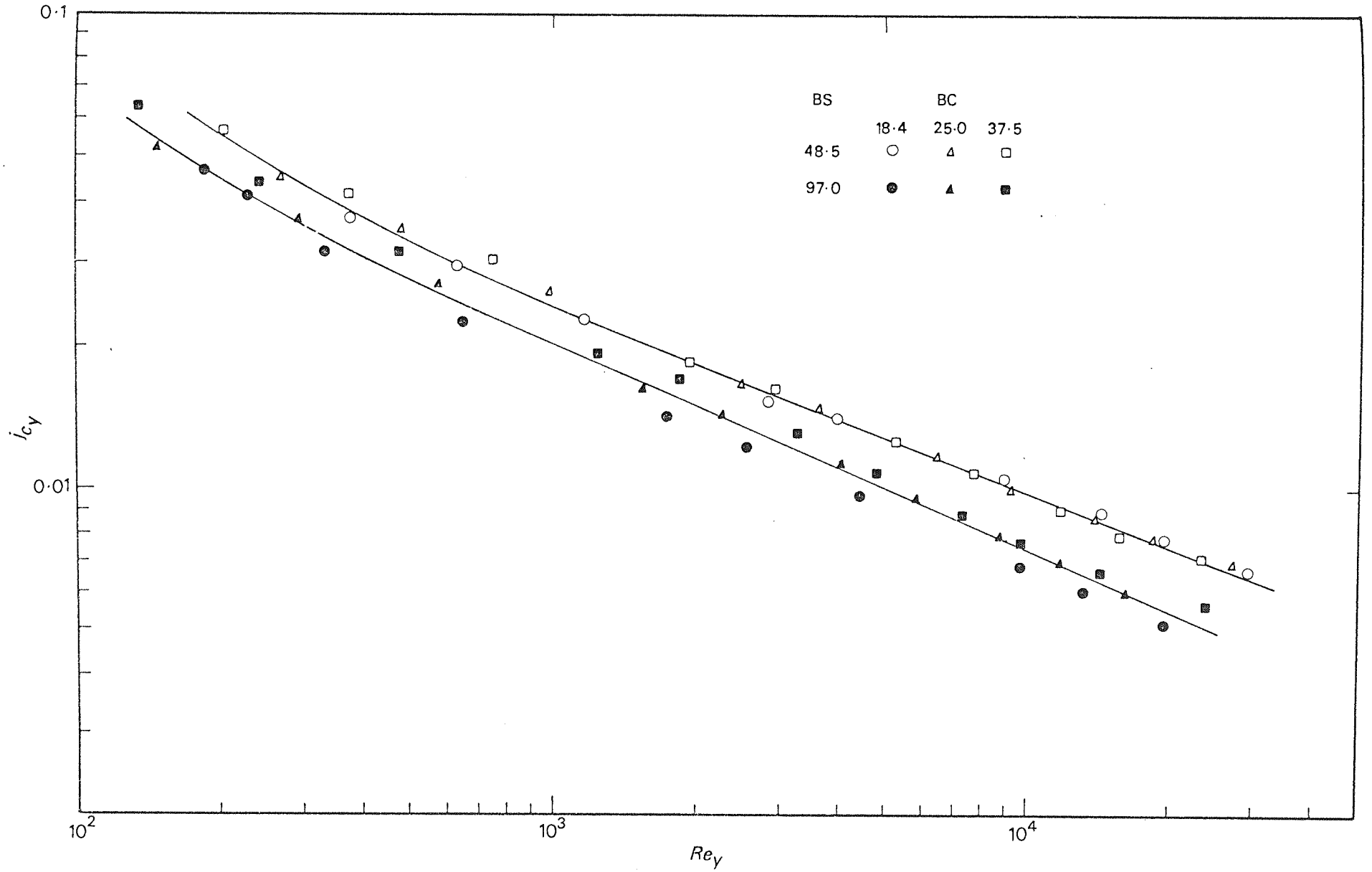

FIG 83 CROSSFLOW ZONAL AVERAGES

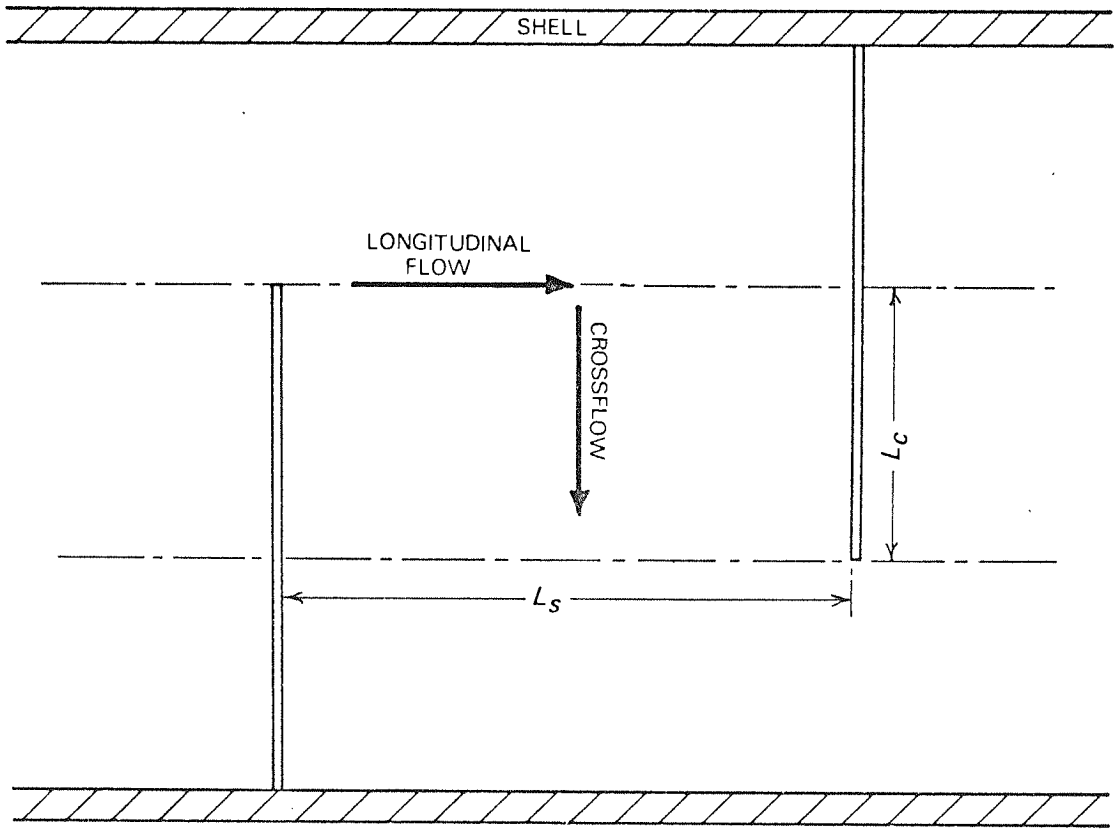

FIG 84 CROSSFLOW ZONE FLOW COMPONENTS

For small values of L_C/L_S, the flow in the crossflow zone would approach longitudinal flow. Values of L_C/L_S were calculated for the six baffle arrangements. These values are tabulated in Appendix 3.3.3.

Re-examination of the crossflow zone data in Fig. 80 revealed that the four sets of data showing good correlation were from baffle arrangements having values for L_C/L_S of less than unity. The short baffle spacing data at the 18.4 and 25.0 per cent baffle cuts had values for L_C/L_S of 1.78 and 1.48 respectively. This feature is better illustrated in Fig. 85. For values of L_C/L_S less than around unity, the crossflow zone average j-factor (based on the crossflow area A_M) is independent of L_C/L_S. For values of L_C/L_S greater than around unity the crossflow j-factor increases with L_C/L_S. Similar characteristics were exhibited at both high and low values of Reynolds numbers.

Fig. 85 indicates that for baffle arrangements having L_C/L_S less than unity, the baffle window dimensions need not be taken into account when predicting the crossflow zone average j-factor. This suggests that the longitudinal flow component is substantially constant in these cases. At values of L_C/L_S greater than around unity the crossflow zone j-factor is a function of both the baffle spacing and the baffle cut. No simple expression has been found in this work to correlate the crossflow zone data for these two effects. There being only two baffle arrangements with L_C/L_S greater than unity, restricts an empirical analysis of these particular data.

TEMA (2) recommends that the baffle spacing be not less than 20 per cent of the shell inside diameter. For the typical commercial baffle cut of 25 per cent, this would correspond to a maximum value of 2.5 for L_C/L_S. However it is common practice in heat exchanger design to use baffle spacings of similar magnitude to the shell ID.

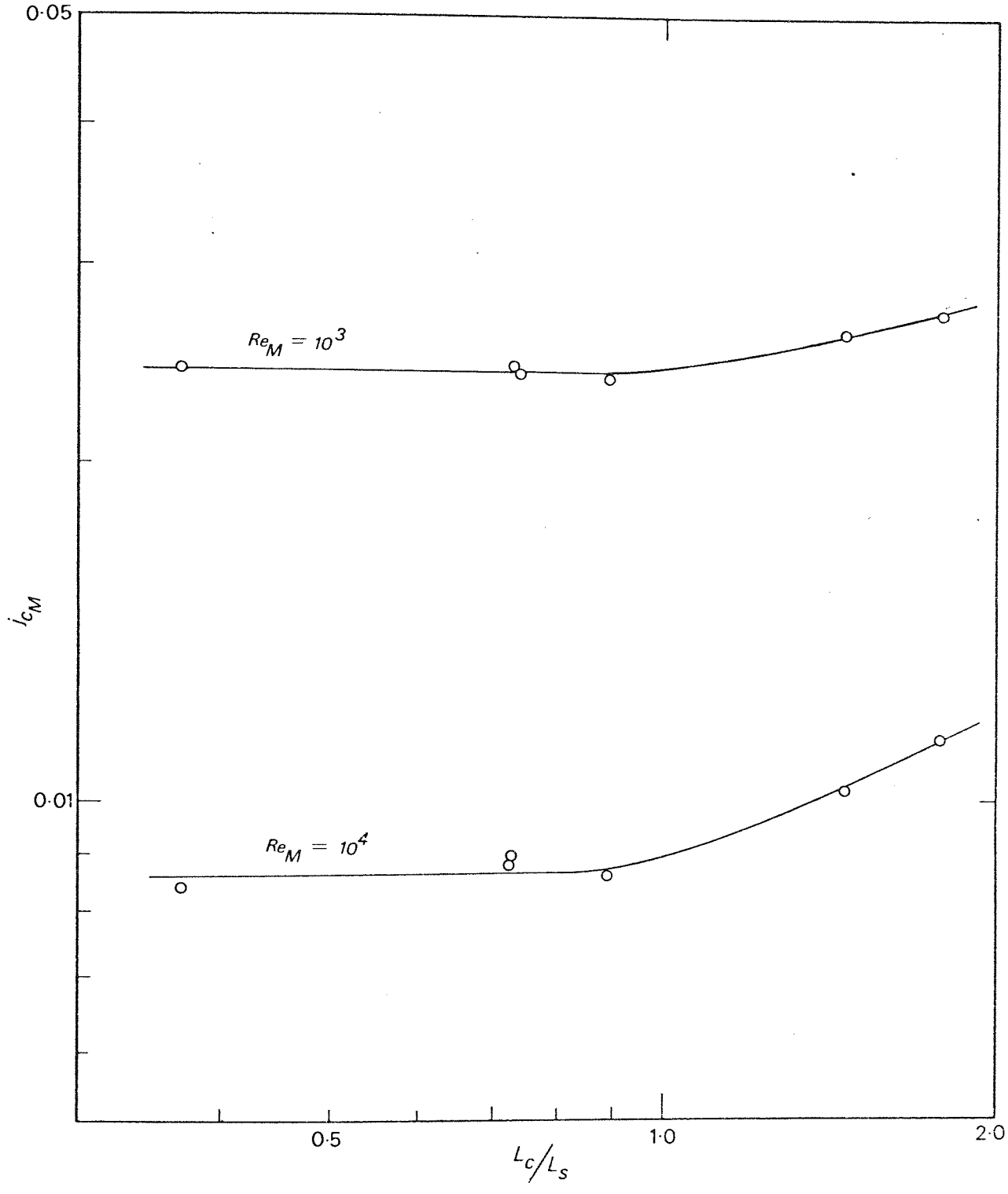

FIG 85 EFFECT OF L_c/L_s ON CROSSFLOW ZONE COEFFICIENTS

This gives a value for L_C/L_S of 0.5 at a 25 per cent baffle cut. The correlation of the crossflow zone j-factor data in Fig. 80 for baffle arrangements with L_C/L_S less than unity, would thus have wide commercial application.

The crossflow zone data of this work were compared with data from ideal tube-banks. The two baffle arrangements chosen for the comparison were those having an 18.4 per cent baffle cut at the short baffle spacing and a 37.5 per cent cut at the long spacing. These baffle arrangements had extreme values of L_C/L_S (viz. 1.78 and 0.37) and had shown the highest and lowest crossflow zone j-factors respectively.

In Fig. 86 these data are compared with the ideal tube-bank data of Bergelin et al. (11) and the Grimison (4) correlation (see Section 1.2). The Bergelin data were compiled in two separate investigations using the same equipment but with different oils as the shell-side fluid. The data from the experiments confined to the lower Reynolds numbers are tabulated in (18) and the other data in (120). Bergelin gave no explanation for the discrepancy between the two sets of data at the low Reynolds numbers.

The short baffle spacing, 18.4 per cent baffle cut, crossflow zone data, show good agreement with the Bergelin data. At the lower Reynolds numbers the data follow the curve of the Bergelin data obtained using the more viscous oil. At the high Reynolds numbers the data fall above the Grimison correlation and show a smaller slope. This could be attributed to fluid jetting which has been shown to be more significant at higher flow rates (see Section 6.3.2). The long baffle spacing, 37.5 per cent baffle cut data, fall well below the Bergelin data in the intermediate Reynolds number range but show good agreement with the viscous oil Bergelin data at the low Reynolds numbers. The data fall below the Grimison correlation. The short

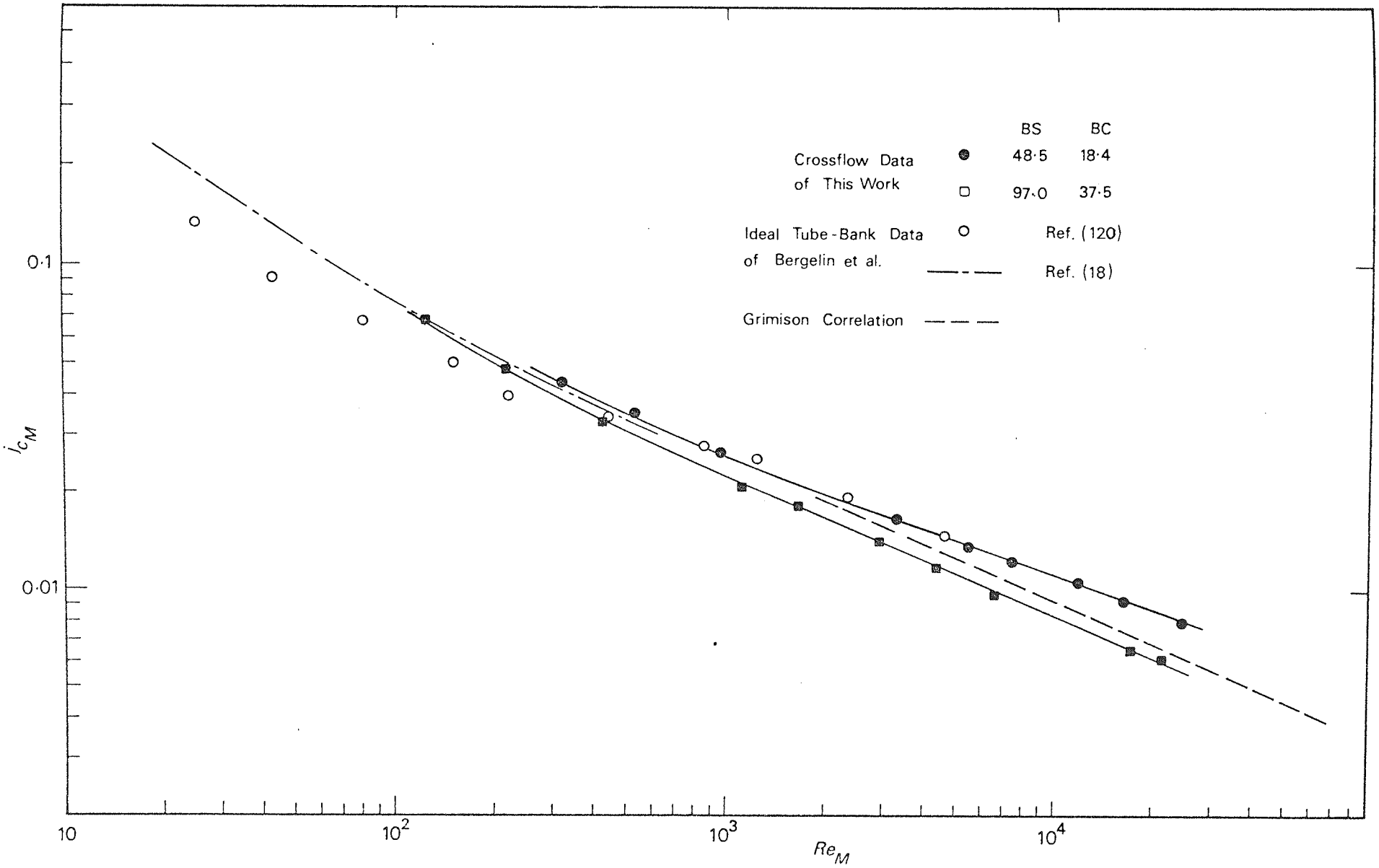

FIG 86 COMPARISON WITH IDEAL TUBE—BANK DATA

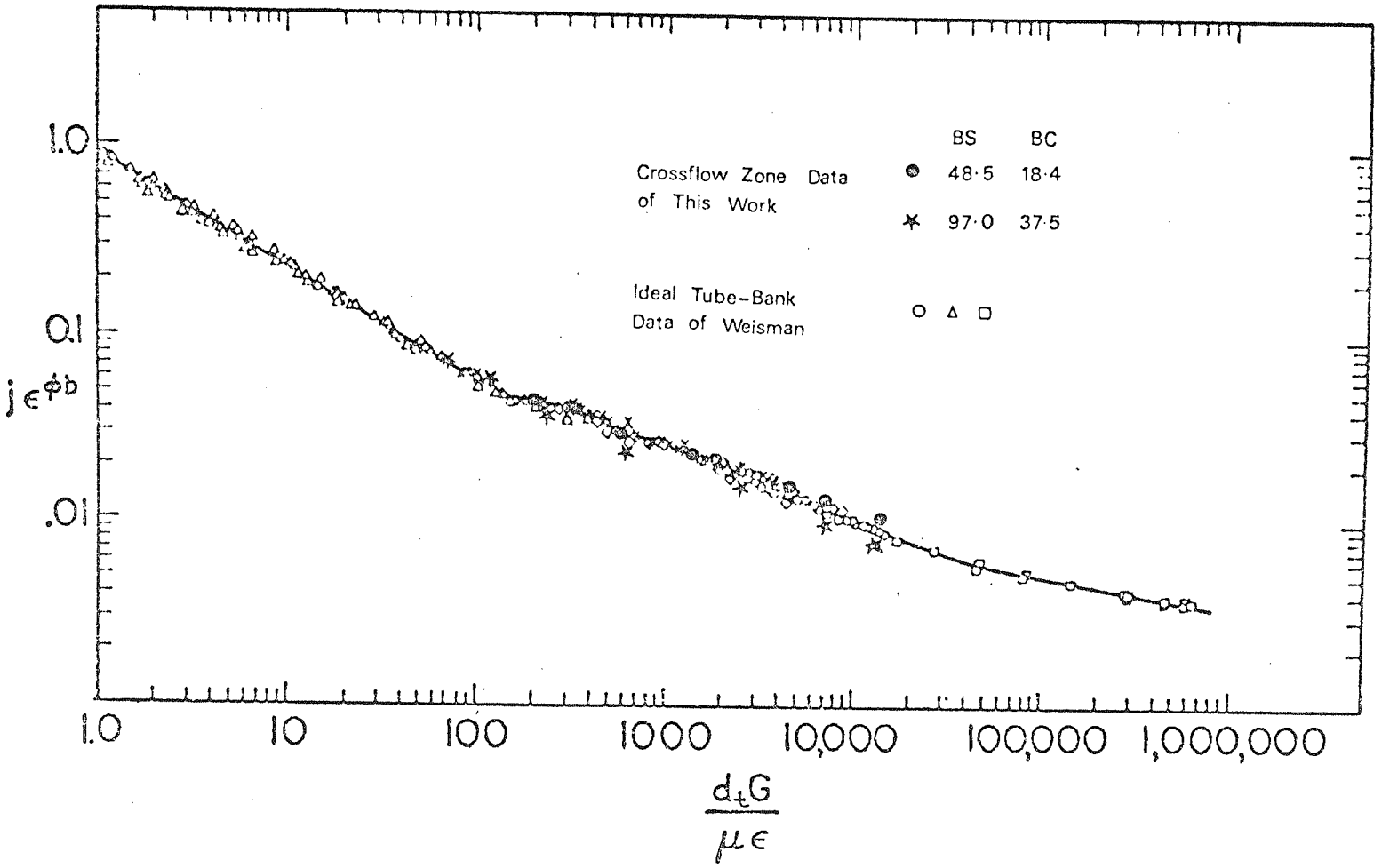

FIG 87 COMPARISON WITH IDEAL TUBE-BANK DATA

baffle spacing, 18.4 per cent baffle cut arrangement, would seem to be most representative of an ideal tube-bank.

The crossflow zone data were correlated in the form recommended by Weisman (14), (see Section 1.2). In Fig. 87 these data are compared with ideal tube-bank data compiled and correlated by Weisman. The short baffle spacing, 18.4 per cent baffle cut data, show good agreement with the ideal tube-bank data for Reynolds numbers (Re_ε) up to 2 000. This corresponds to a value of 3 500 for Re_M. At higher Reynolds numbers the data fall up to 20 per cent above the ideal tube-bank data. The long baffle spacing, 37.5 per cent baffle cut data generally fall below the ideal tube-bank data. There is however good agreement at the very low Reynolds numbers. This method of correlating the crossflow zone data shows no improvement over that based on the crossflow area, A_M in Fig. 80.

6.6 WINDOW ZONE AVERAGE j-FACTORS

The mass or heat transfer coefficients in the window zones are not always inferior to those in the crossflow zone. The analyses of individual tube coefficients in Section 6.3.2, revealed that the baffle geometry has a substantial effect on the distribution of the shell-side flow. The ratio of the crossflow area to the window flow area, A_M/A_W, was shown to characterise these features. While values of A_M/A_W near unity gave high crossflow but low window zone j-factors, the fluid jetting associated with high values of A_M/A_W produced highest j-factors in the inlet window zone. These characteristics are reflected in the zonal average j-factors. Figs. 88 and 89 illustrate this for two extreme baffle arrangements having values for A_M/A_W of 0.65 and 3.45 respectively.

The variation in the shell-side flow distribution with baffle geometry, may be illustrated by the ratio of the average j-factor in the inlet window zone to that in the outlet window zone. This is

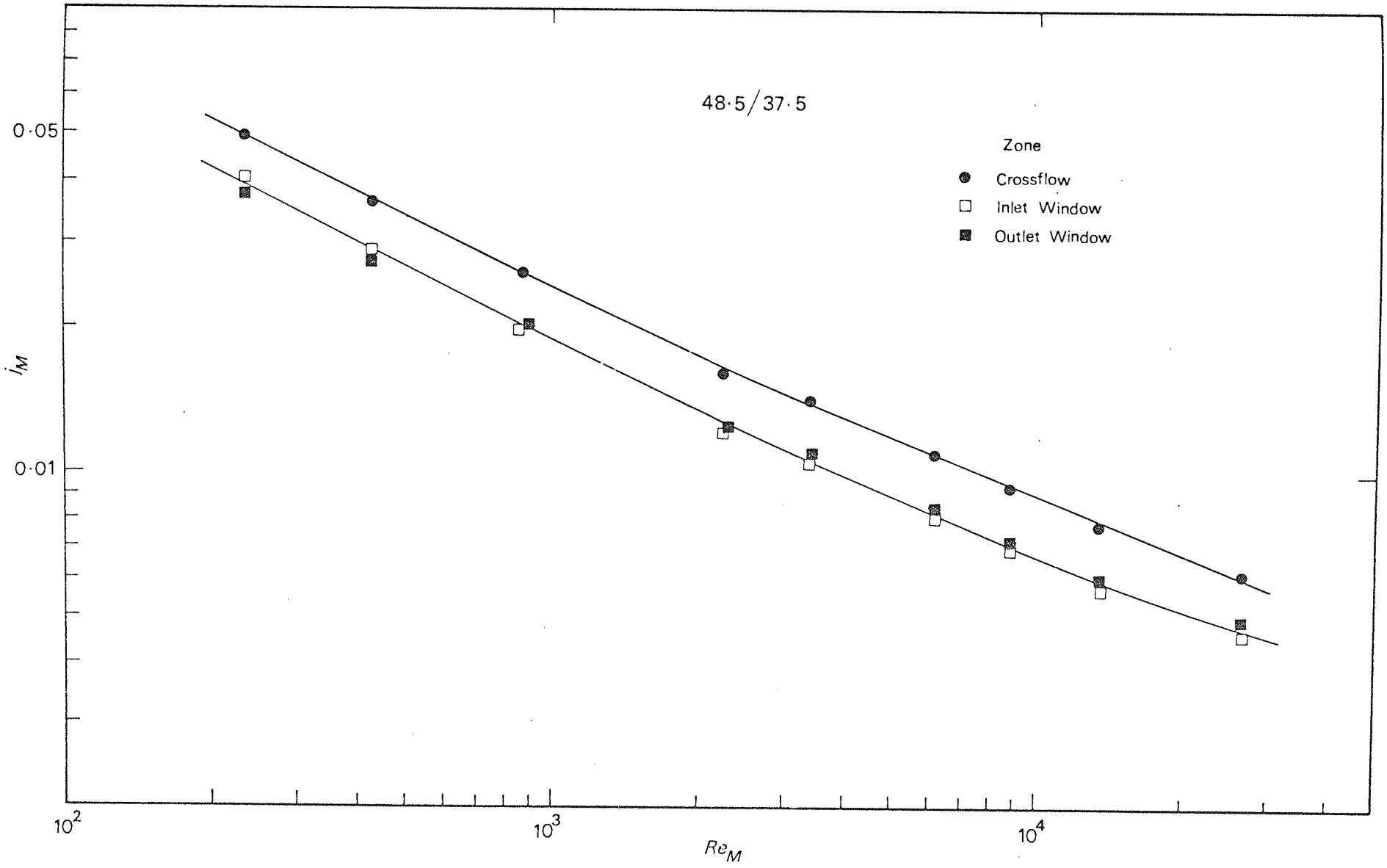

FIG 88 ZONAL AVERAGES

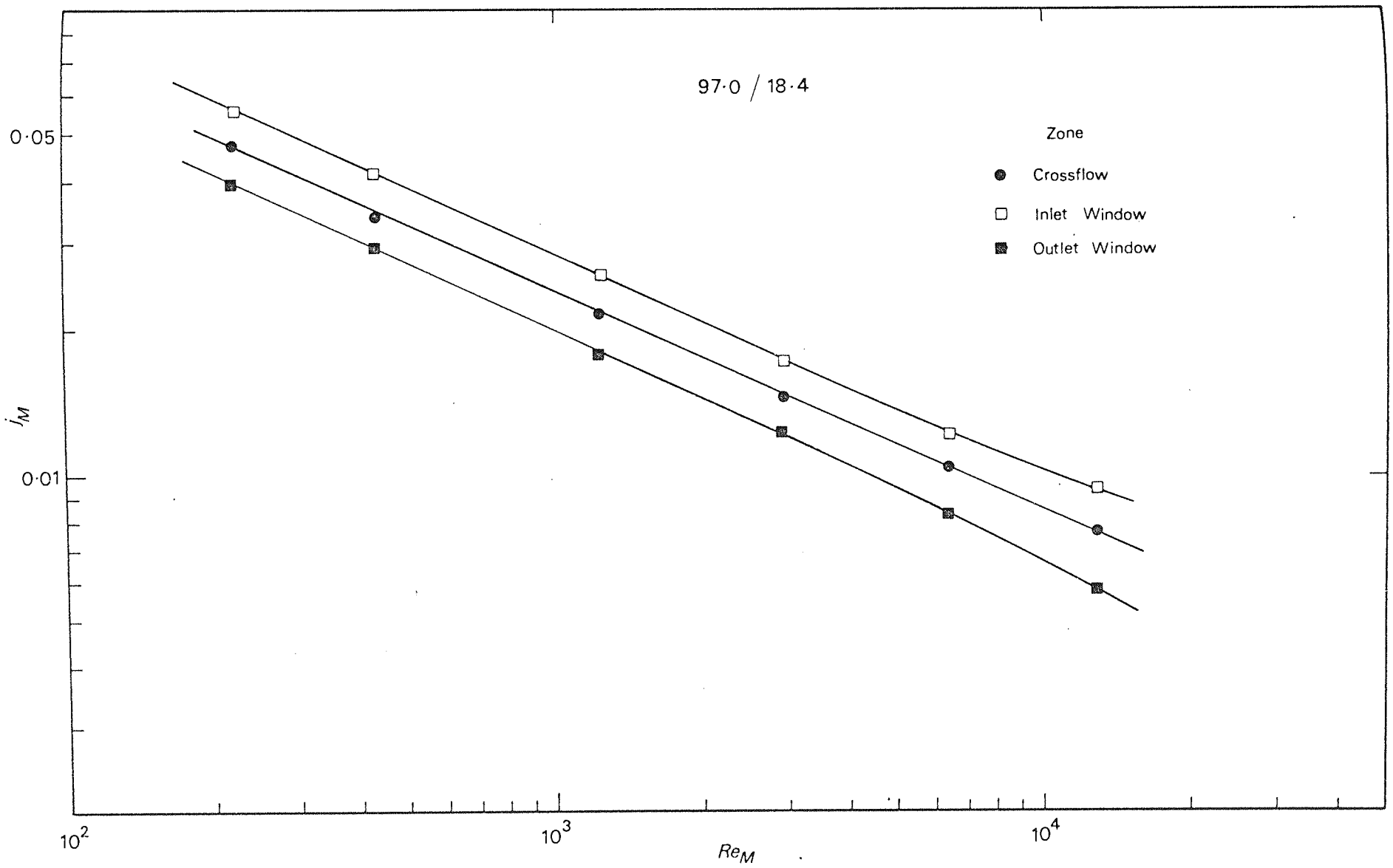

FIG 89 ZONAL AVERAGES

demonstrated for the six baffle arrangements in Fig. 90. All the data at both baffle spacings converge at a value for A_M/A_W of around 1.0. This represents a baffle geometry having a fairly uniform flow area and in consequence negligible fluid jetting. Fig. 90 shows the corresponding value of the ratio of the window zone j-factors to be also near unity. Fluid jetting would occur in the baffle window for baffle arrangements with A_M/A_W greater than 1.0 while in the crossflow zone for arrangements with A_M/A_W less than 1.0. The resulting flow distributions are shown in Fig. 74. Relatively higher coefficients would be expected in the inlet and outlet window zones for the two respective cases. This is shown in Fig. 90.

In the analysis of shell-side heat transfer, the window zone is normally defined as the region contained between alternate baffles and enclosed by the shell wall and a plane parallel to the tubes through the baffle edge. In the absence of baffle leakage the flow patterns in two consecutive baffle compartments are inverted with respect to one another. Hence a window zone average j-factor is obtained from the arithmetic average of the j-factors of the inlet and outlet window zones of a single baffle compartment.

The window zone j-factor data for the six baffle arrangements are shown plotted in Fig. 91. The characteristic velocity was based on the crossflow area A_M. The sets of data show considerable spread. However there is close similarity between some sets of data. The 37.5 per cent baffle cut data at the two baffle spacings show good agreement. Both sets of data at the 25.0 per cent baffle cut and those of the 18.4 per cent cut at the long baffle spacing all fall close to each other. The baffle arrangements in neither of these cases, show similarity in their values of A_M/A_W nor L_C/L_S.

In the window zone, a more characteristic velocity would be that based on the free flow area A_W. The window zone j-factor data

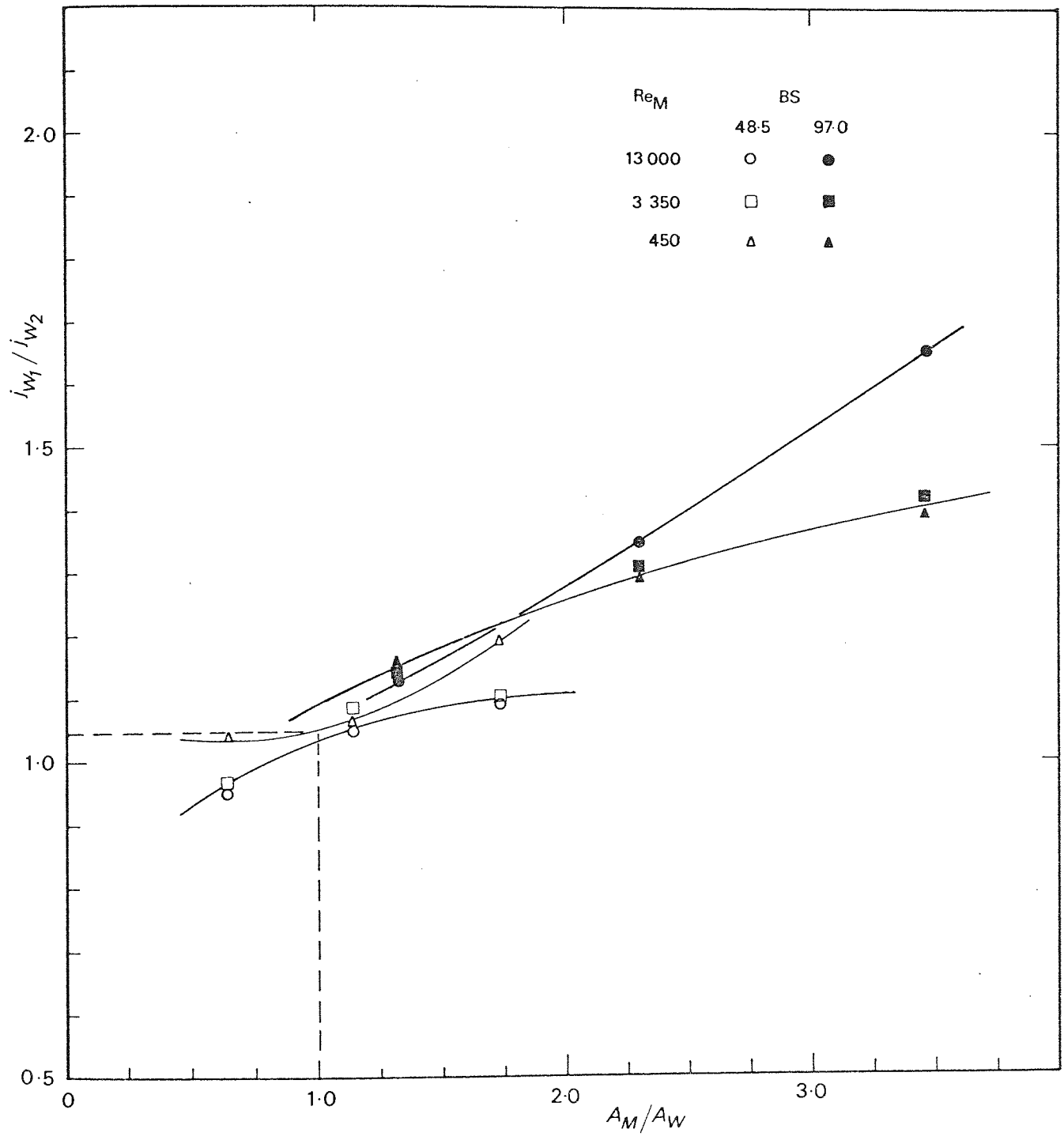

FIG 90 WINDOW ZONE CHARACTERISTICS

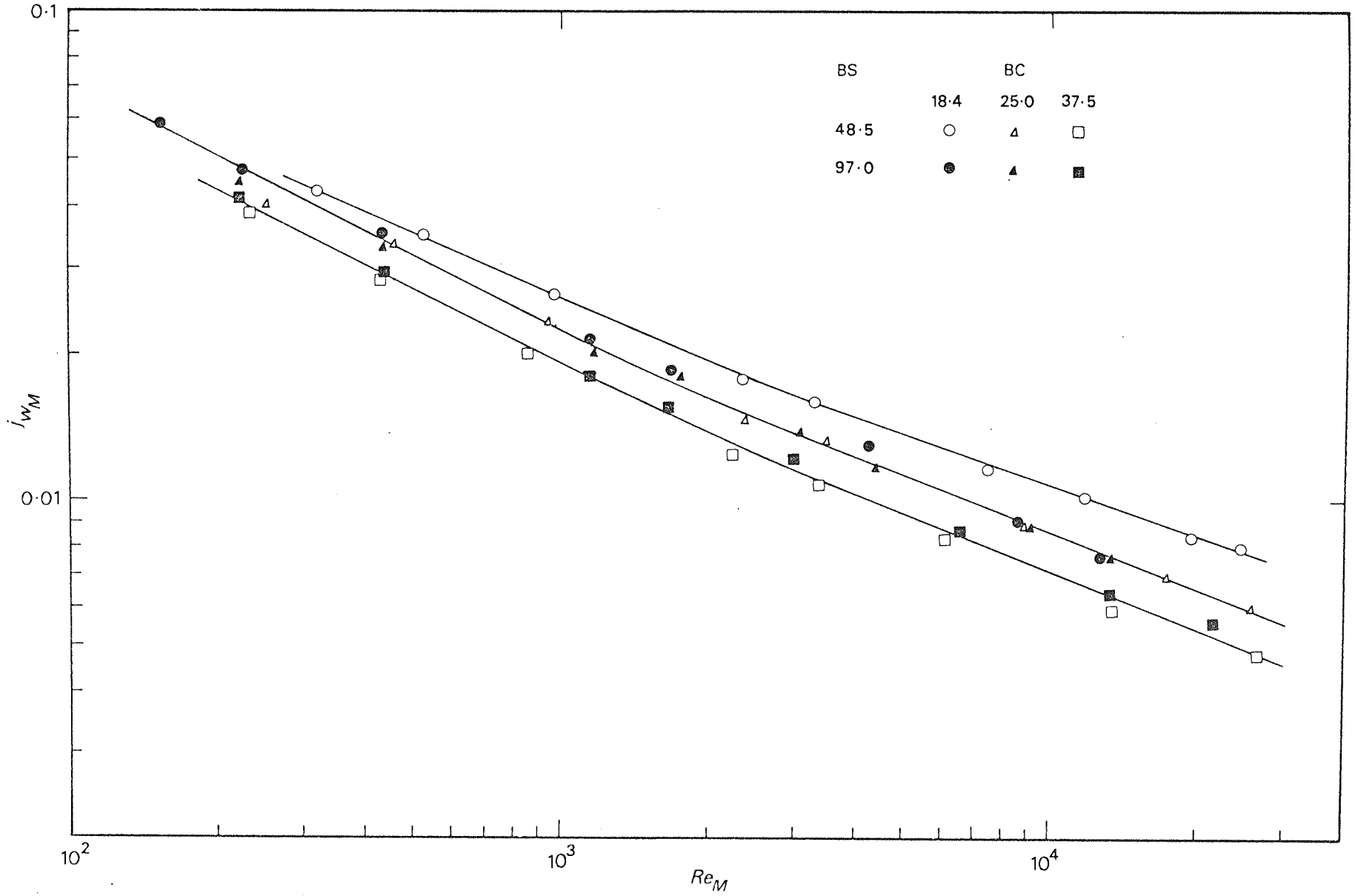

FIG 91 *WINDOW ZONAL AVERAGES*

were analysed in this way and are shown in Fig. 92. The data at the short baffle spacing show correlation to within ± 15 per cent. However the separation of the curves of the data at the long baffle spacing is now substantially greater. Moreover the order of these curves is reversed with the largest baffle cut giving the highest j-factors. Williams (32) observed this same feature when plotting his window zone data in this manner. The reversal indicates that a value of velocity between that in the baffle window and the crossflow zone may reduce the separation.

Williams (32) was able to correlate his window zone j-factor data using the weighted characteristic velocity proposed by Donohue (20). A slightly modified version of this velocity was used in Sections 6.4 and 6.5. The window zone data are analysed in this way in Fig. 93. The data from the two baffle spacings fall onto separate curves. The effect of baffle cut is correlated to within ± 10 per cent for the long baffle spacing but only ± 15 per cent for the short spacing. The short baffle spacing data lie between 15 and 40 per cent above those for the long baffle spacing. The separation is greatest at the higher Reynolds numbers. The investigations of Williams were confined to a single baffle spacing.

An attempt was made to correlate the window zone data in the form recommended by Weisman (14) for ideal tube-banks. The data from the two extreme baffle arrangements are shown plotted in this form in Fig. 94. The data for the 37.5 per cent baffle cut at the long spacing fell around 40 per cent below those of the 18.4 per cent cut at the short spacing. This was no improvement on the other methods of correlation.

No characteristic velocity has been found that adequately correlates the effect of baffle geometry on window zone average j-factors.

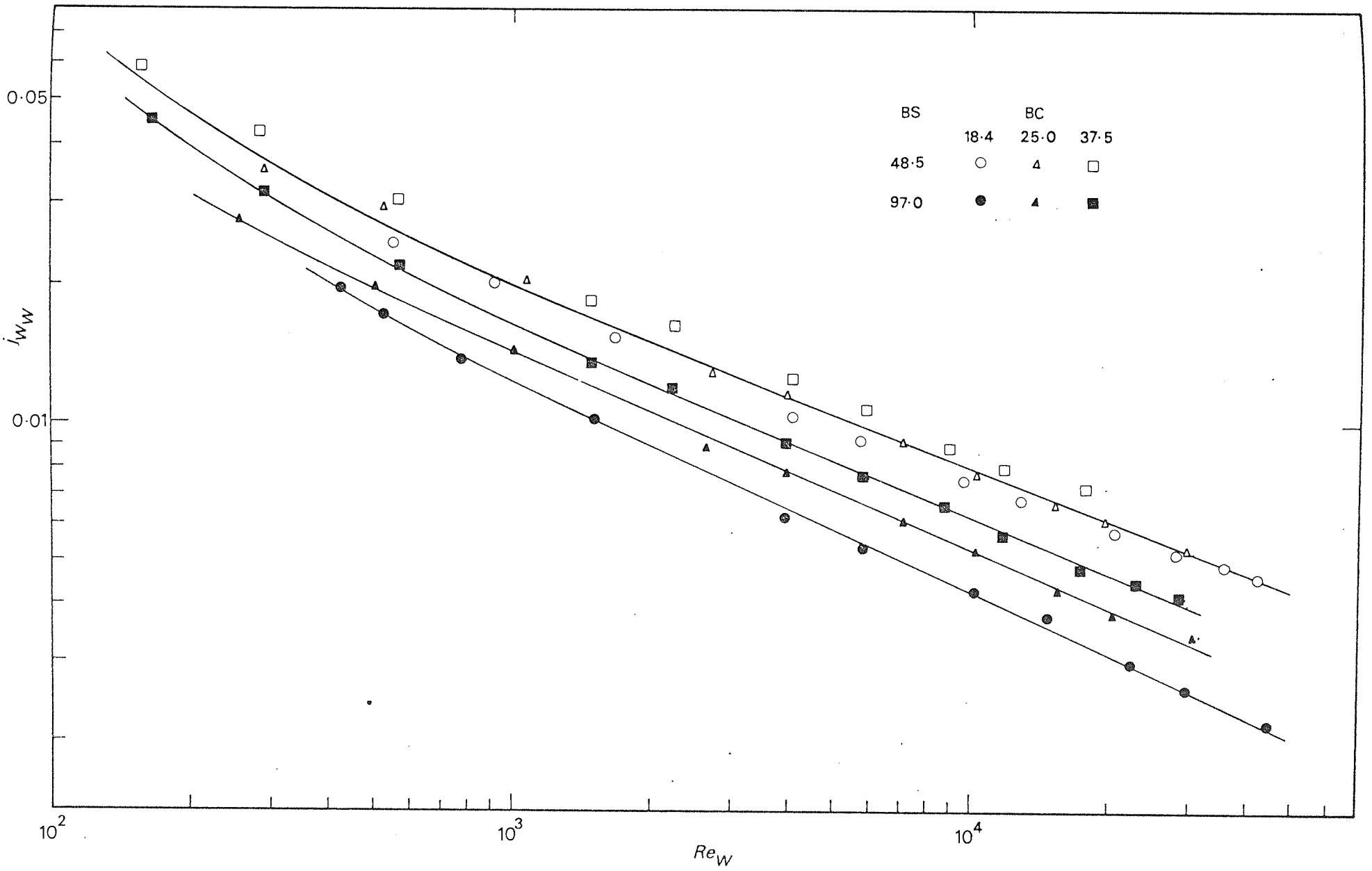

FIG 92 *WINDOW ZONE AVERAGES*

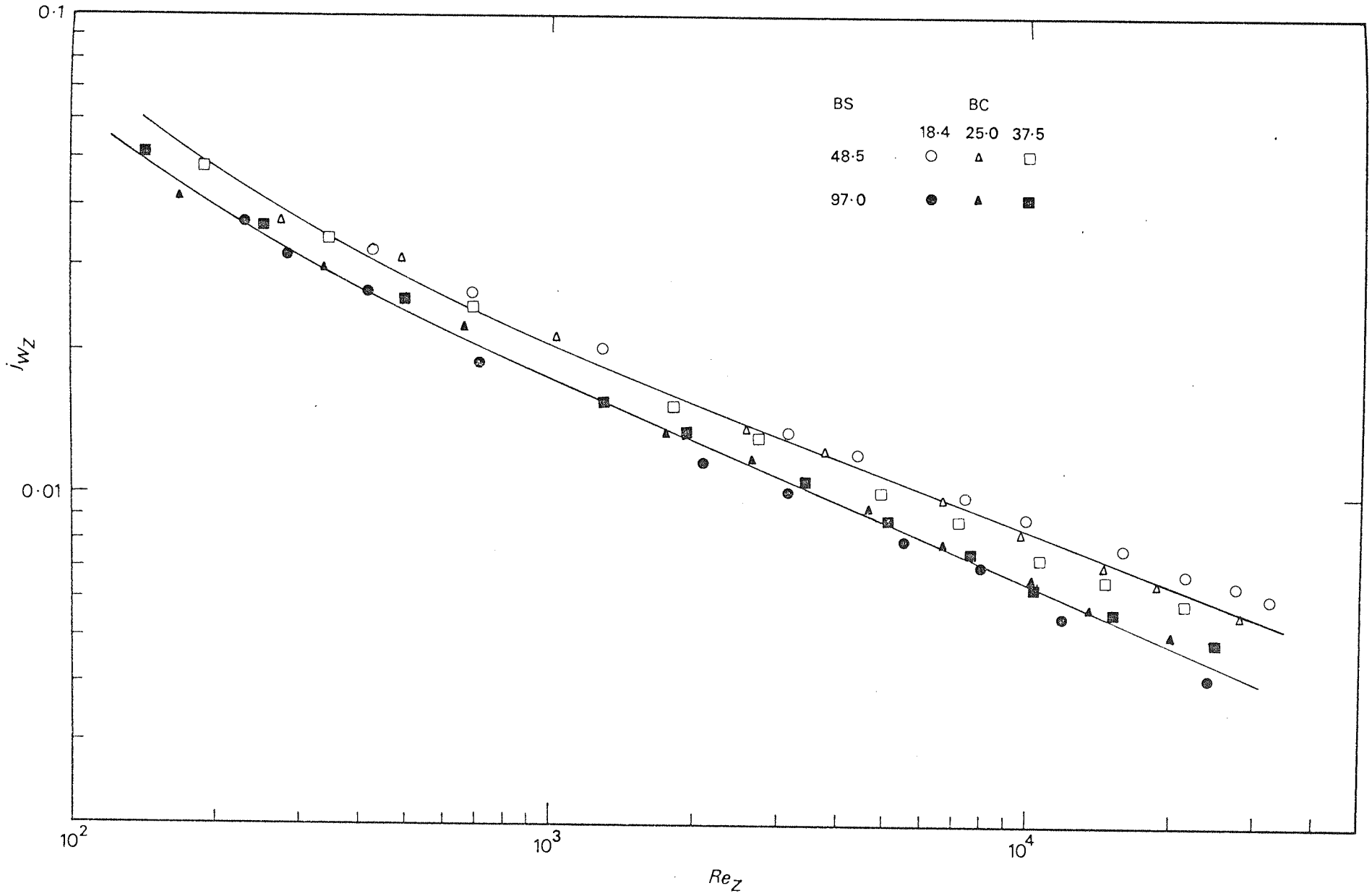

FIG 93 WINDOW ZONAL AVERAGES

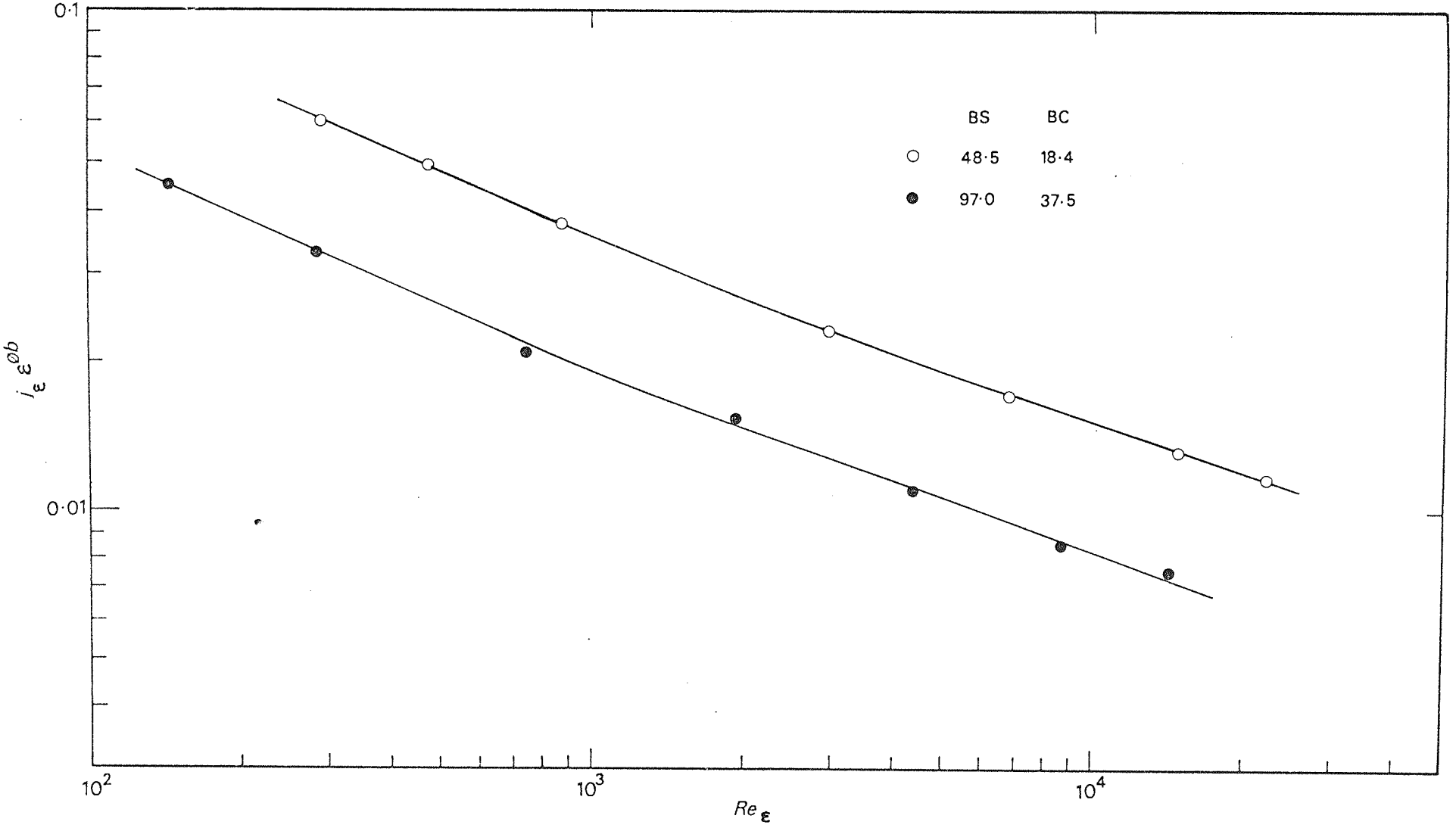

FIG 94 *WINDOW ZONAL AVERAGES*

Individual analyses of the zonal average data have shown no general improvement on the correlation of the shell-side data in terms of baffle compartment average values.

Investigations at other baffle spacings would allow a more detailed analysis of the effect of this geometrical parameter.

6.7 CONCLUSIONS

The results from the no-leakage single segmental baffle investigations are now summarised:-

(i) Distributions of tube j-factors through a baffle compartment have indicated a substantial variation in shell-side flow characteristics with baffle geometry. Fluid "jetting" has been identified with some baffle configurations.

(ii) Little variation was shown in the slopes of individual tube j-factor correlations, suggesting similar flow characteristics throughout the bundle. The true flow characteristics may have been distorted by eddy flow and flow redistributions.

(iii) No simple characteristic velocity was found which could adequately correlate baffle compartment average mass transfer data for the effect of both baffle spacing and baffle cut. Analyses of the crossflow and window zone average data resulted in similar conclusions. However for baffle arrangements having the ratio L_C/L_S less than unity, it was shown that the crossflow zone average data could be correlated in terms of a characteristic velocity based on the crossflow area A_M.

(iv) The crossflow zone average data for the short spacing, 18.4 per cent cut, baffle configuration have shown good agreement with data from ideal tube-banks.

7. SINGLE SEGMENTAL BAFFLES WITH LEAKAGE

7.1 SCOPE OF EXPERIMENTS

The baffles used in these experiments had clearances between the baffle holes and the tubes and between the baffle periphery and the shell wall.

The baffle clearances were typical of those encountered in commercial shell and tube heat exchangers. The baffle clearances recommended by TEMA (2) and British Standard 3274 (formerly BS 2041) were examined in terms of the orifice shape factor used by Bergelin et al. (34) defined by:-

$$Z = \frac{2 \times \text{BAFFLE PLATE THICKNESS}}{\text{DIAMETRICAL CLEARANCE}} \qquad \ldots\ldots (7.1)$$

The details of this examination are given in Appendix 3.3.6. For tube-to-baffle clearance, the value of the shape factor Z_T was found generally to be 8.0. The corresponding shape factor Z_S for shell-to-baffle clearance had an average value of 2.50. The baffles used in the exchanger model had nominal thicknesses of 1/16 and $\frac{1}{8}$ in. (1.59 and 3.18 mm). The corresponding baffle clearances were derived from the recommended values of the orifice shape factors. The nominal and actual baffle clearances are given in the table below. The units are in inches, the units of the micrometer used.

	Shell ID	Baffle Thickness	Baffle Clearances (diametrical) S-B	T-B	Orifice Shape Factor Z_S	Z_T
Nominally	5.250	0.125	0.100	0.031	2.50	8.0
	5.250	0.063	0.050	0.016	2.50	8.0
Actual	5.252	0.122	0.105	0.026	2.32	9.38
	5.252	0.064	0.055	0.013	2.33	9.85

The tubes were allowed to lie on the bottom of the baffle holes and similarly for the baffles in the shell. The eccentric baffle clearances would be typical of those in commercial heat exchangers.

The baffle leakage investigations were confined to a baffle spacing of 1.91 in. (48.5 mm). Studies were made with the shell-side flow weaving up and down through the bundle and with it weaving from side-to-side. For the former flow configuration the baffles were arranged with the windows at the top and bottom of the bundle as shown in Fig. 95. Side-to-side flow was produced by rotating the bundle through ninety degrees. Baffles of both thicknesses with an 18.4 per cent cut were used with the up-and-down flow configuration. The thicker baffles at three cuts were used in the case of the side-to-side flow.

The baffle clearances were found to reduce the rigidity of the 1/16 in. (1.59 mm) thick baffles. In consequence their use was limited to few investigations.

Measurements of mass transfer coefficients were confined to the fifth of nine baffle compartments. In the case of flow up and down through the bundle a complete flow cycle spanned two baffle compartments (see Fig. 95). Measurements were required in two baffle compartments, one with the flow entering at the top and the other with the flow entering at the bottom. The latter configuration was obtained from the former by simply rotating the tube bundle through 180 degrees.

Pressure measurements were made in the fourth, fifth and sixth baffle compartments.

The mass transfer data were expressed in j-factor form using a pseudo no-leakage characteristic velocity based on the crossflow area A_H. The use of a no-leakage characteristic crossflow velocity with leakage data is not strictly justified, for the leakage streams deprive the crossflow stream of fluid. This arbitrary characteristic

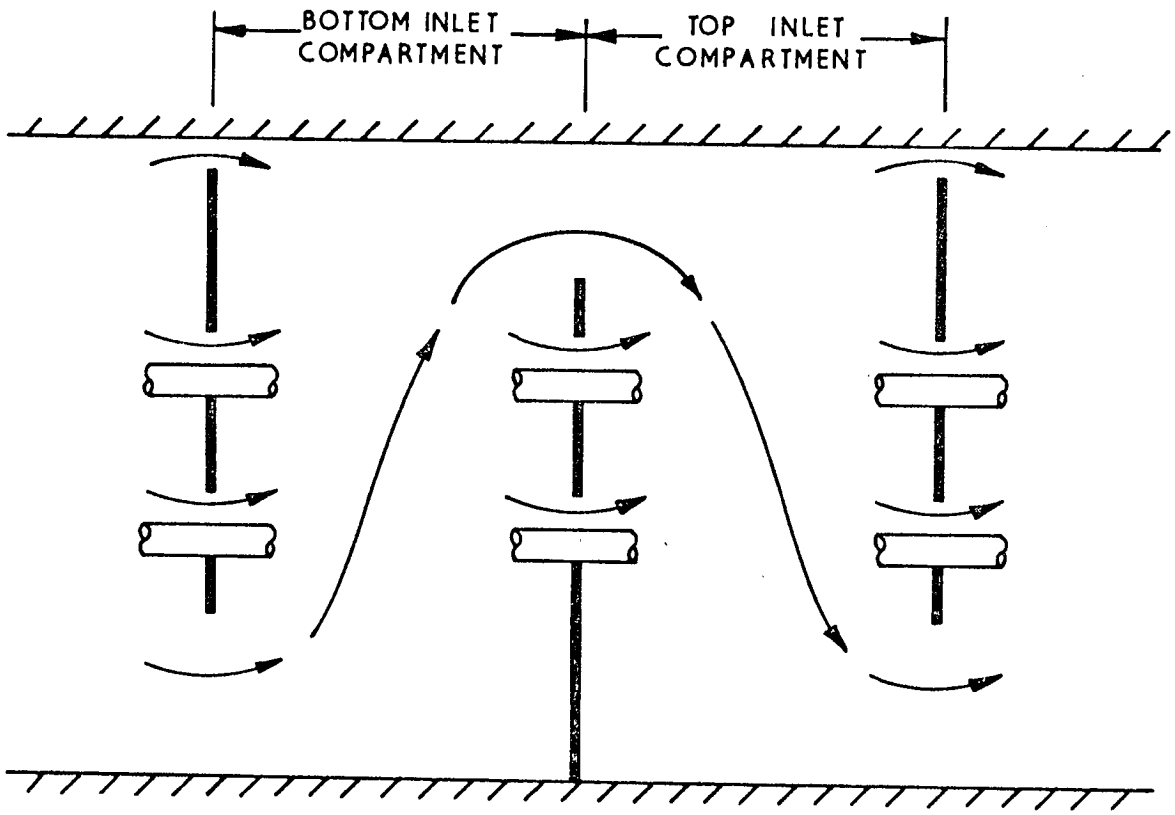

FIG. 95. FLOW CHARACTERISTICS WITH BAFFLE LEAKAGE

velocity does however provide a method of correlating leakage data for a constant baffle spacing in terms of the total shell-side flow rate.

7.2 GENERAL CHARACTERISTICS

This section examines the results of the investigations with the flow weaving up and down through the bundle. The initial leakage experiments were performed with this particular flow configuration as its symmetry about a vertical diameter afforded better identification of the effect of baffle leakage on individual tube and zonal average coefficients.

7.2.1 Compartment Average j-Factors

Compartment average j-factors for the two baffle thicknesses and an 18.4 per cent baffle cut are shown in Fig. 96. The average j-factors for the top and bottom flow inlet compartments (see Fig. 95) are given in each case. The corresponding no-leakage data are also shown.

The presence of leakage is shown to produce a substantial reduction in the baffle compartment average j-factor. In the worst case the leakage data fell 60 per cent below the no-leakage data. These inferior coefficients may be attributed to the general redistribution of the shell-side flow resulting in a greater proportion of longitudinal flow.

The effect of leakage is shown to be greater at higher Reynolds numbers. Bergelin et al. (34) showed the effect of leakage on bundle average coefficients to be greater at low Reynolds numbers. This is discussed in Section 7.3.

The thinner baffles gave the least reduction in the j-factors. In the analysis of pressure drop measurements across a single baffle with clearances, Sullivan (35) showed that the discharge coefficient was a function of the orifice

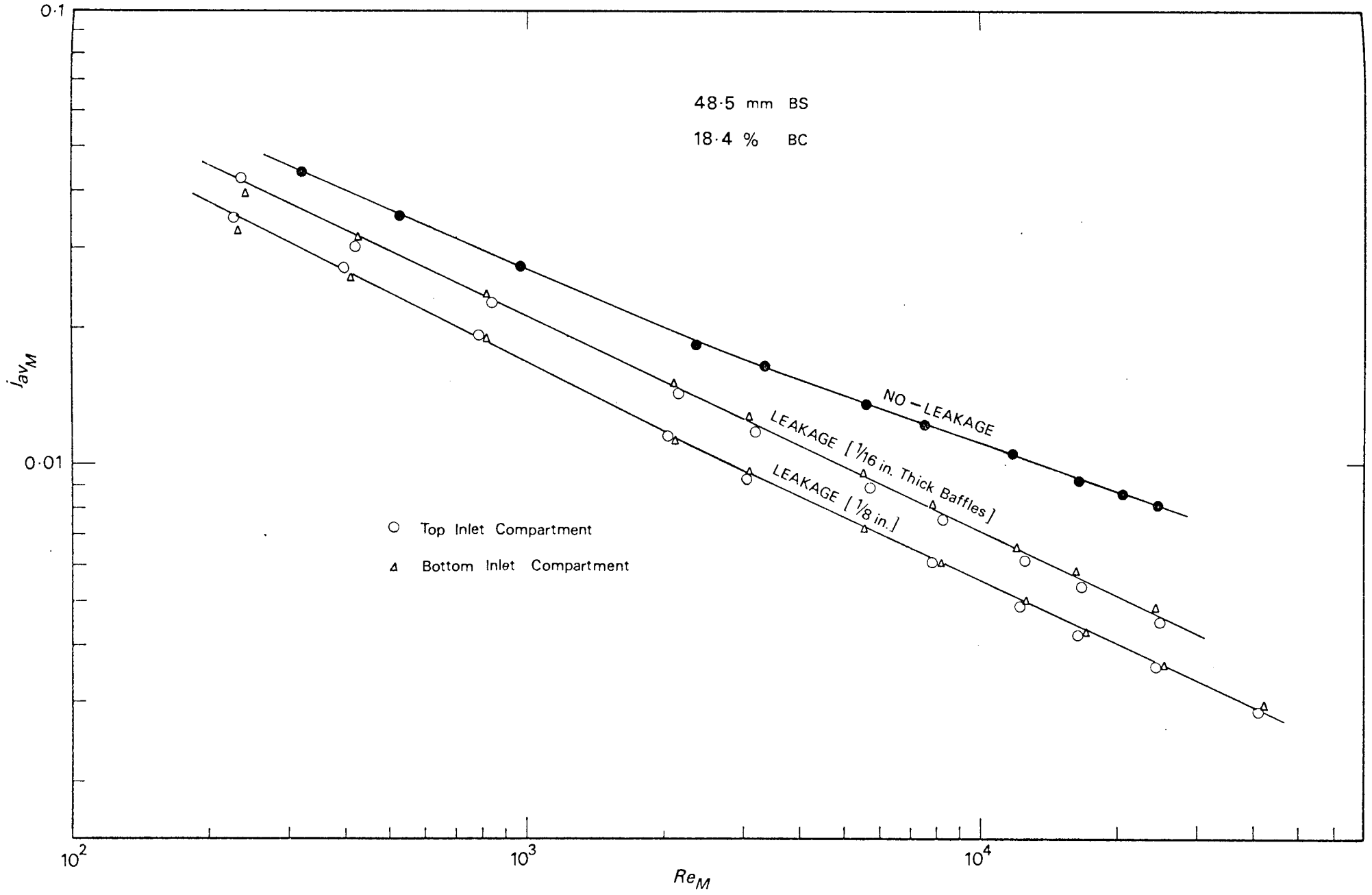

FIG 96 *EFFECT OF LEAKAGE ON COMPARTMENT AVERAGES*

shape factor Z and the orifice Reynolds number. For a given pressure drop the flow through the baffle clearances would be a function of the channel flow area in addition to the two above parameters. The thinner baffles have values of the orifice shape factors similar to those of the thicker baffles but have only about half the leakage channel flow area. The comparison of the j-factor data suggests that the leakage flow with the thicker baffles is the greater, resulting in an inferior mass transfer performance. The relative magnitudes of the leakage flow through the two sets of baffles could be determined only by a detailed analysis of the shell-side pressure drop data. This is the basis of the Stream Analysis prediction method discussed in Section 1.3.3. The experiments with the two sets of leakage baffles were designed to allow the effect of baffle thickness and the orifice shape factor Z on heat transfer and pressure drop to be examined by such an analysis. This is outside the scope of the present work. The leakage studies of Bergelin et al. (34) used baffles of only one thickness.

For both sets of baffles, the j-factors from the two adjacent baffle compartments fall within 10 per cent of each other. The compartment with the fluid entering at the bottom shows the higher coefficients at the higher Reynolds numbers. The reverse is true at the lower Reynolds numbers. This feature is elucidated in the following sections.

7.2.2 Zonal Average j-Factors

Zonal average j-factors are shown for the case of the nominal $\frac{1}{8}$ in. (3.18 mm) thick baffles in Fig. 97. Data are given for the crossflow, inlet window and outlet window zones in the two adjacent baffle compartments.

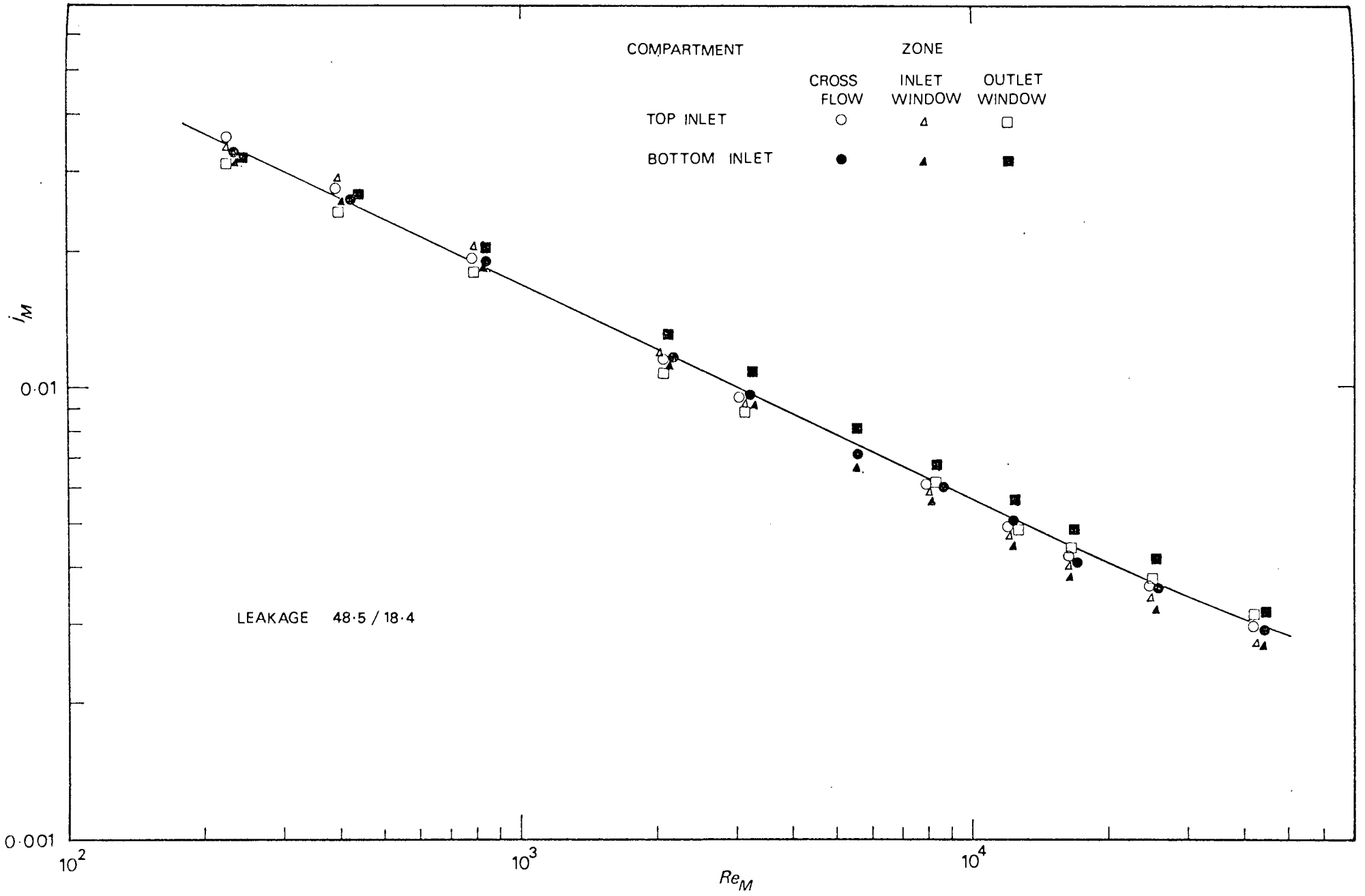

FIG 97 *ZONAL AVERAGES*

The crossflow zone data from the two compartments show close agreement. This suggests that in these compartments, the net upstream and downstream baffle leakages are equal. The highest coefficient is shown in the outlet window zone of the bottom inlet compartment. At the lower Reynolds numbers, the inlet window zone of the adjacent compartment shares this characteristic. These two zones, situated at the top of the bundle would be directly affected by the large leakage stream over the top of the baffles (see Fig. 95). This strong longitudinal flow component would discourage the formation of eddies in the top corner of the baffle compartments. This stream would also make up the fluid lost from the main stream as it passed through the crossflow zone. These combined features would result in the top window zones exhibiting high mass transfer coefficients, superior to those of the crossflow zones.

At the higher Reynolds numbers, the lowest average coefficients are produced by the inlet window zone of the bottom inlet compartment. At the lower Reynolds numbers the outlet window zone of the adjacent compartment shows the lowest coefficient. These two zones are in the region of least shell-to-baffle leakage at the bottom of the bundle. The leakage through the tube-to-baffle clearances may be insufficient to disturb any eddies formed in the corners of these window zones. The alternative flow paths offered by baffle clearances, would reduce fluid jetting in the bundle. These window zones would be expected to reproduce the low coefficients shown by window zones in the absence of baffle leakage and fluid jetting (see Section 6.3.2). The variation with Reynolds number of the window zone giving the lowest coefficients, may be attributed to reproportioning of the flow between the leakage and main streams.

7.2.3 Individual Tube j-Factors

A detailed examination was made of the individual tube j-factor data obtained using the nominal $\frac{1}{8}$ in. (3.18 mm) thick baffles. The data were normalised by dividing the individual tube j-factor by the compartment average value. The distribution of these coefficients for the top inlet baffle compartment are shown over a range of Reynolds numbers in Figs. 98, 99 and 100.

The distributions of the coefficients are shown to be very uniform with very few tubes exhibiting j-factors that do not fall within $\pm$ 10 per cent of the compartment average value. Fig. 98 reveals that at the low Reynolds numbers, the highest j-factors are produced generally in the inlet window zone and the upstream region of the crossflow zone. In the previous section the high j-factors in the inlet window zone were attributed to the large leakage stream over the top of the baffles. It would appear that these effects penetrate into the crossflow zone. The low coefficients in the outlet window zone have already been attributed to the small amount of shell-to-baffle leakage present at the bottom of the bundle.

At the higher Reynolds numbers, substantial redistributions in the tube coefficients are shown to occur (Figs. 99 and 100). The tubes in the inlet window zone are now among those giving the lowest j-factors. Due to its high velocity, the leakage stream over the tops of the baffles may cling to the shell wall without contacting the tube bundle. Thus any beneficial effect from this stream is lost. The coefficients of the remainder of the tubes in the compartment exhibit no distinct distribution characteristics. However with increasing Reynolds numbers, a region of low coefficients is formed across the centre of the

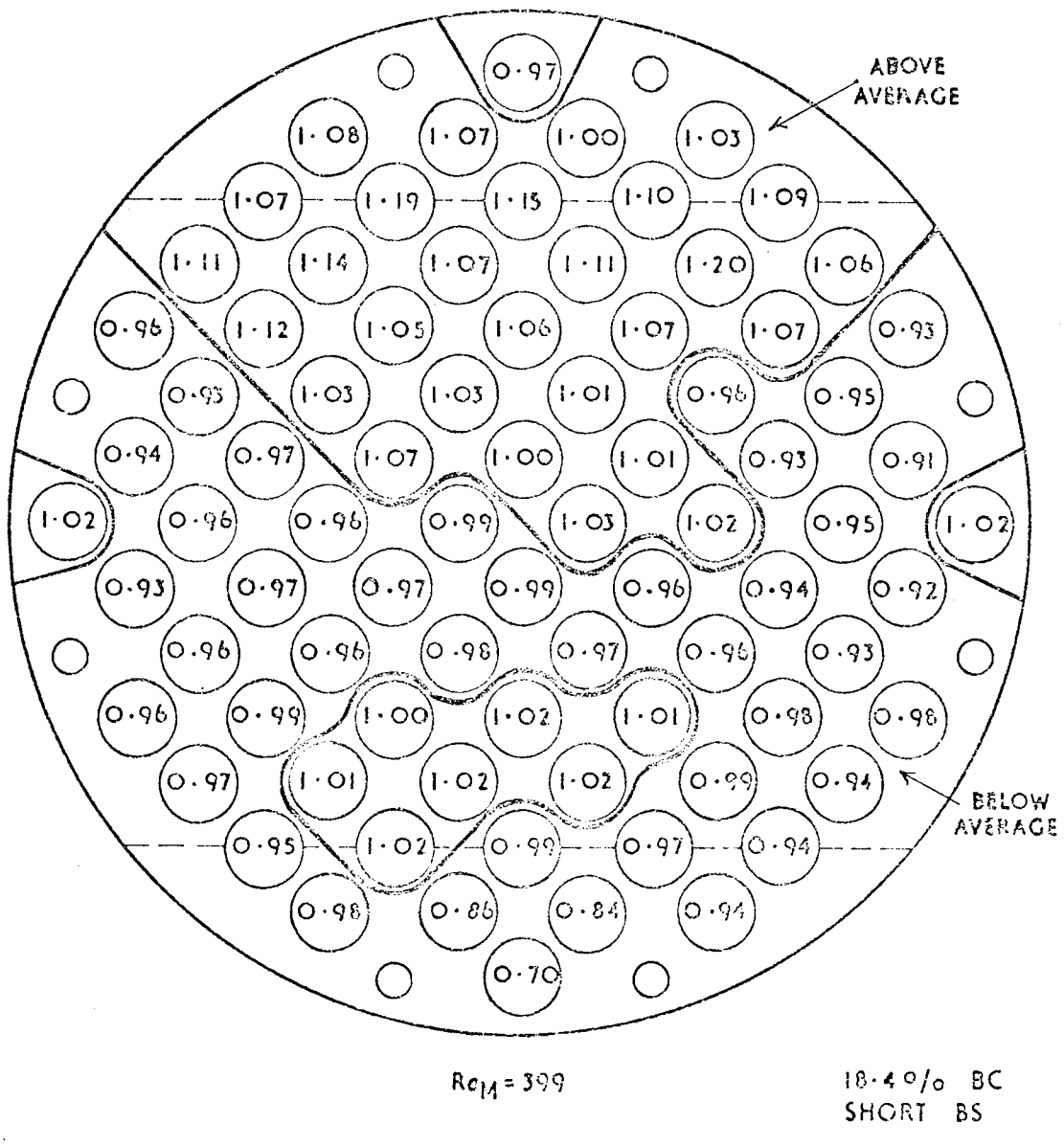

FIG. 98. LEAKAGE

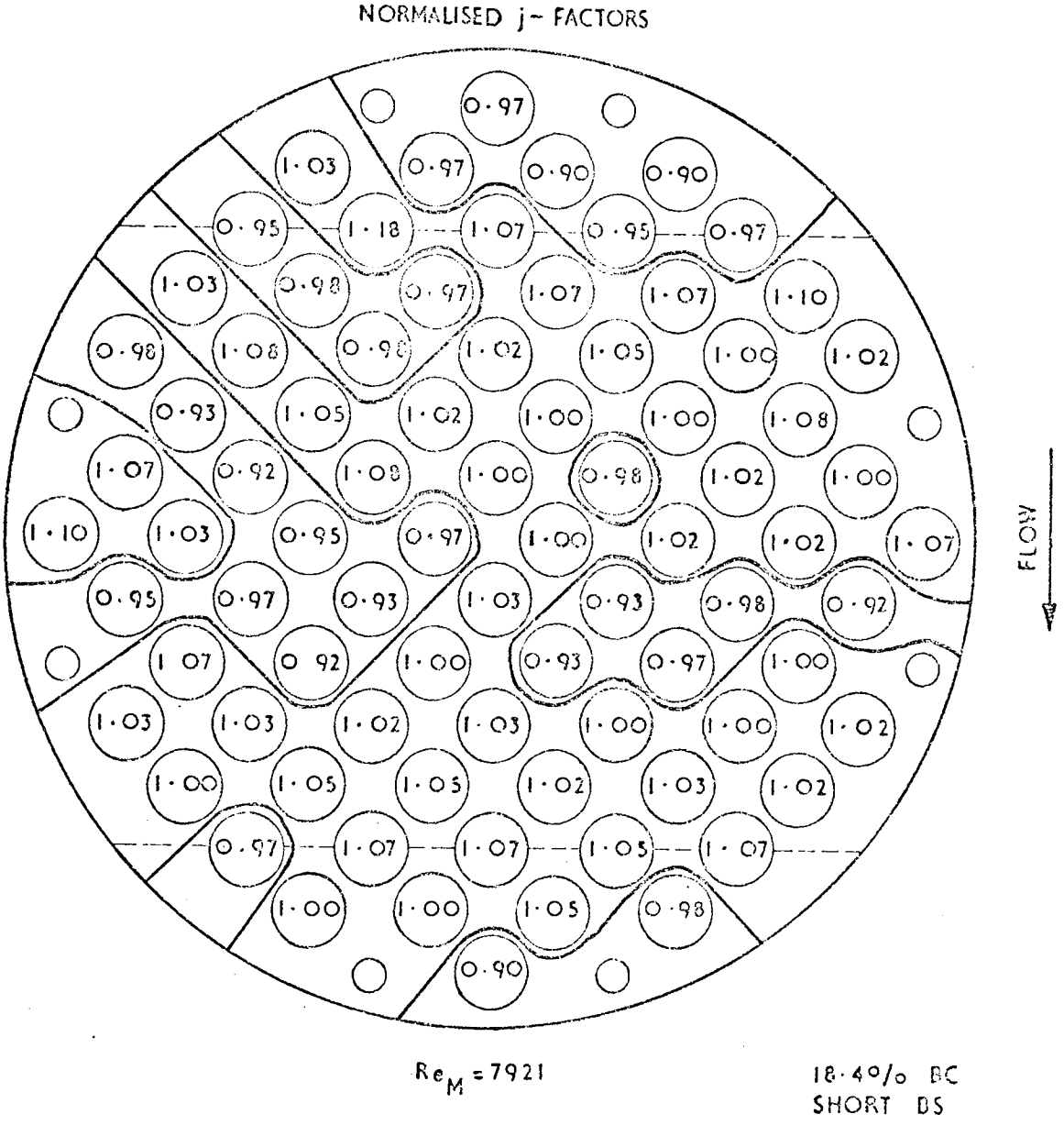

FIG. 99. LEAKAGE

NORMALISED j- FACTORS

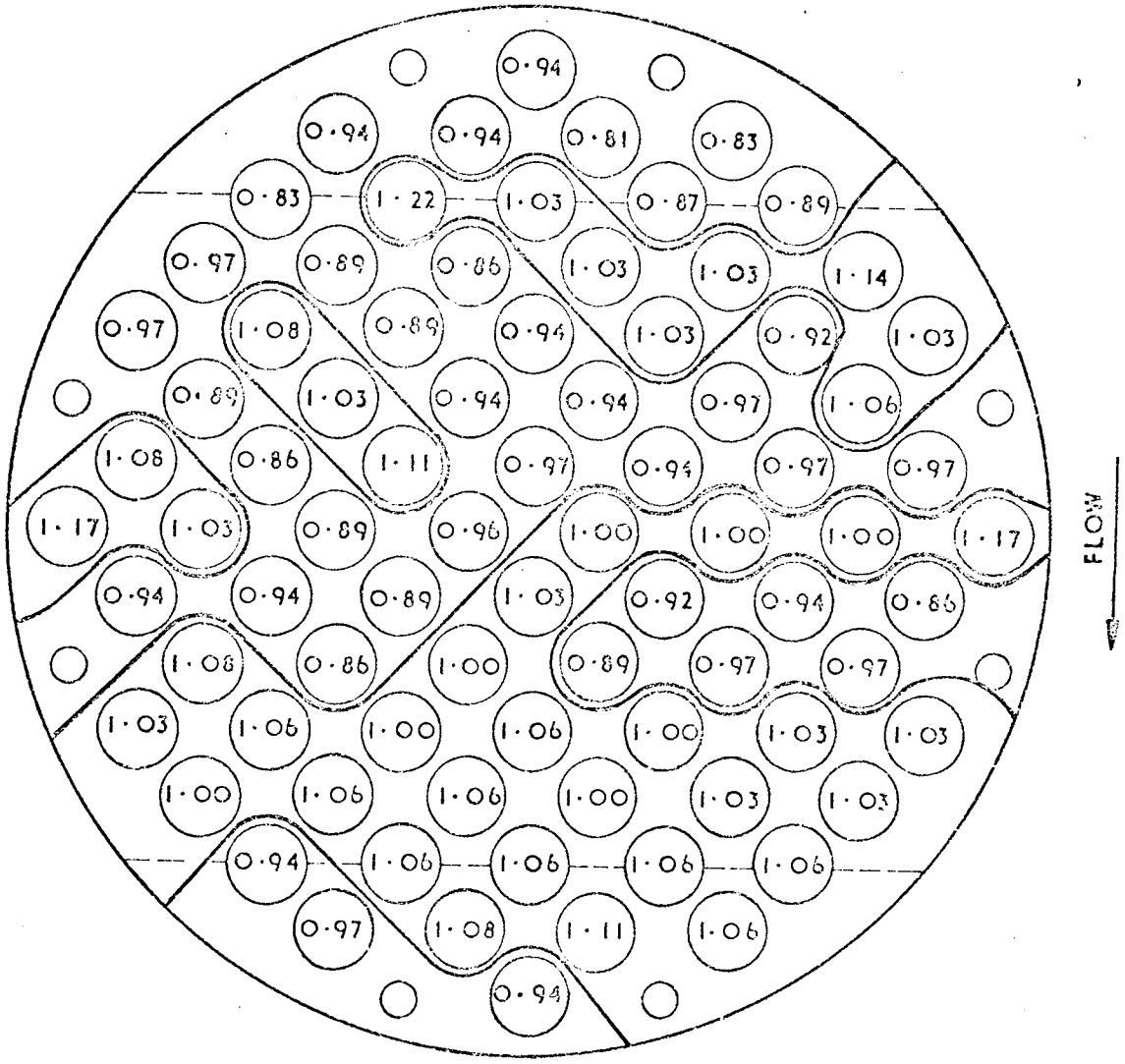

Re_M = 24550

18·4 % BC
SHORT BS

FIG.100. LEAKAGE

crossflow zone. This could be caused by reproportioning of the flow between the crossflow and leakage streams.

Fig. 101 shows the distribution of the normalised j-factors through the bottom inlet baffle compartment at an intermediate Reynolds number. The high outlet window zone tube j-factors indicated by the zonal analysis (Section 7.2.2) are shown to extend into the last three downstream rows of tubes in the crossflow zone. The tubes at the bottom of the bundle show the lowest j-factors. This baffle compartment gives greater evidence of low j-factors in the central tube rows of the crossflow zone.

In both baffle compartments, the j-factors of tubes symmetrically positioned about a vertical diameter were generally within 5 per cent of each other. The average of the j-factors from all the tubes in the two symmetrical halves of the baffle compartments differed by less than one per cent. The no-leakage data exhibited a similar degree of symmetry (see Section 6.3.1).

Figs. 102 and 103 illustrate the change in individual tube j-factors as a result of the leakage. The percentage drop in the j-factors from the no-leakage values are given for the top inlet baffle compartment. At both the high and low Reynolds numbers the change in the tube j-factors is fairly uniform throughout the baffle compartment. At the low Reynolds number, the j-factors of Tubes 1 and 80 at the top and bottom of the bundle, show relatively low and high discrepancies respectively. Leakage is shown to have a greater effect on the tube j-factors at the higher Reynolds number.

The j-factor versus Reynolds number correlation characteristics of individual tubes are shown in Fig. 104. The corresponding no-leakage data are also shown. Tubes 1, 44, 48 and 80 (see Fig. 16) were considered to represent the varying characteristics

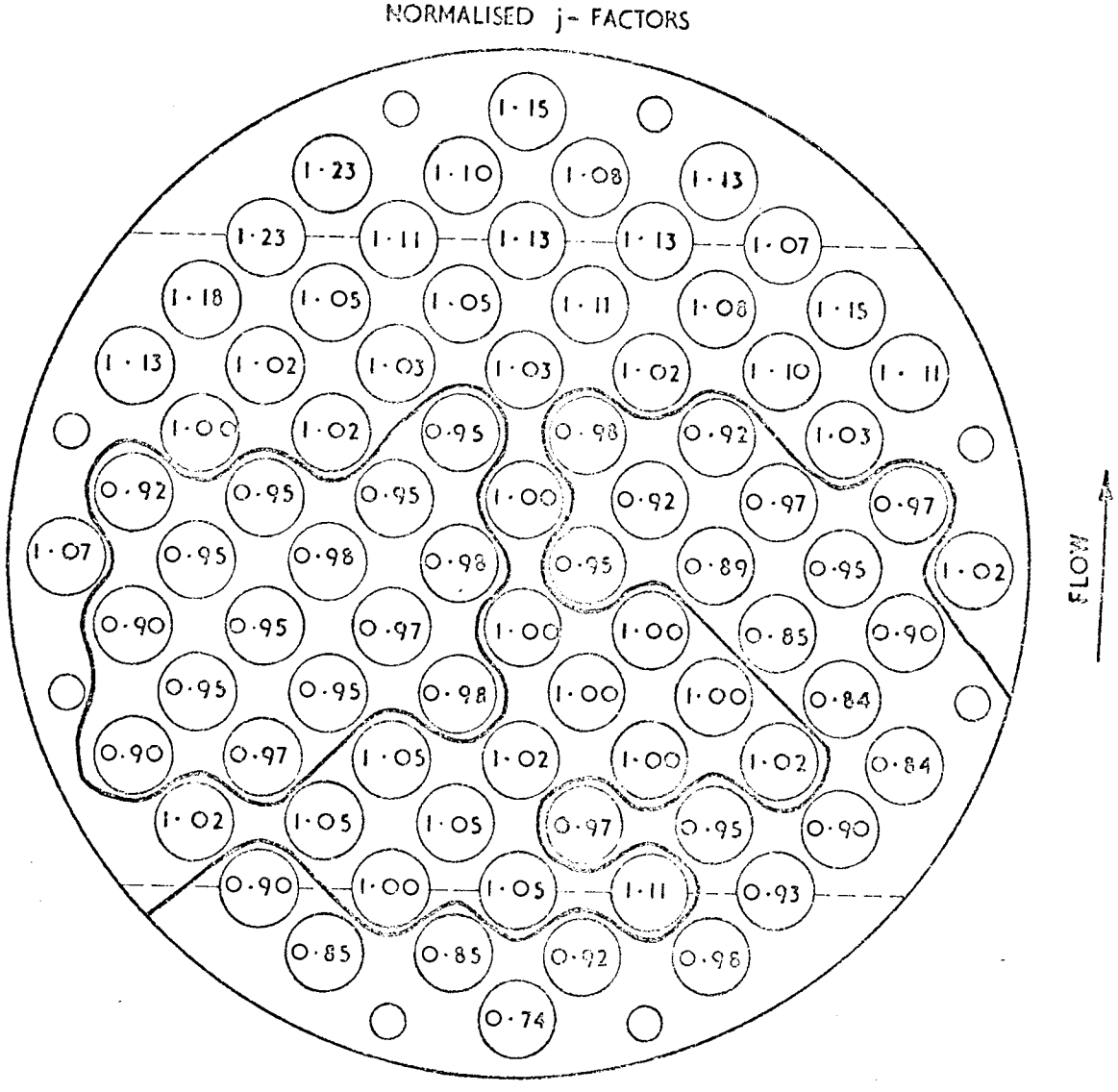

FIG.101. LEAKAGE

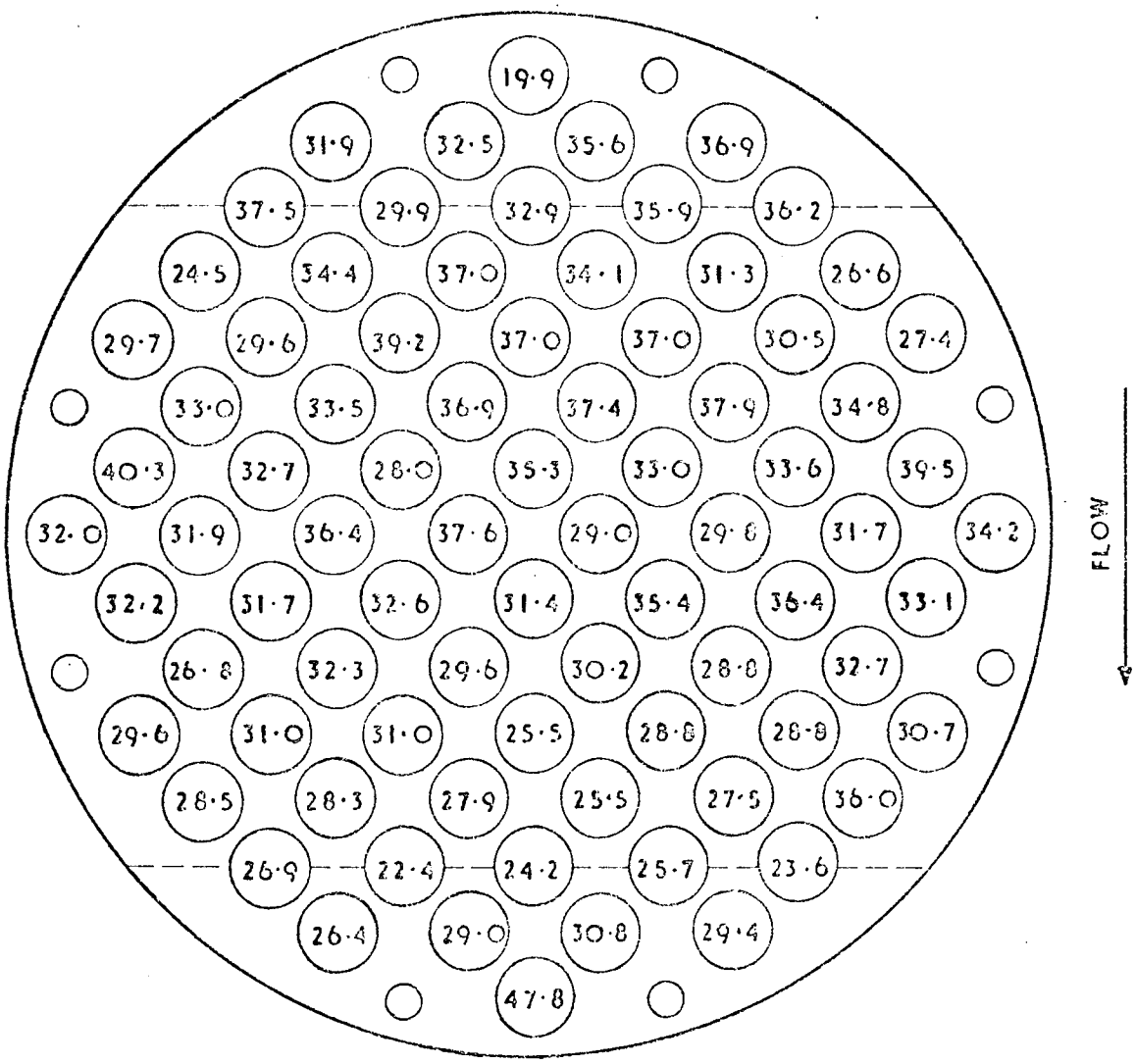

FIG.102. EFFECT OF LEAKAGE

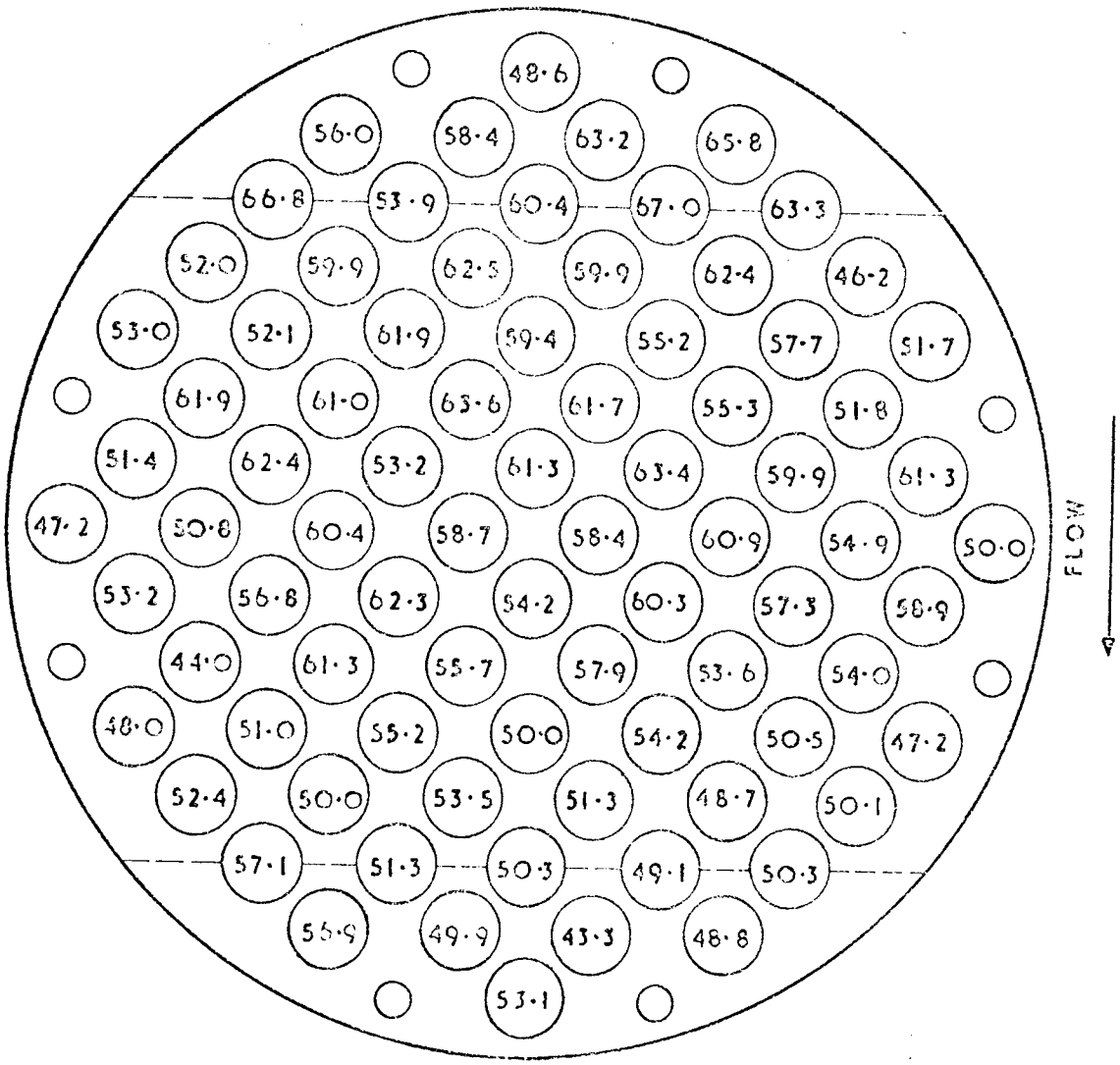

FIG.103. EFFECT OF LEAKAGE

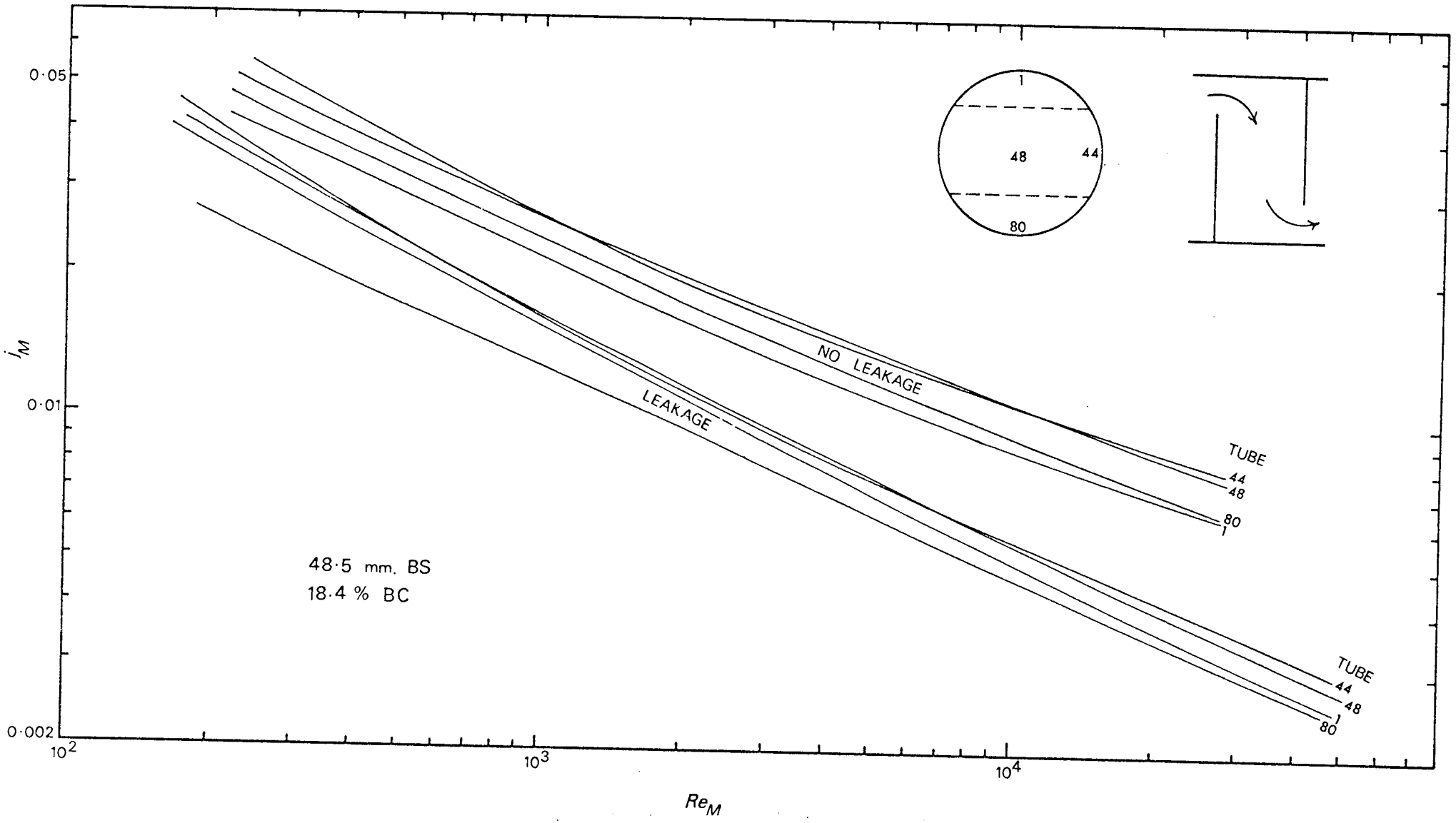

FIG 104

INDIVIDUAL TUBE COEFFICIENTS

through the compartment. These studies were confined to the top inlet baffle compartment. The characteristics of the leakage data should be interpreted in terms of the overall shell-side flow rate; for the characteristic velocity used in these data neglects the loss of fluid from the main flow stream due to leakage.

The variation in the slope of the curves from tube to tube, is greater in the leakage data than in the no-leakage data. This feature indicates that leakage produces a larger variation in flow characteristics through the bundle. The steeper slope of the leakage data suggests a larger proportion of crossflow. However these curves may have been distorted by variations in the distribution of the flow with Reynolds number. The slope of the curve given by Tube 80 is similar to those exhibited by the no-leakage data. It has already been shown in Section 7.2.2 that the tubes in the outlet window zone of this compartment would have characteristics resembling those under no-leakage conditions.

7.3 COMPARISON WITH BUNDLE AVERAGE HEAT TRANSFER DATA

The dimensions of the nominal 1/16 in. (1.59 mm) thick baffles were similar to those of a set of baffles used in the heat transfer experiments of Bergelin et al. (34). The baffle dimensions are compared in the table below. All dimensions are given in inches.

Work	Baffle Thickness	Baffle Clearances (diametrical)	
		Tube	Shell
This work	0.064	0.013	0.055
Bergelin et al.	0.063	0.013	0.063

Bergelin used the 18.4 per cent baffle cut and 1.91 in. (48.5 mm) baffle spacing of this work.

The bundle average j-factor data of Bergelin are compared with the top and bottom inlet baffle compartment average data of this work in Fig. 105. The heat exchanger of Bergelin had fourteen baffle compartments. Bergelin used the same no-leakage characteristic velocity in his leakage j-factor data. The corresponding no-leakage data of this work are also shown. These data have already been shown to be in good agreement with those of Bergelin (see Section 6.2.1).

The compartment average leakage data of this work show general disagreement with the bundle average data of Bergelin. At the low Reynolds numbers the data of this work fall up to 30 per cent above those of Bergelin. At the higher Reynolds numbers the data fall around 15 per cent below the Bergelin data. The two sets of data are coincident at a Reynolds number of 4 000. The discrepancy may be caused by the differing shell-to-baffle clearances. However data of Bergelin obtained with the shell-to-baffle clearance increased to 0.105 in. showed a reduction in the j-factor of only 12 per cent (see Fig. 105). The slopes of these two sets of data were similar. Measurements of the baffle-to-shell clearances showed that there was negligible sagging in the bundle of this work.

The reduction in the compartment average j-factor as a result of the combined tube-to-baffle and shell-to-baffle leakage, is shown to be greater at higher Reynolds numbers. The Bergelin data show the effect of this leakage on the bundle average j-factors to be greater at lower Reynolds numbers. This suggests that with leakage, the characteristics of an internal baffle compartment differ widely from those of the overall bundle. Limited experiments with solely shell-to-baffle leakage (see Section 4.4.2.4), indicated that the effect of this leakage on baffle compartment j-factors was greater at lower

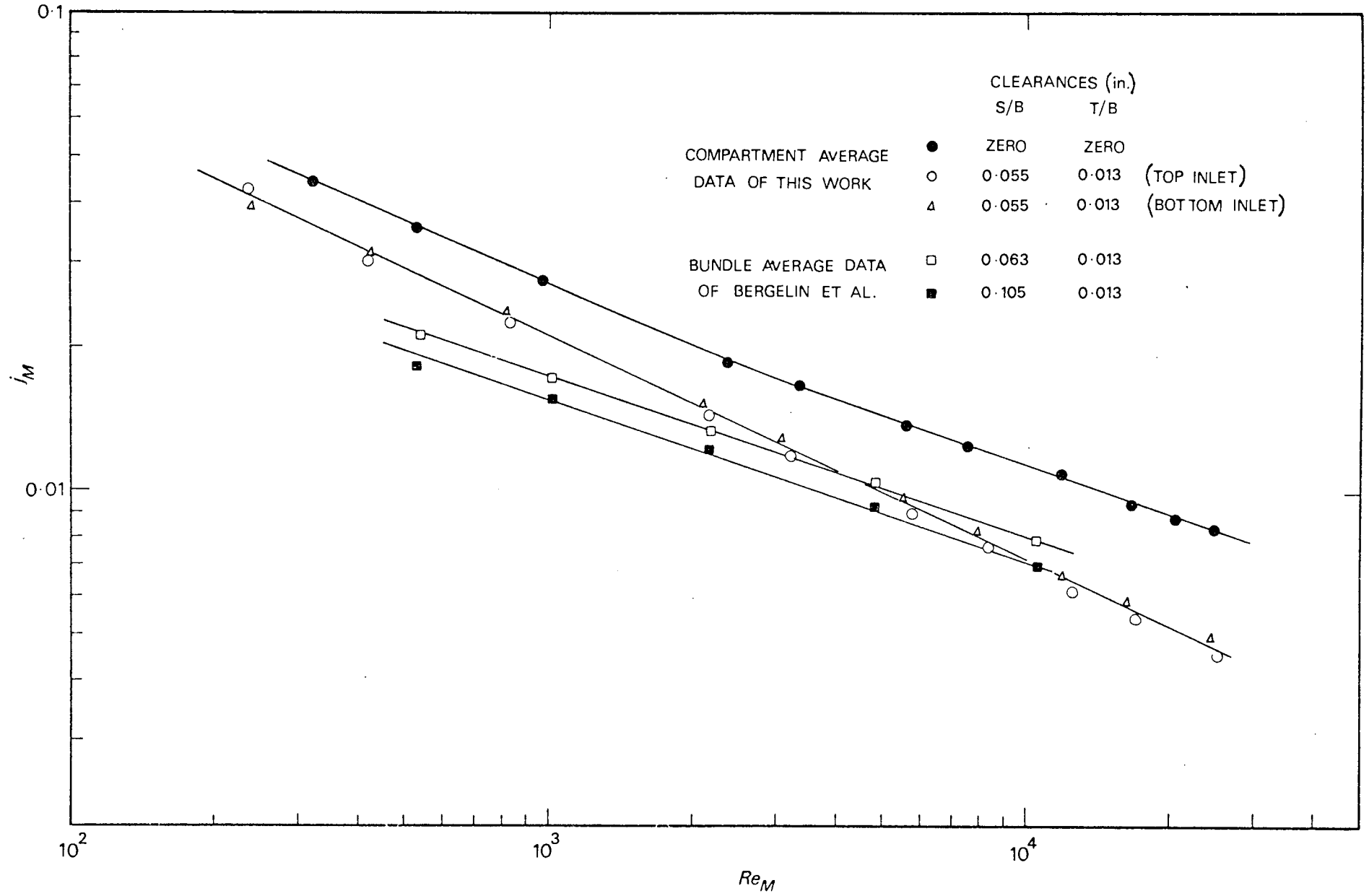

FIG 105 *COMPARISON OF LEAKAGE DATA*

Reynolds numbers. Thus the flow characteristics with shell-to-baffle leakage would appear to be very dissimilar to those with the combined forms of baffle leakage.

The pressure drop measurements of this work were compared with those obtained by Bergelin. Bergelin's measurements were confined to the sixth and seventh baffle compartments of a total of fourteen. The sum of the pressure drop across the crossflow zone in a top inlet compartment and that across a full lower window zone is shown for the two investigations in Fig. 106. The Bergelin pressure drop data fall between 10 and 15 per cent below those of this work. The results of Bergelin show an unusually low data point at a Reynolds number of 10 000; no similar characteristic was observed in Bergelin's pressure data for the increased shell-to-baffle clearance. In recognition of the random instability associated with local pressure measurements, the agreement between the two sets of data would seem satisfactory. The flow characteristics in the internal baffle compartments of the two exchanger models would appear to be similar.

The discrepancy in the baffle compartment average and bundle average j-factor data, could be attributed to the differing flow characteristics in the internal and the end baffle compartments. In the entrance baffle compartment the tube sheet provides no upstream leakage. Similarly there is no downstream leakage in the exit baffle compartment.

Bergelin et al. (34) in other leakage experiments, made pressure measurements throughout the bundle. The results showed that the pressure drops in the end baffle compartments were a factor of five greater than those in internal baffle compartments. The second and the penultimate baffle compartments showed pressure drops that were lower than those of more internal compartments. The excessive pressure

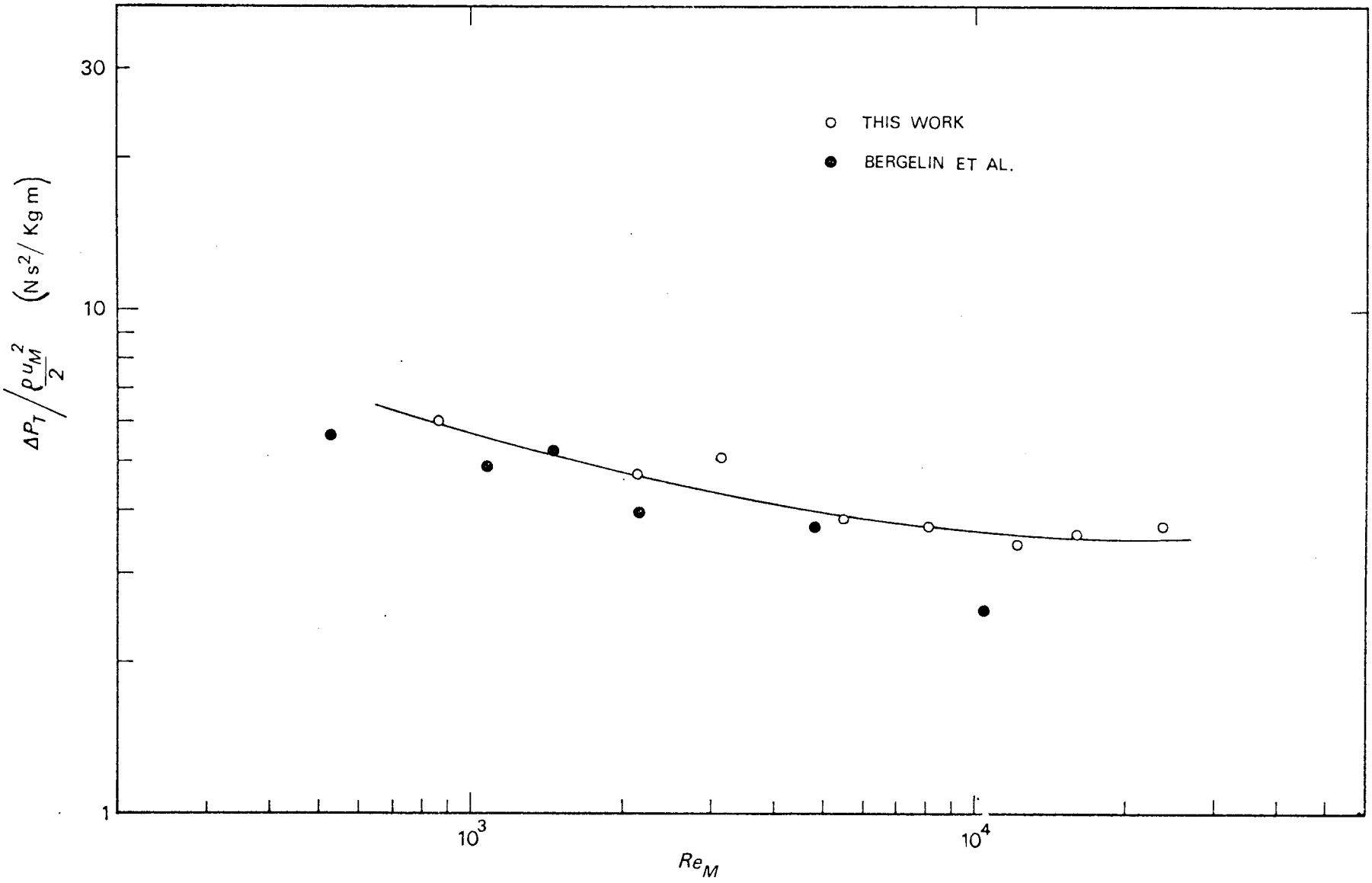

FIG 106 COMPARISON OF COMPARTMENT PRESSURE DROPS

losses in the end compartments were attributed to the smaller leakage area available.

The flow characteristics of an ideal internal baffle compartment may be established in only a few central compartments. The mass transfer characteristics of these compartments would be far from representative of those of the bundle as a whole. The complexity of the shell-side flow prohibits any accurate prediction of the mass transfer characteristics of the end baffle compartments. The need for measurements of mass transfer coefficients in these baffle compartments is thus demonstrated.

7.4 DIRECTION OF FLOW ACROSS THE BUNDLE

In commercial segmentally baffled shell and tube heat exchangers, the baffle openings are normally arranged such that the shell side fluid weaves from side to side through the bundle. This baffle arrangement has definite advantages:-

(i) The bottom corners of the baffle openings provide a liquid drainage channel along the whole length of the bundle. With an up-and-down flow arrangement, the liquid must drain through the baffle clearances. In time these clearances at the bottom of the bundle become blocked by the accumulation of solid deposits.

(ii) The full vertical baffle diameter prevents bundle sagging, thereby reducing the stresses on tie-bars and tubes.

With this baffle arrangement, adjacent baffle compartments have the same flow characteristics, the flow direction merely being reversed. Thus mass transfer measurements can be confined to a single baffle compartment. Furthermore the use of this baffle arrangement in leakage investigations would eliminate the problem of bundle

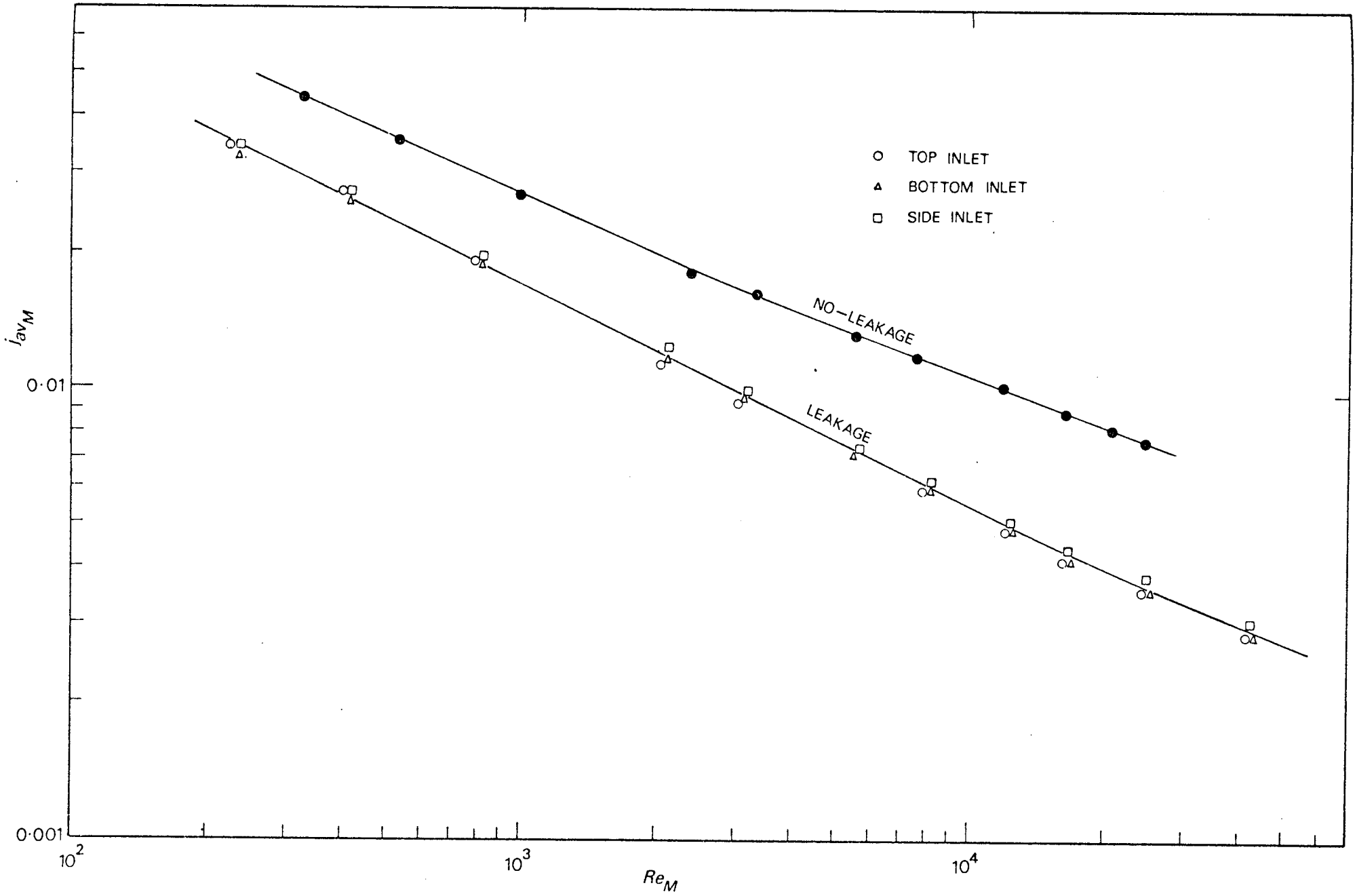

FIG 107 EFFECT OF BAFFLE ORIENTATION

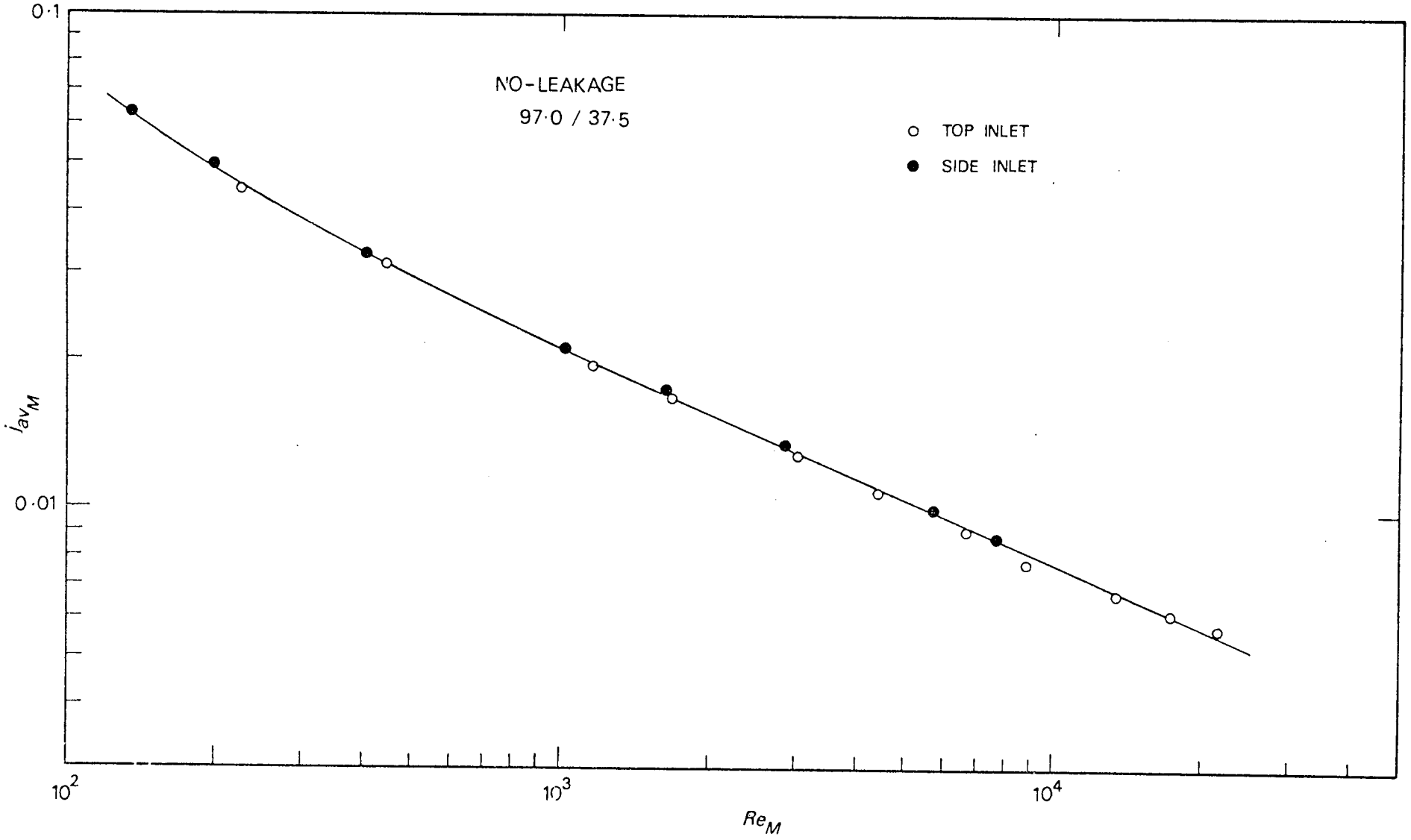

FIG 108 *EFFECT OF BAFFLE ORIENTATION*

sagging. Bundle sagging would have become more serious with the up-and-down flow baffle arrangement at larger baffle cuts.

The eccentric baffle clearances would produce differing flow distributions in the up-and-down and side-to-side flow baffle arrangements. A comparison was made between the mass transfer data from these two baffle arrangements. Compartment average j-factors for an 18.4 per cent baffle cut are shown in Fig. 107. The corresponding no-leakage data are also shown. The side-to-side flow data fall about 8 per cent above the up-and-down flow data. This difference is insignificant in relation to the estimated accuracy of the data. The structural advantages of the side-to-side flow baffle arrangement are not offset by an inferior mass transfer performance.

The mass transfer characteristics of these two flow arrangements would be expected to be identical for the case of no baffle leakage. At low Reynolds numbers natural convection effects may differ very slightly. Compartment average j-factors for the two flow arrangements are compared in Fig. 108. A 3.82 in. (97.0 mm) baffle spacing and a 37.5 per cent baffle cut were used. The two sets of data are shown to be coincident.

7.5 VARIATION IN BAFFLE CUT

For these investigations the nominal $\frac{1}{8}$ in. (3.18 mm) thick baffles were used at a spacing of 1.91 in. (48.5 mm). The baffles were orientated to produce side-to-side flow through the bundle. Three baffle cuts of 18.4, 25.0 and 37.5 per cent were used.

7.5.1 Compartment Average j-Factors

Baffle compartment average j-factors for the three baffle cuts are compared in Fig. 109. The corresponding no-leakage data from Section 6.4 are also shown.

The 18.4 per cent baffle cut is shown to produce the highest and the 37.5 per cent baffle cut by far the lowest mass

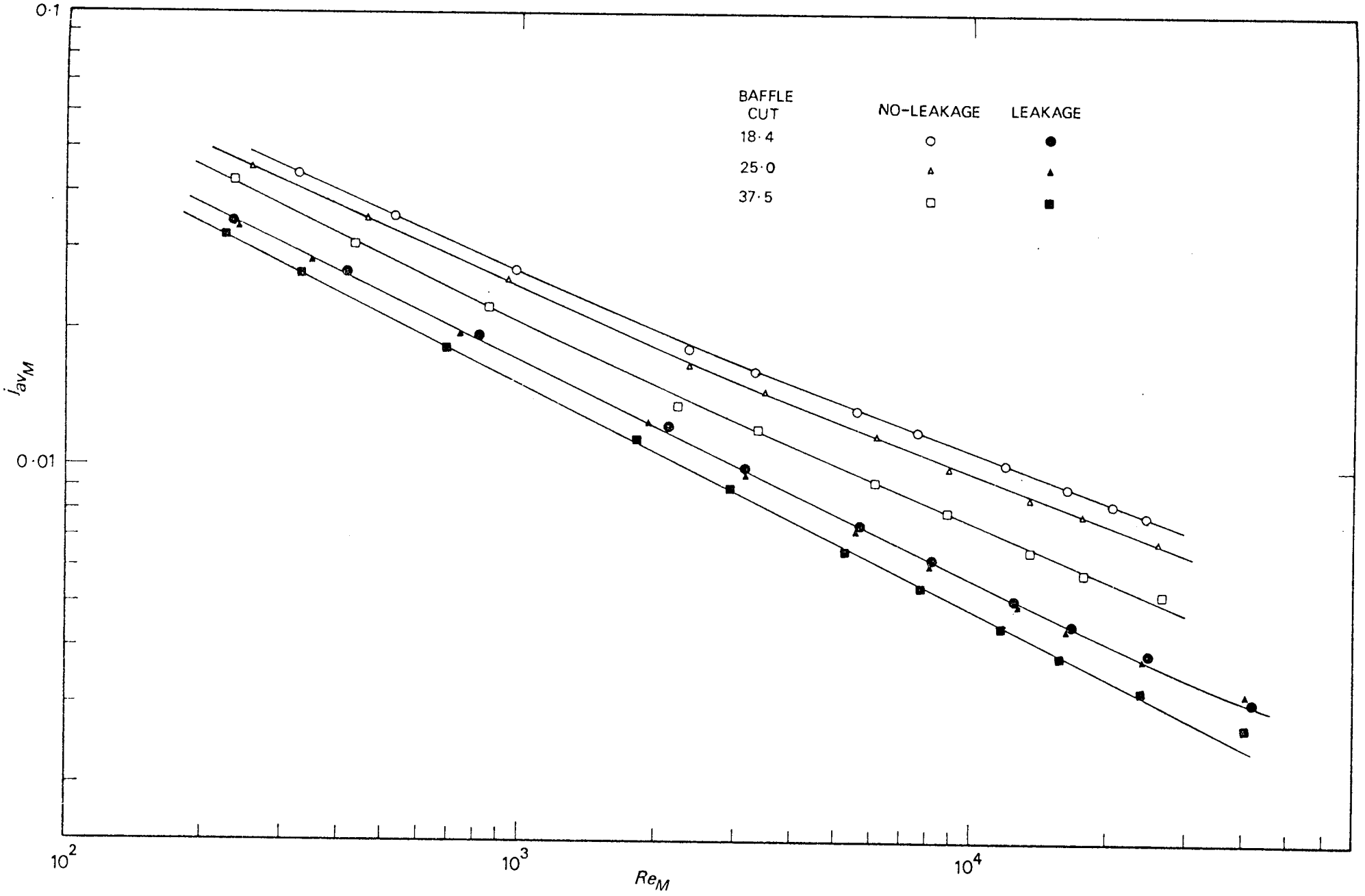

FIG 109 COMPARTMENT AVERAGES

transfer coefficients. The variation in the value of the j-factors with baffle cut is considerably less than that for the case of no-leakage. The difference in the values of the j-factors for the 18.4 and 25.0 per cent cuts is insignificant. At a Reynolds number of 20 000, the j-factor for the 37.5 per cent baffle cut falls 19 per cent below that for the 18.4 per cent cut. The corresponding value for the no-leakage data was 34 per cent. The effect of baffle cut would be expected to be less in the case of leakage for the following reasons:-

(i) A smaller proportion of the shell-side flow actually passes through the baffle window.

(ii) The reduction in the window flow area with decrease in baffle cut is to some extent offset by the associated increase in the available leakage area.

Fig. 109 reveals that for all the baffle cuts, the effect of leakage on the compartment average j-factor is greater at higher Reynolds numbers. A similar characteristic was shown by the up-and-down flow arrangement in Section 7.2.1. The distribution of the shell-side fluid between the various flow streams (see Fig. 3) is controlled by the relative flow resistances of the channels. The flow resistances of the baffle leakage channels may be relatively lower at the higher Reynolds numbers. A greater proportion of the shell-side fluid would be contained in the leakage streams, resulting in a greater departure from the no-leakage situation. This feature is better illustrated in Fig. 110 where the ratio of the j-factor with leakage to that without leakage is plotted against the Reynolds number. The no-leakage data were obtained with up-and-down flow. However in Section 7.4 it was shown that the no-leakage compartment

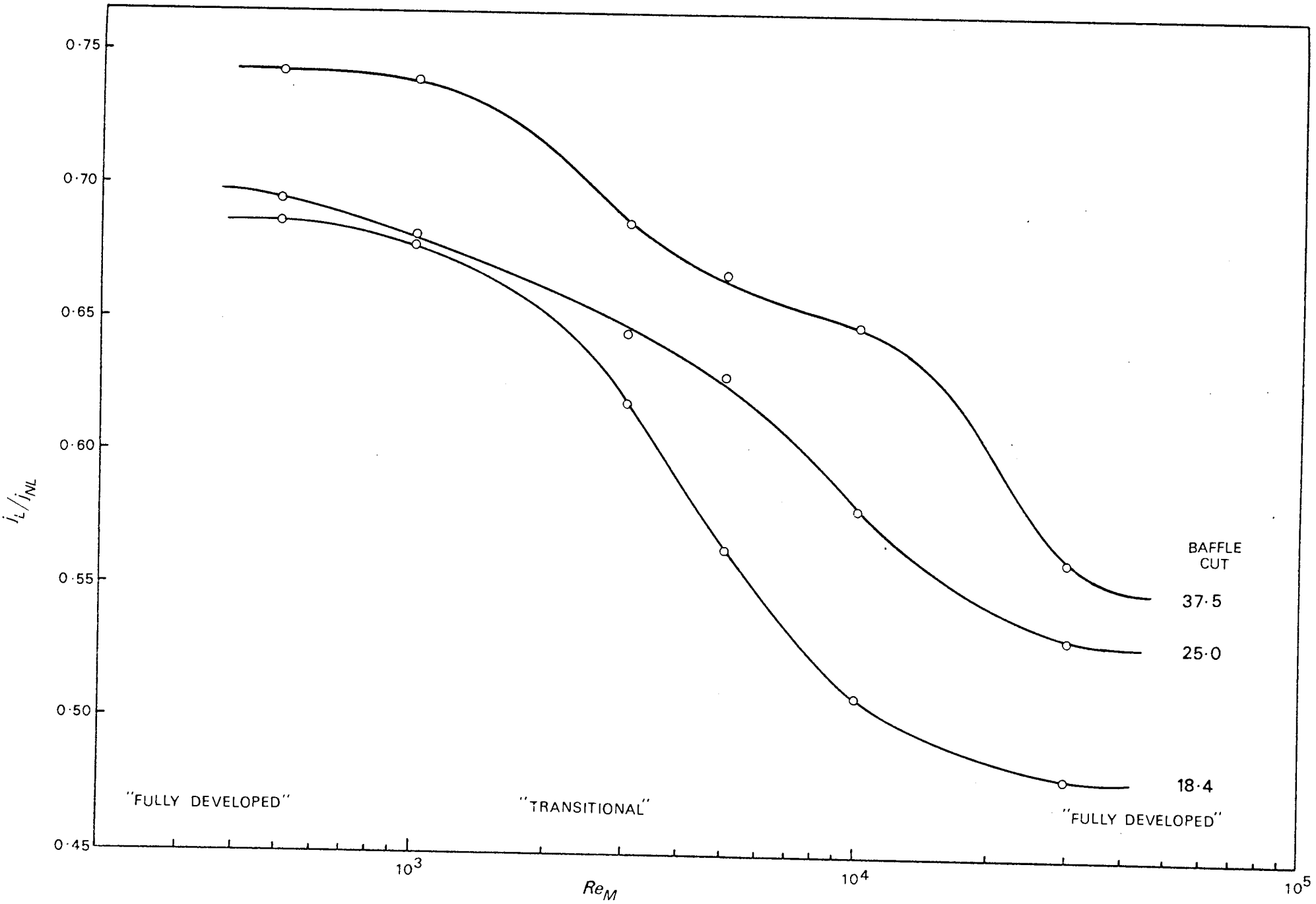

FIG 110 VARIATION IN EFFECT OF LEAKAGE WITH REYNOLDS NUMBER

average j-factors with up-and-down and side-to-side flow were identical.

At either end of the Reynolds number range, the value of the ratio term for each baffle cut, would appear to be independent of the Reynolds number. The variation in the effect of leakage with Reynolds number is confined to an intermediate Reynolds number range of 600 to 30 000. The limits of the estimated accuracy of the data could produce leeway in the data points in Fig. 110, sufficient to invalidate this rigorous interpretation. However it is significant that pairs of data from six independent investigations (viz. three leakage and three no-leakage experiments) have all exhibited similar characteristics.

The constant relative effect of leakage at Reynolds numbers below 600, suggests a stable distribution of the shell-side flow. Previous experiments in the absence of leakage indicated that the flow was fully laminar at Reynolds numbers below 300 (see Section 4.4.2.7). The greater longitudinal flow component with leakage, would extend the shell-side laminar flow regime to higher Reynolds numbers. The Reynolds number of 600 could represent the limit of laminar flow.

The shell-side flow distribution would appear to be fully developed at Reynolds numbers above 30 000. This may represent a region of fully turbulent flow. Pressure drop data have indicated a late transition to turbulent flow (see Section 7.7).

The intermediate range of Reynolds numbers represents a transitional region in which most of the flow redistribution occurs. The differing flow characteristics of the individual streams would produce a very unstable system. While the main crossflow stream may be turbulent, the shell-to-baffle leakage stream may still be fully laminar.

The relative effects of leakage on compartment average j-factors are further analysed in Section 7.6.

7.5.2 Individual Tube j-Factors

The variation in the distribution of individual tube coefficients with baffle cut is illustrated in Figs. 111, 112 and 113. Tube j-factors have been divided by the corresponding compartment average value.

All the three baffle cuts produce low coefficients in the inlet window zone. The values of these coefficients become relatively lower with increase in baffle cut. The coefficients of tubes in the outlet window zone are generally above average. At low Reynolds numbers, the 37.5 per cent baffle cut shows low coefficients in both inlet and outlet window zones (see Fig. 114). This suggests that the high outlet window zone coefficients at the higher Reynolds numbers are caused by fluid jetting through the relatively small crossflow area. The other baffle cuts show little change in the distribution characteristics with Reynolds number.

The 37.5 per cent baffle cut shows high coefficients throughout the crossflow zone. The 18.4 per cent cut and to a lesser extent the 25.0 per cent cut, show a region of low coefficients spreading upwards through the central tube rows in the crossflow zone. The fact that this feature emanates from an area of least shell-to-baffle leakage at the bottom of the bundle, suggests that it is caused by the formation of flow eddies.

The variation in tube j-factors through a baffle compartment was measured in terms of the normalised standard deviation used previously in Section 6.3.2. The variation of this distribution term with baffle cut is shown in Fig. 115. The

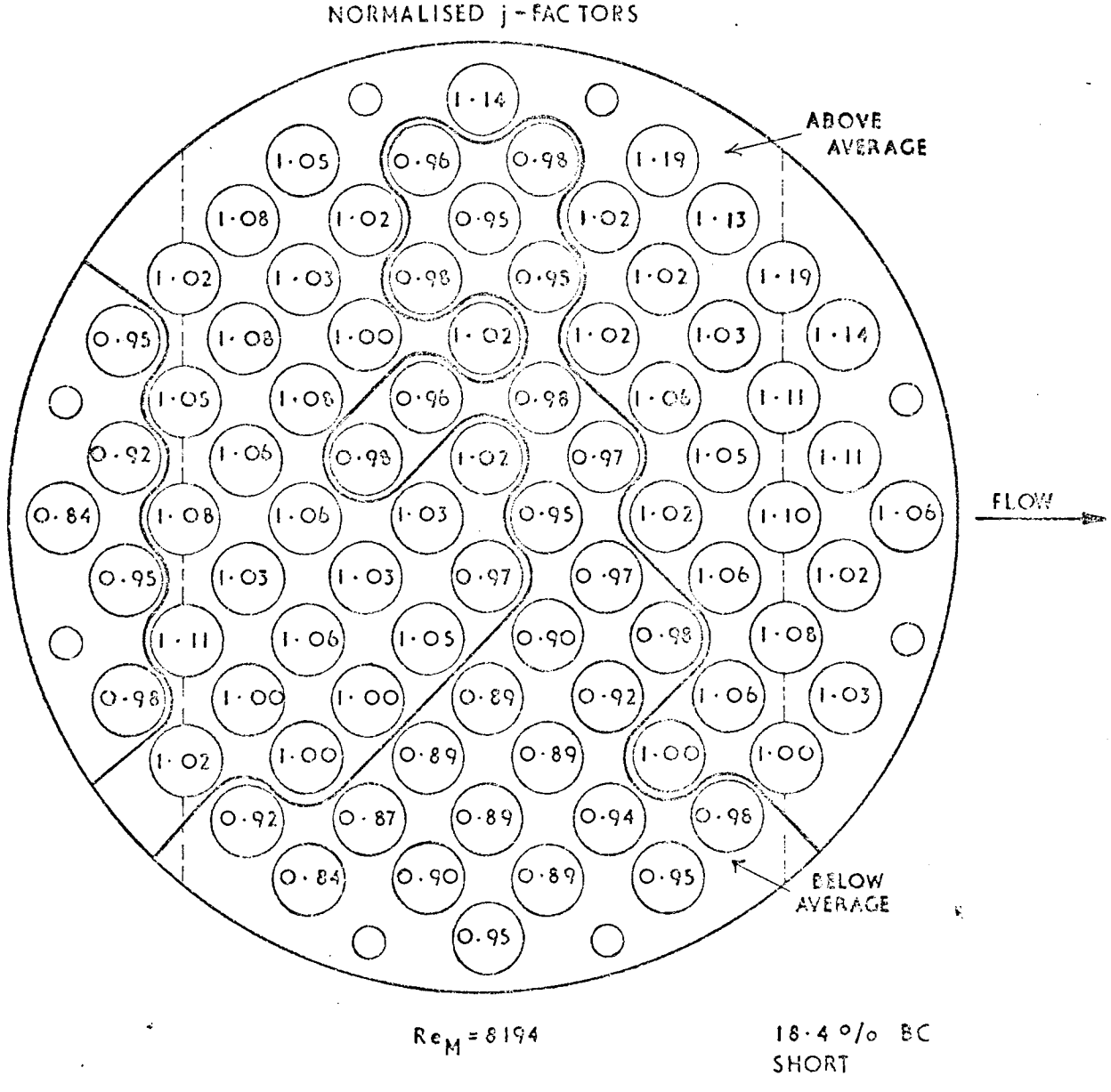

FIG. III. LEAKAGE

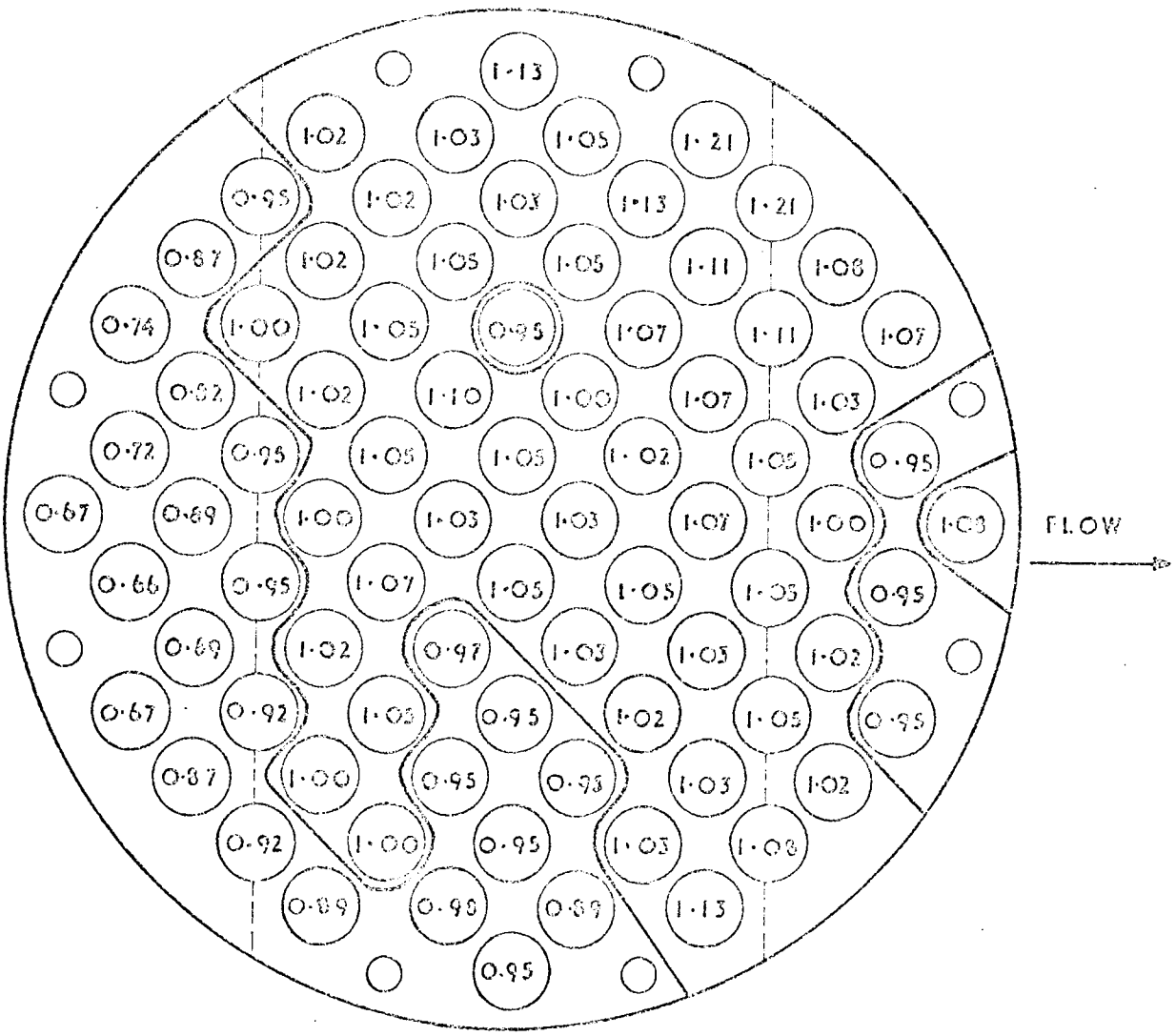

FIG.112. LEAKAGE

NORMALISED j-FACTORS

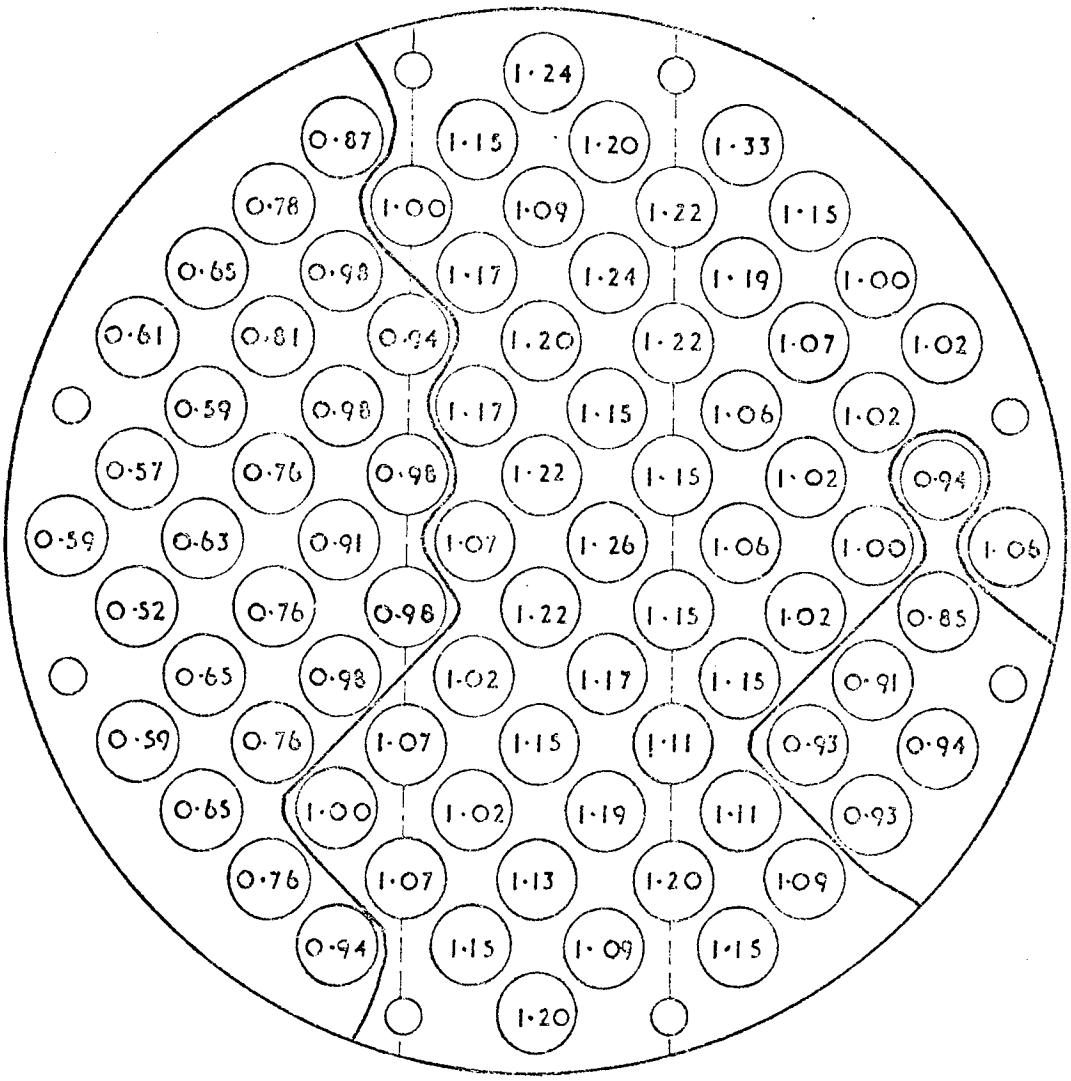

$Re_M = 7659$

37·5 % BC

SHORT BS

FIG.13. LEAKAGE

NORMALISED j FACTORS

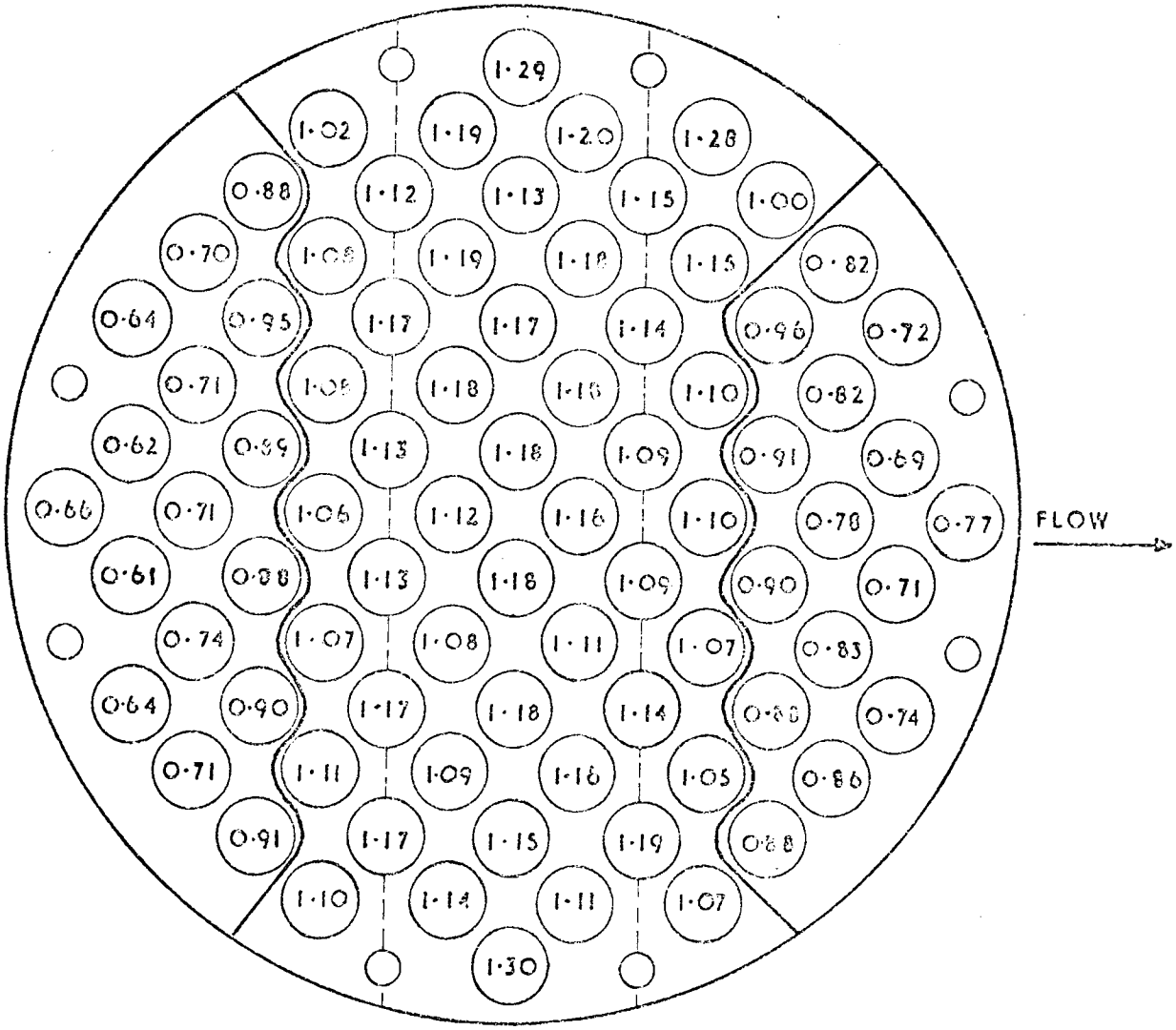

ReM 330 37·5 % BC

SHORT BS

FIG.114. LEAKAGE

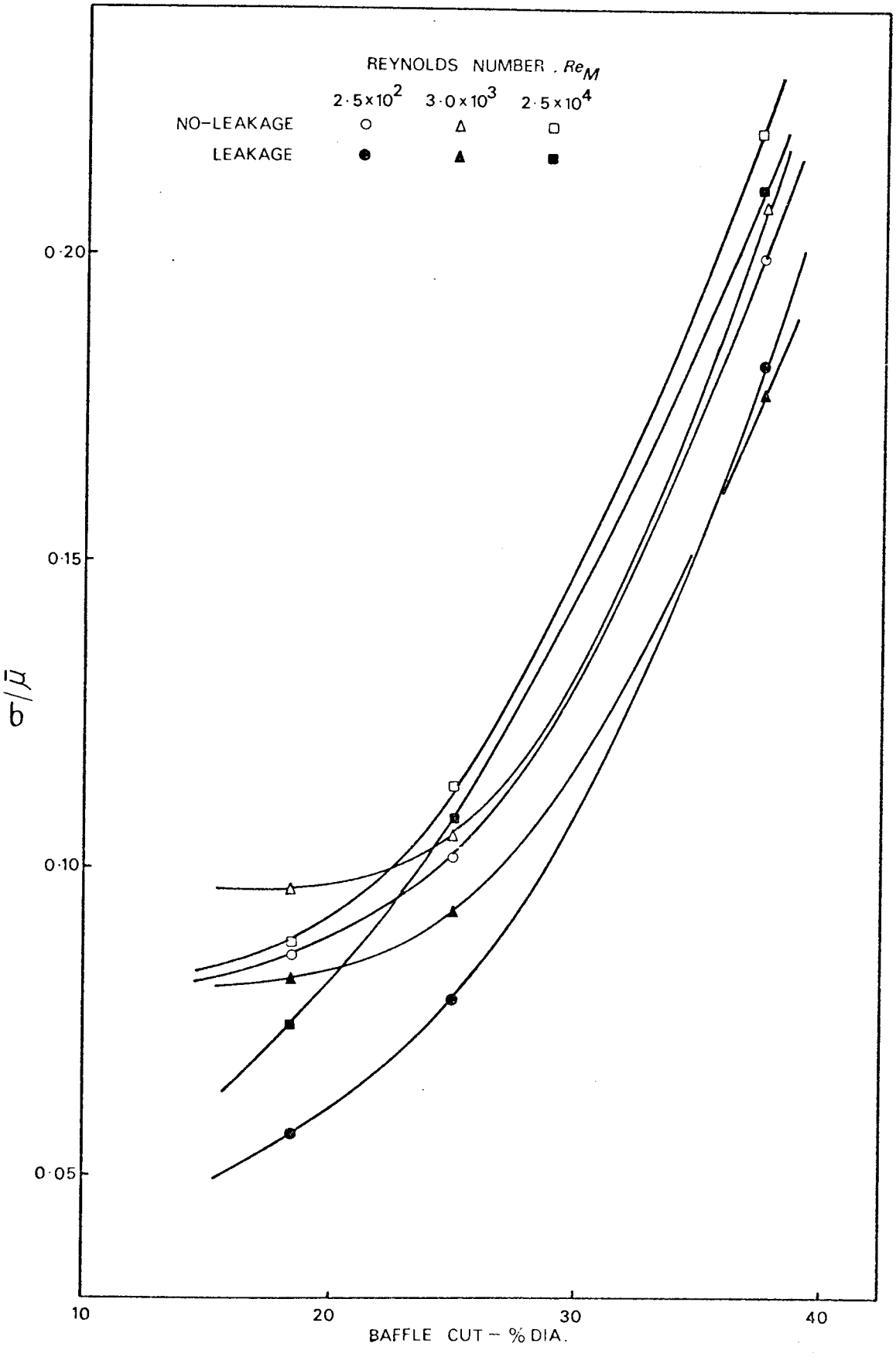

FIG 115 *DISTRIBUTION OF TUBE COEFFICIENTS*

corresponding no-leakage data from Section 6.3.2 are also shown. At each shell-side Reynolds number, the variation in the individual tube coefficients decreases with the baffle cut. The no-leakage data show this same feature. The leakage data generally show a more uniform distribution of tube coefficients, particularly at the lowest Reynolds number. The presence of baffle clearances would discourage the formation of local "hot spots" in the bundle.

7.6 CORRELATION OF THE EFFECT OF LEAKAGE

Any rigorous correlation of leakage heat transfer data with exchanger geometry, requires a knowledge of the relative magnitudes of the individual flow streams. The Stream Analysis prediction method uses this approach (see Section 1.3.3).

A simpler approach is to correlate the relative effect of leakage on the heat transfer data with the leakage flow area. Bell (29) correlated the effect of leakage in this manner (see Section 1.3.2.4). In his experiments both the baffle spacing and the baffle clearances were varied. Bell described this varying baffle geometry by the term A_L/A_M i.e. the ratio of the total leakage area to the crossflow area.

In the leakage studies of this work with the thicker baffles, the baffle cut was the only geometrical variable. The variation with baffle cut in the ratio of the baffle compartment average j-factor with leakage to that without leakage is shown in Fig. 116. The effect of leakage is greater at the smaller baffle cuts. This can be attributed to the increased leakage area associated with a decrease in baffle cut. Leakage is again shown to have a greater effect at higher Reynolds numbers.

The variable baffle geometry may be described by the ratio of the total leakage area to the baffle window flow area i.e. A_L/A_W.

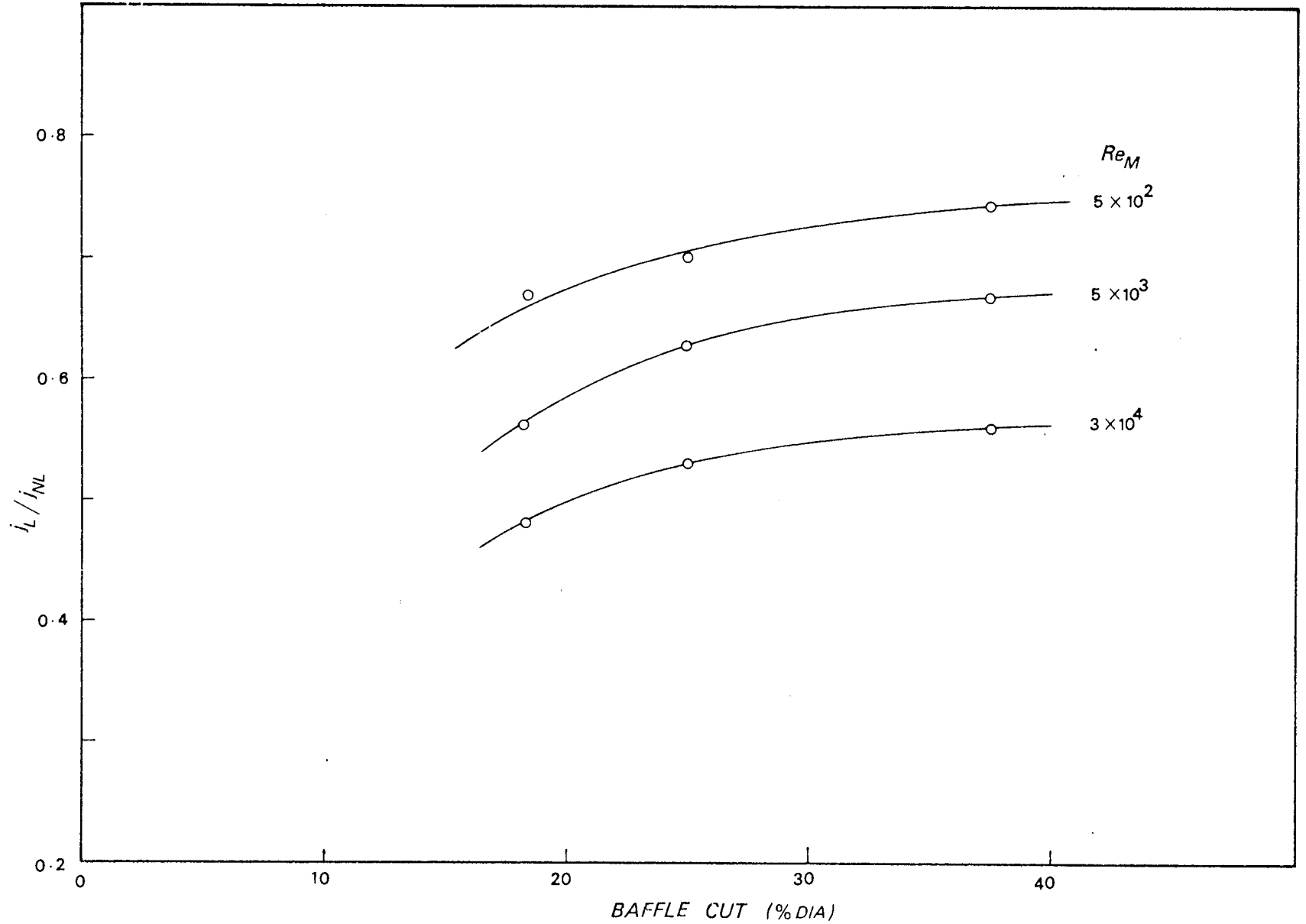

FIG 116 VARIATION IN EFFECT OF LEAKAGE WITH BAFFLE CUT

This term is analogous to that used by Bell. The ratio A_L/A_W represents the additional longitudinal flow area produced by leakage clearances to that available in the absence of leakage. The terms A_L and A_W are not truly independent variables for they are both related to the baffle cut.

The compartment average j-factor data are plotted in this form in Fig. 117. When calculating the shell-to-baffle leakage area it was assumed that the baffles were concentric within the shell. As the baffle cut is increased the term A_L/A_W decreases. For the case of a 100 per cent baffle cut (i.e. no baffles), the term A_L/A_W would be zero and the ratio of the j-factors would be unity. The curves in Fig. 117 have been extrapolated to this point. This form of correlation thus enables the effect of leakage to be estimated for baffle cuts above the experimental limit of 37.5 per cent. The single set of data from the nominal 1/16 in. (1.59 mm) thick baffles are also shown in Fig. 117. These data fall well above the corresponding curves of the thicker baffles. In Section 7.2 it was shown that both the baffle thickness and clearance need to be taken into account when correlating leakage data.

The crossflow and window zone average j-factor data are correlated in this same form in Fig. 118. The averages of the inlet and outlet window zone data are shown. The reduction in the j-factor through leakage, is greater for the crossflow zone than for the window zone, particularly at the higher Reynolds numbers. It has already been shown that leakage diminishes the effective crossflow stream. Leakage also reduces the window flow but would disperse any stagnant fluid in the corners of the window zone. Thus the effect of leakage on the mass transfer in the window zone is not solely detrimental.

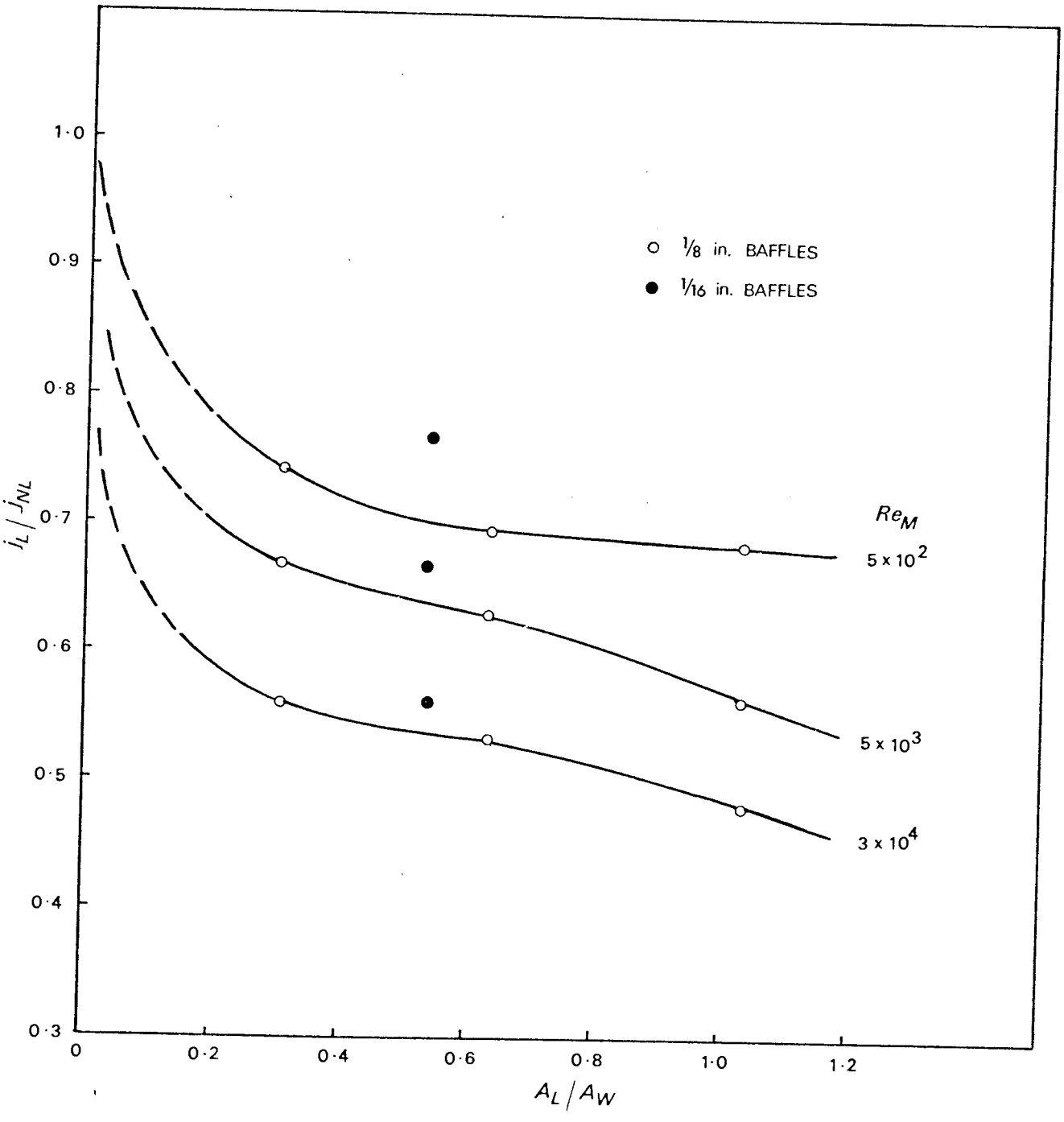

FIG 117 CORRELATION OF LEAKAGE EFFECT

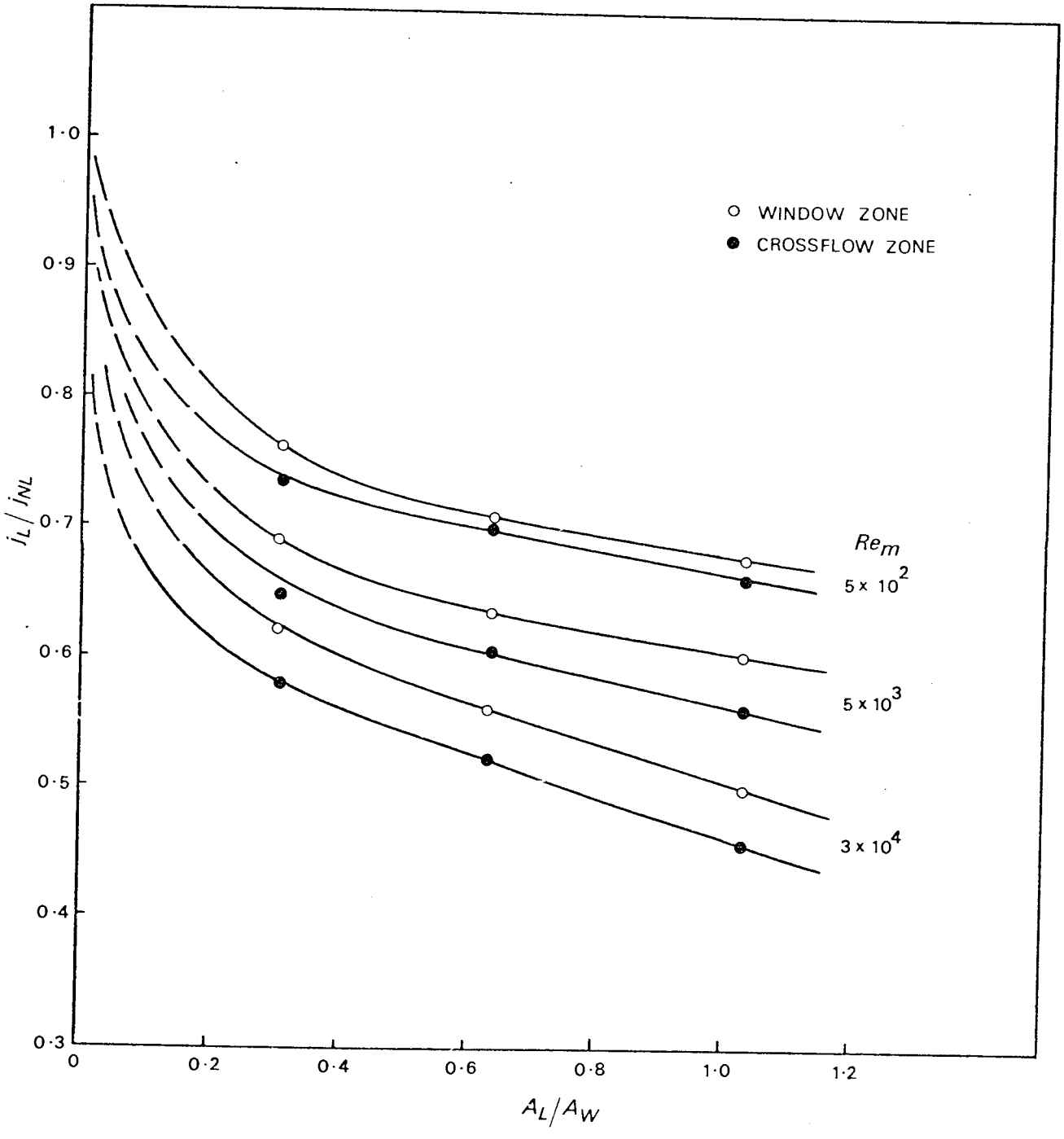

FIG 118 CORRELATION OF LEAKAGE EFFECT

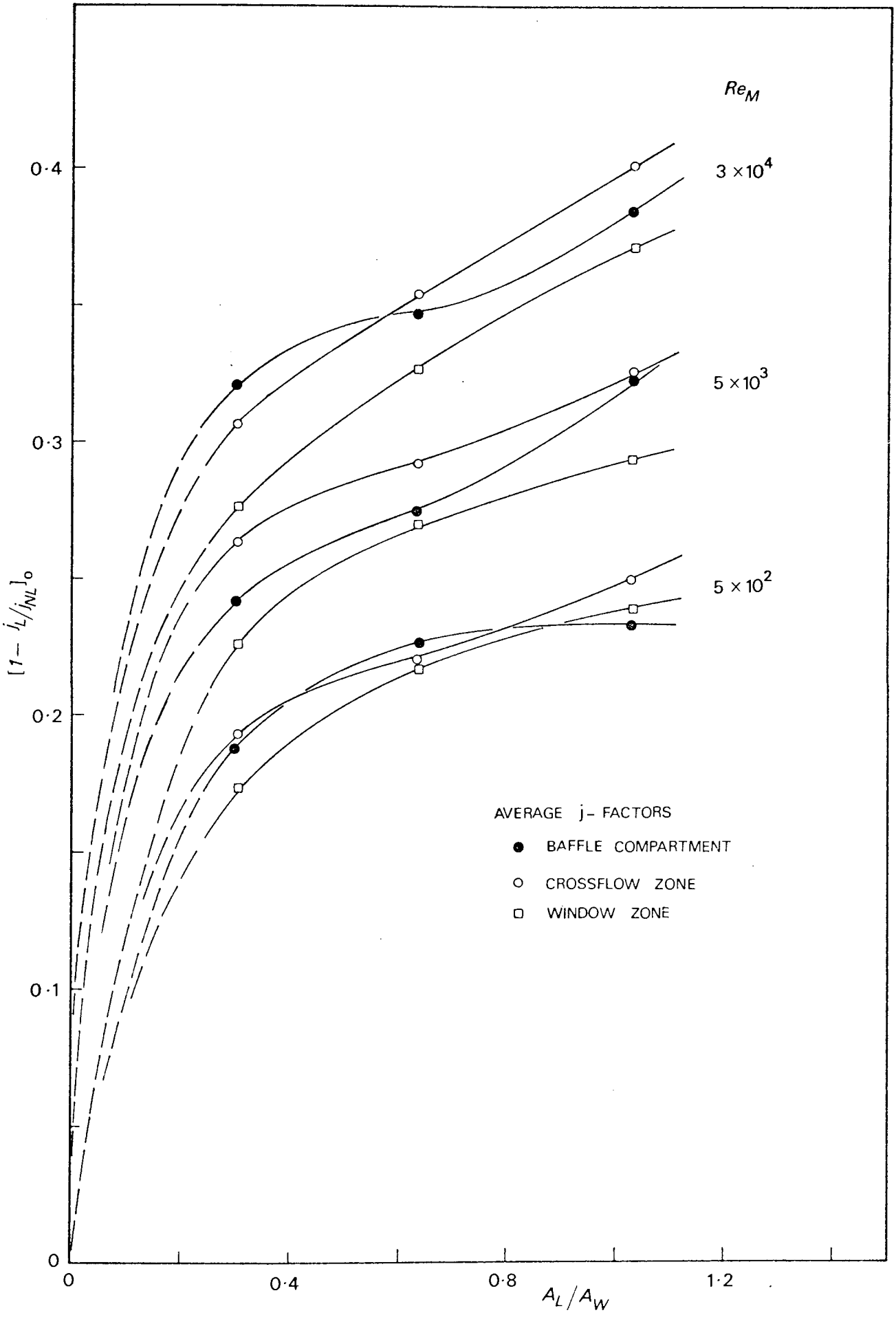

FIG 119 *CORRELATION OF LEAKAGE EFFECT*

Bell (29) found that at a given A_L/A_M, the value of $(1 - h_L/h_{NL})$ for shell-to-baffle leakage was about twice that for tube-to-baffle leakage (see Section 1.3.2.4). Bell proposed an equation for the weighted effect of the two sources of leakage (see Equation (1.27)). The same relationship between the effect of shell-to-baffle and tube-to-baffle leakage was assumed to hold in this work. The analogous equation to Equation (1.27) is:-

$$\left[1 - \frac{j_L}{j_{NL}}\right]_{\substack{\text{COMBINED} \\ \text{LEAKAGE}}} = \left[1 - \frac{j_L}{j_{NL}}\right]_0 \left[\frac{A_{TB} + 2\,A_{SB}}{A_L}\right] \qquad \ldots\ldots (7.2)$$

For a given A_L/A_W, the value of the combined leakage j-factor ratio term is obtained from Fig. 117 or 118. The weighted j-factor ratio term $(1 - j_L/j_{NL})_0$ is then calculated from Equation (7.2). This term, for both baffle compartment and zonal average j-factors, is plotted against A_L/A_W in Fig. 119. This correlation is used in later sections of the work.

7.7 PRESSURE DROP

Pressure drop measurements made using the thicker baffles, side-to-side flow and an 18.4 per cent baffle cut are correlated in Fig. 120. The pressure drop is the sum of the pressure drops across a crossflow zone and a full window zone in the fifth baffle compartment of nine. The corresponding no-leakage data are also shown.

Leakage is shown to reduce the pressure drop across this internal baffle compartment by up to a factor of six. Bergelin et al. (34) found the effect of leakage on pressure drop to be of a similar order (see Section 1.3.2.4).

The onset of fully turbulent flow would appear to occur at a Reynolds number of around 15 000. The slope of the curve is however

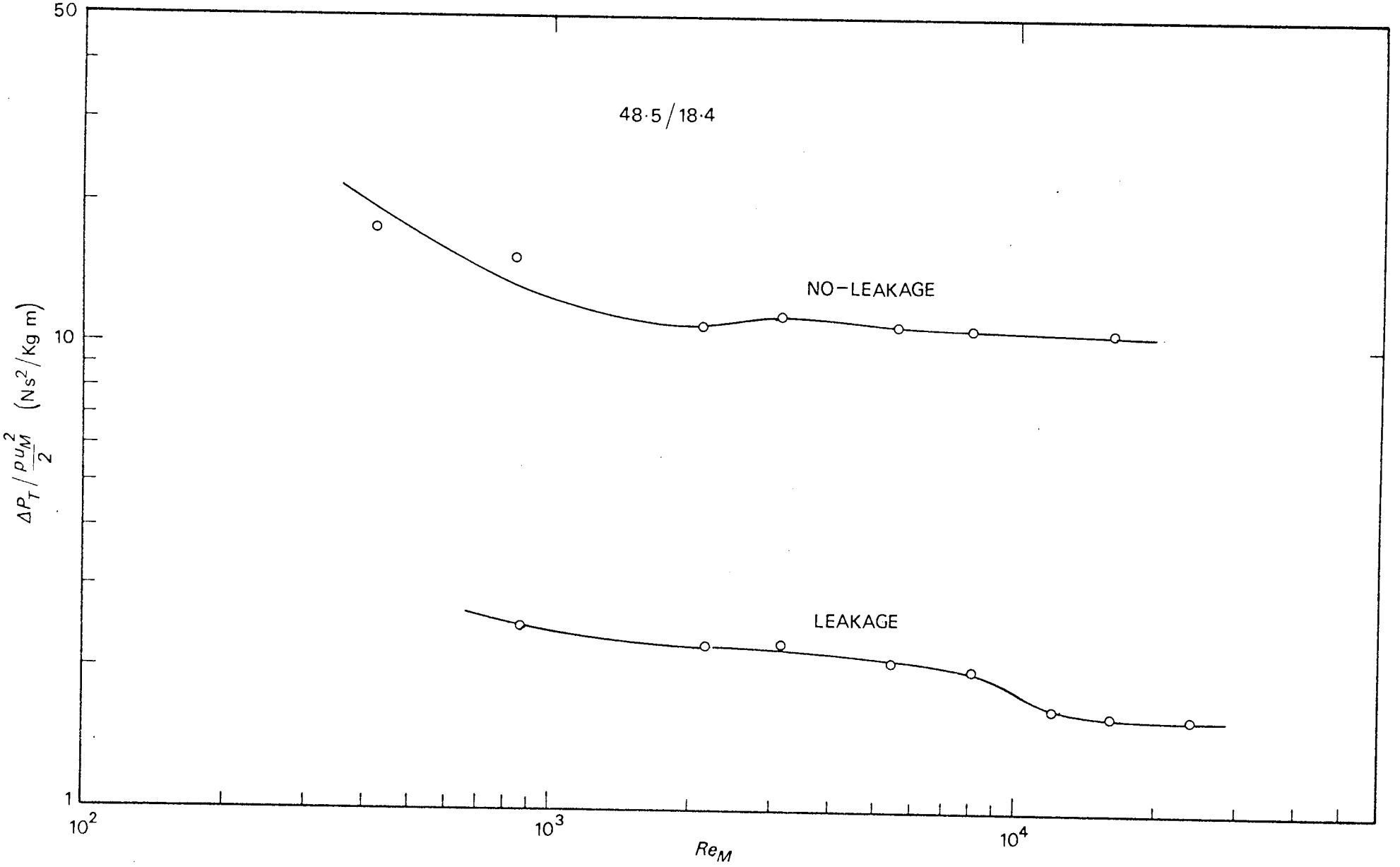

FIG 120 COMPARTMENT PRESSURE DROP

only slight in the Reynolds number range 2 000 to 8 000. The dip in the curve at a Reynolds number of 10 000, may represent a substantial flow redistribution instead of an abrupt transition to fully turbulent flow. The no-leakage data show the flow to be fully turbulent at Reynolds numbers above 5 000. The late transition to turbulent flow indicated by the leakage data could be attributed to the increased longitudinal flow component.

The range of the Reynolds number in the leakage investigations does not permit identification of laminar flow. This would be indicated by a slope of minus one.

The reduction in pressure drop due to leakage is demonstrated in Fig. 121 for three baffle cuts. The sum of the pressure drops across a crossflow zone and a window zone are again compared. The leakage pressure drops vary between 19 and 27 per cent of the no-leakage values. The reduction in pressure drop is shown to be greatest at the 25.0 per cent baffle cut. The 18.4 per cent cut would be expected to exhibit this characteristic as it has the largest leakage area.

The corresponding mass transfer j-factor data are also shown in Fig. 121. The effect of leakage is considerably less; values of compartment average j-factors for leakage being between 48 and 58 per cent of the no-leakage values. The reduction in the j-factor increases with decrease in baffle cut. The presence of leakage would be expected to have a greater effect on pressure drop than on mass (or heat) transfer. The increase in the available flow area provided by the baffle clearances would reduce the average fluid velocity. The pressure drop would vary as the square of the fluid velocity. However the mass transfer coefficient would vary as only the 0.6 to 0.8 power of the fluid velocity; redistribution of the shell-side flow being neglected.

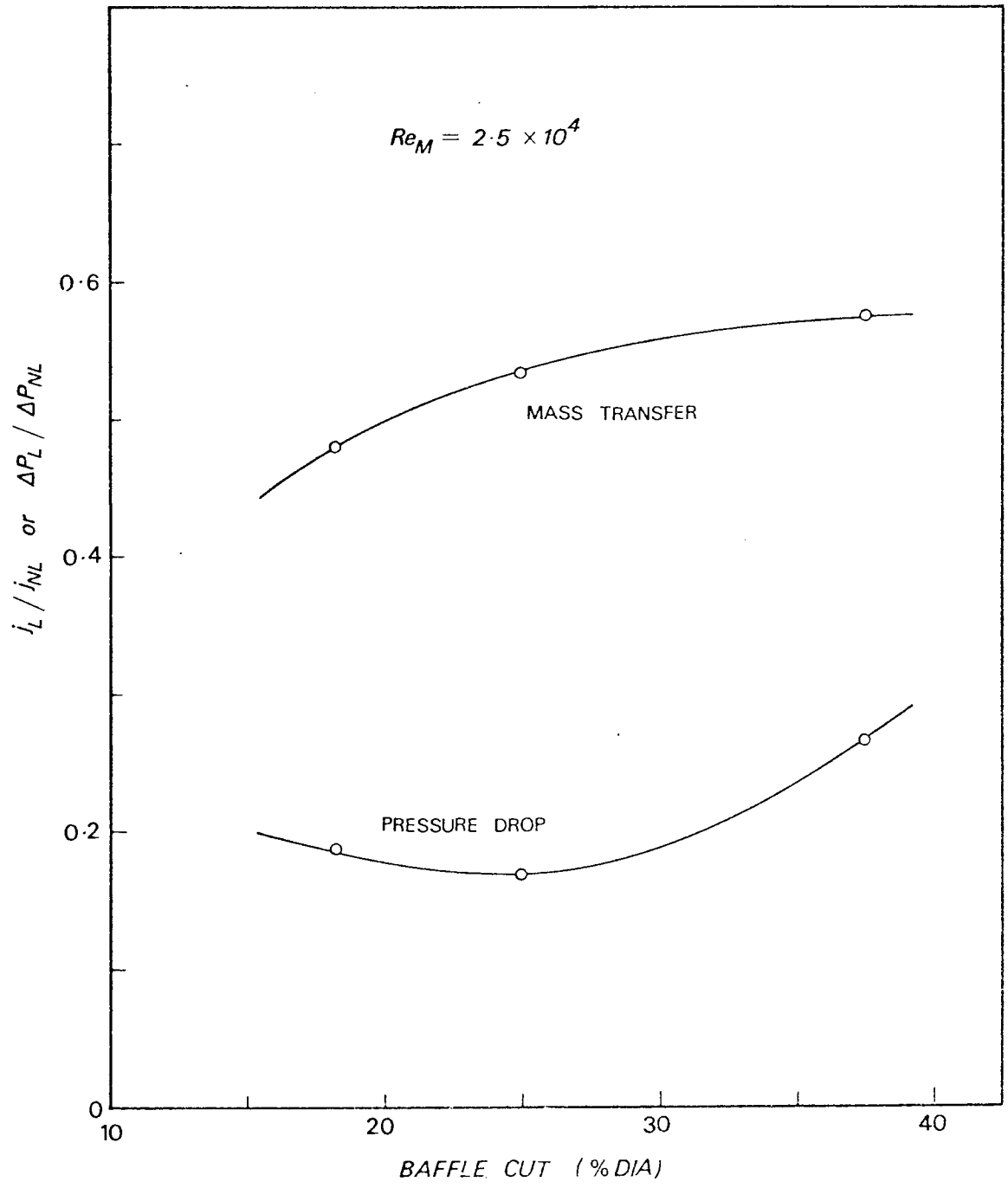

FIG 121 EFFECT OF LEAKAGE ON COMPARTMENT j-FACTOR AND PRESSURE DROP

7.8 CONCLUSIONS

The results from the leakage single segmental baffle investigations are now summarised:-

(i) Baffle leakage has been shown to produce a substantial reduction in the baffle compartment average j-factor. This reduction was as high as 60 per cent. The effect of leakage was greater at high Reynolds numbers. The inferior coefficients with leakage were attributed to the general redistribution of the shell-side flow resulting in a greater proportion of longitudinal flow.

(ii) Distributions of tube coefficients were shown to be far more uniform than those from the no-leakage investigations. Few tubes had coefficients differing by more than 10 per cent from the compartment average value. This greater uniformity was attributed to the dispersal of the eddy flow and the reduction in fluid "jetting".

(iii) Individual tube and zonal average mass transfer data have allowed identification of the localised effects of the leakage streams.

(iv) Up-and-down and side-to-side shell-side flow configurations were shown to produce similar baffle compartment average j-factors.

(v) The effect of baffle cut on compartment average j-factors was shown to be less than that in the case of no-leakage. This was attributed to a reduction in window area being to some extent offset by an increase in the baffle leakage area.

(vi) A correlation was derived describing the reduction in the baffle compartment and zonal average j-factors due to

leakage. The variation in the leakage area resulted out of a change in baffle cut.

(vii) Baffle leakage was shown to have a far greater effect on pressure drop than on the mass transfer coefficients. As a result of the leakage, the baffle compartment pressure drop was reduced by up to a factor of six.

8. DOUBLE SEGMENTAL BAFFLES

8.1 INTRODUCTION

Multiple segmental baffles are replacing the customary single segmental baffles in many commercial shell and tube heat exchangers. The double segmental is the most common of these multiple segmental baffle designs. This baffle arrangement is illustrated in Fig. 122.

The flow path of the shell-side fluid with double segmental baffles is less tortuous than that with single segmental baffles. For the same shell-side flow rate and baffle spacing, the fluid velocity over the tubes contained in the baffle overlap, is halved in the case of double segmental baffles. Considerably lower shell-side pressure drops are thus produced by this baffle design. The shell-side heat transfer coefficients would also be lower than those exhibited by single segmental baffled exchangers.

Shell and tube heat exchangers with double segmental baffles are employed for heat transfer duties requiring a low shell-side pressure drop. Economics make a long double segmental baffled unit of small shell diameter preferable to a short single segmental baffled unit of large shell diameter.

No design data for double segmental baffles have been published. The need for accurate design data for this baffle arrangement has been emphasised by the heat exchange equipment manufacturers indirectly sponsoring this work.

With double segmental baffles, geometrical symmetry exists about a plane through a diameter parallel to the baffle cut. This is shown in Fig. 122. The shell-side flow may be assumed to be equally distributed between these two halves of the bundle. The flow geometry of each of these half-bundles is similar to that of a single segmental baffle arrangement. A double segmental baffled unit may thus be analysed as two equal parallel single segmental baffled units.

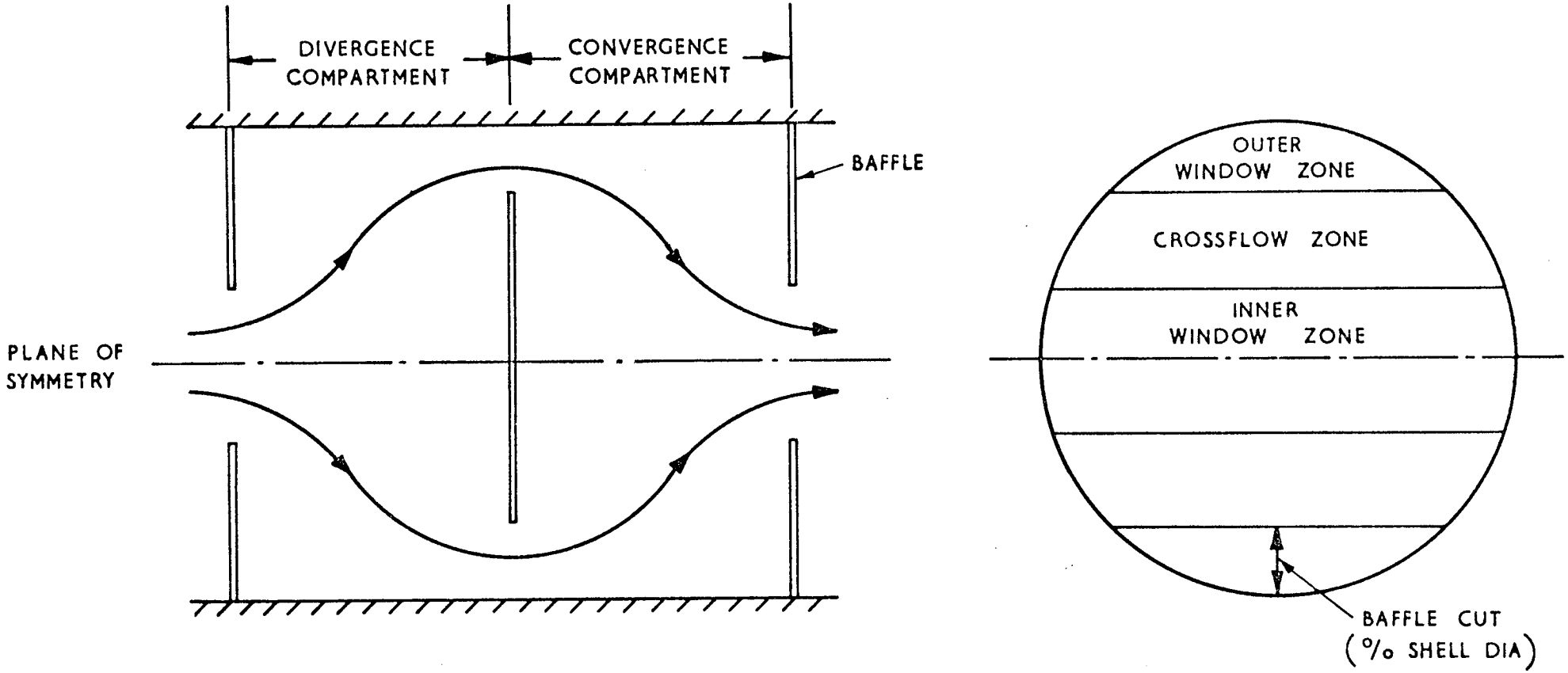

FIG.122. DOUBLE SEGMENTAL BAFFLE ARRANGEMENT

A similar approach was suggested by Kern (21) for predicting the performance of single segmental baffled heat exchangers with multi shell-side passes.

Certain features of these two parallel, half-cylindrical units differ from those of a true single segmental baffled exchanger. A liquid-to-liquid interface exists between the two parallel single segmental baffled units. The small velocity gradient towards this interface would produce far less frictional drag than that incurred at the shell wall in a normal single segmental baffled unit. However in a tube bundle, frictional drag is very small compared with form drag, even at low Reynolds numbers. Intermixing of fluid across the interface may be neglected. Form drag associated with the separation of the flow streams along the interface would be negligible compared with that for flow over all the tubes.

The outer window zone (see Fig. 122) is of identical geometry to that of normal single segmental baffles. The crossflow zone is relatively shallower and shows no symmetry about the central transverse row of tubes. The inner window zone differs most from a normal single segmental baffle window zone. It is of almost rectangular cross-section and is tightly packed with tubes. Furthermore no shell-to-baffle leakage can occur at the interface between the two parallel units.

A single shell inlet and outlet port would produce maldistribution of the flow in the end baffle compartments of a double segmental baffled exchanger. These flow characteristics would propagate into other baffle compartments. Truly symmetrical flow may exist in only a few central baffle compartments.

The experiments of this section of the work were designed to demonstrate the general performance characteristics of double segmental baffle arrangements. The analysis of the results examines

the similarity in the performance of a double segmental baffled exchanger to that of two parallel single segmental baffled units.

8.2 SCOPE OF EXPERIMENTS

Both shell-to-baffle and tube-to-baffle leakage was present in all the experiments. The nominal $\frac{1}{8}$ in. (3.18 mm) thick baffles used in the leakage investigations of Section 7 were cut to a double segmental design.

Measurements were made at two baffle spacings and two baffle cuts. These were:-

Baffle spacing - 1.91, 3.82 in. (48.5, 97.0 mm).

Baffle cut (% diameter) - 18.4, 25.0.

The baffle cut refers to that of the one-piece baffles (see Fig. 122). The cut of the two-piece baffles gave equal superficial areas in the inner and outer windows. This is the normal commercial design.

Only a limited number of the results obtained are reported in this thesis. These discussions are thus restricted to the 1.91 in. (48.5 mm) baffle spacing, 18.4 per cent baffle cut configuration. This baffle geometry is shown in Fig. 123.

The arrangement of the bundle within the shell provided side-to-side flow. This produced the flow symmetry depicted in Fig. 122.

Measurements of mass transfer coefficients were confined to the fourth and fifth of nine baffle compartments. These are shown as the divergence and convergence compartments respectively in Fig. 122. An intermediate bundle rebuild was avoided by using a spacer block to relocate the cathodes in the adjacent baffle compartment.

Pressure measurements were made in the fourth, fifth and sixth baffle compartments. The measurements were confined to one symmetrical half of the bundle. The positions of the pressure tapping tubes are shown in Fig. 123. The tappings were orientated at right angles to the crossflow direction.

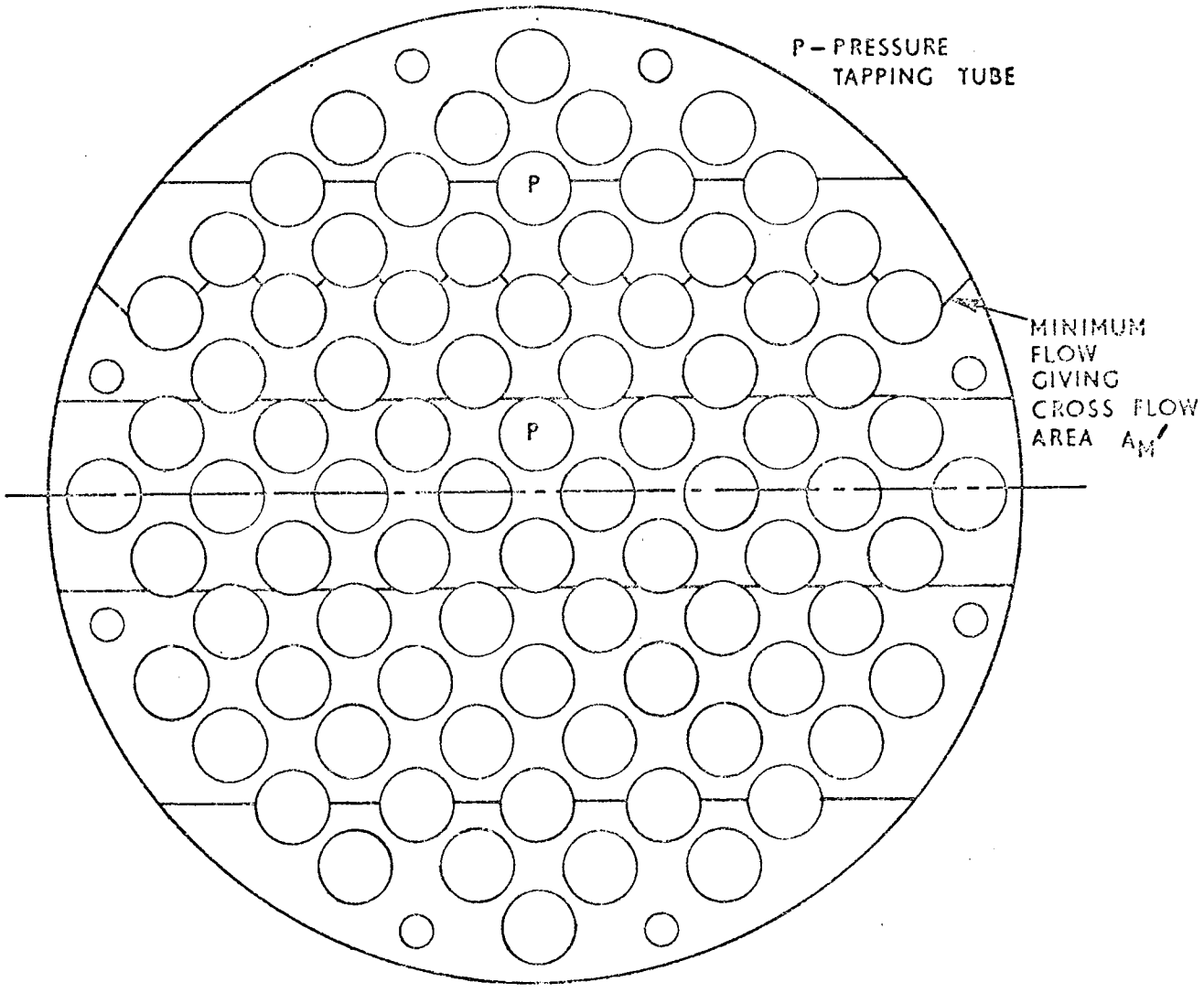

FIG.123. DETAILS OF 18·4% CUT
DOUBLE SEGMENTAL BAFFLES

The mass transfer data were expressed in j-factor form. The shell-side flow was assumed to be equally distributed between the two symmetrical half-bundles. The psuedo no-leakage characteristic velocity of these two flow streams was based on the area A'_M. This is the minimum flow area at the centre row of tubes in the crossflow zone (see Fig. 123). This area is 1.3 per cent less than the corresponding A_M at the centre row of tubes in the bundle. The j-factor data of the two half-bundles could thus be directly compared with the single segmental baffle data.

8.3 DISCUSSION OF EXPERIMENTAL RESULTS

8.3.1 Symmetry

The compartment average j-factors for the two half-bundles are compared in Fig. 124. These data are for the convergence baffle compartment (see Fig. 122). The mass transfer from the centre row of tubes was assumed to be equally distributed between the two streams. The two sets of data fall within 5 per cent of each other. This separation is insignificant. Although not shown, an identical result was obtained from the divergence baffle compartment. Thus the overall mass transfer performances of the two streams are identical. This would suggest equal distribution of the flow between these parallel streams.

The distribution of the individual tube j-factors in the convergence baffle compartment is shown in Fig. 125. The j-factor data has been normalised by dividing individual tube values by the compartment (80 tubes) average value. The coefficients of symmetrically positioned tubes rarely differ by more than 5 per cent. The tube j-factors in the divergence baffle compartment showed a similar degree of symmetry.

Fig. 125 shows that the lowest j-factors occur in the two outer window zones. In the convergence baffle compartment these

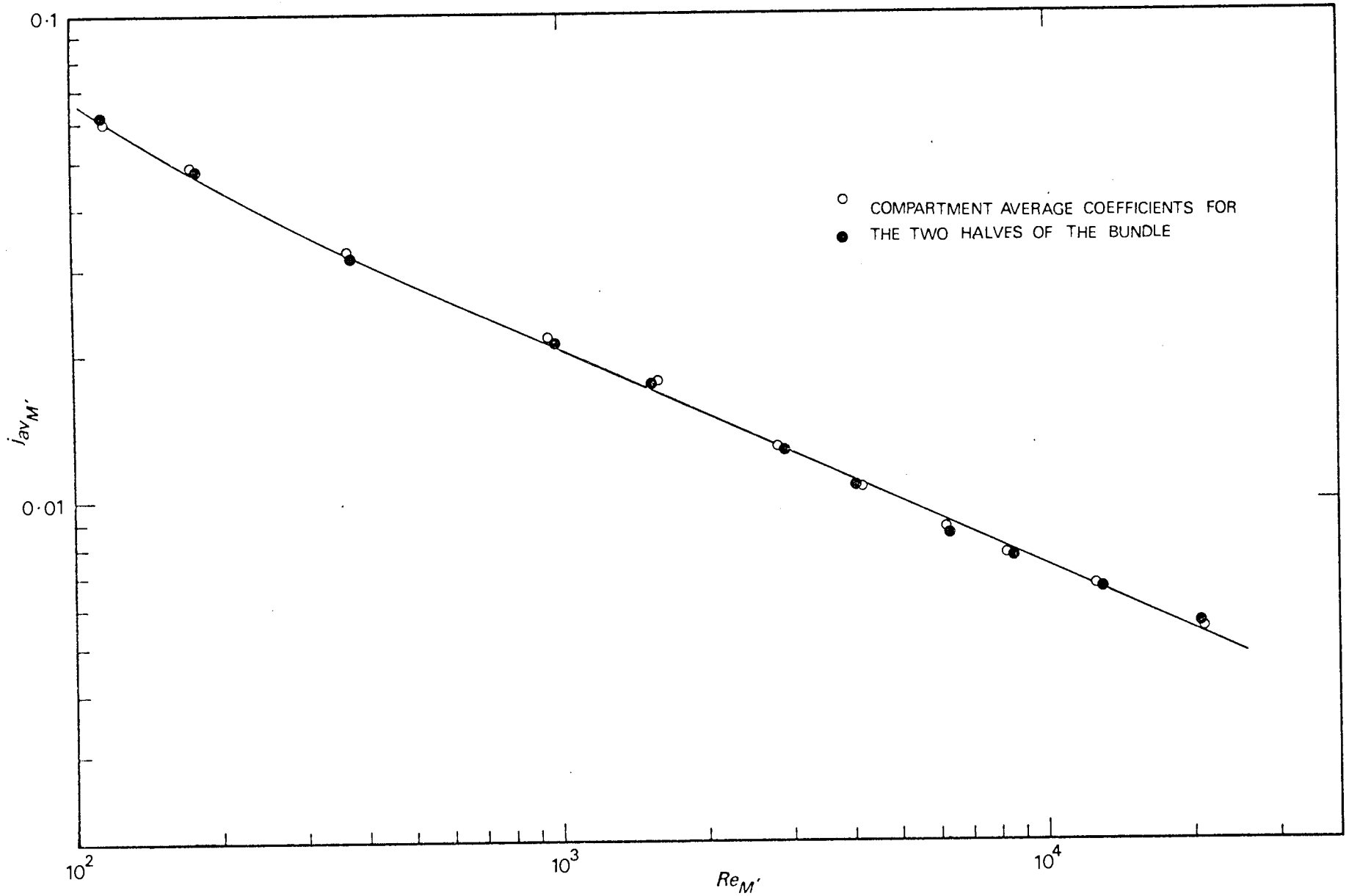

FIG 124

BUNDLE SYMMETRY

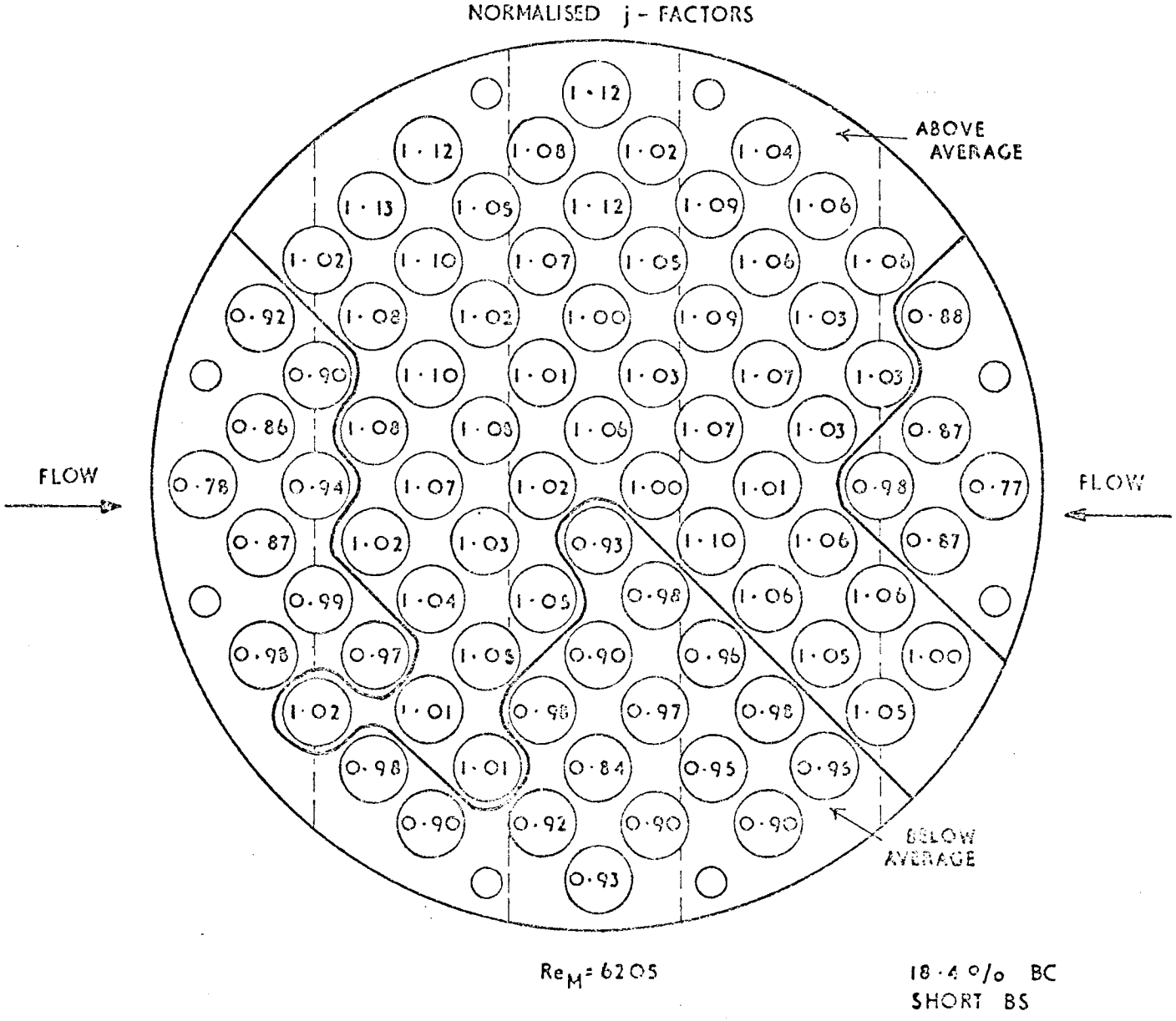

FIG.125. DOUBLE SEGMENTAL CONVERGENCE COMPARTMENT

correspond to flow inlet window zones. The j-factors of tubes in the inner window zones (corresponding to flow outlet window zones) are generally higher than those of the outer window zones and are of near equal magnitude to those of tubes in the crossflow zones. Similar features were shown by the 18.4 per cent baffle cut single segmental data in Section 7.5.2 (see Fig. 111). Both the single and double segmental baffle data show a region of low j-factors spreading upwards through the centre of the bundle. This has been attributed to flow eddies formed as the result of the small shell-to-baffle leakage at the bottom of the bundle.

8.3.2 Convergence and Divergence Baffle Compartments

In adjacent baffle compartments, the shell-side flow converges and diverges respectively (see Fig. 122). While the superficial flow areas of the outer and inner windows are equal, the inner window contains more tubes. The ratio of the free flow area of the outer to that of the inner window is 1.28. Thus in the convergence and divergence baffle compartments, the shell-side fluid encounters a contraction and expansion respectively in the flow area. Differing mass transfer performances would be expected from the two baffle compartments.

The average j-factors for the convergence and divergence baffle compartments are compared in Fig. 126. The two sets of data fall well within 10 per cent of each other. The zonal average j-factors for the two baffle compartments are shown in Fig. 127. The averages are derived from the tubes in both halves of the bundle. The variation in the zonal average j-factors in either baffle compartment is within 15 per cent. In both compartments, the crossflow zone is shown to generally produce the highest average j-factor. The average j-factors of corresponding zones in the two compartments fall within

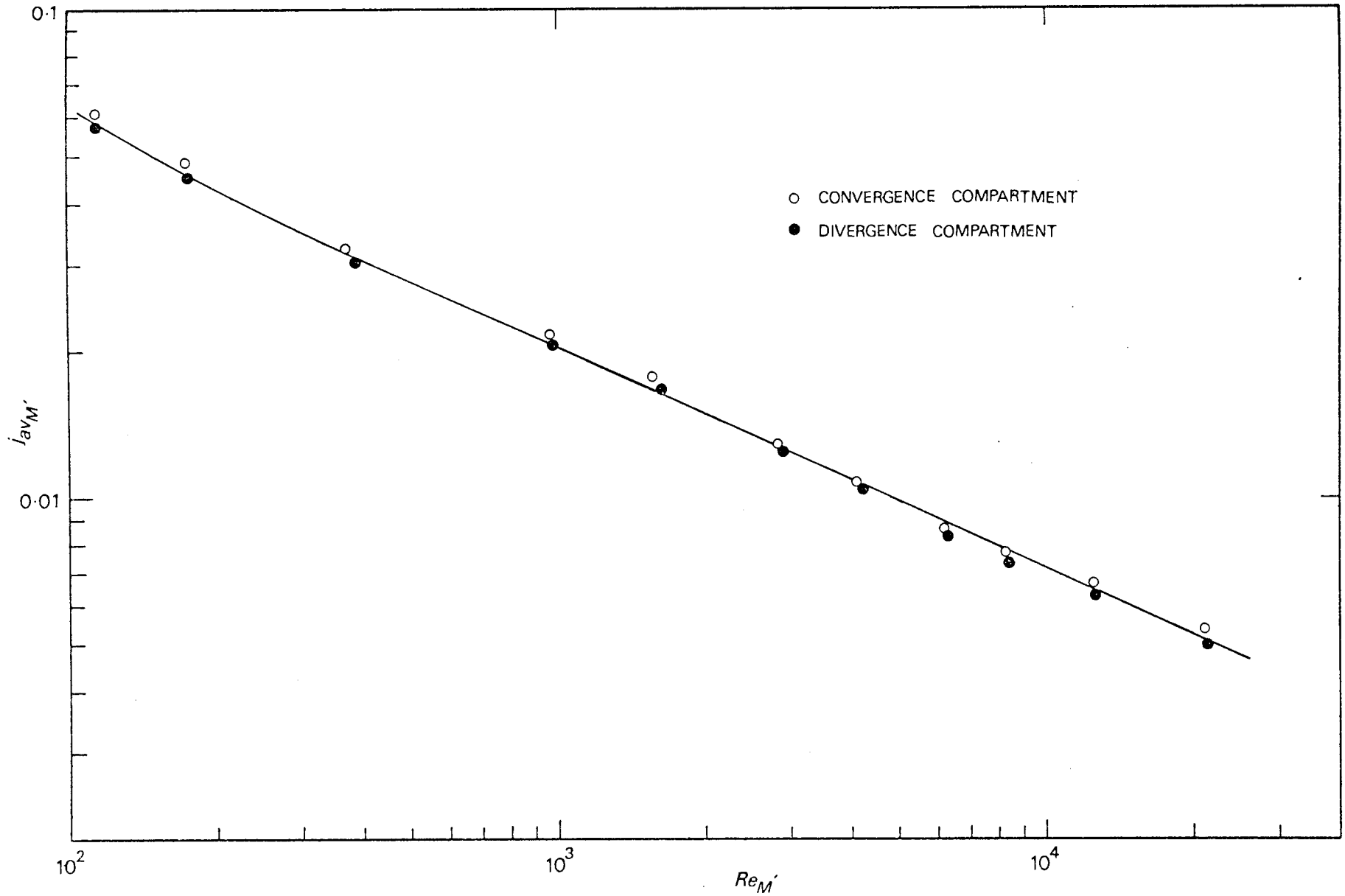

FIG 126 COMPARTMENT AVERAGE COEFFICIENTS

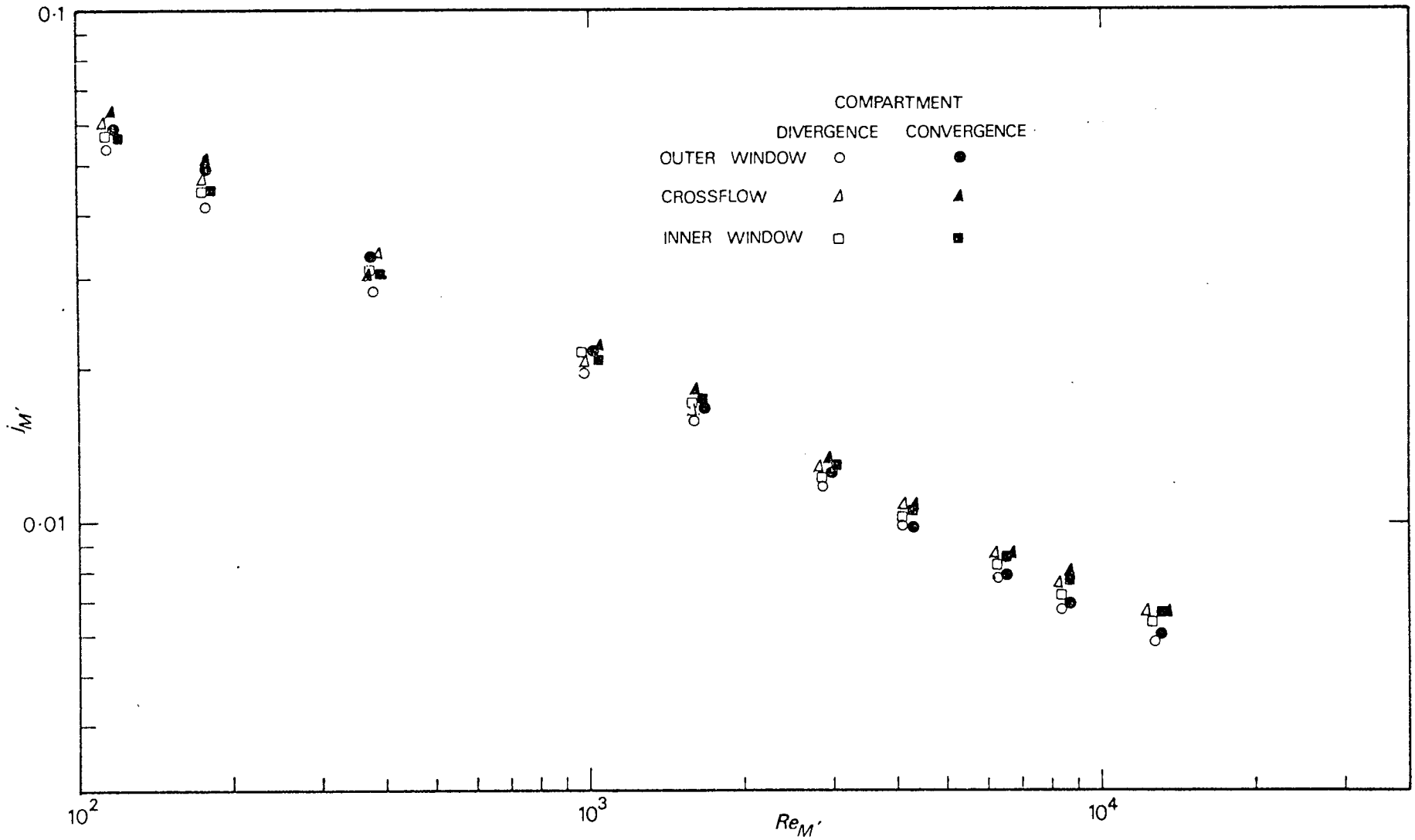

FIG 127 ZONAL AVERAGE COEFFICIENTS

5 per cent of each other. The exception is the case of the outer window zone at low Reynolds numbers. However this discrepancy is only 10 per cent. The differences in the corresponding zonal and compartment average j-factors of the two baffle compartments are barely significant in relation to the estimated accuracy of the data.

In the remaining analyses, the average of the corresponding data from the two adjacent baffle compartments is used.

8.3.3 Performance Prediction using Correlations for Single Segmental Baffles

In this section the mass transfer performance of the double segmental baffled exchanger is compared with that of two parallel single segmental baffled units. The average of the data from the two symmetrical half-bundles is used. The characteristic fluid velocity assumes half the shell-side fluid to flow through the area A_M' (see Fig. 123). These data are compared with the 18.4 per cent baffle cut, single segmental baffle leakage data obtained with side-to-side flow in Section 7.5. The outer window zone of the double segmental baffle arrangement is of identical geometry to that of the window zones in this single segmental baffle configuration. The crossflow and the inner window zones differ from those of the single segmental baffle configuration in the manner already described in Section 8.1.

8.3.3.1 Baffle Compartment

The baffle compartment average j-factors are compared in Fig. 128. The double segmental baffle data fall between 17 and 26 per cent above the single segmental baffle data. The discrepancy is greatest at the high Reynolds numbers. This suggests differing amounts of leakage in the two cases (see Section 7.5.1).

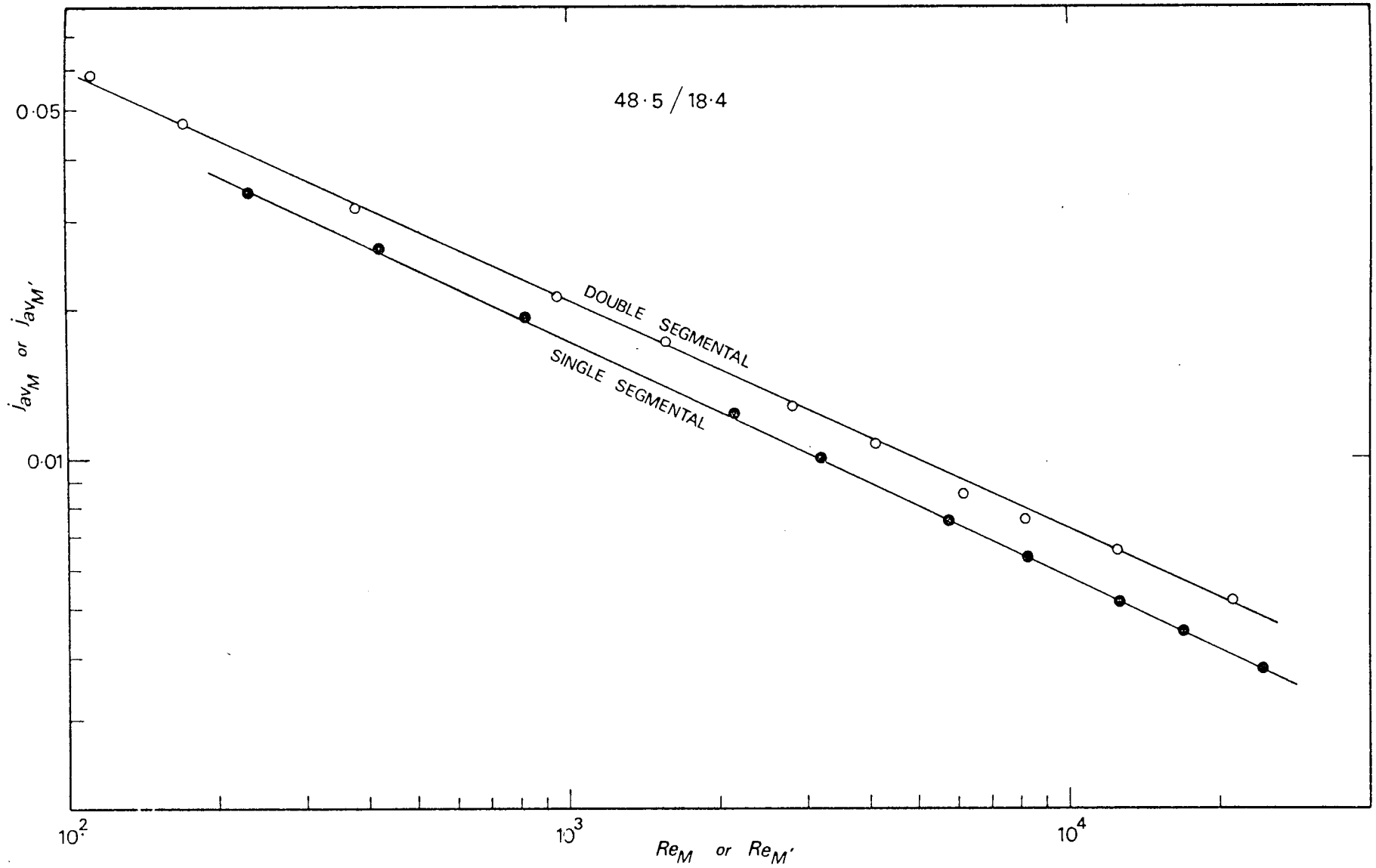

FIG 128 COMPARISON OF COMPARTMENT AVERAGES

The double segmental baffle half-bundle has proportionately less baffle leakage area than the single segmental baffled model. The smaller baffle overlap introduces less tube-to-baffle leakage area. No shell-to-baffle leakage area exists at the interface between the two half-bundles. For a true comparison of the double and single segmental baffle data, these differing leakage areas must be taken into account.

The leakage to window area ratio A_L/A_W used in Section 7.6, was calculated for the case of the double segmental baffle half-bundle. The window area A_W, was taken as the average of the inner and outer window areas. The calculation of the total leakage area A_L is given in Appendix 3.3.5 Values of j_L/j_{NL} corresponding to this value of A_L/A_W were obtained for various Reynolds numbers from Fig. 117. The double segmental data in Fig. 128 were converted to a no-leakage datum by dividing the j-factors by the appropriate value of j_L/j_{NL}. In Fig. 129 these data are compared with the single segmental baffle no-leakage data obtained in Section 6.4. The separation between the two sets of data is reduced with the double segmental data now falling within 10 per cent of the single segmental baffle data. This discrepancy is barely significant.

In a similar analysis the weighted effects of tube-to-baffle and shell-to-baffle leakage were taken into account. Thus values of $\left[1 - j_L/j_{NL} \right]_0$ corresponding to values of A_L/A_W, were obtained for various Reynolds numbers from Fig. 119. These values and the individual leakage areas were inserted into Equation (7.2) to provide values of j_L/j_{NL}. The double segmental baffle data were then

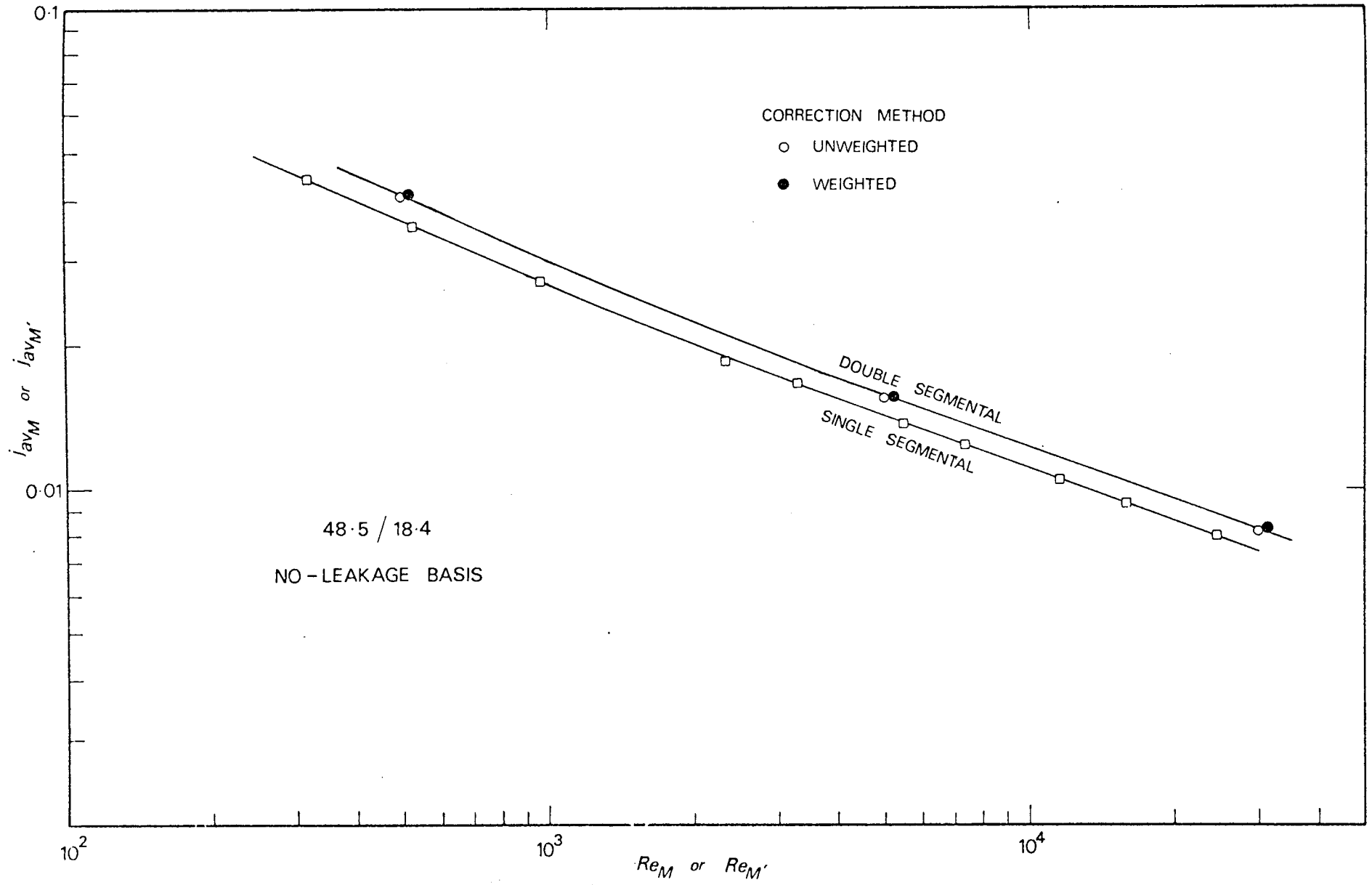

FIG 129 *COMPARTMENT AVERAGES*

converted to a no-leakage datum as before. These data are also shown in Fig. 129. The data show no improvement on those obtained by the first method. The simple unweighted method would seem adequate.

The correlations in Figs. 117 and 119 used above to correct for leakage, describe the effect of a variation in leakage area accompanying a change in baffle cut. No account is taken of the actual distribution of the leakage area within the bundle. The weighted method does distinguish between shell-to-baffle and tube-to-baffle leakage. The relatively smaller leakage areas in the case of the double segmental baffles, would be interpreted as being caused by an increase in the baffle cut. Thus the corrections for leakage should be regarded as only tentative.

The comparison between the double and single segmental baffle data is now extended to individual zones. These analyses would reveal any regional disparities which could have been concealed in the compartment average data.

8.3.3.2 Outer Window Zone

In Fig. 130 the outer window zone average j-factors are compared with those of the single segmental baffle window zone. The latter data are the average of the inlet and outlet window zone j-factors. The double segmental baffle data fall between 11 and 16 per cent above the single segmental baffle data, the discrepancy being greatest at the low Reynolds numbers. This agreement between the data is superior to that shown by the compartment average data. This is to be expected, for the geometry of the outer window zone is identical to that of a single segmental baffle window zone.

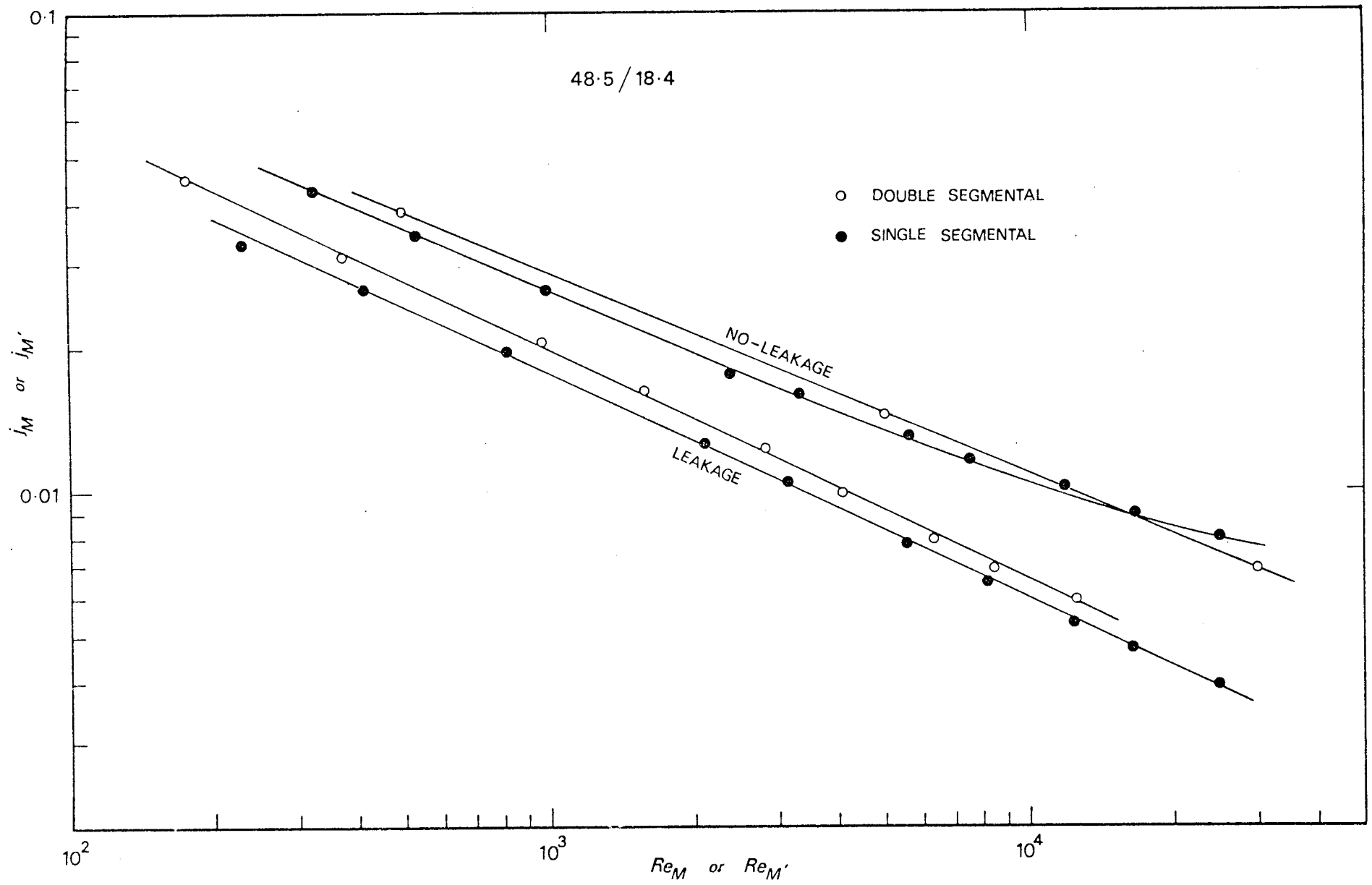

FIG 130 OUTER WINDOW ZONE

The double segmental baffle data were corrected for the weighted effect of leakage as before, using Fig. 119. In Fig. 130 these data are compared with the single segmental baffle window zone no-leakage data. The double segmental baffle data now fall within ± 8 per cent of the single segmental baffle data. This discrepancy is insignificant. The effect of leakage would appear to have been overpredicted at the high Reynolds numbers.

8.3.3.3 Crossflow Zone

Crossflow zone average j-factors are compared in Fig. 131. The double segmental baffle data fall between 23 and 28 per cent above those of the single segmental baffles. This discrepancy is larger than that shown by the compartment average data. The geometries of the crossflow zones differ considerably resulting in that of the double segmental baffles having a relatively smaller leakage area.

The double segmental baffle data were corrected for the weighted effect of leakage. These along with the single segmental baffle crossflow zone no-leakage data are also shown in Fig. 131. At the higher Reynolds numbers the double segmental baffle data fall around 5 per cent above the single segmental baffle data. This discrepancy increases to 15 per cent at lower Reynolds numbers. The correlation of the double and single segmental baffle data would appear to be inadequate at these low Reynolds numbers. The differing values of the geometrical ratio L_C/L_S may need to be taken into account (see Section 6.5).

8.3.3.4 Inner Window Zone

In Fig. 132 the inner window zone average j-factors are compared with those of the single segmental baffle

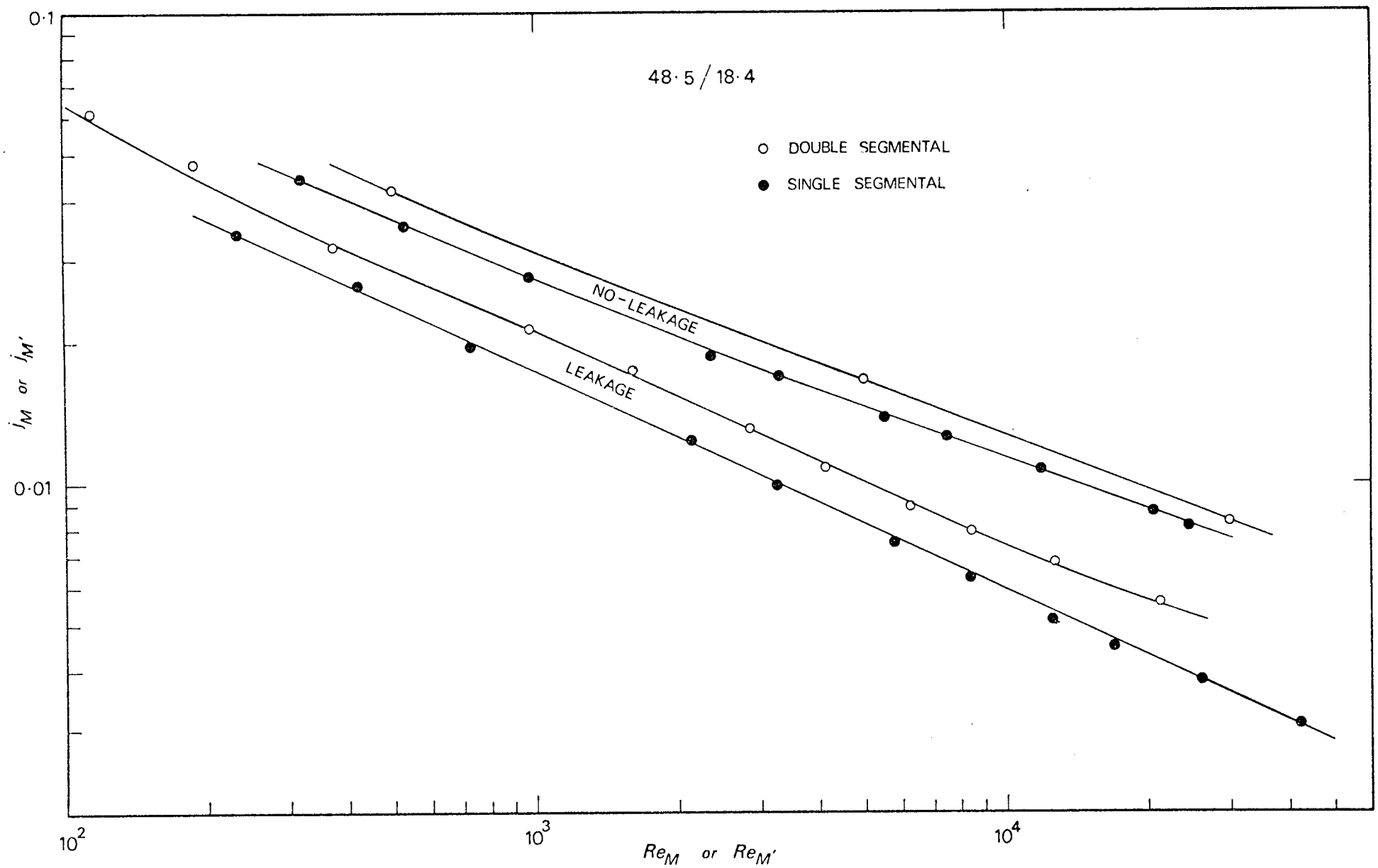

FIG 131

CROSSFLOW ZONE

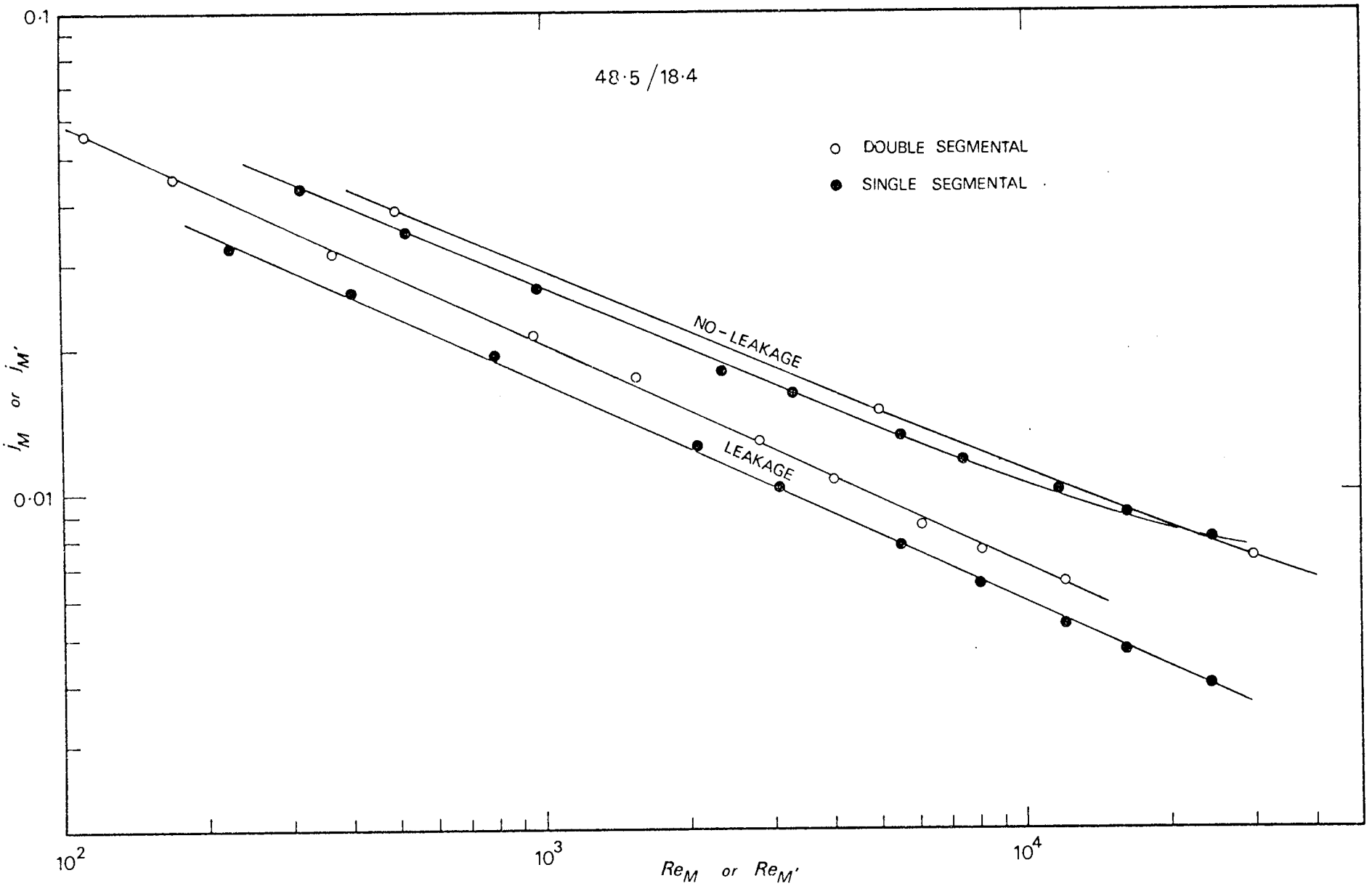

FIG 132

INNER WINDOW ZONE

window zone. The latter data are again the average of the inlet and outlet window zone data. The double segmental baffle data fall consistently around 20 per cent above the single segmental baffle data. After correcting for the weighted effect of leakage, the data fall within 10 per cent of the single segmental baffle no-leakage data. This discrepancy is barely significant. This agreement between the single and double segmental baffle data is almost as good as that shown by the outer window zone. The geometry of the inner window zone however differs far more from that of a single segmental baffle window zone.

8.3.3.5 Conclusions

The mass transfer characteristics of a double segmental baffled exchanger have been shown to be similar to those of two parallel single segmental baffled units. The investigations have been confined to a central internal baffle compartment. The normal port geometry with double segmental baffle units would present asymmetry in the end baffle compartments. The method used in correcting for the effect of leakage is only tentative.

The zonal analyses indicated that the crossflow zone data were least similar to those of the single segmental baffles. The dissimilarity was significant only at the low Reynolds numbers. The correction for leakage may have been inadequate.

8.3.4 Advantages of Double Segmental Baffles

On a total shell-side flow rate basis, the mass transfer performance of the 18.4 per cent baffle cut, double segmental baffles was found to be very similar to that of the 37.5 per cent cut single segmental baffles with the same baffle clearances.

No correction was made for the differing available leakage areas. The two sets of data are compared in Fig. 133. The area A_M and the total shell-side volumetric flow rate were used in calculating the characteristic velocity in both baffle arrangements. The double and single segmental baffle data are shown to be well within 10 per cent of each other.

The baffle spacing of the two baffle arrangements is the same. The total window flow area with the double segmental baffles is 30 per cent less than that of the single segmental baffles. However the double segmental baffles have a 14 per cent higher baffle leakage area. The additional leakage area would compensate for some of the deficit in the window flow area.

Pressure drop measurements from the two baffle arrangements are compared in Fig. 134. The pressure drop is that across two adjacent baffle compartments. The double segmental baffle pressure measurements were confined to one half of the bundle (see Fig. 123). Similar pressure drops would be expected from the two symmetrical half-bundles. Mass transfer measurements have already suggested symmetry within the fluid flow. The data are compared on the basis of the volumetric flow rate, pressure measurements having been made at similar fluid temperatures. The double segmental baffle pressure drop data fall within 10 per cent of those of the single segmental baffles. At the high flow rates the double segmental baffle data fall slightly above the single segmental baffle data. The reverse is true at the low flow rates. A similar feature was exhibited by the mass transfer data in terms of Reynolds numbers in Fig. 133.

These two particular baffle configurations have been shown to produce similar mass transfer and pressure drop performances. In this situation there would appear to be no advantage in

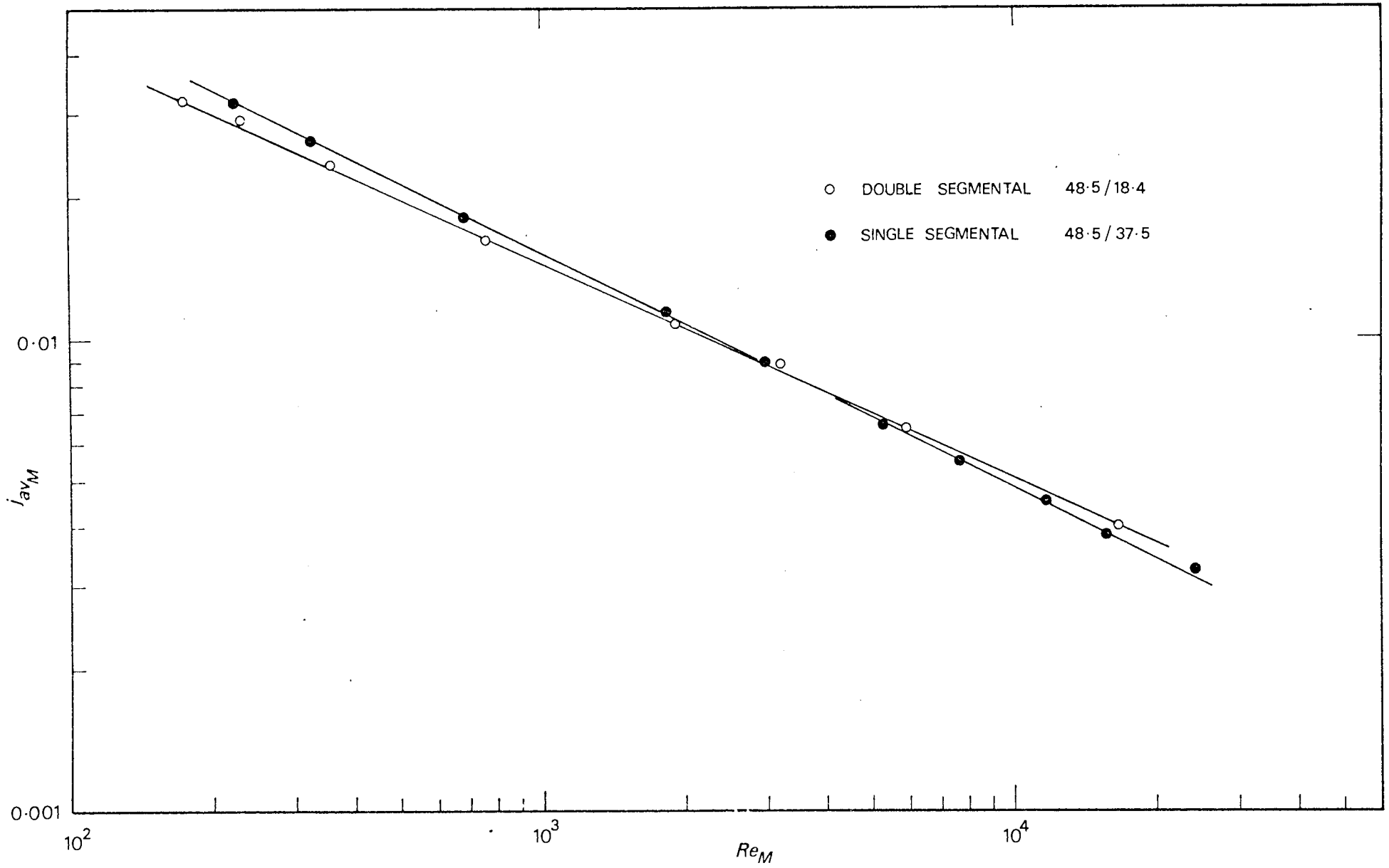

FIG 133 COMPARISON OF COMPARTMENT AVERAGE COEFFICIENTS

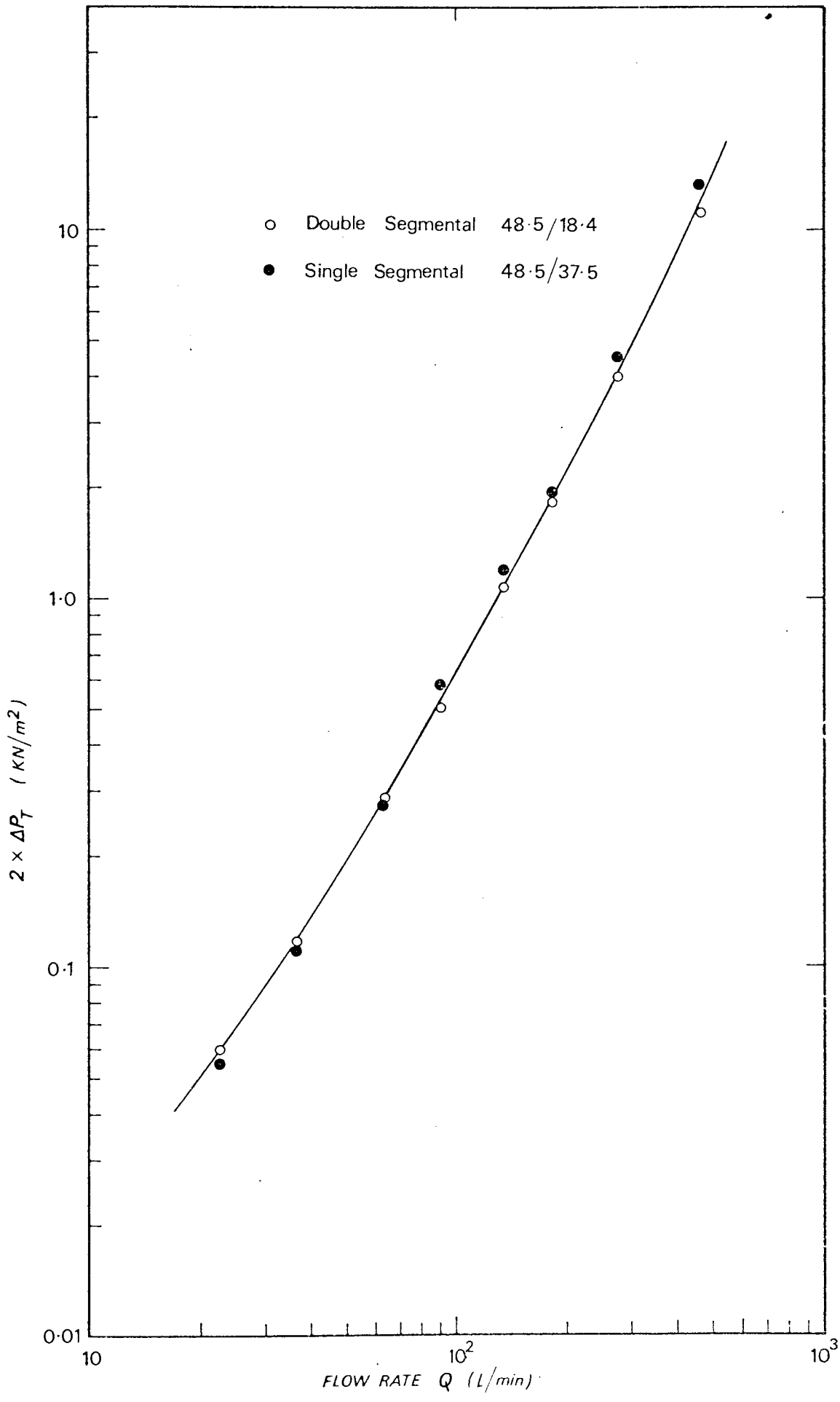

FIG 134 COMPARISON OF PRESSURE DROP

replacing the single segmental baffles by the double segmental baffle arrangement. However this large cut single segmental baffle arrangement has been shown to produce a maldistribution of tube j-factors (see Section 7.5.2). In Fig. 135, the variations in tube j-factors through a baffle compartment for the single and double segmental baffle arrangements, are compared in terms of a normalised standard deviation. The Reynolds number is that used above. A convergence and a divergence compartment were analysed in the case of the double segmental baffles. The double segmental baffles are shown to produce a far more uniform distribution of tube j-factors, indicating that better use is being made of the available transfer surface. On the basis of this characteristic, the double segmental baffles would appear to be superior to the single segmental baffles in this particular situation.

This isolated comparison suggests that for any single segmental baffle configuration, there exists a design of double segmental baffles which has both a similar mass transfer and pressure drop performance to those of the single segmental baffles. For a low shell-side pressure drop requirement it has been shown above that double segmental baffles would be preferable to single segmental baffles with a large baffle cut.

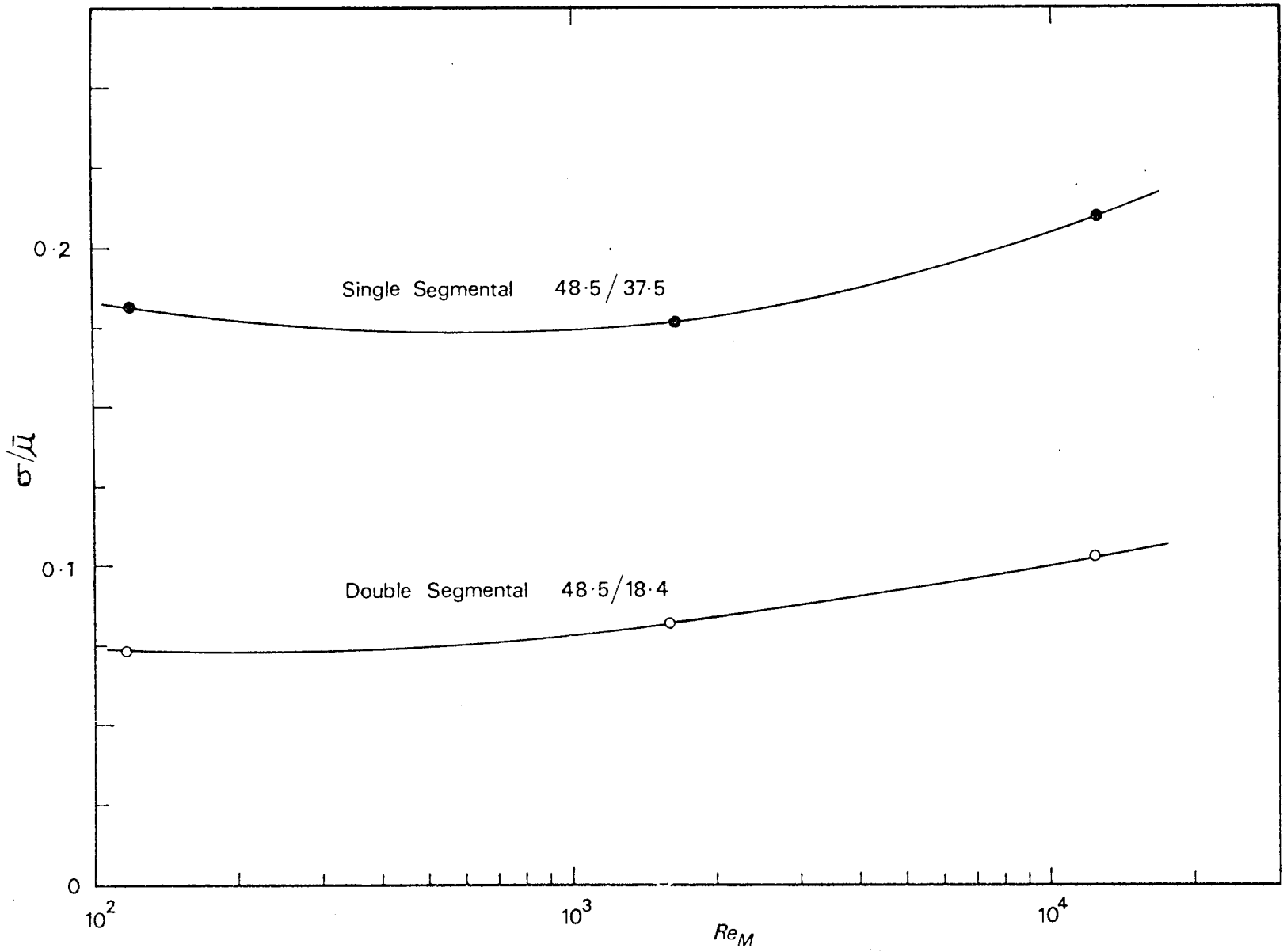

FIG 135 *DISTRIBUTION OF TUBE COEFFICIENTS*

9. GENERAL CONCLUSIONS

9.1 APPRAISAL OF THE MASS TRANSFER MODELLING TECHNIQUE

The electrochemical mass transfer technique has been shown through the Chilton and Colburn analogy, to predict shell-side heat transfer data which are consistent with actual heat transfer measurements and also data from another mass transfer modelling technique.

The suitability of the electrochemical technique for rapid data acquisition has been demonstrated in this work. Over a six month experimental period, thirty one different shell-side geometries were examined incorporating over 21 000 measurements of tube mass transfer coefficients.

The electrochemical technique has many advantages over other mass transfer modelling techniques and methods of direct heat transfer measurement. These have already been listed in Section 3.

9.2 SIMILARITY IN PERFORMANCE OF ALL THE BAFFLE ARRANGEMENTS

The combined heat transfer and pressure drop performances constitute the overall shell-side performance. The similarity shown in both the shell-side mass transfer and pressure drop data of a single and a double segmental baffle arrangement (see Section 8.3.4), suggests that any specified shell-side performance may be fulfilled by more than one baffle design.

In Fig. 136 the mass transfer and pressure drop data for all the baffle configurations examined in this work are compared at a particular shell-side flow rate. Data at other flow rates exhibited similar features. The baffle compartment average mass transfer coefficient is shown. The pressure drop has been obtained by dividing the baffle compartment pressure drop by the baffle spacing. The data fall near to a single curve. The data for the no-leakage, 18.4 per cent cut, 97.0 mm spacing, baffle configuration is the

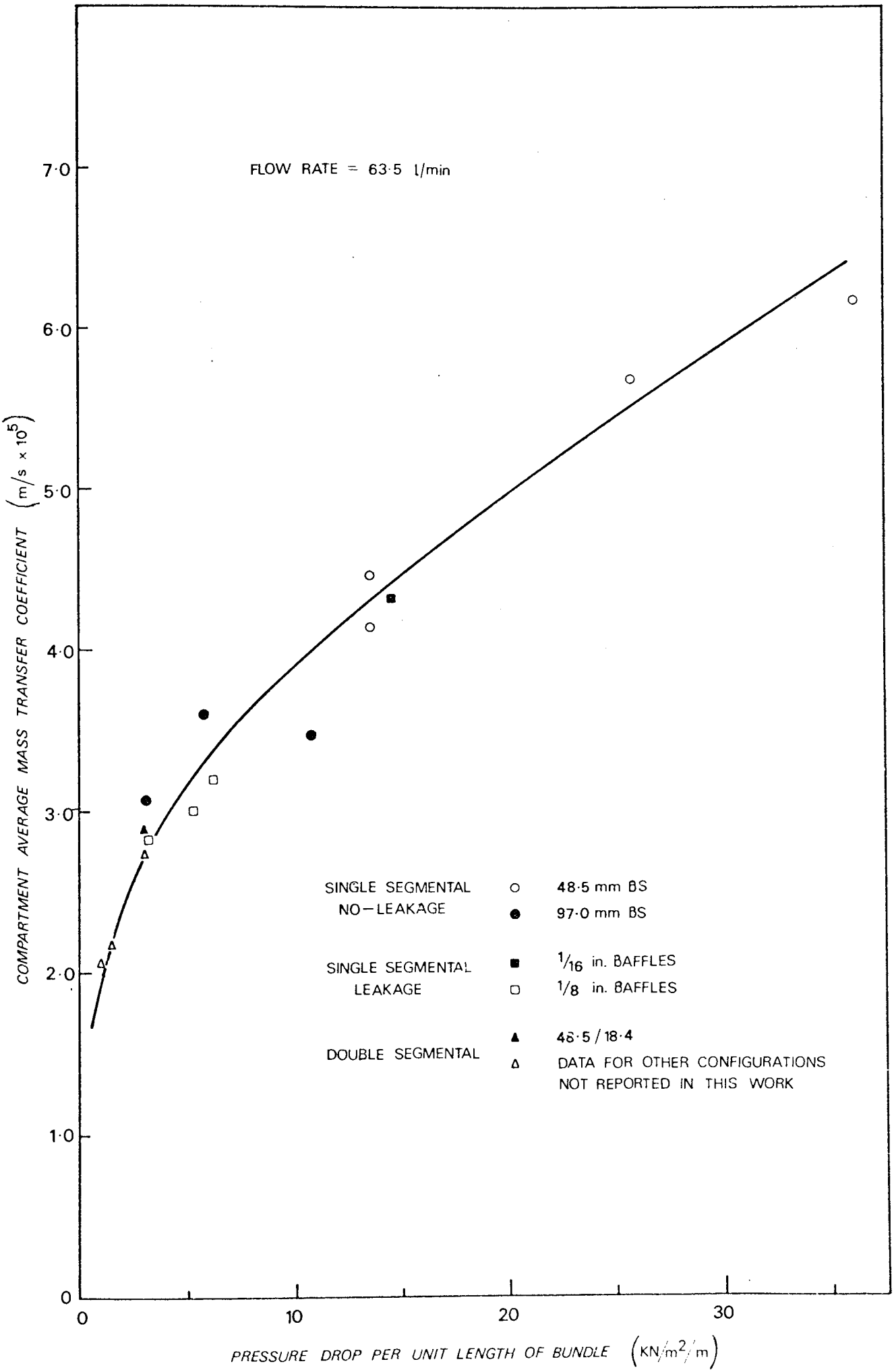

FIG 136 PERFORMANCE COMPARISON

exception. This particular configuration has been shown to be of bad design; the large value of A_M/A_W causes serious fluid "jetting" (see Section 6.3.2).

The no-leakage, short baffle spacing, single segmental baffle data fall at the top end of the curve. The double segmental baffle data fall at the bottom end of the curve. The long baffle spacing no-leakage and the leakage single segmental baffle data fall in an intermediate region. Overlap occurs between the sets of data. The following conclusions may be drawn from this analysis:-

(i) Baffles of differing designs can have similar overall performances.

(ii) Any improvement in the heat transfer performance through a change in baffle design, results in an increase in the pressure drop.

(iii) A specified overall performance may be obtained with single segmental baffles by altering only the baffle spacing, baffle cut or baffle clearances.

(iv) For a low shell-side pressure drop duty, double segmental baffles could be replaced by single segmental baffles with large baffle clearances, baffle cut or baffle spacing.

This interchangeability of baffles suggests that the ultimate criterion for the choice of baffle design may be the uniformity in the distribution of the shell-side heat transfer coefficients. The data from this work provide this information.

10. RECOMMENDATIONS FOR FUTURE WORK

The following investigations are recommended for future work:-

(i) Measurements of mass transfer coefficients and pressure drops in the end baffle compartments. The differing characteristics between end and internal baffle compartments could be identified. Various port geometries could be investigated. The data would allow the derivation of a bundle average j-factor.

(ii) Investigations at larger baffle spacings. The inability to correlate the no-leakage single segmental baffle data for the effect of both spacing and baffle cut may be confined to the relatively small baffle spacings examined in this work. The results from the investigations of Short (22) suggest that this may be the case (see Section 6.4).

(iii) Extension of the single segmental baffle leakage investigations to other baffle spacings and baffle clearances. The data from these investigations would allow a more thorough analysis of the effect of leakage.

(iv) Detailed investigations into the variation in the mass transfer coefficient along tube lengths (see Section 4.4.5). These studies may identify sections of tubes having particularly abnormal coefficients. This information would aid the design of more efficient shell-side geometries.

(v) Further development of the electrochemical technique in studies of distributions of residence times in the shell-side fluid (see Appendix 2.5). Residence time studies would provide valuable information about the features of shell-side flow, in particular the degree of intermixing of the shell-to-baffle leakage and the bundle-bypass streams with the main flow stream. An accurate correction factor for the LMTD (see Section 1.3.3) could be derived.

Investigations into other features of shell-side geometry have already been included in the future experimental programme at AEE Winfrith (see Section 5.1).

NOMENCLATURE

A	Shell-side flow area	m^2
A_B, A_M	Minimum crossflow area at centre row of tubes	m^2
A_L	Total baffle leakage area	m^2
$A_{M'}$	Minimum crossflow area at centre row of tubes in double segmental baffle crossflow zone	m^2
A_{max}	Maximum crossflow area in crossflow zone	m^2
A_{min}	Minimum crossflow area in crossflow zone	m^2
A_{SB}	Shell-to-baffle leakage area	m^2
A_{TB}	Tube-to-baffle leakage area	m^2
b	Coefficient in Weisman correlation	
C	Concentration	Kg mole/m^3
C_b	Bulk ferricyanide ion concentration	Kg mole/m^3
C_p	Specific heat evaluated at bulk temperature	KJ/Kg.^oc
C_s	Ferricyanide ion concentration at the cathode surface	Kg mole/m^3
D, D_v	Diffusion coefficient	m^2/s
D_e	Shell equivalent diameter	m
D_h	Shell hydraulic mean diameter	m
D_s	Shell inside diameter	m
d_t	Tube outside diameter	m
E	Oxidation potential	V
F	Faraday's constant	
F_{BP}	Fraction of A_M in bypass channel	
F_E	End-space factor	
G	Shell-side fluid mass velocity	$Kg/m^2.s$
G_C	Crossflow mass velocity through widest section of shell	$Kg/m^2.s$
G_K	Mass velocity defined by Kern	$Kg/m^2.s$
g	Gravitational acceleration	m/s^2
Gr	Grashof Number	
h	Heat transfer coefficient	$KW/m^2.^oc$

h_B	Average shell-side heat transfer coefficient for the crossflow zone	$KW/m^2.^oc$
h_o	Bundle average shell-side heat transfer coefficient	$KW/m^2.^oc$
h_W	Average shell-side heat transfer coefficient for the window zone	$KW/m^2.^oc$
I	Electrical current	A
I_L	Limiting (or diffusion) current	A
j	Individual tube mass transfer j-factor	
jav	Baffle compartment average mass transfer j-factor	
jc	Crossflow zone average mass transfer j-factor	
jh	Heat transfer j-factor, $\frac{h}{C_p \rho u} Pr^{2/3}$	
jm	Mass transfer j-factor $\frac{K_C}{u} S_c^{2/3}$	
jw	Window zone average mass transfer j-factor	
j_{w1}	Inlet window zone average mass transfer j-factor	
j_{w2}	Outlet window zone average mass transfer j-factor	
K	Flow resistance factor	
K_C	Mass transfer coefficient	m/s
K_M	Arithmetic mean of mass transfer coefficients from incremental cathodes	m/s
K_S	Mass transfer coefficient for baffle-spacing length cathode	m/s
k	Thermal conductivity evaluated at bulk temperature	$W/m.^oc$
L_C	Baffle overlap	m
L_E	Cathode length	m
L_S	Baffle spacing	m
m	Exponent	
N	Rate of mass transfer	Kg mole/m^2.s
N_B	Number of baffles	
N_C	Number of tube rows in crossflow zone	
$N_{C'}$	Total effective number of crossflow tubes	
N_S	Number of sealing strips	

N_T	Number of tube rows	
N_W	Number of tube rows in window zone	
n	Exponent	
n_e	Valency of an ion	
Nu	Nusselt number, $\frac{h\ d_t}{k}$	
P	Tube pitch	m
Pr	Prandtl Number, $\frac{Cp\ \mu}{k}$	
ΔP	Pressure drop	N/m^2
ΔP_C	Crossflow zone shell-side pressure drop	N/m^2
ΔP_T	Baffle compartment shell-side pressure drop	N/m^2
ΔP_W	Window zone shell-side pressure drop	N/m^2
Q	Shell-side fluid volumetric flow rate	m^3/s
Q'	Equilibrium constant	
R	Gas constant	
r	Ratio S_W/S_T	
Ra	Rayleigh number, GrPr	
Re	Shell-side Reynolds number, $\frac{\rho u\ d_t}{\mu}$	
S	Cathode surface area	m^2
S_B	Total external surface area of tubes in crossflow zone	m^2
S_T	Total tube external surface area of bundle	m^2
S_W	Total external surface area of tubes in window zone	m^2
Sc	Schmidt Number $\frac{\mu}{\rho\ D_v}$	
St	Stanton Number, $\frac{Nu}{Re\ Pr}$	
T	Temperature	^oc
u	Fluid velocity	m/s
u_{AV}	$\frac{1}{3}(u_{min} + u_{max} + u_W)$	m/s

u_M	Shell-side velocity based on A_M	m/s
$u_{M'}$	Shell-side velocity based on $A_{M'}$	m/s
u_W	Shell-side velocity based on A_W	m/s
u_y	$(u_M^2 . u_W)^{1/3}$	m/s
u_z	$(u_M . u_W)^{1/2}$	m/s
W	Shell-side fluid mass flow rate	Kg/s
y	Distance	m
Z	Orifice shape factor	
Z_S	Orifice shape factor for shell-to-baffle clearance	
Z_T	Orifice shape factor for tube -to-baffle clearance	

α	Proportionality constant	
α'	Effectiveness factor	
β	Proportionality constant	
β'	Effectiveness factor	
β_h	Thermal coefficient of expansion	$/^\circ c$
γ	Tube-row correction factor	
γ'	Effectiveness factor	
ε	Voidage fraction in tube bundle	
ε_D	Molecular eddy diffusivity	m^2/s
ε_ψ	Electrostatic potential eddy diffusivity	m^2/s
ζ	Bundle bypass stream correction factor	
ζ'	Effectiveness factor	
η	Kinematic viscosity, μ/ρ	m^2/s
λ	Baffle leakage correction factor	
μ	Fluid viscosity evaluated at bulk temperature	Ns/m^2
μ_W	Fluid viscosity evaluated at the wall temperature	Ns/m^2

$\bar{\mu}$	Arithmetic mean	
ν	Ratio of velocity at edge of laminar sublayer to the stream velocity	
ρ	Fluid density evaluated at bulk temperature	Kg/m^3
σ	Standard deviation	
τ	Shear stress	N/m^2
$\varnothing$	Baffle window correction factor	
ϕ	Coefficient in Weisman correlation	
Ψ	Electrostatic potential	V

Subscripts:

AV	Based on u_{AV}
BP	Bundle bypass stream
f	Evaluated at film temperature
h	Heat transfer process
I	Ideal tube-bank
IW	Inner window zone
L	For baffle leakage
m	Mass transfer process
M	Based on u_M
M'	Based on $u_{M'}$
max	Based on u_{max}
min	Based on u_{min}
NL	Without baffle leakage
OW	Outer window zone
W	Based on u_W
y	Based on u_y
z	Based on u_z
ε	Based on ε

BIBLIOGRAPHY

1 TABOREK J
"Fouling - The Major unresolved Problem in Heat Transfer, Parts I and II"
C.E.P. Symp. Series Nos. 2 and 7 68 (1972)

2 STANDARDS OF THE TUBULAR EXCHANGER MANUFACTURERS ASSOCIATION
Fourth Edition (1959)

3 COLBURN A P
"A Method of correlating Forced Convection Heat Transfer Data and a comparison with Fluid Friction".
Trans. AIChE 29 174 (1933)

4 GRIMISON E D
"Correlation and Utilisation of New Data on Flow Resistance and Heat Transfer for Cross Flow of Gases over Tube Banks".
Trans. ASME 59 (7) 583 (1937)

5 HUGE E C
"Experimental Investigation of Effects of Equipment size on Convection Heat Transfer and Flow Resistance in Cross Flow of Gases over Tube Banks".
Trans. ASME 59 (7) 573 (1937)

6 PIERSON O L
"Experimental Investigation of the Influence of Tube Arrangement on convection Heat Transfer and Flow Resistance in Cross Flow of Gases over Tube Banks".
Trans. ASME 59 (7) 563 (1937)

7 McADAMS W H
"Heat Transmission"
Third Edition, Mcgraw Hill (1954)

8 SHEEHAN T V, SCHOMER R T, DWYER O E
"Heat Transfer for Cross Flow of Water through a Tube Bank at Reynolds Numbers up to a Million".
Paper No. 54-F-19 ASME meeting, New York (1954)

9 BERGELIN O P, DAVIS E S, HULL H L
"A study of Three Tube Arrangements in Unbaffled Tubular Heat Exchangers".
Trans. ASME 71 369 (1949)

10 BERGELIN O P, BROWN G A, HULL, SULLIVAN
"Heat Transfer and Fluid Friction during Viscous Flow across Banks of Tubes-Part III".
Trans. ASME 72 881 (1950)

11 BERGELIN O P, BROWN G A, DOBERSTEIN S C
"Heat Transfer and Fluid Friction during Flow across Banks of Tubes-Part IV".
Trans. ASME 74 953 (1952)

12 BELL K J
"Final Report of the Co-operative Research Programme on Shell and Tube Heat Exchangers".
University of Delaware Engineering Experimental Station, Bulletin No 5 (1963)

13 ZUKAUSKAS A
"Heat Transfer from Tubes in Crossflow".
Advances in Heat Transfer 8 93 (1972)

14 WEISMAN J
"Effect of Void Volume and Prandtl Modules on Heat Transfer in Tube Banks and Packed Beds".
AIChE JL 1 342 (1955)

15 KAYS W M, LONDON A L, LO R K
"Heat Transfer and Friction characteristics for Gas Flow Normal to Tube Banks - The Use of a Transient-Test Technique".
Trans. ASME 76 387 (1954)

16 WHITAKER S
"Forced Convection Heat Transfer Correlations for Flow in Pipes, Past Flat Plates, Single Cylinders, Single Spheres, and for Flow in Packed Beds and Tube Bundles".
AIChE JL 18 (2) 361 (1972)

17 FAIRCHILD H N, WELCH C P
"Convection Heat Transfer and Pressure Drop of Air Flowing across In-Line Tube Banks at Close Back Spacings".
Paper No 61-WA-250 ASME meeting, Cornell University (1961)

18 BERGELIN O P, COLBURN A P, HULL H L
"Heat Transfer and Pressure Drop during Viscous Flow across Unbaffled Tube Banks".
University of Delaware Engineering Experimental Station, Bulletin No. 2 (1950)

19 ZUKAUSKAS A, MAKAREVICIUS V J, SLANCIAUSKAS A
"Heat Transfer in Banks of Tubes in Crossflow of Fluid".
Mintis, Vilnius (1968) (In Russian)

20 DONOHUE D
"Heat Transfer and Pressure Drop in Heat Exchangers".
Ind. Eng. Chem. 41 2499 (1949)

21 KERN D Q
"Process Heat Transfer"
First Edition McGraw Hill (1950)

22 SHORT B E
"Heat Transfer and Pressure Drop in Heat Exchangers".
University of Texas Publication No 4324 (1943)

23 HEINRICH E, STUCKLE R
Ver. deut. Ing., Mitt. Forech. Gebiete
Ingenieurw., Heft 271 (1925) (In German)

24 BOWMAN, R A
"Investigation of Heat Transfer Rates on the External Surface of baffled Tube Banks"
Unpublished ASME paper No 28, New York (1936)

25 GARDNER H S, SILLER I
"Shell-side coefficients of Heat Transfer in a Baffled Heat Exchanger".
Trans. ASME 69 (6) 687 (1947)

26 TINKER T
"Shell Side Characteristics of Shell and Tube Heat Exchangers".
Paper No 47-A-130 ASME Meeting New York (1947)

27 BRITISH SHIPBUILDING RESEARCH ASSOCIATION
"A Correlation of Current Data on Heat Transfer and Pressure Drop in Segmentally Baffled Shell-and-Tube Heat Exchangers".
Report No 148 (1955)

28 TINKER T
"Shell Side Characteristics of Shell and Tube Heat Exchangers (Parts I and II)".
General Discussions on Heat Transfer, ASME and Inst. Mech. Engrs. London (1952)

29 BELL K J
"Exchanger Design Based on the Delaware Research Programme".
Petrol. Engr. 32 (11) C26 and C40a (1960)

30 BERGELIN O P, BROWN G A, DOBERSTEIN S C
"Heat Transfer and Fluid Friction during Flow across Banks of Tubes-Part V".
Trans. ASME 76 841 (1954)

31 BROWN G A
"Heat Transfer and Fluid Friction during Turbulent Flow through a Baffled cylindrical shell and Tube Heat Exchanger".
Ph. D Thesis, University of Delaware (1956)

32 WILLIAMS T A
"A Mass Transfer Study of Local Transfer Coefficients on the shell-side of a cylindrical shell and Tube Heat Exchanger Fitted with Segmental Baffles".
Ph. D. Thesis, University of Manchester (1962)

33 BERGELIN O P, BELL K J, LEIGHTON M D
"Heat Transfer and Fluid Friction during Flow across Banks of Tubes - Part VII".
C.E.P. Symp. Series 55 (29) 45 (1959)

34 BERGELIN O P, BELL K J, LEIGHTON M D
"Heat Transfer and Fluid Friction during Flow across Banks of Tubes - Part VI".
Trans ASME 80 53 (1958)

35 SULLIVAN F W, BERGELIN O P
"Heat Transfer and Fluid Friction in a Shell and Tube Exchanger with a single Baffle".
C.E.P. symp. series 52 (18) 85 (1956)

36 PALEN J W, TABOREK J
"Solution of Shell-side Flow Pressure Drop and Heat Transfer by Stream Analysis Method".
C.E.P. Symp. Series 65 (92) 53 (1968)

37 PARKER R O, MOK Y I
"Shell-side Pressure Loss in Baffled Heated Exchangers".
Brit. Chem. Eng. 13 124 (1968)

38 DEVORE A
"Try This Simplified Method for Rating Baffled Exchangers".
Petrol. Refiner 40 (5) 221 (1961)

39 AMBROSE T W, KNUDSEN J G
"Local Shell-Side Heat Transfer Coefficients in Baffled Tubular Heat Exchangers".
AIChE JL. 4 332 (1958)

40 GURUSHANKARIAH M S, KNUDSEN J G
"Local Shell-Side Heat Transfer Coefficients in the Vicinity of segmental Baffles in Tubular Heat Exchangers".
C.E.P. Symp. series 55 (29) 29 (1959)

41 SHORT B E
"Shell and Tube Heat Exchangers - Effect of By-Pass and Clearance streams on the Main Stream Temperature".
Paper No 60-HT-16 presented at ASME/AIChE Heat Transfer Conference Buffalo New York (1960)

42 PARKER R O, FISHER J
"New ideas on Heat Exchanger Design".
Hydrocarbon Processing 48 (7) 147 (1969)

43 PATANKAR S V, SPALDING D B
"A Calculation Procedure for the Transient and Steady-State Behaviour of Shell and Tube Heat Exchangers".
Paper presented at 1972 International Seminar, Trogir, Yugoslavia organised by International Centre for Heat and Mass Transfer.

44 TABOREK J
"Design Methods for Heat Transfer Equipment - A Critical Survey of the State of the Art".
Ibid.

45 EMERSON W H
"Shell Side Heat Transfer and Pressure Drop with Turbulent Flow in Segmentally Baffled Shell and Tube Heat Exchangers - A Survey".
National Engineering Laboratory, Report No 45 East Kilbride, Glasgow.

46 GUNTER A Y, SENNSTROM, KOPP
"A Study of Flow Patterns in Baffled Heat Exchangers".
Paper No 47-A-103 presented at meeting of ASME Atlantic City N.J (1947)

47 GUPTA R K, KATZ D L
"Flow Patterns for Predicting Shell-side Heat Transfer Coefficients for Baffled Shell and Tube Exchangers".
Ind. Eng. Chem. 49 998 (1957)

48 MILLER P, BYRNES J J, BENFORADO D M
"Heat Transfer to Water Flowing Parallel to a Rod Bundle".
AIChE J. 2 (2) 226 (1956)

49 ENGINEERING SCIENCES DATA UNIT
Item 69004 -" Convective Heat Transfer during Forced crossflow of Fluids over a cylinder, including Free convection Effects".

50 STACHIEWICZ J W, SHORT B E
"Local Shell-Side Heat Transfer Coefficients in a Leak-Proof Heat Exchanger".
International Developments in Heat Transfer, Colorado,959 (1961)

51 NARAYANAN K
"Local and Overall Heat Transfer Coefficients in Baffled Heat Exchangers".
PhD Thesis, Oregon State University (1962)

52 GAY B, WILLIAMS T A
"Heat Transfer on the Shell-Side of a Cylindrical Shell and Tube Heat Exchanger Fitted with Segmental Baffles - Part I"
Trans. Instn Chem. Engrs 46 95 (1968)

53 WHITE R R, CHURCHILL S W
"Experimental Foundations of Chemical Engineering".
AIChE JL 5 354 (1959)

54 ROBERTS P C O
"Individual Tube Transfer Coefficients in a Segmentally Baffled Shell and Tube Exchanger".
Ph.D Thesis, University of Aston (1969)

55 GAY B, ROBERTS P C O
"Heat Transfer on the Shell-side of a Cylindrical Shell-and-Tube Heat Exchanger Fitted with segmental Baffles-Part II".
Trans. Instn chem. Engrs. 48 3 (1970)

56 CHILTON T H,COLBURN A P
"Mass Transfer (Absorption) Coefficients".
Ind. Eng. Chem. 26 1183 (1934)

57 REYNOLDS O
Proc. Manchester Lit. Phil. Soc. 14 7 (1874)

58 TAYLOR G I
Great Britain Advisory Comm. Aeronaut.
Report Memo 2272 (1916)

59 PRANDTL L
Physik Z, 29 487 (1928)

60 SHERWOOD T K
Trans. AIChE 36 817 (1940)

61 LUCAS D M, DAVIES R M
"Mass Transfer Modelling Techniques in the Prediction of convective Heat Transfer Coefficients in Industrial Heating Processes".
Paper presented at 4th International Heat Transfer Conference, Versailles (1970)

62 MURPHREE E V
Ind. Eng. Chem. 24 726 (1932)

63 VON KARMAN T
Trans. ASME 61 705 (1939)

64 LIN C S , MOULTON R W, PUTNAM G L
"Mass Transfer between Solid Wall and Fluid Streams"
Ind. Eng. Chem. 45 636 (1953)

65 DEISSLER R G
"Analysis of Turbulent Heat Transfer, Mass Transfer, and Friction in Smooth Tubes at High Prandtl and Schmidt Numbers"
N.A.C.A. Report No 1210 (1955)

66 MIZUSHINA T, OGINO F, OKA Y, FUKUDA H
"Turbulent Heat and Mass Transfer between Wall and Fluid Streams of Large Prandtl and Schmidt Numbers".
Int. J.Heat Mass Transfer 14 1705 (1971)

67 MIXON F O, CARBERRY J J
"Diffusion within a Developing Boundary Layer - Mathematical Solution for Arbitrary Velocity Distribution".
Chem. Eng. Sci 13 30 (1960)

68 HUBBARD D W, LIGHTFOOT E N
"Correlation of Heat and Mass Transfer Data for High Schmidt and Reynolds Numbers".
Ind. Eng. Chem. Fundls. 5 (3) 370 (1966)

69 VIETH W R, PORTER J H, SHERWOOD T K
Ind. Eng. Chem. Fundls 2 1 (1963)

70 VOGTLANDER P H, BAKKER C
"An Experimental Study of Mass Transfer from a Liquid Flow to Wires and Gauges".
Chem. Eng. Sci 18 583 (1963)

71 LEVICH V G
"The Theory of Concentration Polarisation".
Disc. Faraday Soc. 1 37 (1947)

72 AGAR J N
"Diffusion and Convection at Electrodes".
Disc. Faraday Soc. 1 26 (1947)

73 MIZUSHINA T
"The Electrochemical Method".
Advances in Heat Transfer 7 87 (1971)

74 ARVIA A J, CARROZZA J S W
"Mass Transfer in the Electrolysis of Copper Sulphate in Aqueous Solutions under Limiting Current and Forced Convection Employing a Cylindrical Cell with Rotating Electrodes".
Electrochim. Acta 7 65 (1962)

75 EISENBERG M, TOBIAS C W, WILKE
"Ionic Mass Transfer and Concentration Polarisation at Rotating Electrodes".
J Electrochem. Soc. 101 306 (1954)

76 SHAW P V, REISS, HANRATTY
"Rates of Turbulent Transfer to a Pipe Wall in the Mass Transfer Entry Region".
AIChE J. 9 362 (1963)

77 GRASSMANN P, IBL N, TRUB J
"Electrochemical Measurement of Mass Transfer Coefficients".
(Translation from German)
Chem. Ing. Tech. 33 529 (1961)

78 SUTTON F
"Volumetric Analysis" 12th Edition
Blakiston and Co., Philadelphia (1935)

79 COSTELLO J
"Flow and Transfer Processes at Abrupt Expansions".
Ph.D Thesis, University of Aston (1969)

80 BAZAN J C, ARVIA A J
"Ionic Mass Transfer in Flowing Solutions. Electrochemical Reactions under Ionic Mass Transfer Rate Control on Cylindrical Electrodes".
Electrochim. Acta 9 667 (1964)

81 LIN C S, DENTON, GASKILL, PUTNAM
"Diffusion - Controlled Electrode Reactions".
Ind. Eng. Chem. 43 2136 (1951)

82 ROSS T K, WRAGG A A
"Electrochemical Mass Transfer Studies in Annuli".
Electrochim. Acta 10 1093 (1965)

83 DOBRY R, FINN R K
"Mass Transfer to a Cylinder at Low Reynolds Number".
Ind. Eng. Chem. 48 1540 (1956)

84 MIZUSHINA T, VEDA H, UMEMIYA N
"Effect of Free-Stream Turbulence on Mass Transfer from a Circular Cylinder in Crossflow".
Int. J. Heat Mass Transfer 15 769 (1972)

85 GLEN J B, KEEY R B
"Mass Transfer by Forced Convection at the Front Pole of a Sphere".
Chem. Eng. Sci 20 444 (1965)

86 NOORDSIJ P, ROTTE J W
"Mass Transfer Coefficients to a Rotating and to a Vibrating Sphere".
Chem. Eng. Sci. 22 1475 (1967)

87 HICKS R E, MANDERSLOOT W G B
"The Effects of Viscous Forces on Heat and Mass Transfer in Systems with Turbulence promoters and in Packed Beds".
Chem. Eng. Sci. 23 1201 (1968)

88 JOLLS K R, HANRATTY T J
"Use of Electrochemical Techniques to Study Mass Transfer Rates and Local Skin Friction to a Sphere in a Dumped Bed".
AIChE J. 15 (2) 199 (1969)

89 KING D H, SMITH J W
"Wall Mass Transfer in Liquid-Fluidised Beds.".
Can. J. Chem. Eng. 45 329 (1967)

90 SUTEY A M, KNUDSEN J G
"Mass Transfer at the Solid-Liquid Interface for climbing Film Flow in an Annular Duct".
AIChE J. 15 719 (1969)

91 IRIBARNE A, GOSMAN, SPALDING D B
"A Theoretical and Experimental Investigation of Diffusion-Controlled Electrolytic Mass Transfer between a Falling Liquid Film and a Wall".
Int.J. Heat Mass Transfer 10 1661 (1967)

92 WRAGG A
"Mass Transfer between a Falling Liquid Film and a Plane Vertical Surface".
Int. J. Heat Mass Transfer 11 1287 (1968)

93 RUNCHAL A K
"Transfer Processes in Steady 2-Dimensional Separated Flows".
Ph.D Thesis, Imperial College, London (1969)

94 FENECH E J, TOBIAS C W
"Mass Transfer by Free Convection at Horizontal Electrodes".
Electrochim. Acta 2 311 (1960)

95 FOUAD M G, GOUDA T
"Natural Convection Mass Transfer at Vertical Electrodes".
Electrochim. Acta 9 1071 (1964)

96 WILKE C R, TOBIAS C W, EISENBERG M
"Free convection Mass Transfer at Vertical Plates",
C.E.P. 49 663 (1953)

97 LLOYD J R, SPARROW E M, ECKERT E
"Laminar, Transition and Turbulent Natural Convection Adjacent to Inclined and Vertical Surfaces".
Int. J. Heat Mass Transfer 15 (3) 457 (1972)

98 RAVOO E, ROTTE J W, SEVENSTERN F W
"Theoretical and Electrochemical Investigation of Free Convection Mass Transfer at Vertical Cylinders".
Chem. Eng. Sci. 25 1637 (1970)

99 SCHUTZ G
"Natural Convection Mass Transfer Measurements on Spheres and Horizontal Cylinders by an Electrochemical Method".
Int. J. Heat Mass Transfer 6 873 (1963)

100 SHULMAN Z P POKRYVAILO, KORDONSKY, NESTEROV
"Mass Transfer Peculiarities of a Disc Rotating in a Non-Newtonian Fluid".
Int. J. Heat Mass Transfer 16 1339 (1973)

101 GAY B, JENKINS J D, MACKLEY N V
"Design Data for Shell-Side Heat Transfer in Shell and Tube Heat Exchangers - The Use of a Mass Transfer Modelling Technique".
Paper presented at 1972 International Seminar "Recent Developments in Heat Exchangers" Trogir Yugoslavia, organised by the International Centre for Heat and Mass Transfer.

102 MITCHELL J E, HANRATTY J J
"A Study of Turbulence at a Wall using an Electrochemical Wall Shear-Stress Meter".
J Fluid Mechn. 26 199 (1966)

103 VAN DER HEGGE ZIJNEN B G
Appl. Sci. Res., Sect. A7, 205 (1958)

104 COMINGS E W, CLAPP J T, TAYLOR J F
"Air Turbulence and Transfer Process-Flow Normal to Cylinders".
Ind. Eng. Chem. 40 1076 (1948)

105 HILPERT R
"Warmeabgabe von geheizten Drahten und Rohnen im Luftstrom".
Forsch. Geb. Ing-wes 4 215 (1933)

106 NERNST W
Z Physik. Chem. 47 52 (1904)

107 SUTEY A M, KNUDSEN G
"Effect of Dissolved Oxygen on Redox Method for Measurement of Mass Transfer Coefficients".
Ind. Eng. Chem. Fundls. 6 (1) 132 (1967)

108 WILKE C R, EISENBERG M, TOBIAS C W
"Correlation of Limiting Currents under Free Convection Conditions".
J Electrochem. Soc. 100 513 (1953)

109 KOLTHOFF I M, PEARSON
"Stability of Potassium Ferrocyanide Solutions".
Ind. Eng. Chem. (Anal) 3 381 (1931)

110 EISENBERG M, TOBIAS C W, WILKE C R
"Selected Physical Properties of Ternary Electrolytes Employed in Ionic Mass Transfer Studies".
J Electrochem. Soc. 103 413 (1956)

111 DAWSON D A, TRASS O
"Mass Transfer at Rough Surfaces"
Int. J. Heat Mass Transfer 15 1317 (1972)

112 CARMODY W R, ROHAN J J
"Polarisation at Oxidation-Reduction Electrodes".
Trans. Electrochem. Soc. 83 9pp preprint (1943)
(Chemical Abstracts 37 29977)

113 LANDOLT-BORNSTEIN
"Zahlenwerte und Funktionen aus Physik, Chemie, Astronomie, Geophysik, Technik".
Vol II Part 5 p. 316

114 BAZAN J C, ARVIA A J
"The Diffusion of Ferri and Ferrocyanide Ions in Aqueous Solutions of Sodium Hydroxide".
Electrochim. Acta 10 1025 (1965)

115 KOLTHOFF I M, LINGANE J J
"Polarography" Vol 1
New York Interscience Publishers (1941)

116 NATIONAL ENGINEERING LABORATORY
Report No 137
"The Thermal Conductivity of Liquids".

117 THORPE
"Dictionary of Applied Chemistry"
Fourth Edition.

118 PASCAL P
"Nouveau Traité De Chemie Minérale". Vol. II

119 AKERS J B
Ph.D Thesis, University of Aston (1967)

120 BERGELIN O P, LEIGHTON, LAFFERTY, PIGFORD
"Heat Transfer and Pressure Drop during Viscous and Turbulent Flow Across Baffled and Unbaffled Tube Banks".
University of Delaware Engineering Experimental Station,
Bulletin No. 4 (1958)

APPENDICES

APPENDIX 1

EXPERIMENTAL DEVELOPMENT OF THE ELECTROCHEMICAL TECHNIQUE

The following sections describe aspects of the experimental development work on adapting the electrochemical technique for use in shell and tube heat exchanger studies. In particular the experimental features of the potassium ferri-ferrocyanide redox electrochemical system are investigated.

A1.1 STABILITY OF THE ELECTROLYTE SOLUTION

Previous users of the potassium ferri-ferrocyanide system have recommended that a fresh batch of electrolyte solution be used every couple of days. In the present work this would have necessitated a change of solution for every exchanger configuration studied. The cost of materials and labour for a change of electrolyte batch at AEE Winfrith was in the order of £30. Thus simple economics justified the examination of methods for prolonging the operational lives of electrolyte batches.

A1.1.1 Effect of Sunlight

Solutions of both ferricyanide and ferrocyanide ions are known to decompose in sunlight, this being more significant in the case of the latter ion.

Kolthoff and Pearson (109) proposed that the decomposition of the ferrocyanide ion took the form:-

$$Fe(CN)_6^{4-} + H_2O \underset{\text{DARK}}{\overset{\text{LIGHT}}{\rightleftharpoons}} \left[Fe(CN)_5 \cdot H_2O\right]^{3-} + CN^- \quad \ldots\ldots \text{(A1)}$$

$$CN^- + H_2O \rightleftharpoons HCN + OH^- \quad \ldots\ldots \text{(A2)}$$

It is believed that a similar expression describes the decomposition of the ferricyanide ion.

Both sunlight and heat favour the decomposition. The stability of the solutions in sunlight is dependent upon the pH; alkaline conditions as encountered in the presence of excess hydroxyl "indifferent" ions, moving the equilibrium to the left and making the solution more stable.

In the electrochemical system involving the cathodic reduction of potassium ferricyanide, a slight reduction in the concentration of the ferrocyanide ions due to decomposition can be tolerated. However the cyanide ions formed as a result of this decomposition poison the electrodes.

Previous users of this electrochemical system have normally taken the precaution of using freshly made-up solutions and not exposing these solutions to the ultra violet rays in sunlight.

In the absence of quantitative data on the electrolyte decomposition by sunlight, it was thought worthwhile to perform simple experiments which would provide valuable information for equipment design and operating procedure.

Two identical samples of the electrolyte solution used in this work, were stored in clear glass bottles. Nitrogen had previously been bubbled through the solutions to remove any dissolved oxygen. Aluminium foil was wrapped around one of the bottles to exclude the sunlight. The two bottles were placed in direct sunlight and the ferri- and ferrocyanide ion concentrations were determined at regular intervals by titration over a period of two days. While there were long periods of sun in the daytime, during the night there would have been virtually no ultra violet rays. The results of these tests are shown in Fig. 42.

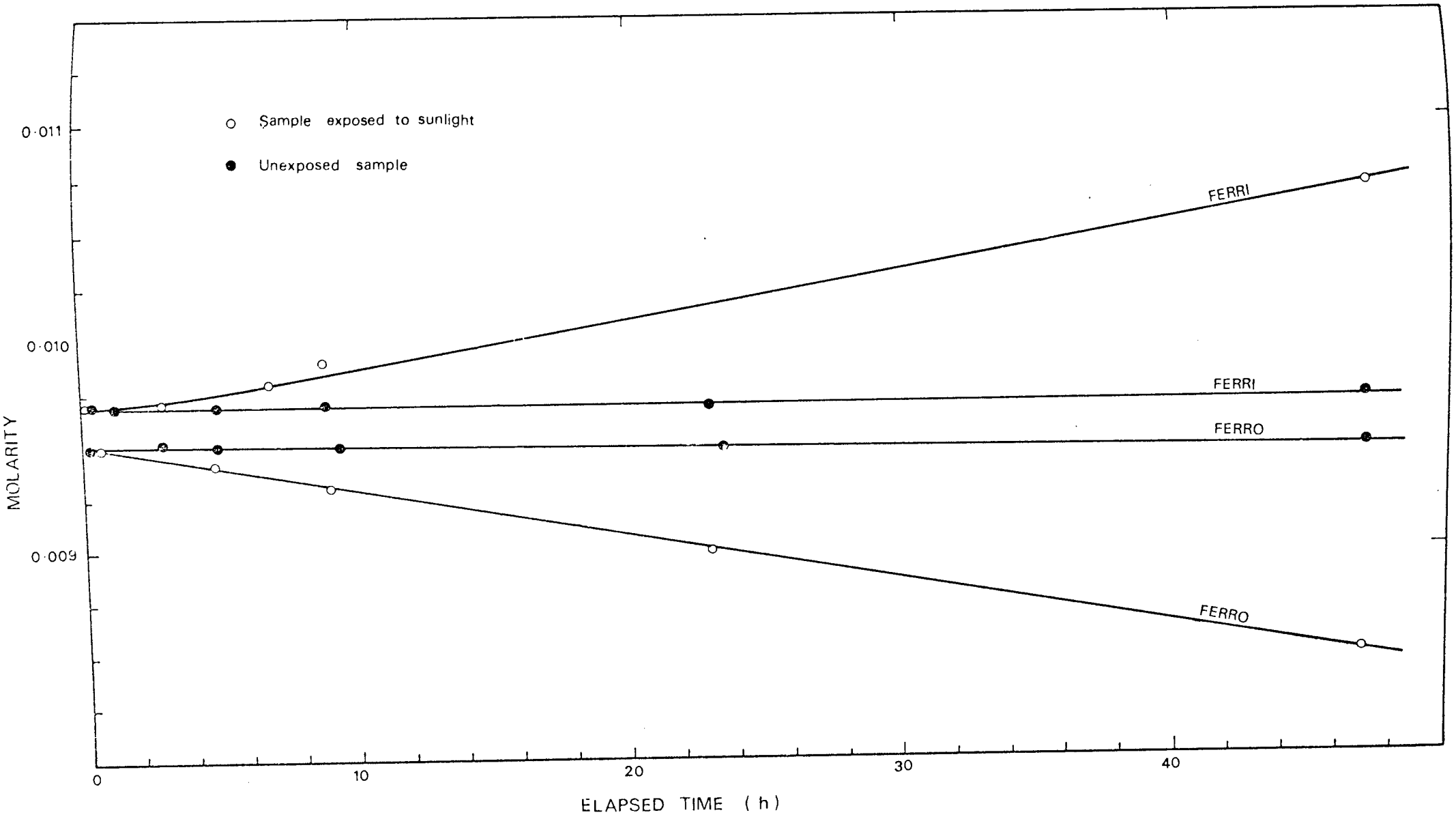

FIG 42 EFFECT OF SUNLIGHT

While decomposition had been completely avoided in the sample protected by aluminium foil, the concentrations of both the ferri- and ferrocyanide ions had changed appreciably in the other sample. As predicted by Equation (A1) the ferrocyanide ion had decomposed, its concentration having dropped by over 10 per cent during the 48 hour period. The ferricyanide ion however showed a corresponding increase in concentration over this period. This suggests that an oxidation process occurs whereby the ferrocyanide is converted to ferricyanide.

A1.1.2 Effect of Dissolved Oxygen

The effect of dissolved oxygen in redox electrolyte solutions is very complex, generally producing abnormally low limiting currents. The low limiting currents may arise from a depletion in the reacting ions by chemical decomposition. More favoured explanations for the effect of dissolved oxygen are the contamination of the electrode surfaces and the occurrence of competing electrochemical reactions.

The reduction of oxygen at the cathode would interfere with the redox electrochemical reactions. However as the oxygen activation polarisation on most electrodes is very high, it is improbable that actual electrochemical reaction involving oxygen occurs in the voltage range employed with the redox system. When dissolved in water, oxygen can give rise to mixed potentials. In the ferri-ferrocyanide (Fe^{3+}/Fe^{2+}) system the oxygen can become electro-active in place of the Fe^{3+} and a Fe^{2+}/O_2 mixed potential is produced.

In the presence of dissolved oxygen, the decomposition of the ferrocyanide ion yields iron oxide.

The accumulation of the oxide on the electrode surfaces reduces the effective surface available for electrochemical

reaction. Chemical polarisation may become significant as the surface concentration of the reacting ions departs from zero. Oxide films have been apparent in this work when dismantling the tube bundle after long periods of exposure to untreated electrolyte.

Sutey and Knudsen (90) investigated the time dependence of the effect of dissolved oxygen. They found that if test solutions were first saturated with nitrogen, future exposure to air for short periods of time did not greatly affect the value of the limiting current. Moreover, for a solution with 70 per cent oxygen saturation, the limiting current dropped by only 5 per cent over an operating period of 275 minutes.

Experiments were performed to investigate the effects of dissolved oxygen on limiting currents in the present work. In one test ordinary distilled water was used in the electrolyte solution, while that used in another test was pretreated by bubbling nitrogen through it for about an hour. The experimental results are presented in Fig. 43. It is evident that without the oxygen removal treatment, the electrochemical system would give highly inaccurate transient results.

The consistent diffusion current values over the 40 hour period indicate that the de-oxygenation method was adequate. The initial slight fall in current is due to heterogeneity in the electrolyte solution. Experimental results on other occasions showed no adverse effects from electrolyte batches of over four days old.

In the development work at the University of Aston the same sodium hydroxide solution was used for the activation process (see Appendix 1.2) and the experimental measurements. The reacting ions were added to the solution after the activation

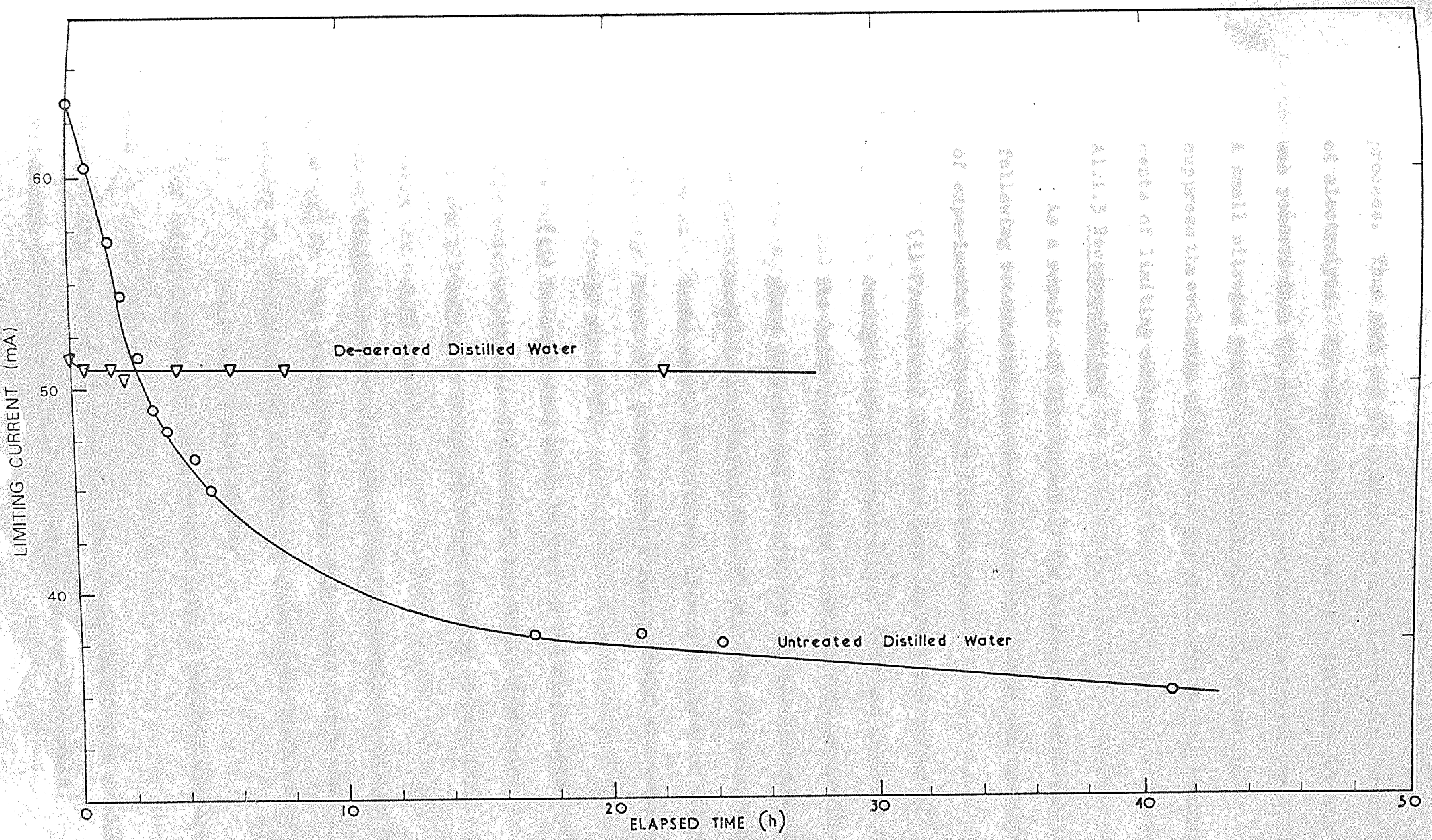

FIG 43 EFFECT OF DISSOLVED OXYGEN

process. Thus each set of experiments required a fresh batch of electrolyte. The oxygen produced in the activation process was removed from the solution by a continuous nitrogen purge. A small nitrogen pressure was maintained in the system to suppress the evolution of gases at the electrodes during measurements of limiting currents.

A1.1.3 Recommendations

As a result of this aspect of the development work the following recommendations were made for the design and operation of experimental equipment at AEE Winfrith:-

(i) Precautions should be taken against the influx of sunlight into the electrolyte. This was achieved on the Aston rig by wrapping aluminium foil around the glass pipework and encasing the perspex heat exchanger model in hardboard. The PVC pipework and polypropylene tanks of the Winfrith rig however required no attention. The perspex heat exchanger model was encased in rigid PVC.

(ii) De-oxygenated water be used in the electrolyte solutions. AEE Winfrith had boiler feed water available having an oxygen content of less than 0.02 ppm.

(iii) A separate flow circuit and electrolyte solution for the activation process. This would remove the necessity of changing the electrolyte batch after each set of experiments.

(iv) The system should be kept under a positive nitrogen pressure.

The adoption of these recommendations resulted in a need to change electrolyte batches only every four or five weeks.

A1.2 PRETREATMENT OF ELECTRODES

Past users of the ferri-ferrocyanide system have found that chemical polarisation was an occasional problem unless the electrode surfaces were treated prior to operation. Eisenberg et al. (110) proposed a series of pretreatment processes which have since been generally adopted. The nickel surface is first polished with a fine emery cloth followed by washing in carbon tetrachloride to remove any grease. A cathode activation process then follows in which hydrogen is evolved at the electrode surface. Eisenberg advocated the use of a 5 per cent sodium hydroxide electrolyte solution passing a current density of 20 mA/cm^2 for 12 to 15 minutes. Some workers e.g. (68) have found that the activation process was unnecessary.

Dawson and Trass (111) in their studies of mass transfer at rough surfaces, found that for such electrode surface conditions the limiting current value was very dependent on the electrode pretreatment process. They observed that rinsing the surface with dilute sulphuric acid followed by washing with a commercial cleanser and finally 30 minutes of cathodic activation treatment produced limiting currents of up to 15 per cent higher than those obtained using the generally accepted treatment process without the polishing stage.

In the present work satisfactory results were obtained by first polishing the electrodes with number 400 grade wet-and-dry paper followed by cathodic treatment with a current density of about 0.1 mA/mm^2 for 4 to 5 minutes. No degreasing process was thought necessary as sodium hydroxide itself possesses this very characteristic.

The comparatively mild treatment found to be adequate in this work is attributable to the simple electrode geometry, the precautions taken against electrolyte decomposition and the actual operational period for any electrode being usually only a few hours.

Although most previous users of this electrochemical system have restricted the pretreatment processes to the cathode, in this work the cathodic activation process was extended to the anode. This was justified particularly in situations where the use of multiple cathodes meant that the anode-to-cathode area ratio was greatly reduced.

When a series of experimental tests necessitated removal of the bundle but not disassembly of the tubes, an alternative to the emery paper polishing treatment was used. Instead the whole bundle was first thoroughly rinsed with distilled water to remove any traces of electrolyte and was then immersed in a 10 per cent solution of hydrochloric acid for 1 to 2 minutes. After removal, the bundle was again thoroughly washed with distilled water prior to replacement in the rig.

A1.3 ANODE GEOMETRY

The surface area and location of the anode relative to the cathode affects:-

(i) Control of the overall electrochemical process.

(ii) Distribution of the potential field.

(iii) Ohmic potential.

The complex geometry of the model heat exchanger necessitated a careful examination of both anode position and surface area. Previous use of the electrochemical technique has been confined to geometrically simple systems where symmetry and small separation of the electrodes were possible.

Three nickel plate anode arrangements were investigated, the details of which are shown in the table below.

ANODE	POSITION	SURFACE AREA (mm^2)	ANODE/CATHODE* AREA RATIO
A	Shell Wall	7 730	2.63
B	Sides of Outlet Port	5 820	1.98
C	Top and Bottom of Outlet Port	11 640	3.96

*A single rod electrode.

The Anode A was on the wall of the shell in the baffle compartment under investigation. Anodes B and C each consisted of two plates attached to the two sides and top and bottom faces respectively of the rectangular outlet port of the exchanger model. The nickel plates were adhered to the perspex using Araldite. Copper electrical leads were soldered to the backs of the plates, passing through holes drilled in the heat exchanger body. The pairs of plates in both Anodes B and C were connected in parallel. The anode arrangements are shown in Fig. 44.

The shell wall Anode A, while providing a low ohmic resistance because of its close proximity to the cathodes, would produce a non-uniform potential field around the tubular cathodes. The two port Anodes B and C, because of their distance from the cathodes, would exhibit larger ohmic resistances but a more uniform potential field. The areas of the three anodes were all of the same order of magnitude and larger than that of the cathode. Measurements made using an Avometer confirmed that the port anodes gave higher ohmic resistances. Using the cathode on tube Number 48 (see Fig. 16 for tube layout), the port Anode C produced an ohmic resistance of 20 ohms while the shell Anode A only 15 ohms. The corresponding currents while being equal, were not however recorded.

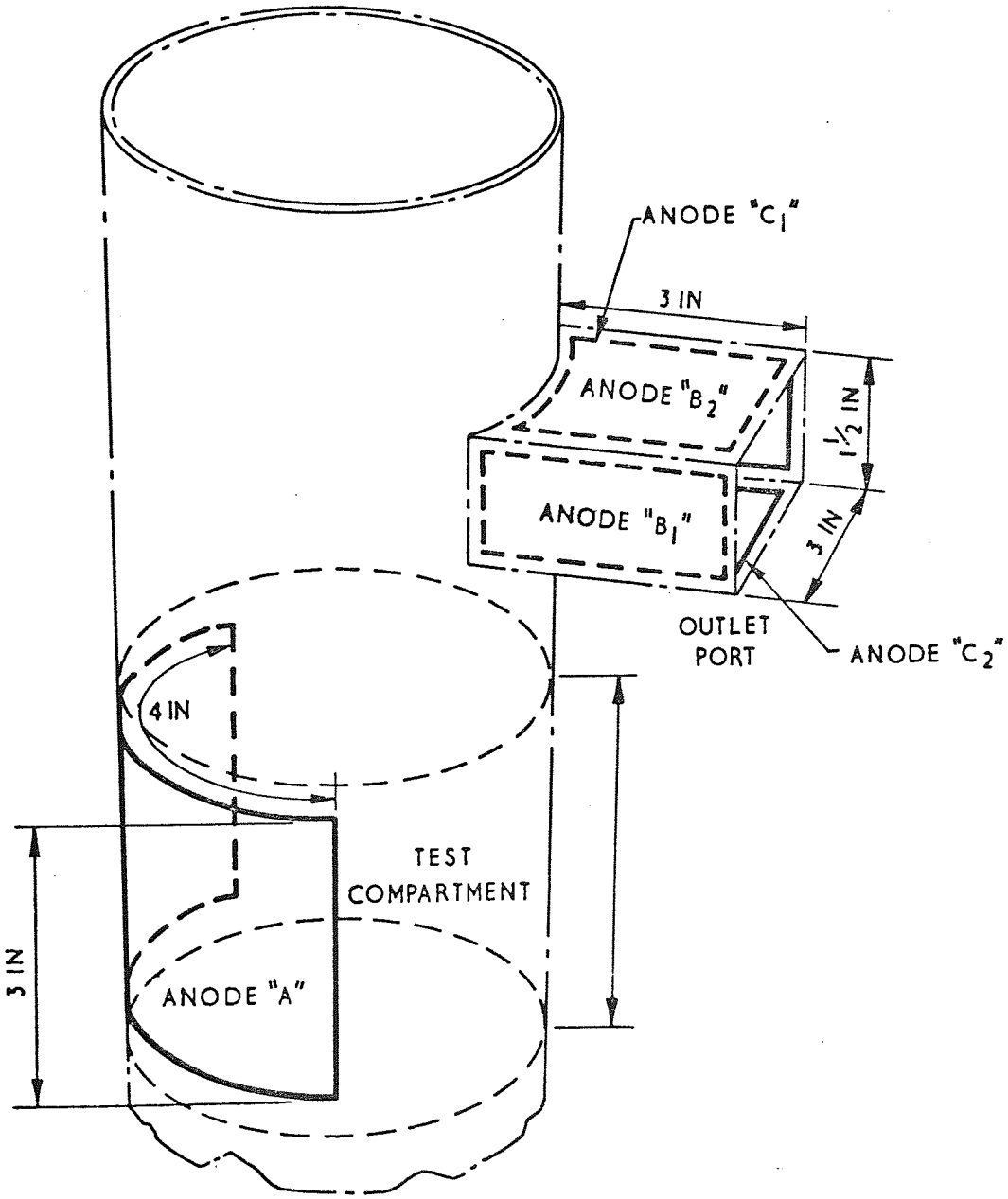

FIG. 44 ANODE ARRANGEMENTS

The performances of the three anode arrangements were compared by measuring limiting currents from various tubes in the bundle. The particular tubes chosen were tube numbers 1, 44, 48 and 80. These represented extreme positions in the bundle (see Fig. 16). For each tube the three anode arrangements produced identical limiting currents; no difference being detected by the current measuring equipment. The characteristics of the polarisation curves were also identical except for a slight shift of the plateau in the case of the shell-anode. This as already discussed in Section 3.5.2, is attributable to the lower ohmic potential associated with this electrode. The polarisation curves are shown in Fig. 45.

These experimental results agree with theoretical predictions. The effect of ohmic resistance on limiting currents has already been discussed in Section 3.5.2. In the presence of an indifferent electrolyte any non-uniformity in the potential distribution is automatically corrected by the indifferent ions.

The effect of the anode-to-cathode area ratio on the control of the electrochemical process is discussed in Apprendix 1.6.

As a result of these tests, the anode arrangement C was adopted as the operating anode in all future investigations. The shell Anode A was dispensed with as its position hindered the removal of the tube bundle. The other port anode arrangment B was used as a "sacrificial" anode in electrode activation processes.

A1.4 ELECTRODE MATERIALS OF CONSTRUCTION

Nickel electrodes have been generally adopted for the potassium ferricyanide reduction process. Platinum cathodes have been found to produce chemical polarisation (112). Copper electrodes were used by Dobry and Finn (83) with success. However there is scepticism about the long-term compatibility of copper and the potassium ferri-ferrocyanide electrolyte solution. There are reports of the use of

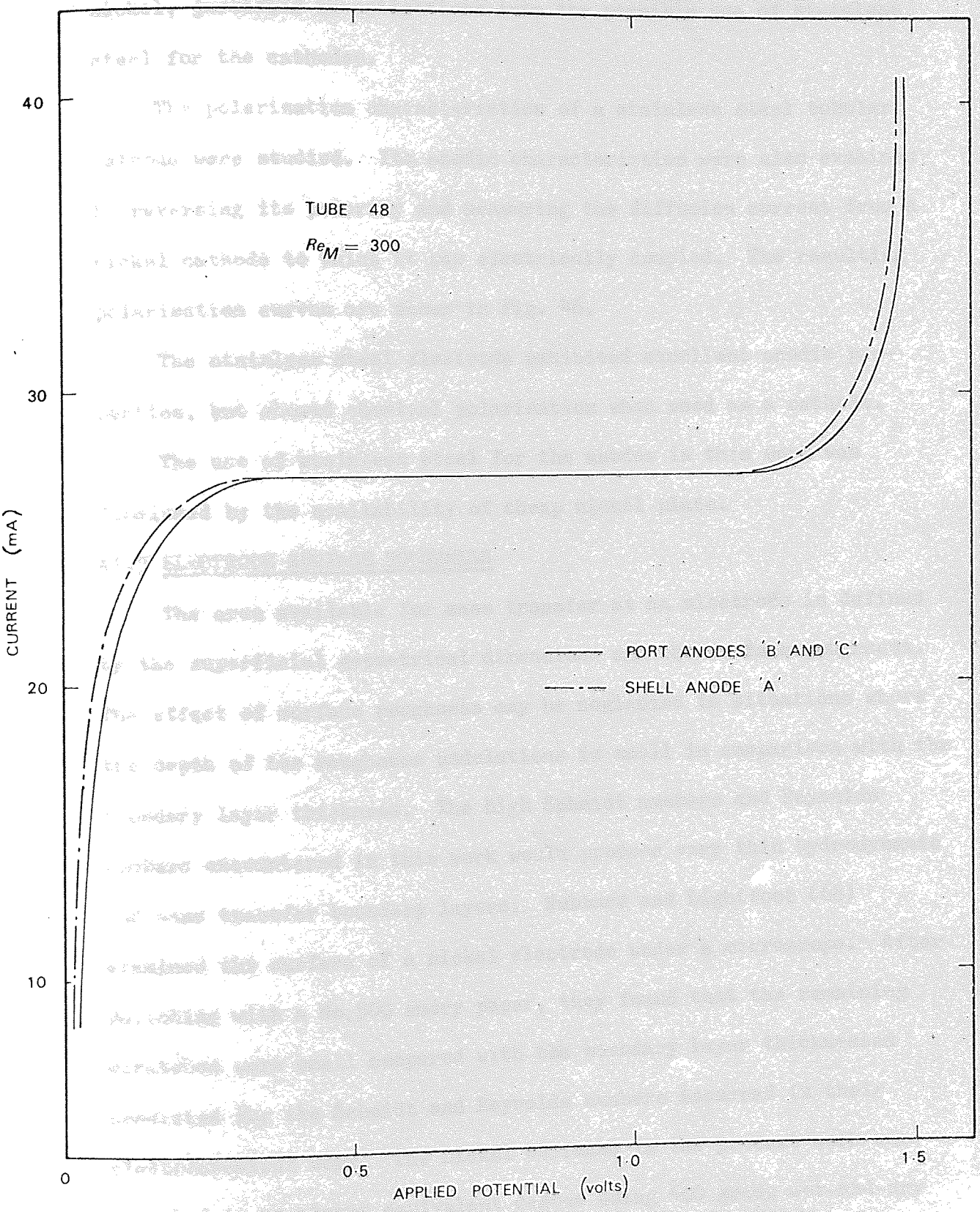

FIG 45 POLARISATION CURVES

stainless steel as the anode (107) but not as the cathode.

The material cost and machining difficulties associated with nickel, justified investigations into the possible use of stainless steel for the cathodes.

The polarisation characteristics of a stainless steel tubular cathode were studied. Its anodic characteristics were also examined by reversing its polarity and measuring the diffusion current from a nickel cathode to which it was electrically coupled. The resulting polarisation curves are shown in Fig. 46.

The stainless steel electrode exhibited excellent anodic properties, but showed chemical polarisation when used as a cathode.

The use of stainless steel for the anodes in this work was dismissed by the availability of cheap nickel plate.

A1.5 ELECTRODE SURFACE ROUGHNESS

The area available for mass transfer at an electrode is defined by the superficial geometrical dimensions and the surface roughness. The effect of surface roughness may be neglected in situations where the depth of the roughness undulations is small in comparison with the boundary layer thickness. The high Schmidt numbers and Reynolds numbers encountered in this work would produce very thin hydrodynamic and mass transfer boundary layers. Hubbard and Lightfoot (68) examined the surface of a nickel electrode under a microscope. After polishing with a No.500 emery paper, they found that the remaining scratches were small compared with the boundary layer thicknesses predicted for the Schmidt and Reynolds numbers incurred in their electrochemical work. The nickel surfaces in the present work were polished to an almost equivalent degree using 400 grade wet-and-dry paper.

A simple test was performed to examine the sensitivity of the measured limiting current to variations in surface roughness.

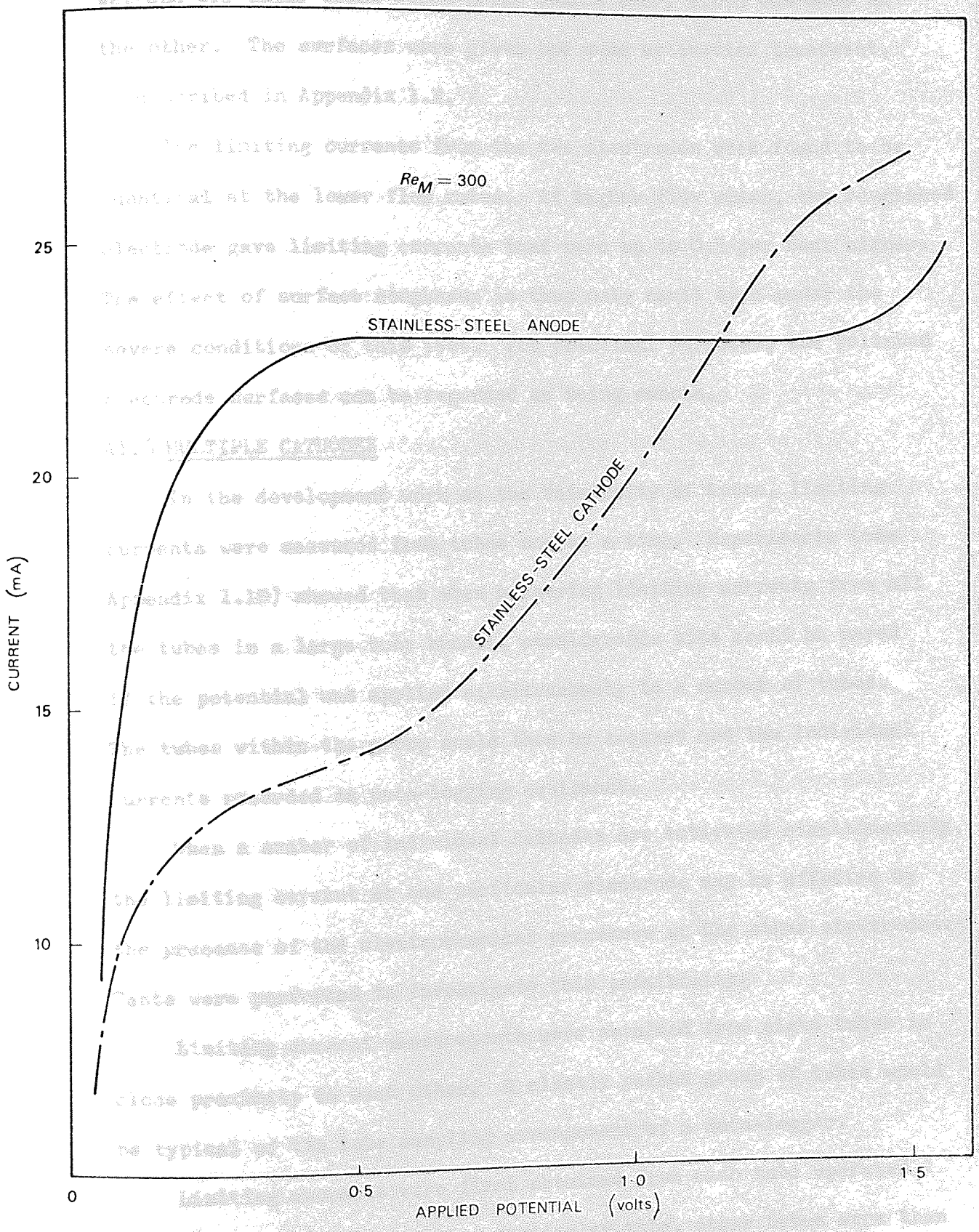

FIG 46 STAINLESS—STEEL ELECTRODE CHARACTERISTICS

Comparative tests were performed on two tubular nickel cathodes; the surface of one electrode had been polished using No.400 grade wet-and-dry paper while No.40 grade coarse emery cloth was used on the other. The surfaces were given the same activation treatment, as described in Appendix 1.2.

The limiting currents from the two electrodes were found to be identical at the lower flow rates. At higher flow rates, the roughened electrode gave limiting currents that were up to 0.5 per cent higher. The effect of surface roughness is thus only small even under the severe conditions of this test. For practical purposes, the polished electrode surfaces can be regarded as being smooth.

A1.6 MULTIPLE CATHODES

In the development work at the University of Aston, limiting currents were measured from tubes one at a time. Experiments (see Appendix 1.10) showed that when measuring limiting currents from all the tubes in a large tube bundle, considerable time could be saved if the potential was applied simultaneously to a number of tubes. The tubes within the group could then be scanned and the individual currents recorded on data-logging equipment.

When a number of individual cathodes are activated simultaneously, the limiting current at one particular electrode may be affected by the presence of the electrochemical processes at the other electrodes. Tests were performed to investigate this possibility.

Limiting current measurements were obtained from eight tubes in close proximity to each other. A closely packed group of tubes would be typical of the tube sampling arrangement of a data-logger.

Limiting currents were first obtained from each tube operated individually. Starting with a particular tube, other tubes were then progressively coupled to it and the net limiting current from each

group was measured. Thus the combined effect of 1, 2, 3 up to 8 tubes was investigated.

The net limiting currents were compared with the values obtained by summing the limiting currents from the group's constituent tubes when operated individually. The results are recorded in Appendix 3.1.5. The discrepancies between the net and the additive limiting current values were less than one per cent. This discrepancy can be attributed to inaccuracies of the experimental measurements. The polarisation curves from the multiple electrodes are shown in Fig. 47.

A1.7 PRESENCE OF ELECTRICAL CONDUCTORS

The initial experimental work at the University of Aston used the baffles and dummy tubes originally employed by Roberts (54). These were all constructed of chromium plated mild steel. Subsequent experimental work utilised an entirely plastic tube bundle comprising perspex dummy tubes and polypropylene baffles. The stainless steel tie-rods and nuts were retained.

The presence of electrical conductors in an electrochemical system provides a preferential path for the transfer of electrical charge from one electrode to the other. Electrochemical reactions must occur at the conductor surfaces to convert the ionic charges into electronic charges. In the absence of data on the discharge potentials of ferricyanide and ferrocyanide ions at chromium electrodes, it may be assumed that electrochemical reactions occur at the conductor surfaces in the operating range of applied potential. If the surface area of the conductors were small, a slow reaction rate on these surfaces could cause the onset of chemical polarisation. Furthermore the conditions at this surface could control the overall electrochemical process thus removing the diffusion control from the cathode.

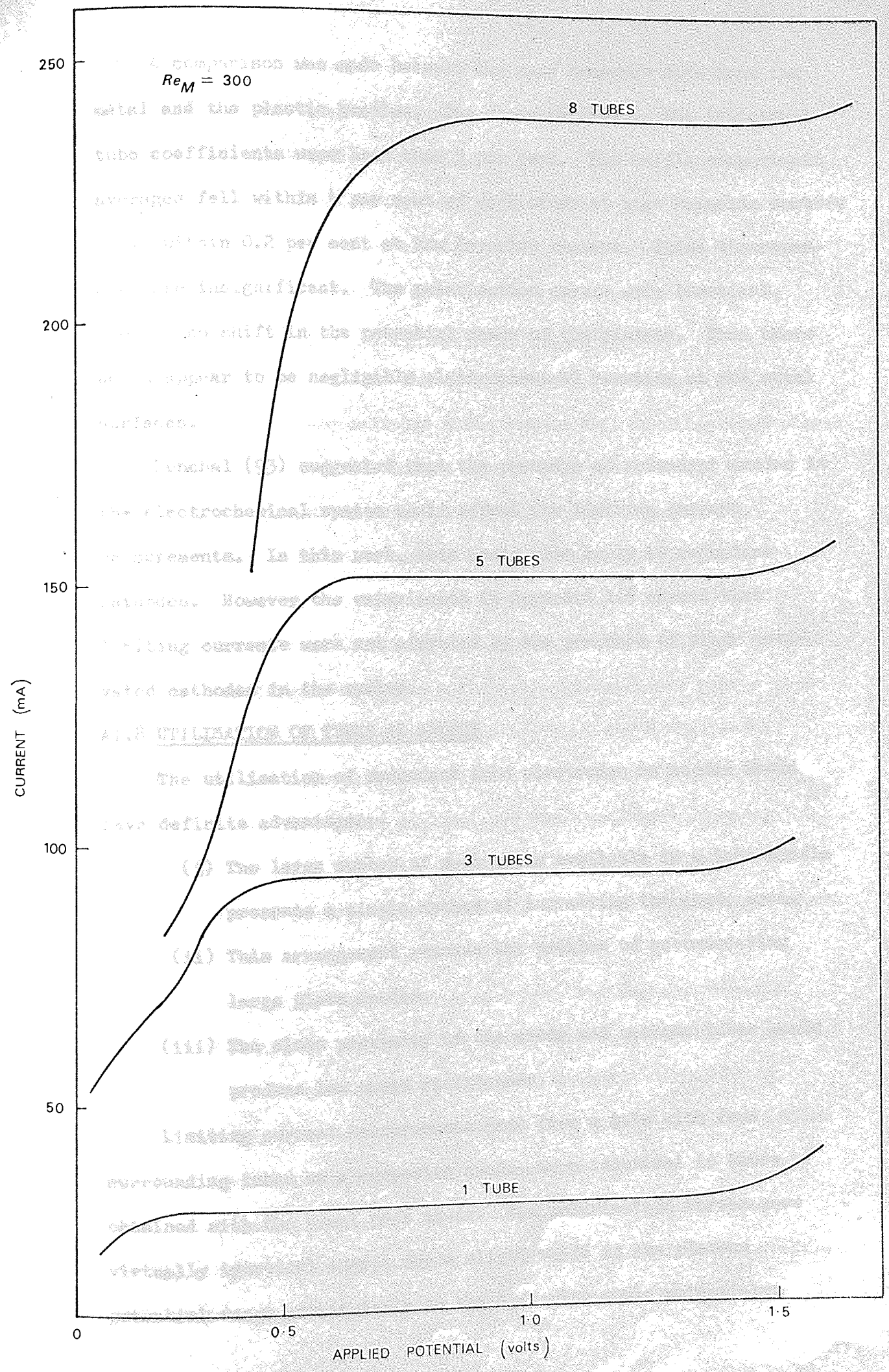

FIG 47 MULTIPLE CATHODES

A comparison was made between the mass transfer data from the metal and the plastic bundles. The discrepancies in the individual tube coefficients were less than 5 per cent. The baffle compartment averages fell within 4 per cent of each other at high Reynolds numbers while within 0.2 per cent at low Reynolds numbers. These discrepancies are insignificant. The polarisation curves were identical, showing no shift in the potential range of the plateau. Thus there would appear to be negligible electrochemical reaction at the metal surfaces.

Runchal (93) suggested that the presence of redundant anodes in the electrochemical system would affect the limiting current measurements. In this work, this could also apply to redundant cathodes. However the experiments in Appendix 1.6 showed that limiting currents were not affected by the presence of other activated cathodes in the system.

A1.8 UTILISATION OF TUBES AS ANODES

The utilisation of redundant tube electrodes as anodes would have definite advantages:-

(i) The large number of such tubes available in a tube bundle presents a simple method of increasing the anode area.

(ii) This arrangement removes the problem of accommodating large plate anodes.

(iii) The close proximity of the anode and cathode tubes would produce low ohmic resistances.

Limiting current measurements made from a tube with four surrounding tubes as a composite anode, were identical to those obtained with the usual port anode. The polarisation curves were virtually identical except for a slight shift in the plateau potential range attributable to the differing ohmic potentials.

The anode-to-cathode area ratios of the two systems were similar; being 4.0 with the composite anode and 3.96 with the port anode.

Although showing these attributes, this anode arrangement was not adopted in the model exchanger at AEE Winfrith. The system would have necessitated intricate electromechanical modifications to the already complex data-logging and ancillary equipment.

A1.9 FERRICYANIDE/FERROCYANIDE ION CONCENTRATION RATIO

Some previous users of the electrochemical technique (61, 111) claim to have improved cathodic diffusion-control in situations where the anode-to-cathode ratio is not appreciably above unity, by increasing the potassium ferrocyanide ion concentration. The multiple cathodes in this work represent a case of a low anode-to-cathode area ratio.

Experiments were performed to investigate the effect of increasing the potassium ferrocyanide concentration. Polarisation curves were obtained for multiple cathodes containing 1, 4 and 8 electrodes. Ferrocyanide ion concentrations of 0.01, 0.02 and 0.05 molar were used. The same port anode was employed for every test as was a Reynolds number of 1 500 and a ferricyanide concentration of 0.01 M.

The sets of polarisation curves for the three cathodes are shown in Fig. 48.

For every anode-to-cathode area ratio, the ferrocyanide ion concentration had no effect on the actual limiting current value, but improved the polarisation curve plateau. This was particularly evident for the lowest anode-to-cathode area ratio. The improvement in the plateau was virtually insignificant in the case of the 3.96 anode-to-cathode area ratio. The independence of the limiting current on the ferrocyanide ion concentration shows that the overall process was cathodically controlled for all the anode-to-cathode

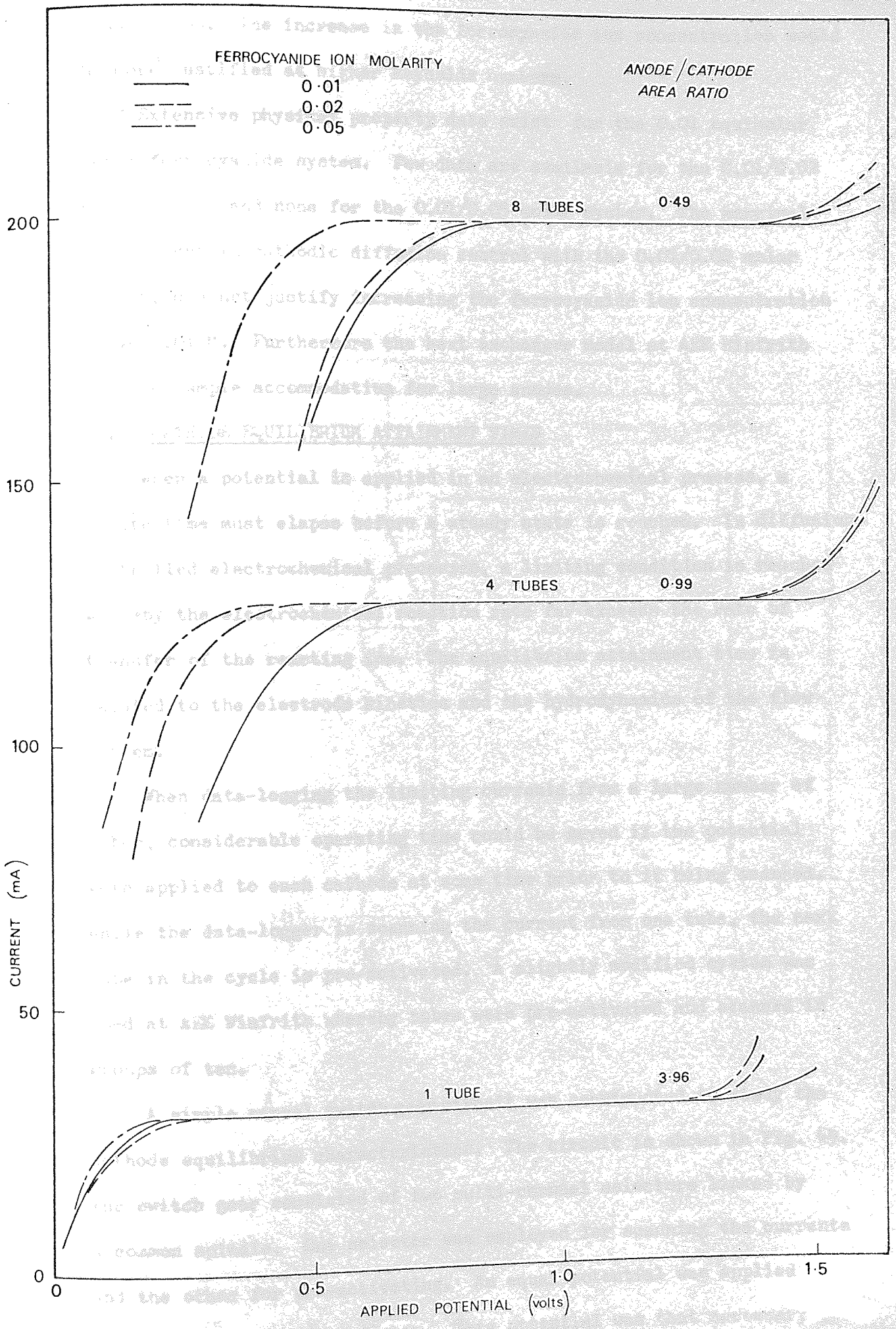

FIG 48 EFFECT OF FERROCYANIDE ION CONC^{N}

area ratios. The increase in the ferrocyanide ion concentration would be more justified at higher Reynolds numbers.

Extensive physical property data exist for the 0.01 equimolar ferri-ferrocyanide system. Few data are available for the 0.01/0.02 molar system and none for the 0.01/0.05 molar system. The marginal improvement in cathodic diffusion control with the 0.01/0.02 molar system, did not justify increasing the ferrocyanide ion concentration above 0.01 M. Furthermore the heat exchanger model at AEE Winfrith provided ample accommodation for large anodes.

A1.10 CATHODE EQUILIBRIUM ATTAINMENT TIMES

When a potential is applied in an electrochemical process, a finite time must elapse before a steady state is reached. In diffusion-controlled electrochemical processes, a limiting condition is reached whereby the electrochemical reaction rate far exceeds the rate of transfer of the reacting ion. The equilibrium attainment time is related to the electrode kinetics and the hydrodynamics of the flow system.

When data-logging the limiting currents from a large number of tubes, considerable operating time could be saved if the potential were applied to each cathode at some time prior to it being scanned. While the data-logger is scanning the current from one tube, the next tube in the cycle is pre-activated. A slightly modified system was used at AEE Winfrith whereby tubes were pre-activated and scanned in groups of ten.

A simple manual switch gear circuit was constructed to study the cathode equilibrium characteristics. The circuit is shown in Fig. 49. The switch gear consisted of two multi-channel selectors linked by a common spindle. One selector was employed for scanning the currents and the other for pre-activating. An equal potential was applied through both selector switches. This potential was that necessary

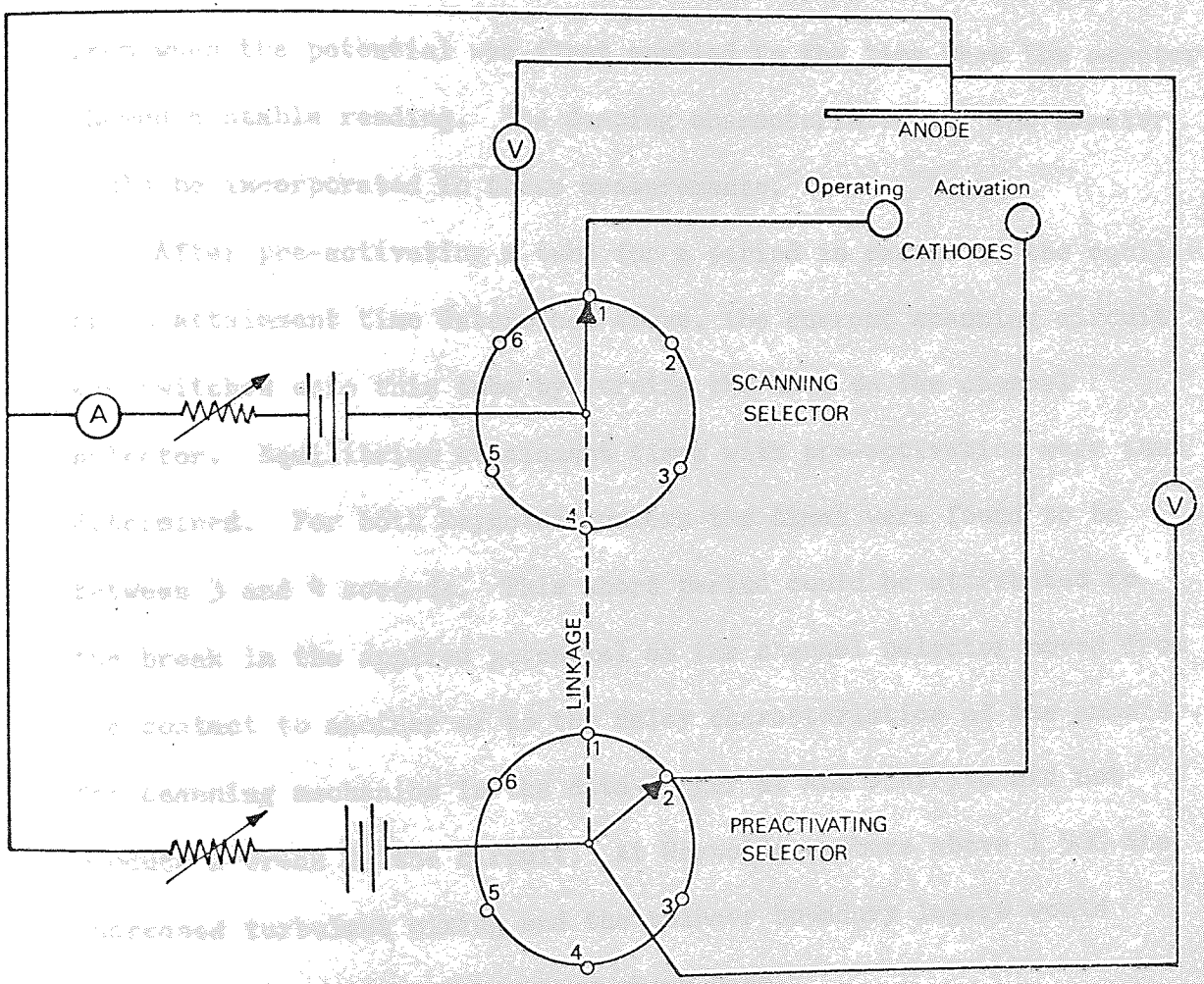

FIG 49 SWITCH-GEAR CIRCUITRY

for diffusion-controlled conditions. The two sets of selector channels were connected to six tubes in a cyclic manner such that the second tube was pre-activated while the first tube had its limiting current measured. Studies were made at Reynolds numbers of 150 and 1 500. At the low Reynolds number, equilibrium attainment times without pre-activation were found to be between 12 and 14 seconds. The corresponding values at the high Reynolds number were around 5 seconds. The equilibrium attainment time was taken as the period from when the potential was first applied to the time when the ammeter showed a stable reading. The damping characteristics of the ammeter would be incorporated in these measurements.

After pre-activating a tube for a period in excess of the equilibrium attainment time determined above, the current scanning circuit was switched onto this tube by turning the knob on the channel selector. Equilibrium attainment times with pre-activation were thus determined. For both Reynolds numbers the times were found to be between 3 and 4 seconds. This short period could be attributed to the break in the applied potential as the channel selector moved from one contact to another or to the delay characteristics of the ammeter. The scanning mechanism in the data-logger at AEE Winfrith did not produce a break in the circuit. At Reynolds numbers above 1 500 the increased turbulent mixing and the thinner boundary layers would produce shorter times than those shown here.

The tests thus demonstrated the reduction in experimental time as a result of pre-activating the cathodes. The total time taken for measurements from 80 tubes at a Reynolds number of 150 could be reduced from 18 to 5 minutes.

A1.11 CORRECTION FOR TEMPERATURE

The mass transfer j-factor utilised in this work is defined by:-

$$j_m = \frac{I_L}{C_b S n_e F u} \left[\frac{\mu}{\rho D_V}\right]^{2/3} \quad \ldots\ldots (A3)$$

also

$$j_m = \text{function } \left(\frac{\rho u d_t}{\mu}\right) \quad \ldots\ldots (A4)$$

The physical properties μ , ρ and D_V are all temperature dependent.

In the experimental work at AEE Winfrith, interpolation formulae were used to account for the effect of temperature on the electrolyte physical properties (see Appendix 1.13).

A simpler form of temperature correction was favoured in the development work. A correction factor was derived accounting for the combined effect of temperature on all of the physical properties. Limiting currents obtained at various temperatures were corrected to a datum of 25°C at which temperature the physical properties had been evaluated.

At a constant flow rate and electrolyte concentration, the variation in limiting current with temperature was investigated over the temperature range 22.5 to 28.5°C. For each temperature, the discrepancy between the limiting current value and that at 25°C was calculated. The variation of this correction with temperature is shown in Fig. 50. This is compared with a corresponding correction factor determined from the physical property data given in Appendix 1.13. The rotameter calibration did not require correction over this small temperature range. The difference between the two

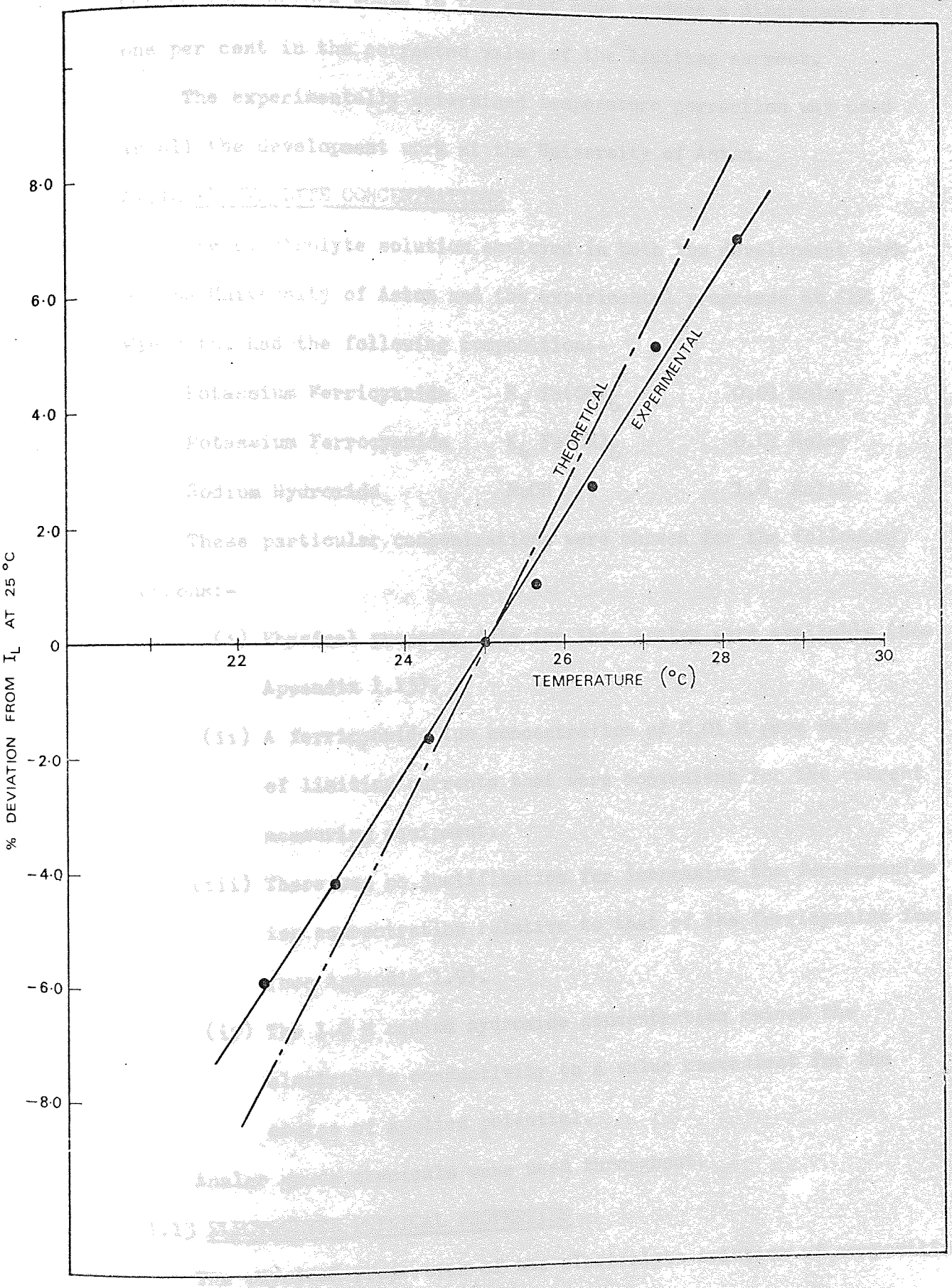

FIG 50 VARIATION IN LIMITING CURRENT WITH TEMPERATURE

correction factors would in the worst case produce a discrepancy of one per cent in the corrected value of the limiting current.

The experimentally determined temperature correction was used in all the development work at the University of Aston.

A1.12 ELECTROLYTE CONCENTRATIONS

The electrolyte solution employed in both the development work at the University of Aston and the experimental programme at AEE Winfrith, had the following composition:-

Potassium Ferricyanide	$K_3 Fe(CN)_6$	0.01 Molar
Potassium Ferrocyanide	$K_4 Fe(CN)_6$	0.01 Molar
Sodium Hydroxide	NaOH	1.0 Molar

These particular concentrations were chosen for the following reasons:-

(i) Physical property data for this system were available (see Appendix 1.13).

(ii) A ferricyanide ion concentration of 0.01 M gave values of limiting currents that were convenient for the current measuring equipment.

(iii) There was no justification for increasing the ferrocyanide ion concentration relative to that of the ferricyanide ion (see Appendix 1.9).

(iv) The 1.0 M sodium hydroxide concentration raised the electrolyte conductivity to a value convenient for the source of applied potential.

Analar grade chemicals were used throughout.

A1.13 ELECTROLYTE PHYSICAL PROPERTIES

The physical properties of the electrolyte solution of composition given in Appendix 1.12, were determined for the temperature range 15° to 35°C.

Density

Density data used were based on experimental values for aqueous solutions of sodium hydroxide given in the International Critical Tables. Allowance was made for the small amounts of potassium ferri- and ferrocyanide by assuming that negligible volume change occurs when these compounds are added to the molar caustic solution.

The accuracy of the density data is estimated to be within 0.5 per cent.

Viscosity

Viscosity data for a molar sodium hydroxide solution were obtained from Landolt-Bornstein (113). These data showed close agreement with experimental data of Bazan and Arvia (114) and with some laboratory measurements made in the present work using a Cannon-Fenske viscometer. In both these cases the potassium salts were present in the electrolyte solution.

The accuracy of the viscosity data is estimated to be within 1 per cent.

Diffusion Coefficient

The diffusion coefficient for the ferricyanide ion in the electrolyte solution has been obtained in three ways:-

(i) Using the Nernst Equation (115).

(ii) Using the Levich Equation (114).

(iii) By direct measurement (110).

The electrolyte solutions in the above three references were of slightly differing compositions. The diffusion coefficients were compared using the Stokes-Einstein Equation:-

$$\frac{D_V \mu}{T} = \text{constant} \qquad \ldots\ldots (A5)$$

where

D_V = Diffusion coefficient (m^2/s)

μ = Dynamic viscosity (Ns/m^2)

T = Temperature (^oK)

The values of the constants thus obtained are tabulated below.

Method	Value of Constant
(i)	2.68×10^{-15}
(ii)	2.52×10^{-15}
(iii)	2.50×10^{-15}

The direct method of measurement (Method (iii)) is considered likely to be the most accurate. A value of 2.50×10^{-15} for the above constant is thus recommended.

Diffusion coefficients are obtained from Stokes-Einstein Equation using the recommended value for the constant.

The Stokes-Einstein Equation is assumed to hold over the temperature range 15° to 35°C.

The accuracy of the diffusion coefficient data is estimated to be within 3 per cent, this being the sum of possible errors incurred in the Stokes-Einstein constant and the viscosity.

Thermal Conductivity

Thermal conductivity data for a molar sodium hydroxide solution were obtained from Landolt-Bornstein (113). A National Engineering Laboratory report (116) gives a method for calculating the effect on thermal conductivity of different components in aqueous solutions of electrolytes. This method has been applied to estimate the effect of the potassium salts. The calculation shows the effect to be negligible. The accuracy of the data is estimated to be within 1 per cent.

Specific Heat

Specific heat data were obtained from two textbook sources (117, 118) both sets being in good agreement with each other. A method

of allowing for the presence of the potassium salts has not been found, but the effect is unlikely to be significant.

The accuracy of the data is estimated to be within one per cent.

Schmidt Number

The Schmidt number defined by:-

$$Sc = \frac{\mu}{\rho \, D_V}$$

has been calculated over the temperature range 15° to 35°C.

For computation purposes the variation of the Schmidt number with temperature has been represented by an interpolation formula:-

$$Sc = 0.595 \times 10^{4} - 0.319 \times 10^{3} \, T + 0.790 \times 10 \, T^{2}$$

$$- 0.983 \times 10^{-1} \, T^{3} + 0.496 \times 10^{-3} \, T^{4} \qquad \ldots\ldots \text{(A6)}$$

where temperature T is in °C.

The polynomial was obtained by a least squares technique.

The accuracy of the Schmidt number data is estimated from summation of component errors to be within 4.5 per cent.

Prandtl Number

The Prandtl number defined by:-

$$Pr = \frac{C_p \, \mu}{k}$$

for the temperature range 15° to 35°C has been represented by the interpolation formula:-

$$Pr = 0.144 \times 10^{2} - 0.443 \, T + 0.701 \times 10^{-2} \, T^{2}$$

$$- 0.450 \times 10^{-4} \, T^{3} \qquad \ldots\ldots \text{(A7)}$$

The accuracy of the Prandtl number data is estimated from summation of component errors to be within 4 per cent.

Kinematic Viscosity

The kinematic viscosity defined by:-

$$\eta = \frac{\mu}{\rho}$$

for the temperature range 15° to 35°C is represented by the interpolation formula:-

$$\eta = 0.205 \times 10^{-5} - 0.598 \times 10^{-7}\, T + 0.943 \times 10^{-9}\, T^2 - 0.608 \times 10^{-11}\, T^3 \qquad (m^2/s) \quad \ldots\ldots (A8)$$

The accuracy of these data is estimated to be within 2.5 per cent.

A1.14 FERRI-FERROCYANIDE ION DETERMINATION

The concentrations of the ferricyanide and ferrocyanide ions in the electrolyte solution were determined by titration. Some users of this electrochemical system (61) have made these determinations by colorimetric analysis employing commercial absorptiometers. Investigations in the present work revealed that these instruments gave poor repeatability and did not provide the required accuracy.

The ferricyanide ion concentration was determined by iodometric titration with a thiosulphate. The ferrocyanide ion concentration was determined by simple titration with a permanganate under acidic conditions. Details of both these methods are given in (78). The accuracy of the ferricyanide determinations was estimated to be within ± 1.2 per cent (see Appendix 2.2).

A1.15 MATERIALS OF CONSTRUCTION

Literature studies revealed that the materials of construction most commonly used with the redox electrochemical system were:-

glass, perspex, stainless steel, neoprene rubber

Compatibility charts indicated that both polyvinyl chloride (PVC) and polypropylene were unaffected by sodium hydroxide solutions. Laboratory tests were performed to confirm the compatibility of these plastics with the redox electrolyte solution.

APPENDIX 2

A2.1 VERIFICATION OF THE SCHMIDT NUMBER EXPONENT

A2.1.1 Introduction

The value of 2/3 for the Schmidt number exponent in the Chilton and Colburn mass transfer j-factor was verified experimentally in this work.

The mass transfer j-factor is given by:-

$$j_m = \frac{K_C}{u} Sc^{2/3} \qquad \text{..... (2.5)}$$

Inserting the definition for the mass transfer coefficient in the electrochemical technique given by Equation (3.6):-

$$j_m = \frac{I_L}{u\, C_b\, S\, F\, n_e} Sc^{2/3} \qquad \text{..... (A2.1)}$$

Rearranging and incorporating the Reynolds number Re_M gives:-

$$j_m = \left[\frac{d_t}{S\, F\, n_e}\right] \frac{I_L\, \rho}{C_b\, \mu\, Re_M} Sc^{2/3} \qquad \text{..... (A2.2)}$$

For a given system the terms within the brackets will all be constants.

At a given Reynolds number and for a constant value of j_m, from Equation (A2.2):-

$$\left[\frac{I_L\, \rho}{C_b\, \mu}\right] \propto Sc^{-2/3} \qquad \text{..... (A2.3)}$$

Thus the experimental value of the Schmidt number exponent is obtained as the absolute value of the gradient from a logarithmic plot of $\left[\frac{I_L\, \rho}{C_b\, \mu}\right]$ versus Schmidt number.

A2.1.2 Experimental

The Schmidt number of the mass transfer system was varied by adjusting the concentration of the sodium hydroxide in the electrolyte solution. An increase in the molarity of the sodium hydroxide from 0.5 to 7.0 produced a corresponding increase in the Schmidt number from 1 272 to 31 770 at 25°C. In the absence of physical property data for such electrolyte solutions, densities and viscosities were determined experimentally. A Cannon-Fenske viscometer was used for viscosity measurements. The Stokes-Einstein Equation (see Appendix 1.13) was assumed to hold over the whole viscosity range. The rotameters were recalibrated for each electrolyte solution.

Limiting current measurements were made from Tubes 1, 9, 41, 44 and 74 (see Fig. 16 for tube layout) over a range of Reynolds numbers. Five different electrolyte solutions with sodium hydroxide molarities of 0.5, 1.0, 2.0, 4.0 and 7.0 were used. The results were analysed in terms of the limiting currents from the individual tubes and the average value from all the five tubes investigated. Tube 41 was chosen to illustrate the individual tube results in these discussions. The experimental results are tabulated in Appendix 3.1.7 and are represented graphically in Figs. 137 and 138. Straight lines were fitted to these data using a method of least squares. The data showed excellent correlation in each case, with coefficients of correlation never falling below 0.997 (cf unity for a perfect correlation). The values of the slopes of these straight lines are given in Figs. 137 and 138. The averaged limiting current data from the five tubes showed the same characteristics as those from the individual tubes. The value of the Schmidt number exponent varied slightly with Reynolds number, ranging from 0.63 to 0.67. The low value of 0.63, obtained at the highest Reynolds number,

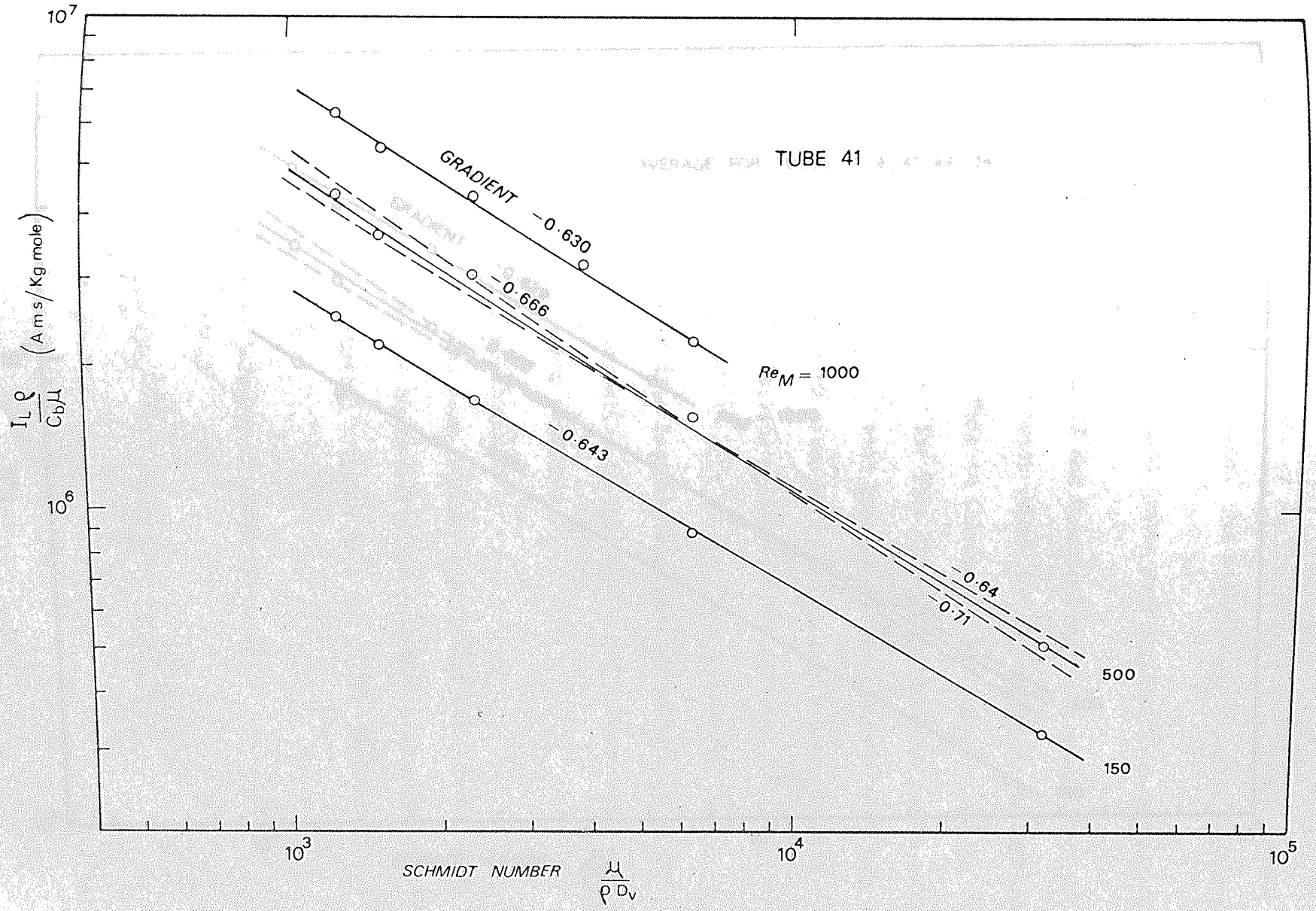

FIG 137 SCHMIDT NUMBER EXPONENT

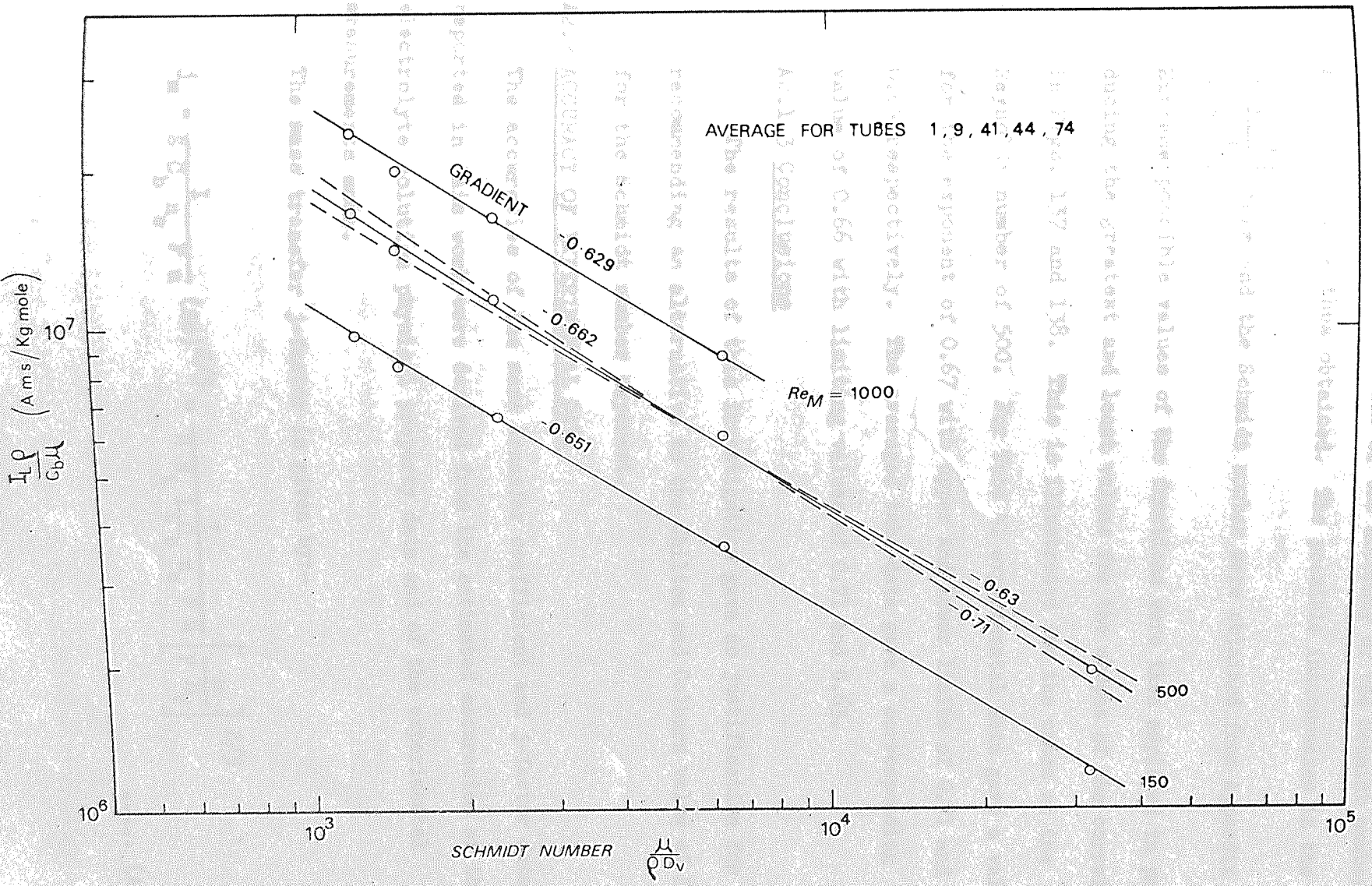

FIG 138 SCHMIDT NUMBER EXPONENT

must however be regarded as tentative, for the sizes of the rotameters did not allow investigations for Schmidt numbers above 6 300 at this flow rate.

An estimation was made of the accuracy of the Schmidt number exponent values thus obtained. The possible inaccuracies in the $\left[\frac{I_L \rho}{C_b \mu}\right]$ term and the Schmidt number were obtained from Appendix 2.2. Extreme possible values of the functions were then employed in producing the greatest and least values for the slopes of the correlations in Figs. 137 and 138. This is illustrated for the cases at the Reynolds number of 500. For Tube 41 experimental data gave a value for the exponent of 0.67 with upper and lower limits of 0.71 and 0.64 respectively. The averaged tube data gave a corresponding value of 0.66 with limiting values of 0.71 and 0.63.

A2.1.3 Conclusions

The results of this investigation gave no justification for recommending an alternative to the Chilton and Colburn value of 2/3 for the Schmidt number exponent.

A2.2 ACCURACY OF EXPERIMENTAL DATA

The accuracies of the mass transfer coefficient and j-factor data reported in this work were derived from the estimated accuracies of the electrolyte solution physical property data and of the experimental measurements made.

The mass transfer j-factor is given by:-

$$j_m = \frac{I}{S\, C_b\, n_e\, F\, u} (Sc)^{2/3} = \frac{I}{\Pi\, d_t\, L_E C_b\, n_e\, F\, u} \left[\frac{\mu}{\rho\, D_V}\right]^{2/3} \quad \ldots\ldots (A2.4)$$

and the mass transfer coefficient by:-

$$K_C = \frac{I}{S\, C_b\, n_e\, F} = \frac{I}{\Pi\, d_t\, L_E\, n_e\, F} \qquad \ldots\ldots (A2.5)$$

The possible errors in each component term are now examined.

(i) Electrolyte physical properties.

In Appendix 1.13 the accuracies of these data were estimated to be:-

Viscosity, μ	$\pm$ 1%
Density, ρ	$\pm$ 0.5%
Diffusion coefficient, D_V	$\pm$ 3%

The accuracy of the Schmidt number was estimated from the summation of these component errors to be within 4.5 per cent. The accuracy of $Sc^{2/3}$ would thus be $\pm$ 3.0 per cent.

(ii) Electrode surface area, S.

Measurements made of the nickel cathode dimensions revealed the following variations:-

Length, L_E	3.890 in. (99 mm)	$\pm$ 0.005 in.
Diameter, d_t	0.375 in. (9.5 mm)	$\pm$ 0.001 in.

The accuracy of the dimensions were thus $\pm$ 0.1 per cent and $\pm$ 0.3 per cent for the length and diameter respectively. The accuracy of the surface area was estimated from the summation of these two component errors to be $\pm$ 0.4 per cent.

(iii) Velocity, u.

The accuracy of the rotameter calibrations in both the development and subsequent work was estimated to be within $\pm$ 3.0 per cent. The accuracy of the measurement of the minimum crossflow area was estimated to be about $\pm$ 0.5 per cent. Thus possible errors in the velocity were considered to be less than $\pm$ 3.5 per cent.

(iv) Current, I.

The calibration of the Sangamo Weston ammeter used at Aston University was quoted by the manufacturers as being accurate to within ± 0.1 per cent. The standard resistor and digital voltmeter instrumentation at AEE Winfrith was designed to an accuracy of ± 0.1 per cent.

(v) Electrolyte temperature measurement.

Temperature measurements in both the experimental rigs were considered to have been accurate to within 0.2°C at 25°C. Examination of the physical property data revealed the following possible errors:-

Density, ρ	± 0.1%
Viscosity, μ	± 0.2%
Diffusion Coefficient, D_V	± 0.3%

The corresponding possible error in the Schmidt number was estimated by summation to be ± 0.6 per cent and hence ± 0.4 per cent for $Sc^{2/3}$. The rotameter calibration was essentially inert to changes in the electrolyte viscosity. Thus any inaccuracies in velocity measurements would have been the same as those incurred in the density term.

(vi) Potassium Ferricyanide concentration, C_b

The repeatability of the ferricyanide determination titrations was found to be within 0.2 ml in 25 ml i.e. ± 0.8 per cent. The titrations for the standardisation of the thiosulphate solution were estimated to be accurate to within 0.1 ml in 25 ml i.e ± 0.4 per cent. The accuracy of the measurement of the potassium ferricyanide bulk concentration was estimated from the summation of the two component errors to be within ± 1.2 per cent.

(vii) Mass transfer data.

By summation of the constituent errors, the accuracies of the mass transfer data were estimated to be:-

Mass transfer j-factor $\pm$ 8.6 per cent

Mass transfer coefficient, K_C $\pm$ 1.7 per cent

These values represent the most severe case for some constituent errors could cancel others out.

(viii) Reynolds number, $\frac{d_t u \rho}{\mu}$.

By summation of the constituent errors, the accuracy of the Reynolds number was estimated to be $\pm$ 5.6 per cent.

A2.3 REPRODUCIBILITY OF EXPERIMENTAL DATA

The reproducibility of the experimental mass transfer data was estimated from measurements made from a nominally identical shell-side geometry on two occasions nearly two months apart. Several bundle rebuilds had been made within the intermediate period.

The no-leakage single segmental baffles were used having a 1.91 in. (48.5 mm) spacing and a 37.5 per cent cut. The electrolyte ferricyanide ion concentrations in the two experiments were 0.0110 and 0.0102 molar respectively.

Baffle compartment average j-factors are compared in Fig. 139. The j-factors are plotted on a linear scale in order to emphasise any separation in the data. The two sets of data fall within $\pm$ 5 per cent of a mean.

The discrepancies between individual tube j-factors at a particular Reynolds number are shown in Fig. 140. The j-factors from the two experiments fall generally within $\pm$ 10 per cent of each other. This degree of variation may be attributed to random redistributions in the shell-side flow. These results give a measure of the consistency of the bundle rebuilds.

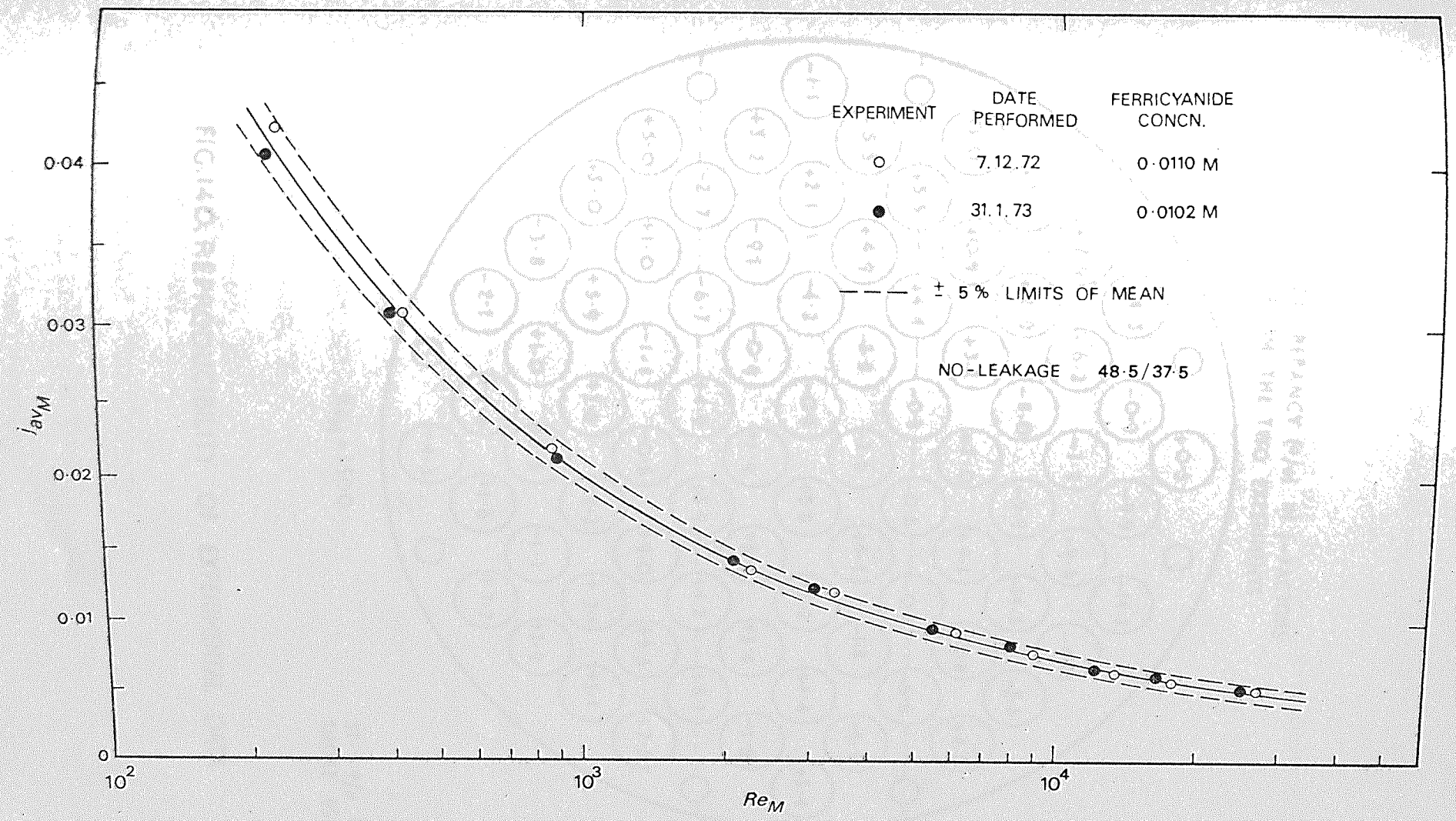

FIG 139 *REPEATABILITY TEST*

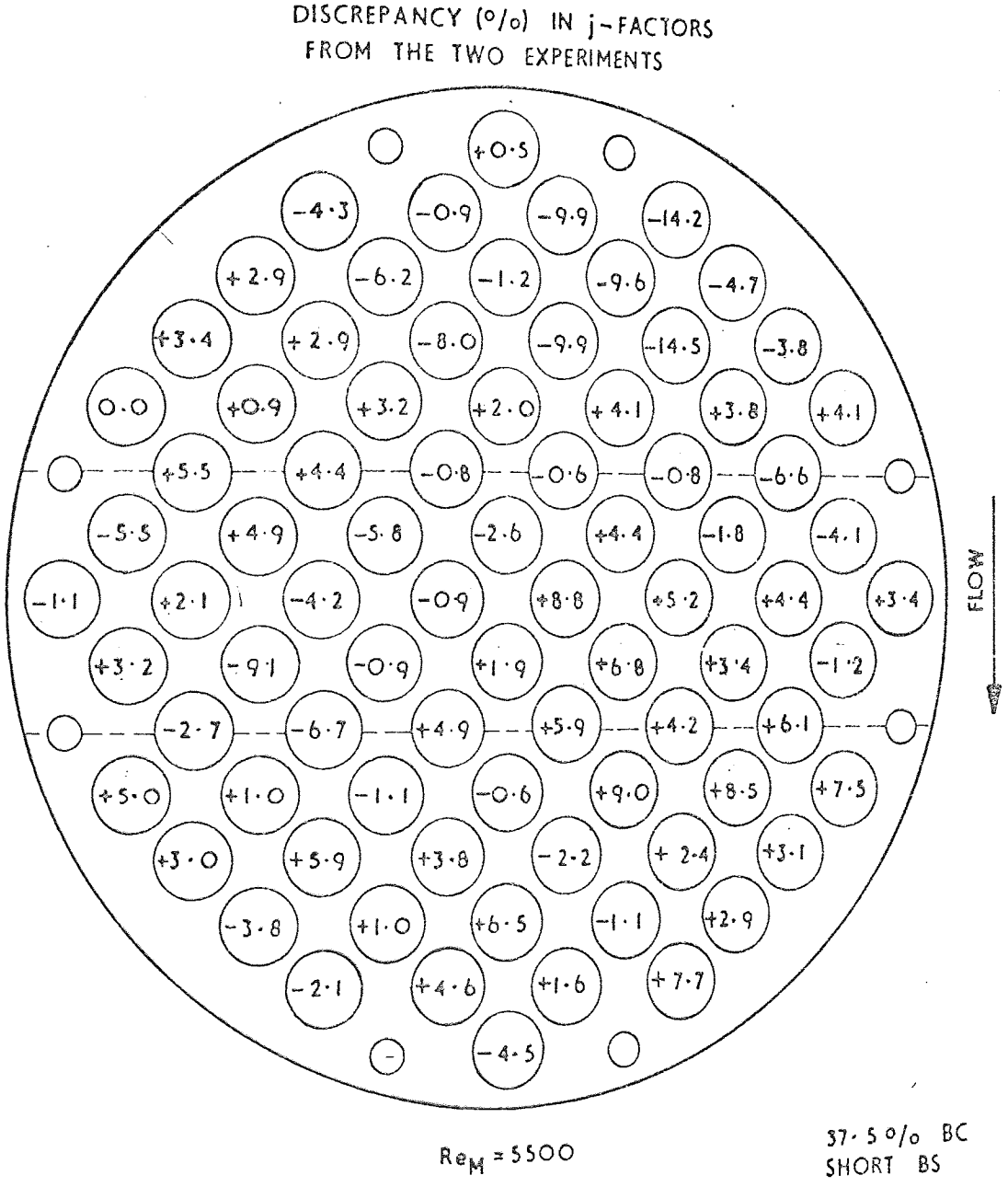

FIG.140. REPRODUCIBILITY OF EXPERIMENTAL DATA

A2.4 DATA PROCESSING

All experimental data at AEE Winfrith were recorded on punched paper tape and then processed by computer.

A2.4.1 Data Input Format

For every experimental run the following data were recorded on 8-hole punched tape:-

RUN NUMBER (M)

DVM OUTPUT - Logged data from 80 tubes (volts)

FLOW RATE (M) - Rotameter reading (gal/min)

DVM RANGE LEVEL (M)

AMPLIFIER GAIN (M)

ELECTROLYTE TEMPERATURE (M) - From chart recorder (^{o}C)

FERRI ION CONCENTRATION (M) - From titration

BAFFLE SPACING (M)

BAFFLE CUT (M)

SHELL-TO-BAFFLE CLEARANCE (M)

TUBE-TO-BAFFLE CLEARANCE (M)

(M) refers to manual input onto punched tape.

A2.4.2 Scope of Computer Program

The computer program was written in EGDON (FORTRAN 2). The program was run on an English Electric KDF9 computer.

The program gave the following output data:-

CHARACTERISTIC VELOCITY, u_M (m/s)

REYNOLDS NUMBER, Re_M

SCHMIDT NUMBER, Sc

PRANDTL NUMBER, Pr

MASS TRANSFER j-FACTORS, j_m

(i) Individual Tube

(ii) Zonal Average

(iii) Baffle Compartment Average

HEAT TRANSFER COEFFICIENTS, h ($KW/m^2\ ^oC$)

(i) Zonal Average

(ii) Baffle Compartment Average

The calculation procedures of the computer program are shown as a flow diagram in Fig. 141. Details of the calculations are given below.

A specimen computer printout is shown in Fig. 142.

A2.4.3 Calculation Procedures

A2.4.3.1 Definition of Parameters

The following formulae were used in processing the experimental data:-

$$\text{CURRENT, } I = \frac{\text{DVM OUTPUT}}{\text{STANDARD RESISTANCE}} \cdot \frac{\text{DVM RANGE LEVEL}}{\text{AMPLIFIER GAIN}} \quad \ldots\ldots (A2.6)$$

$$\text{FLOW AREA, } A_M = L_S \cdot \text{FLOW PATH LENGTH} \quad \ldots\ldots (A2.7)$$

$$\text{VELOCITY, } u_M = \frac{Q}{A_M} \quad \ldots\ldots (A2.8)$$

$$\text{REYNOLDS NUMBER, } Re_M = \frac{u_M \rho d_t}{\mu} \quad \ldots\ldots (A2.9)$$

MASS TRANSFER AREA

(i) No tube-to-baffle leakage : $S = L_S \Pi d_t$ ..... (A2.10)

(ii) Tube-to-baffle leakage : $S = L_E \Pi d_t$ ..... (A2.11)

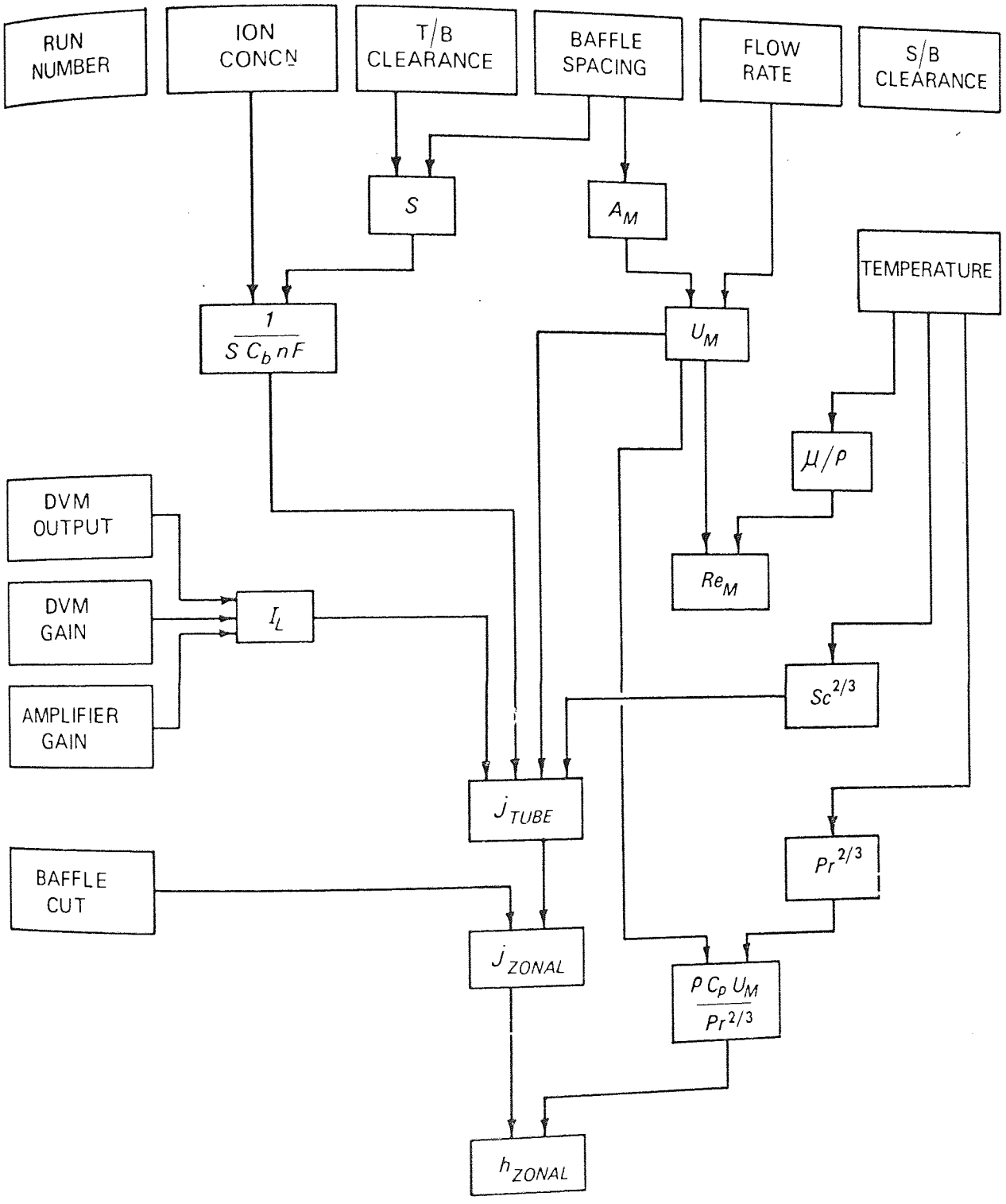

FIG 141 DATA PROCESSING

RUN NUMBER 73
SHELL DIA (MM) = 133 BAFFLE SPACING (MM) = 48.5 BAFFLE CUT (0/0) = 25.0
S/B CLEARANCE (MM) = 0.00 T/B CLEARANCE (MM) = 0.00
FLOW RATE (IPGM) = 14.0 TEMP (DEG.C) = 34.1 VELOCITY (M/S) = 0.559
REYNOLDS NUMBER = 0.6158E+04 SCHMIDT NUMBER = 1026 PRANDTL NUMBER = 5.7

INDIVIDUAL TUBE COEFFICIENTS

TUBE	JM	TUBE	JM	TUBE	JM	TUBE	JM
1	0.8414E-02	21	0.1317E-01	41	0.1262E-01	61	0.1149E-01
2	0.9981E-02	22	0.1329E-01	42	0.1236E-01	62	0.1192E-01
3	0.9284E-02	23	0.1137E-01	43	0.1163E-01	63	0.1166E-01
4	0.8675E-02	24	0.1311E-01	44	0.1178E-01	64	0.1175E-01
5	0.9255E-02	25	0.1285E-01	45	0.1187E-01	65	0.1181E-01
6	0.1204E-01	26	0.1323E-01	46	0.1140E-01	66	0.1210E-01
7	0.1132E-01	27	0.1279E-01	47	0.1192E-01	67	0.1137E-01
8	0.1094E-01	28	0.1297E-01	48	0.1192E-01	68	0.1137E-01
9	0.1088E-01	29	0.1248E-01	49	0.1221E-01	69	0.1088E-01
10	0.1181E-01	30	0.1250E-01	50	0.1152E-01	70	0.1091E-01
11	0.1227E-01	31	0.1265E-01	51	0.1143E-01	71	0.1108E-01
12	0.1239E-01	32	0.1303E-01	52	0.1137E-01	72	0.1042E-01
13	0.1262E-01	33	0.1277E-01	53	0.1172E-01	73	0.9894E-02
14	0.1262E-01	34	0.1268E-01	54	0.1172E-01	74	0.1013E-01
15	0.1265E-01	35	0.1227E-01	55	0.1192E-01	75	0.1088E-01
16	0.1236E-01	36	0.1207E-01	56	0.1184E-01	76	0.9487E-02
17	0.1137E-01	37	0.1233E-01	57	0.1187E-01	77	0.9284E-02
18	0.1320E-01	38	0.1213E-01	58	0.1201E-01	78	0.9545E-02
19	0.1335E-01	39	0.1192E-01	59	0.1213E-01	79	0.9313E-02
20	0.1332E-01	40	0.1250E-01	60	0.1184E-01	80	0.8878E-02

ZONAL AVERAGE COEFFICIENTS

JW1 = 0.1077E-01 JC = 0.1220E-01 JW2 = 0.1024E-01 JAV = 0.1165E-01

ZONAL AVERAGE HEAT TRANSFER COEFFICIENTS (KW/M^2,DEG.C)

HW1 = 0.7875E+01 HC = 0.8920E+01 HW2 = 0.7486E+01 HAV = 0.8517E+01

FIG 142

SPECIMEN COMPUTER PRINTOUT

MASS TRANSFER j-FACTOR

$$j_m = \left[\frac{I_L}{S\ C_b\ n_e\ F}\right]\left[\frac{1}{u_M}\right] Sc^{2/3} \qquad \ldots\ldots (A2.12)$$

HEAT TRANSFER COEFFICIENT

$$h = j_m \frac{\rho\ C_p\ u_M}{Pr^{2/3}} \qquad \ldots\ldots (A2.13)$$

A2.4.3.2 Physical Property Data

The electrolyte physical properties at the operating temperature were evaluated using the interpolation formulae given in Appendix 1.13.

A2.4.3.3 j-Factors of Dummy Tubes

The j-factors of the tubes in which pressure measurements were made, were estimated from those of adjacent tubes. Details are given in the tables below. The tube numeration is that given in Fig. 16. Thus j(8) refers to the j-factor for Tube 8.

(i) Single Segmental Baffles.

BAFFLE CUT (%)	FORMULA
18.4	$j(8) = \left[j(9) + j(7)\right]/2$ $j(73) = \left[j(72)+j(74)\right]/2$
25.0	$j(13) = j(14)$ $j(67) = j(68)$
37.5	$j(26) = j(27)$ $j(54) = j(55)$

(ii) Double Segmental Baffles.

BAFFLE CUT (%)	FORMULA
18.4	$j(8) = [j(9) + j(7)] /2$ $j(33) = [j(32)+j(34)] /2$
25.0	$j(13) = j(14)$ $j(26) = j(27)$

A2.4.3.4 Average j-Factors

(i) Baffle Compartment Average.

This average j-factor was derived as the arithmetic average of the j-factors from all the 80 tubes.

(ii) Zonal Average.

This average j-factor was derived as the arithmetic average of the j-factors from all the tubes contained within the particular zone.

In cases where the edge of the baffle bisected a tube row, the mass transfer from the tubes in this row was divided equally between the two zones.

A2.5 RESIDENCE TIME STUDIES

Limited development work was performed on the use of the electrochemical technique in studies of residence time distributions within the shell-side fluid. Local concentration disturbances produced by injections of the reacting ions were measured by the limiting currents from micro-electrodes.

Limiting currents from electrodes are associated with concentration gradients across the boundary layer. The use of micro-electrodes allows measurements of very local concentration disturbances. With the established conductivity methods, the response is from conductivity disturbances in a relatively large volume of liquid between two cell electrodes.

Injections were made at five points on the exchanger shell using a hypodermic syringe. These injection points are identified as bulkhead fittings in Fig. 13. 1 ml samples of a 0.10 molar potassium ferricyanide solution were injected into the flow of the electrolyte solution. The combination of this small volume of liquid and a large bore hypodermic needle, afforded on almost ideal pulse input disturbance. Cylindrical nickel cathodes $\frac{1}{8}$ in. (3.18 mm) long were located on various tubes midway between the baffles in the normal test baffle compartment (third of four). A micro-electrode tube is shown in Fig. 12. The outlet port anode was used. The response from a cathode was recorded on a Kent chart recorder, shunted to give a current readout.

With diffusion-controlled conditions at the cathode, an injection was made at a precise moment in time. The response of the cathode to this disturbance in the ferricyanide ion concentration was shown as a peak in the recorded limiting current such as those shown in Fig. 143. The injection points on the inlet port and in the inlet window zone of the second baffle compartment were favoured as these allowed a greater time interval between the injection and the response.

Analysis of experiments with no-leakage baffles showed that the time interval between the injection and the onset of the response peak agreed closely with that estimated for an element of fluid travelling from the point of injection to the cathode through the loci of the centres of all the crossflow and window zone channels. This agreement is illustrated in the table below. A Reynolds number (Re_M) of 300 was used throughout.

INJECTION POINT	CATHODE TUBE NO	ONSET OF PEAK(s)	TOP OF PEAK(s)	ESTIMATED TIME(s)
INLET PORT	38	14.1	18.8	14.6
INLET PORT	48	14.1	19.4	14.2
SECOND COMPARTMENT	38	8.2	9.1	7.8
SECOND COMPARTMENT	73	6.2	8.2	6.3

The initial response will be due to the element of fluid which takes the least time to travel from the point of injection to the cathode surface. Although there are shorter fluid paths than that mentioned above, the velocity of fluid travelling along these paths would appear to be lower. Integration of the response curves would given an indication of the distribution of the shell-side fluid between different streams.

In investigations with shell-to-baffle leakage a smaller response peak emerged before the main peak. An example is shown in Fig. 143. The main peak corresponded to that produced in the no-leakage investigations. This suggests that the main peak was caused by concentration disturbances carried in the main flow stream and the smaller peak by those carried in the shell-to-baffle leakage stream which bypasses the baffles.

The transfer of the concentration disturbance from the injection point to the cathode is assumed to be due only to convection in the shell-side fluid. The potential field in the electrolyte upstream of the cathode would be negligible.

The results from these limited investigations suggest the following uses for this aspect of the electrochemical technique in studies of shell-side phenomena:-

(i) Identification of baffle leakage and bundle-bypass streams.

(ii) Quantitative measurements could indicate the relative magnitudes of the shell-side flow streams.

(iii) Provide information on the intermixing of the shell-side flow streams. This would allow an accurate approach to calculating a true log mean temperature difference term (see Section 1.3.3).

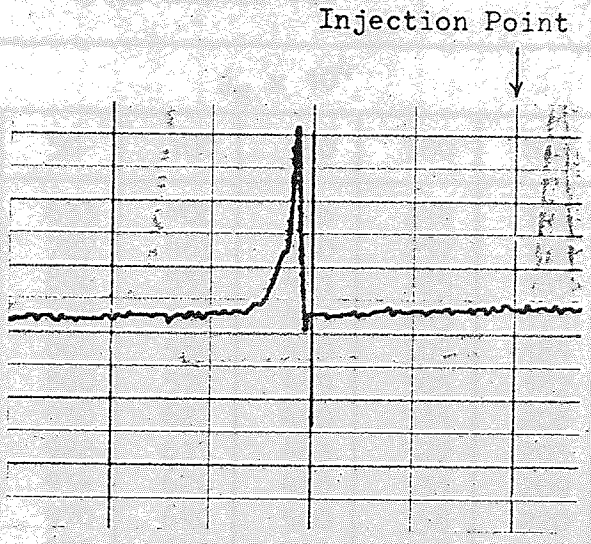

TYPICAL RESPONSE CURVE

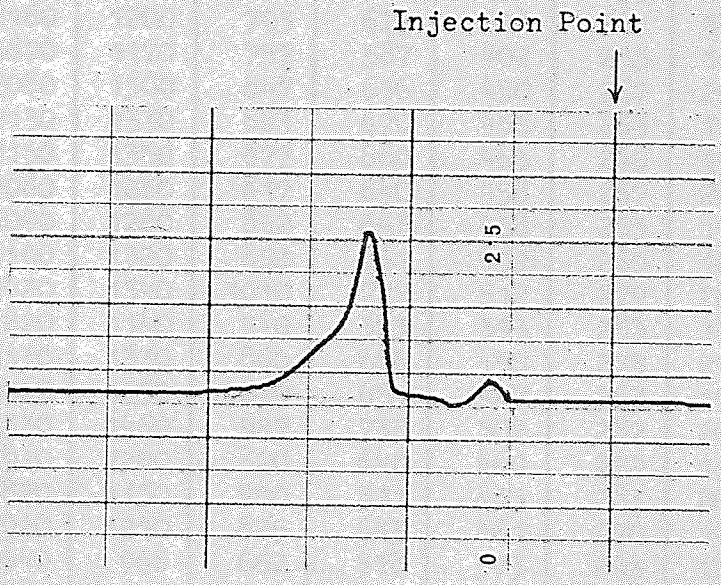

RESPONSE CURVE WITH SHELL-TO-BAFFLE LEAKAGE

Chart Speeds = 34 mm/s

Fig 143 RESPONSE CURVES

APPENDIX 3 TABULATED EXPERIMENTAL DATA

A 3.1 DEVELOPMENT WORK

A 3.1.1 Individual Tube j-Factors

43.7% Baffle Cut

Tube No	$j_M \times 10^4$						
Re_M =	24	50	100	150	300	800	1500
1	1250	633	408	328	218	132	95
4	1310	727	483	380	257	156	110
5	1450	806	535	421	285	165	116
8	1450	808	538	423	285	171	123
9	1630	860	580	450	305	184	133
10	1630	860	570	449	305	182	130
14	1690	938	622	490	331	208	150
15	1660	922	613	483	327	203	147
16	1680	934	620	488	331	209	153
20	1830	970	640	500	358	220	157
21	1820	970	642	506	358	220	158
22	1620	958	637	502	359	231	164
23	1710	1060	703	561	361	219	160
27	2070	1150	763	602	407	252	179
28	2130	1180	783	617	418	253	182
29	2160	1200	793	627	424	261	188
33	1870	1170	757	587	402	253	183
34	2080	1300	847	656	450	267	200
35	2130	1330	863	670	458	263	195
36	2150	1350	877	680	465	265	192
41	2080	1280	817	640	458	267	202
42	2090	1280	832	643	458	263	190
43	2100	1320	852	661	452	260	186
44	2420	1540	1010	777	512	279	200
48	1820	1140	740	573	393	253	186
49	2130	1330	860	666	450	275	200
50	2060	1290	839	651	447	262	192
51	2330	1460	947	732	502	287	202
55	1910	1200	820	640	460	272	190
56	1820	1150	740	571	453	283	206
57	1920	1210	825	643	461	270	191
61	1540	968	662	518	373	243	178
62	1780	1120	770	601	432	263	190
63	1680	1060	723	565	407	242	172
64	1890	1190	815	637	458	260	186
68	1470	923	632	494	355	215	160
69	1280	807	551	431	310	209	147
70	1250	789	540	422	304	193	142
73	1060	667	456	356	256	166	123
74	1110	760	530	419	265	172	125
75	995	626	428	334	240	162	127
78	910	572	392	307	220	149	111
79	970	610	419	328	236	150	115
80	923	470	403	322	212	135	96

31.0% Baffle Cut

Tube No	$j_M \times 10^4$		
Re_M =	300	800	1500
1	284	182	136
4	372	223	162
5	402	234	166
8	415	250	179
9	439	271	198
10	444	274	203
14	475	287	209
15	488	303	221
16	485	305	222
20	485	317	236
21	445	302	213
22	462	297	220
23	344	167	202
27	470	297	226
28	426	275	196
29	397	234	162
33	460	298	226
34	430	272	196
35	421	254	174
36	440	276	203
41	460	298	220
42	454	294	221
43	437	272	202
44	490	297	217
48	410	250	160
49	437	289	214
50	443	283	211
51	442	270	195
55	457	295	226
56	450	291	215
57	428	278	203
61	454	293	221
62	436	292	217
63	454	293	223
64	470	299	222
68	414	270	207
69	408	267	203
70	406	267	196
73	385	252	178
74	359	236	171
75	366	250	185
78	315	198	147
79	333	221	155
80	278	187	133

A 3.1.2 Zonal and Baffle Compartment Average j-Factors

43.7% Baffle Cut

Re_M	j-Factor* x 10			
	j_{w1_M}	j_{c_M}	j_{w2_M}	j_{av_M}
24	1.72	2.13	1.43	1.73
50	0.954	1.34	0.900	1.04
100	0.634	0.863	0.619	0.692
150	0.500	0.670	0.483	0.539
300	0.350	0.462	0.358	0.374
800	0.213	0.269	0.221	0.226
1500	0.153	0.194	0.160	0.164

31.0% Baffle Cut

Re_M	j-Factor* x 10			
	j_{w1_M}	j_{c_M}	j_{w2_M}	j_{av_M}
300	0.436	0.445	0.382	0.427
800	0.270	0.283	0.251	0.272
1500	0.196	0.208	0.185	0.200

* Average j-factors derived from all the tubes in the bundle assuming symmetry about a vertical diameter.

A 3.1.3 Individual Tube j-Factors from Test with Shell-to-Baffle Leakage.

31.0% Baffle Cut

Tube No	j_M x 10^4	
Re_M =	300	1500
1	252	116
10	360	170
14	405	188
42	345	195
44	355	159
48	365	195
51	285	150
68	325	164
70	363	162
80	279	102

A 3.1.4 Mass Transfer Coefficients for Composite Cathodes

All Data for 31.0% Baffle Cut

Tube 23

Re_M	$K_C \times 10^5$ (m/s)				K_M † $\times 10^5$ (m/s)	K_S $\times 10^5$ (m/s)
Increment =	1*	2	3	4		
300	0.80	1.07	1.11	1.18	1.04	1.06
500	1.07	1.36	1.43	1.49	1.34	1.41
1200	1.54	2.14	2.39	2.40	2.12	2.16
1500	1.75	2.33	2.66	2.70	2.36	2.42

† $K_M = \frac{1}{4}\Sigma K_C$

Tube 48

Re_M	$K_C \times 10^5$ (m/s)			
Increment =	1*	2	3	4
300	0.96	1.22	1.38	1.40
500	1.18	1.55	1.85	1.82
1200	1.58	2.48	3.07	3.05
1500	1.70	2.78	3.50	3.48

Tube 23 Shell-to-Baffle Leakage

Re_M	$K_C \times 10^5$ (m/s)			
Increment =	1*	2	3	4
300	0.57	0.71	0.67	0.82
800	1.06	1.13	1.24	1.46
1500	1.59	1.46	1.78	2.12

* Upstream Increment

A 3.1.5 Limiting Current Data for Multiple Cathodes

Operating as Individual Cathodes

Tube No	I_L^* (mA)
21	30.4
22	31.7
27	32.2
28	29.1
29	27.1
34	29.3
35	28.8
36	30.0

Operating as Multiple Cathodes

Tubes in Multiple Cathode	$I_{L_{Mult}}^*$ (mA)	$\Sigma I_{L_{Single}}$ (mA)
21	30.3	30.4
21, 22	61.8	62.1
21, 22, 27	94.3	94.3
21, 22, 27, 28	124.0	123.4
21, 22, 27, 28, 29	152.0	150.5
21, 22, 27, 28, 29, 34	181.1	179.8
21, 22, 27, 28, 29, 34, 35	209.8	208.6
21, 22, 27, 28, 29, 34, 35, 36	239.8	238.6

* Corrected to 25°C (using Figure 50)

A 3.1.6 Pressure Drop Data

43.7% Baffle Cut

Re_M	u_M x 10 (m/S)	ΔP (in W)	$\frac{\Delta P/\rho u_M^2}{2}$ ($N\ s^2/Kg\ m$)
300	0.34	0.03	13.0
800	0.90	0.15	8.86
1000	1.12	0.21	7.92
1200	1.34	0.28	7.44
1500	1.68	0.41	6.90
2000	2.24	0.67	6.35
3000	3.36	1.43	6.00

31.0% Baffle Cut

Re_M	$u_M \times 10$ (m/S)	ΔP (in W)	$\Delta P/\rho u_M^2$ $(N\ s^2/Kg\ m)$
300	0.34	0.05	20.5
800	0.90	0.22	12.9
1000	1.12	0.36	13.5
1200	1.34	0.50	12.9
1500	1.68	0.72	12.1
2000	2.24	1.18	11.2
3000	3.36	2.53	10.7

A 3.1.7 Verification of the Schmidt Number Exponent

Tube 41

Sc	$C_b\mu/\rho \times 10^9$ (Kg mole/m.s)	I_L (mA)		
		Re_M = 150	500	1000
1272	9.65	24.2	42.1	60.8
1528	10.48	23.2	39.0	56.3
2348	11.00	18.7	33.5	48.1
6300	17.60	15.7	27.7	39.8
31770	37.60	12.3	19.0	-

Multiple Cathode using Tubes 1, 9, 41, 44, 74

Sc	$C_b\mu/\rho \times 10^9$ (Kg mole/m.s)	I_L (mA)		
		Re_M = 150	500	1000
1272	9.65	93.3	161.6	228.7
1528	10.48	89.0	149.2	210.0
2348	11.00	73.2	125.5	177.8
6300	17.60	63.5	107.8	155.6
31770	37.60	44.2	72.8	-

A 3.2 EXPERIMENTAL WORK AT AEE WINFRITH

A 3.2.1 Summary of the Experiments

Run Number		Baffle* Thickness (in)	S-B Clearance (in)	T-B Clearance (in)	Baffle Spacing (in)	Baffle Cut (% dia)	Compart-ment Tested	Flow Inlet To Compart-ment Tested
44- 56	SINGLE SEGMENTAL NO-LEAKAGE	0.0625	0	0	1.91	18.4	5th of 9	TOP
57- 67		0.0625	0	0	3.82	18.4	3rd of 5	TOP
68- 77		0.0625	0	0	1.91	25.0	5th of 9	TOP
78- 87		0.0625	0	0	3.82	25.0	3rd of 5	TOP
88- 97		0.0625	0	0	1.91	37.5	5th of 9	TOP
98-109		0.0625	0	0	3.82	37.5	3rd of 5	TOP
184-193		0.0625	0	0	1.91	37.5	2nd of 6	TOP
194-205		0.0625	0	0	1.91	37.5	5th of 9	TOP
357-364		0.0625	0	0	3.82	37.5	3rd of 5	SIDE
132-141A	SINGLE SEGMENTAL LEAKAGE	0.0625	0.055	0.013	1.91	18.4	5th of 9	TOP
141B-150		0.0625	0.055	0.013	1.91	18.4	5th of 9	BOTTOM
151-161		0.125	0.105	0.026	1.91	18.4	5th of 9	TOP
162-172		0.125	0.105	0.026	1.91	18.4	5th of 9	BOTTOM
173-183		0.125	0.105	0.026	1.91	18.4	5th of 9	SIDE
206-216		0.125	0.105	0.026	1.91	25.0	5th of 9	SIDE
217-227	DOUBLE SEGMEN-TAL	0.125	0.105	0.026	1.91	37.5	5th of 9	SIDE
228-238		0.125	0.105	0.026	1.91	18.4	5th of 9	SIDE
239-249		0.125	0.105	0.026	1.91	18.4	4th of 9	SIDE

* Nominal - see Appendix 3.3.1 for actual thicknesses

The quantity of data from these experiments has meant that only zonal and baffle compartment average j-factors are tabulated in this thesis.

Individual tube j-factor data in the format of the data sheet shown in Figure 142 are in the custody of Dr B Gay, Department of Chemical Engineering, University of Aston, in Birmingham.

A 3.2.2 Single Segmental Baffles without Leakage.
Zonal and Compartment Average j-Factors

Run Number	Re_M	j-Factor x 10^2			
		j_{w1_M}	j_{c_M}	j_{w2_M}	j_{av_M}
44	7450	1.23	1.24	1.11	1.22
45	5550	1.38	1.38	1.24	1.36
46	3310	1.67	1.69	1.52	1.67
47	2350	1.88	1.85	1.67	1.84
48	972	2.82	2.73	2.52	2.72
49	524	3.79	3.55	3.19	3.54
50	320	4.73	4.42	3.84	4.39
51	11900	1.05	1.07	0.955	1.05
52	16200	0.939	0.941	0.845	0.932
53	20600	0.873	0.870	0.804	0.864
54	7380	1.25	1.26	1.12	1.24
55	19400	0.891	0.860	0.776	0.855
56	24300	0.840	0.810	0.758	0.808
57	153	6.74	6.27	5.11	6.20
58	123	7.63	7.11	6.13	7.06
59	223	5.55	4.73	3.99	4.73
60	434	4.17	3.40	2.91	3.42
61	1130	2.58	2.13	1.78	2.14
62	1680	2.20	1.86	1.55	1.86
63	2960	1.72	1.46	1.26	1.46
64	4280	1.48	1.25	1.11	1.26
65	6440	1.21	1.03	0.829	1.03
66	8600	1.11	0.913	0.706	0.912
67	12800	0.939	0.774	0.571	0.770
68	257	4.25	4.70	3.75	4.46
69	462	3.45	3.65	3.26	3.50
70	950	2.49	2.71	2.16	2.58
71	2380	1.55	1.74	1.39	1.66
72	3500	1.37	1.55	1.27	1.47
73	6160	1.08	1.22	1.02	1.17
74	8890	0.908	1.05	0.839	0.993
75	13300	0.774	0.904	0.728	0.854
76	17500	0.695	0.822	0.680	0.779
77	26000	0.587	0.717	0.609	0.678
78	113	6.98	6.88	5.63	6.70
79	224	5.12	4.89	3.96	4.78
80	440	3.83	3.59	2.87	3.51
81	1170	2.31	2.17	1.76	2.13
82	1740	2.05	1.94	1.56	1.89
83	3090	1.59	1.51	1.21	1.48
84	4430	1.35	1.27	1.02	1.25
85	6700	1.13	1.06	0.853	1.04
86	8920	1.01	0.927	0.754	0.912
87	13200	0.883	0.791	0.652	0.783

Run Number	Re_M	j-Factor x 10^2			
		$jw1_M$	j_{cM}	$jw2_M$	j_{avM}
88	236	3.99	4.90	3.76	4.24
89	430	2.86	3.61	2.75	3.09
90	862	1.99	2.61	2.00	2.21
91	2240	1.21	1.62	1.24	1.37
92	3390	1.06	1.43	1.10	1.21
93	6090	0.807	1.10	0.854	0.926
94	8860	0.686	0.935	0.725	0.786
95	13400	0.568	0.781	0.602	0.654
96	17900	0.507	0.694	0.535	0.582
97	26700	0.456	0.619	0.491	0.525
98	125	6.27	6.90	5.61	6.28
99	221	4.47	4.84	3.85	4.39
100	435	3.14	3.44	2.67	3.09
101	1130	1.93	2.16	1.68	1.93
102	1670	1.68	1.88	1.48	1.68
103	2980	1.29	1.44	1.14	1.29
104	4370	1.08	1.19	0.950	1.08
105	6580	0.904	0.987	0.792	0.897
106	8770	0.795	0.851	0.692	0.781
107	13100	0.684	0.727	0.596	0.670
108	17400	0.633	0.658	0.547	0.614
109	21700	0.592	0.616	0.521	0.577
184	242	3.68	4.65	3.55	3.98
185	435	2.74	3.39	2.63	2.93
186	862	1.92	2.54	2.03	2.18
187	2250	1.20	1.60	1.24	1.35
188	3390	1.01	1.34	1.06	1.14
189	6020	0.772	1.01	0.801	0.864
190	8720	0.655	0.853	0.678	0.732
191	13200	0.529	0.688	0.550	0.591
192	17700	0.456	0.583	0.465	0.503
193	26600	0.395	0.492	0.404	0.432
194	226	3.75	4.80	3.60	4.05
195	405	2.85	3.65	2.73	3.10
196	787	2.10	2.63	2.07	2.28
197	2090	1.27	1.69	1.31	1.43
198	3100	1.11	1.48	1.14	1.25
199	5540	0.845	1.15	0.875	0.963
200	8020	0.734	0.997	0.763	0.835
201	12200	0.609	0.839	0.626	0.695
202	16400	0.528	0.736	0.540	0.605
203	24800	0.462	0.637	0.478	0.529
204	5940	0.818	1.10	0.825	0.917
205	2390	1.20	1.60	1.22	1.35
357	133	6.11	6.99	5.65	6.27
358	199	4.92	5.50	4.34	4.93
359	405	3.27	3.70	2.87	3.29
360	1020	2.09	2.41	1.88	2.13
361	1630	1.76	2.04	1.58	1.80
362	2870	1.34	1.56	1.21	1.38
363	3710	1.23	1.41	1.10	1.25
364	5710	0.982	1.14	0.878	1.00
365	7730	0.882	1.01	0.793	0.898
366	11800	0.769	0.877	0.696	0.783

3.2.3 Single Segmental Baffles with Leakage.

Zonal and Compartment Average j-Factors

Run Number	Re_M	j-Factor x 10^2			
		j_{w1_M}	j_{c_M}	j_{w2_M}	j_{av_M}
132	237	4.25	4.32	4.05	4.29
133	420	3.14	3.02	2.75	3.01
134	832	2.34	2.28	2.20	2.28
135	2160	1.41	1.41	1.38	1.42
136	3180	1.16	1.19	1.16	1.18
137	5620	0.852	0.899	0.896	0.894
138	8190	0.718	0.763	0.768	0.759
139	12400	0.570	0.616	0.635	0.613
140	16600	0.501	0.540	0.564	0.539
141A	24900	0.414	0.450	0.480	0.450
141B	242	3.85	3.95	3.90	3.93
142	425	3.33	3.17	3.10	3.17
143	820	2.55	2.32	2.39	2.35
144	2110	1.51	1.51	1.61	1.51
145	3100	1.25	1.27	1.39	1.28
146	5510	0.902	0.957	1.04	0.960
147	7990	0.753	0.817	0.895	0.818
148	12100	0.598	0.657	0.727	0.658
149	16300	0.531	0.579	0.649	0.581
150	24600	0.467	0.484	0.537	0.487
151	225	3.49	3.51	3.11	3.48
152	399	2.91	2.75	2.47	2.74
153	790	2.07	1.92	1.81	1.92
154	2050	1.18	1.13	1.09	1.13
155	3020	0.947	0.944	0.890	0.939
157	7920	0.585	0.607	0.605	0.604
158	12000	0.467	0.490	0.493	0.488
159	16200	0.399	0.419	0.436	0.419
160	24600	0.335	0.357	0.372	0.356
161	41400	0.266	0.287	0.310	0.287
162	234	3.11	3.30	3.24	3.27
163	415	2.56	2.60	2.61	2.60
164	815	1.86	1.90	2.04	1.90
165	2100	1.11	1.16	1.32	1.17
166	3110	0.919	0.964	1.09	0.971
167	5550	0.675	0.720	0.807	0.724
168	8080	0.557	0.609	0.609	0.612
169	12300	0.447	0.496	0.568	0.498
170	16800	0.377	0.422	0.486	0.424
171	24500	0.322	0.360	0.415	0.362
172	42400	0.273	0.290	0.325	0.291

Run Number	Re_M	j-Factors x 10^2			
		j_{w1_M}	j_{c_M}	j_{w2_M}	j_{av_M}
173	231	3.31	3.45	3.28	3.43
174	416	2.75	2.69	2.59	2.69
175	819	2.02	1.95	1.96	1.96
176	2120	1.26	1.23	1.29	1.24
177	3170	1.01	0.995	1.08	1.00
178	5630	0.728	0.745	0.799	0.748
179	8190	0.613	0.631	0.681	0.634
180	12400	0.497	0.511	0.550	0.513
181	16800	0.432	0.444	0.480	0.446
182	25200	0.383	0.384	0.410	0.386
183	42300	0.312	0.312	0.325	0.313
206	235	2.95	3.56	3.10	3.38
207	350	2.57	2.94	2.56	2.82
208	741	1.80	2.01	1.85	1.95
209	1930	1.12	1.28	1.22	1.25
210	3130	0.841	0.997	0.981	0.969
211	5570	0.608	0.746	0.748	0.724
212	8070	0.498	0.626	0.630	0.606
213	12300	0.404	0.517	0.523	0.499
214	16500	0.356	0.457	0.466	0.442
215	24800	0.304	0.389	0.402	0.377
216	41400	0.257	0.323	0.340	0.315
217	223	2.82	3.71	3.02	3.20
218	330	2.36	3.08	2.50	2.65
219	696	1.63	2.09	1.70	1.81
220	1810	0.978	1.30	1.12	1.14
221	2950	0.753	1.02	0.902	0.896
222	5280	0.528	0.743	0.676	0.651
223	7660	0.424	0.619	0.572	0.540
224	11700	0.343	0.510	0.477	0.445
225	15800	0.289	0.433	0.413	0.380
226	24100	0.247	0.367	0.353	0.323
227	40500	0.202	0.297	0.294	0.265

A 3.2.4 Double Segmental Baffle Zonal and Compartment Average j-Factors

Divergence Compartment

Run Number	$Re_{M'}$	j-Factor* x 10^2			
		$j_{OW_{M'}}$	$j_{C_{M'}}$	$j_{IW_{M'}}$	$j_{av_{M'}}$
228	115	5.34	6.07	5.61	5.81
229	178	4.23	4.72	4.43	4.45
230	375	2.91	3.15	3.12	3.09
231	976	2.02	2.11	2.13	2.10
232	1600	1.63	1.70	1.68	1.68
233	2850	1.22	1.28	1.21	1.24
234	4120	1.03	1.08	1.01	1.05
235	6350	0.830	0.875	0.816	0.850
236	8410	0.728	0.773	0.719	0.750
237	12600	0.606	0.672	0.638	0.650
238	21200	0.485	0.531	0.524	0.521

Convergence Compartment

Run Number	$Re_{M'}$	j-Factor* x 10^2			
		$j_{OW_{M'}}$	$j_{C_{M'}}$	$j_{IW_{M'}}$	$j_{av_{M'}}$
239	117	6.01	6.33	5.71	6.10
240	176	4.96	5.05	4.44	4.87
241	371	3.34	3.32	2.99	3.23
242	962	2.19	2.20	2.09	2.17
243	1590	1.69	1.77	1.71	1.74
244	2820	1.23	1.31	1.26	1.28
245	4090	0.985	1.09	1.04	1.06
246	6210	0.793	0.888	0.851	0.860
247	8340	0.710	0.799	0.772	0.775
248	12600	0.614	0.688	0.671	0.670
249	21100	0.496	0.563	0.553	0.547

* Average j-factors derived from tubes in both symmetrical halves of the bundle

A 3.2.5 Pressure Drop Data

Single-segmental, no-leakage
(corresponding to Runs 44-56)

Re_M	u_M x 10 (m/s)	ΔP_C* (in W)	ΔP_W* (in W)	$\Delta P_C/\frac{\rho u_M^2}{2}$ (N_s^2/Kg m)	$\Delta P_W/\frac{\rho u_M^2}{2}$ (N_s^2/Kg m)
445	0.47	0.052	0.034	11.01	7.22
863	0.88	0.14	0.11	8.22	6.84
2150	2.20	0.51	0.61	5.03	5.90
3130	3.20	1.06	1.43	4.92	6.64
5490	5.60	3.10	4.15	4.76	6.25
8020	8.00	6.05	8.70	4.54	6.45
12000	12.00	12.70	18.30	4.21	6.01

* Test baffle compartment

Single-segmental Baffles with Leakage
(corresponding to Runs 141B-150)

Re_M	u_M x 10 (m/s)	ΔP_C* (in W)	ΔP_W+ (in W)	$\Delta P_T/\frac{\rho u_M^2}{2}$ (N_s^2/Kg m)
863	0.88	0.04	0.06	6.20
2150	2.20	0.17	0.32	4.76
3130	3.20	0.45	0.65	5.13
5490	5.60	1.10	1.49	3.85
8020	8.00	2.30	2.77	3.76
12000	12.00	4.72	5.57	3.40
16000	16.01	9.27	10.20	3.61
24000	24.20	24.70	22.30	3.81

* Top inlet compartment

\+ Bottom window zone

Single-segmental Baffles with Leakage
(corresponding to Runs 173-183)

Re_M	u_M x 10 (m/s)	ΔP_C* (in W)	ΔP_W* (in W)	$\Delta P_T/\frac{\rho u_M^2}{2}$ (N_s^2/Kg m)
863	0.88	-0.07	0.11	2.45
2150	2.20	0.04	0.19	2.23
3130	3.20	0.19	0.30	2.28
5490	5.60	0.67	0.71	2.09
8020	8.00	1.34	1.36	2.00
12000	12.00	2.48	2.57	1.66
16000	16.01	4.32	4.35	1.60
24000	24.20	10.01	9.00	1.58

* Test baffle compartment

Single-segmental Baffles with Leakage
(corresponding to Runs 217-227)

Q (l/min)	ΔP_C* (in W)	ΔP_W* (in W)	2 x ΔP_T (KN/m^2)
22.7	0.022	0.086	0.055
36.3	0.065	0.15	0.11
63.5	0.19	0.37	0.28
90.8	0.48	0.69	0.58
136.0	0.95	1.45	1.20
182.0	1.49	2.33	1.90
272.0	3.73	5.48	4.58
454.0	10.40	16.12	13.20

* Test baffle compartment

Double-segmental Baffles
(corresponding to Runs 228-238)

Q (l/min)	ΔP (in W)				$\Sigma\Delta P$* KN/m^2
	ΔP_{C_1}	ΔP_{W_1}	ΔP_{C_2}	ΔP_{W_2}	
22.7	0.033	0.033	0.086	0.11	0.060
36.3	0.065	0.13	0.086	0.19	0.12
63.5	0.17	0.37	0.17	0.43	0.28
90.8	0.37	0.65	0.33	0.71	0.51
136.0	0.76	1.38	0.76	1.36	1.06
182.0	1.25	2.46	1.30	2.25	1.80
272.0	2.49	5.55	2.65	5.22	3.95
454.0	6.70	16.20	7.30	14.70	11.20

* $\Sigma\Delta P = \Delta P_{C_1} + \Delta P_{W_1} + \Delta P_{C_2} + \Delta P_{W_2}$

Other pressure drop data not analysed in this thesis are in the custody of Dr B Gay, Department of Chemical Engineering, University of Aston in Birmingham.

A 3.3 PHYSICAL DIMENSIONS

A 3.3.1 Baffle Thickness

Type of Baffle	Nominal Thickness (in)	Actual Thickness (in)
No-leakage	1/16	0.059 ± 0.001
Leakage	1/16	0.064 ± 0.001
Leakage	1/8	0.122 ± 0.004

A 3.3.2 Flow Areas

i Minimum crossflow area at centre row of tubes

Baffle Spacing (mm)	Flow Area (mm^2)	
	A_M	A_M'
48.5	1896	1870
97.0	3792	3740

ii Window flow area (Single segmental baffles)

Baffle Cut (% Dia)	A_W (mm^2)
18.4	1097
25.0	1660
37.5	2870

iii Window flow area (Double segmental baffles with cut of 18.4%)

Window	A_W* (mm^2)
Inner	883
Outer	1130

* One symmetrical half of the bundle

iv Minimum and maximum crossflow areas (Independent of baffle cut)

Baffle Spacing (mm)	Area (mm^2)	
	A_{min}*	A_{max}
48.5	1896	3110
97.0	3792	6220

* In fact $A_{min} = A_M$

v Longitudinal flow area in crossflow zone.
(Used in Weisman correlation)

Baffle Cut (% Dia)	A_{CL} (mm^2)
18.4	5980
37.5	2400

iv Superficial flow area in crossflow and window zones (used in Weisman correlation)

Baffle Spacing (mm)	Baffle Cut (% Dia)	A_{sup} (mm^2)	
		Crossflow Zone	Window Zone
48.5	18.4	5770	3100
97.0	37.5	12200	9450

A 3.3.3 Crossflow Zone Dimensions

Baffle Spacing L_S (mm)	Baffle Cut (% Dia)	Baffle Overlap L_C (mm)	L_C/L_S
48.5	18.4	86.3	1.78
48.5	25.0	71.3	1.47
48.5	37.5	35.4	0.73
97.0	18.4	86.3	0.89
97.0	25.0	71.3	0.73
97.0	37.5	35.4	0.37

A 3.3.4 Baffle Leakage Areas (Single segmental baffles)

A 3.3.4.1 Tube-to-Baffle Leakage

Leakage Area per Tube

Nominal Baffle Thickness (in)	A_{TB} (mm^2)
1/16	5.0
1/8	10.2

Total leakage area per baffle

Baffle Cut (% Dia)	No. Tube Holes in Baffle	A_{TB} (mm^2)	
		1/16 in. Baffles	1/8 in. Baffles
18.4	72.5	363	740
25.0	67	335	683
37.5	54	270	551

A 3.3.4.2 Shell-to-Baffle Leakage

Leakage area per full-face baffle (ie no window)

Nominal Baffle Thickness (in)	A_{SB} (mm^2)
1/16	316
1/8	548

Leakage area per baffle

Baffle Cut (% Dia)	% Circumference available for Leakage	Leakage Area A_{SB} (mm^2)	
		1/16in. Baffles	1/8in. Baffles
18.4	71.5	226	392
25.0	67.2	212	368
37.5	58.1	184	318

A 3.3.5 Baffle Leakage Areas (Double segmental baffles)

48.5 mm Baffle spacing, 18.4% baffle cut
Defined for one symmetrical half of the bundle

Baffle (See Fig 122)	No. of Tubes Holes	% Circumference* available for Leakage
1 - Piece	32.5	22.5
2 - Piece	29	43.9
Average =	30.75	33.2

* Assuming no leakage at interface between the two symmetrical half units

Whence

Leakage Area (mm^2)		
A_{TB}	A_{SB}	A_T
313	182	495

A 3.3.6 Baffle Design Standards

Reccommended Baffle Clearances
(Dimensions in Inches)

Design Standard	Class or Grade	Shell Dia	Baffle Thickness	Clearances		Orifice Shape Factor	
				S-B	T-B	Z_S	Z_T
TEMA	R	8-13	1/8	0.100	1/32*	2.5	8.0
					1/64	2.5	16.0
	C	6-13	1/16	0.100	1/32	1.25	4.0
					1/64	1.25	8.0
	B	6-13	1/8	0.100	1/32	2.5	8.0
					1/64	2.5	16.0
BS 2041 Later BS 3274	1	8-25	1/8	0.125	1/32	2.0	8.0
					1/64	2.0	16.0
	2 (Liq)	8-14	1/8	0.100	1/32	2.5	8.0
	(gas)		1/8	0.188	1/64	1.33	16.0

* 1/32 in T-B clearances for unsupported tube lengths of 36 in. or less.
1/64 in T-B clearances for those greater than 36 in.

A 3.4 SPECIMEN CALCULATIONS

A 3.4.1 Mass Transfer j-Factor in the Development Work

Example: No-leakage, 43.7% baffle cut

Tube 1, $Re_M = 300$

Current $I_L = 15.3$ mA

Electrolyte temperature = 23.7°C

Ferricyanide ion concentration, $C_b = 0.0106$ kg mole/m^3

Correcting current to 25°C datum using Fig 50 gives:

$$I_{L\ 25^oC} = 15.8 \text{ mA}$$

From equation (A 2.2)

$$j_M = \frac{I_L}{C_b\ Re_M} \left[\frac{Sc^{2/3} \rho\ d_t}{S\ F\ n_e \mu} \right]$$

Evaluating electrolyte physical property data at 25°C (Appendix 1.13) and the electrode surface area S from equation (A 2.10) gives (in SI units):

$$j_M = \frac{15.8 \times 10^{-3}}{0.0106 \times 300} \left[\frac{1570^{2/3} \times 1045 \times (9.5 \times 10^{-3})}{(99.0 \times \Pi \times 9.5 \times 10^{-6}) \times 9.65 \times 10^7 \times 1 \times (1.11 \times 10^{-3})} \right]$$

$$= 2.18 \times 10^{-2}$$

A 3.4.2 Natural Convection Data

A 3.4.2.1 Grashof Numbers

For horizontal cylinders in crossflow, the Grashof number for natural convection heat transfer is given by:

$$Gr_h = \frac{d_t^3\ \rho^2\ g\ \beta_h \Delta T}{\mu^2} \qquad \ldots (A\ 3.1)$$

For vertical cylinders the tube length is the characteristic dimension.

The analogous Grashof number for natural convection mass transfer is given by:

$$Gr_m = \frac{d_t^3 \rho^2 g}{\mu^2} \left(\frac{\Delta\rho}{\rho} \right) \qquad \ldots (A\ 3.2)$$

where $\Delta\rho$ is the density difference brought about by differences in concentration.

The value of the densification term $\Delta\rho$ for the electrochemical system used in this work was taken as that reported by Fouad and Gouda (95) for a 0.01 M ferricyanide, 0.01 M ferrocyanide, 2.0 M sodium hydroxide electrolyte solution (cf. 0.01/0.01/1.0 M solution of this work). Data for solutions of other reacting ion concentrations showed the sodium hydroxide concentration to have little effect on the value of the densification term.

Grashof numbers for horizontal cylinders derived for the heat and mass transfer processes (See Section 4.4.2.8) are tabulated below:

Work	Sc or Pr	Grashof Number
Tompkins*	1150	12.1
Brown*	29.2	1.54×10^4
Williams	1.22	3.8×10^{-4}
This Work+	1570	3.9×10^4

* Average of the data for the heating and cooling experiments.

\+ Physical property data at 25°C

This work gave a value of 5.7×10^7 for the Grashof number for vertical cylinders. The characteristic length was 3.89 in (99.0 mm).

A 3.4.2.2 Natural Convection Components

Natural convection components were derived from baffle compartment or

bundle average j-factor data assuming a negligible natural convection component in Williams' data. Corresponding Nusselt or Sherwood numbers were calculated from the equations:

$$Nu = j_h \, Re \, Pr^{1/3} \qquad \ldots (A\ 3.3)$$

and $$Sh = j_m \, Re \, Sc^{1/3} \qquad \ldots (A\ 3.4)$$

Example: 3.89 in. (99.0 mm) baffle spacing,

43.7% baffle cut.

$Re_M = 20$ (extrapolating data in Fig 17 accordingly)

Work	j_{av}	j_{av} Natural Convection	Nu or Sh
Williams	0.0125	ZERO	-
Tompkins	0.0154	0.029	6.08
This Work	0.0194	0.069	16.0

The results of all the analyses are tabulated below:

Work	Nu or Sh		
Re_M =	20	60	100
Tompkins	6.08	10.3	-
This Work:			
Aston	16.0	14.8	-
Aston*	182	169	
Winfrith	-	-	14.9

* Using correlation for vertical cylinders